


December 2015

Predictive Modeling of Terrestrial Radiation Exposure from Geologic Materials

Daniel A. Haber
University of Nevada, Las Vegas

Follow this and additional works at: <https://digitalscholarship.unlv.edu/thesesdissertations>

 Part of the [Geochemistry Commons](#), [Nuclear Commons](#), and the [Remote Sensing Commons](#)

Repository Citation

Haber, Daniel A., "Predictive Modeling of Terrestrial Radiation Exposure from Geologic Materials" (2015).
UNLV Theses, Dissertations, Professional Papers, and Capstones. 2537.
<http://dx.doi.org/10.34917/8220105>

This Thesis is protected by copyright and/or related rights. It has been brought to you by Digital Scholarship@UNLV with permission from the rights-holder(s). You are free to use this Thesis in any way that is permitted by the copyright and related rights legislation that applies to your use. For other uses you need to obtain permission from the rights-holder(s) directly, unless additional rights are indicated by a Creative Commons license in the record and/or on the work itself.

This Thesis has been accepted for inclusion in UNLV Theses, Dissertations, Professional Papers, and Capstones by an authorized administrator of Digital Scholarship@UNLV. For more information, please contact digitalscholarship@unlv.edu.

PREDICTIVE MODELING OF TERRESTRIAL RADIATION EXPOSURE FROM GEOLOGIC
MATERIALS

By

Daniel A. Haber

Bachelor of Science – Geoscience

University of Nevada, Las Vegas

2013

A thesis submitted in partial fulfillment
of the requirements for the

Master of Science - Geoscience

Department of Geoscience

College of Sciences

The Graduate College

University of Nevada, Las Vegas

December 2015



Thesis Approval

The Graduate College
The University of Nevada, Las Vegas

October 30, 2015

This thesis prepared by

Daniel Haber

entitled

Predictive Modeling of Terrestrial Radiation Exposure from Geologic Materials

is approved in partial fulfillment of the requirements for the degree of

Master of Science – Geoscience
Department of Geosciences

Pamela C. Burnley, Ph.D.
Examination Committee Chair

Kathryn Hausbeck Korgan, Ph.D.
Graduate College Interim Dean

Elisabeth Hausrath, Ph.D.
Examination Committee Member

Russell Malchow, Ph.D.
Examination Committee Member

Ralf Sudowe, Ph.D.
Graduate College Faculty Representative

Abstract

Aerial gamma ray surveys are an important tool for national security, scientific, and industrial interests in determining locations of both anthropogenic and natural sources of radioactivity. There is a relationship between radioactivity and geology and in the past this relationship has been used to predict geology from an aerial survey. The purpose of this project is to develop a method to predict the radiologic exposure rate of the geologic materials in an area by creating a model using geologic data, images from the Advanced Spaceborne Thermal Emission and Reflection Radiometer (ASTER), geochemical data, and pre-existing low spatial resolution aerial surveys from the National Uranium Resource Evaluation (NURE) Survey. Using these data, geospatial areas, referred to as background radiation units, homogenous in terms of K, U, and Th are defined and the gamma ray exposure rate is predicted. The prediction is compared to data collected via detailed aerial survey by our partner National Security Technologies, LLC (NSTec), allowing for the refinement of the technique.

High resolution radiation exposure rate models have been developed for two study areas in Southern Nevada that include the alluvium on the western shore of Lake Mohave, and Government Wash north of Lake Mead; both of these areas are arid with little soil moisture and vegetation. We determined that by using geologic units to define radiation background units of exposed bedrock and ASTER visualizations to subdivide radiation background units of alluvium, regions of homogenous geochemistry can be defined allowing for the exposure rate to be predicted.

Soil and rock samples have been collected at Government Wash and Lake Mohave as well as a third site near Cameron, Arizona. K, U, and Th concentrations of these samples have been determined using inductively coupled mass spectrometry (ICP-MS) and laboratory counting using radiation detection equipment. In addition, many sample locations also have

concentrations determined via *in situ* radiation measurements with high purity germanium detectors (HPGe) and aerial survey measurements. These various measurement techniques have been compared and found to produce consistent results.

Finally, modeling using Monte Carlo N-Particle Transport Code (MCNP), a particle physics modeling code, has allowed us to derive concentration to exposure rate coefficients. These simulations also have shown that differences in major element chemistry have little impact on the gamma ray emissions of geologic materials.

Acknowledgements

I would like to thank the Canadian Geologic Survey for their help in the field and their insights into this project as well as NSTec for providing funding and principal support.

Kara Marsac, thank you for spearheading this project and giving me the confidence to take on this challenge. Having you around to bounce ideas off of was a tremendous asset to my work and the project as a whole. You have been a great friend as well as a great colleague.

Christopher Adcock, thank you for providing all the remote sensing imagery and the great advice. The shadow reduction technique you came up with turned Lake Mohave into a success.

Racheal Johnson, thank you for your unique insight into petrology and the chemistry of igneous rocks. Thank you also for the great advice and help at every turn.

I would also like to thank my family for supporting me over the last six years. I want to especially thank my brother Robert whose love of science rivals my own.

To my wife Erin, thank you for being there for me these six long years through school. You have fully supported me every step of the way and I can't thank you enough. This past decade with you has been the best time of my life. I can't wait to see what the next decade bring us.

I would also like to thank my committee:

Ralf Sudowe, I learned so much from your careful patient teaching. You are a tremendous educator and a kind person; thank you.

Libby Hausrath, thank you for guiding me through all of this complex chemistry and the advice you provided to us all.

Rusty Malchow, I learned so much from you that it's frankly immeasurable. Thank you for constantly checking this geologist's math and for rushing to get our work through the STIP process.

Finally, Pamela Burnley, you have been an amazing advisor and mentor. Thank you so much for bringing me onto this project. Through dedicated guidance and, at times, forcing me to be independent you have turned this student into a scientist. In the paraphrased words of Carl Sagan: science is more than a body of knowledge, it is a way of thinking; you have taught me how to think like a scientist and for that I will be forever grateful.

This research was supported by National Security Technologies, LLC, under Contract No. DE-AC52-06NA25946 with the U.S. Department of Energy and by the Site-Directed Research and Development Program. The United States Government retains and the publisher, by accepting this document for publication, acknowledges that the United States Government retains a non-exclusive, paid-up, irrevocable, world-wide license to publish or reproduce the published form of this manuscript, or allow others to do so, for United States Government purposes, DOE/NV/25946--2680.

Table of Contents

Abstract	iii
Acknowledgements	v
Table of Contents	vii
List of Tables	xii
List of Figures	xiii
List of Equations	xvi
Chapter One	1
Introduction	1
Figures	5
Chapter Two	8
Background	8
Aerial Gamma Ray Surveys	8
Radioactivity	8
Terrestrial Sources of Radiation	9
Disequilibrium	12
Other Effects	13
Gamma Ray Spectra	14
Exposure Rate Calculation and Spectral Stripping	16
Manuscripts	17
Tables	18

Figures	19
Chapter Three: Monte Carlo Simulations of the Gamma-Ray Screening Properties of	
Common Rocks	22
Abstract	22
Introduction.....	23
Background	24
Methods.....	26
Rock Materials	27
Density.....	27
Two-Layer Model.....	27
Results	28
Rock Materials	28
Density.....	28
Two-Layer Model.....	29
Discussion	29
Rock Materials	29
Density.....	30
Two-Layer Model.....	30
Conclusions	31
Tables.....	32
Figures	35
Chapter Four: Comparing Multiple Techniques of Measuring Naturally Occurring	
Radionuclides in Geologic Materials	38

Abstract	38
Introduction.....	39
Background	40
Methods.....	41
AMS Data	41
Sampling.....	42
In Situ Measurements.....	43
Laboratory Counting	44
ICP-MS	45
Results	45
Sample Descriptions.....	45
Southern Nevada.....	46
Cameron	47
Calibration Pads	47
Discussion	47
Southern Nevada.....	47
Cameron	49
Calibration Pads	50
Conclusions	51
Acknowledgments	52
Tables.....	53
Figures	58
Chapter Five: Modeling Background Radiation in Southern Nevada	74

Abstract	74
Introduction.....	75
Background	77
Methods.....	78
Defining Background Radiation Units	78
AMS Data	80
Geochemical Data	81
NURE Data	82
Results	82
Government Wash GMTG	83
Government Wash GMN	84
Government Wash 2/1N	84
Government Wash 2/1,6,10N	85
Lake Mohave GMTG	86
Lake Mohave GMN.....	87
Lake Mohave 2,7,13N.....	87
Lake Mohave 2,6,10N.....	88
Discussion	89
GMTG Models	89
GMN Models.....	90
ASTER Based Models.....	90
Geochemical Data	91
NURE Data	92
Conclusions.....	93

Tables.....	94
Figures	101
Appendix A: Government Wash Unit Report	130
Appendix B: Lake Mohave Unit Report	256
References	395
Curriculum Vitae.....	399

List of Tables

Table 2-1: K, U, and Th Stripping Ratios	18
Table 3-1: Concentration to Exposure Rate Coefficients for Common Rocks	32
Table 3-2: Concentration to Exposure Rate Coefficients with Increasing Density	33
Table 3-3: Concentration to Exposure Rate Coefficients for Two-Layer Models	34
Table 4-1: K, U, and Th Values of Samples in Southern Nevada	53
Table 4-2: Exposure Rate Values of Samples in Southern Nevada	54
Table 4-3: K, U, and Th Values of Samples near Cameron, Arizona	55
Table 4-4: Exposure Rate Values of Samples near Cameron, Arizona	56
Table 4-5: Exposure Rate, K, U, and Th Values of Samples from Calibration Pads	57
Table 5-1: Geochemical Data by Geologic Unit.....	94
Table 5-2: AMS and NURE Exposure Rate, K, U, and Th Values by Geologic Unit.....	95
Table 5-3: Summary of AMS Whole Survey	98
Table 5-4: AMS and NURE K, U, and Th Values for Government Wash Remote Sensing Units	99
Table 5-5: AMS and NURE K, U, and Th Values for Lake Mohave Remote Sensing Units	100

List of Figures

Figure 1-1: Location of Government Wash and Lake Mohave	5
Figure 1-2: Geologic Map of Government Wash	6
Figure 1-3: Geologic Map of Lake Mohave	7
Figure 2-1: Decay Scheme of K-40	19
Figure 2-2: Decay Scheme of U and Th Series	20
Figure 2-3: Schematic Drawing of Gamma Spectral Features	21
Figure 3-1: X/Z Cross Section of MCNP Template	35
Figure 3-2: Change in Exposure Rate with Increasing Density	36
Figure 3-3: Change in Exposure Rate as Top Layer Thickens	37
Figure 4-1: Location of Samples in Southern Nevada	58
Figure 4-2: Location of Samples near Cameron, Arizona	59
Figure 4-3: HPGe Detector	60
Figure 4-4: Photo of Sample Collection at Government Wash	61
Figure 4-5: K (wt%) Values of Various Measurment Techniques, Southern Nevada	62
Figure 4-6: U ppm Values of Various Measurment Techniques, Southern Nevada	63
Figure 4-7 Th ppm Values of Various Measurment Techniques, Southern Nevada	64
Figure 4-8: Exposure Rate Values of Various Measurment Techniques, Southern Nevada	65
Figure 4-9: K (wt%) Values of Various Measurment Techniques, Cameron, Arizona	66
Figure 4-10: U ppm Values of Various Measurment Techniques, Cameron, Arizona	67
Figure 4-11: Th ppm Values of Various Measurment Techniques, Cameron, Arizona	68
Figure 4-12: Exposure Rate Values of Various Measurment Techniques, Cameron, Arizona	69
Figure 4-13: K (wt%) Values of ICP-MS and Published Chemistry, Calibration Pads	70
Figure 4-14: U ppm Values of ICP-MS and Published Chemistry, Calibration Pads	71
Figure 4-15: Th ppm Values of ICP-MS and Published Chemistry, Calibration Pads	72

Figure 4-16: Exposure Rate of ICP-MS and Published Chemistry, Calibration Pads	73
Table 5-2B: AMS and NURE K, U, and Th Values for Government Wash Geologic Units	96
Figure 5-1: Comparison of Published and Altered Geologic Map, Government Wash	101
Figure 5-2: Unclassified and Classifies 2/1 ASTER Image, Government Wash	102
Figure 5-3: Unclassified and Classifies 2/1,6,10 ASTER Image, Government Wash	103
Figure 5-4: Unclassified and Classifies 2,7,13 ASTER Image, Lake Mohave	104
Figure 5-5: Unclassified and Classifies 2,6,10 ASTER Image, Lake Mohave	105
Figure 5-6: AMS Data at Government Wash	106
Figure 5-7: AMS Data at Lake Mohave	107
Figure 5-8: Geochemical and NURE Data, Government Wash	108
Figure 5-9: Geochemical and NURE Data, Lake Mohave	109
Figure 5-10: AMS to NURE Data Comparison, Lake Mohave	110
Figure 5-11: AMS to NURE Data Comparison, Government Wash	111
Figure 5-12: Predicted vs AMS Exposure Rate by Geologic Unit, Government Wash	112
Figure 5-13: Point Difference Map, Geochemical Data, Government Wash	113
Figure 5-14: Plot of K (wt%) Prediction vs AMS, Governemnt Wash	114
Figure 5-15: Plot of U ppm Prediction vs AMS, Governemnt Wash	115
Figure 5-16: Plot of Th ppm Prediction vs AMS, Governemnt Wash	116
Figure 5-17: Point Difference Map, GMN Model, Government Wash	117
Figure 5-18: Predicted Exposure Rate, ASTER Units, Government Wash	118
Figure 5-19: Point Difference Map, 2/1N Model, Government Wash	119
Figure 5-20: Point Difference Map, 2/1,6,10N Model, Government Wash	120
Figure 5-21: Predicted vs AMS Exposure Rate by Geologic Unit, Lake Mohave	121
Figure 5-22: Point Difference Map, Geochemical Data, Lake Mohave	122
Figure 5-23: Plot of K (wt%) Prediction vs AMS, Lake Mohave	123
Figure 5-24: Plot of U ppm Prediction vs AMS, Lake Mohave	124

Figure 5-25: Plot of Th ppm Prediction vs AMS, Lake Mohave	125
Figure 5-26: Point Difference Map, GMN Model, Lake Mohave	126
Figure 5-27: Predicted Exposure Rate, ASTER Units, Lake Mohave	127
Figure 5-28: Point Difference Map, 2,7,13N Model, Lake Mohave	128
Figure 5-29: Point Difference Map, 2,6,10N Model, Lake Mohave	129

List of Equations

Equation 2-1: Calculation of Exposure Rate from Counts	16
Equation 2-2: Calculation of n_{3Th}	16
Equation 2-3: Calculation of n_{2U}	16
Equation 2-4: Calculation of n_{1K}	17
Equation 2-5: Calculation of Th Concentration	17
Equation 2-6: Calculation of U Concentration	17
Equation 2-7: Calculation of K Concentration	17
Equation 3-1: Beer-Lambert Law	25
Equation 3-2: Calculation of Exposure Rate from Monte Carlo Simulation	26
Equation 4-1: Calculation of Exposure Rate from K, U, and Th Concentrations	40

Chapter One

Introduction

Aerial gamma ray surveys have a variety of purposes whether they are scientific, industrial or security related. National Security Technologies, LLC. (NSTec), our collaborator in this project, conducts these surveys primarily as a means of detecting errant anthropogenic radiologic sources; but also for other scientific purposes such as snow water equivalent analysis. Typically, when an aerial gamma ray survey is flown in an area, a local body of water is also measured to correct for background gamma radiation from cosmic rays, atmospheric radon and equipment related sources. However, presently there is not a similar method to correct for geologic sources of gamma radiation when the purpose is to measure anthropogenic sources.

The purpose of this project is to develop a method to predict the terrestrial radiation of geologic materials so that geologic sources of radiation can be accounted for during an aerial survey. Currently, if a gamma ray survey is being flown in an area, the only way to account for geologic sources of gamma rays is to have flown the area previously (Dickson and Scott 1997), or to conduct extensive ground surveying, both of which are prohibitively expensive and generally impractical.

In this study, two survey areas in Southern Nevada, Government Wash, located east of Las Vegas and north of Lake Mead, and the western shore of Lake Mohave near Searchlight, Nevada have been examined (Figure 1-1). Both areas were chosen primarily because they are frequently surveyed by the Aerial Measurement System (AMS) section of NSTec and therefore have aerial radiologic data available which can be used to test model predictions.

Government Wash lies within the Las Vegas Valley Shear Zone; a right lateral fault system that experienced significant tectonic activity during the Cenozoic with displacement

between 23 and 69 km (Langenheim, Jachens et al. 1997). The area of interest (AOI) contains modern alluvial fans as well as sedimentary and volcanic units. The two primary formations that occur in the AOI are the Muddy Creek Formation and the Horse Spring Formation both of which were deposited after the cessation of displacement during the Miocene (Figure 1-2) (Duebendorfer 2003).

The Muddy Creek Formation is middle to late Miocene in age and is composed of clastic sedimentary rocks ranging from claystone to conglomerate. There are three primary members of this formation within the AOI. Tmcl is the lower member of the formation and is composed of claystone, siltstone, and gypsiferous siltstone that ranges in color from tan to red-brown with an angular unconformity that separates Tmcl from the sub-member that lies above Tmcg (Duebendorfer 2003). Tmcg is the middle sub-unit of the Muddy Creek Formation and is composed of white to grey or pale yellow gypsum. There are variable amounts of silt and clay intermixed with the gypsum deposits. Tmcg is weakly resistant to erosion but more resistant than the lower member Tmcl and therefore forms ledges on top of Tmcl (Duebendorfer 2003). Tmcu is the upper member of the Muddy Creek Formation and is composed of a poorly sorted boulder conglomerate with minor sandstone and siltstone that are tan to light brown in color. Conglomerate clasts are composed of a heterogeneous mix of Paleozoic, Mesozoic and Miocene age rocks sourced from surrounding units (Duebendorfer 2003).

The Horse Spring Formation is early Miocene in age and consists primarily of an ancient alluvial fan that was fed by a wide variety of rock types. The Thl/Thlv member consists of clasts of white limestone, calcareous and tuffaceous sandstone and siltstone. Thlv also contains basalt and basaltic andesite from interbedded volcanic flows and sills (Duebendorfer 2003). The Tht/Thtb member consists of conglomerate, megabreccia, sandstone, siltstone, limestone, calcareous sandstone, tuff, and tuffaceous sandstone. The Thtb sub-member consists of megabreccia debris flow and avalanche deposits that are composed of a variety of rock types

including: leucogranite, megacrystic granite, garnet-biotite gneiss and schist, hornblende schist, amphibolite and gabbro (Duebendorfer 2003).

There are other minor units in the Government Wash AOI. Trs is a Miocene age red sandstone unit that is interbedded with Tvc, a series of basaltic andesite volcanic flows, and contains some localized contact metamorphism. The Tvc flows range from aphyric to porphyritic with phenocrysts of olivine, clinopyroxene, and plagioclase. Finally, Ti is an intrusive sill in the Tht member of the Horse Spring Formation. It is a basaltic sub-volcanic diabase composed largely of hornblende and plagioclase.

Lake Mohave is an artificial lake on the Colorado River located south of Lake Mead and east of Searchlight, Nevada. The mountain range west of the lake is part of the Eldorado Mountains and was created by volcanic activity during the Miocene. On the western shore of Lake Mohave there are extensive alluvial deposits that are composed of materials derived from the plutonic, volcanic, and metamorphic rocks that have eroded from the mountains to the west (Figure 1-3) (House and Faulds 2008).

In the southern portion of the source mountain range there is a mix of Proterozoic age crystalline basement and Miocene age felsic and intermediate igneous rocks (House and Faulds 2008). The crystalline basement rocks are composed of metamorphic rocks that are granitic to dioritic in composition (House and Faulds 2008). The felsic and intermediate igneous rocks are composed of rhyolite, diorite and tuff and are intermixed in overlapping flows and veins (House and Faulds 2008).

In the center of the range there are intermediate and mafic, igneous rocks such as andesite, dacite, and basalt that are Miocene in age and occur as a mix of volcanic flows, dikes, and sills (Hinz, Faulds et al. 2012). There are also Proterozoic age metamorphic rocks such as amphibolite and schist (Hinz, Faulds et al. 2012). The northern section is dominated by felsic igneous and metamorphic rocks including quartz monzonite, granite, gneiss, and contains minor

mafic rocks that are all Miocene in age (Hinz, Faulds et al. 2012). These rocks occur primarily as plutons with some dikes, sills, and volcanic flows.

The pattern expressed by the rocks in the mountain range is also expressed in the alluvial fans near the shore of Lake Mohave. Alluvial deposits consist primarily of metamorphic rocks as well as felsic and intermediate igneous rocks in the southern portion of the fans. Intermediate and mafic igneous rocks primarily compose the rocks in the center; while felsic igneous rocks are dominate in the northern portion. However, there are no hard boundaries between rock types in the fans as they have been heavily mixed and therefore the change in rock types is gradational from south to north. Older alluvial surfaces tend to have strong desert pavement development as well as caliche formation at depth. Younger surfaces are sandy or loosely consolidated and have little desert pavement or caliche development.

Aside from materials derived from the mountain range to the west the alluvium also has components related to past fluvial deposits. Lake Mohave sits above the recent flood plain of the Colorado River; however, there are deposits related to the river's recent past intermixed with alluvium as late as early Holocene in age. This material is composed of a wide range of rock types from further upstream including loose sand, sandstone, limestone, and rocks of igneous origin. Generally, these deposits sit near the shore of Lake Mohave, with some cases of material further inland.

Figures

Figure 1-1: Location of Government Wash and Lake Mohave

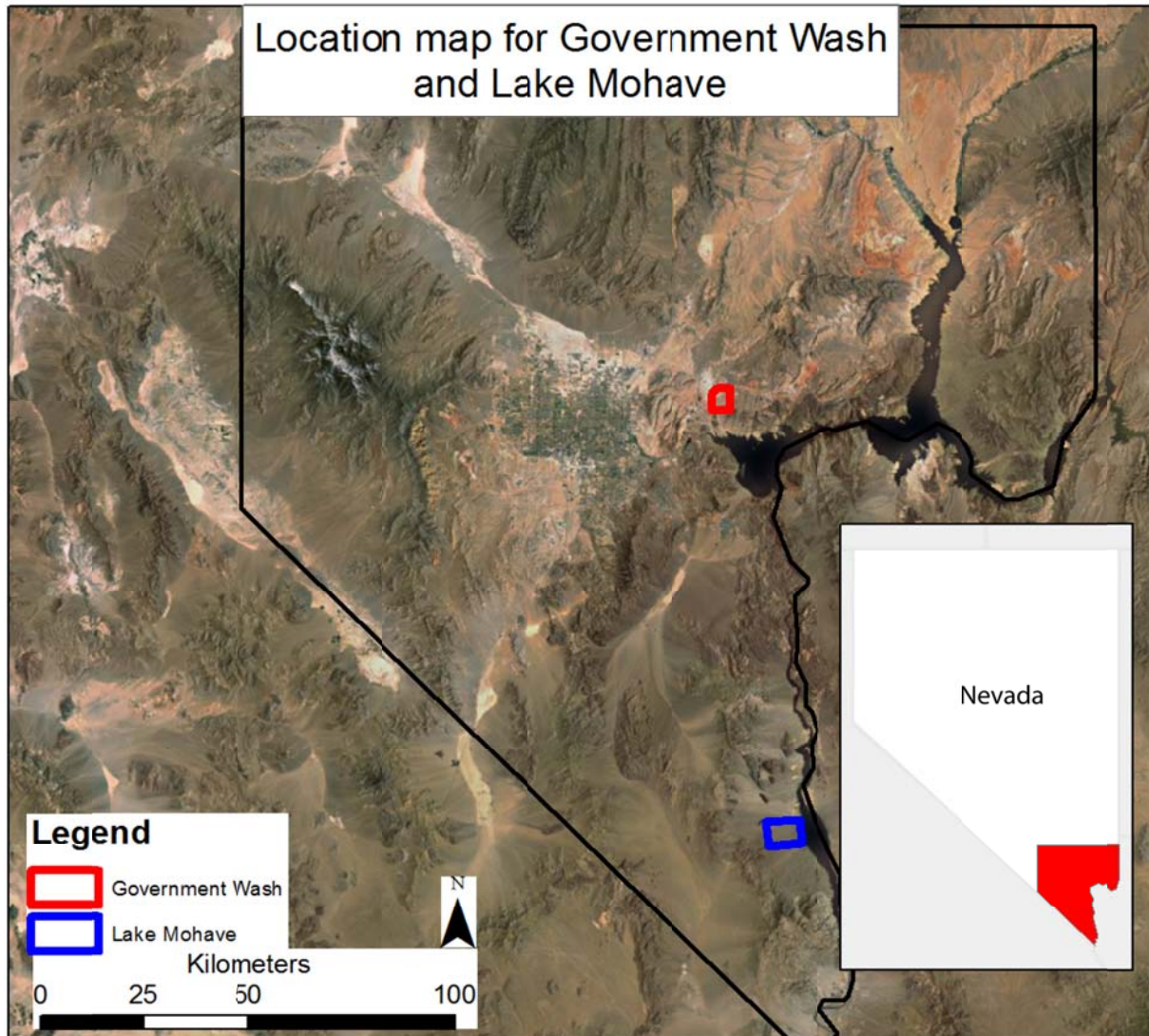


Figure 1-1: The general location of the Government Wash and Lake Mohave study areas.

Figure 1-2: Geologic Map of Government Wash

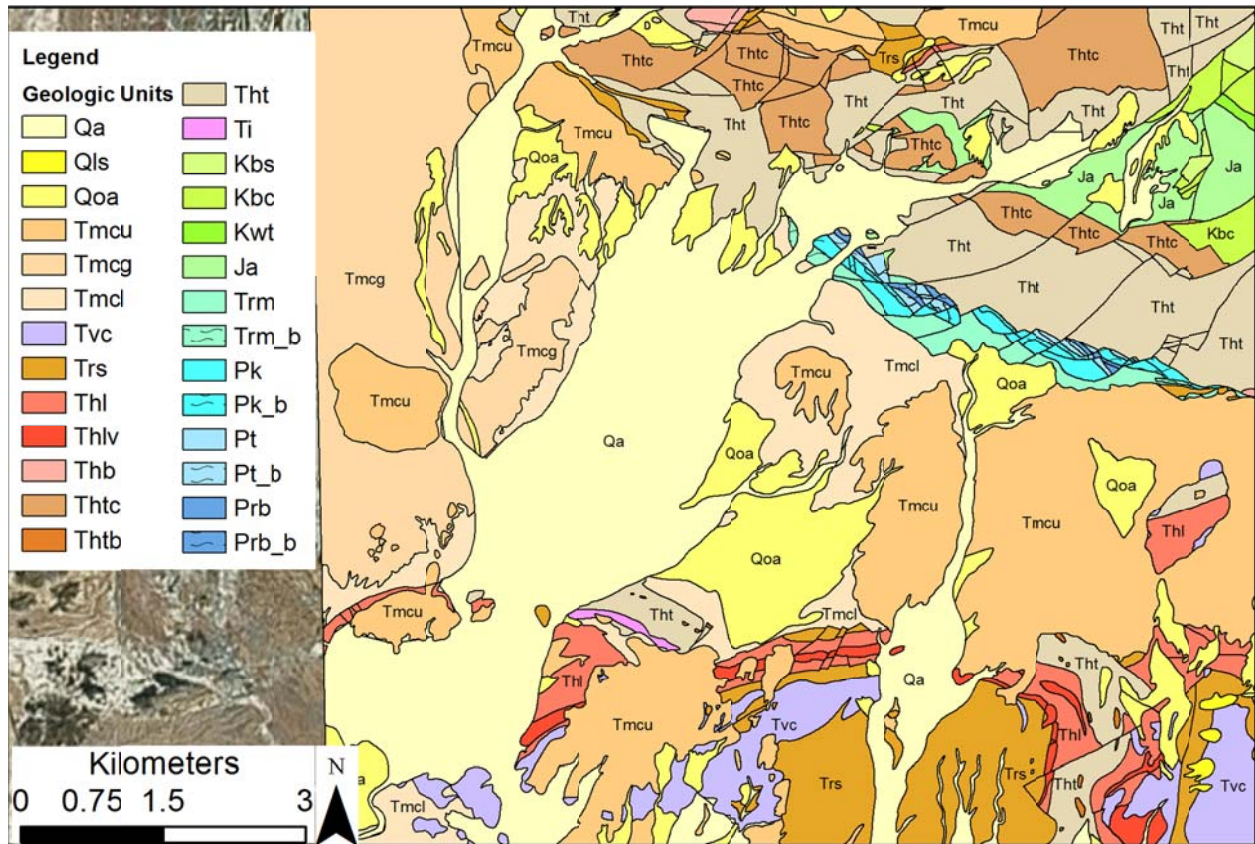


Figure 1-2: Geologic map of Government Wash published by the Nevada Bureau of Mines and Geology (Duebendorfer 2003).

Figure 1-3: Geologic Map of Lake Mohave

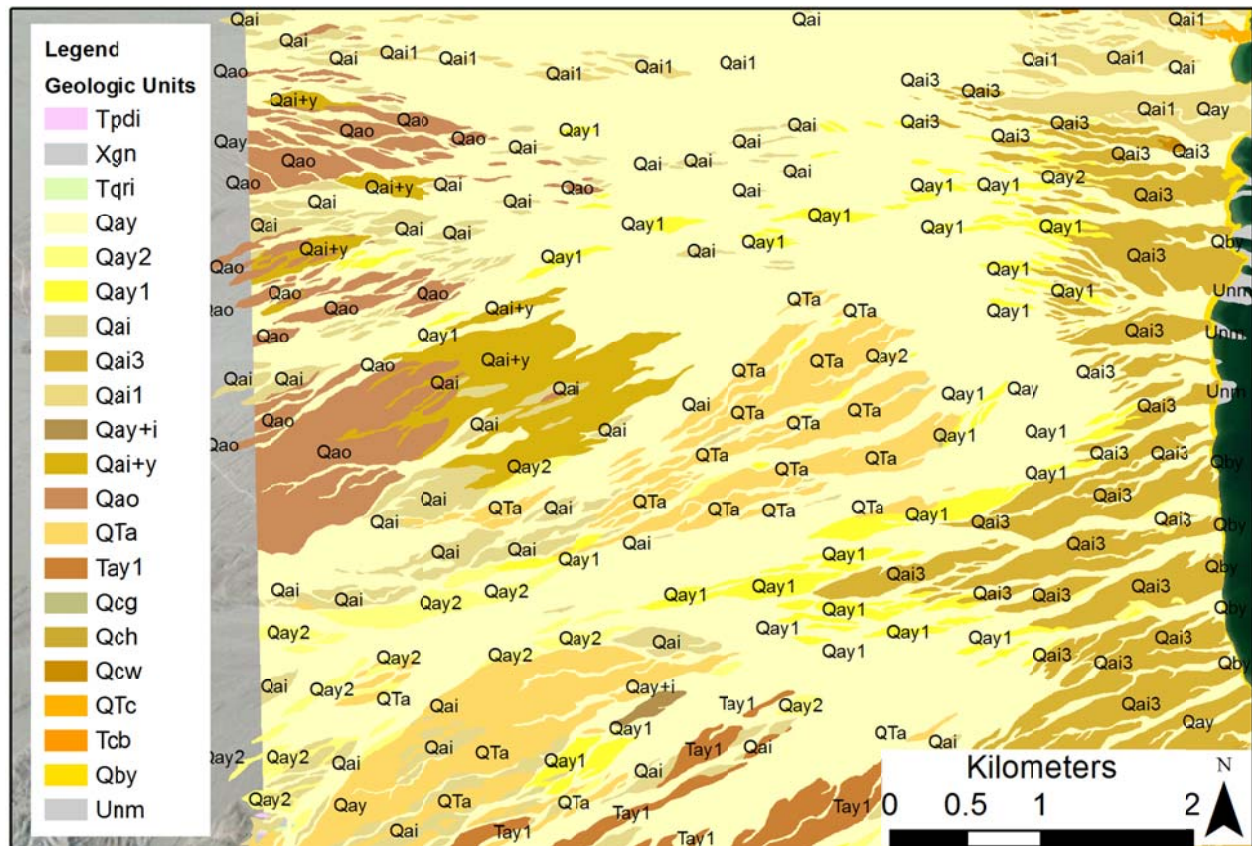


Figure 1-3: Geologic map of Lake Mohave published by the Nevada Bureau of Mines and Geology (House and Faulds 2008).

Chapter Two

Background

Aerial Gamma Ray Surveys

Aerial gamma ray surveys are conducted by aircraft, such as helicopters, flying in a linear pattern across the AOI at a constant altitude; usually about 100 meters off the surface. These aircraft are typically equipped with sodium iodide (NaI) scintillation detectors that measure incident gamma ray photon energy and intensity levels, producing a spectra (Minty, 1997). The raw data are corrected for atmospheric attenuation down to a standard one meter off the surface. The data are also corrected for known atmospheric, cosmic, and equipment related sources of gamma rays (Minty 1997; IAEA 2003). From the corrected spectra, the activity concentration of the constituent gamma emitting elements can be determined. In responding to a radiologic incident, AMS can use these data to pinpoint anthropogenic sources of gamma ray emissions after the proper corrections for background radiation have been made.

Radioactivity

Radioactive decay is a spontaneous naturally occurring process by which a given isotope of a given element releases energy or mass in an effort to stabilize an unstable nuclear system. The energy that is released interacts with the surrounding environment damaging chemical bonds. The atom that released the energy usually becomes a new element that itself may or may not be stable.

Radioactive isotopes decay in a stochastic fashion; that is any one atom may spontaneously decay at any time. However, over time a mass of radioactive atoms will decay at a predictable rate. This rate is measured in terms of half-lives. A half-life is simply the amount of time that must pass for half of a given amount of radioactive material to decay into what are known as daughter products.

There are several modes of radioactive decay. Alpha decay occurs when the nucleus of the radioactive isotope releases an alpha particle. An alpha particle is composed of 2 protons and 2 neutrons and reduces the atomic number of the emitting element by 2. Beta decay occurs in one of three ways. Beta plus decay involves a proton transforming into a neutrino and a positron that are emitted from the nucleus, decreasing the atomic number. Beta minus decay involves a neutron transforming into a proton accompanied by the emission of an antineutrino and an electron increasing the atomic number by one. Electron capture is a form of beta decay in which an inner electron is absorbed by a proton rich nucleus, changing a proton to a neutron while emitting an electron neutrino. Alpha and beta decay release charged particles that are quickly attenuated by Coulomb interactions (i.e. interactions based on electric charge) with surrounding materials. An alpha particle is typically attenuated by the atmosphere after a few centimeters, while a beta particle may travel up to a few meters (Minty 1997).

Gamma ray emissions release an energetic neutral photon at discrete energy levels that do not interact via Coulomb forces. These emissions typically occur when an element has already undergone another form of decay, usually beta decay, and the nucleus is left in an excited state. The nucleus can then move to a lower energy state by the emission of a gamma photon. Gamma rays are capable of penetrating up to 30 cm of geologic material and several hundred meters of atmosphere (Dickson and Scott 1997; Minty 1997).

Terrestrial Sources of Radiation

In geologic materials, there are three major radioactive elements that contribute to the detectable gamma ray signal: potassium, uranium, and thorium. Each of these elements have radioactive isotopes that decay and release energy. Potassium and thorium each have one abundant naturally occurring radioactive isotope; potassium-40 (^{40}K) and thorium-232 (^{232}Th) respectively. There are two primary radioactive isotopes of uranium that occur in nature; uranium-235 (^{235}U) and uranium-238 (^{238}U).

^{40}K makes up approximately 0.0117% of all potassium. The activity of ^{40}K , which is a measure of the number of decays over time, is relatively low; however it occurs in great abundance in the Earth's crust making it as detectable as uranium and thorium (Minty 1997). ^{40}K is a long lived isotope with a half-life of 1.2Ga. This isotope is capable of beta minus decay that produces calcium-40 (^{40}Ca) and an electron capture decay that produces argon-40 (^{40}Ar) and a gamma ray (Figure 2-1). Of all the ^{40}K decays, the beta minus decay to ^{40}Ca accounts for close to 90% while the gamma ray producing decay to ^{40}Ar accounts for a little more than 10%. When ^{40}K decays into ^{40}Ar , a single photon is emitted with an energy of 1.46 MeV. Because of this, the gamma spectral profile for ^{40}K decay shows a peak at 1.46 MeV that is easily identifiable.

Potassium occurs in a wide range of rock types with an average crustal abundance of approximately 2% (Minty 1997). It is most abundant in felsic igneous rocks where it is contained in micas and feldspars (Dickson and Scott 1997). When these sources of potassium weather out of the parent material, they can become constituent parts of sedimentary rocks such as sandstone or be incorporated into soils and clays (Dickson and Scott 1997). Potassium is also abundant in the metamorphic products of felsic igneous rocks.

^{235}U and ^{238}U have half-lives of 704Ma and 4.468Ga respectively. Uranium isotopes do not emit high energy gamma rays when they decay. Instead, uranium has a complex decay chain in which its daughter isotopes, which are also radioactive, go through their own decay, emitting gamma rays (Figure 2-2 A&B). ^{235}U occurs in low abundance (<1% of all U) and is typically not considered when conducting a radiation survey. Therefore, when estimating the concentration of uranium from the gamma spectra, daughter isotopes of ^{238}U such as ^{214}Bi , ^{214}Pb , ^{210}Pb , and ^{234}Th are used to estimate the concentration of uranium and is reported as equivalent uranium (eU) (Minty 1997; IAEA 2003).

Uranium occurs at about 3 parts per million in the Earth's crust, and is widely distributed in many rock and mineral types. In rocks, it occurs in an oxidized and reduced form; U^{+6} and U^{+4} respectively. The oxidized form is more soluble than the reduced and as a result it more readily stays in solution, increasing its mobility (Dickson and Scott 1997). U^{+6} is typically reduced in the presence of organic compounds and therefore tends to accumulate in hydrocarbon sinks such as organic rich shales (Dickson and Scott 1997). There are many uranium bearing minerals, such as uraninite and coffinite, that contain uranium as a primary constituent (Burns and Finch 1999). However, uranium occurs more frequently as an external coating on pre-existing mineral grains. Uranium can be found as a coating on minerals such as zircon, monazite and xenotime (Dickson and Scott 1997; Burns and Finch 1999).

^{232}Th has a half-life of 14.02Ga and is the only abundant naturally occurring isotope of thorium. Other isotopes of thorium are short-lived and occur within decay chains of other elements. Like uranium, thorium does not emit high energy gamma rays during decay (Figure 2-2 C). Thorium also has a chain of daughter isotopes including ^{208}Tl , ^{212}Pb , ^{212}Bi , and ^{228}Ac that decay and release gamma rays. Thus, concentration values derived from gamma spectra are reported as equivalent thorium (eTh) (Dickson and Scott 1997; Minty 1997).

Thorium is more abundant than uranium, occurring at an average of 12 parts per million in Earth's crust, and occurs in many of the same rocks and minerals as uranium (Dickson and Scott 1997; Minty 1997). Some of the more important thorium-bearing minerals are monazite, zircon and xenotime (Dickson and Scott 1997). Thorium has a single valence state (Th^{+4}), and therefore its mobility is unaffected by redox conditions. Thorium is fairly insoluble in basic conditions but can be soluble in acidic or neutral conditions; the latter when it is organically complexed (Wilford and Minty 2007). Thorium tends to concentrate in insoluble heavy minerals such as heavy mineral sands (Dickson and Scott 1997).

Disequilibrium

Because uranium and thorium do not directly contribute to the gamma ray emissions of geologic material, an assumption must be made with respect to whether or not uranium and thorium are in secular equilibrium with their decay chain when measuring their concentration from a gamma ray survey. Secular equilibrium is a state in which the daughter isotopes have a significantly shorter half-life than the parent and 8-10 half-lives of the longest living daughter isotope have passed. Assuming 8-10 half-lives of the longest lived daughter has passed, the activity of the parent and daughter isotopes are equal and an estimate of the concentration of the parent can be made from the activity of the daughter (Minty 1997).

It is possible for daughter isotopes to be differentially transported relative to their parent because of the varying solubilities of the daughters (Dickson and Scott 1997; Minty 1997). This can enrich one area in daughter isotopes and deplete another. Under such conditions, the activity of the daughter isotopes will not be equal with the activity of the parent and the calculated concentrations of eU and eTh will not represent the true concentrations in the ground.

In active alluvial units, uranium and thorium disequilibrium can have an effect on the measured gamma ray emissions. Surfaces older than 40 years should be in equilibrium with respect to thorium (Minty 1997). This means that only the most recent surfaces will have the thorium series in disequilibrium. The uranium series however, can take up to 1.2 million years to come to equilibrium with its daughter isotopes (Minty 1997). This lengthy time means that all but the oldest alluvial surfaces will have some degree of disequilibrium in the uranium decay chain.

Radon exhalation is a major contributor to uranium disequilibrium in geologic materials (Grasty, Carson et al. 1984). Radon is a noble gas and a member of the uranium decay chain. There are a number of factors that influence the exhalation of radon from natural materials and each material will be controlled by different factors (e.g., presence of rock fractures, porosity

and permeability, degree of saturation). The isotope of radon, radon-222, is a member of the ^{238}U series and is relatively long lived compared to other isotopes of radon, with a 3.8 day half-life. Since radon is non-reactive and long lived it can easily escape from permeable geologic material into the atmosphere (Grasty, Carson et al. 1984). Therefore, areas with high radon exhalation will have lower gamma ray activity from the uranium series than would be predicted from the uranium concentration.

Generally, a decay chain in disequilibrium means a lower overall exposure rate because the combined activity of all the daughter products is lower than if it were in equilibrium (Minty 1997). However, in a 1995 study, Dickson found that disequilibrium in arid Australian soils was of minimal consequence. This result has been attributed to the fact that uranium channel data from aerial surveys are noisy due to the down scattering of higher energy gamma rays (Dickson 1995). In addition, the uranium decay series only contributes to approximately 20% of the total exposure rate under crustal average conditions (Grasty, Carson et al. 1984; Dickson 1995). Therefore, small differences in actual vs measured concentrations of uranium have minimal impact on the resulting exposure rate.

Other Effects

Abundant vegetation poses another challenge to modeling gamma ray exposure rate from geologic materials. The primary reason why vegetation affects the gamma signal is because of the water content in plants, as well as the associated increase in soil and atmospheric moisture (Grasty, Carson et al. 1984; Minty 1997). Water attenuates gamma rays very efficiently and the water content in dense vegetation is enough to have a significant impact on aerial measurements (Grasty, Carson et al. 1984; Minty 1997). This is because water has about 1.11 times the electrons per gram as most natural materials allowing for more effective Compton Scattering (Grasty, Carson et al. 1984; Beamish 2013). Plants also take up minerals into their bodies to grow. Thus a significant amount of potassium as well as daughter products

of uranium and thorium can be drawn into the plant's bodies and potentially transported from the system (Minty 1997; Ulbrich, Ulbrich et al. 2009).

Gamma Ray Spectra

The raw spectral data from a NaI detector used during an aerial gamma ray survey consist of a series of spectra taken every second. The energy range is from about 30 keV to 3 MeV. When a radionuclide decays and releases a gamma ray, the energy of the gamma ray is unique and predictable and is used to understand the concentrations of the various radionuclides being measured. Recorded ionizations, called pulses, are stored and presented as a histogram with the number of events plotted against the energy. There are three types of gamma ray interactions with matter that each have different implications for the spectra.

Photoelectric absorption is a process whereby the incoming photon interacts with an outer shell electron and imparts the entirety of its energy on the electron. The photoelectron is then ejected from the atom where it can be collected and measured. When this type of interaction occurs the entire energy of the incoming photon can easily be measured and shows up in the spectra as a full energy peak (Figure 2-3)(Knoll 2000).

Compton scattering is a process where an incoming photon interacts with an outer shell electron and imparts only a portion of its energy onto that electron resulting in the ejection of a photoelectron. In this type of interaction the photon preserves a portion of its energy and is scattered at an angle. This complicates the interpretation of spectra because the deflected gamma ray may not fully deposit its energy within the detector (Knoll 2000). In this case, the information related to the full energy of the initial photon is lost. This produces what is known as a "Compton continuum" (Figure 2-3) within the spectra where a continuum of lower energy electrons are recorded leading up to the maximum energy that can be deposited in a Compton event called the "Compton edge" (Knoll 2000).

The final interaction mechanism occurs at energy levels above 1.022 MeV and is called pair production. Pair production is a process where an incoming photon is absorbed by the nucleus and converted into an electron, positron pair (Knoll 2000). Energy in excess of 1.022 MeV goes into kinetic energy that is shared between the electron and positron. The electron and positron will eventually slow down and interact with detector materials. The positron will annihilate with an electron and release two 511 keV photons. If these photons escape the detector volume it will create a single and or double escape peak in the spectra located at 511 and 1022 keV less than the full energy peak respectfully (Figure 2-3)(Knoll 2000).

There are a number of other phenomena that can cause a loss of recorded energy in the spectra. Aside from escaping the detector volume electrons can lose energy through the emission of bremsstrahlung radiation (Figure 2-3)(Knoll 2000). Bremsstrahlung, also known as braking radiation, is created when a charged particle slows down and changes course when it is deflected by another charged particle. The bremsstrahlung photon can escape the detector. In this case the information related to the energy of the bremsstrahlung radiation is lost even if the emitting electron is recorded (Knoll 2000). Characteristic X-rays can be created during photoelectric absorption when an electron from a higher shell moves down to fill the space left open by the photoelectron. Typically, these X-rays are readily absorbed, but may escape if the interaction occurs near the detector surface. Any escaping X-Rays will create an X-ray escape peak at an energy unique to the emitting element (Knoll 2000).

There are also effects related to secondary radiation from materials and sources that surround the detector. Bremsstrahlung, positron annihilation radiation, and scattered gamma rays from outside sources can interact with the detector and add to the spectra (Knoll 2000). These sources can be corrected for by measuring background radiation over water, high in the atmosphere, or previously measured territory (IAEA 2003).

Exposure Rate Calculation and Spectral Stripping

$$X = \sum_{i=8}^{1009} (C_i - B_i) * e^{\mu h} * (3.17E - 4) \quad \text{Equation 2-1}$$

Exposure rate, K, eU, and eTh concentrations have been calculated from raw spectra provided by AMS. The spectra consist of 1024 bins that contain counts that correspond to energy. To calculate the exposure rate, counts from energies of approximately 24keV to 3MeV that are in bins ranging from 8 to 1009 were summed, corrected for dead time, and background subtracted. The background is obtained by averaging counts at survey altitude over water. The air attenuation coefficient, which allows for the correction of counts to 1m off the surface, was determined by analyzing altitude spiral data and plotting the counts against altitude and fitting an exponential curve to the data. Finally, a count to exposure rate ($\mu\text{R/h}$) conversion coefficient of $3.17\text{E}-4$ was provided by AMS and was originally determined by measuring calibration pads in Grand Junction, Colorado. The exposure rate is given by Equation 2-1. Where C_i are the counts in each bin, B_i are the average counts in each bin over water, μ is the air attenuation coefficient, h is the altitude of the flight and X is the exposure rate in $\mu\text{R/h}$.

K, eU, and eTh were calculated by the spectral stripping routine published by the IAEA in 2003. To obtain these concentrations AMS provided spectral stripping ratios listed in Table 2-1. Counts were summed, dead time corrected, and background subtracted under each spectral window and concentration was determined by the following series of equations obtained from the IAEA (2003) document:

$$n_{3\text{Th}} = (C_{t\text{Th}} - (\alpha * C_{t\text{U}})) / (1 - (\alpha * a)) \quad \text{Equation 2-2}$$

$$n_{2\text{U}} = C_{t\text{U}} - (\alpha * n_{3\text{Th}}) \quad \text{Equation 2-3}$$

$$n_{1K} = Ct_K - (\beta * n_{3Th}) - (\gamma * n_{2U}) \quad \text{Equation 2-4}$$

$$C_{Th} = n_{3Th} / s_{3Th} \quad \text{Equation 2-5}$$

$$C_U = n_{2U} / s_{2U} \quad \text{Equation 2-6}$$

$$C_K = n_{1K} / s_{1K} \quad \text{Equation 2-7}$$

Where α is the ratio between s_{2Th} and s_{3Th} , a is the ratio between s_{3U} and s_{2U} , β is the ratio between s_{1Th} and s_{3Th} , and γ is the ratio between s_{1U} and s_{2U} . $s_{1(K,U,Th)}$, $s_{2(K,U,Th)}$, and $s_{3(K,U,Th)}$ are defined in Table 2-1. C_{Th} , C_U , and C_K are the resulting concentrations in ppm and weight percent respectively.

Manuscripts

The following chapters explore three aspects of modeling background radiation from geologic materials and are presented in manuscript format. The Chapter 3 discusses modeling that was performed of geologic materials using the particle physics modeling software Monte Carlo N-Particle Transport. Using this software differences in rock chemistry, density, and layering of different geologic materials were explored in terms of their effect on gamma ray attenuation and exposure. Chapter 4 discusses samples collected at three field sites in the Southwestern United States and compares various techniques of measuring radionuclide concentration. Finally Chapter 5 outlines the development of high resolution models of the distribution of K, U, Th, and exposure rate at Government Wash and Lake Mohave.

Tables

Table 2-1: K, U, and Th Stripping Ratios

Sensitivities	$s1_{(K,U,Th)}$	$s2_{(K,U,Th)}$	$s3_{(K,U,Th)}$
Counts/1wt% K	15.7935	0	0
Counts/1ppm eU	1.3813	1.3509	0.106
Counts/1ppm eTh	0.4397	0.3009	0.6621

Table 2-1: Table displaying the spectral stripping ratios provided by AMS used to calculate K, eU, and eTh concentrations from the raw gamma spectra also provided by AMS.

Figures

Figure 2-1: Decay Scheme of K-40

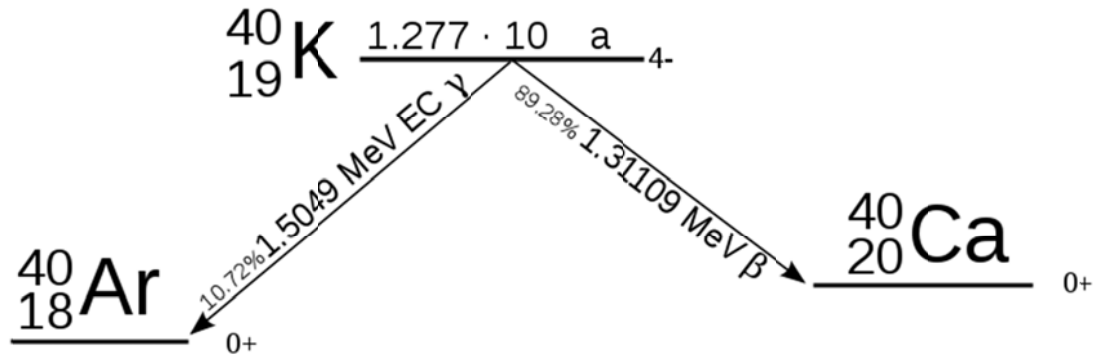


Figure 2-1: The decay scheme of ^{40}K ; 89.28% of ^{40}K decays are a beta decay to ^{40}Ca while 10.72% of decays are an electron capture decay to ^{40}Ar with an associated release of a 1.46MeV gamma ray (Tubas 2011).

Figure 2-2: Decay Scheme of U and Th Series

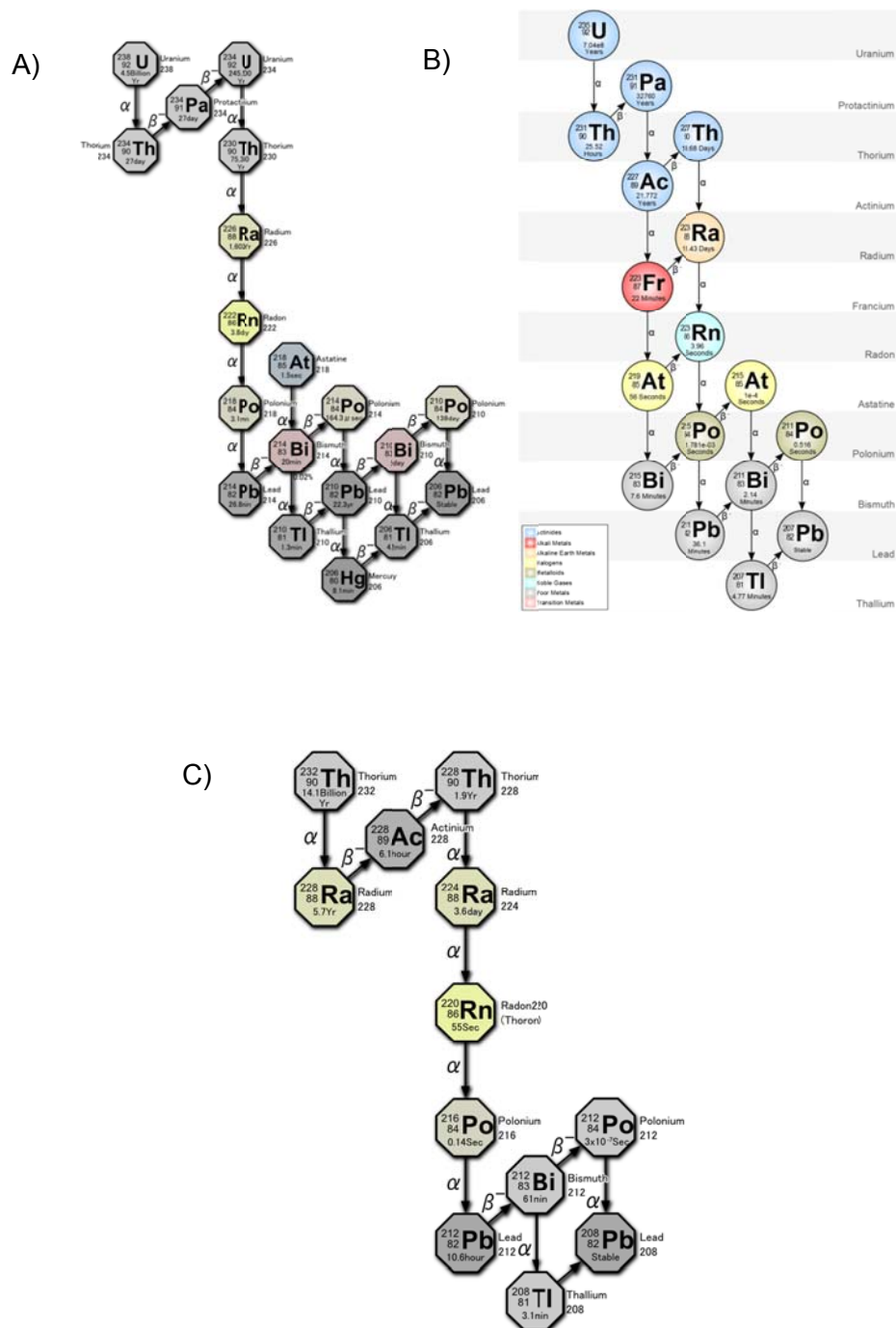


Figure 2-2: Decay series of: A) Uranium-238 (Tosaka 2014), B) Uranium-235 (YBG 2013), C) Thorium-232 (Tosaka 2008)

Figure 2-3: Schematic Drawing of Gamma Spectral Features

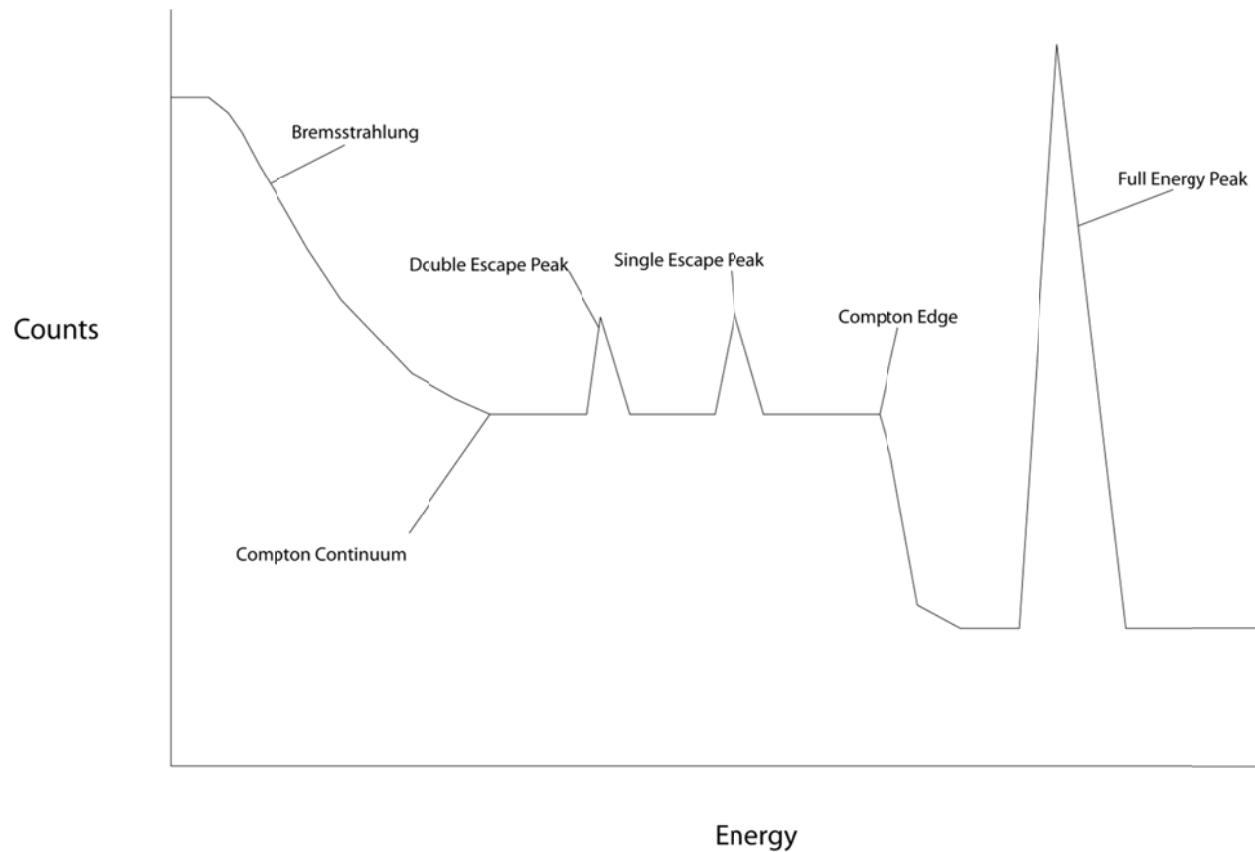


Figure 2-3: Schematic drawing of features found in a gamma spectra. Bremsstrahlung radiation arises from escaping photons that are emitted when particles such as electrons slow down due to Coulomb interaction. The Compton continuum is produced when a gamma ray interacts in a stochastic fashion with the outer shell electron of an atom, scattering the photon, which subsequently escapes the detector. The single and double escape peaks arise from the escape of annihilation radiation produced when positrons created by Pair Production annihilate with an electron releasing two 511keV photons and are therefore located at 511 and 1022keV less than the full energy peak. The Compton edge represents the maximum energy that can be deposited during a single Compton event within the detector. The Full Energy Peak is the peak produced by recording the entire energy of an incoming photon.

Chapter Three

Monte Carlo Simulations of the Gamma-Ray Screening Properties of Common Rocks

Abstract

This study is part of a larger study that attempts to forward model the results of an aerial gamma ray survey by modeling the geologic contribution to the gamma ray signal. In geologic materials, ^{40}K , ^{238}U , and ^{234}Th are responsible for most gamma ray production. If the concentration of these radioelements and attenuation factors such as degree of water saturation are known, an estimate of the gamma ray exposure rate can be made. In order to understand the attenuation properties of rock types, Monte Carlo simulations have been created for major rock types. We have shown that there are no significant differences in gamma ray screening between major rock types. Additionally, we have determined that rock density is the largest controlling factor in terms of gamma ray attenuation when the total number of nuclides remains constant. Finally, we tested the effects of layering a geologic material and found that the depth of a layered material can be estimated if the radionuclide content of both materials are known.

Introduction

In geologic materials there are three primary radioisotopes that are responsible for the emission of gamma rays; those radioisotopes are ^{40}K , ^{238}U , and ^{234}Th . While ^{238}U and ^{234}Th do not directly emit detectable gamma rays, they decay into radioactive daughter isotopes, some of which produce detectable gamma rays. Exposure rate is a measure of the number of ionizations produced in a quantity of air by photon radiation per unit time. There is a linear relationship between the concentration of these radioelements and the gamma ray exposure rate (Beck, DeCampo et al. 1972; Løvborg and Kirkegaard 1974; Grasty, Carson et al. 1984; Gasser, Nachab et al. 2014). Because of this linear relationship, if the exposure rate contribution of each nuclide is understood, then the total exposure rate can be determined by simply summing the contribution from each nuclide. However, differences in screening properties of the radiation source can have an effect on the resulting exposure rate. Therefore, this study attempts to quantify how differences in rock bulk chemistry and density affect the exposure rate of those materials by deriving concentration to exposure rate coefficients for various rock types.

This study is part of a larger research and development project, with our corporate partner National Security Technologies, LLC. (NSTec), that attempts to predict the gamma ray exposure rate of geologic materials. To help achieve that goal, we used Monte Carlo N-Particle Transport Code v6 (MCNP) software to simulate the interaction of gamma ray photons with geologic materials based on known physics (Pelowitz 2008). We have created a series of simple simulations using MCNP to test the screening properties of various rock types as well as ideas regarding differences in density and the effects of layering of materials.

MCNP is code developed by Los Alamos National Laboratory for analyzing the transport of gamma ray photons and neutrons over a broad range of energies. The code simulates the transport of these particles and any secondary particles created from interactions within the simulation such as electrons and positrons. MCNP operates by a random number generator that

decides, for each simulated particle, the initial vector as well as the vector at each stage of the simulation whose sum is referred to as a track. At each stage of the simulation, the status of each particle is calculated by stochastic probabilities to determine if the particle has interacted with any of the chemistry present in its current location. In the case of gamma rays, the photon may interact by means of: photoelectric absorption, which would terminate the track of the particle and produce an electron; Compton scattering, which would scatter the particle at an angle and produce an electron; or pair production, which replaces the particle with an electron positron pair. If the particle has not interacted it continues on its current track. The secondary particles created by the interaction mechanisms have their own tracks that are calculated by similar means.

The MCNP input file consists of a series of “cards” that define the parameters of the simulation. The geometry of the simulation is defined by “cell cards” and “surface cards”. The “cell cards” define the shape of each object and the “surface cards” define the placement of chemistry in the cell. “Material cards” define the chemistry of each cell based on mass fractions, which is homogeneously distributed within the cell. Radiation sources are assigned with an “sdef card” and may encompass more than one cell. Within the “sdef card” the range and probability distribution of particle energies (i.e. branching ratios) is defined to simulate particle emissions from a particular source (e.g., ^{238}U). A “tally” region is also defined that counts the energy deposited within that region. The simulation generates a user defined type and number of particles and terminates when those particles have been generated and have reached the end of their track by either losing all of their energy due to interactions or by leaving the simulated space.

Background

There is a long history of deriving exposure rate or dose coefficients for concentrations of ^{40}K , ^{238}U (sometimes reported as ^{226}Ra) and ^{234}Th (Beck, DeCampo et al. 1972; Løvborg and

Kirkegaard 1974; Gasser, Nachab et al. 2014). Beck et al. (1972) was the first to derive exposure rate coefficients for nuclide concentrations by comparing NaI detector activity measurements of K, and U and Th daughter isotopes in a soil to available branching ratios and assuming homogenous distribution of nuclides. In 1974, Løvborg et al. also derived similar coefficients by theoretical calculation, using computer code they designed and branching ratios determined by a statistically weighted average of twelve previously published studies.

In 2014, Gasser et al. updated previous coefficients to reflect new branching ratios and also took into account different soil chemistries and levels of water saturation. All of Gasser et al. (2014) simulations are of generic soil chemistries at a density of 1.6 g/cm³. To date no known studies have examined to what degree variations in common rock chemistry and density might alter the gamma ray screening properties. Therefore, our rock simulations represent a first attempt to derive exposure rate coefficients for common rocks.

The Beer-Lambert law is a simple model that describes attenuation of electromagnetic radiation as it passes through a homogenous material (Lambert 1760). The equation is as follows:

$$I = I_0 e^{-\mu X} \quad \text{Equation 3-1}$$

Where I_0 is the initial intensity of the radiation, μ is the linear attenuation coefficient specific to the material, and X is the thickness of the material. Gamma ray attenuation in geologic materials should then follow this basic principal when attenuation factors such as rock chemistry, water saturation, and air in void spaces are considered (Beamish 2013). While MCNP simulations do not use the Beer-Lambert law to calculate interactions, we expect a successful simulation to fit this model.

In natural environments, there are processes that can create small scale layering of materials with different radiologic properties. Alluvial processes bring eroded material from

topographic highs and fill in topographic lows. Another process is eolian addition, whereby windblown material, often from regional or global sources, settles on the surface of geologic material (Reheis, Budahn et al. 2009). No matter the sedimentary process, the deposited material may have little if any relationship to the material it overlies in terms of chemistry, density, and radiogenic properties.

Methods

A geometry template composed of a cylindrical rock slab 50 cm thick with a 10 m radius, and an atmosphere 10 m in thickness directly above was applied to each simulation (Figure 3-1). Two layer simulations to investigate the effects of layered material were similarly composed; however, the rock cylinder's thickness was reduced and an additional cylinder was placed on top to represent the deposited material. The total thickness of both cylinders remained 50 cm even as the thickness of the top material was increased. The geometry of the template was chosen using results published by Gasser et al. in 2014, who demonstrated that asymptotic values for their coefficients were reached using a cylindrical source with a 50 cm soil depth and a 10 m radius.

Bulk chemistry and radionuclides were homogenously distributed within each source (i.e. the rock or top layer material). One meter off the surface there is a 50 cm sphere that is also composed of atmosphere. In each simulation, $1e10$ gamma ray photons are generated for each nuclide using energies and branching ratios provided to us by NSTec. Energy deposited in the sphere is placed into 1024 bins and integrated; exposure rate is calculated by the following equation:

$$X = \int_{d=1}^{1024} (1.837 \times 10^{-8}) (M f_i A_i N_A \lambda_i Y_j E_d) / (N_{A_{ri}} M_{air}) \quad \text{Equation 3-2}$$

Where, X is the exposure rate in $\mu\text{R/h}$; M is the mass of the rock slab; f_i is the mass fraction of

the element, A_i is the relative abundance of the nuclide, N_A is the Avogadro constant, λ_i is the decay constant of the nuclide, E_d is the energy deposited in each bin in the detection sphere in keV, N is the total number of photons generated, A_{ri} is the relative atomic mass of the isotope in g/mol, and M_{air} is the mass of the atmosphere in the energy detection sphere.

Rock Materials

To test the gamma ray screening of various rock types, worldwide averages were used for bulk chemistry and density of common rocks. The following rock types were tested: basalt, gabbro, rhyolite, granite, limestone, and gypsum rich siltstone. Bulk chemistry and density for basalt, rhyolite, and limestone were taken from Winter, 2010. Chemistry and density for gabbro and granite were taken from Hess, 1989. For the gypsum rich siltstone, the chemistry was obtained from Pabco Gypsum, Inc (Sloan 2011); a company that is actively mining a radiologically cool gypsum deposit in Southern Nevada.

K, U, and Th rhyolite test was performed several times with different random number seeds to assess the reproducibility of results. The maximum difference between the simulations is approximately 1%.

Density

To test the effects of density the absolute number of radionuclides was held constant while the density was increased by an order of magnitude. Densities of 1, 2, 3, 4, 5, 7, 9, and 10 g/cm³ were tested using rhyolite lithology. The concentration of ⁴⁰K is 2.99E-2 (mol/m³), ²³⁸U is 4.20E-3 (mol/m³), and ²³²Th 4.31E-3 (mol/m³).

Two-Layer Model

To test how the presence of layers of different composition can affect the exposure rate, a two-layer model was created according to the scheme described above for two different material types. The underlying rock unit is composed of basalt in both sets of simulations. In the

first series of simulations the overlying material is composed of regional dust chemistry from the Desert Southwest provided by Reheis et al., 2008, at a density of 1.6 g/cm^3 . The second series of simulations used the same gypsum rich siltstone tested in the rock materials test, and also has a density of 1.6 g/cm^3 . In these series of simulations, the thickness of the top material was increased from a thickness of 0.5 cm to 40 cm at intervals of 0.5 cm from 0.5-1cm, 1 cm from 1-5 cm, 5 cm from 5-10 cm, and 10 cm from 10-40 cm. For each simulation, the exposure rate contribution was assessed for 1 wt% K, 1 U ppm, and 1 Th ppm from each source and plotted against the top layer thickness.

Results

Rock Materials

The concentration to exposure rate coefficients derived from the various rock materials simulations are reported in Table 3-1. The K coefficients range from 1.22 to 1.25 ($\mu\text{R/h}$) per wt% K with uncertainties ranging from 0.010 to 0.011. U coefficients range from 0.40 to 0.42 ($\mu\text{R/h}$) per ppm with uncertainties ranging from .0047 to .0055. Th coefficients range from 0.21 to 0.22 ($\mu\text{R/h}$) per ppm with uncertainties ranging from 0.0028 to 0.0031.

Density

The results of the density tests are reported in Table 3-2 and Figure 3-2. At a density of $1 \text{ (g/cm}^3\text{)}$ the combined exposure is $1.76 \pm 0.011 \text{ } \mu\text{R/h}$. At a density of $2 \text{ (g/cm}^3\text{)}$ the combined exposure is $0.92 \pm 0.006 \text{ } \mu\text{R/h}$. At a density of $3 \text{ (g/cm}^3\text{)}$ the combined exposure is $0.63 \pm 0.007 \text{ } \mu\text{R/h}$. At a density of $4 \text{ (g/cm}^3\text{)}$ the combined exposure is $0.47 \pm 0.003 \text{ } \mu\text{R/h}$. At a density of $5 \text{ (g/cm}^3\text{)}$ the combined exposure is $0.38 \pm 0.0053 \text{ } \mu\text{R/h}$. At a density of $7 \text{ (g/cm}^3\text{)}$ the combined exposure is $0.27 \pm 0.004 \text{ } \mu\text{R/h}$. At a density of $9 \text{ (g/cm}^3\text{)}$ the combined exposure is $0.21 \pm 0.004 \text{ } \mu\text{R/h}$. Finally, at a density of $10 \text{ (g/cm}^3\text{)}$ the combined exposure is $0.19 \pm 0.0037 \text{ } \mu\text{R/h}$.

Two-Layer Model

Exposure rate coefficients for the layered material tests are reported in Table 3-3 and Figure 3-3. Coefficients for the rock layer range from 1.25 to 0.013 ($\mu\text{R/h}$) per wt% K; 0.41 to 0.003 ($\mu\text{R/h}$) per U ppm; 0.22 to 0.0023 ($\mu\text{R/h}$) per Th ppm; as the rock thickness is decreased from 50 cm to 10 cm. Exposure rate coefficients for the top layer range from 0.08 to 1.20 ($\mu\text{R/h}$) per wt% K; 0.03 to 0.39 ($\mu\text{R/h}$) per U ppm; 0.015 to 0.20 ($\mu\text{R/h}$) per Th ppm; as the top material thickness is increased from 0 cm to 40 cm.

Discussion

Rock Materials

Our simulations show that there is little difference between rock types in terms of gamma ray screening. Even the gypsum rich material, which is significantly hydrated, produced very similar results. This is consistent with the findings of Gasser et al. (2014) whose tests on various soil types deviated very little from each other. The average coefficients from our simulations (all reported as $\mu\text{R/h}$ per K wt% or (U,Th)ppm) are 1.24 (0.0113), 0.414 (0.0051), and 0.217 (0.0029) for ^{40}K , ^{238}U , and ^{232}Th respectively. Our coefficients compare with those originally published by Beck et al.: 1.49, 0.62 and 0.31; and by Løvborg et al.: 1.52, 0.63 and 0.31 for ^{40}K , ^{238}U and ^{232}Th respectively. Gasser et al., 2014, reported coefficients in the form of (nGy/h)/(Bq/kg) as 0.036, 0.357 and 0.482 for ^{40}K , ^{226}Ra and ^{232}Th respectively. Converting Gasser's coefficients to the form of (nGy/h) per wt% or ppm and ^{226}Ra to ^{238}U yields coefficients of 11.18, 3.60 and 1.96 for ^{40}K , ^{238}U and ^{232}Th respectively. Using a conversion factor of 0.1 between coefficients for nGy/h and $\mu\text{R/h}$ (Cember and Johnson 2009) our results report coefficients that are in between the older works and the 2014 work by Gasser et al.

Density

Our density simulations in combination with our rock materials simulations show that indeed rock density is the largest controlling factor in terms of gamma ray attenuation from geologic material. Therefore, a change in density without a corresponding change in the total number of nuclides is a much greater controlling factor than bulk rock chemistry in any geologic system. An example of a rock material that changes in density while some radionuclides remain in place is a saprolite which forms when rock is chemically weathered in place and many major elements, including K, are removed. However, U and Th tend to remain in secondary iron oxides and therefore increase in concentration due to the overall loss of mass (Michel 1984; Patino, Velbel et al. 2003; Lee and Baik 2009) and would therefore be expected to produce a higher gamma ray exposure rate from U and Th sources.

Two-Layer Model

Our two-layer model simulations have shown that as the lower density top material thickens due to deposition, the exposure rate from the rock drops off exponentially and exposure rate from the top material increases logarithmically (Figure 3-3). The summed exposure of both materials remains constant because both materials have the same nuclide concentrations. The results of both the eolian material and the gypsum rich material are statistically identical and therefore only the results of the gypsum rich siltstone simulations are presented here. These results are consistent with the Beer-Lambert law described above (Equation 3-1). The linear attenuation coefficient of the top material derived from these simulations is 0.108. Using these data, an estimate of the thickness of overlying material can be made in conjunction with aerial or ground based survey data. However, the attenuation coefficient will vary with density and therefore it should not be assumed that the coefficient derived from these simulations is universally applicable without modifications for change in density.

Conclusions

We have shown that the gamma ray screening properties are constant across many common rocks. Coefficients determined from our simulations to translate the concentrations of ^{40}K , ^{238}U and ^{232}Th into gamma ray exposure rate ($\mu\text{R/h}$) are analogous to previous studies. We have also shown that density, not rock chemistry, is the determining factor in terms of gamma ray screening efficiency in geologic materials. Finally, we have shown that the depth of layered material can be estimated based on the Beer-Lambert law when properties (e.g., K, U, and Th concentrations and attenuation coefficient) of the rock media and layered material are known.

Tables

Table 3-1: Concentration to Exposure Rate Coefficients for Common Rocks

Rock Type/Density (g/cm ³)	Total K Energy keV	Exp Rate (μR/h) per K wt	Total U Energy keV	Exp Rate (μR/h) per U ppm	Total Th Energy keV	Exp Rate (μR/h) per Th ppm
Basalt/2.90	8032.6	1.2526 (0.0119)	3840.3	0.4166 (0.0054)	4575.2	0.2198 (0.0030)
Gabbro/3.0	7722.3	1.2457 (0.0121)	3700.8	0.4154 (0.0055)	4393.4	0.2183 (0.0031)
Rhyolite/2.50	9253.6	1.2440 (0.0110)	4489.5	0.4199 (0.0050)	5271.9	0.2183 (0.0028)
Granite/2.70	8567.8	1.2439 (0.0114)	4120.4	0.4162 (0.0052)	4904.3	0.2193 (0.0029)
Limestone/2.50	9081.6	1.2208 (0.0109)	4328.7	0.4049 (0.0049)	5133.3	0.2126 (0.0028)
Gypsum rich siltstone/2.30	9869.9	1.2207 (0.0105)	4755.3	0.4092 (0.0047)	5585.3	0.2128 (0.0027)

Table 3-1: Table reporting the exposure rate coefficients (μR/h per K wt% or (U,Th)ppm) determined via Monte Carlo simulations for each rock type tested and total energy deposited in the detection sphere in each simulation. Basalt, rhyolite, gabbro, granite and limestone chemistry taken from world averages (Hess 1989; Winter 2010). Gypsum rich siltstone chemistry was obtained from Sloan, 2011.

Table 3-2: Concentration to Exposure Rate Coefficients with Increasing Density

Density (g/cm ³)	Nuclide	Total Energy (keV)	Exp Rate (μR/h) per K wt% or (U,Th)ppm
1	K	21610.13	1.162018 (0.006749)
	U	10483.4	0.392191 (0.003007)
	Th	12268	0.203201 (0.001693)
2	K	11301.21	0.607688 (0.0048399)
	U	5584.54	0.208921 (0.002211)
	Th	6576.48	0.108929 (0.001246)
3	K	7740.401	0.416216 (0.004027)
	U	3756.307	0.140526 (0.00182)
	Th	4459.512	0.073865 (0.001025)
4	K	2853.98	0.311242 (0.003487)
	U	2818.118	0.106769 (0.00158)
	Th	3241.43	0.053689 (0.000872)
5	K	4612.906	0.248045 (0.003118)
	U	2259.163	0.084517 (0.001419)
	Th	2622.883	0.043444 (0.000785)
7	K	3255.717	0.175066 (0.002611)
	U	1623.475	0.060735 (0.00121)
	Th	1881.3	0.031161 (0.000667)
9	K	2525.581	0.135805 (0.002295)
	U	1252.533	0.046858 (0.001056)
	Th	1455.11	0.024102 (0.000583)
10	K	2278.011	0.122493 (0.002177)
	U	1121.338	0.04195 (0.001004)
	Th	1295.982	0.021466 (0.000555)

Table 3-2: Table reporting the exposure rate coefficients determined via Monte Carlo simulations as density was increased and the number of radionuclides was held constant. Rock chemistry is rhyolite worldwide average (Winter 2010).

Table 3-3: Concentration to Exposure Rate Coefficients for Two-Layer Models

Thickness of Top Material (cm)	Exp Rate ($\mu\text{R/h}$) per K (wt%)	Exp Rate ($\mu\text{R/h}$) per U ppm	Exp Rate ($\mu\text{R/h}$) per Th ppm
Rock			
0	1.252591	0.416641	0.219767
0.5	1.174976	0.382381	0.203996
1	1.099157	0.355874	0.189551
2	0.96521	0.313072	0.168239
3	0.863188	0.280413	0.150074
5	0.696955	0.214352	0.11992
10	0.430641	0.127379	0.071216
20	0.16533	0.047851	0.030596
30	0.07179	0.018511	0.012236
40	0.013114	0.003329	0.0023
Top Material			
0.5	0.079141	0.029787	0.014624
1	0.150054	0.055963	0.027509
2	0.272879	0.09994	0.049601
3	0.375071	0.136383	0.067533
5	0.535808	0.191896	0.095524
10	0.795834	0.275784	0.140826
20	1.02965	0.353512	0.180406
30	1.137149	0.383465	0.196792
40	1.180287	0.390865	0.204403

Table 3-3: Table reporting the results of the dual-layer models with basalt rock overlain by gypsum rich siltstone. Basalt chemistry was obtained from worldwide averages (Winter 2010) and gypsum rich siltstone chemistry was obtained from Sloan, 2011. Exposure rates for the rock material drop off exponentially as the gypsum material thickens. Similarly, the exposure rates from the gypsum rich siltstone increase logarithmically as the gypsum rich siltstone thickens.

Figures

Figure 3-1: X/Z Cross Section of MCNP Template

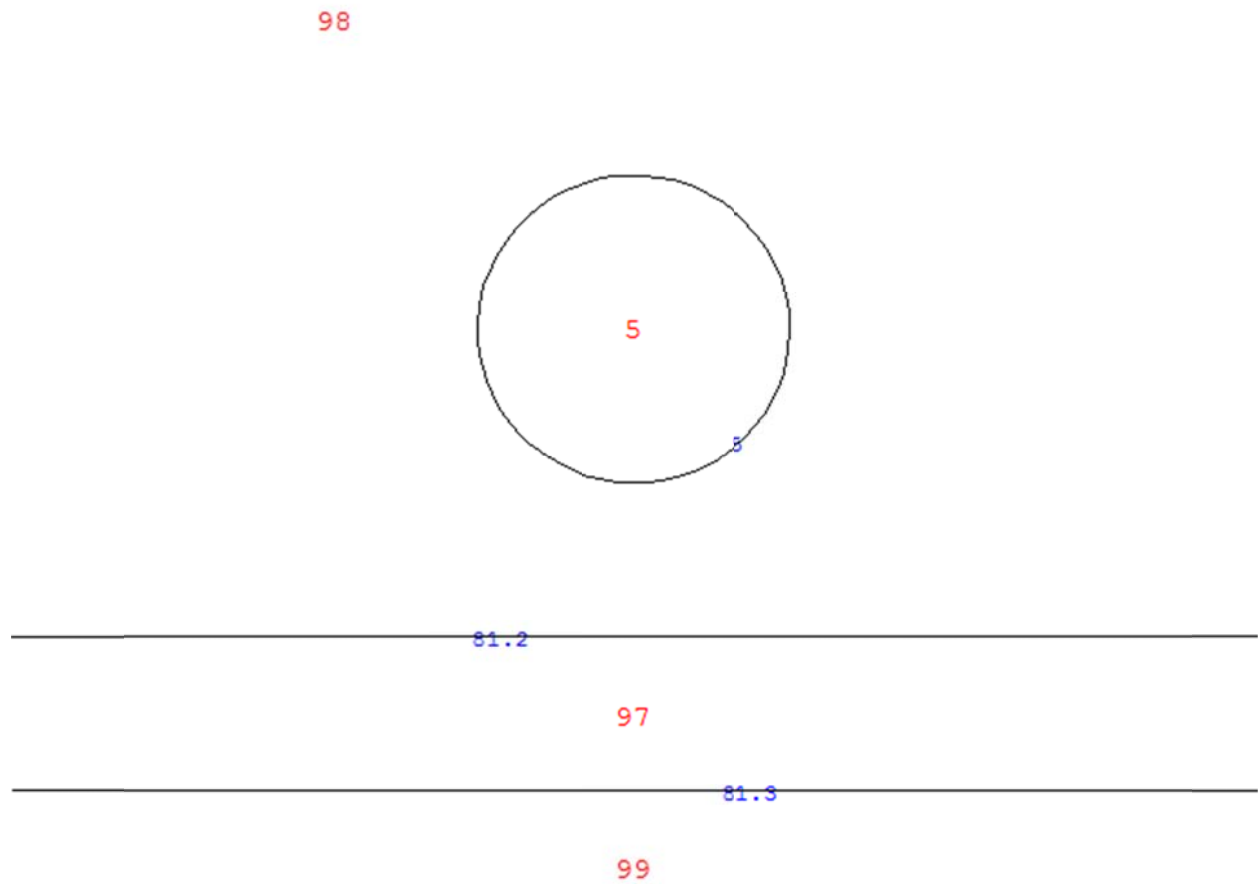


Figure 3-1: X/Z cross section of the simple template model used in all MCNP simulations. Rock media is 97, atmosphere is 98, detection sphere is 5, and the outer universe is 99. In multi-layer models the rock media (97) is reduced in height and another layer is introduced on top.

Figure 3-2: Change in Exposure Rate with Increasing Density

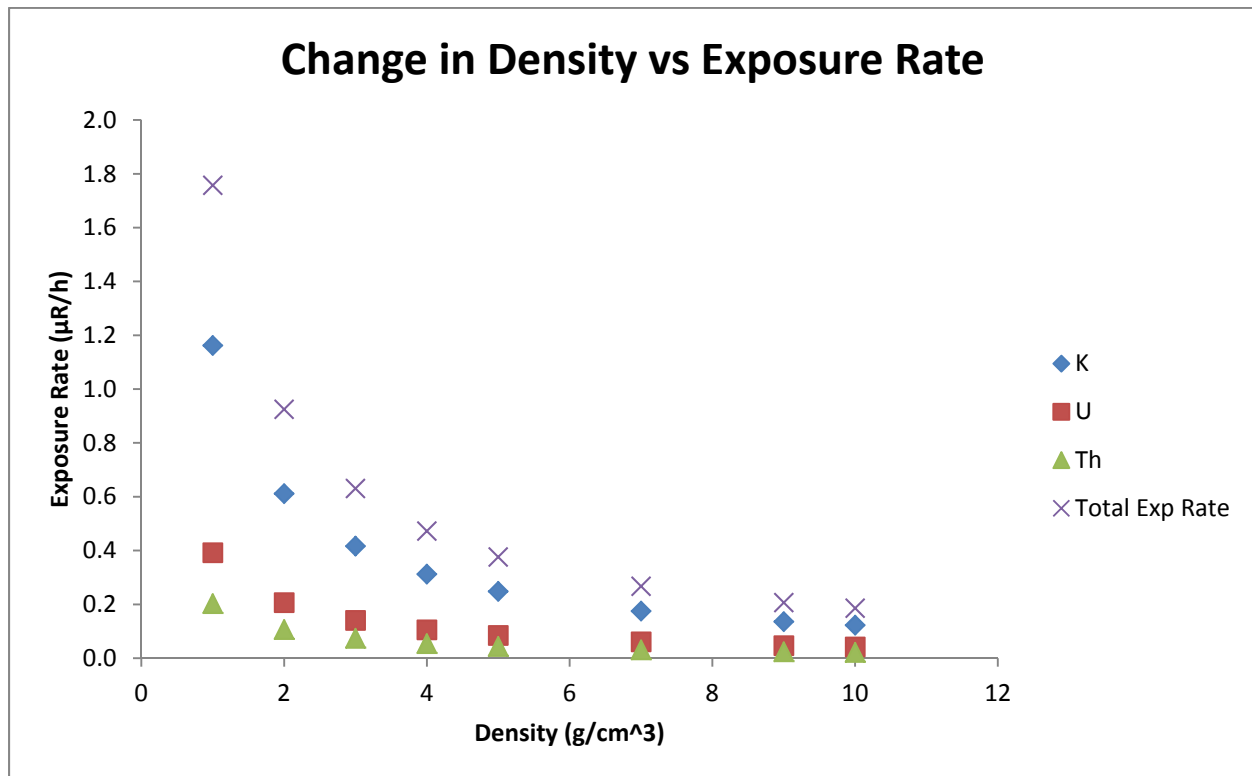


Figure 3-2: Figure showing the drop off of exposure rate as density increases in a rock without a corresponding increase in radionuclides. K, U, and Th values are 1 wt% and 1 ppm respectively at a density of 1 g/cm³.

Figure 3-3: Change in Exposure Rate as Top Layer Thickens

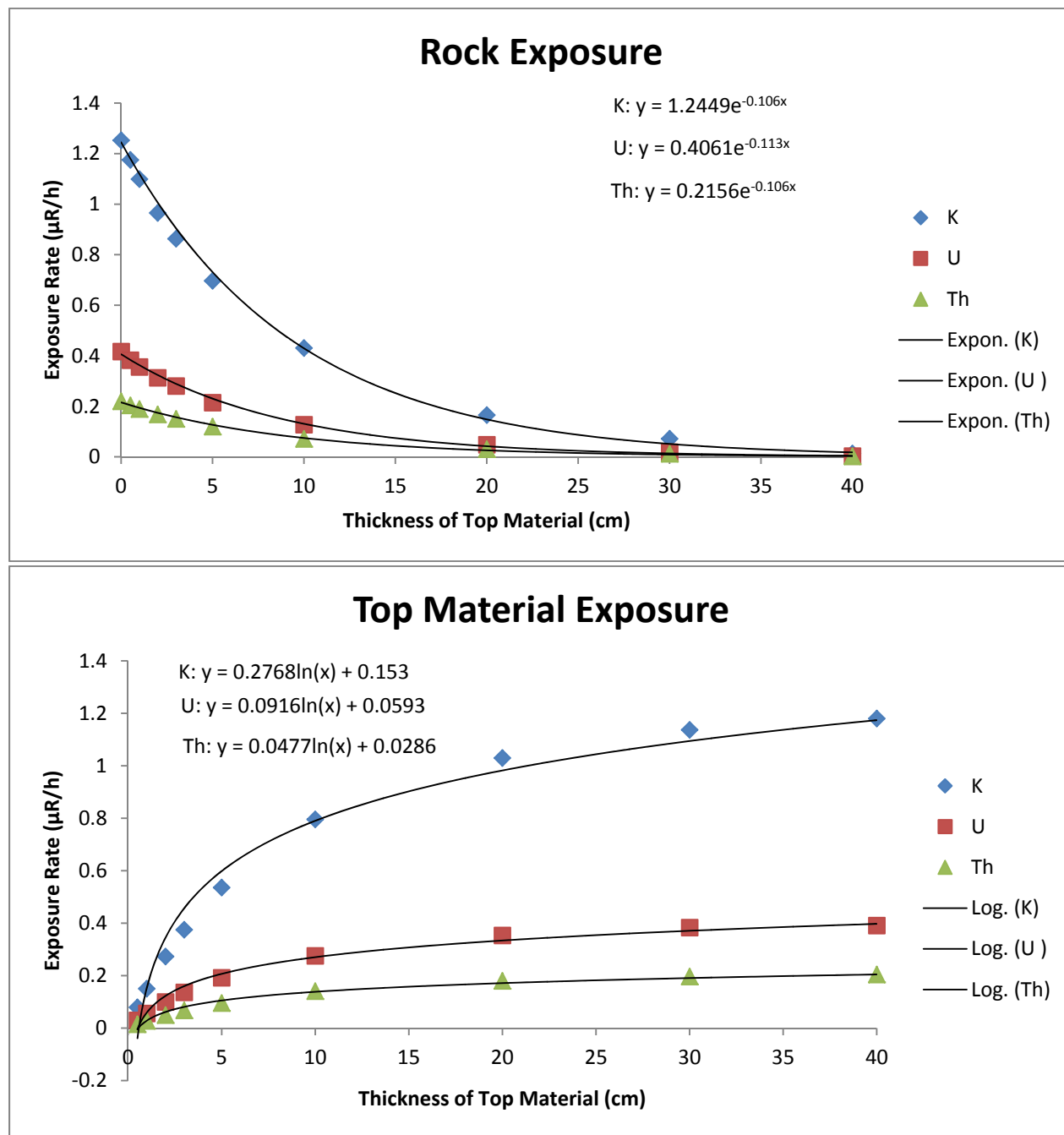


Figure 3-3: The behavior of the rock (top) and top material (bottom) exposure rate as the thickness of the top material increases. This relationship fits with the expectations of the Beer-Lambert law of attenuation. K, U, and Th values are 1 wt% and 1 ppm respectively.

Chapter Four

Comparing Multiple Techniques of Measuring Naturally Occurring Radionuclides in Geologic Materials

Abstract

Aeroradiometric surveys are an effective tool to map the distribution of radioelements across a large area. This study is part of a larger study that attempts to forward model the results of an aeroradiometric survey by modeling the geologic contribution to the gamma ray signal by using geologic and geochemical data. To that end we compare the results of several means of determining radioelement concentration including: ICP-MS, laboratory gamma ray counting, in situ HPGe measurements, and aeroradiometric surveying to determine the consistency of results between the techniques. Three field locations, two in Southern Nevada and one in central Arizona, were chosen for this study due to the availability of high resolution aeroradiometric data. In addition, we have acquired pieces of several concrete calibration pads from Grand Junction Colorado that are routinely used to calibrate radiation detection equipment. We have found that each technique produces similar results when effects of detector footprint and in-situ conditions are considered.

Introduction

Aeroradiometric surveys are an effective means of determining the distribution of radioelements across a large area. Low flying aircraft equipped with scintillation detectors collect gamma spectral data, and by using stripping ratios determined by measuring known sources (IAEA 2003), the concentrations of K, eU, and eTh can be determined. Previous studies have compared the relationship between aeroradiometric surveys and ground based radiometric surveying techniques (Grasty, Carson et al. 1984). The purpose of this study is to compare the results of inductively coupled mass spectrometry (ICP-MS) to three aeroradiometric surveys, ground based radiometric techniques and laboratory based counting of samples and in order to determine the consistency of results between techniques.

This study is part of a larger study that attempts to forward model the results of an aeroradiometric survey using pre-existing geochemical data to predict the distribution of K, U, and Th. It was quickly discovered that existing geochemistry in online databases was problematic in terms of the geolocation and quality of the metadata; particularly with older data points taken before the ubiquitous use of GPS equipment. Additionally, many pre-existing geochemical data points did not correspond to the aerial survey results and as a result field work was performed to assess the differences, if any existed, between the various measurement techniques.

Another goal of this work was to evaluate the presence and potential of disequilibrium in the U series decay chain. Many of the sample points are within contemporarily active alluvial units that may exhibit considerable disequilibrium. In a 1995 study, Dickson found that U-series disequilibrium in arid Australian soils was of minimal consequence largely due to the fact that uranium signal from aerial surveys is noisy and estimation of U from an aerial survey has a large uncertainty. Additionally, uranium usually contributes only about 20% to the total exposure

rate under crustal average conditions so small variations in U may have little effect on the total gamma ray exposure rate (Grasty, Carson et al. 1984; Dickson 1995).

Background

When AMS performs an aerial survey of a particular area they are primarily concerned with the gamma ray exposure rate rather than exact K, U, and Th concentrations. To that end, we compare measured exposure rates to exposure rates calculated from K, U, and Th concentration. Exposure rate is a measure of the number of ionizations produced in a quantity of air by photon radiation per unit time. There is a linear relationship between radioelement concentration and exposure rate given by the following equation:

$$E=1.32*K + 0.548*eU + 0.227*eTh \quad \text{Equation 4-1}$$

(Beck, DeCampo et al. 1972; Løvborg and Kirkegaard 1974; Duval, Carson et al. 2005)

Where K is the concentration of K in weight percent, eU is equivalent U in parts per million, eTh is equivalent Th in parts per million and E is the exposure rate in $\mu\text{R(Roentgen)}/\text{h}$. This equation was first derived by Beck et al. in 1972 using NaI measurements of activity of K, and U and Th daughter isotopes in a soil and comparing that to available branching ratios assuming a homogenous distribution of nuclides in the soil. In 1974, Løvborg et al. also derived similar coefficients by theoretical calculation, using computer code they designed and branching ratios determined by a statistically weighted average of twelve previously published studies. Coefficients were updated by Duval in 2005 to reflect units of dose and used here assuming a 0.1 factor between nGy/h and $\mu\text{R}/\text{h}$. We assume this factor because the conversion from roentgen to rad is about 1 and 1 Gy is equal to 100 rad (Cember and Johnson 2009).

K, U, and Th values from aerial spectral data are determined by spectral stripping coefficients. These coefficients are derived by comparing spectra to a source with a known concentration of nuclides. AMS uses calibration pads located in Grand Junction, Colorado, as

their known source to calibrate their detectors and derive these coefficients. These pads were installed in the 1970's and were doped with radioelement bearing minerals. Potassium feldspar in the form of a pink, orthoclase granite provided K; U was provided by pitchblende; and Th was provided by monazite sand (Ward 1978). A desired concentration level for each radionuclide was obtained in each pad by chemical assay and blending of the sources into the concrete (Ward 1978). A portion of concrete from each pad was reserved and chemically tested to determine concentration levels. K was determined by atomic absorption spectroscopy, U was determined by fluorometric analysis, and Th was determined by x-ray fluorescence (George, Novak et al. 1985). If these concentrations are not representative of the pads then detector calibrations based on these data are in doubt.

Methods

AMS Data

AMS provided us with high spatial resolution aerial gamma ray survey data for both Government Wash and Lake Mohave. These data are comprised of a series of spectra taken at one second intervals along the flight line. The flight lines are grouped close together so that the data points fill the area of interest. The raw spectral data were corrected for dead time, background subtracted, and corrected for air attenuation down to one meter off the surface. Dead time was accounted for by dividing the counts by the live time. The spectra were corrected for background signal by removing counts collected over either Lake Mead or Lake Mohave. Air attenuation was accounted for by plotting an altitude spiral against count rate and obtaining an exponential fit. Exposure rate was calculated by using Equation 2-1.

The data were then processed to provide K, eU, and eTh values in each area of interest according to the spectral stripping technique outlined in the 2003 IAEA Tech Doc using the activity of ^{214}Bi to calculate eU ppm and activity of ^{208}Tl to calculate eTh ppm values and

Equation 2-2 through Equation 2-7. Spectral stripping coefficients were provided by AMS (Table 2-1).

NSTec also provided us with exposure rate data points from an aerial survey of Cameron, Arizona, but the original spectral data has been lost. Therefore, aerial data at Cameron can only be compared on the basis of exposure rate.

When comparing data derived from an aerial survey to results from sample analysis or in-situ measurements, a consideration must be made for the detector's footprint. The aerial surveys conducted by NSTec at an altitude of 100m have a footprint of ~100m radius around each point. Thus the spectra is an average of all the material within that radius. While AMS provided us with a dense set of points, there are no spectra directly above the locations of field measurements. Therefore, to compare aerial data with other methods, an average of the nearest points within the same geologic unit was chosen with maximum distances of 200m at Cameron and 50m in Southern Nevada. An additional comparison were made to the average exposure rate within the geologic unit that the field measurement was taken.

Uncertainty in the data provided by NSTec is not well understood. Therefore, we have used $1/\sqrt{n}$ with n being the average counts over water at Government Wash and Lake Mohave of 1211. This is equal to approximately 3% uncertainty.

Sampling

Twenty-two soil and rock samples were collected from three field sites in the Southwestern United States. Two sites are in Southern Nevada; the first site, Government Wash, located east of Las Vegas and north of Lake Mead, and the second on the western shore of Lake Mohave near the town of Searchlight (Figure 4-1). The third site is near Cameron, Arizona (Figure 4-2). Fourteen samples were collected in Southern Nevada (Figure 4-1) and eight were collected in Cameron (Figure 4-2). These sites were primarily chosen due to readily available high resolution aeroradiometric surveys from the Aerial Measurement System (AMS)

section of our corporate partner National Security Technologies, LLC (NSTec). At Government Wash and Lake Mohave the Remote Sensing Lab (RSL) of NSTec conducted the ground truth survey with us and provided a high purity germanium (HPGe) detector to measure radionuclide concentrations at the sampling sites (Figure 4-3).

All samples from Southern Nevada and Cameron, Arizona were collected according to ASTM Standards (ASTM 2005). Briefly, one square meter is measured out; rings with a diameter of 4 inches and a depth of 2 inches are placed in each corner and directly in the middle and are hammered into the ground with a rubber mallet. The material within the rings was removed and placed into a plastic bucket (Figure 4-4). Each location had either significant soil development, was very friable or was composed of alluvium. Because of this, all samples are composed of soil or soil like material with a few large pieces of rock. Plant material was removed using metal tweezers by visual inspection.

In addition to the twenty-two soil and rock samples, we obtained five samples from the concrete calibration pads located in Grand Junction Colorado. These samples come from portions of the pads that have broken off the surface and were therefore susceptible to weathering. The least weathered pieces that were at least 5 cm in size were used in this analysis to minimize the effects of weathering.

In Situ Measurements

The RSL HPGe detector was placed at a height of 1 meter off the surface at each sampling location in Southern Nevada. The HPGe detectors collected spectra at each point for 15 minutes to minimize counting uncertainty. Instead of providing us with raw spectra, RSL provided us with activity concentrations derived from the spectra for gamma emitting elements in the ground. The activity of ^{40}K was used to calculate K weight percent. Activity values for ^{214}Bi were used to calculate eU and activity values for ^{208}Tl were used to calculate eTh. Uncertainty is

not understood for these data. Exposure rates were calculated from the HPGe data by using Equation 4-1.

Laboratory Counting

In preparation for counting, pieces larger than 1 cm in each sample were crushed. The large fraction was retained because we are interested in understanding the K, U, and Th concentration of the surface as a whole. Water was removed from the samples by placing them in a 110°C oven for 24 hours. The samples were then sealed for 28 days prior to counting to allow for the ingrowth of Ra daughters. The Cameron samples were sieved into the following size fractions: <500µm, <2mm and >2mm. These size fractions were tested separately to better understand the distribution of K, U, and Th within the size fractions.

Samples collected at Lake Mohave and Government Wash were counted at Test America Inc. Samples from Cameron, AZ were counted at the Environmental Radiochemistry Laboratory at the University of Nevada Las Vegas. The Environmental Radiochemistry Laboratory counted the samples with high purity germanium (HPGe) detectors Canberra Model GR4019 and Canberra Model GX3519 using a version of EPA Method 901.1 modified for soil samples. The detectors were calibrated using a reference standard (Analytix 78730-602) consisting of a sieved soil in a 500 mL Marinelli Beaker. Test America used HPGe detectors and ASTM procedures for sample analysis (ASTM 2004). Both labs counted blanks before and after counting the series of samples and background corrected the results. Test America counted the samples for 12 hours while the UNLV lab counted the samples for 24 hours. Because Cameron samples were counted for twice the length as the Southern Nevada samples, they have a lower level of uncertainty than the Southern Nevada samples.

Both laboratories provided us with activity concentrations for gamma emitting radioisotopes. The activity concentration of ^{40}K was used to calculate K weight percent. eU and eTh concentrations were determined by counting their daughter isotopes and assuming

equilibrium. Average activity values for ^{226}Ra , ^{214}Bi , ^{214}Pb , ^{234}Th and ^{210}Pb were used to calculate eU. Average activity values for ^{212}Bi , ^{228}Ac , ^{212}Pb , ^{228}Ra and ^{208}Tl were used to calculate eTh.

Weighted exposure rates for the Cameron samples were calculated by first multiplying the K, U, and Th values in each size fraction by the ratio between the mass of the size fraction and the total mass of the sample to obtain weighed K, U, and Th values; then by summing together the weighted K, U, and Th values an exposure rate was calculated with Equation 4-1.

ICP-MS

To prepare all the samples for ICP-MS they were first homogenized and reduced in volume according to the cone and quarter method (Schumacher, Shines et al. 1990), then randomly subsampled using a spoon, and weighed to obtain a representative 20g sample. The 20g sample was then crushed into rock flour using a Bico shatter box. The samples were then processed through ICP-MS by four acid digestion (BrooksRand 2007) (HF, HClO_4 , HNO_3 , and HCl) at the Environmental Soil Analysis Laboratory, UNLV. Blanks were run prior to the batch analysis to determine background levels. National Institute of Standards and Technology (NIST) standards SRM2711a Montana soil and 8704 Buffalo River Sediment were used to check the consistency of results. Both of these standards offer known K, U, and Th concentration values. Exposure rates derived from the ICP-MS analysis are calculated using Equation 4-1. The sieved samples from Cameron were not recombined for ICP-MS; instead each size fraction was tested separately to compare with the size fraction counting results.

Results

Sample Descriptions

The samples Tmcg2, Tmcg3, Tmcl2, and Tmcl3 from Government Wash are composed of highly friable grey to red siltstone bedrock with some pieces of gypsum >1cm. Tmcu1 is

composed of grey sandy material with some larger pieces of conglomerate and limestone up to 2cm. The Qa1, Qa4, and Qoa1 sample point are located on alluvial material that range in size from sand to boulder with clasts of limestone, basalt, and sandstone.

Samples Qay1, Qay2, A3, A5, A7, and A9 from Lake Mohave are located on alluvial material with varying amounts of sand and silt and gravel. Qay1 and Qay2 consist of well-developed desert pavements with interlocking clasts of tuff that are 1 to 2cm in size and eolian dust beneath. A3 is a well-developed desert pavement consisting of clasts of granite and tuff that are 1 to 2 cm in size with eolian dust beneath. A5 and A7 are composed of loose gravels and sand with <1mm clasts of granitic rock and tuff. A9 is composed of loose gravel with <1cm clasts of tuff, granite, amphibolite, and vesicular basalt.

At the Cameron site the Qps sample site consists of a brown mud cracked surface scattered with lag deposits of basalt that are between 1 and 5 cm in size. The Ql site consists of eolian sands and large >10cm basalt lag pieces. The TRcp site consists of a blue-grey mud cracked silty dust with some clasts of chert between 1 and 5cm in size. The TRcs site is composed of white and red medium grain sandstone with soil development on top of the sandstone. There are clasts of sandstone <5cm in size intermixed with the sampled soil. TRmss is a fine grained thin bedded sandstone with thin soil development on top mixed with clasts of sandstone <3cm in size. TRmw is composed of a dark red decomposed friable sandstone with some large indurated >10m ripple marked lag deposits.

Southern Nevada

The K (wt%) values determined by ICP-MS, laboratory counting, HPGe measurement, and aerial survey are reported in Table 4-1 and Figure 4-5. The U ppm values determined by ICP-MS, laboratory counting, HPGe measurement, and aerial survey are reported in Table 4-1 and Figure 4-6. The Th ppm values determined by ICP-MS, laboratory counting, HPGe measurement, and aerial survey are reported in Table 4-1 and Figure 4-7. Exposure rate

comparisons between ICP-MS, HPGe, laboratory counting and AMS data are reported in Table 4-2 and Figure 4-8.

Cameron

The K (wt%) values determined by ICP-MS and laboratory counting are reported in Table 4-3 and Figure 4-9. The U ppm values determined by ICP-MS and laboratory counting are reported in Table 4-3 and Figure 4-10. The Th ppm values determined by ICP-MS and laboratory counting are reported in Table 4-3 and Figure 4-11. Exposure rate comparisons between ICP-MS, laboratory counting and AMS data are reported in Table 4-4 and Figure 4-12.

Calibration Pads

The K (wt%), U, and Th ppm values determined by ICP-MS are compared to published chemistry in Table 4-5 and Figure 4-13, Figure 4-14, and Figure 4-15 respectively. Exposure rates calculated from ICP-MS and published K, U, and Th values are compared to exposure rates measured by NSTec using a PIC in Table 4-5 and Figure 4-16.

Discussion

To evaluate whether data from a particular measurement agree with other measurements on the same sample, we examine whether or not a K, U, or Th value will cause the exposure rate to change by more than $\pm 1 \mu\text{R/h}$ outside of uncertainty, against any other measurement technique according to Equation 4-1. A K weight percent difference that is > 0.75 , a U ppm difference of > 1.82 , and a Th ppm difference of > 3.67 will cause the exposure rate to vary by $\pm 1 \mu\text{R/h}$.

Southern Nevada

K, U, and Th values for Tmcg2 agree with the exception of the lab counting value which reports a higher K and exposure rate than all other techniques. The high exposure rate is controlled by the K value. This sample was counted twice with different K, U, and Th values on

each run. The reason for this discrepancy is not understood, however the second K result agrees with the other techniques. Tmcu1 is in a small outcrop of Tmcu that is 90m across in the direction of the AMS survey, surrounded by a radiologically cooler unit. In addition, the Tmcu1 sample point is only 20 m from the geologic boundary with the cooler unit. The AMS K, Th, and exposure rate values of Tmcu1 are below the values of the other analytical techniques. The AMS data for Tmcu is therefore likely influenced by the surrounding unit.

The Tmcg3 sample location is geographically within the geologic unit it represents yet the AMS close point and whole unit averages are consistently lower in U, Th, and exposure rate than other analytical techniques. A possible explanation for this result is that this represents a region of Tmcg, smaller than the footprint of the detector, which has thinned due to erosion and is being influenced by the hotter unit that occurs stratigraphically below. Other portions of Tmcg have thinned to the extent that the lower unit is exposed. Images from the field collection appear to show the red unit that underlies Tmcg just below the surface (Figure 4-4).

The HPGe data for Qay1, Qay2, Qoa1, A3, and A5 consistently report higher U concentrations than other techniques. This may arise from the fact that the HPGe data are not corrected for atmospheric radon which has the largest effect on the U channel (Grasty, Carson et al. 1984; Minty 1997).

Tmcl2 ICP-MS K value is higher than other techniques but near our standard for agreement. It is possible that this is a sampling bias.

Exposure rate comparisons are reflective of the differences in K, U, and Th concentrations. For Qoa1, the difference between the AMS exposure rate is reported as 1.75 $\mu\text{R/h}$ while the AMS unit average is 3.36 $\mu\text{R/h}$. The AMS unit average is $< \pm 1$ $\mu\text{R/h}$ relative to exposure rates from the other techniques.

As a general trend, the AMS data reports lower K, U, Th, and exposure rate values, even when those values are within our standard for agreement. This discrepancy is especially

pronounced in the K, Th, and exposure rate data; U data is spread out between over and under reporting against other techniques. This may be related to the detector calibration performed using the Grand Junction Calibration pads; it may also be an issue related to the detector footprint. In either case, the differences are often within our desired range.

Cameron

The K weight percent values for the Cameron samples are in agreement between the ICP-MS and counting data. However, there are some significant differences with the U and Th data. The coarse fraction of the Qps Hot sample has considerably more U and Th reported by the counting than by the ICP-MS. A U value of 0.90 ppm is reported by the ICP-MS and 6.58 ppm is reported by counting while Th values are 3.22 and 43.66 ppm for ICP-MS and counting respectively. Calculated exposure rate values for the coarse fraction are 2.46 and 23.32 $\mu\text{R/h}$ for the ICP-MS and counting respectively. However, the coarse fraction only represents 10% of the total mass of the sample and weighted exposure rates are both comparable to the AMS close point and unit averages. This is the most significant variation in the Cameron samples and may be explained by the presence of petrified wood enriched in radioelements present in the parent material of the unit (Billingsley, Priest et al. 2007). The pieces of petrified wood are small and sparse within the sample and may not have been subsampled for the ICP-MS analysis. The laboratory counting of the coarse fraction of the TRcp and TRcs units, which also have a petrified wood component, also have high U ppm values compared to ICP-MS and may also suffer from a subsampling bias.

Figure 4-12 displays the exposure rate values of the ICP-MS data against the various techniques used to determine an exposure rate. The large outlier at about 23 $\mu\text{R/h}$ is the Qps hot sample, which is driven by the high U and Th values reported by the lab counting. The lab counted samples that are significantly below and above the one to one line are the TRcp and

TRcs samples discussed previously. The rest of the samples fall within ± 1 $\mu\text{R/h}$ of the ICP-MS exposure rate.

There are few discernable patterns in terms of the distribution of K, U, and Th among the size fractions in these samples (Table 4-3). In some cases, the radionuclides are concentrated in the coarse fraction (e.g., TRcs Ave U and Th values), while in other cases the radionuclides are concentrated in the fine fraction (e.g., TRcp Hot K and Th values). The fine fractions tend to have the most K overall but there are no clear patterns for U and Th.

Calibration Pads

ICP-MS results agree with the original published chemistry of the Grand Junction calibration pads (Table 4-5). In pads 1 and 2, there is a significant difference between our analysis and the published Th values. There are also significant differences between the U values for pad 5 and the K values for pad 4. Considering the general agreement between our values and the published values, these variations may be related to weathering of the pieces of the pads that were analyzed.

Exposure rates derived from ICP-MS analysis and published geochemistry both agree and disagree with PIC data provided by NSTec (Figure 4-16). Pad 1 PIC data reports an exposure rate of 11.1 $\mu\text{R/h}$. The published chemistry agrees with this exposure rate with an exposure rate of 10.63 $\mu\text{R/h}$ while the exposure rate from our ICP-MS analysis is 4.86 $\mu\text{R/h}$. The exposure rates for pad 2 are similar to pad 1 in that the published chemistry is in closer agreement with the PIC data. However, pad 3 has a PIC exposure rate of 19.1 $\mu\text{R/h}$ which is in better agreement with our ICP-MS derived exposure rate of 20.92 $\mu\text{R/h}$; the published chemistry exposure rate is 29.97 $\mu\text{R/h}$. Pads 4 and 5 both have PIC data that are in between our analysis and the published chemistry with the published data in better agreement for pad 4 and our analysis in better agreement with pad 5.

With this exposure rate data some judgments can be made as to the accuracy of each data set's concentration values. The major outlier in terms of differences between values for pads 1 and 2 is the Th concentration data and since the PIC data agree with the exposure rate derived from the published data it can be surmised that the published Th data is better representative of the whole pad. The concentration and exposure rate values for pad 3 agree both with each other and with the NSTec PIC data suggesting that these data are representative of the actual pad concentrations. For pad 4 the exposure rate calculated from the published values is in better agreement with the PIC data than the ICP-MS derived exposure rate. K values for pad 4 are higher in the ICP-MS analysis suggesting that the published K concentration may be more representative of the pad. Finally, the PIC exposure rate for pad 5 is in better agreement with the ICP-MS derived exposure rate suggesting that the ICP-MS values may be more representative; although the difference between the published and ICP-MS derived exposure rates are small.

Conclusions

We have shown that multiple techniques for measuring naturally occurring radionuclides in geologic materials are equally viable and produce similar results when effects of detector footprint and in-situ conditions are considered. We have also shown that ICP-MS derived values for K, U, and Th can be used to successfully predict the exposure rate of a geochemically homogenous unit. As Dickson reported in 1995, U disequilibrium appears to be of minimal significance despite the young age of some of these surfaces. Therefore, U series disequilibrium can largely be ignored in arid conditions.

There are no significant patterns in terms of the size fraction distribution of K, U, and Th concentrations in the samples from Cameron other than a tendency for there to be more K in the fine fractions.

Finally, we have shown that the assumed chemical concentrations of the Grand Junction Calibration Pads used to calibrate detectors are correct when comparing exposure rates calculated from published chemistry to NSTec PIC measurements.

Acknowledgments

We want to thank NSTec for providing us with data as well as HPGe detectors to make field measurements, and the DOE office of Legacy Management for providing the samples of the calibration pads.

We also wanted to give special thanks to Dr. Ralf Sudowe and his students, for joining us in the field and providing soil sampling equipment and for counting the samples we brought back.

Tables

Table 4-1: K, U, and Th Values of Samples in Southern Nevada

Sample	ICP-MS K (wt%)	HPGe K (wt%)	Lab Count K (wt%)	AMS K (wt%)	ICP-MS U (ppm)	HPGe U (ppm)	Lab Count U (ppm)	AMS U (ppm)	ICP-MS Th (ppm)	HPGe Th (ppm)	Lab Count Th (ppm)	AMS Th (ppm)
Qa1	0.80 (0.02)	0.67	0.77 (0.11)	0.55 (0.017)	1.65 (0.01)	3.13	1.88 (0.29)	1.51 (0.05)	4.31 (0.09)	3.34	5.17 (1.58)	3.25 (0.1)
Qa4	0.58 (0.02)	0.65	0.46 (0.07)	0.62 (0.018)	1.43 (0.01)	2.47	1.19 (0.18)	1.87 (0.06)	2.50 (0.05)	2.79	1.81 (0.61)	2.21 (0.07)
Tmcg2	0.35 (0.01)	0.30	1.33 (0.18)	0.27 (0.008)	0.44 (0.002)	2.31	2.05 (0.34)	0.79 (0.02)	1.35 (0.03)	1.81	5.77 (1.57)	0.79 (0.02)
Tmcg2 Rerun			0.39 (0.10)				1.26 (0.88)				1.45 (1.72)	
Tmcg3	1.30 (0.04)	0.91	1.23 (0.18)	0.47 (0.014)	1.54 (0.01)	2.98	2.44 (0.43)	0.53 (0.02)	6.52 (0.13)	5.45	6.19 (2.02)	1.95 (0.06)
Tmcl1	2.18 (0.07)	1.74	2.30 (0.28)	0.43 (0.013)	2.45 (0.01)	2.62	1.85 (0.33)	3.05 (0.09)	7.23 (0.14)	5.84	7.53 (2.05)	1.93 (0.06)
Tmcl2	1.45 (0.04)	0.64	0.81 (0.16)	0.51 (0.015)	2.23 (0.01)	2.91	2.05 (0.35)	2.93 (0.09)	5.32 (0.11)	4.78	4.21 (1.52)	3.49 (0.1)
Tmcl3	1.44 (0.04)	1.48	1.30 (0.18)	1.09 (0.033)	1.91 (0.01)	2.71	1.75 (0.32)	2.72 (0.08)	4.83 (0.10)	4.75	3.74 (1.50)	3.36 (0.1)
Qoa1	0.89 (0.03)	0.56	0.78 (0.12)	0.23 (0.007)	2.49 (0.01)	3.08	2.18 (0.34)	0.7 (0.02)	5.06 (0.10)	2.93	3.50 (1.36)	3.3 (0.1)
Qay1	3.55 (0.11)	3.22	3.34 (0.37)	3.38 (0.101)	2.59 (0.01)	4.72	2.68 (0.37)	1.35 (0.04)	15.67 (0.31)	14.34	12.09 (2.21)	17.15 (0.51)
Qay2	3.27 (0.10)	3.32	3.25 (0.36)	3.14 (0.094)	2.46 (0.01)	4.31	2.92 (0.38)	0.78 (0.02)	14.90 (0.30)	14.76	16.18 (2.94)	11.6 (0.35)
A3	3.21 (0.10)	3.23	3.25 (0.36)	2.91 (0.087)	2.23 (0.01)	4.51	2.51 (0.36)	2.24 (0.07)	12.51 (0.25)	13.12	12.36 (2.10)	11.31 (0.34)
A5	3.58 (0.11)	3.30	3.29 (0.37)	2.69 (0.081)	1.84 (0.01)	4.26	1.92 (0.29)	3.33 (0.1)	11.70 (0.23)	11.21	11.18 (2.16)	9.47 (0.28)
A7	3.33 (0.10)	3.18	2.80 (0.33)	2.78 (0.083)	2.09 (0.01)	3.72	2.43 (0.40)	2.39 (0.07)	14.88 (0.30)	14.09	17.76 (3.30)	11.39 (0.34)
A9	3.28 (0.10)	3.35	3.08 (0.35)	2.98 (0.089)	1.92 (0.01)	3.38	2.33 (0.35)	2.38 (0.07)	15.34 (0.31)	15.57	14.57 (3.10)	12.19 (0.37)

Table 4-1: K, U, and Th values of the various measurement techniques in Southern Nevada.

Table 4-2: Exposure Rate Values of Samples in Southern Nevada

Sample	ICP-MS Exp (μR/h)	HPGe Exp (μR/h)	Lab Counting Exp (μR/h)	AMS Exp (μR/h)	AMS Unit Average
Qa1	3.29 (0.06)	3.50	3.46 (0.74)	2.61	2.68
Qa4	2.35 (0.04)	2.97	1.75 (0.35)	2.41	
Tmcg2	1.12 (0.02)	2.15	4.45 (0.86)	1.29	2.03
Tmcg3	4.54 (0.09)	4.31	4.64 (1.03)	1.65	
Tmcl1	6.46 (0.13)	5.33	6.1 (1.11)	2.48	3.20
Tmcl2	4.8 (0.09)	4.57	3.76 (0.82)	3.90	3.56
Tmcl3	4.47 (0.08)	4.73	3.7 (0.81)	3.86	
Qoa1	4.13 (0.07)	3.23	3.17 (0.71)	1.75	3.36
Qay1	10.79 (0.22)	10.13	9.17 (1.28)	9.52	8.69
Qay2	10.12 (0.2)	10.16	10.29 (1.49)	9.33	
A3	9.22 (0.19)	9.65	9.02 (1.24)	8.78	8.64
A5	9.25 (0.2)	9.09	8.44 (1.23)	7.75	8.69
A7	9.98 (0.21)	9.41	9.85 (1.55)	9.19	
A9	9.94 (0.2)	9.86	9.3 (1.5)	9.96	8.62

Table 4-2: Exposure rate values of the various measurement techniques in Southern Nevada.

Table 4-3: K, U, and Th Values of Samples near Cameron, Arizona

Sample	ICP-MS K (wt%)	Lab Counting K (wt%)	ICP-MS U (ppm)	Lab Counting U (ppm)	ICP-MS Th (ppm)	Lab Counting Th (ppm)
QI Cool Fine	1.63 (0.05)	2.34 (0.15)	1.91 (0.01)	2.96 (0.12)	8.39 (0.17)	7.86 (0.35)
QI Cool medium	0.77 (0.02)	1.09 (0.07)	1.42 (0.01)	2.18 (0.1)	4.35 (0.09)	4.6 (0.32)
QI Cool Coarse	0.68 (0.02)	0.9 (0.06)	0.94 (0.005)	2.56 (0.09)	3.2 (0.06)	3.02 (0.22)
Qps Hot Fine	0.91 (0.03)	1.15 (0.08)	3.56 (0.02)	4.34 (0.16)	13.39 (0.27)	14.63 (0.7)
Qps Hot Medium	0.6 (0.02)	0.74 (0.05)	4.87 (0.02)	4.89 (0.17)	22.81 (0.46)	21.24 (0.75)
Qps Hot Coarse	0.35 (0.01)	0.35 (0.22)	0.9 (0.004)	6.58 (0.91)	3.22 (0.06)	43.66 (2.75)
TRcp Hot Fine	2.28 (0.07)	2.52 (0.16)	7.17 (0.04)	8.19 (0.25)	12.98 (0.26)	10.03 (0.47)
TRcp Hot Medium	1.29 (0.04)	1.7 (0.11)	9.08 (0.05)	13.01 (0.35)	10.2 (0.2)	10.6 (0.53)
TRcp Hot Coarse	1.11 (0.03)	1.09 (0.08)	12.92 (0.06)	21.35 (0.57)	8.56 (0.17)	8.02 (0.62)
TRcp Ave Fine	1.74 (0.05)	1.92 (0.13)	6.85 (0.03)	5.28 (0.19)	17.41 (0.35)	14.54 (0.63)
TRcp Ave medium	1.61 (0.05)	1.92 (0.12)	8.66 (0.04)	6.94 (0.21)	15.73 (0.31)	15.51 (0.6)
TRcp Ave Coarse	1.68 (0.05)	2.06 (0.13)	12.45 (0.06)	9.55 (0.28)	14.04 (0.28)	14.45 (0.64)
TRcs Hot Fine	2.65 (0.08)	2.32 (0.15)	4.95 (0.02)	4.79 (0.14)	11.41 (0.23)	6.74 (0.29)
TRcs Hot Medium	1.9 (0.06)	1.92 (0.12)	4.82 (0.02)	5.46 (0.18)	9.46 (0.19)	7.15 (0.39)
TRcs Hot Coarse	1.59 (0.05)	1.4 (0.19)	11.02 (0.06)	17.72 (0.86)	9.07 (0.18)	8.7 (2.11)
TRcs Ave Fine	0.71 (0.02)	0.76 (0.05)	3.2 (0.02)	3.17 (0.1)	15.51 (0.31)	11.88 (0.41)
TRcs Ave Medium	0.44 (0.01)	0.48 (0.04)	4.51 (0.02)	3.88 (0.15)	20.85 (0.42)	14.39 (0.53)
TRcs Ave Coarse	0.22 (0.01)	0.27 (0.03)	5.28 (0.03)	5.2 (0.19)	19.41 (0.39)	13.15 (0.59)
TRmss Fine	2.05 (0.06)	2.44 (0.16)	2.07 (0.01)	2.82 (0.11)	7.55 (0.15)	6.63 (0.31)
TRmss Medium	1.38 (0.04)	1.59 (0.11)	1.99 (0.01)	2.5 (0.11)	5.79 (0.12)	5.14 (0.89)
TRmss Coarse	1.27 (0.04)	1.28 (0.08)	1.91 (0.01)	1.96 (0.07)	2.5 (0.05)	2.18 (0.26)
TRmw Fine	4.2 (0.13)	4.49 (0.29)	2.98 (0.01)	2.74 (0.13)	10.9 (0.22)	7.74 (0.43)
TRmw Medium	3.89 (0.12)	4.79 (0.3)	3.02 (0.02)	2.54 (0.11)	10.5 (0.21)	8.78 (0.42)
TRmw Coarse	2.09 (0.06)	2.43 (0.15)	2.04 (0.01)	1.92 (0.08)	5.41 (0.11)	4.5 (0.24)

Table 4-3: K, U, and Th values of the various measurement techniques in Cameron, AZ.

Table 4-4: Exposure Rate Values of Samples near Cameron, Arizona

Sample	ICP-MS Exp (μR/h)	ICP-MS Weighted Exp (μR/h)	Lab Counting Exp (μR/h)	Lab Counting Weighted Exp (μR/h)	AMS Closest Points Exp (μR/h)	AMS Unit Average Exp (μR/h)
QI Cool Fine	5.73 (0.11)	3.99	6.85 (0.18)	4.99	4.11	4.49
QI Cool medium	3.13 (0.05)		3.88 (0.12)			
QI Cool Coarse	2.4 (0.04)		3.42 (0.09)			
Qps Hot Fine	7.17 (0.11)	8.28	7.88 (0.19)	10.23	10.23	6.78
Qps Hot Medium	10.22 (0.14)		9.43 (0.18)			
Qps Hot Coarse	2.46 (0.03)		23.32 (0.45)			
TRcp Hot Fine	11.06 (0.17)	10.82	10.55 (0.24)	11.96	10.42	10.01
TRcp Hot Medium	10.08 (0.12)		12.26 (0.24)			
TRcp Hot Coarse	11.65 (0.12)		15.32 (0.29)			
TRcp Ave Fine	11.41 (0.17)	12.24	9.38 (0.22)	10.58	11.24	
TRcp Ave medium	11.83 (0.16)		10.56 (0.22)			
TRcp Ave Coarse	13.71 (0.16)		11.89 (0.25)			
TRcs Hot Fine	9.78 (0.17)	9.32	7.52 (0.17)	7.60	10.44	9.47
TRcs Hot Medium	8.14 (0.13)		7.47 (0.18)			
TRcs Hot Coarse	11.31 (0.13)		13.93 (0.65)			
TRcs Ave Fine	7.29 (0.11)	8.190235	5.97 (0.12)	6.34	10.27	
TRcs Ave Medium	9.23 (0.12)		6.68 (0.14)			
TRcs Ave Coarse	8.98 (0.11)		6.79 (0.16)			
TRmss Fine	6.15 (0.12)	4.81	6.57 (0.18)	4.92	5.68	6.18
TRmss Midium	4.7 (0.09)		4.87 (0.22)			
TRmss Coarse	3.57 (0.07)		3.36 (0.11)			
TRmw Fine	10.55 (0.22)	8.07	9.53 (0.28)	7.79	5.68	7.98
TRmw Medium	10.04 (0.21)		10.1 (0.29)			
TRmw Coarse	5.57 (0.11)		5.48 (0.16)			

Table 4-4: Exposure rate values of the various measurement techniques in Cameron, AZ. AMS closest points are an average of points in the same geologic unit within 200m of the sample point. Unit average is the average exposure rate of the entire geologic unit.

Table 4-5: Exposure Rate, K, U, and Th Values of Samples from Calibration Pads

Sample	ICP-MS K (wt%)	Pub Chem K (wt%)	ICP-MS U (ppm)	Pub Chem U (ppm)	ICP-MS Th (ppm)	Pub Chem Th (ppm)	ICP-MS Exp (μR/h)	Pub Chem Exp (μR/h)	NSTec PIC Exp (μR/h)
Pad1	1.88 (0.06)	1.6 (0.05)	1.78 (0.04)	2.5 (0.55)	5.15 (0.03)	14.3 (2.43)	4.86 (0.1)	10.63 (0.93)	11.1 (0.4)
Pad2	5.97 (0.18)	5.1 (0.26)	4.07 (0.08)	5.8 (2.03)	8.07 (0.04)	14.5 (5.08)	12.31 (0.29)	16.26 (2.61)	15.3 (0.3)
Pad3	2.7 (0.08)	2.2 (0.07)	5.1 (0.1)	4.4 (1.28)	53.52 (0.27)	47.2 (6.14)	20.92 (0.22)	18.15 (2.19)	19.1 (0.3)
Pad4	4.11 (0.12)	2.2 (0.06)	32.13 (0.64)	35.3 (8.47)	13.86 (0.07)	15 (4.5)	26.81 (0.53)	20.73 (5.74)	22 (0.3)
Pad5	5.23 (0.16)	4.3 (0.12)	18.74 (0.37)	24.3 (8.02)	21.89 (0.11)	22.1 (6.19)	23.13 (0.44)	24.4 (5.96)	21.8 (0.7)

Table 4-5: K, U, and Th values of the ICP-MS analysis and published chemistry of the Grand Junction calibration pads.

Figures

Figure 4-1: Location of Samples in Southern Nevada

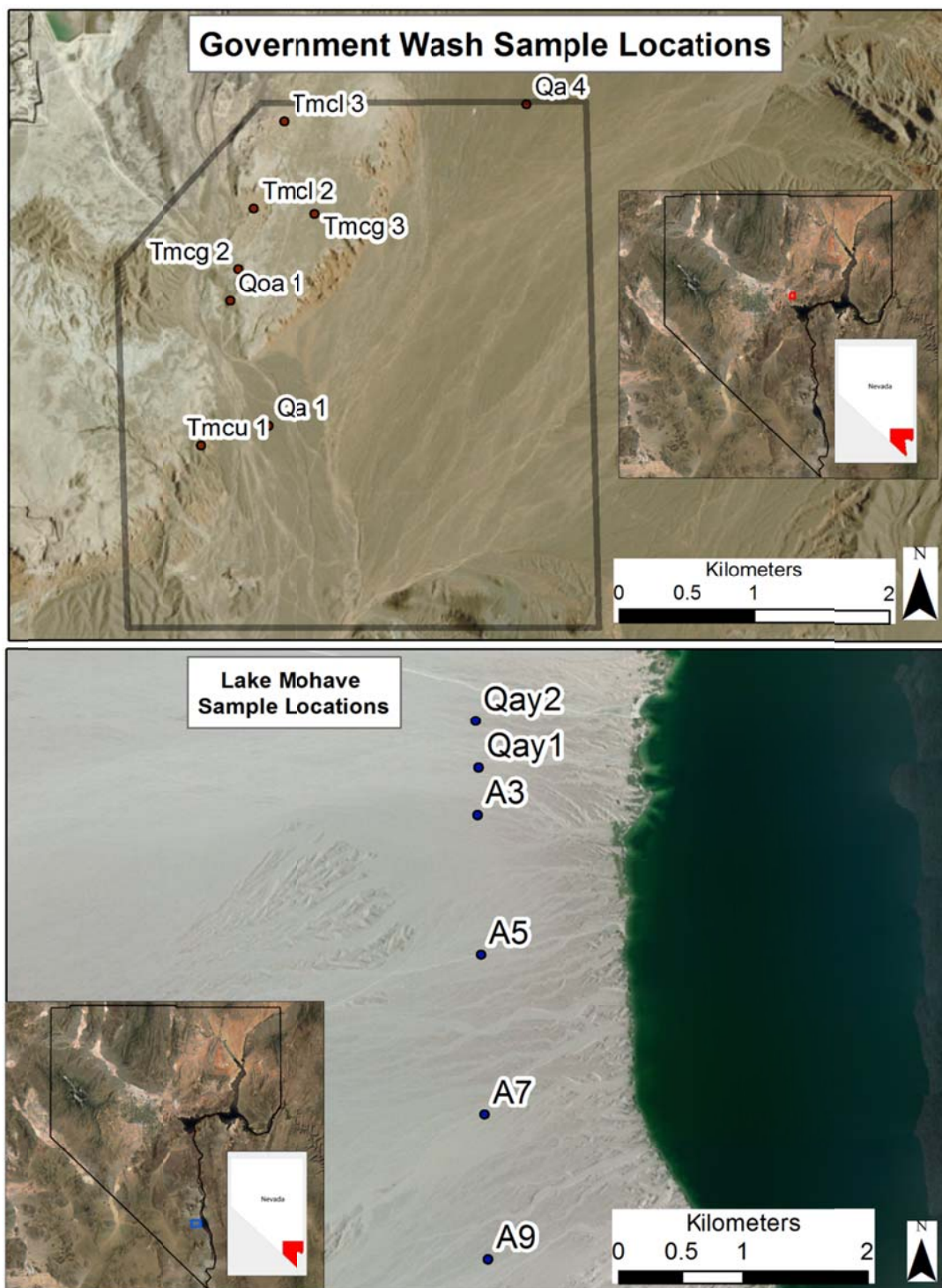


Figure 4-1: Sample locations at Government Wash (above) and Lake Mohave (below)

Figure 4-2: Location of Samples near Cameron, Arizona

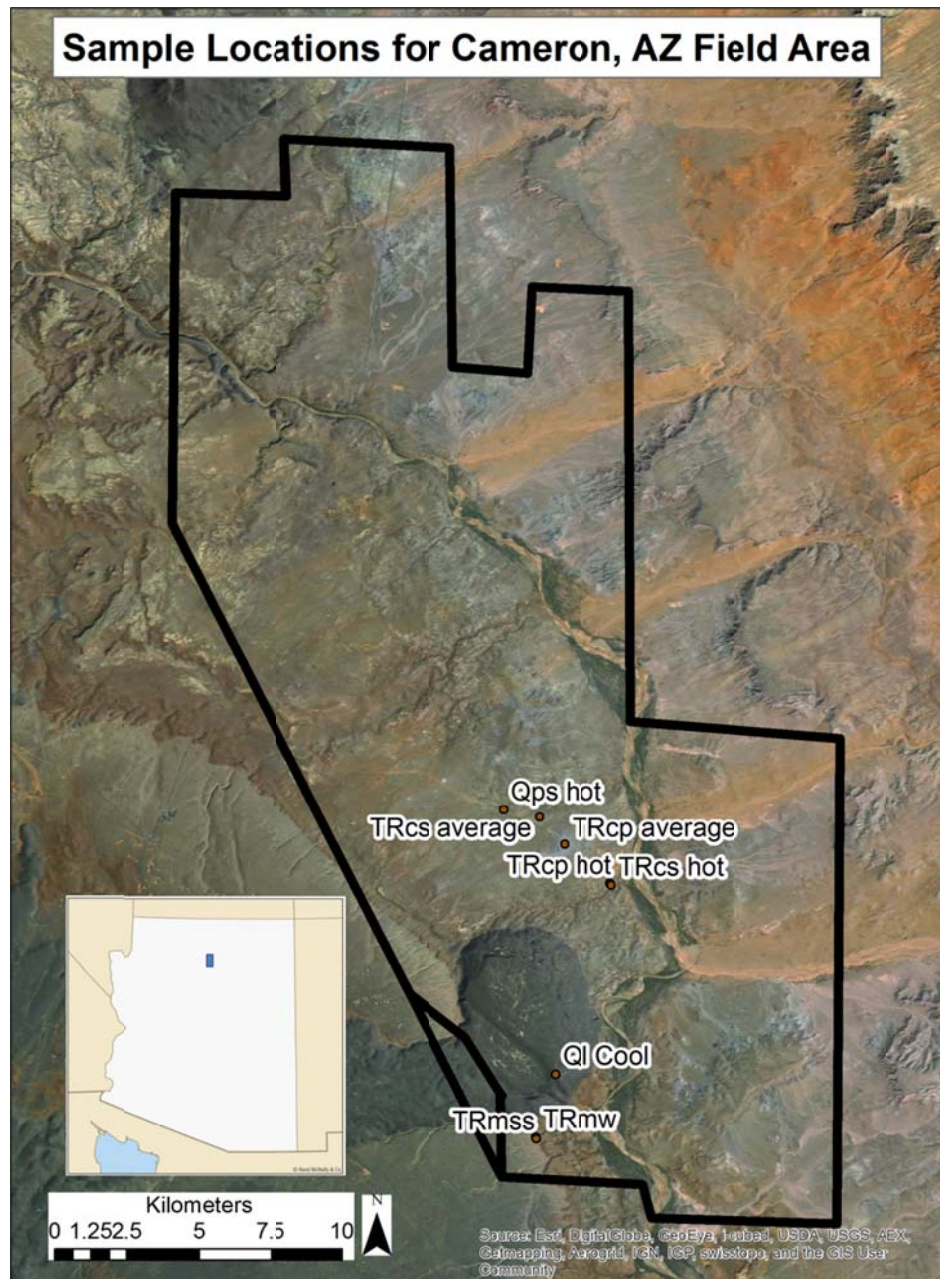


Figure 4-2: The location of the Cameron, AZ study area and the location of the sampling points.

Figure 4-3: HPGe Detector



Figure 4-3: HPGe detector at Government Wash

Figure 4-4: Photo of Sample Collection at Government Wash



Figure 4-4: Sample collection of Tmcg3 (above) and the red colored siltstone in sample collection ring (below).

Figure 4-5: K (wt%) Values of Various Measurement Techniques, Southern Nevada

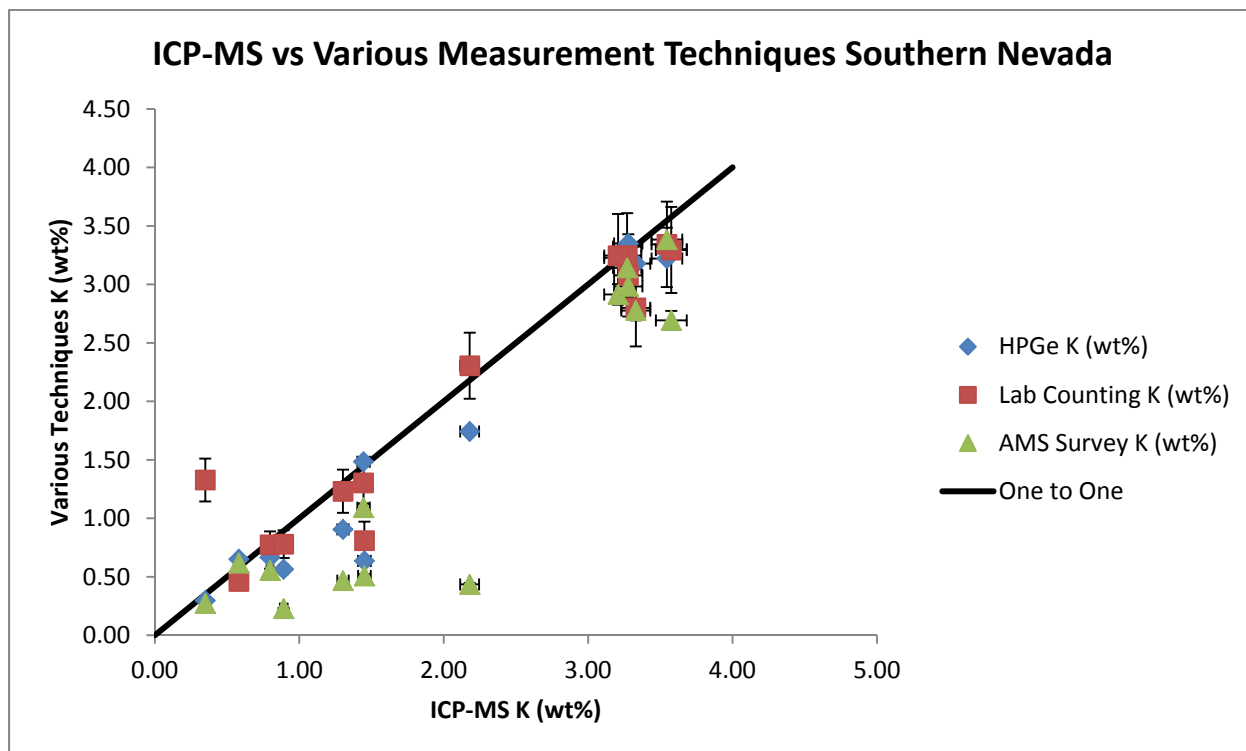


Figure 4-5: ICP-MS K (wt%) values compared against K (wt%) values obtained by HPGe, laboratory counting, and aerial survey.

Figure 4-6: U ppm Values of Various Measurement Techniques, Southern Nevada

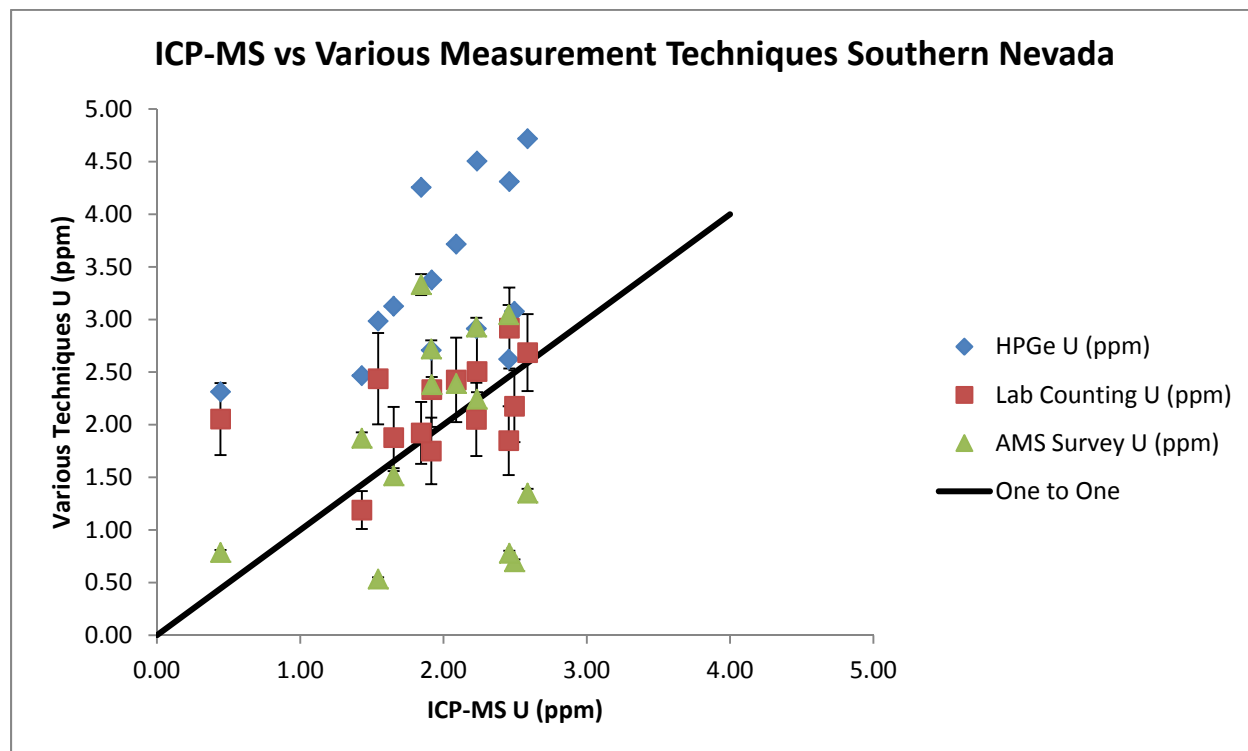


Figure 4-6: ICP-MS U ppm values compared against U ppm values obtained by HPGe, laboratory counting, and aerial survey.

Figure 4-7 Th ppm Values of Various Measurement Techniques, Southern Nevada

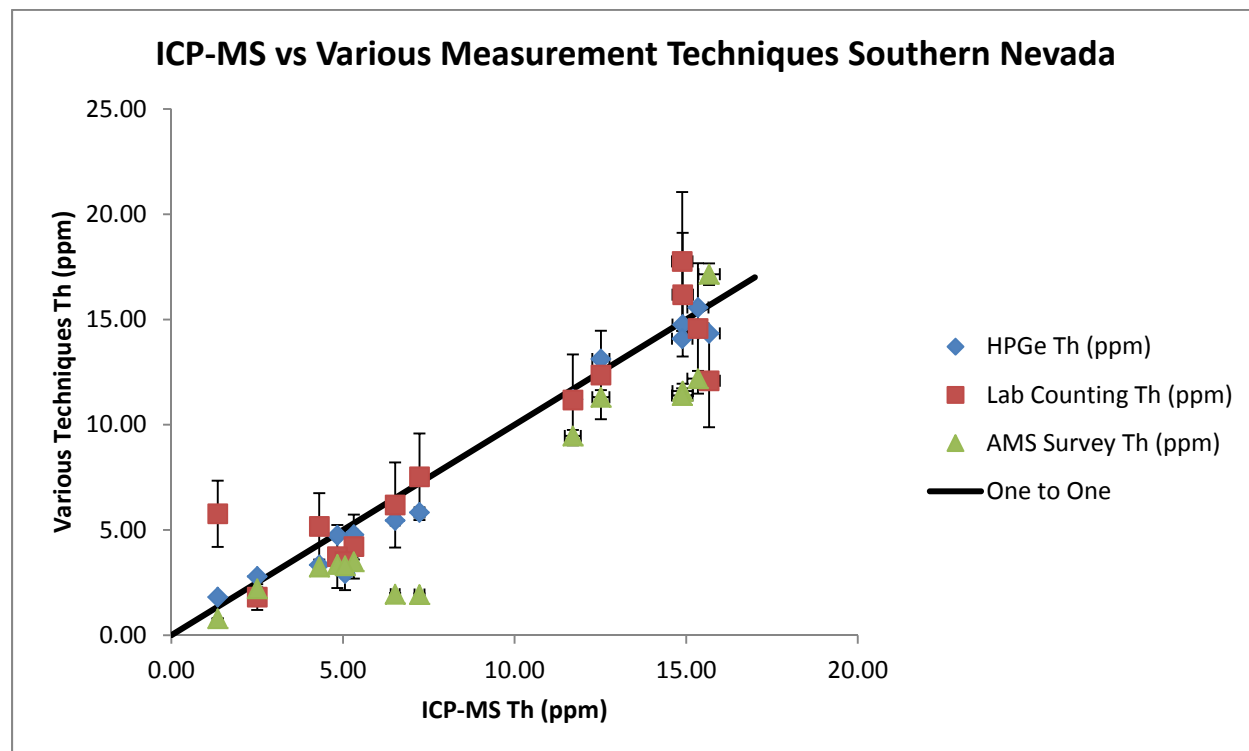


Figure 4-7: ICP-MS Th (ppm) values compared against Th ppm values obtained by HPGe, laboratory counting, and aerial survey.

Figure 4-8: Exposure Rate Values of Various Measurement Techniques, Southern Nevada

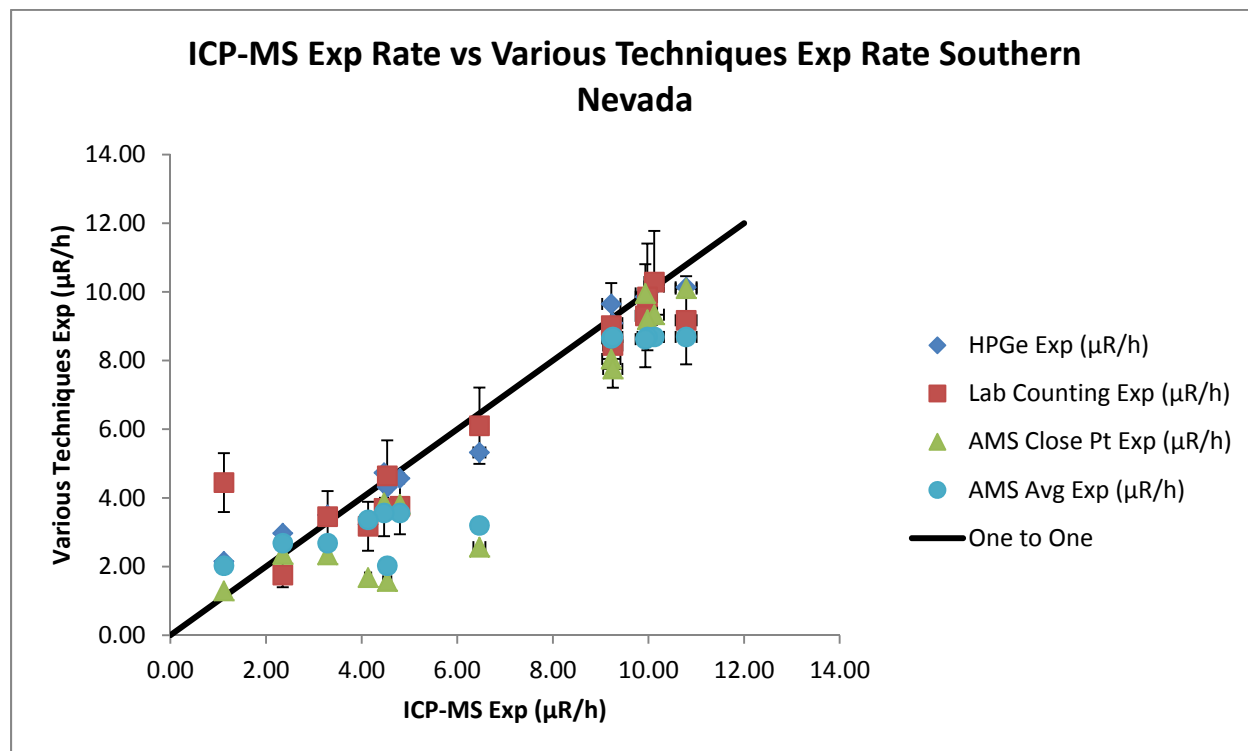


Figure 4-8: Exposure rate values calculated by equation 1 using ICP-MS K, U, and Th values compared against exposure rate values obtained by the same calculation using HPGe derived K, U, and Th values, laboratory counting derived K, U, and Th values, and aerial survey exposure rate data. Aerial survey closet points data was calculated by averaging the closest aerial point in the same geologic unit within 50m of the sample location. The AMS average exposure rate is the average exposure rate value for the entire geologic unit.

Figure 4-9: K (wt%) Values of Various Measurement Techniques, Cameron, Arizona

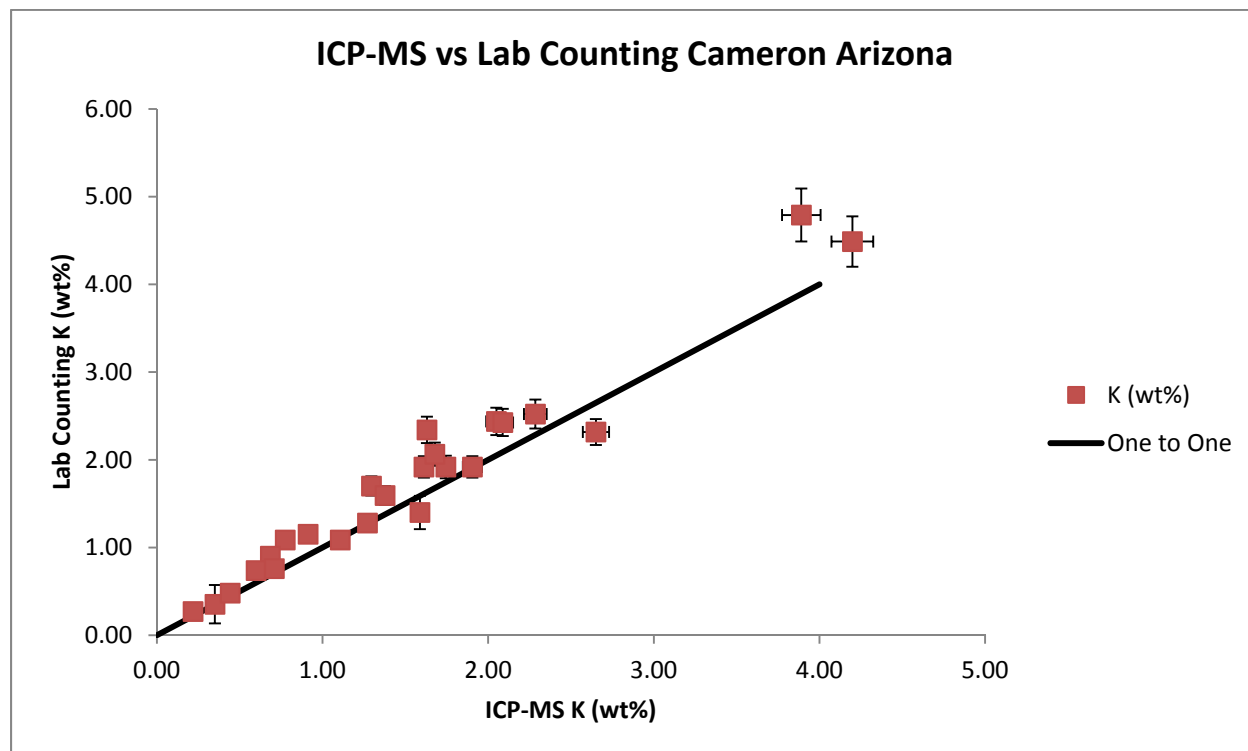


Figure 4-9: ICP-MS K (wt%) values compared against K (wt%) values obtained from laboratory counting.

Figure 4-10: U ppm Values of Various Measurement Techniques, Cameron, Arizona

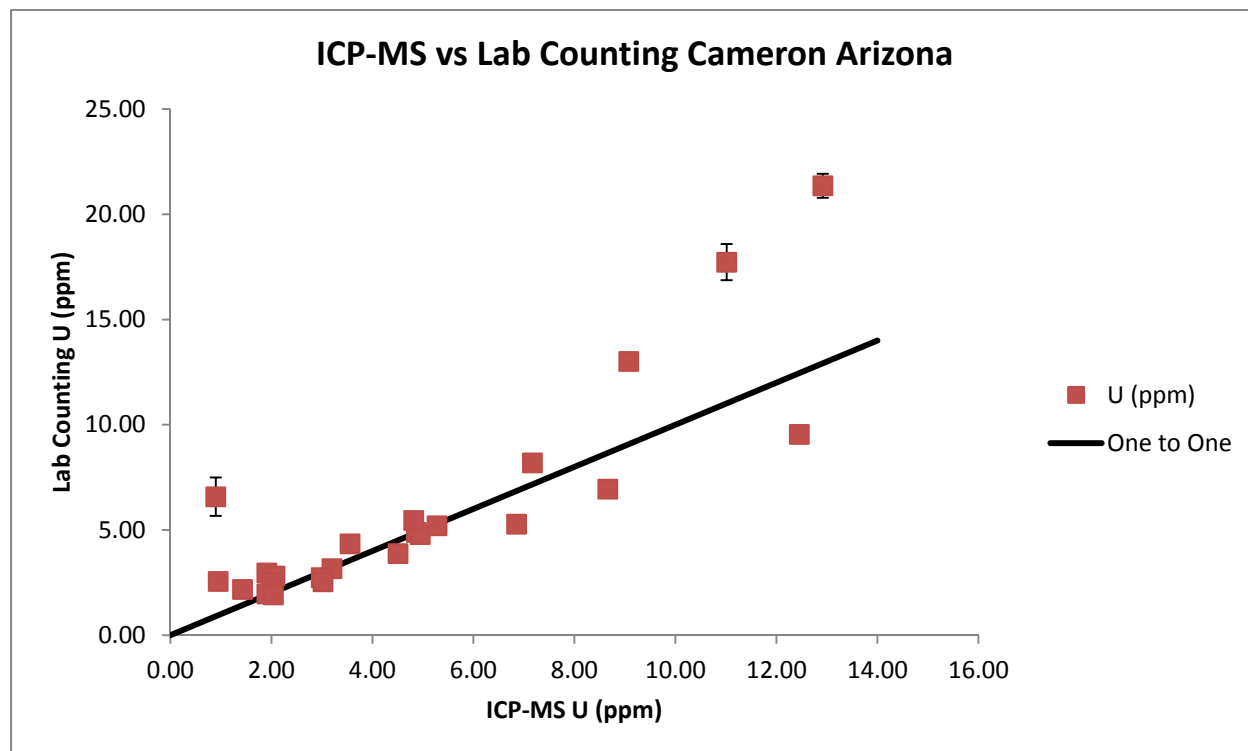


Figure 4-10: ICP-MS U ppm values compared against U ppm values obtained from laboratory counting.

Figure 4-11: Th ppm Values of Various Measurment Techniques, Cameron, Arizona

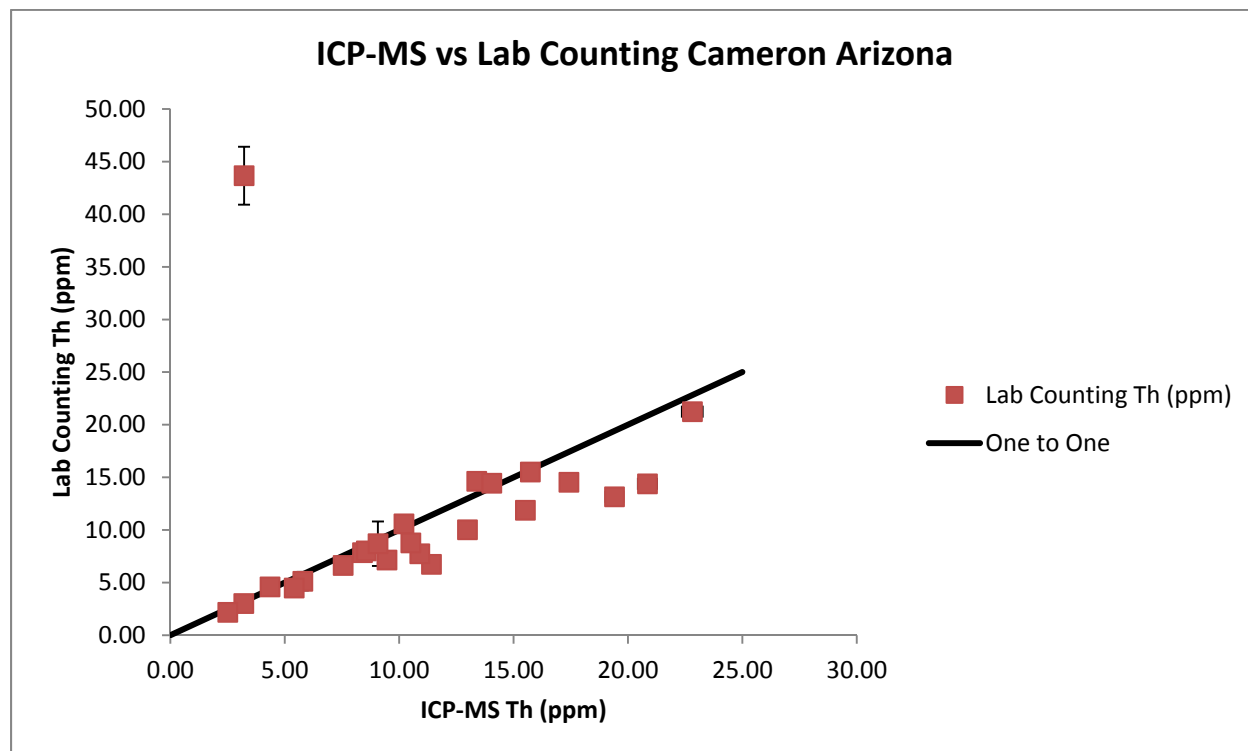


Figure 4-11: ICP-MS Th ppm values compared against Th ppm values obtained from laboratory counting.

Figure 4-12: Exposure Rate Values of Various Measurement Techniques, Cameron, Arizona

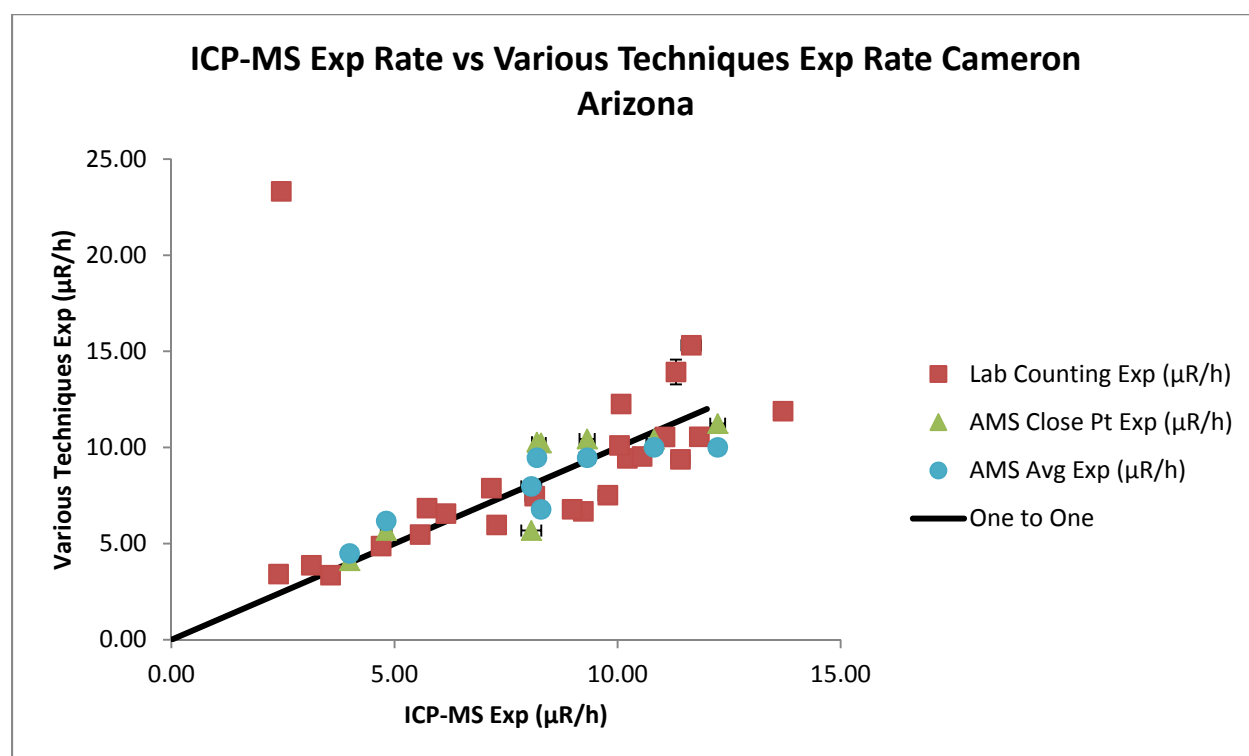


Figure 4-12: Exposure rate values calculated by equation 1 using ICP-MS K, U, and Th values compared against exposure rate values obtained by the same calculation using laboratory counting derived K, U, and Th values, and aerial survey exposure rate data. Aerial survey closet points data was calculated by averaging the closest aerial point in the same geologic unit within 200m of the sample location. The AMS average exposure rate is the average exposure rate value for the entire geologic unit.

Figure 4-13: K (wt%) Values of ICP-MS and Published Chemistry, Calibration Pads

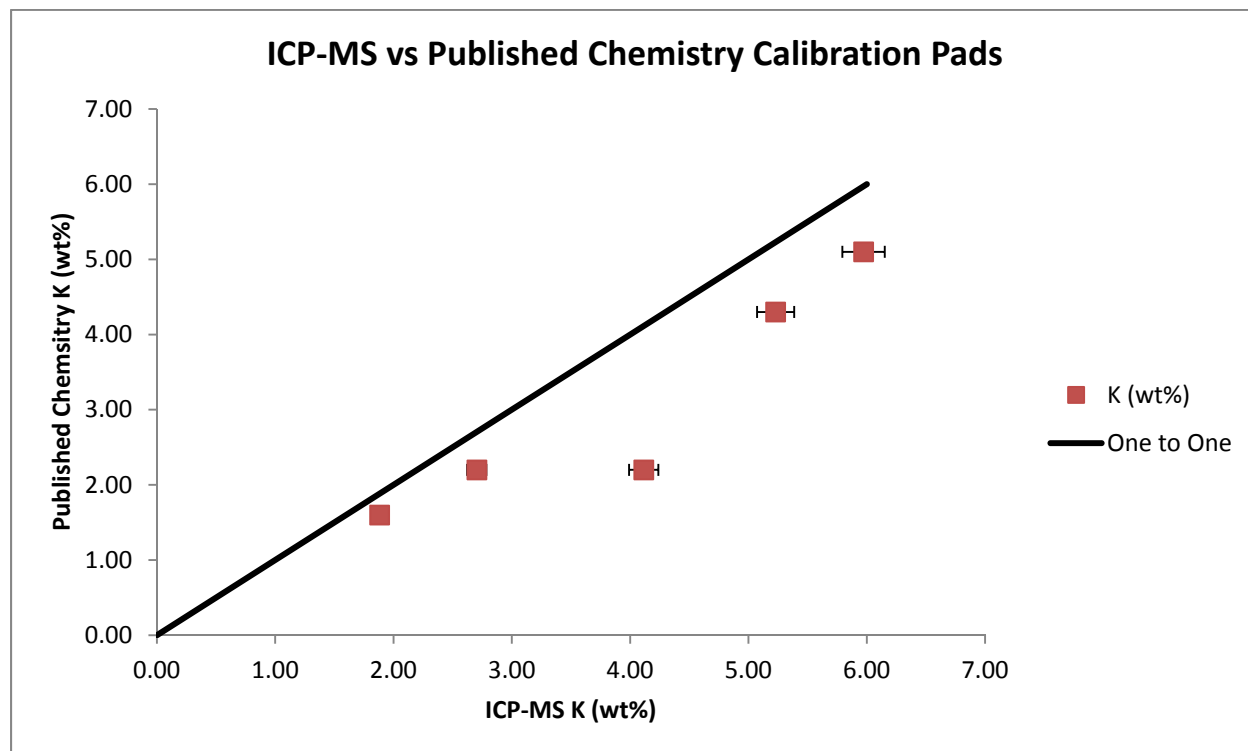


Figure 4-13: Comparison of K (wt%) values from our ICP-MS analysis and the published chemistry of the Grand Junction Calibration Pads when the pads were installed.

Figure 4-14: U ppm Values of ICP-MS and Published Chemistry, Calibration Pads

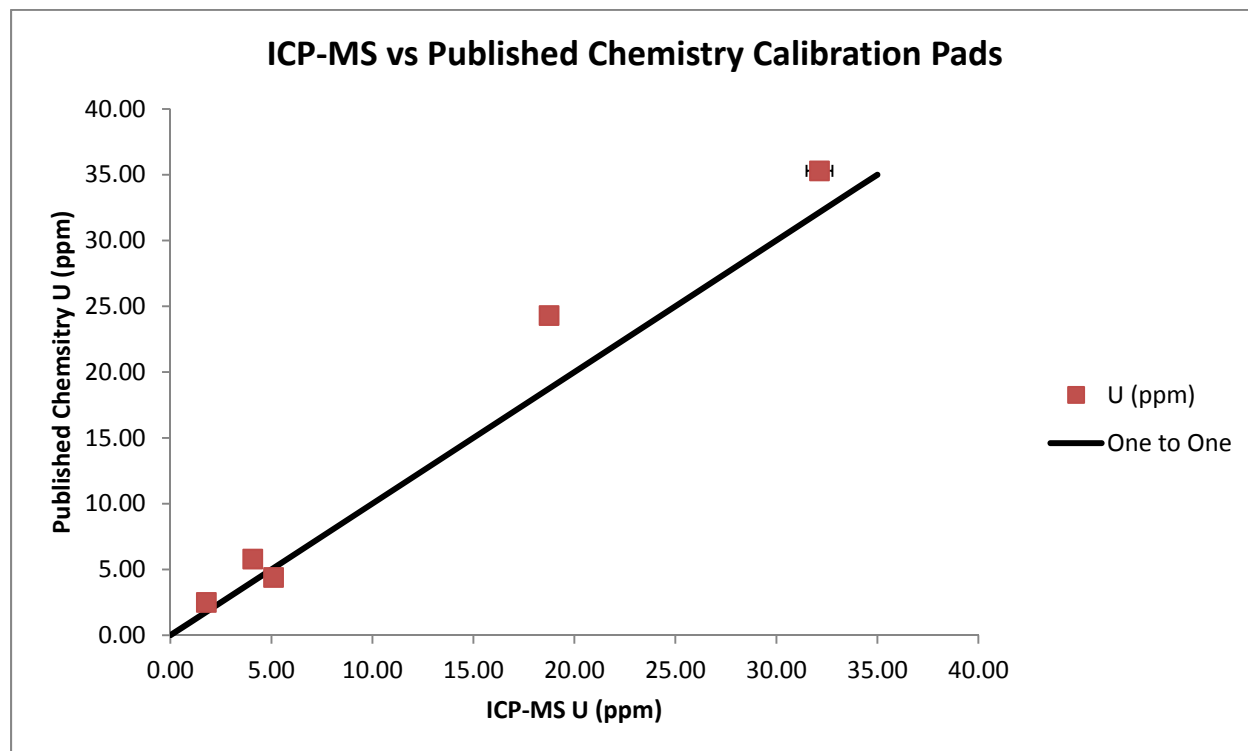


Figure 4-14: Comparison of U ppm values from our ICP-MS analysis and the published chemistry of the Grand Junction Calibration Pads when the pads were installed.

Figure 4-15: Th ppm Values of ICP-MS and Published Chemistry, Calibration Pads

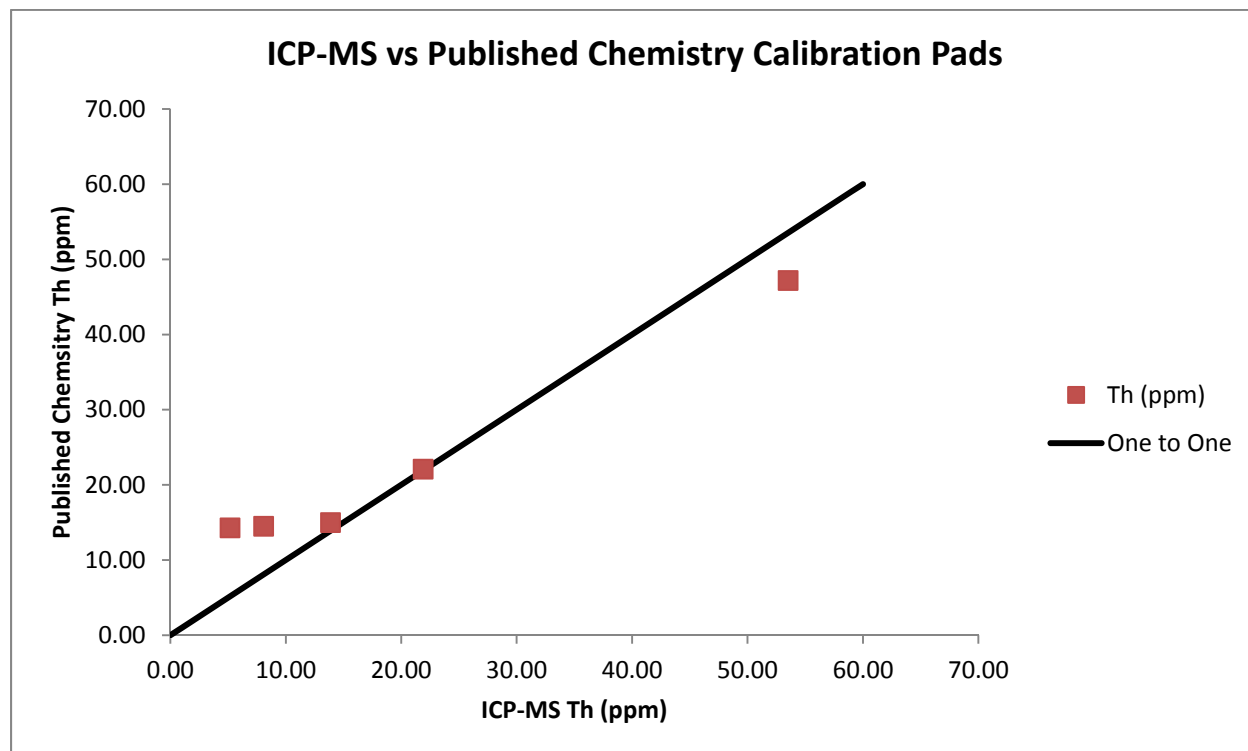


Figure 4-15: Comparison of Th ppm values from our ICP-MS analysis and the published chemistry of the Grand Junction Calibration Pads when the pads were installed.

Figure 4-16: Exposure Rate of ICP-MS and Published Chemistry, Calibration Pads

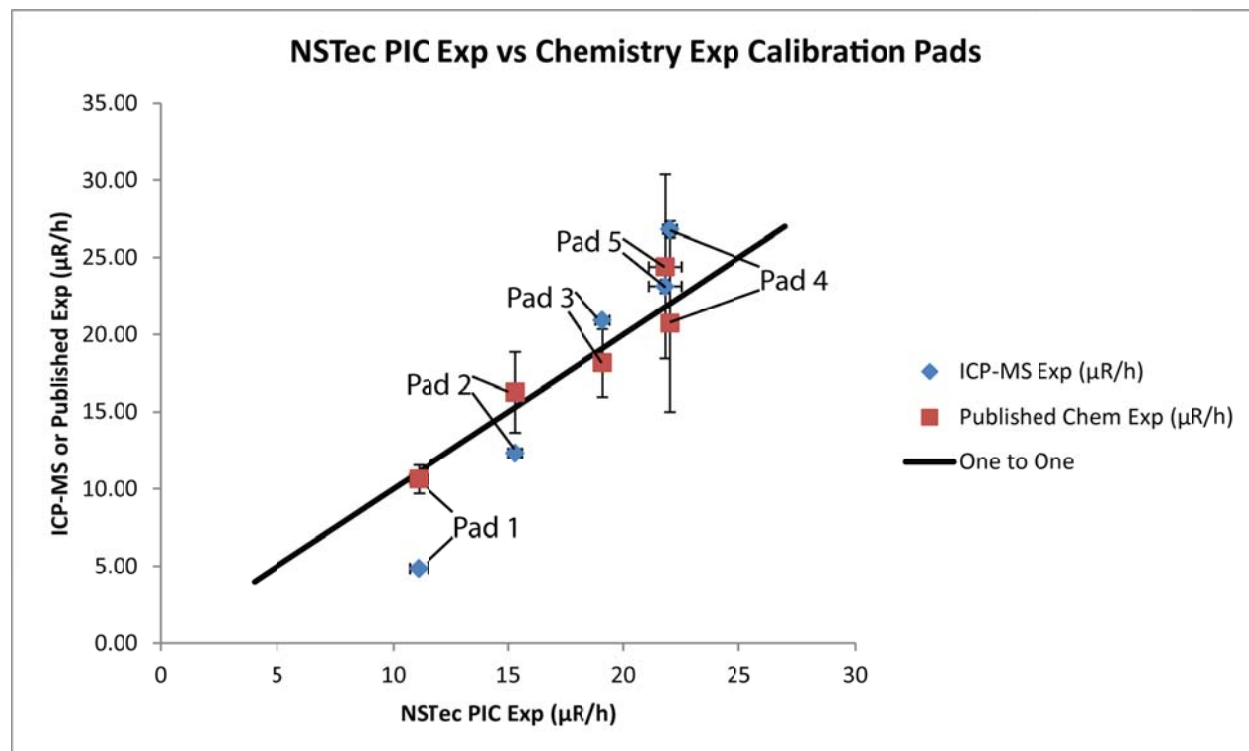


Figure 4-16: Comparison of the PIC exposure rate measurements provided by NSTec against exposure rates calculated by equation 1 using published K, U, and Th values and those derived from our ICP-MS analysis.

Chapter Five

Modeling Background Radiation in Southern Nevada

Abstract

Aerial gamma ray surveys are an important tool for national security, scientific, and industrial interests in determining locations of both anthropogenic and natural sources of radioactivity. There is a relationship between radioactivity and geology and in the past this relationship has been used to predict geology from an aerial survey. The purpose of this project is to develop a method to predict the radiologic exposure rate of the geologic materials in an area by creating a model using geologic data, images from the Advanced Spaceborne Thermal Emission and Reflection Radiometer (ASTER), geochemical data, and pre-existing low resolution aerial surveys from the National Uranium Resource Evaluation (NURE) Survey. Using these data, geospatial areas, referred to as background radiation units, homogenous in terms of K, U, and Th are defined and the gamma ray exposure rate is predicted. The prediction is compared to data collected via detailed aerial survey by our partner National Security Technologies, LLC (NSTec), allowing for the refinement of the technique.

High resolution gamma ray exposure rate models have been developed for two study areas in Southern Nevada that include the alluvium on the western shore of Lake Mohave, and Government Wash north of Lake Mead; both of these areas are arid with little soil moisture and vegetation. We determined that by using geologic units to the define radiation background units of exposed bedrock and ASTER visualizations to subdivide and define radiation background units of alluvium, regions of homogenous geochemistry can be defined allowing for the exposure rate to be predicted.

Introduction

The Aerial Measuring System (AMS) section of National Security Technologies, LLC (NSTec), performs high resolution aerial gamma ray surveys for national security and scientific purposes. Aerial gamma ray surveys are performed by low flying aircraft equipped with scintillation radiation detectors. When AMS performs an aerial gamma ray survey they are typically looking for anomalies related to anthropogenic sources of gamma rays. There are robust techniques to correct for background radiation from sources such as atmospheric radon, cosmic rays, and equipment related sources of gamma rays (IAEA 2003). Typically, these sources of gamma rays are corrected for by flying over an open body of water, flying high in the atmosphere above the influence of ground based sources, or by flying over previously measured territory (IAEA 2003). However, currently there is no accepted way of correcting for the signal from geologic sources when the purpose is to measure anthropogenic sources.

In natural materials, there are three radioelements that are responsible for gamma rays: Potassium (K), Uranium (U) and Thorium (Th). These three elements either generate gamma rays directly when they decay (e.g., ^{40}K) or they decay to daughter isotopes that are also radioactive which subsequently decay and generate gamma rays. There is a direct relationship between the concentration of the primary radioelements and gamma ray exposure rate (Beck, DeCampo et al. 1972; Løvborg and Kirkegaard 1974; Grasty, Carson et al. 1984). This study focuses on three of the primary isotopes of these elements: potassium-40 (^{40}K), uranium-238 (^{238}U) and thorium-232 (^{232}Th).

Previous studies have found a strong link between the gamma ray exposure rate and geology (Griscom and Peterson 1961; Books 1962; Moxham 1963; Pitkin, Bates et al. 1964; Grasty, Carson et al. 1984; Wilford, Bierwirth et al. 1997). Many of the early studies were performed around nuclear power plants to serve as a baseline so that future surveys could assess any change in background levels of radioactivity. During these surveys they observed a

consistent change in counts as the geology changed across the surface (Griscom and Peterson 1961; Books 1962; Moxham 1963; Pitkin, Bates et al. 1964). It was also determined that some geologic structures, such as faults, could be detected due to high levels of radon emanation from the fractured rock (Pitkin, Bates et al. 1964). The purpose of our project is to produce a means of predicting the gamma ray exposure rate of geologic sources in an area so that the geologic signal may be understood in the results of an aerial gamma ray survey.

Exposure rate is a measure of the number of ionizations produced in a quantity of air by photon radiation per unit time. In order to predict an exposure rate, there must be a means of translating radioelement concentration to exposure rate. There is a linear correlation between radioelement concentration and exposure rate that is given by Equation 4-1.

In this study, models of the distribution of K, U, Th, and exposure rate for two field areas in Southern Nevada, Government Wash and Lake Mohave, were created as a means of predicting the results of an aerial survey. Government Wash is located north of Lake Mead, and east of Las Vegas, while Lake Mohave is located east of Searchlight Nevada (Figure 1-1). These areas were chosen primarily because the AMS section of our collaborator NSTec had surveyed these areas numerous times making aerial gamma ray data readily available for comparison.

The most challenging task associated with forward modeling an aerial gamma ray survey is defining geospatial areas that are homogenous in terms of their radiogenic properties so that they may be assigned a single K, U, Th, and exposure rate value. We refer to these geospatial areas as background radiation units. This study used two primary means of defining background radiation units. The first is to use geologic units defined by published geologic maps. The second method uses multispectral imaging data from spacecraft to define background radiation units consisting of similar spectral features. Once these regions are defined, K, U, and Th values can be assigned to them and an exposure rate can be calculated.

The arid climate of our study areas simplifies attenuation problems related to soil moisture and vegetation. However, arid environments present their own unique set of challenges including eolian dust deposition and alluvial processes. Eolian dust occurs on regional and global transport scales and has little to no connection with local bedrock (Reheis, Budahn et al. 2009). In addition, alluvial material is composed of eroded rock from the surrounding environment and may not represent the bedrock it overlies.

Background

Government Wash lies within the Las Vegas Valley Shear Zone which has experienced 23 to 69 km of displacement since the Miocene (Langenheim, Jachens et al. 1997) (Figure 1-2). All of the geologic units in the area of interest (AOI) were deposited after the cessation of displacement 8.5 Ma (Langenheim, Jachens et al. 1997). The primary geologic formation in the area is the Muddy Creek Formation which is middle to late Miocene in age and primarily composed of clastic sedimentary rocks ranging from siltstone to conglomerate (Duebendorfer 2003). Portions of this formation also contain significant gypsum deposits that are currently being mined by Pabco Gypsum, Inc. The other major geologic formation in Government Wash is the Horse Spring Formation. The Horse Spring Formation is early Miocene in age and consists primarily of an ancient alluvial fan that was fed by limestone as well as a variety of igneous and metamorphic parent rocks to the north and northeast (Duebendorfer 2003). There are also minor volcanic and sedimentary units in the area. For more information on the geology of Government Wash please see Appendix A.

The Lake Mohave field area consists of the northern two thirds of the western shore of Lake Mohave (Figure 1-3). The geologic surfaces at Lake Mohave are alluvial in nature, consisting of material primarily derived from the mountain range to the west. The mountain range was created by volcanic activity during the Miocene and is composed of a variety of metamorphic and igneous rocks (House and Faulds 2008). The rock types in this mountain

range vary from north to south and can be described by breaking the range into three regions. The northern most region is composed of felsic igneous and metamorphic rocks with some minor mafic intrusions. The central region is composed of mafic and intermediate igneous rocks and the southern portion is a mix of Proterozoic age crystalline basement and Miocene age felsic and intermediate igneous rocks. The spatial trends in the source rocks are also expressed in the alluvial material in the AOI. Near-shore there are also deposits related to past flood events of the Colorado River. For more information on the geology of Lake Mohave please see Appendix B.

Methods

Defining Background Radiation Units

Geographic information systems (GIS) based geologic maps were downloaded from the Nevada Bureau of Mines and Geology for both Lake Mohave (House and Faulds 2008) and Government Wash (Duebendorfer 2003). Based on field observations and satellite photos, some of the geologic boundaries at Government Wash were altered. Figure 5-1 shows the alteration of the boundaries between geologic units Tmcg and Tmcu as well as boundaries between Tmcg and Tmcl.

The Terra satellite has a multispectral instrument package known as the Advanced Spaceborne Thermal Emission and Reflection Radiometer (ASTER) that collects spectral data across 14 sensors referred to as bands. The bands occur at discrete wavelengths ranging from visual to thermal infrared. ASTER data, like other forms of multispectral imagery, occur as multiple rasters representing each band. Like any raster, the pixels of the ASTER image are assigned unit-less digital number (DN) values from 0 to 255 based on the intensity of the pixel. Simple visualizations that place bands in the red, blue and green channels can be used to create false color images of an area (Meer, Werff et al. 2011). Math can also be performed on

the different bands to emphasize spectral features within the data that have been shown to correspond to mineralogical trends on the surface (Meer, Werff et al. 2011).

Each set of bands have different spatial resolution and when mixing bands of different resolution the data must be either undersampled or oversampled. Bands 1-4 have a spatial resolution of 15m, bands 5-10 have a spatial resolution of 30m, and bands 10-14 have a spatial resolution of 90m. In this analysis bands 5-14 have been oversampled to a spatial resolution of 15m using the Environment for Visualizing Images (ENVI) software package.

When using ASTER data, appropriate bands must be chosen to highlight the mineralogical features of interest. Simple visualization images are used to distinguish general lithological differences (Meer, Werff et al. 2011). In this study, visualizations using bands 2, 7, 13 and 2, 6, 10 were used at Lake Mohave to distinguish broad lithological trends. Ratio images can also be used to accentuate spectral absorptions in certain bands. Previous studies have shown that during weathering U and Th tend to associate with secondary iron oxides (Koons, Helmke et al. 1980; Michel 1984; Patino, Velbel et al. 2003; Lee and Baik 2009; Breithner, Osán et al. 2014). The band ratio 2/1 highlights differences in ferric iron concentration (Meer, Werff et al. 2011). We used this band ratio as a proxy for K, U, and Th variation in alluvial materials at Government Wash. Ratio images can also be used as part of a visualization to bring out trends in ferric iron as well as lithology. To that end a 2/1, 6, 10 visualization was also used at Government Wash. These images are then classified into regions of common spectral characteristics.

The primary classification algorithm we used for ASTER images is the Iso Cluster Unsupervised Classification tool in ESRI's software package ArcGIS. Quaternary alluvium was clipped from the ASTER data prior to classification to reduce the influence from surrounding materials. Models have been created using this method for the following images: 2/1 (Figure

5-2) and 2/1, 6, 10 (Figure 5-3) at Government Wash and the 2, 7, 13 (Figure 5-4) at Lake Mohave.

An alternate means of classification was pursued to reduce the effects of noise and shadows which are discussed later. The 2, 6, 10 image (Figure 5-5) at Lake Mohave was classified by first normalizing all the pixel values by using the Histogram Equalize tool. Then, using the Segment Mean Shift tool, tonal differences were reduced between pixels. Finally, the image was classified with the Reclassify tool using natural breaks with a 20 pixel minimum cluster size. This image was not clipped prior to classification.

Clipped images were divided into 5 usable classes with a sixth class added to account for surface water at Lake Mohave. The 2, 6, 10 image was classified into 10 classes to account for the much larger coverage area. Classified images were then turned into vector based polygons using the Raster to Polygon tool for ease of manipulation.

ASTER based models were only used to subdivide alluvium into radiation background units. This is because alluvium is classified by age rather than composition and therefore can be geochemically heterogeneous over a surface. Bedrock is typically more geochemically homogenous and therefore geologic maps have been used to define those radiation background units.

All ASTER based models used NURE data to predict the exposure rate. A geochemical model was not created because of the fact that geolocation problems preclude the possibility of accurately placing the data in any particular class and it is difficult to say whether a particular geochemical point compositionally matches the unit defined by the ASTER image.

AMS Data

AMS provided us with high resolution aerial gamma ray survey data for both Government Wash and Lake Mohave (Figure 5-6 & Figure 5-7). These data are comprised of a

series of spectra taken at one second intervals along the flight path so that the data points fill the AOI. Each point has a footprint of approximately 100m and the spacing between flight lines is also approximately 100m. The raw spectral data were background subtracted by removing counts collected over either Lake Mead or Lake Mohave and an exposure rate was calculated by summing the total dead time corrected counts and applying a count to exposure rate conversion factor provided by AMS (Equation 2-1) (IAEA 2003). The data were then processed to provide K, eU, and eTh values in each AOI by using spectral stripping ratios provided by AMS and the technique outlined in the 2003 IAEA Tech Doc (Equation 2-2 through Equation 2-7). These data are then sorted according to the background radiation unit they spatially occur in and reduced to representative statistics (e.g., mean, median, standard deviation, range).

Geochemical Data

Geolocated geochemical data was obtained from several online databases including: the National Uranium Resource Evaluation (NURE) Survey (geochemical section), Geochemical Rock Database (GeoRoc), and Integrated Earth Data Applications (IEDA). Figure 5-8 and Figure 5-9 show the geochemical data available at Government Wash and Lake Mohave respectively. These data provide K, U, and Th values at each point as well as geolocation and compositional metadata (i.e. rock type). The geochemical data were unified into one single dataset and sorted into the geologic unit they occur in. The compositional metadata were used in addition to geolocation to determine if the sample matched the geologic unit it was located in. In some cases, the geolocation metadata was imprecise and compositional metadata was solely used to place the data.

After sorting the data into the appropriate geologic unit there were a total of 35 data points for units present in Government Wash and 47 data points for units present at Lake Mohave. Statistical representations (Table 5-1) and exposure rates (Table 5-2A) were calculated for each unit. In some cases, large outliers skewed mean values therefore median

values were used to calculate exposure rate (e.g., Tht U ppm value). All exposure rates were calculated using Equation 4-1.

NURE Data

NURE aerial gamma ray survey data consists of K, eU, and eTh concentrations derived from a national scale aerial gamma ray survey conducted in the 1970's by the Atomic Energy Commission (Duval, Carson et al. 2005). For each point, exposure rates were calculated using Equation 4-1. The specific dataset used in this study was compiled by Duval (2005) and was obtained through the USGS (Figure 5-8 & Figure 5-9). The NURE dataset occurs as either east-west or north-south trending flight lines with approximately 1-10 km spacing. At Government Wash there are two east-west lines spaced 4.5 km apart that provide 518 data points. Lake Mohave has 8 east-west lines with spacing between 0.75 and 2.5 km and one north-south line that provide a combined 1262 data points. In the dataset there are many data points with zeros or negative values for K, eU, or eTh; these values were removed before analysis. The NURE data were joined to the background radiation unit that each point resides in. Statistical representations of each unit were calculated and exposure rates were determined by using the statistical mean (Table 5-2 A&B).

In addition to sorting the data into background radiation units comparisons were made in areas where AMS data overlaps with NURE data (e.g., Figure 5-10 & Figure 5-11). Because the points do not directly overlap they were compared within a distance of 20 meters.

Results

By comparing the standard deviations of AMS data of the entire survey to the standard deviations of the AMS data within a particular background radiation unit, an assessment can be made whether or not the radiation background unit is more homogenous than the entire area. A background radiation unit with a lower standard deviation than that of the whole survey can be considered successful because variance within the unit is lower than the whole survey. Our

measure of success of an exposure rate prediction for a background radiation unit is whether the prediction is within ± 1 $\mu\text{R/h}$ of the AMS mean within that unit. Additionally, if more than 80% of the AMS exposure rate data within the total AOI are within ± 1 $\mu\text{R/h}$ of the predictions we consider the whole model to be successful. Table 5-3 displays the summary statistics of the whole survey of the AMS data points that occur at Government Wash and Lake Mohave.

For both Government Wash and Lake Mohave, models have been created using geologic maps and traditional geochemistry (GMTG) as well as NURE data (GMN). At Government Wash there are two models using ASTER and NURE data (alluvium only): 2/1 image ratio (2/1N) and 2/1,6,10 visualization (2/1,6,10N). Finally, at Lake Mohave there are also two models using ASTER and NURE data: 2, 7, 13 visualization (2,7,13N) and 2, 6, 10 visualization (2,6,10N).

Government Wash GMTG

Predicted exposure rates using geochemistry and the Government Wash geologic map are reported in Table 5-2A and Figure 5-12. Exposure rate predictions range from 2.48 to 11.05 $\mu\text{R/h}$. Standard deviations of AMS data sorted into geologic units range from 0.3 to 1.03 $\mu\text{R/h}$ with most of the units below the AMS whole survey standard deviation of 0.8 $\mu\text{R/h}$ (Table 5-3). Absolute differences between geochemical exposure rate predictions and AMS averages are also reported in Table 5-2A and range from 0.2 to 7.49 $\mu\text{R/h}$. The average difference between predicted and observed exposure rates among all units is 2.05 $\mu\text{R/h}$. Using this predictive map 49.5% of the AMS exposure rate data are predicted within ± 1 $\mu\text{R/h}$ (not including data over units with no geochemical data) (Figure 5-13).

Predicted K weight percent values range from 0.63 to 4.01 (Table 5-1) and are compared with AMS averages that range from 0.41 to 1.25 (Table 5-2B & Figure 5-14). Standard deviations for AMS K weight percent sorted into geologic units range from 0.14 to 0.34 (Table 5-2B) which compare with the whole survey standard deviation of 0.27 (Table 5-3).

Predicted U ppm values range from 1.26 to 28.45 (Table 5-1) and are compared with AMS averages that range from 1.52 to 2.83 (Table 5-2B & Figure 5-15). Standard deviations for AMS U ppm sorted into geologic units range from 0.66 to 0.88 (Table 5-2B) which compare with the whole survey standard deviation of 0.75 (Table 5-3). Predicted Th ppm values range from 2.62 to 11.86 (Table 5-1) and are compared with AMS averages ranging from 1.98 to 7.10 (Table 5-2B & Figure 5-16). Standard deviations for AMS Th ppm sorted into geologic units range from 1.00 to 2.75 (Table 5-2B) which compare with the whole survey standard deviation of 1.55 (Table 5-3).

Government Wash GMN

Exposure rate predictions using the NURE data and the Government Wash geologic map are reported in Table 5-2A and Figure 5-12. Using these data predictions range from 1.50 to 5.06 $\mu\text{R/h}$ with absolute differences that range from 0.09 to 2.18 $\mu\text{R/h}$. Using this predictive model 48% of the AMS data are successfully predicted if the alluvial units are included. If Quaternary alluvium is excluded then 78% of the data are predicted within ± 1 $\mu\text{R/h}$. Further, if paleo-alluvial units are not considered then 84% of the AMS exposure rate data are predicted within ± 1 $\mu\text{R/h}$ (Figure 5-17).

Predicted K weight percent values range from 0.25 to 1.26 and are compared with AMS averages that range from 0.41 to 1.25 (Table 5-2B & Figure 5-14). U ppm values range from 1.47 to 2.96 and are compared with AMS averages that range from 1.52 to 2.83 (Table 5-2B & Figure 5-15). Th ppm values range from 1.50 to 5.87 and are compared with AMS averages ranging from 1.98 to 7.10 (Table 5-2B & Figure 5-16). Because GMN uses the same geospatial areas as GMTG the standard deviations of the AMS data are the same.

Government Wash 2/1N

The 2/1 ASTER ratio image was used to subdivide the Quaternary alluvium (Qa and Qoa) in Government Wash. AMS data and NURE predictions for 2/1N are reported in Table 5-4

and Figure 5-18. Exposure rate predictions range from 2.65 to 3.43 $\mu\text{R/h}$. Standard deviations of the AMS data in these classes range from 0.36 to 0.47 $\mu\text{R/h}$ which are almost all lower than the survey standard deviation over Quaternary units of 0.43 $\mu\text{R/h}$. Absolute differences of the AMS mean and the prediction range from 0.09 to 0.16 $\mu\text{R/h}$. Using this predictive map 98% of the AMS exposure rate data over the Quaternary alluvium are predicted within ± 1 $\mu\text{R/h}$ (Figure 5-19).

Predicted K weight percent values range from 0.73 to 0.82 and are compared with AMS averages that range from 0.62 to 0.67 (Table 5-4 & Figure 5-14). Standard deviations for AMS K weight percent sorted into ASTER units range from 0.15 to 0.16 (Table 5-4) which compare with the survey standard deviation over the Quaternary units of 0.16. Predicted U ppm values range from 1.48 to 2.38 and are compared with AMS averages that range from 1.88 to 2.25 (Table 5-4 & Figure 5-15). Standard deviations for AMS U ppm sorted into ASTER units range from 0.66 to 0.70 (Table 5-4) which compare with the survey standard deviation over the Quaternary units of 0.69. Predicted Th ppm values range from 3.40 to 4.40 and are compared with AMS averages ranging from 2.70 to 3.28 (Table 5-4 & Figure 5-16). Standard deviations for AMS Th ppm sorted into ASTER units range from 0.98 to 1.27 (Table 5-4) which compare with the survey standard deviation over the Quaternary units of 1.12.

Government Wash 2/1,6,10N

The ASTER visualization 2/1,6,10 was used to subdivide the Quaternary alluvium (Qa and Qoa) at Government Wash. Table 5-4 and Figure 5-18 report the exposure rate, K, U, and Th values of the AMS and NURE data in five classes. Exposure rate predictions range from 2.47 to 3.66 $\mu\text{R/h}$. Standard deviations of the AMS data in these classes range from 0.30 to 0.55 $\mu\text{R/h}$ which compares to the survey standard deviation over Quaternary units of 0.43 $\mu\text{R/h}$. Absolute differences of the AMS mean and the NURE based prediction range from 0.18 to 0.73

μR/h. Using this predictive map 95% of the AMS data are predicted within ±1 μR/h (Figure 5-20).

Predicted K weight percent values range from 0.65 to 1.09 and are compared with AMS averages that range from 0.61 to 0.77 (Table 5-4 & Figure 5-14). Standard deviations for AMS K weight percent sorted into ASTER units range from 0.14 to 0.17 (Table 5-4) which compare with the survey standard deviation over the Quaternary units of 0.16. Predicted U ppm values range from 0.86 to 1.90 and are compared with AMS averages that range from 1.85 to 2.54 (Table 5-4 & Figure 5-15). Standard deviations for AMS U ppm sorted into ASTER units range from 0.19 to 0.75 (Table 5-4) which compare with the survey standard deviation over the Quaternary units of 0.69. Predicted Th ppm values range from 2.50 to 5.35 and are compared with AMS averages ranging from 2.68 to 3.79 (Table 5-4 & Figure 5-16). Standard deviations for AMS Th ppm sorted into ASTER units range from 0.19 to 1.19 (Table 5-4) which compare with the survey standard deviation over the Quaternary units of 1.12.

Lake Mohave GMTG

AMS data and exposure rate predictions for GMTG at Lake Mohave are reported in Table 5-2A and Figure 5-21. Exposure rate predictions range from 8.2 to 12.73 μR/h. AMS exposure rate standard deviations are also listed in Table 5-2A and range from 0.07 to 0.98 μR/h and compare to the AMS total survey standard deviation of 0.54 μR/h (Table 5-3). Absolute differences between the AMS mean and the prediction in each unit range from 0.09 to 3.73 μR/h. Using this predictive model 10% of the AMS data are predicted within ±1 μR/h (Figure 5-22).

Predicted K weight percent values range from 4.14 to 5.38 (Table 5-1) and are compared with AMS averages that range from 1.95 to 3.13 (Table 5-2C & Figure 5-23). Standard deviations for AMS K weight percent sorted into geologic units range from 0.15 to 0.40 (Table 5-2C) which compare with the whole survey standard deviation of 0.25 (Table 5-3).

Predicted U ppm values range from 1.60 to 2.91 and are compared with AMS averages that range from 2.33 to 3.18 (Table 5-2C & Figure 5-24). Standard deviations for AMS U ppm sorted into geologic units range from 0.69 to 1.22 (Table 5-2C) which compare with the whole survey standard deviation of 0.89 (Table 5-3). Predicted Th ppm values range from 6.79 to 18.82 and are compared with AMS averages ranging from 8.30 to 13.50 (Table 5-2C & Figure 5-25). Standard deviations for AMS Th ppm sorted into geologic units range from 0.79 to 2.10 (Table 5-2C) which compare with the whole survey standard deviation of 1.91 (Table 5-3).

Lake Mohave GMN

Exposure rate predictions using the Lake Mohave geologic map and NURE data are found in Table 5-2A and Figure 5-21. Exposure rate predictions range from 7.21 to 9.98 $\mu\text{R/h}$. Absolute differences between the NURE prediction and the AMS mean in each unit range from 0.19 to 1.75 $\mu\text{R/h}$. Using this predictive model 68% of the AMS data are predicted within ± 1 $\mu\text{R/h}$ (Figure 5-26).

Predicted K weight percent values range from 2.45 to 3.17 and are compared with AMS averages that range from 1.95 to 3.13 (Table 5-2C & Figure 5-23). U ppm values range from 1.73 to 4.20 and are compared with AMS averages that range from 2.33 to 3.18 (Table 5-2C & Figure 5-24). Th ppm values range from 9.25 to 14.72 and are compared with AMS averages ranging from 8.30 to 13.50 (Table 5-2C & Figure 5-25). Standard deviations in the AMS data for these units are the same as the GMTG model because they share the same unit definitions.

Lake Mohave 2,7,13N

Table 5-5 and Figure 5-27 report exposure rate, K, U, and Th predictions for the 2,7,13N model. Exposure rate predictions range from 6.23 to 9.74 $\mu\text{R/h}$. The AMS standard deviations for the units defined using this image range from 0.31 to 0.86 $\mu\text{R/h}$ and compare to the AMS whole survey standard deviation of 0.54 $\mu\text{R/h}$ (Table 5-3). Absolute differences between the

AMS mean and the NURE prediction for each unit range from 0.13 to 1.3 $\mu\text{R/h}$. This model predicts 69% of the AMS data within ± 1 $\mu\text{R/h}$ (Figure 5-28).

Predicted K weight percent values range from 2.00 to 3.12 and are compared with AMS averages that range from 2.28 to 3.02 (Table 5-5 & Figure 5-23). Standard deviations for AMS K weight percent sorted into ASTER units range from 0.21 to 0.41 (Table 5-5) which compare with the whole survey standard deviation of 0.25 (Table 5-3). Predicted U ppm values range from 1.93 to 3.29 and are compared with AMS averages that range from 2.01 to 2.63 (Table 5-5 & Figure 5-24). Standard deviations for AMS U ppm sorted into geologic units range from 0.26 to 0.90 (Table 5-5) which compare with the whole survey standard deviation of 0.89 (Table 5-3). Predicted Th ppm values range from 8.61 to 14.07 and are compared with AMS averages ranging from 10.45 to 13.06 (Table 5-5 & Figure 5-25). Standard deviations for AMS Th ppm sorted into geologic units range from 1.74 to 2.59 (Table 5-5) which compare with the whole survey standard deviation of 1.91 (Table 5-3).

Lake Mohave 2,6,10N

Table 5-5 and Figure 5-27 report exposure rate, K, U, and Th predictions for the 2,6,10N model. Exposure rate predictions range from 6.86 to 9.03 $\mu\text{R/h}$. The AMS standard deviations for the units defined using this image range from 0.34 to 1.00 $\mu\text{R/h}$ compared to the AMS whole survey standard deviation of 0.54 $\mu\text{R/h}$ (Table 5-3). Absolute differences between the AMS mean and the NURE prediction for each unit range from 0.08 to 1.59 $\mu\text{R/h}$. This model predicts 95.5% of the AMS data within ± 1 $\mu\text{R/h}$ (Figure 5-29).

Predicted K weight percent values range from 2.07 to 2.63 and are compared with AMS averages that range from 1.90 to 3.08 (Table 5-5 & Figure 5-23). Standard deviations for AMS K weight percent range from 0.21 to 0.45 (Table 5-5) which compare with the whole survey standard deviation of 0.25 (Table 5-3). Predicted U ppm values range from 2.53 to 3.15 and are compared with AMS averages that range from 2.23 to 2.63 (Table 5-5 & Figure 5-24). Standard

deviations for AMS U ppm range from 0.62 to 0.98 (Table 5-5) which compare with the whole survey standard deviation of 0.89 (Table 5-3). Predicted Th ppm values range from 10.26 to 14.23 and are compared with AMS averages ranging from 8.22 to 13.31 (Table 5-5 & Figure 5-25). Standard deviations for AMS Th ppm range from 1.64 to 2.04 (Table 5-5) which compare with the whole survey standard deviation of 1.91 (Table 5-3).

Discussion

Using the criteria for success outlined earlier it can be said that the bedrock units defined on the geologic map at Government Wash were successful at making a prediction with the NURE data and the Quaternary alluvium was successfully modeled with both 2/1N and 2/1,6,10N models. At Lake Mohave the only truly successful model was 2,6,10N.

GMTG Models

The geochemical models using geologic maps were the least successful models at both Government Wash and Lake Mohave. Government Wash has better data coverage with 66% of the geologic units having enough data to create a model. At Lake Mohave only about 43% of the units were able to be modeled. Of the units modeled, the vast majority are outside of the desired ± 1 $\mu\text{R/h}$ range when comparing AMS exposure rate averages to predictions. At Government Wash, only 49.5% of the AMS exposure rate data is predicted within ± 1 $\mu\text{R/h}$ on a point by point basis. This percentage is higher than the GMN model when the Quaternary alluvium is included; however, this arises because the geochemical prediction is closer to the mean of the AMS data in the Quaternary alluvium than the NURE data. In other words, if you remove the alluvium from both models the percentage of successful data points declines for GMTG rather than increasing as with GMN. At Lake Mohave only 10% of the AMS data are predicted within ± 1 $\mu\text{R/h}$ making this model the least successful.

GMN Models

At Government Wash the GMN model was successful at predicting the exposure rates of bedrock units. With the exception of Quaternary alluvial and paleo-alluvial units (e.g., ThI, ThIV and ThT) the NURE data sorted into geologic units successfully predicted 84% of the data. AMS standard deviations are smaller than for the whole survey in bedrock units and differences between predicted and AMS mean exposure rates are $<1 \mu\text{R/h}$.

The GMN model at Lake Mohave on the other hand was less successful than at Government Wash. This is due to the fact that the entire modeling area is alluvial with a range of source rocks and long history of deposition, incision and flood deposits from the Colorado River. Standard deviations are mixed with some lower and some higher than the general survey and on average are near that of the whole survey. Additionally, only 68% of the AMS exposure rate data points are successfully predicted. This model had some success however, as most of the units fall within $\pm 1 \mu\text{R/h}$ when comparing AMS mean exposure rates to predictions.

ASTER Based Models

At Government Wash a total of 90% of the AMS data are successfully modeled when using the bedrock and paleo-alluvial geologic units and the 2/1N model for the Quaternary alluvium. Standard deviations for this model are below the whole survey standard deviation and absolute differences between the predictions and AMS means are below $1 \mu\text{R/h}$. Similarly, using 2/1,6,10N to model the Quaternary alluvium and the GMN to model the bedrock the percentage of successfully predicted AMS data points is 88.5%. The 2/1,6,10N model also has low standard deviations and low absolute differences between AMS means and predictions. Both models greatly improve upon the prediction based on the geologic boundaries of the Quaternary alluvium alone.

At Lake Mohave the 2,7,13N model had some success as the standard deviations are mostly near the whole survey standard deviation and absolute differences between AMS means

and predictions are almost exclusively below 1 $\mu\text{R}/\text{h}$. Despite these successes only 69% of the AMS exposure rate data were successfully predicted. The effects of shadows in the 2, 7, 13 image become apparent upon close examination of the classified image and it may be that this image would be more successful if further processed to reduce those effects. It should also be noted that unit 1 is composed of water and is therefore removed from this analysis.

The 2, 6, 10N model was the most successful at Lake Mohave. Standard deviations are high on some units (e.g., units 2-4), however those units occur very close to the shore of the lake and likely represent nearshore vegetation. These units occupy only a 1.7% of the model. Units 5-8 represent the vast majority of the survey area and the AMS standard deviations of those units are below that of the whole survey. Unit 9 is the smallest of the significant units and is the only significant unit to fall outside of the success range. Unit 1 represents water and unit 10 occurs outside of the survey area and therefore they are not considered in this analysis. This model is the most successful model at Lake Mohave with 95.5% of the AMS exposure rate data successfully modeled.

Strong shadows can become their own artificial class with no correlation to actual composition. In addition, natural variation on the ground, the oversampling of images and atmospheric effects can introduce noise into the image and interfere with classification. By reducing tonal differences between pixels and forcing classes to be at least 20 pixels in size shadows and noise on the 2, 6, 10 image at Lake Mohave were significantly reduced and the resulting model was much more successful.

Geochemical Data

A number of factors lead to the general failure of the use of geochemistry for these models. One of the most difficult impediments to using geochemistry to create a model is the lack of data available for many units (e.g., Units: Ti, Qai3). Additionally, the quality of the metadata in these datasets is not consistent making it difficult to determine where many data

points should reside. Many data points have little or no lithologic information (i.e., rock type) and still others have imprecise geolocation information (e.g., points only report latitude and longitude to the second decimal).

Processes related to soil formation and eolian deposition can also complicate the use of geochemical data. Soil forming processes can alter radioelement concentrations through enrichment or depletion (Michel 1984; Wilford, Bierwirth et al. 1997). In addition regional or global dust deposited by eolian processes may be either enriched or depleted in radioelements relative to the underlying lithology (Reheis, Budahn et al. 2009).

NURE Data

The NURE data has some significant advantages over traditional geochemistry as a source dataset for K, U, and Th concentrations. There are many more NURE data points to work with making any prediction more statistically robust. In addition, we are comparing the results of two aerial gamma ray surveys and therefore differences between soil and bedrock chemistry are incorporated into the data.

However, we have encountered some geolocation problems with the NURE data. When comparing the NURE lines that occur over the areas surveyed by AMS, in some instances there is little to no correlation between the datasets. Although the NURE data at Lake Mohave are well correlated to the AMS data (Figure 5-10), at Government Wash the data are not well correlated (Figure 5-11). The bedrock units at Government Wash solely use data from the northern line which is not tested against AMS data. However, the Horse Spring units, and a small portion of the aster based units do obtain data from this line. This may explain some of the discrepancy between the predictions for the Horse Spring units and the AMS data over those units.

A possible source of this error is the fact that the NURE survey was not conducted with GPS equipment and instead position was determined via sighting techniques from the aircraft

(Duval, Carson et al. 2005). It may be possible to reposition any given NURE line by observing how K, U, and Th values change as the line goes over an open body of water; however, that is beyond the scope of this study.

Conclusions

This study has shown that in places where NURE survey data or the equivalent exists (e.g., Canada and Australia) it is possible to predict the background radiation emanating from geology to within $\pm 1 \mu\text{R/h}$. Geochemical data was not successful as a base for modeling. This is due to several factors including: a limited availability of data for many geologic units, and poor metadata quality including compositional and location data.

While the use of bedrock geologic units to sort the NURE data is successful at predicting the exposure rate; multispectral imagery, is far more successful for modeling complex surfaces like alluvium. Further work into the manipulation of multispectral imagery will allow for the reduction of shadows and noise and improve future modeling.

Tables

Table 5-1: Geochemical Data by Geologic Unit

Government Wash – Geochemical Data

Unit	Number of Points	Mean K (wt%)	Median K (wt%)	Standard Deviation K	Mean U (ppm)	Median U (ppm)	Standard Deviation U	Mean Th (ppm)	Median Th (ppm)	Standard Deviation Th
Qa	10	1.38	1.34	0.49	1.66	1.69	0.22	3.10	2.77	1.27
Qoa	2	1.35	1.35	0.64	2.37	2.37	0.86	3.60	3.60	2.43
Thl	1	0.63	0.63	N/A	1.71	1.71	N/A	2.62	2.62	N/A
Tht	6	1.68	1.51	0.70	28.45	2.17	52.78	3.89	4.67	1.60
Tmcl	5	4.01	4.01	0.99	4.62	4.62	0.00	11.86	12.22	7.16
Tmcu	3	0.97	0.96	0.12	1.60	1.59	0.03	3.09	3.09	0.45
Tvc	5	2.84	3.09	0.31	N/A	N/A	N/A	N/A	N/A	N/A
Tmcg	1	2.72	N/A	N/A	1.26	N/A	N/A	4.19	N/A	N/A

Lake Mohave – Geochemical Data

Qai	6	5.38	4.54	1.89	1.97	1.88	0.53	18.82	20.25	4.43
Qai1	2	4.39	4.39	0.31	2.91	2.91	0.11	18.00	18.00	0.48
Qao	2	5.54	5.54	0.00	2.25	2.25	0.05	15.42	15.42	1.07
Qay	15	4.80	4.72	0.64	2.08	2.22	0.65	16.40	16.07	2.37
Qay2	2	4.26	4.26	0.44	2.24	2.24	N/A	13.60	13.60	N/A
QTa	1	4.14	4.14	N/A	1.60	1.60	N/A	6.79	6.79	N/A

Table 5-1: Summary statistics of the geochemical data obtained for each geologic unit from national databases

Table 5-2 A: AMS and NURE Exposure Rates by Geologic UnitGovernment Wash Geologic Units Exposure Rate $\mu\text{R/h}$

Unit	AMS Mean	AMS Median	AMS STD	AMS Low	AMS High	NURE Mean	NURE Median	NURE STD	NURE Low	NURE High	Abs Diff AMS-NURE	GC Exp	Abs Diff AMS-GC
Qa	2.68	2.66	0.30	1.47	4.52	3.96	3.76	1.53	1.02	7.05	1.28	3.58	0.90
Qoa	3.36	3.39	0.39	1.37	5.04	4.06	3.91	1.63	1.24	8.16	0.70	4.06	0.70
Tmcg	2.03	1.93	0.53	1.11	4.12	1.50	1.56	0.38	0.52	2.35	0.56	5.41	3.39
Tmcl	3.56	3.52	0.65	2.04	5.88	3.86	2.24	1.48	1.07	6.90	0.58	11.05	7.49
Tmcu	3.20	3.06	0.55	1.52	4.97	3.69	4.22	1.19	2.15	7.74	0.65	3.00	0.20
Thl	4.81	4.87	0.82	2.79	6.85	3.59	3.40	1.10	1.96	6.85	1.27	2.48	2.32
Thlv	4.77	4.86	0.45	3.63	5.56	2.59	2.60	0.30	2.05	3.00	2.18	N/A	N/A
Tht	4.92	4.66	1.03	3.08	6.90	3.32	3.52	0.87	1.71	5.41	1.60	4.46	0.45
Thtb	3.98	N/A	N/A	N/A	N/A	3.88	N/A	N/A	N/A	N/A	0.09	N/A	N/A
Ti	5.04	4.99	0.93	3.44	6.49	N/A	N/A	N/A	N/A	N/A	N/A	N/A	N/A
Trs	4.53	4.74	0.78	2.76	5.53	5.06	4.93	0.52	4.47	6.01	0.66	N/A	N/A
Tvc	4.71	4.55	0.28	4.44	5.22	4.67	4.85	0.52	3.50	5.18	0.24	3.75	0.96

Lake Mohave Geologic Units Exposure Rate $\mu\text{R/h}$

Qai	8.76	8.72	0.51	6.36	9.85	9.81	9.93	1.21	3.39	12.61	1.06	12.14	3.39
Qai+y	8.35	8.34	0.14	8.07	8.92	9.65	9.67	0.54	8.72	10.42	1.31	N/A	N/A
Qai1	8.55	8.72	0.86	5.55	9.41	9.47	9.57	1.60	3.39	13.62	0.92	12.29	3.73
Qai3	8.62	8.65	0.63	4.92	9.77	8.82	8.65	1.53	4.04	12.41	0.20	N/A	N/A
Qao	9.36	9.51	0.44	8.36	9.66	9.99	10.12	0.56	8.81	11.07	0.63	12.74	3.38
Qay	8.69	8.61	0.53	5.45	9.95	7.90	8.26	1.57	3.39	10.64	0.79	11.94	3.25
Qay+i	8.82	8.83	0.10	8.68	8.98	7.87	9.58	3.15	4.23	9.79	0.95	N/A	N/A
Qay1	8.64	8.49	0.50	7.94	9.83	8.98	8.98	1.40	4.06	12.06	0.34	N/A	N/A
Qay2	8.75	8.68	0.52	7.52	9.82	9.43	9.73	1.39	3.81	12.06	0.68	10.55	1.80
Qby	6.24	6.53	0.99	4.04	7.69	7.22	7.96	2.49	0.54	11.31	0.98	N/A	N/A
Qta	8.27	8.27	0.24	7.46	9.07	9.42	9.40	1.34	6.63	13.01	1.15	8.18	0.09
Qch	7.46	7.35	0.46	6.89	8.59	8.97	9.25	1.44	6.04	11.19	1.51	N/A	N/A
Qcw	9.14	9.14	0.07	9.05	9.23	7.38	8.30	2.71	3.39	10.56	1.76	N/A	N/A
Tay1	8.33	8.33	0.28	7.79	8.88	8.74	8.65	0.95	7.30	10.11	0.41	N/A	N/A

Table 5-2A: AMS, NURE and Geochemical exposure rate data by geologic unit.

Table 5-2B: AMS and NURE K, U, and Th Values for Government Wash Geologic Units

Government Wash Geologic Units

K Weight Percent

Unit	AMS Mean	AMS Median	AMS STD	AMS Low	AMS High	NURE Mean	NURE Median	NURE STD	NURE Low	NURE High
Qa	0.60	0.60	0.14	0.02	1.53	1.02	0.97	0.47	0.12	2.18
Qoa	0.74	0.74	0.16	0.24	1.64	1.14	1.09	0.55	0.24	3.03
Tmcg	0.41	0.38	0.18	0.02	1.42	0.25	0.24	0.12	0.12	0.48
Tmcl	0.92	0.87	0.29	0.23	2.09	0.84	0.73	0.51	0.24	1.94
Tmcu	0.66	0.64	0.21	0.05	1.53	1.11	1.09	0.45	0.12	2.18
Thl	1.25	1.26	0.34	0.42	2.27	0.88	0.73	0.38	0.24	1.69
Thlv	1.19	1.21	0.23	0.76	1.56	0.46	0.42	0.12	0.36	0.61
Tht	1.16	1.19	0.28	0.53	1.85	0.90	0.85	0.26	0.36	1.69
Thtb	0.81	N/A	N/A	N/A	N/A	N/A	N/A	N/A	N/A	N/A
Ti	1.17	1.18	0.32	0.64	1.91	N/A	N/A	N/A	N/A	N/A
Trs	1.12	1.15	0.27	0.52	1.70	1.23	1.27	0.18	0.97	1.45
Tvc	1.23	1.20	0.17	0.98	1.52	1.26	1.21	0.11	1.09	1.45

eU ppm

Qa	1.92	1.89	0.67	0.05	6.03	2.45	2.38	0.98	0.57	4.85
Qoa	2.29	2.27	0.66	0.19	4.73	2.01	1.90	0.95	0.10	5.13
Tmcg	1.51	1.47	0.73	0.07	4.78	1.47	1.52	0.65	0.10	3.04
Tmcl	2.18	2.12	0.78	0.01	7.92	1.44	1.33	0.97	0.10	3.61
Tmcu	2.32	2.28	0.78	0.28	6.60	2.30	2.28	0.59	0.76	4.18
Thl	2.83	2.78	0.88	0.95	5.18	2.13	2.09	0.65	0.48	3.42
Thlv	2.72	2.64	0.73	1.10	4.58	2.42	2.47	0.19	2.09	2.57
Tht	2.59	2.52	0.81	0.79	4.98	1.97	1.90	0.90	0.57	4.37
Thtb	2.75	N/A	N/A	N/A	N/A	N/A	N/A	N/A	N/A	N/A
Ti	2.53	2.69	0.61	1.32	3.92	N/A	N/A	N/A	N/A	N/A
Trs	2.47	2.44	0.73	0.71	4.12	2.96	2.85	1.25	1.43	4.94
Tvc	2.31	2.16	0.77	1.26	4.07	2.59	2.71	0.50	1.52	3.04

eTh ppm

Qa	2.71	2.63	1.00	0.07	6.80	4.83	4.36	2.44	0.85	10.65
Qoa	3.72	3.69	1.11	0.34	7.29	5.53	5.69	2.74	0.24	13.19
Tmcg	1.98	1.89	1.10	0.00	13.69	1.50	1.45	0.74	0.61	3.87
Tmcl	3.77	3.63	1.29	0.55	9.79	3.47	2.78	2.24	1.09	9.32
Tmcu	3.13	3.02	1.26	0.03	7.22	5.20	4.96	2.35	0.85	12.34
Thl	5.58	5.29	1.69	2.69	9.64	4.63	4.48	2.31	0.85	10.65
Thlv	5.90	5.92	1.25	3.37	8.54	2.40	2.42	0.72	1.57	3.51
Tht	7.10	6.44	2.75	2.46	14.16	3.88	3.87	1.46	0.48	7.74
Thtb	4.59	N/A	N/A	N/A	N/A	N/A	N/A	N/A	N/A	N/A
Ti	7.89	7.61	2.76	3.25	14.24	N/A	N/A	N/A	N/A	N/A
Trs	5.62	5.42	1.78	2.69	9.99	6.68	6.29	2.18	4.72	10.65
Tvc	6.78	6.84	1.05	4.52	8.13	5.87	5.75	1.82	2.42	8.71

Table 5-2B: AMS and NURE K weight %, U and Th ppm by geologic unit at Government Wash.

Table 5-2C: AMS and NURE K, U, and Th Values for Lake Mohave Geologic Units

Lake Mohave Geologic Units
K Weight Percent

Unit	AMS Mean	AMS Median	AMS STD	AMS Low	AMS High	NURE Mean	NURE Median	NURE STD	NURE Low	NURE High
Qai	2.85	2.89	0.28	1.79	3.44	3.08	3.10	0.40	0.50	3.90
Qai+y	2.78	2.78	0.19	2.28	3.27	3.06	3.05	0.29	2.60	3.50
Qai1	2.73	2.77	0.37	1.63	3.39	3.17	3.20	0.80	0.50	6.40
Qai3	2.84	2.86	0.26	1.33	3.65	2.85	2.90	0.58	1.10	4.40
Qao	3.13	2.99	0.29	2.79	3.49	3.11	3.10	0.29	2.30	3.60
Qay	2.91	2.91	0.24	1.57	3.67	2.47	2.60	0.55	0.50	3.30
Qay+i	2.87	2.87	0.15	2.51	3.04	2.77	3.40	1.27	1.30	3.60
Qay1	2.93	2.93	0.21	2.10	3.57	2.90	2.90	0.49	1.40	3.90
Qay2	2.86	2.86	0.24	2.29	3.37	2.90	2.90	0.40	1.30	3.70
Qby	1.95	2.05	0.40	0.96	2.44	2.41	2.60	0.77	0.10	3.30
Qta	2.78	2.77	0.19	2.16	3.35	2.94	2.90	0.47	1.90	6.20
Qch	2.32	2.31	0.25	1.79	2.88	2.81	2.80	0.41	1.90	3.50
Qcw	2.84	2.86	0.18	2.65	3.01	2.45	3.05	1.20	0.50	3.60
Tay1	2.46	2.46	0.23	2.03	2.98	2.71	2.70	0.38	2.10	3.40

eU ppm

Qai	2.74	2.86	0.89	0.35	5.16	3.52	3.40	1.37	0.40	6.90
Qai+y	2.46	2.56	0.83	0.55	4.49	3.33	3.70	1.58	1.00	5.30
Qai1	2.33	2.28	0.90	0.20	4.16	3.33	3.45	1.37	0.40	6.40
Qai3	2.63	2.62	0.89	0.00	5.62	3.12	3.15	1.18	0.50	6.30
Qao	3.18	2.88	1.22	1.98	5.06	4.20	4.30	1.64	0.60	6.80
Qay	2.59	2.56	0.89	0.01	6.14	3.28	3.10	1.09	1.60	6.00
Qay+i	3.14	3.08	0.83	1.97	4.35	1.73	1.90	0.86	0.80	2.50
Qay1	2.59	2.59	0.91	0.09	5.12	2.89	2.70	1.35	0.50	6.30
Qay2	2.57	2.67	0.84	0.64	4.71	3.49	3.40	1.28	0.70	6.20
Qby	2.39	2.52	0.79	0.79	3.90	3.02	2.85	1.24	0.20	6.00
Qta	2.50	2.51	0.92	0.36	5.76	3.04	2.90	1.16	0.90	6.50
Qch	2.35	2.26	1.00	0.56	4.76	2.32	2.60	0.77	0.90	3.40
Qcw	3.06	3.08	0.69	2.23	3.86	2.97	3.05	1.00	1.40	4.90
Tay1	2.97	2.94	0.94	0.81	5.47	2.98	3.00	1.14	1.40	4.90

eTh ppm

Qai	12.97	13.07	2.10	6.07	18.90	14.07	14.00	2.98	3.40	25.40
Qai+y	11.79	11.64	1.63	7.73	15.80	13.93	12.85	2.42	11.30	17.20
Qai1	12.13	12.65	2.04	5.99	16.49	12.74	13.10	2.75	3.40	18.20
Qai3	12.88	12.89	2.06	4.44	18.93	12.29	12.15	2.69	3.70	23.00
Qao	13.39	14.28	1.72	10.02	14.71	13.16	12.70	2.16	8.10	18.50
Qay	12.54	12.47	1.84	5.93	18.87	11.51	11.60	3.15	3.40	17.20
Qay+i	13.54	13.61	1.51	10.53	16.47	12.00	14.90	6.83	4.20	16.90
Qay1	12.58	12.50	1.77	8.51	18.22	13.12	13.10	2.86	5.50	22.10
Qay2	12.84	12.67	1.84	7.76	17.19	13.74	12.80	3.21	6.30	20.90
Qby	8.30	8.04	1.56	4.12	11.39	11.75	10.70	4.93	0.70	18.70
Qta	11.75	11.64	1.62	7.54	16.29	14.27	13.70	3.19	7.80	23.70
Qch	10.62	11.12	1.44	7.42	13.18	14.72	14.90	3.53	6.70	19.40
Qcw	11.95	11.61	0.80	11.45	13.14	9.25	9.90	4.20	3.40	15.40
Tay1	13.50	13.62	1.74	10.19	17.75	12.98	13.30	2.45	8.70	17.50

Table 5-2C: AMS and NURE K weight %, U and Th ppm by geologic unit at Lake Mohave.

Table 5-3: Summary of AMS Whole Survey

Area of Interest	Total AMS Data Points	Measurement	Mean AMS	Median AMS	STD AMS	Low AMS	High AMS
Government Wash	7655	Exposure Rate ($\mu\text{R/hr}$)	3.00	2.85	0.80	1.11	6.89
		K (wt%)	0.69	0.64	0.27	0.05	2.27
		eU ppm	2.04	2.00	0.76	0.07	7.92
		eTh ppm	3.16	2.92	1.55	0.004	14.23
Lake Mohave	6662	Exposure Rate ($\mu\text{R/hr}$)	8.63	8.55	0.54	5.45	9.95
		K (wt%)	2.87	2.88	0.25	1.63	3.67
		eU ppm	2.59	2.58	0.89	0.001	6.13
		eTh ppm	12.53	12.48	1.91	4.12	18.93

Table 5-3: The summary statistics of AMS exposure rate, K, U, and Th concentration of the whole survey at Government Wash and Lake Mohave.

Table 5-4: AMS and NURE K, U, and Th Values for Government Wash Remote Sensing Units

Government Wash Remote Sensing Units

2/1 Image Ratio - Exposure Rate $\mu\text{R/h}$

Unit	AMS Mean	AMS Median	AMS STD	AMS Low	AMS High	NURE Mean	NURE Median	NURE STD	NURE Low	NURE High	Abs Diff AMS-NURE
1	3.15	3.27	0.47	2.02	4.52	3.28	3.43	0.78	2.47	4.41	0.13
2	2.98	2.93	0.45	1.47	4.84	2.83	2.73	1.10	1.28	5.22	0.15
3	2.88	2.79	0.45	1.47	4.23	3.04	2.85	1.05	1.60	5.06	0.16
4	2.74	2.72	0.37	1.37	4.23	2.83	2.67	0.91	1.02	4.90	0.09
5	2.69	2.67	0.36	1.65	4.28	2.73	2.65	0.24	2.50	3.09	0.03

K Weight Percent

1	0.67	0.65	0.16	0.33	1.20	0.82	0.97	0.34	0.36	1.21	0.15
2	0.64	0.62	0.16	0.02	1.60	0.78	0.73	0.35	0.12	1.57	0.14
3	0.64	0.63	0.16	0.24	1.23	0.76	0.67	0.40	0.12	1.57	0.12
4	0.63	0.62	0.15	0.18	1.36	0.79	0.79	0.29	0.24	1.33	0.16
5	0.62	0.61	0.15	0.25	1.53	0.73	0.73	0.17	0.48	0.97	0.10

eU ppm

1	2.25	2.36	0.67	0.63	3.71	2.38	1.81	1.79	0.38	5.13	0.13
2	2.15	2.16	0.70	0.33	5.51	1.73	1.62	0.82	0.67	3.33	0.42
3	2.04	2.00	0.67	0.19	6.03	1.78	1.66	0.75	0.57	3.23	0.26
4	1.91	1.90	0.66	0.09	5.22	1.65	1.52	0.98	0.10	4.85	0.26
5	1.88	1.86	0.66	0.26	4.69	1.48	1.81	0.79	0.19	2.19	0.40

eTh ppm

1	3.28	3.27	1.27	0.45	7.29	4.40	4.11	1.12	3.27	6.05	1.13
2	3.13	3.01	1.17	0.12	6.95	3.62	3.33	2.25	0.24	7.99	0.49
3	2.98	2.86	1.13	0.10	6.80	3.96	3.63	1.98	1.09	8.71	0.98
4	2.84	2.75	1.04	0.11	6.67	3.40	3.03	1.81	0.85	7.14	0.56
5	2.70	2.61	0.98	0.15	6.92	3.53	3.63	0.73	2.42	4.36	0.83

2/1,6,10 Visualization - Exposure Rate $\mu\text{R/h}$

1	3.39	3.39	0.44	3.07	3.70	2.81	2.81	0.48	2.47	3.15	0.58
2	2.93	2.78	0.55	1.78	4.20	3.66	3.58	0.83	2.31	5.22	0.73
3	3.10	3.16	0.45	1.65	4.52	2.65	2.39	1.06	1.51	4.98	0.45
4	2.88	2.80	0.43	1.37	5.04	2.62	2.57	0.91	1.02	4.90	0.25
5	2.65	2.64	0.30	1.62	4.28	2.47	2.53	0.55	1.24	3.30	0.18

K Weight Percent

1	0.77	0.77	0.16	0.65	0.88	1.09	1.09	0.17	0.97	1.21	0.32
2	0.66	0.62	0.17	0.29	1.11	0.93	0.97	0.34	0.36	1.57	0.27
3	0.66	0.65	0.16	0.26	1.20	0.73	0.73	0.45	0.12	1.57	0.06
4	0.64	0.63	0.17	0.02	1.64	0.65	0.61	0.29	0.24	1.33	0.01
5	0.61	0.60	0.14	0.05	1.53	0.73	0.73	0.15	0.48	0.97	0.13

eU ppm

1	2.54	2.54	0.19	2.41	2.68	0.86	0.86	0.67	0.38	1.33	1.69
2	2.00	1.99	0.75	0.48	4.73	1.90	1.66	1.08	0.48	5.13	0.10
3	2.22	2.24	0.66	0.36	4.53	1.59	1.52	0.71	0.67	2.95	0.63
4	2.04	2.00	0.68	0.09	5.90	1.87	1.66	0.86	0.57	4.85	0.17
5	1.85	1.83	0.65	0.05	6.03	1.49	1.66	0.81	0.10	2.85	0.36

eTh ppm

1	3.79	3.79	0.19	3.66	3.93	3.33	3.33	0.43	3.03	3.63	0.47
2	3.21	3.07	1.03	0.56	6.43	5.35	5.57	1.58	2.78	8.71	2.14
3	3.32	3.25	1.19	0.58	7.29	3.44	3.15	1.95	0.85	7.99	0.12
4	2.96	2.85	1.13	0.12	6.92	2.94	2.78	1.61	0.61	7.14	0.03
5	2.68	2.60	0.97	0.07	6.80	2.50	2.30	1.25	0.24	4.36	0.18

Table 5-4: AMS and NURE exposure rate, K weight %, U and Th ppm for remote sensing models of alluvium at Government Wash

Table 5-5: AMS and NURE K, U, and Th Values for Lake Mohave Remote Sensing Units

Lake Mohave Remote Sensing Units 2,7,13 Visualization - Exposure Rate $\mu\text{R/h}$

Unit	AMS Mean	AMS Median	AMS STD	AMS Low	AMS High	NURE Mean	NURE Median	NURE STD	NURE Low	NURE High	Abs Diff AMS-NURE
2	8.52	8.45	0.55	6.22	9.74	8.65	8.65	1.24	6.15	13.01	0.13
3	8.49	8.45	0.36	6.65	9.82	9.35	9.33	1.07	6.30	12.61	0.86
4	9.13	9.31	0.48	6.44	9.95	9.75	9.91	1.32	0.71	13.62	0.62
5	8.05	8.29	0.86	6.36	9.55	9.36	9.50	1.85	0.51	12.37	1.31
6	7.41	7.41	0.31	7.18	7.63	6.75	6.80	1.33	3.94	9.47	0.66

K Weight Percent

2	2.82	2.83	0.21	1.91	3.35	2.79	2.70	0.69	1.80	6.80	0.03
3	2.84	2.85	0.21	2.03	3.58	2.93	2.90	0.31	1.90	4.00	0.09
4	3.02	3.04	0.25	1.79	3.67	3.12	3.20	0.48	0.10	6.40	0.10
5	2.53	2.58	0.37	1.69	3.13	3.09	3.20	0.63	0.10	4.20	0.56
6	2.28	2.28	0.34	2.04	2.52	2.21	2.20	0.50	1.40	3.20	0.07

eU ppm

2	2.59	2.63	0.90	0.15	5.01	2.93	2.90	1.17	0.20	5.60	0.34
3	2.61	2.60	0.90	0.00	6.14	3.09	3.00	1.26	0.10	6.50	0.48
4	2.59	2.57	0.90	0.13	5.89	3.29	3.10	1.31	0.50	6.80	0.70
5	2.32	2.25	0.80	0.86	3.95	3.18	3.00	1.34	0.10	6.90	0.85
6	2.01	2.01	0.26	1.83	2.19	2.72	2.70	1.07	0.10	5.00	0.71

eTh ppm

2	12.27	12.04	1.76	7.92	18.93	12.40	12.45	2.41	6.60	18.10	0.14
3	12.43	12.33	1.88	5.93	18.90	13.99	13.70	2.86	7.00	24.60	1.56
4	13.06	13.06	1.74	7.56	18.87	14.07	13.90	3.08	0.70	25.40	1.01
5	11.53	11.25	2.23	6.07	18.16	13.05	13.40	3.16	0.60	20.90	1.53
6	11.46	11.46	2.59	9.63	13.29	8.61	9.10	2.45	4.00	13.90	2.85

2,6,10 Visualization - Exposure Rate $\mu\text{R/h}$

2	5.99	5.92	1.00	4.04	7.60	6.87	7.00	2.59	0.77	16.56	0.88
3	7.34	7.39	0.72	6.07	8.66	7.49	7.53	2.55	0.68	18.09	0.16
4	7.89	7.98	0.76	5.84	9.37	7.80	7.91	2.56	0.64	17.91	0.09
5	8.44	8.48	0.51	4.92	9.62	8.07	8.07	2.29	0.54	20.89	0.37
6	8.49	8.46	0.38	5.23	9.82	8.41	8.36	2.21	0.45	18.42	0.08
7	8.71	8.74	0.60	5.45	9.95	8.53	8.44	2.24	0.65	18.65	0.18
8	9.30	9.35	0.34	6.36	9.95	8.73	8.62	2.36	0.51	21.41	0.56
9	7.44	7.18	0.63	6.55	8.57	9.03	8.96	2.91	0.54	21.44	1.59

K Weight Percent

2	1.90	2.01	0.45	0.96	2.73	2.07	2.10	0.75	0.30	6.40	0.17
3	2.35	2.44	0.33	1.57	3.03	2.19	2.20	0.77	0.10	6.70	0.16
4	2.64	2.70	0.33	1.58	3.24	2.27	2.30	0.76	0.10	6.80	0.37
5	2.77	2.79	0.26	1.62	3.39	2.37	2.30	0.68	0.10	6.20	0.40
6	2.84	2.85	0.21	1.62	3.65	2.48	2.50	0.63	0.20	6.10	0.35
7	2.91	2.91	0.26	1.63	3.67	2.49	2.50	0.60	0.10	6.40	0.42
8	3.08	3.09	0.22	1.79	3.67	2.55	2.50	0.61	0.10	5.90	0.53
9	2.28	2.24	0.27	1.69	2.72	2.63	2.60	0.68	0.10	5.40	0.34

eU ppm

2	2.25	2.23	0.62	1.21	3.12	2.53	2.40	1.35	0.10	8.40	0.28
3	2.32	2.17	0.98	0.85	4.72	2.78	2.70	1.35	0.10	9.50	0.46
4	2.23	2.16	0.77	0.81	3.96	2.85	2.70	1.38	0.10	10.10	0.62
5	2.63	2.65	0.93	0.05	5.07	2.90	2.80	1.37	0.10	10.00	0.27
6	2.62	2.60	0.89	0.00	6.14	3.00	2.90	1.40	0.10	9.40	0.38
7	2.57	2.56	0.90	0.13	5.58	3.05	2.90	1.43	0.10	9.90	0.48
8	2.54	2.50	0.88	0.27	5.89	3.07	2.90	1.43	0.10	11.50	0.53
9	2.31	2.19	0.85	0.86	3.94	3.15	3.00	1.52	0.10	10.00	0.84

eTh ppm

2	8.22	8.04	1.73	4.12	10.53	10.26	10.20	4.70	0.10	29.90	2.04
3	11.00	10.86	2.04	7.44	14.67	11.41	11.00	4.86	0.60	39.90	0.42
4	11.49	11.73	1.93	6.71	15.48	12.06	11.80	4.98	0.90	41.10	0.56
5	12.44	12.33	1.96	5.98	18.93	12.43	12.20	4.47	0.60	52.60	0.01
6	12.43	12.33	1.89	5.93	18.90	12.92	12.70	4.35	0.10	41.50	0.49
7	12.44	12.43	1.84	6.20	18.87	13.24	12.80	4.67	1.50	41.70	0.80
8	13.31	13.28	1.70	6.07	18.85	13.65	13.10	5.17	0.30	46.00	0.34
9	10.58	10.83	1.64	7.42	13.65	14.23	13.40	6.67	0.10	49.10	3.66

Table 5-5: Exposure rate, K weight %, eU and eTh ppm for remote sensing models at Lake Mohave

Figures

Figure 5-1: Comparison of Published and Altered Geologic Map, Government Wash

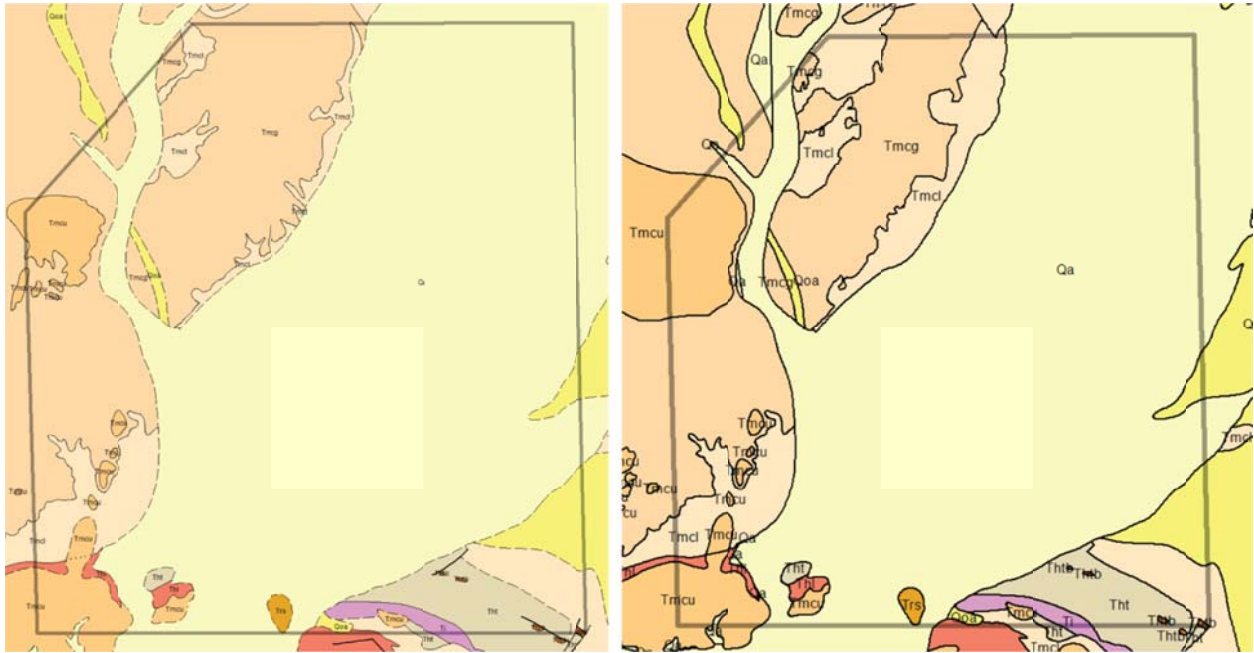


Figure 5-1: A comparison between the unaltered published geologic map (left) and the corrected map (right) of Government Wash (Duebendorfer 2003).

Figure 5-2: Unclassified and Classifies 2/1 ASTER Image, Government Wash

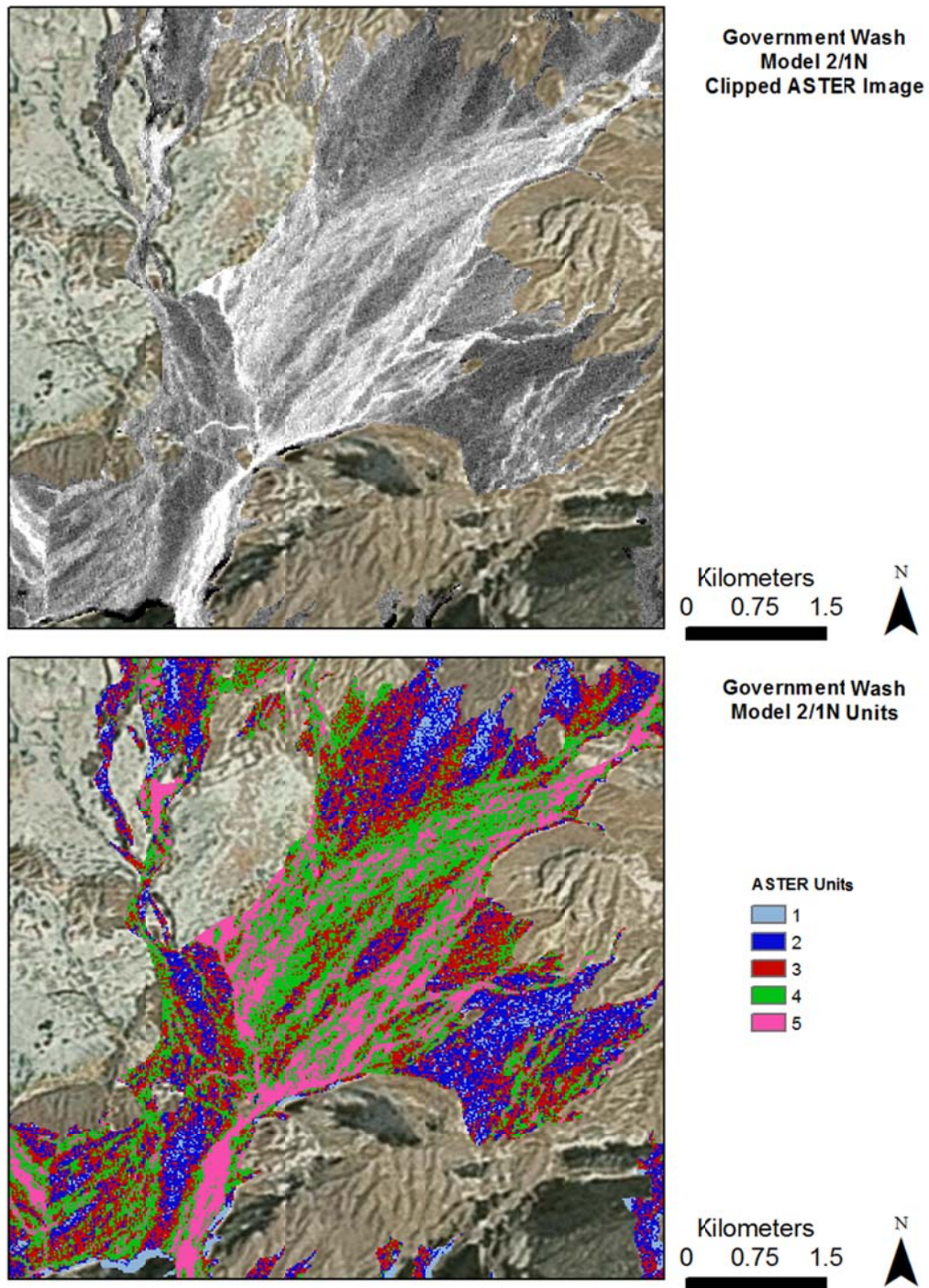


Figure 5-2: 2/1 clipped ASTER image (Abrams 2000) over Quaternary alluvium (top) and the classified image (bottom) at Government Wash

Figure 5-3: Unclassified and Classifies 2/1,6,10 ASTER Image, Government Wash

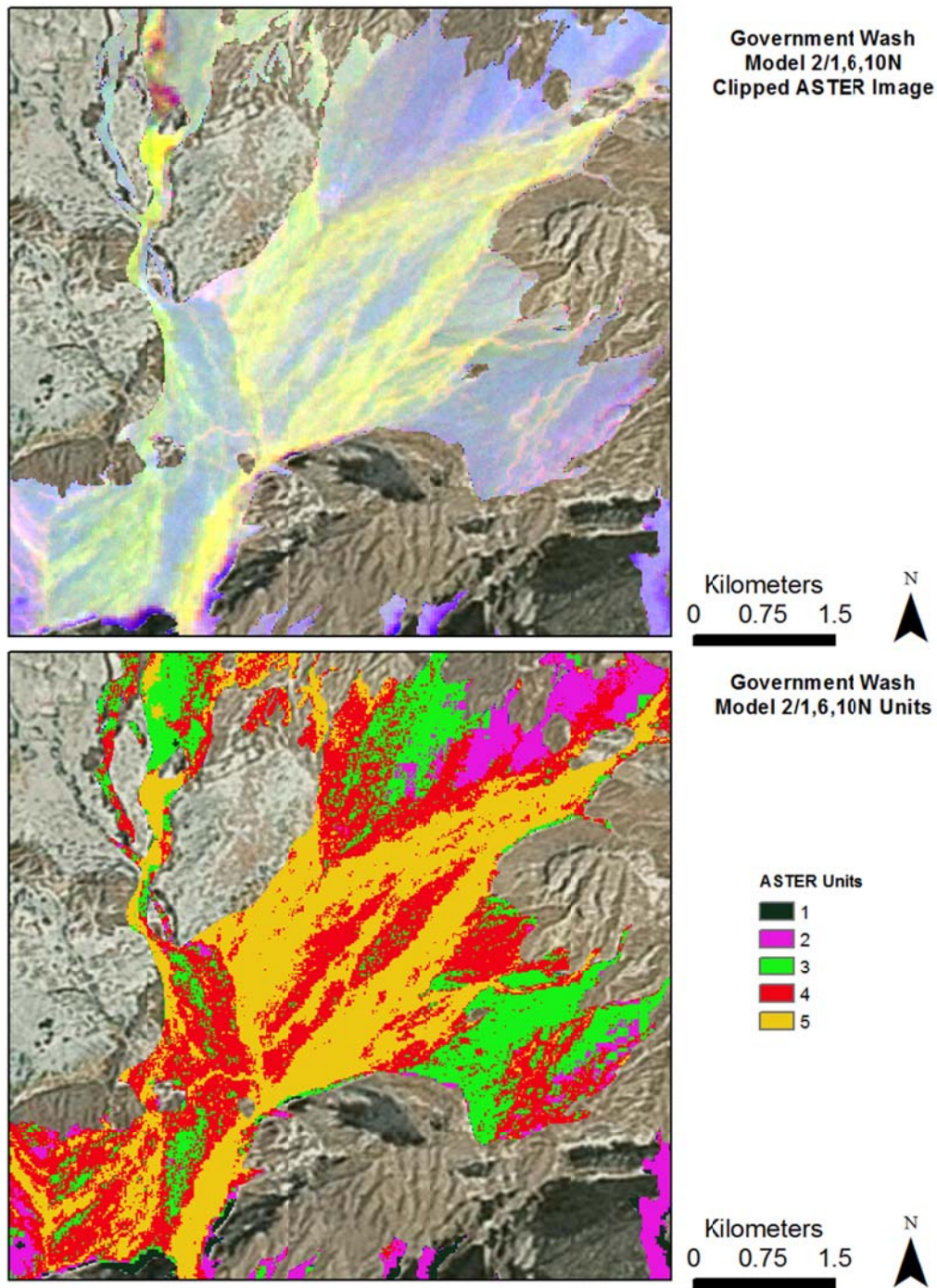


Figure 5-3: 2/1, 6, 10 clipped ASTER image (Abrams 2000) over Quaternary alluvium (top) and the classified image (bottom) at Government Wash.

Figure 5-4: Unclassified and Classifies 2,7,13 ASTER Image, Lake Mohave

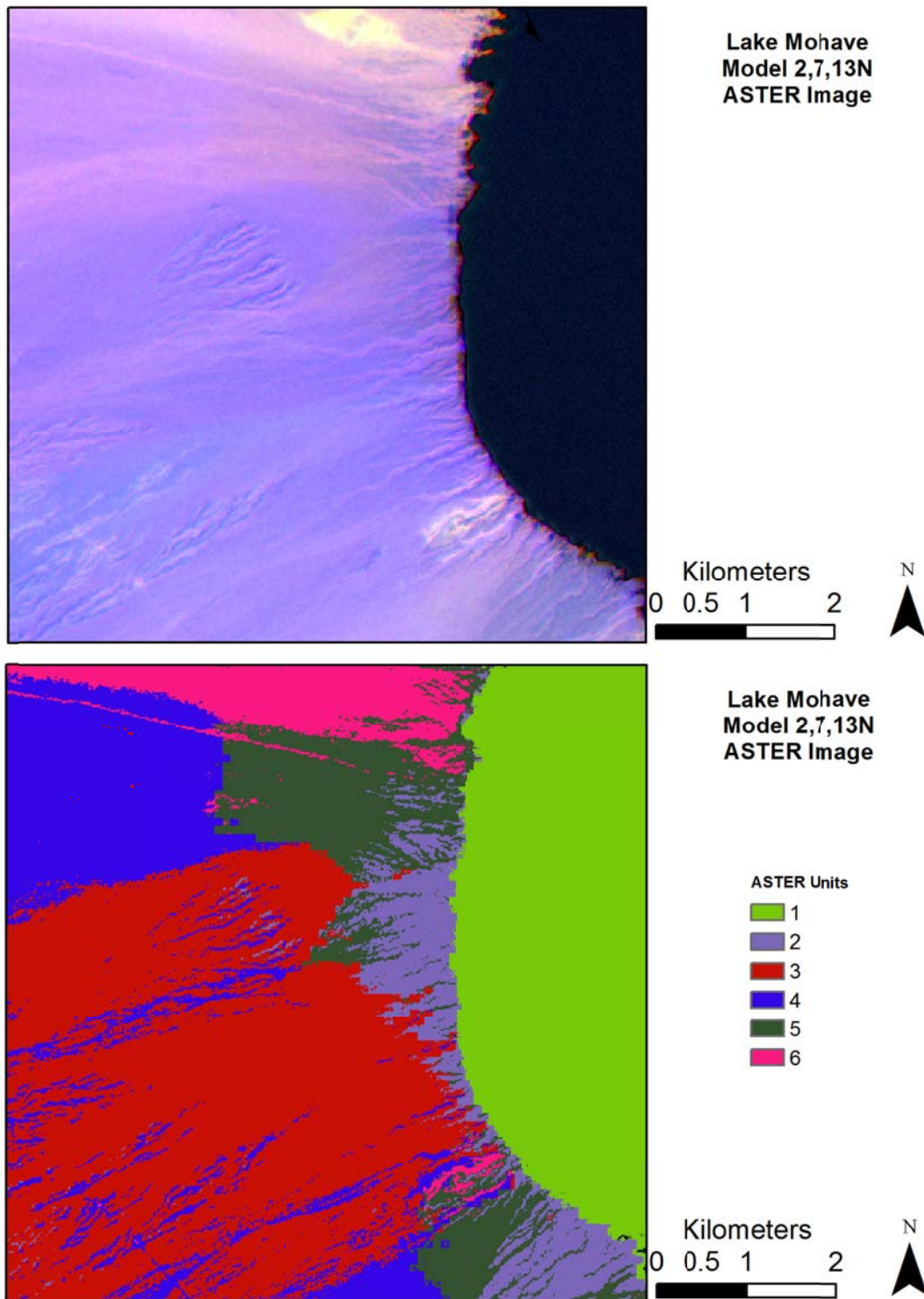


Figure 5-4: 2, 7, 13 clipped ASTER image (Abrams 2000) (top) and the classified image (bottom) at Lake Mohave.

Figure 5-5: Unclassified and Classifies 2,6,10 ASTER Image, Lake Mohave

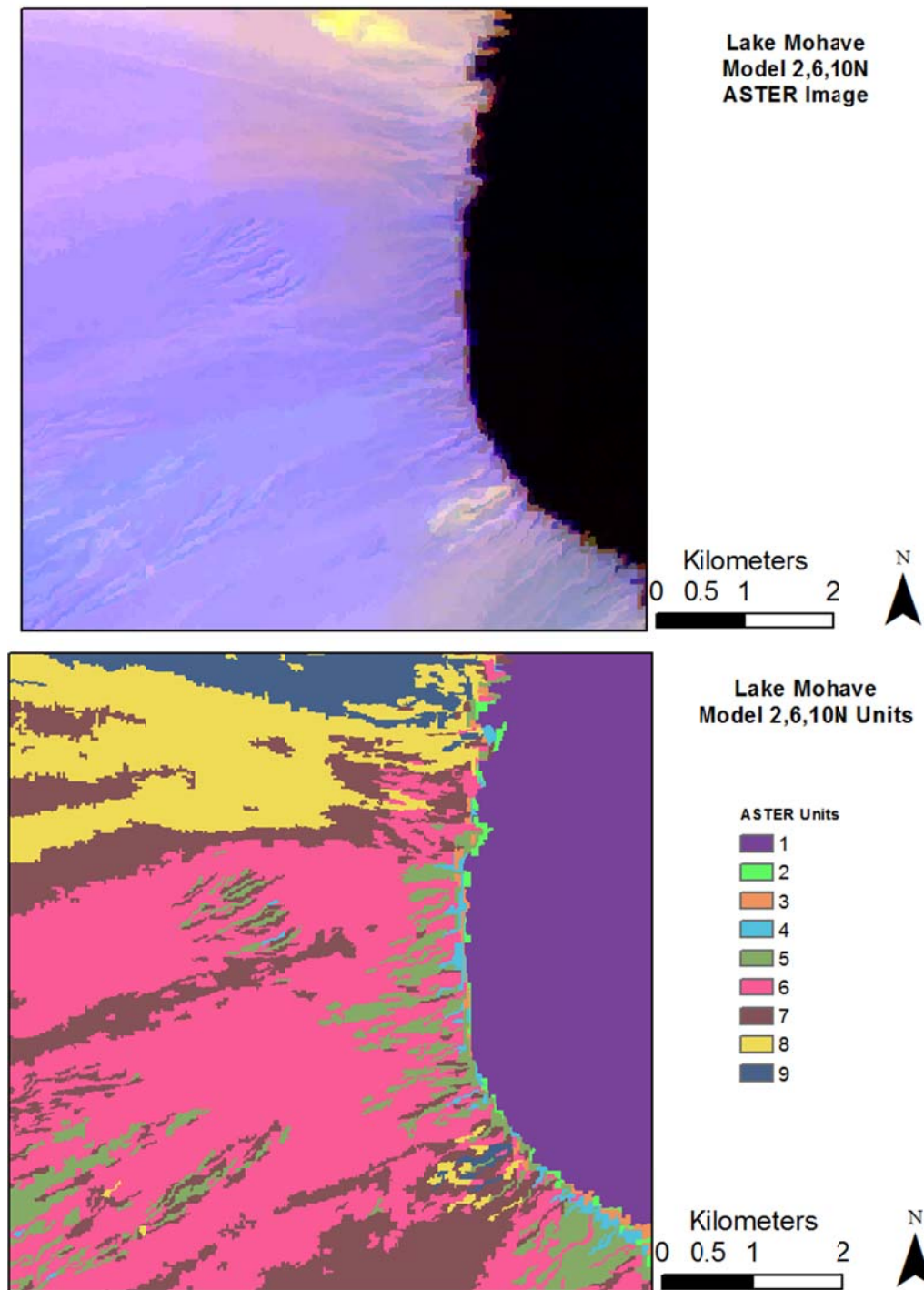


Figure 5-5: 2, 6, 10 ASTER image (Abrams 2000) (top) and the classified image (bottom) at Lake Mohave.

Figure 5-6: AMS Data at Government Wash

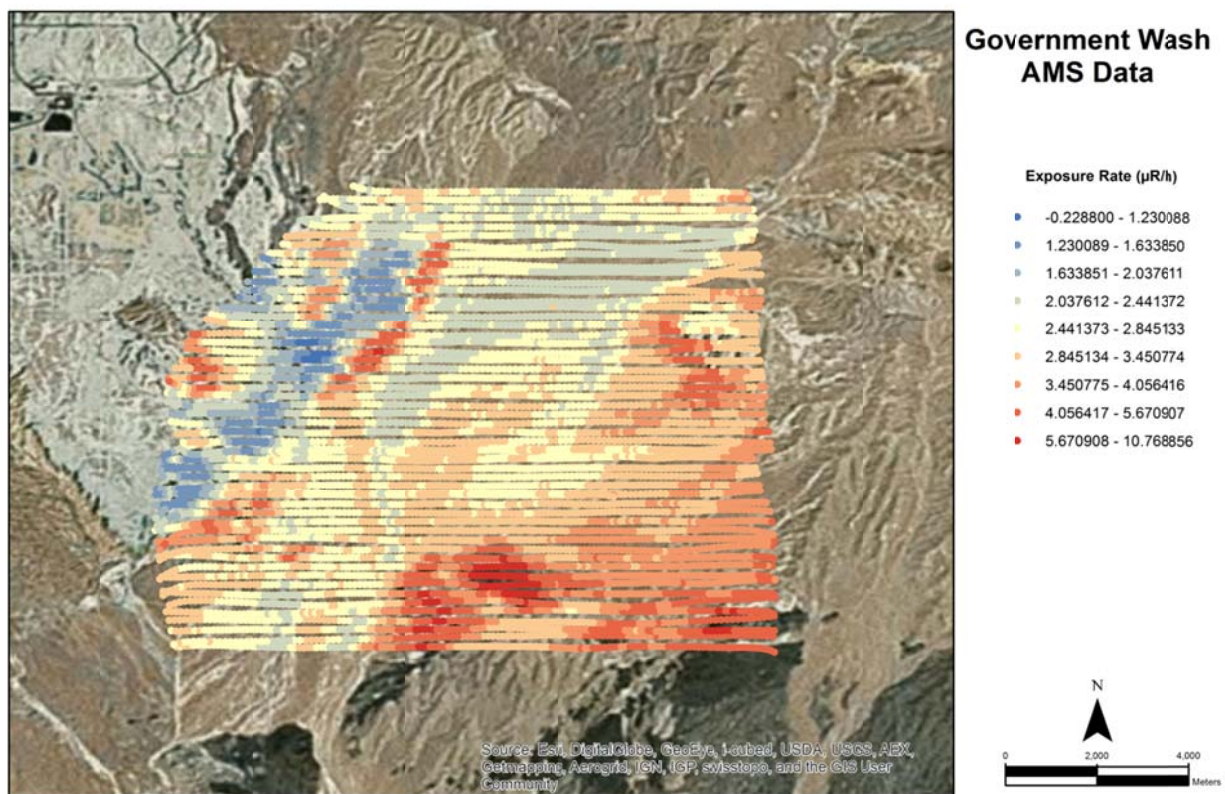


Figure 5-6: AMS exposure rate data at Government Wash.

Figure 5-7: AMS Data at Lake Mohave

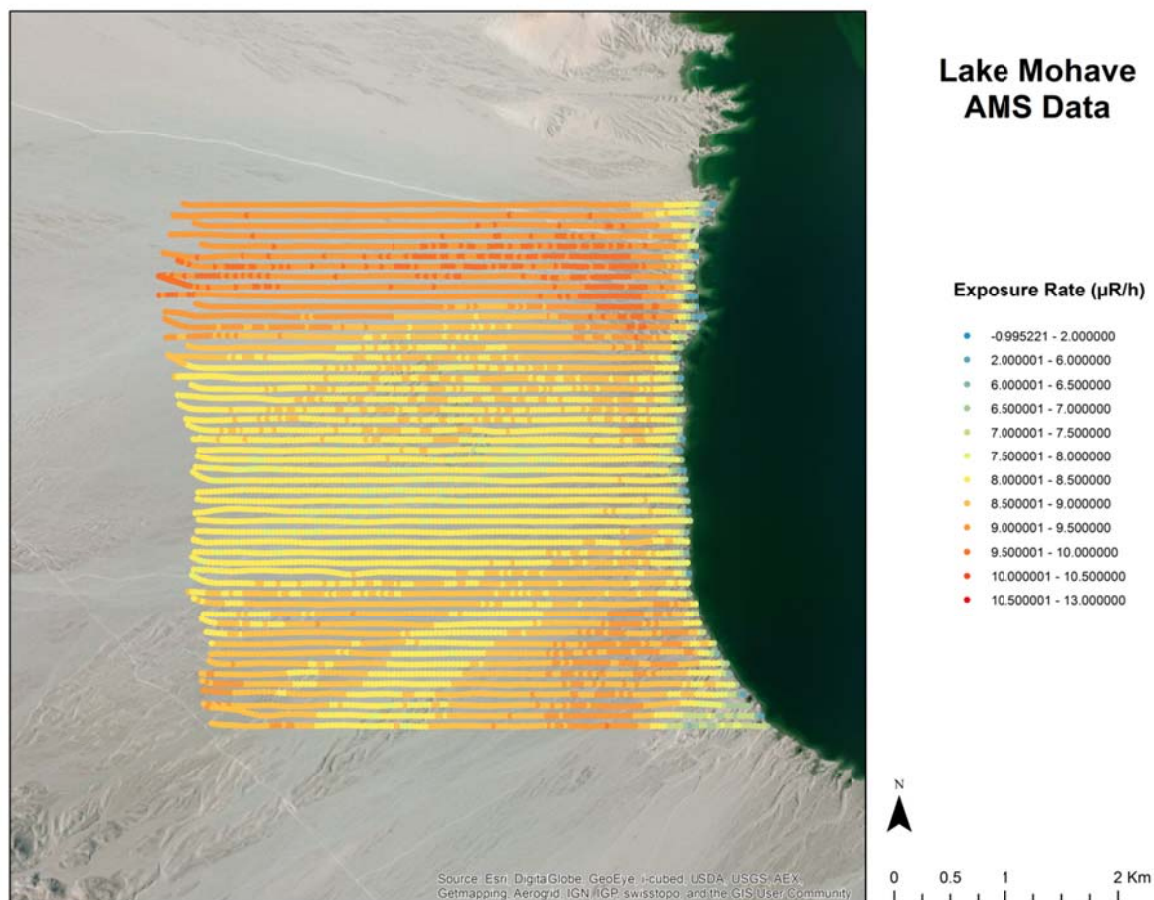


Figure 5-7: AMS data in the form of exposure rate at Lake Mohave.

Figure 5-8: Geochemical and NURE Data, Government Wash

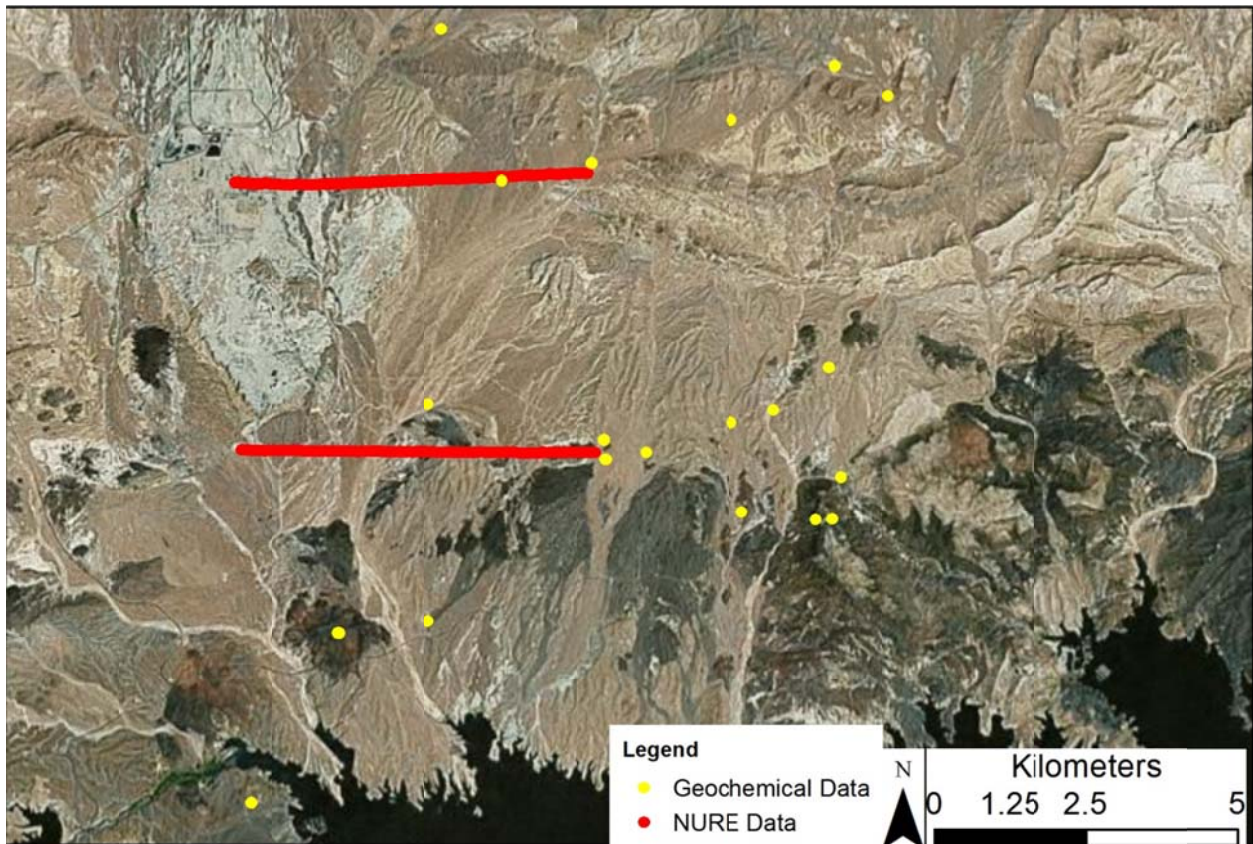


Figure 5-9: Geochemical and NURE data points located around the Government Wash modeling area. Geochemical data points are positioned according to their collection location. NURE data points occur as flight lines with 5 km spacing.

Figure 5-9: Geochemical and NURE Data, Lake Mohave

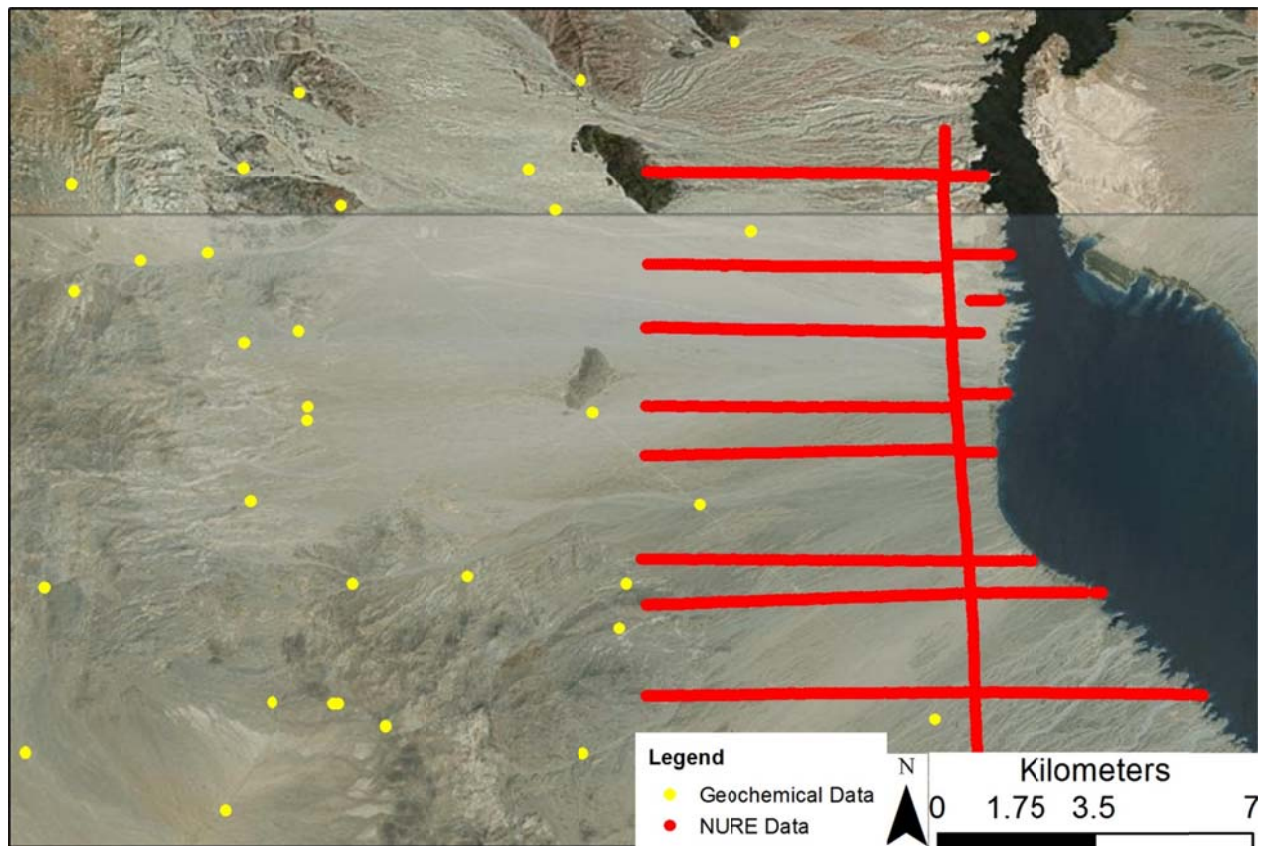


Figure 5-9: Geochemical and NURE data points located around the Lake Mohave modeling area. Geochemical data points are positioned according to their collection location. NURE data points occur as flight lines with 1-4 km spacing.

Figure 5-10: AMS to NURE Data Comparison, Lake Mohave

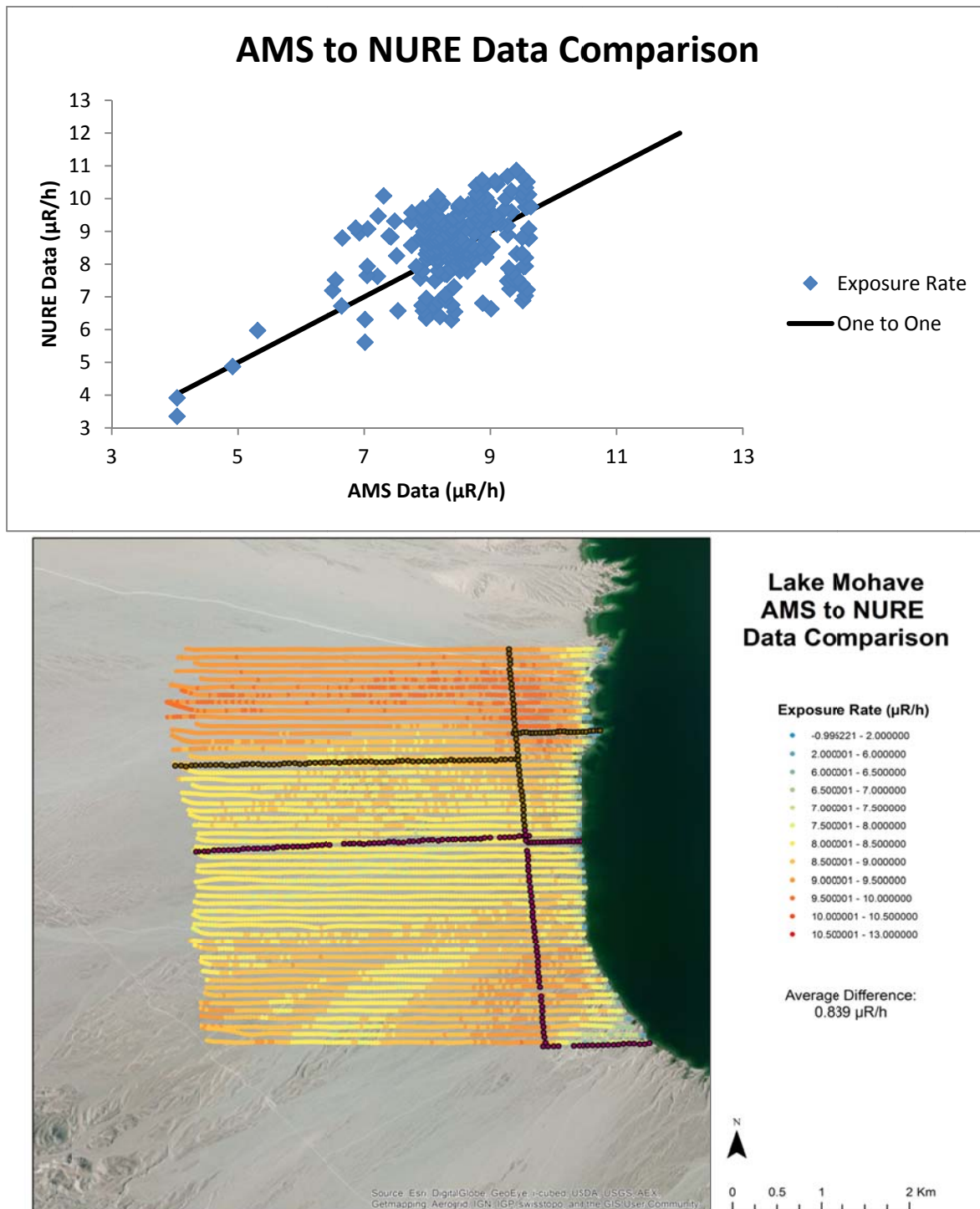


Figure 5-10: Plot (top) showing the relationship between the NURE line and the underlying AMS data (bottom) at Lake Mohave

Figure 5-11: AMS to NURE Data Comparison, Government Wash

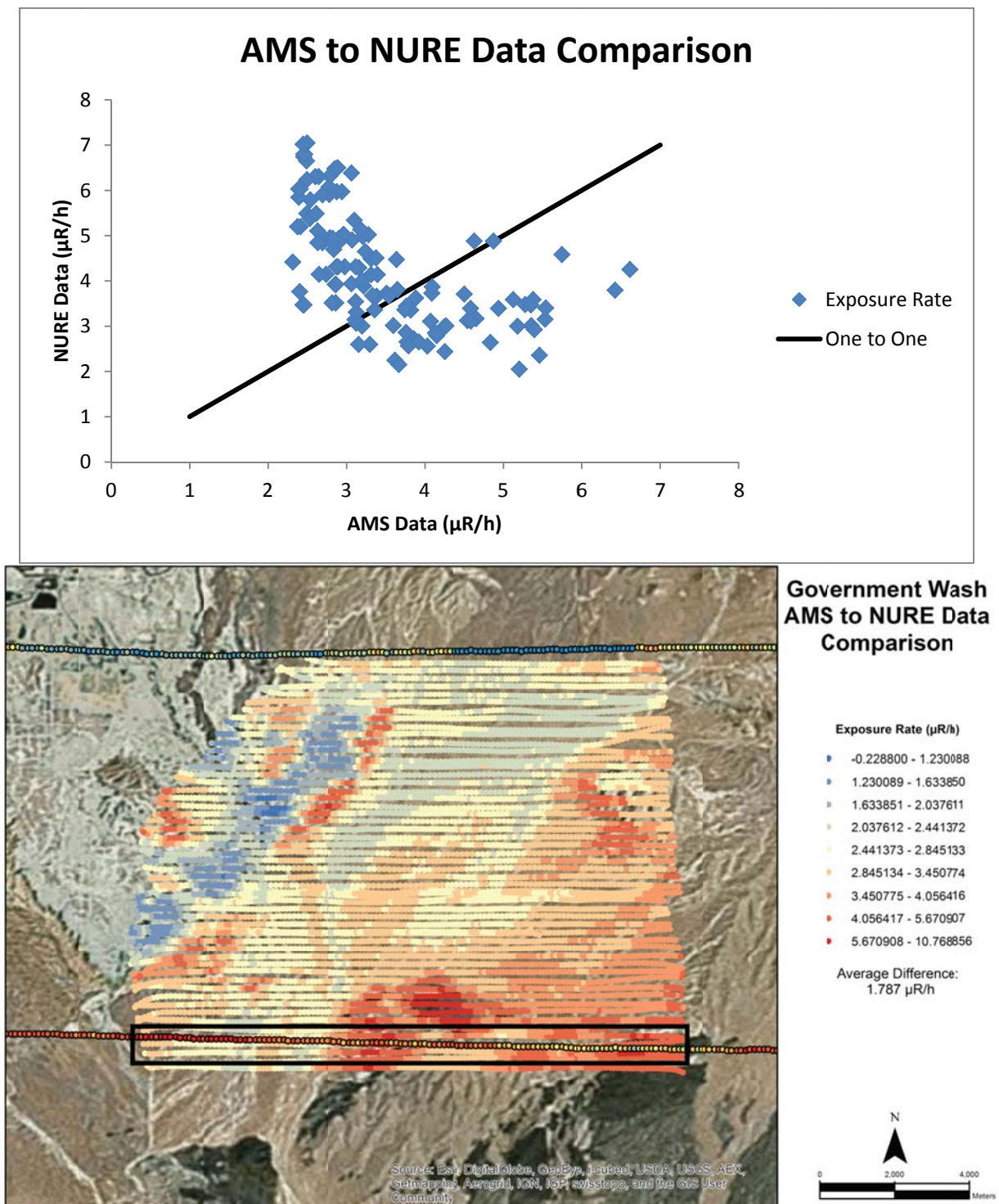


Figure 5-11: Plot (top) showing the relationship between the NURE line and the underlying AMS data (bottom) at Government Wash.

Figure 5-12: Predicted vs AMS Exposure Rate by Geologic Unit, Government Wash

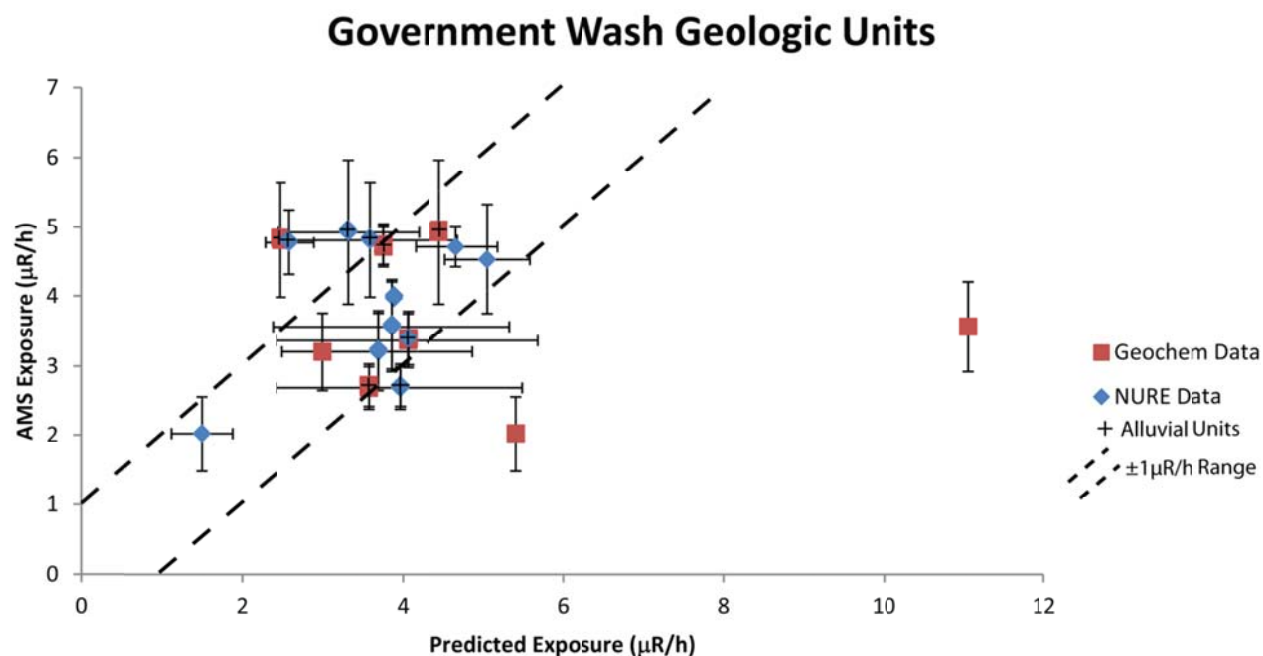


Figure 5-12: Plot showing the relationship between the predicted exposure rates and AMS mean exposure rates at Government Wash using geochemical and NURE data and geologic units to define radiation background units. Error bars are one standard deviation.

Figure 5-13: Point Difference Map, Geochemical Data, Government Wash

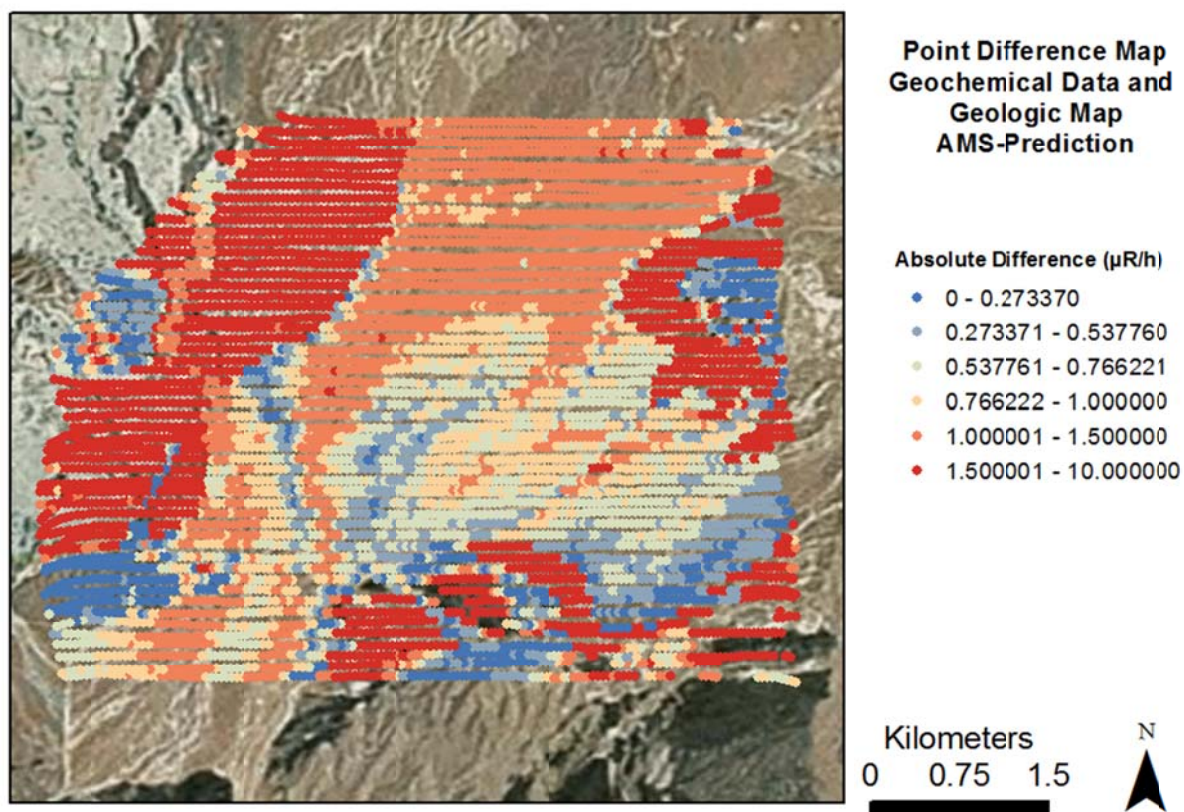


Figure 5-13: Absolute difference between AMS exposure rate data points and exposure rate prediction using geochemistry and geologic maps units at Government Wash.

Figure 5-14: Plot of K (wt%) Prediction vs AMS, Governemnt Wash

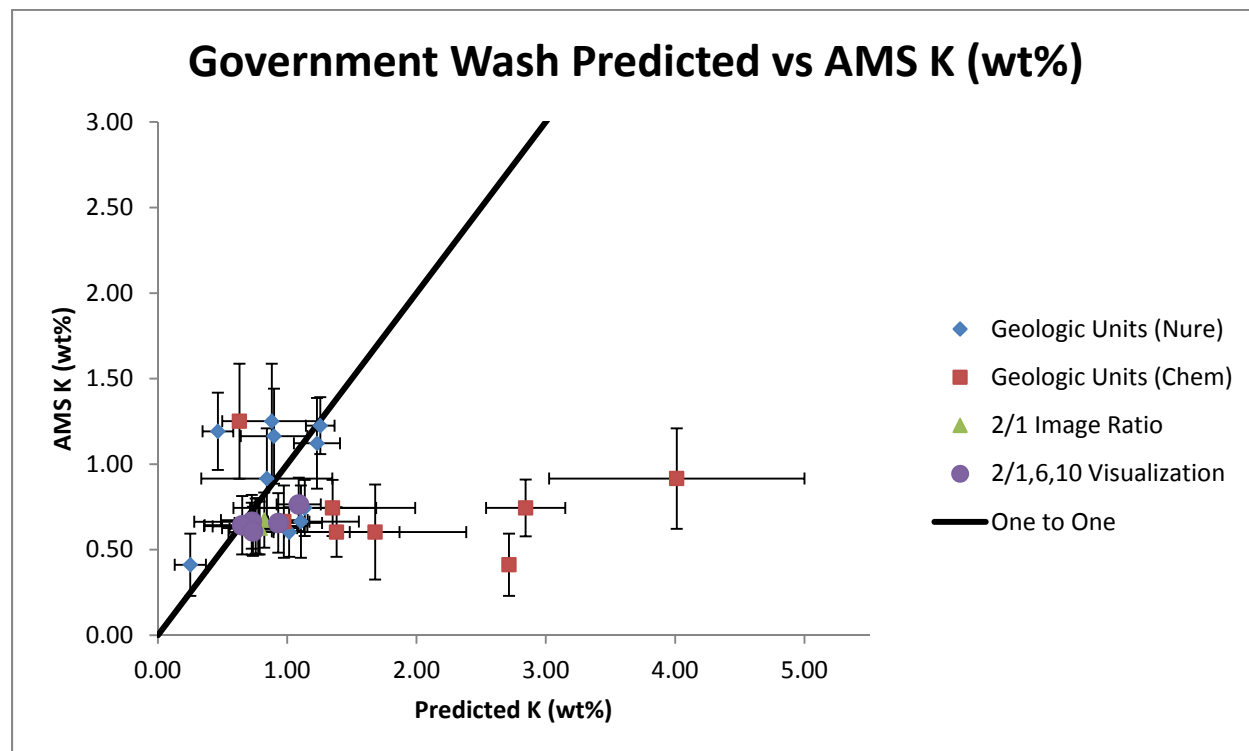


Figure 5-14: Plot showing the relationship between the predicted K (wt%) concentration and AMS mean concentration at Government Wash using geochemical (geologic units only) and NURE data with geologic units and ASTER imagery to define radiation background units. Error bars are one standard deviation.

Figure 5-15: Plot of U ppm Prediction vs AMS, Governemnt Wash

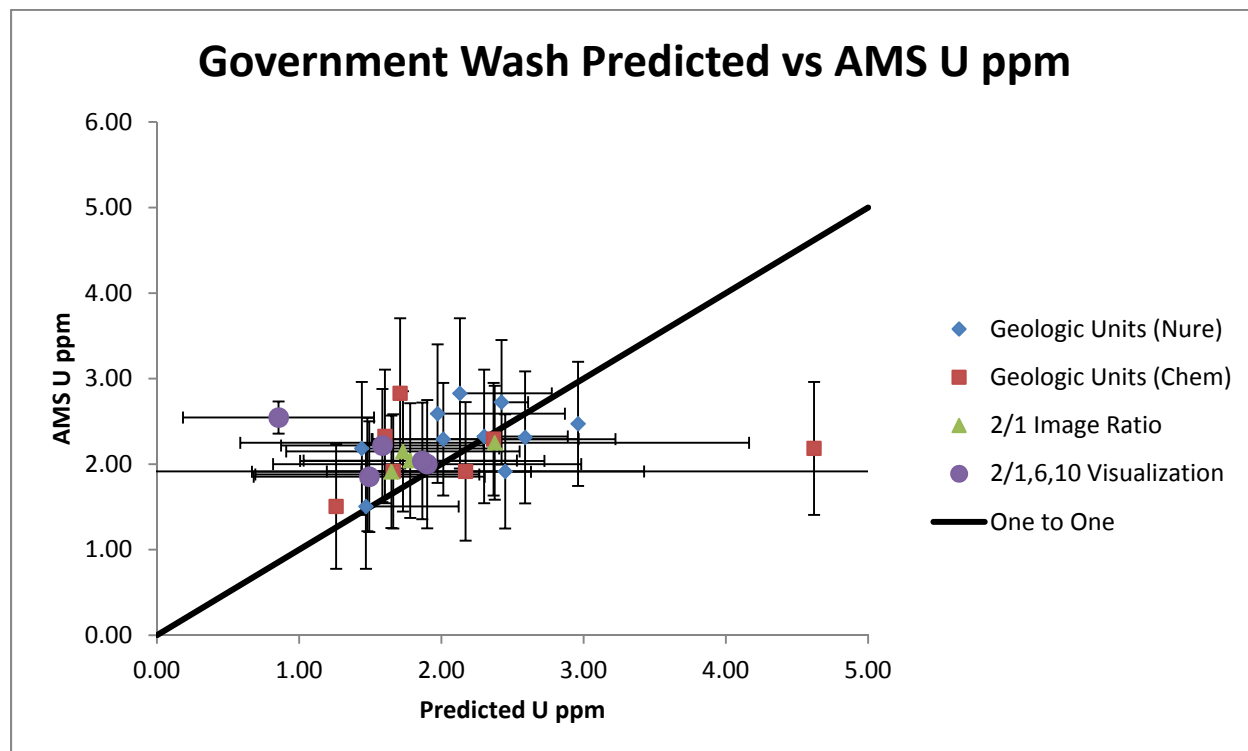


Figure 5-15: Plot showing the relationship between the predicted U ppm concentration and AMS mean concentration at Government Wash using geochemical (geologic units only) and NURE data with geologic units and ASTER imagery to define radiation background units. Error bars are one standard deviation.

Figure 5-16: Plot of Th ppm Prediction vs AMS, Governemnt Wash

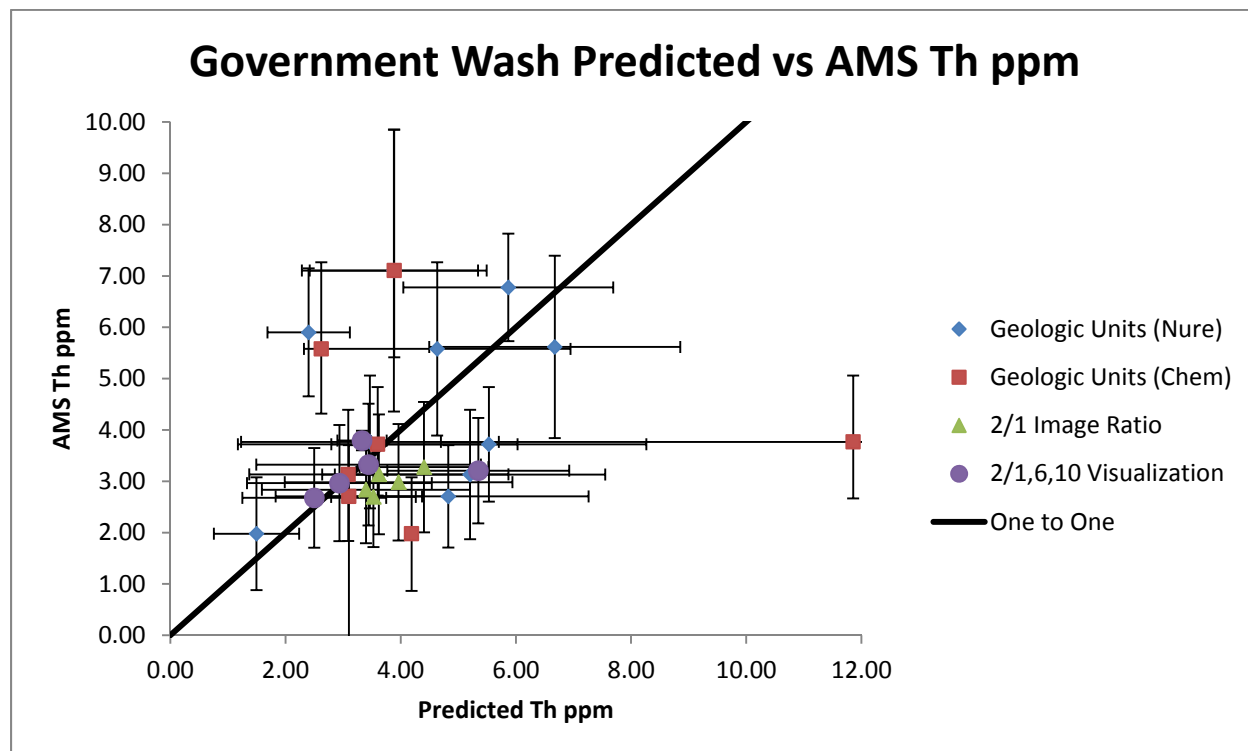


Figure 5-16: Plot showing the relationship between the predicted Th ppm concentration and AMS mean concentration at Government Wash using geochemical (geologic units only) and NURE data with geologic units and ASTER imagery to define radiation background units. Error bars are one standard deviation.

Figure 5-17: Point Difference Map, GMN Model, Government Wash

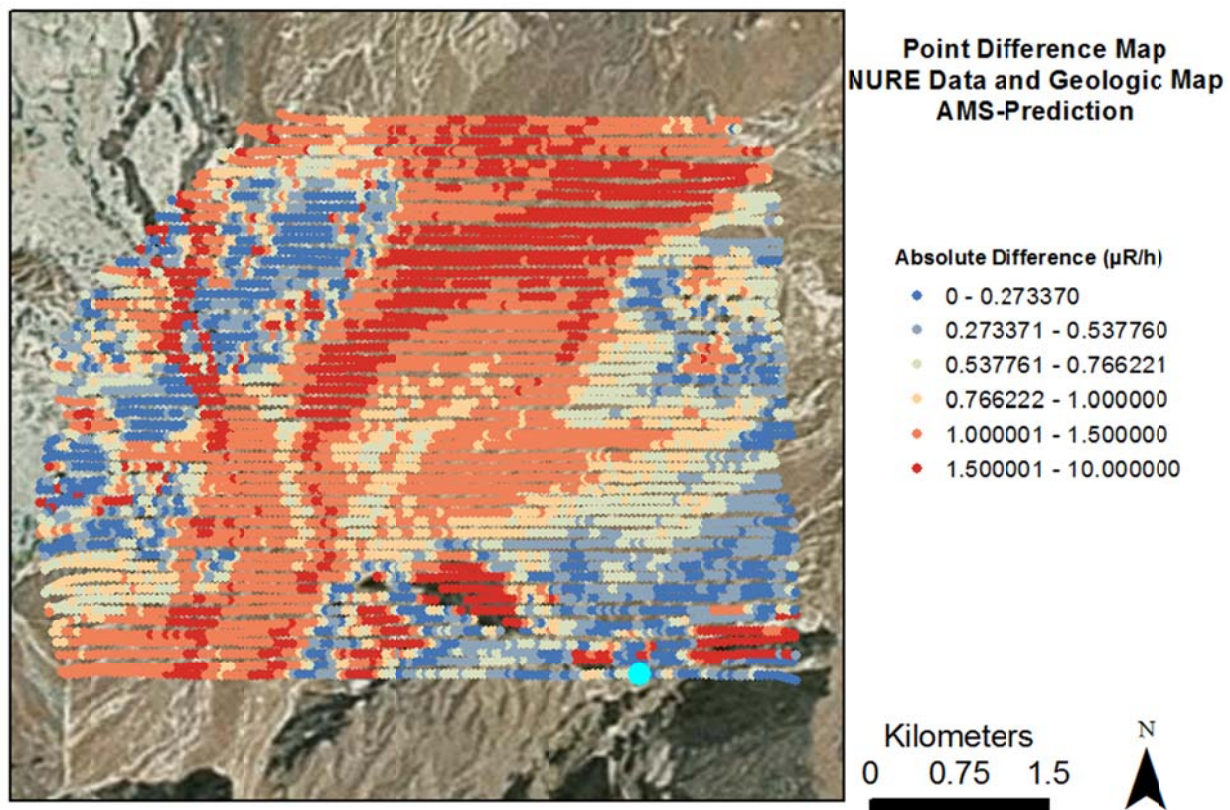


Figure 5-17: Absolute difference between AMS exposure rate data points and exposure rate prediction using NURE data and geologic maps units at Government Wash.

Figure 5-18: Predicted Exposure Rate, ASTER Units, Government Wash

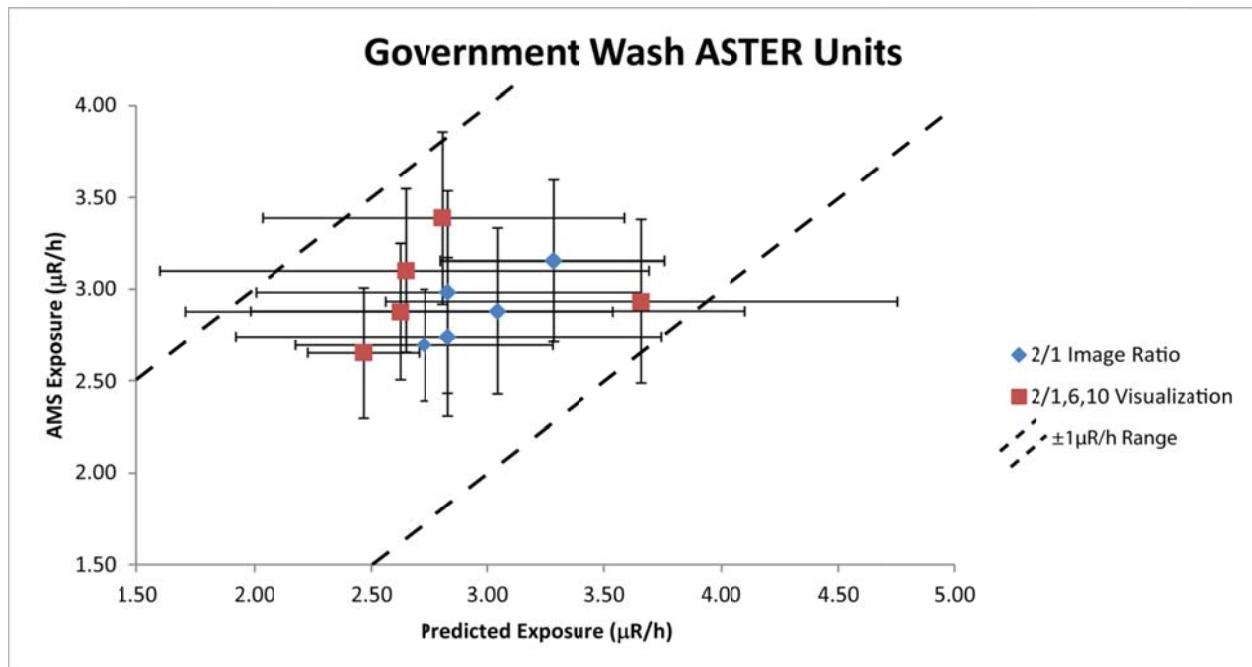


Figure 5-18: Plot showing the relationship between the AMS mean exposure rate data and exposure rate prediction using ASTER images to subdivide the Quaternary alluvium at Government Wash. Error bars are one standard deviation.

Figure 5-19: Point Difference Map, 2/1N Model, Government Wash

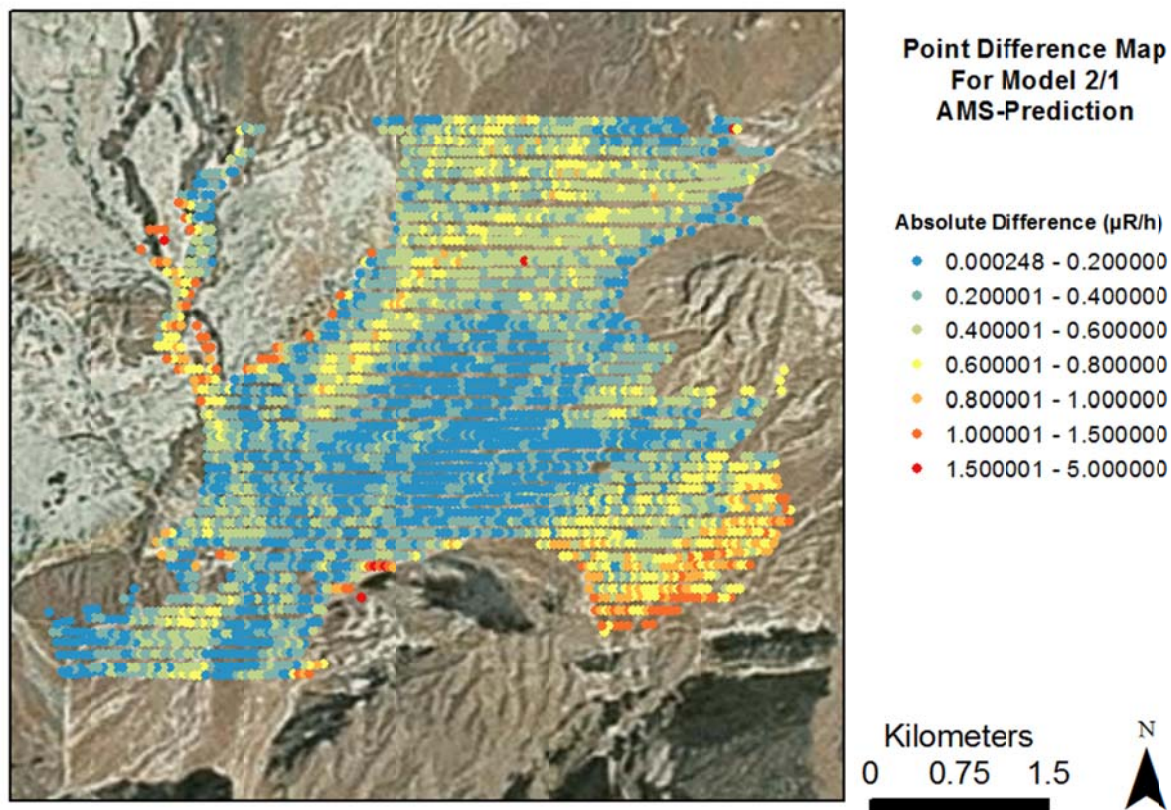


Figure 5-19: Absolute difference between AMS data points and exposure rate prediction for the 2/1N model at Government Wash.

Figure 5-20: Point Difference Map, 2/1,6,10N Model, Government Wash

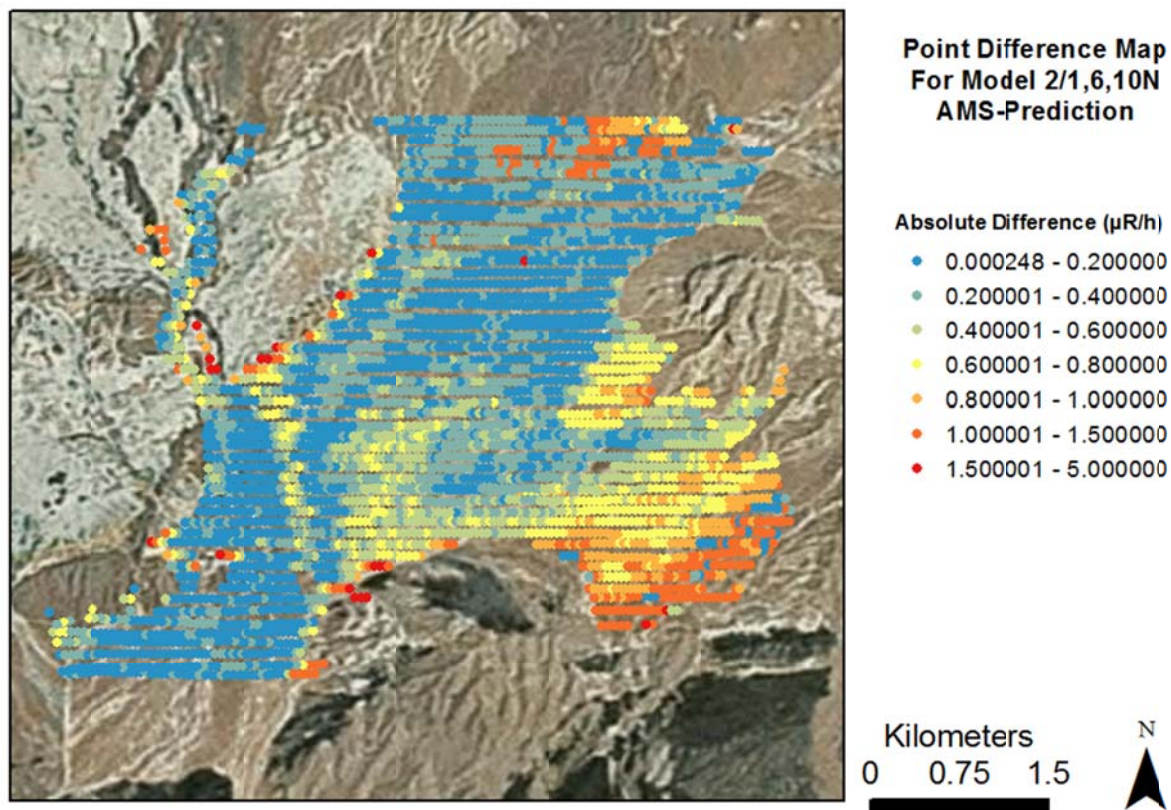


Figure 5-20: Absolute difference between AMS exposure rate data points and exposure rate prediction for the 2/1,6,10N model at Government Wash.

Figure 5-21: Predicted vs AMS Exposure Rate by Geologic Unit, Lake Mohave

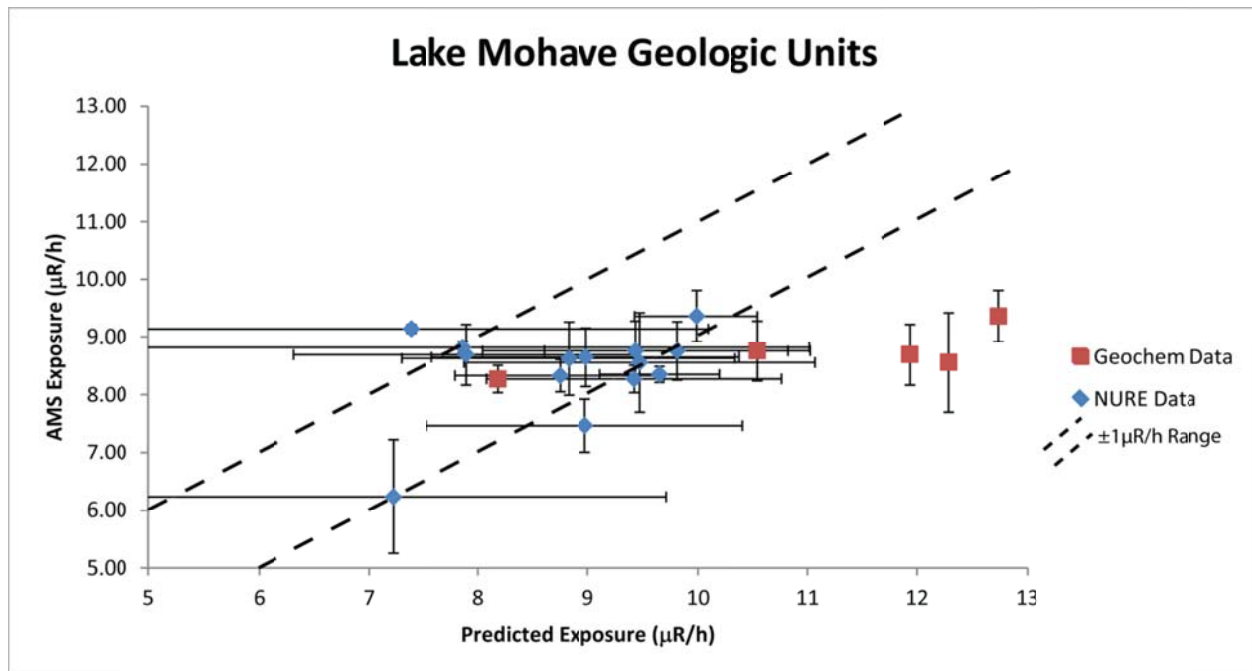


Figure 5-21: Plot showing the relationship between the predicted exposure rates and AMS mean exposure rates at Lake Mohave using geochemical and NURE data and geologic units to define radiation background units. Error bars are one standard deviation.

Figure 5-22: Point Difference Map, Geochemical Data, Lake Mohave

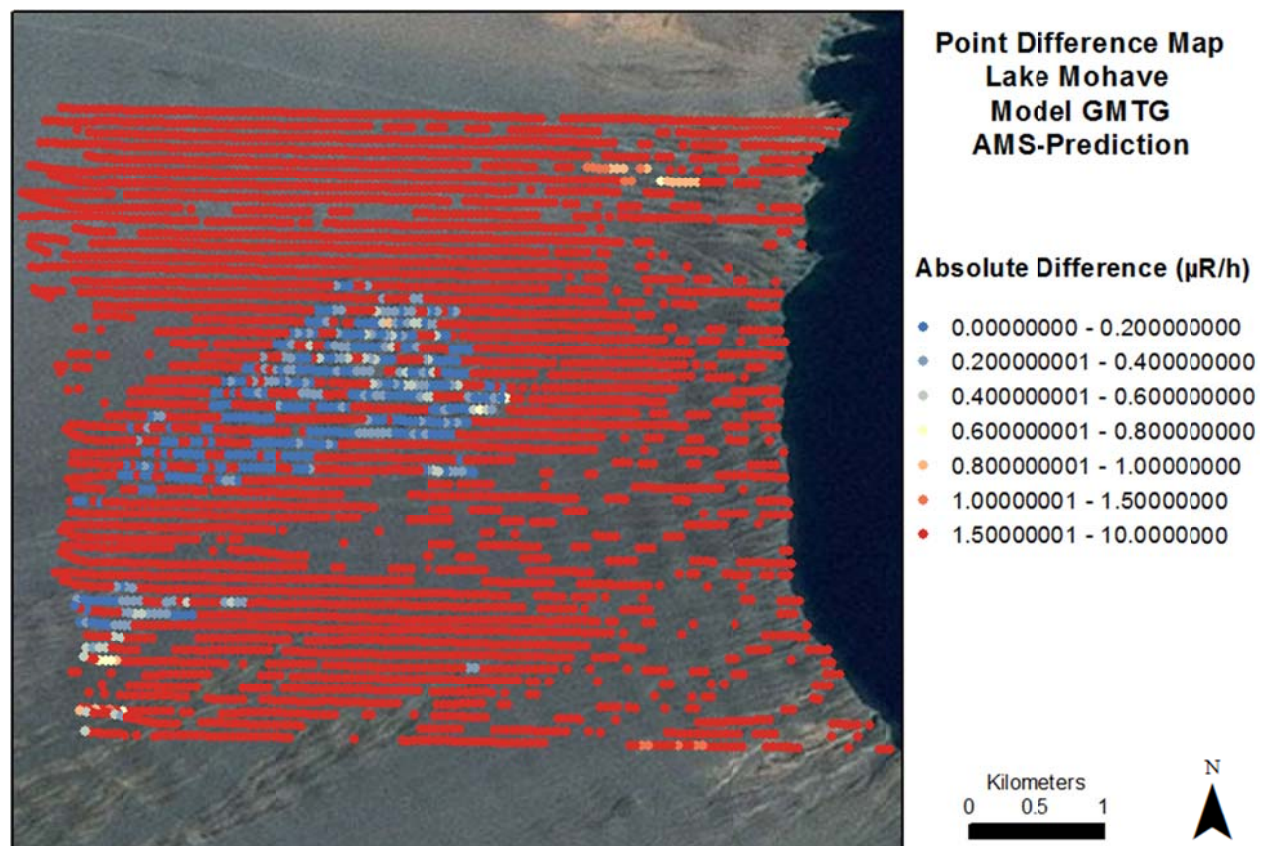


Figure 5-22: Absolute difference between AMS exposure rate data points and exposure rate prediction using for the GMTG model at Lake Mohave.

Figure 5-23: Plot of K (wt%) Prediction vs AMS, Lake Mohave

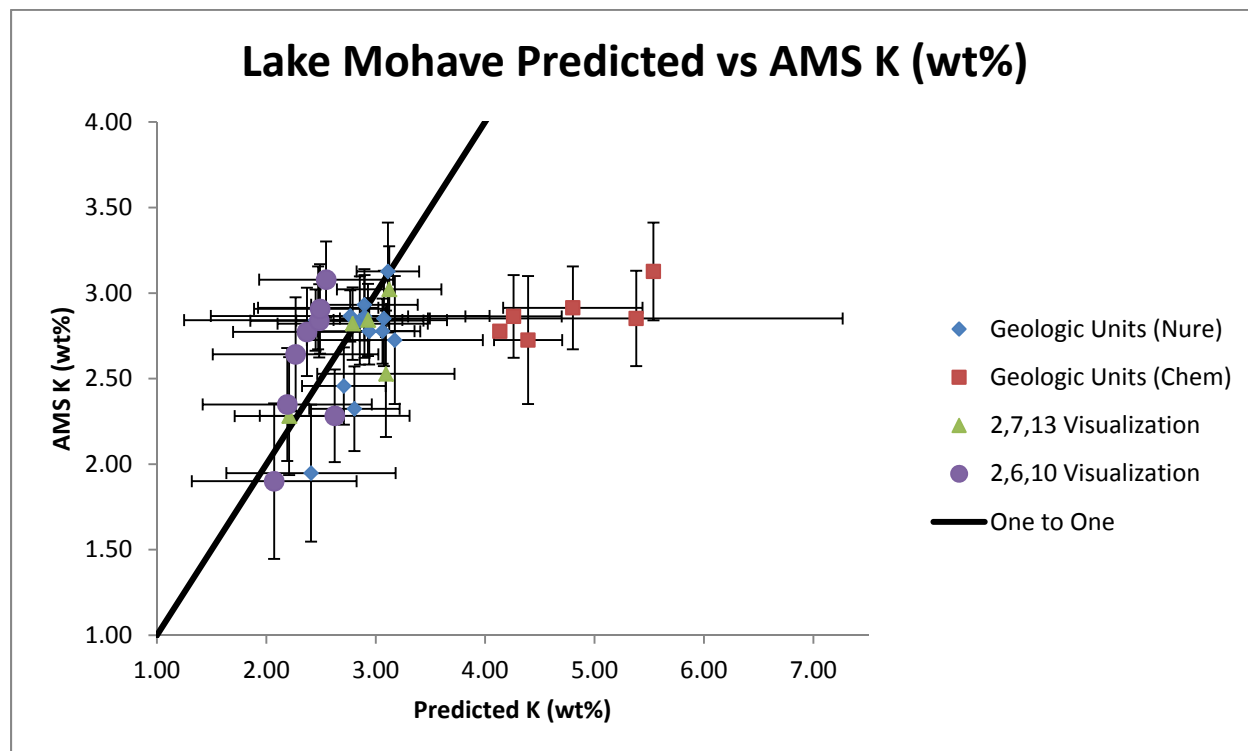


Figure 5-23: Plot showing the relationship between the predicted K (wt%) concentration and AMS mean concentration at Lake Mohave using geochemical (geologic units only) and NURE data with geologic units and ASTER imagery to define radiation background units. Error bars are one standard deviation.

Figure 5-24: Plot of U ppm Prediction vs AMS, Lake Mohave

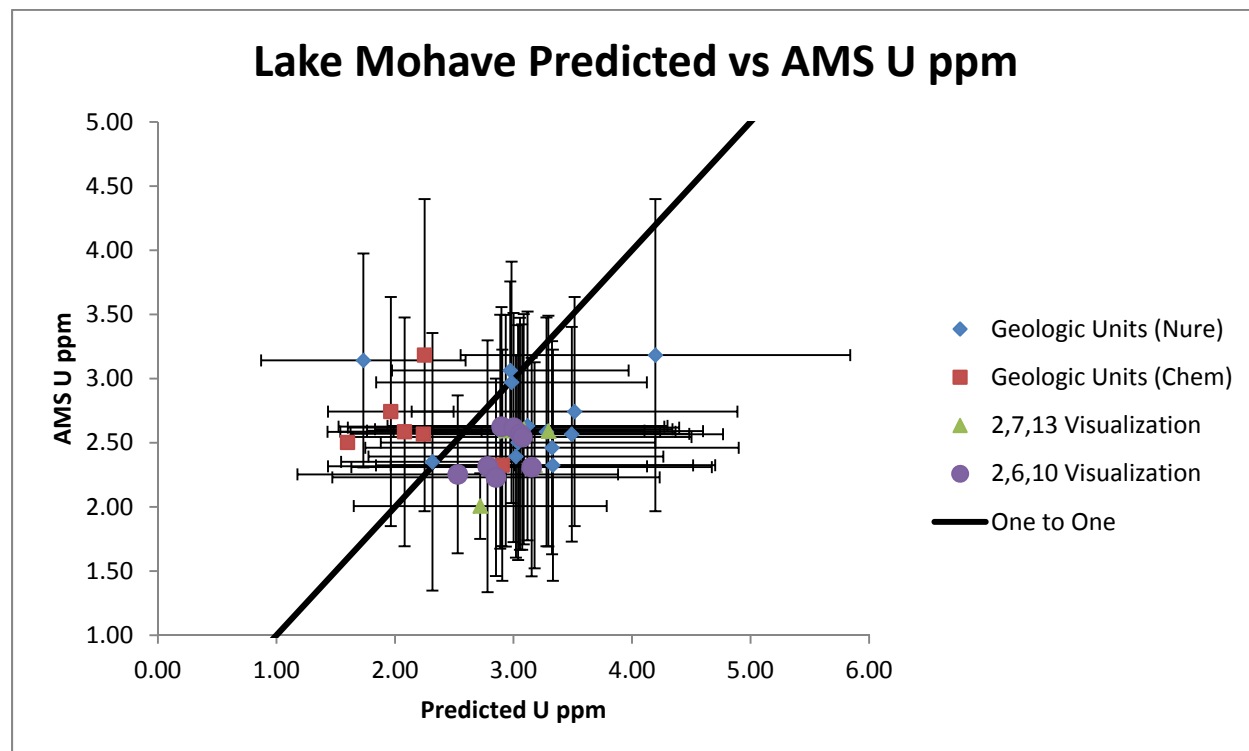


Figure 5-24: Plot showing the relationship between the predicted U ppm concentration and AMS mean concentration at Lake Mohave using geochemical (geologic units only) and NURE data with geologic units and ASTER imagery to define radiation background units. Error bars are one standard deviation.

Figure 5-25: Plot of Th ppm Prediction vs AMS, Lake Mohave

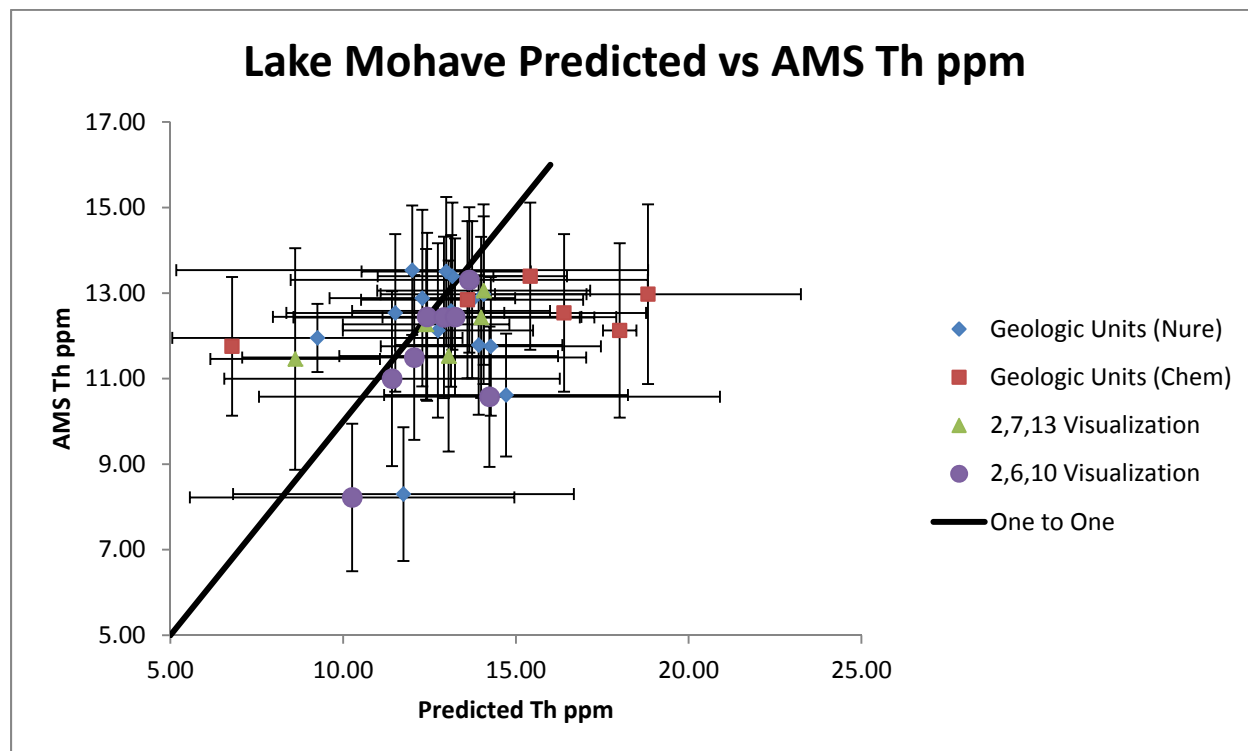


Figure 5-25: Plot showing the relationship between the predicted U ppm concentration and AMS mean concentration at Lake Mohave using geochemical (geologic units only) and NURE data with geologic units and ASTER imagery to define radiation background units. Error bars are one standard deviation.

Figure 5-26: Point Difference Map, GMN Model, Lake Mohave

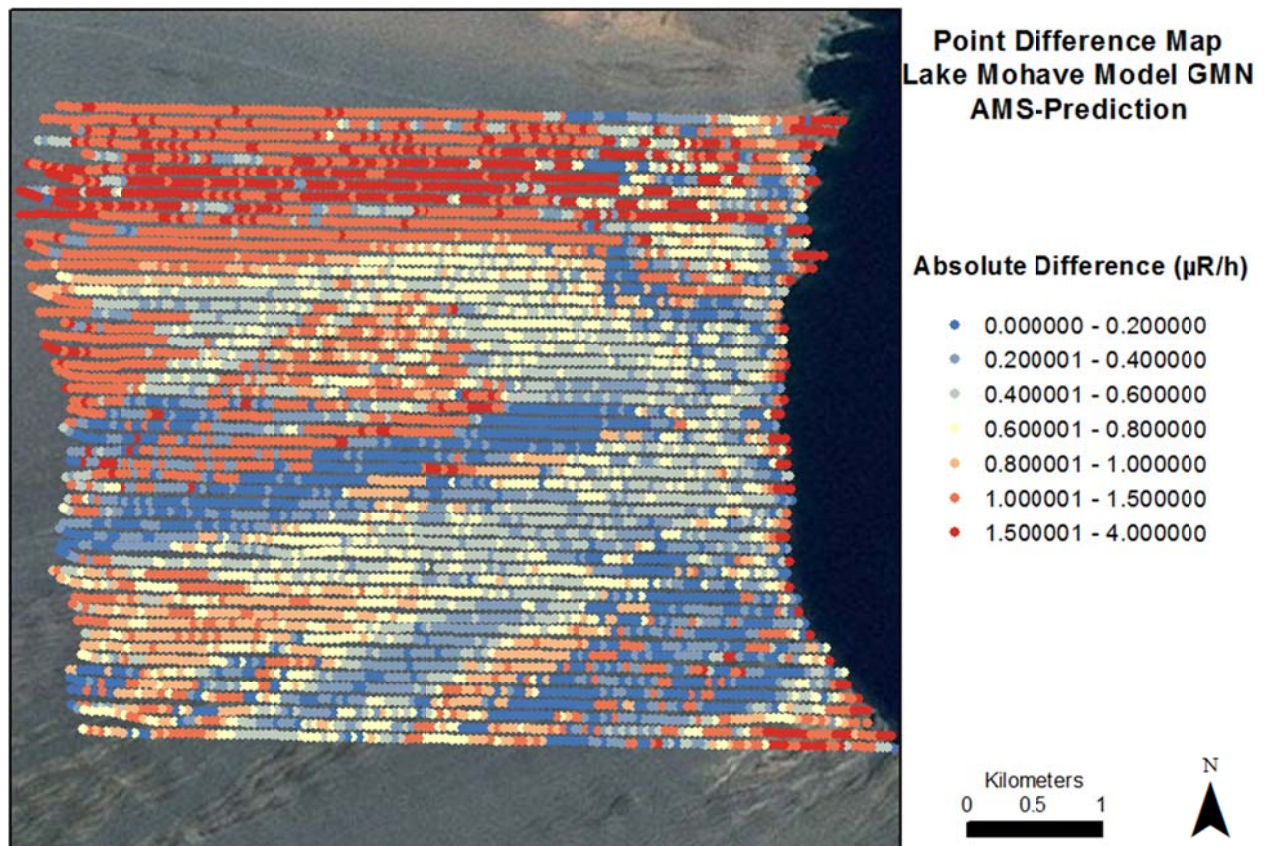


Figure 5-26: Absolute difference between AMS exposure rate data points and exposure rate prediction using for the GMN model at Lake Mohave.

Figure 5-27: Predicted Exposure Rate, ASTER Units, Lake Mohave

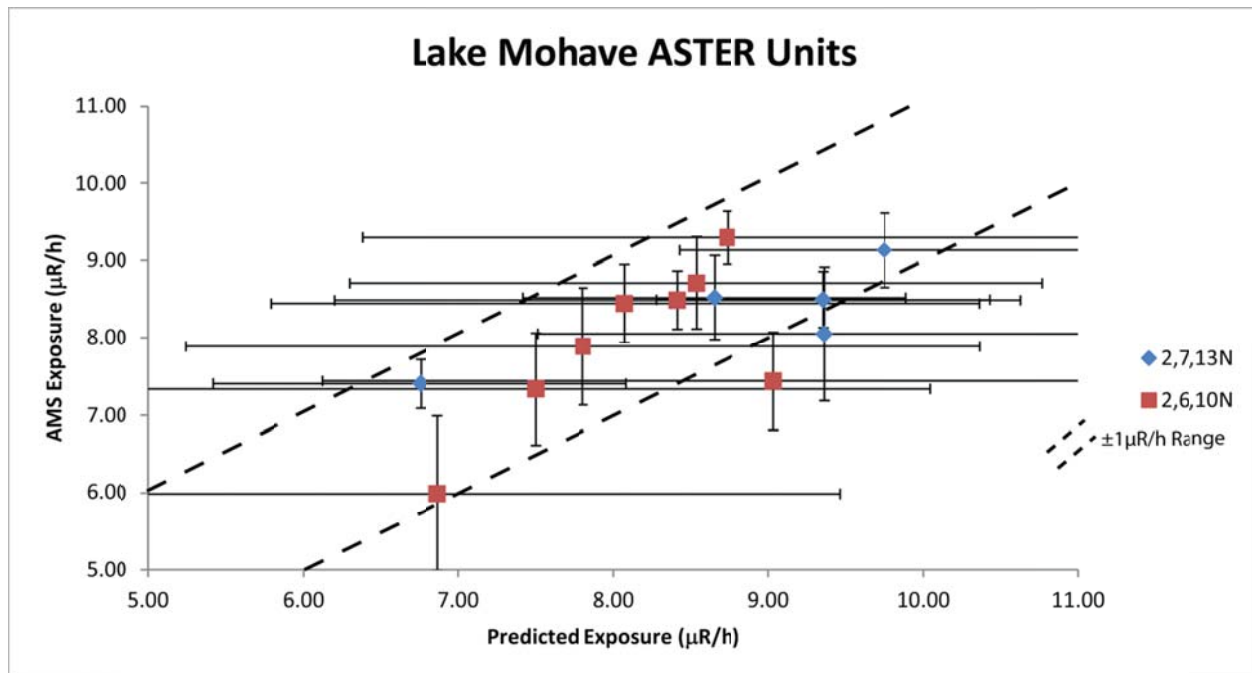


Figure 5-27: Plot showing the relationship between the AMS data and prediction using ASTER images at Lake Mohave. Error bars are one standard deviation.

Figure 5-28: Point Difference Map, 2,7,13N Model, Lake Mohave

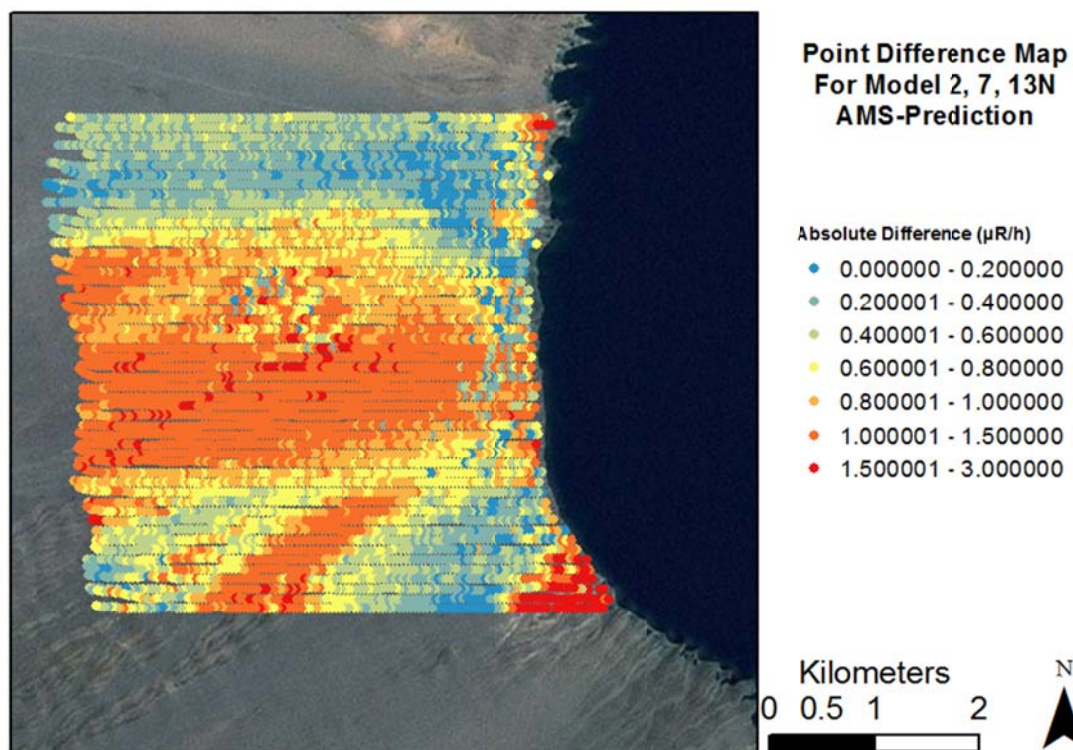


Figure 5-28: Absolute difference between AMS exposure rate data points and exposure rate prediction for the 2,7,13N model at Lake Mohave.

Figure 5-29: Point Difference Map, 2,6,10N Model, Lake Mohave

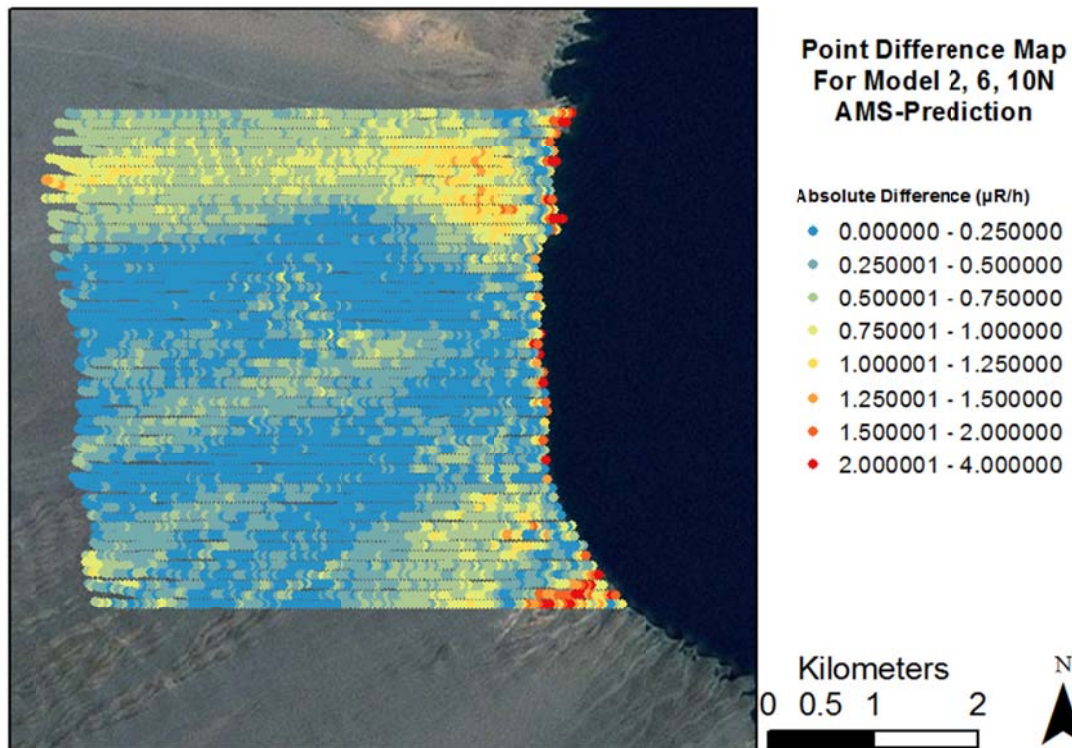


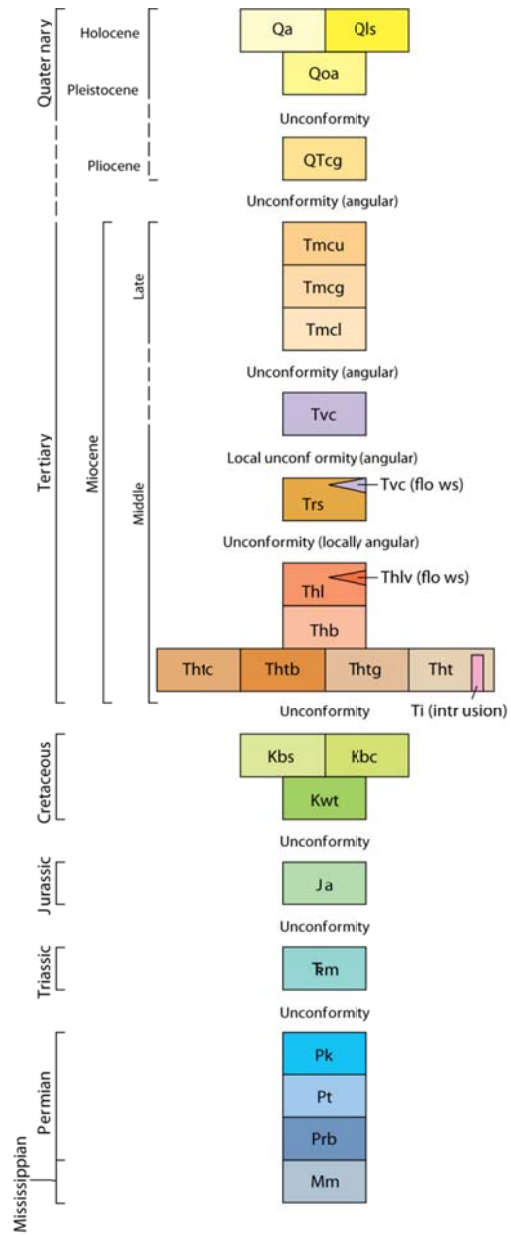
Figure 5-29: Absolute difference between AMS exposure rate data points and exposure rate prediction for the 2,6,10N model at Lake Mohave.

Appendix A: Government Wash Unit Report

Abstract

Government Wash lies within the Las Vegas Valley Shear Zone as mapped by Ernest Duebendorfer (2003) for the Nevada Bureau of Mines. This area has experienced between 23 and 69 km of displacement since the Miocene (Langenheim, Jachens and Schmidt). Most of the geologic units within the study area were deposited after the displacement ceased 8.5 Ma, and are a product of the paleo-erosion and transport (Langenheim, Jachens and Schmidt). Because of this, the Horse Spring and Muddy Creek Formations, the major formations in the area of interest, consist of materials derived from the previously displaced older units. As a result, many of the units are a fairly heterogeneous mix of rock types as they are a product of variable source material.

In the following analysis, all predicted exposure rates are calculated using Equation 4-1 from geochemical and NURE data points. Comparative data has been provided by the Aerial Measurement System (AMS) section of National Security Technologies, LLC (NSTec). The exposure rates presented are statistical representations derived from the AMS and NURE data points that occur within each unit. Units have been defined by referencing published descriptions by Duebendorfer (2003) as well as field observations. Units are listed in stratigraphic order.



Introduction

Government Wash is an area in Southern Nevada north of Lake Mead that lies within the Las Vegas Valley Shear Zone. On a larger scale this area experienced tectonic activity during the Cenozoic with displacement between 23 and 69 km (Langenheim, Jachens and Schmidt). The area of interest contains modern alluvial fans as well as sedimentary and volcanic units. The two major formations that occur in Government Wash are the Muddy Creek Formation and the Horse Spring Formation (Duebendorfer, 2003). The Muddy Creek Formation is middle to late Miocene in age and primarily composed of clastic sedimentary rocks ranging from siltstone to conglomerate. Portions of this formation also contain significant gypsum deposits such that they are currently being mined. The Horse Spring Formation is early Miocene in age and consists primarily of an ancient alluvial fan that was fed by carbonate as well as felsic and mafic igneous and metamorphic parent rocks. There are also interbeds of tuffaceous materials and basaltic flows from volcanic activity that was occurring during that time.

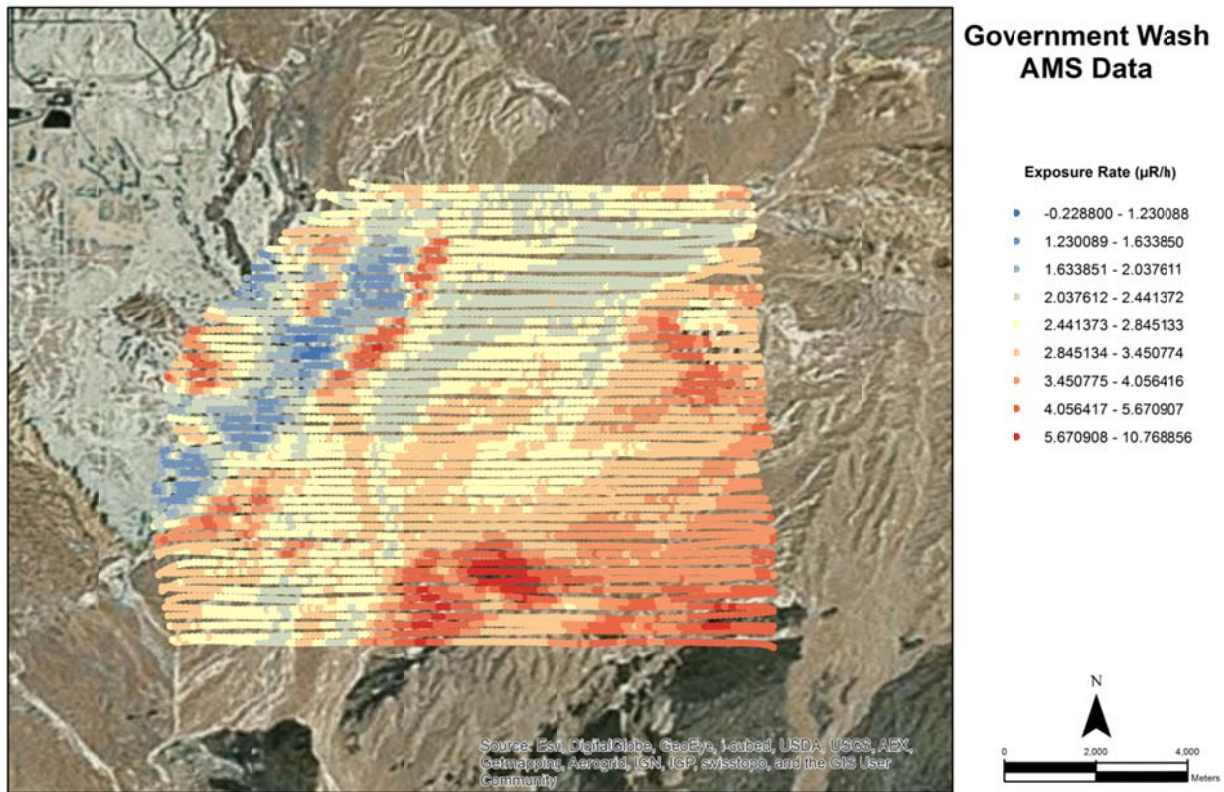
Outside of the area of interest there are older rocks that are Permian to Cretaceous in age that served as parent material for the younger units within the area of interest. The Willow Tank Formation is a late Cretaceous unit that is the remnant of a fluvial system and occurs northeast of the area of interest. This formation contains rocks from siltstones to rounded conglomerates but is primarily composed of medium grained sandstone. The Aztec Sandstone is also present in the northeast; it is the remnant of a Jurassic age erg that encompassed much of the American Southwest. It is entirely composed of eolian sands. The Moenkopi Formation also occurs in the northeast and is an early to middle Triassic age formation that is composed of fine sand deposited in a shallow marine environment. Finally, there are several Permian age limestone units which also occur north east of the area of interest. The Kaibab Formation, Toroweap Formation, and Monte Cristo Formation are a heavily

faulted but compositionally similar set of limestone formations. They are composed of thick grey featureless limestone with significant chert formation.

General Trends

There are general trends in the AMS data that appear to follow geologic trends. For example, exposure rates are highest in the southeast portion of the area of interest which is dominated by the Horse Spring Formation and coolest in the northwest which is dominated by the gypsum rich Muddy Creek Formation. Indeed, in many cases, geologic boundaries as well as weathering patterns are apparent in the AMS data. This is pronounced where there is high contrast between units like the hotter Tmcl that is exposed from under Tmcg which is much cooler. The sliver of Tmcl that is exposed also shows a weathering pattern that trails off southward.

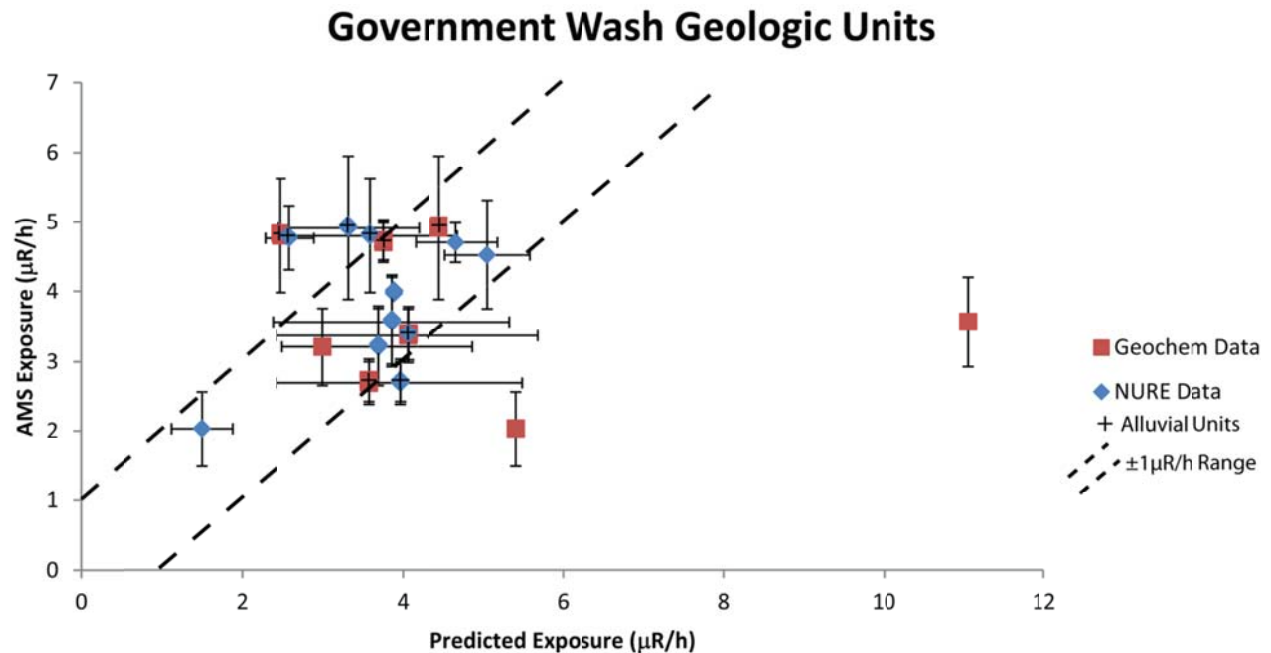
Alluvium units are typically defined by age rather than composition. Therefore, each alluvial unit may contain material from multiple sources that all have unique chemical compositions. This is expressed in the AMS data as heterogeneity in concentrations of K, U, and Th as well as exposure rate. Similar to the recent Quaternary age alluvium, the Horse Spring units are largely composed of ancient alluvium and shows considerable heterogeneity.



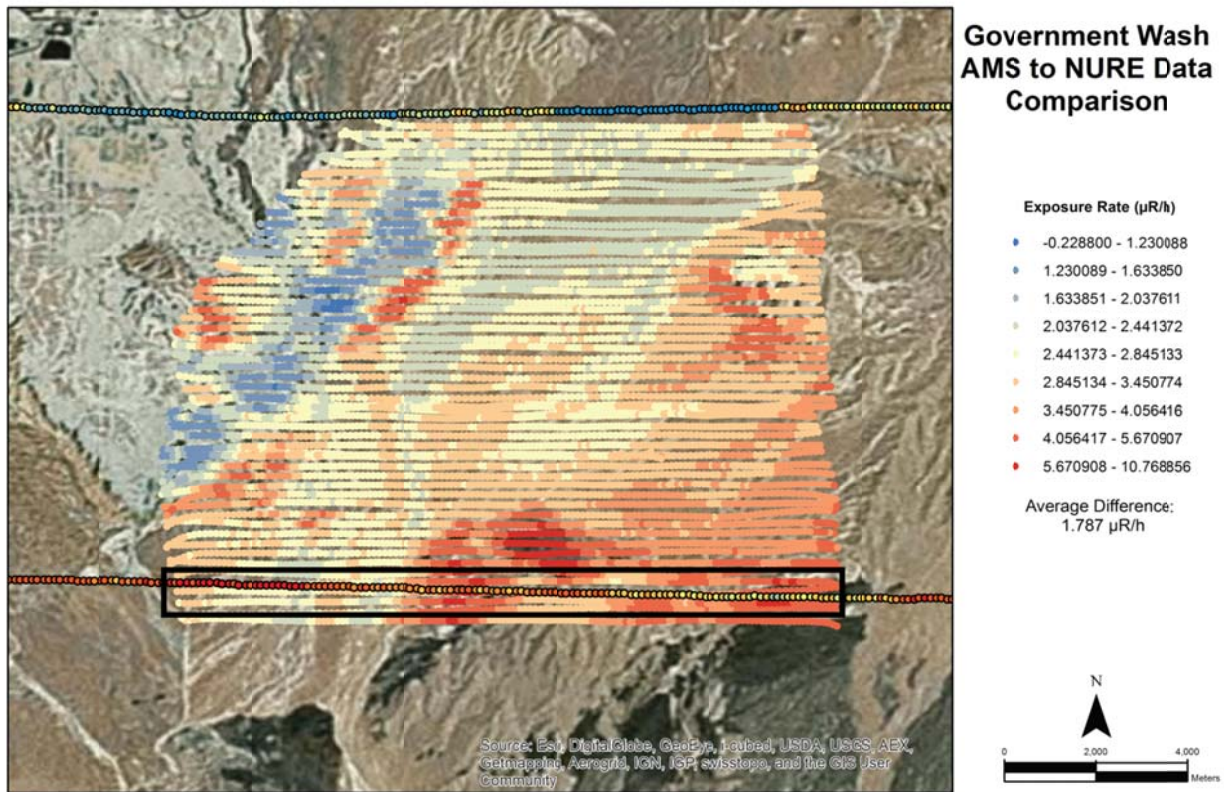
Data Sources

There are two major sources of geochemical data used in this study. In general we refer to the two major sources of data as traditional geochemistry, and NURE data. Traditional geochemistry is sourced from several online databases including: the National Uranium Resource Evaluation (NURE) Survey (geochemical section), Geochemical Rock Database (GeoRoc), and Integrated Earth Data Applications (IEDA). NURE aerial survey data consists of data derived from a national scale aerial gamma ray survey. Since the traditional geochemistry and NURE data are derived using different techniques they are used to create separate models.

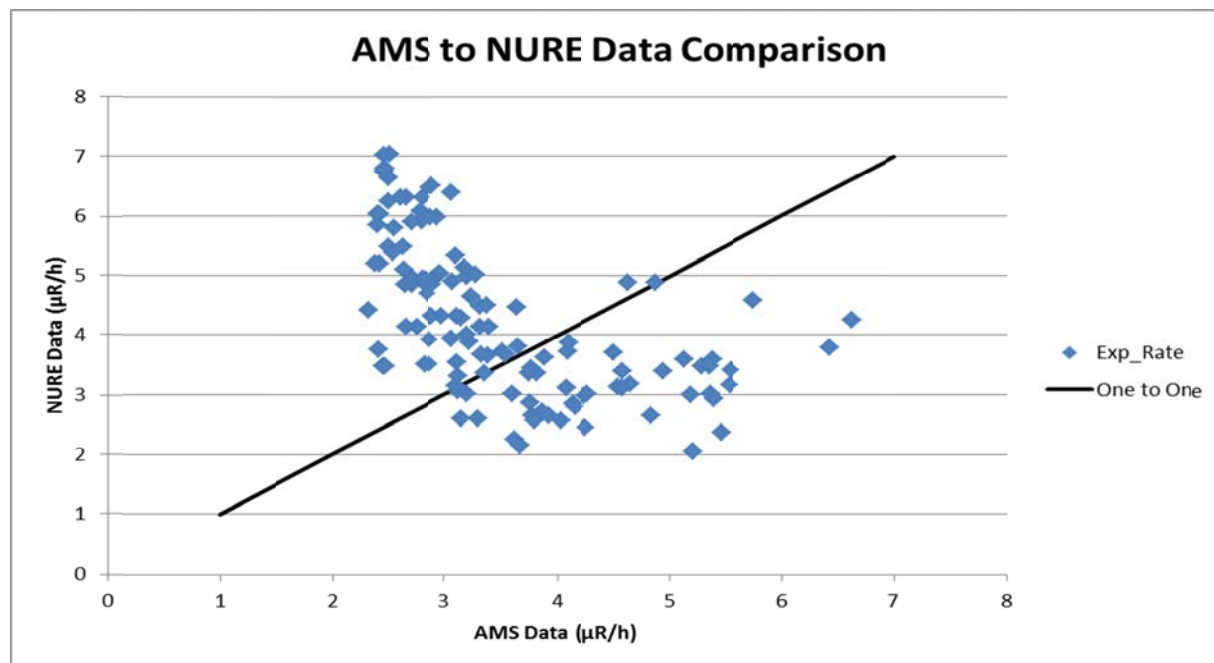
In the figure below, the predicated exposure rate for each geologic unit is plotted against the mean of the AMS data within that unit; error bars represent one standard deviation. The traditional geochemistry is generally more spread out when compared to the NURE data. Generally, the NURE data is within the “success range” defined as $\pm 1\mu\text{R/h}$. The exceptions to this are modern or paleo alluvial units which are mostly just outside of this range.



The NURE data is the result of a series of aerial gamma ray surveys flown in the 1970's to assess the distribution of U across the contemporaneous United States. One NURE flight line overlaps with the AMS survey in Government Wash and a comparison was made between these two datasets. In the figure below there is a NURE data line that occurs in the southern portion of the area of interest. By visual inspection it appears that the data in the line have very little correlation with the AMS dataset that it overlies.

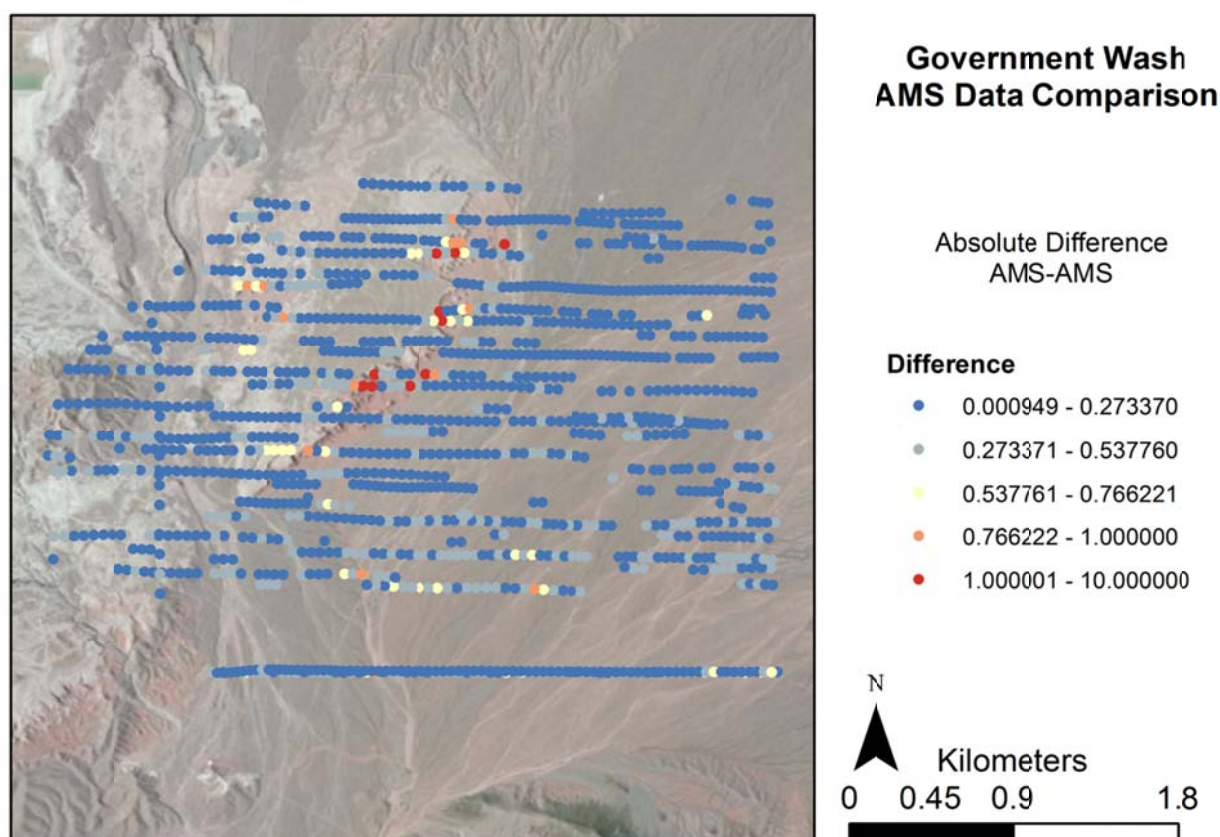


When the NURE data in the south is compared to the closest AMS data point (within 50m) in the figure below it becomes clear that there is no relationship between these data.



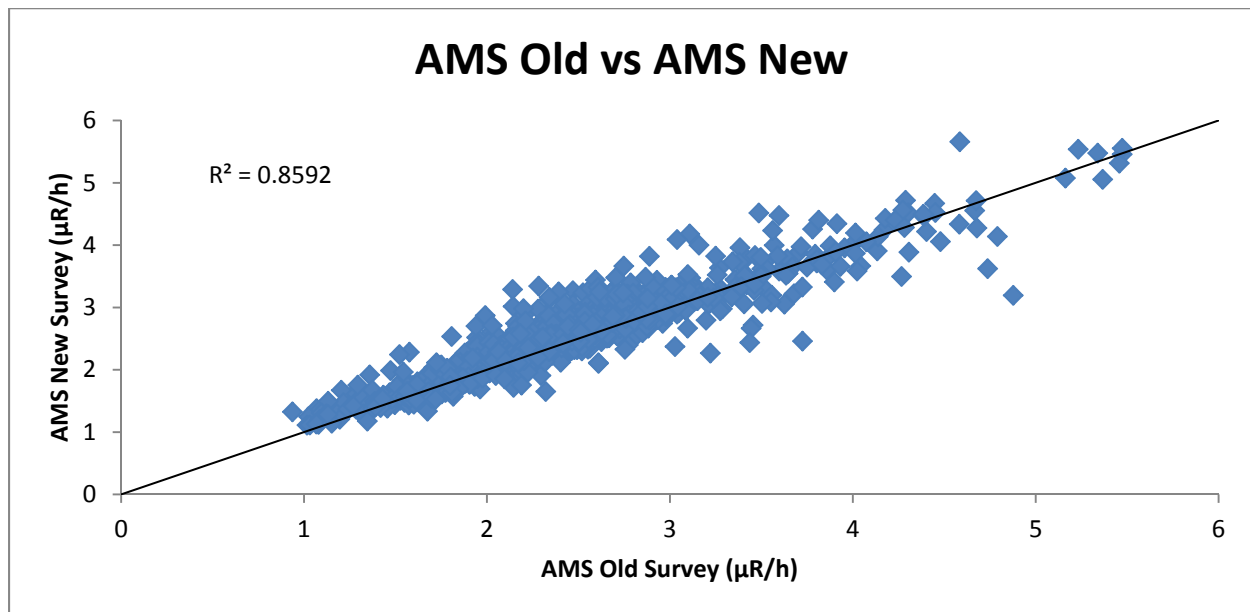
Reproducibility of AMS Data

One of the questions surrounding the AMS surveys in general is how reproducible the dataset is from one flight to another. There are two datasets provided by AMS over Government Wash from two separate flights. The earlier flight covers a smaller spatial area than the later flight. To compare the two datasets the points were joined using the Spatial Join tool in ArcGIS set to join points that are within 25m of each other which is within the resolution of the detector. The figures below show the results of this comparison.

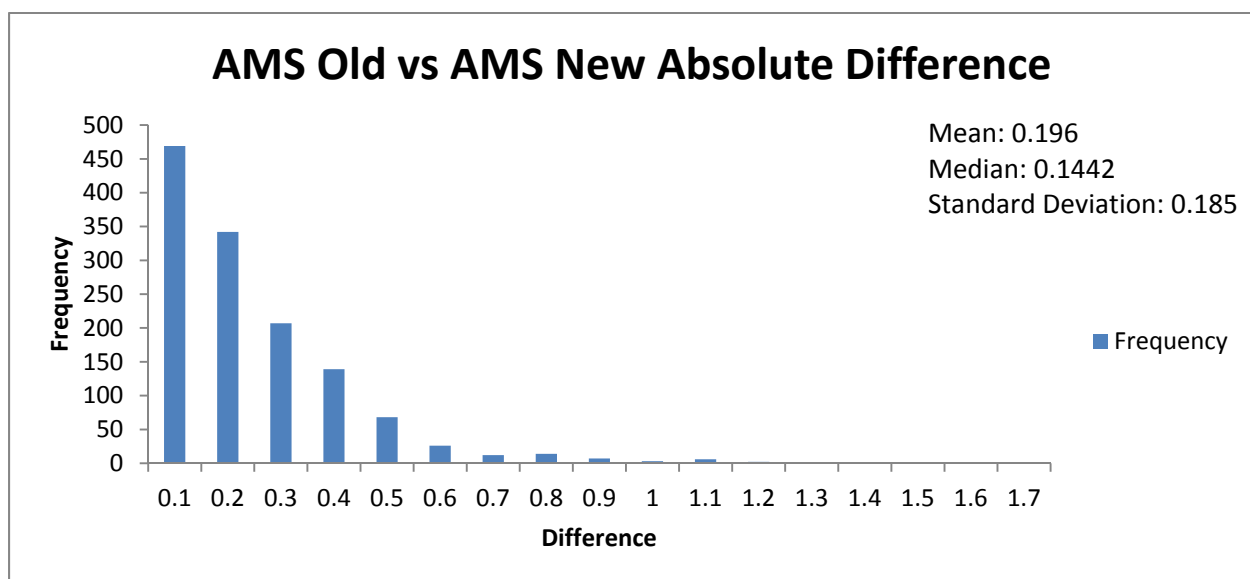


The two datasets show fairly good agreement between the two flights with most of the data having an absolute difference of less than 0.25 μ R/h. There are outliers that are near the border of the units Tmcg and Tmcl with exposure differences of greater than 1 μ R/h. This can be explained by the fact that Tmcl is considerably hotter in terms of exposure rate than Tmcg and the geologic boundary between the units is sharp. The footprint of the detector (~100m) may

mean that even though the points occur within 25m of each other they may be picking up a primary signal that is dominated by one particular unit.

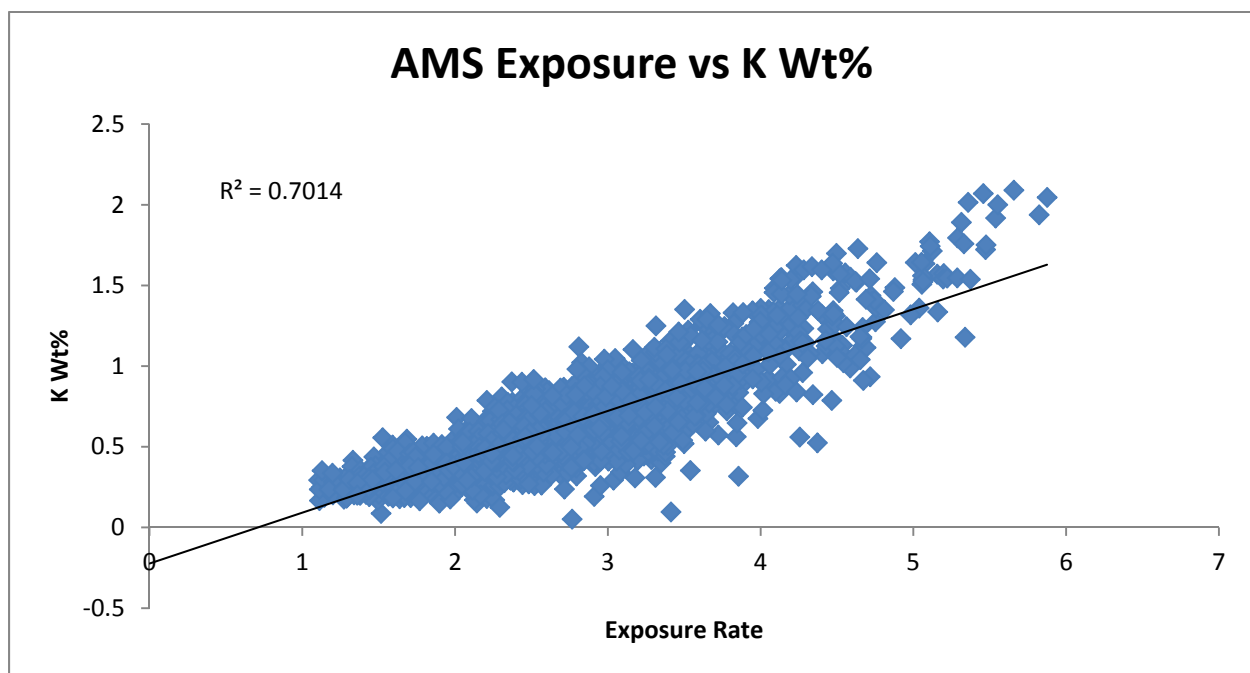


The R^2 value of the relationship between the surveys is 0.859 which suggests a good relationship between the datasets. The mean difference is rather low at 0.196 µR/h however the standard deviation of the difference is 94% of the mean suggesting that the mean is not a good representation of this dataset. The median is lower than the mean at 0.1442 µR/h and may be more representative of the real difference between these data.

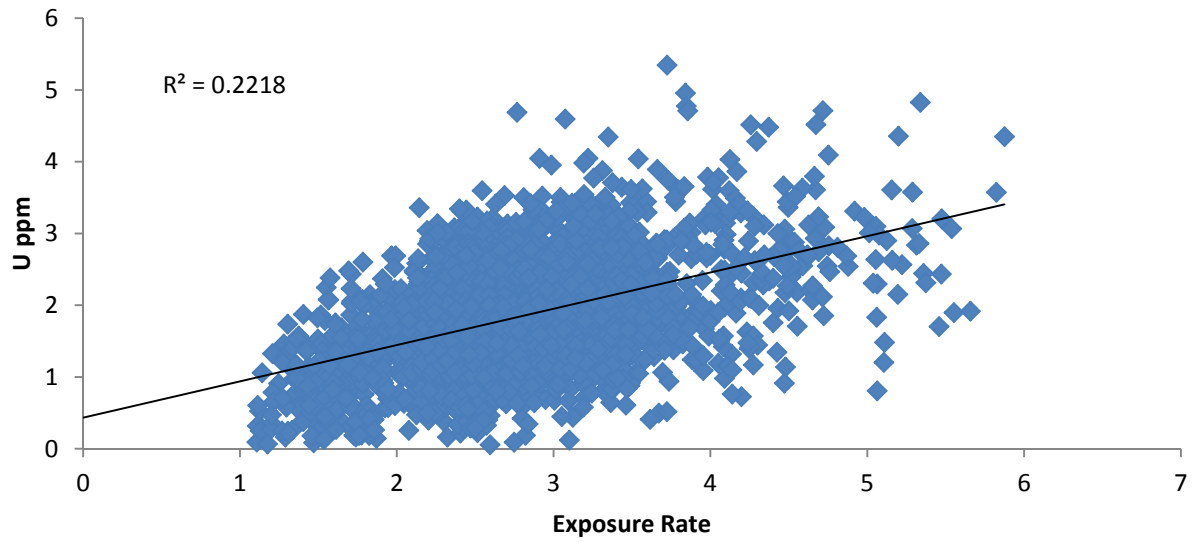


K, U, and Th Distribution

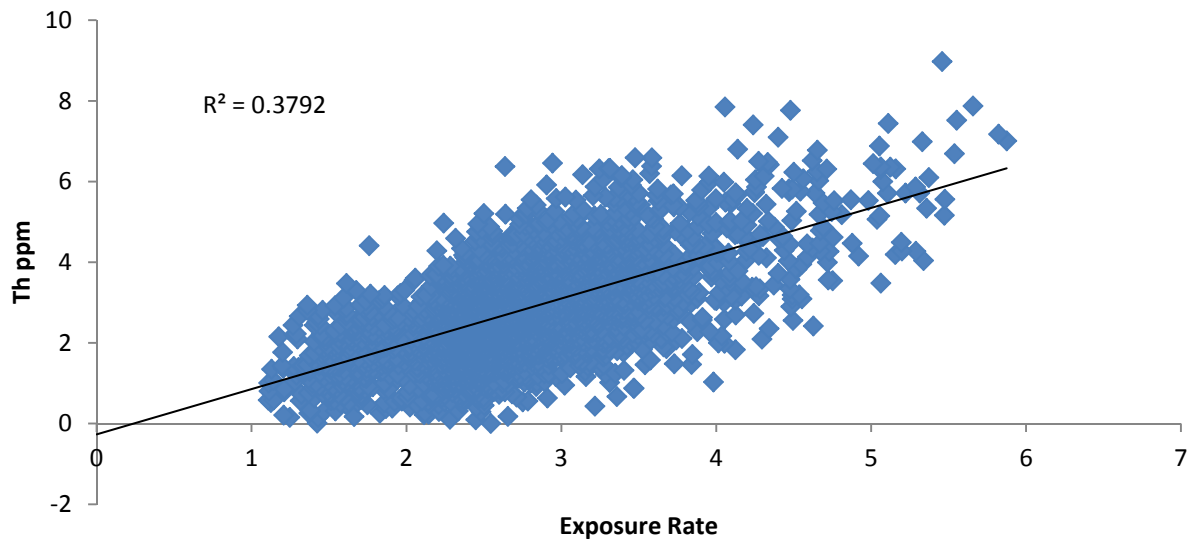
In general, exposure rate is most highly correlated with K concentration having an R^2 value of 0.7014. The relationship between Th and exposure is also significant with an R^2 of 0.39, but much less so than K. U has very little correlation with exposure with an R^2 of 0.2218. Indeed in this relationship is clear in the concentration maps below. Generally, the hotter parts of the area have the most K and Th; and U seems to be fairly homogenous throughout the area. K and Th tend to covary across the area which can be seen in the Th/K image.



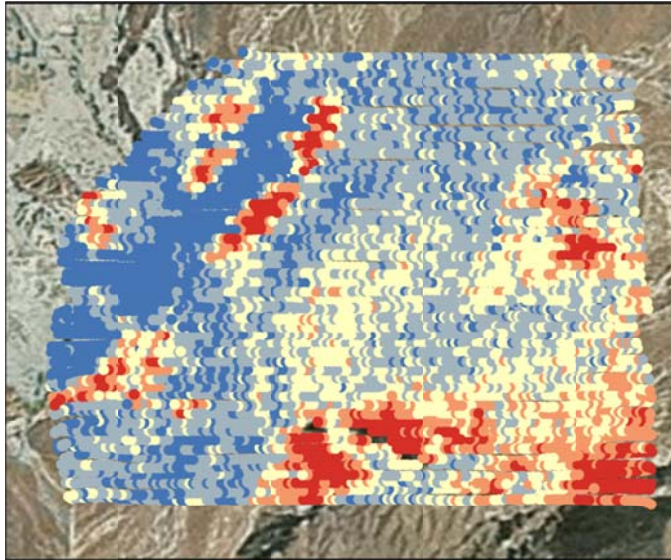
AMS Exposure vs U ppm



AMS Exposure vs Th ppm

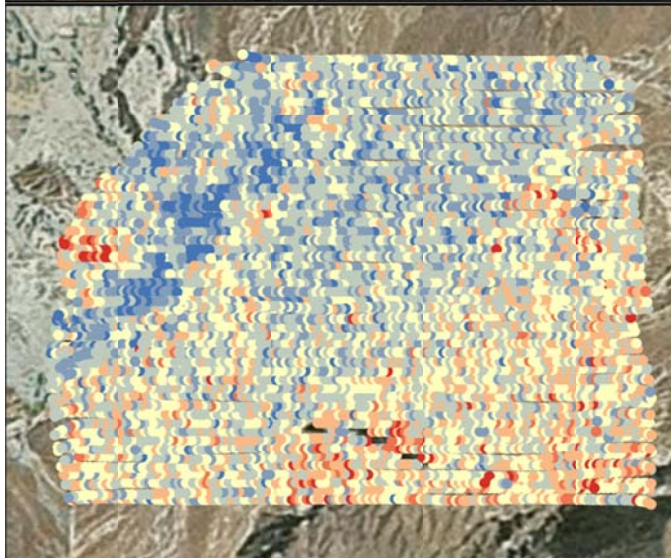


Government Wash Radioelement Concentration Images



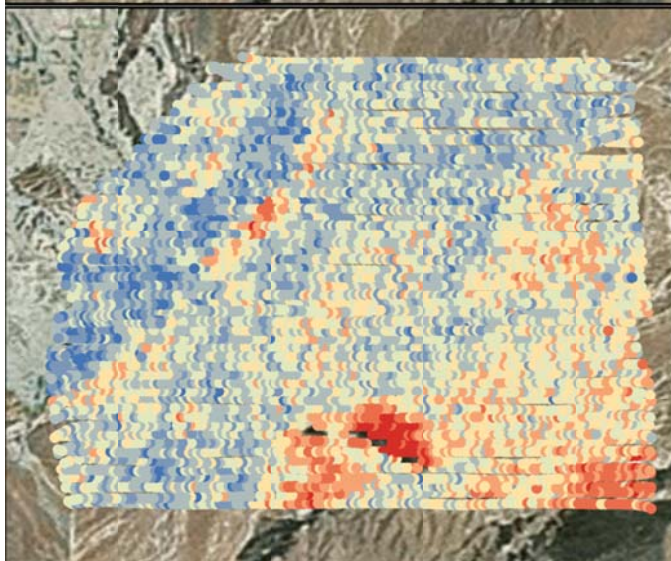
K Wt%

- 0 - 0.485574
- 0.485575 - 0.679890
- 0.679891 - 0.902579
- 0.902580 - 1.234061
- 1.234062 - 2.271017



U PPM

- 0 - 0.818232
- 0.818233 - 1.415482
- 1.415483 - 2.069242
- 2.069243 - 2.679219
- 2.679220 - 3.502989
- 3.502990 - 4.043893
- 4.043894 - 7.910720



Th PPM

- 0 - 0.942384
- 0.942385 - 1.784504
- 1.784505 - 2.810072
- 2.810073 - 3.763784
- 3.763785 - 4.843144
- 4.843145 - 6.364771
- 6.364772 - 8.949389
- 8.949390 - 14.238856



0 0.5 1 2
Kilometers

Government Wash Radioelement Ratio Images

U/K Ratio

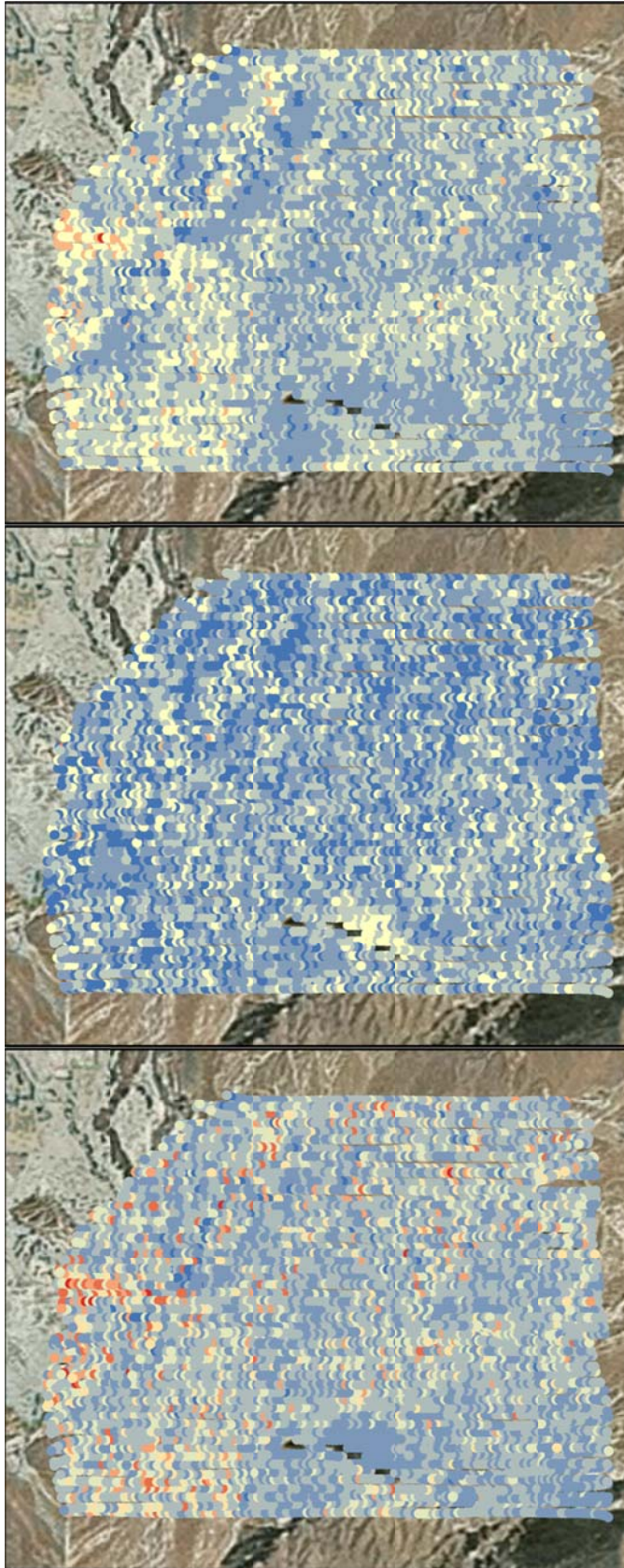
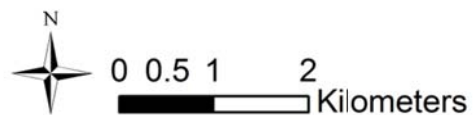
- 0 - 1.000000
- 1.000001 - 2.776200
- 2.776201 - 4.814531
- 4.814532 - 9.199804
- 9.199805 - 26.562074
- 26.562075 - 67.621020
- 67.621021 - 229.055746

Th/K Ratio

- 0 - 3.307556
- 3.307557 - 5.092326
- 5.092327 - 7.271497
- 7.271498 - 15.387768
- 15.387769 - 38.153590
- 38.153591 - 74.386013
- 74.386014 - 164.297821

U/Th Ratio

- 0 - 0.100000
- 0.100001 - 0.500000
- 0.500001 - 1.000000
- 1.000001 - 1.500000
- 1.500001 - 2.000000
- 2.000001 - 3.000000
- 3.000001 - 9.114520
- 9.114521 - 242.489933



Unit Data Summary

Unit	AMS Mean	AMS Median	AMS STD	AMS Low	AMS High	NURE Exp	Avg ABS Diff	Avg Diff
Qa	2.681	2.664	0.3045	1.472	4.522	3.96	1.2814	-1.2803
Qoa	3.360	3.392	0.386	1.375	5.042	4.058	0.7045	-0.6971
Tmcg	2.025	1.927	0.526	1.107	4.123	1.504	0.5634	0.5211
Tmcl	3.561	3.52	0.6451	2.035	5.875	3.858	0.5758	-0.2969
Tmcl	3.201	3.064	0.553	1.523	4.971	3.692	0.6526	-0.4914
Thl	4.805	4.873	0.817	2.788	6.850	3.59	1.267	1.2147
Thlv	4.771	4.863	0.454	3.629	5.563	2.592	2.1793	2.1793
Tht	4.918	4.659	1.032	3.075	6.895	3.322	1.602	1.596
Thtb	3.978	3.978	N/A	3.978	3.97	3.884	0.094	0.0937
Ti	5.035	4.985	0.931	3.436	6.49	N/A	N/A	N/A
Trs	4.527	4.739	0.778	2.762	5.531	5.062	0.6574	-0.5345
Tvc	4.7101	4.548	0.283	4.445	5.225	4.672	0.2378	0.0381

Qa

Composition

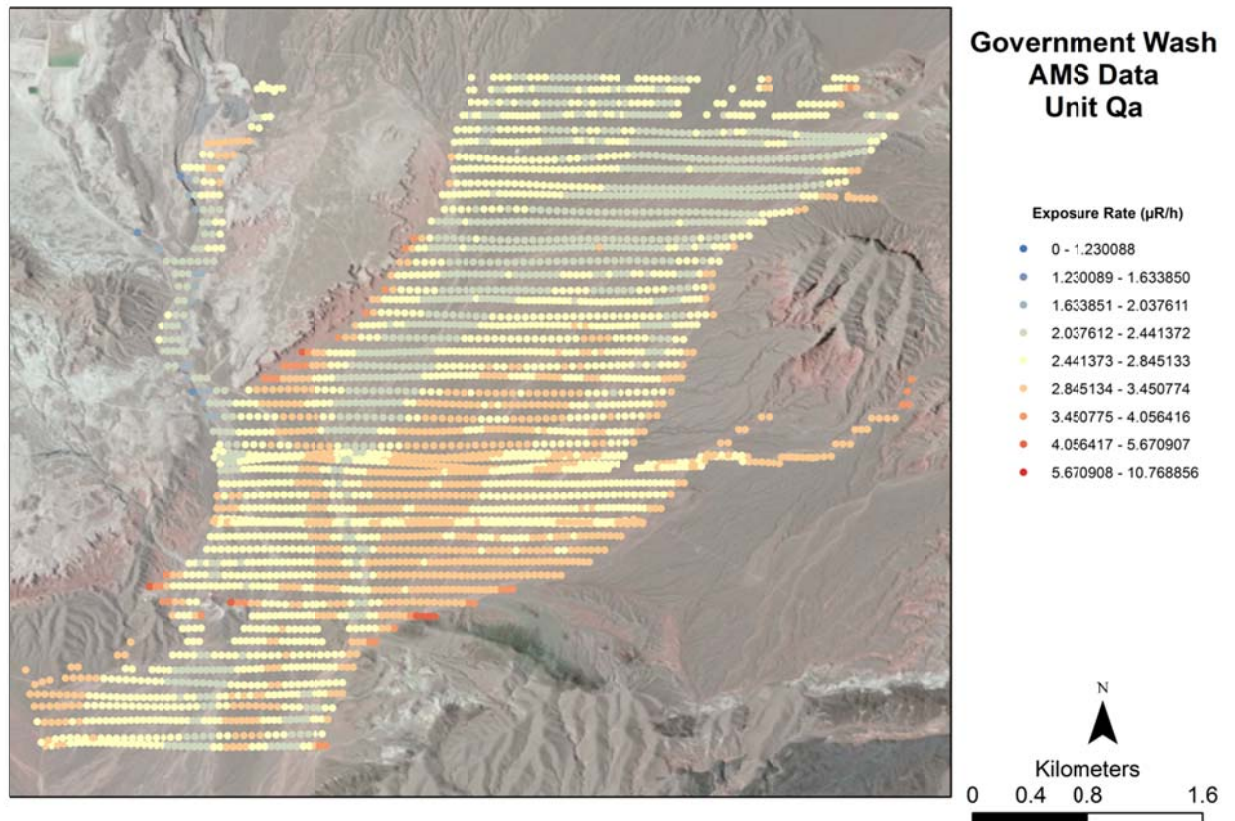
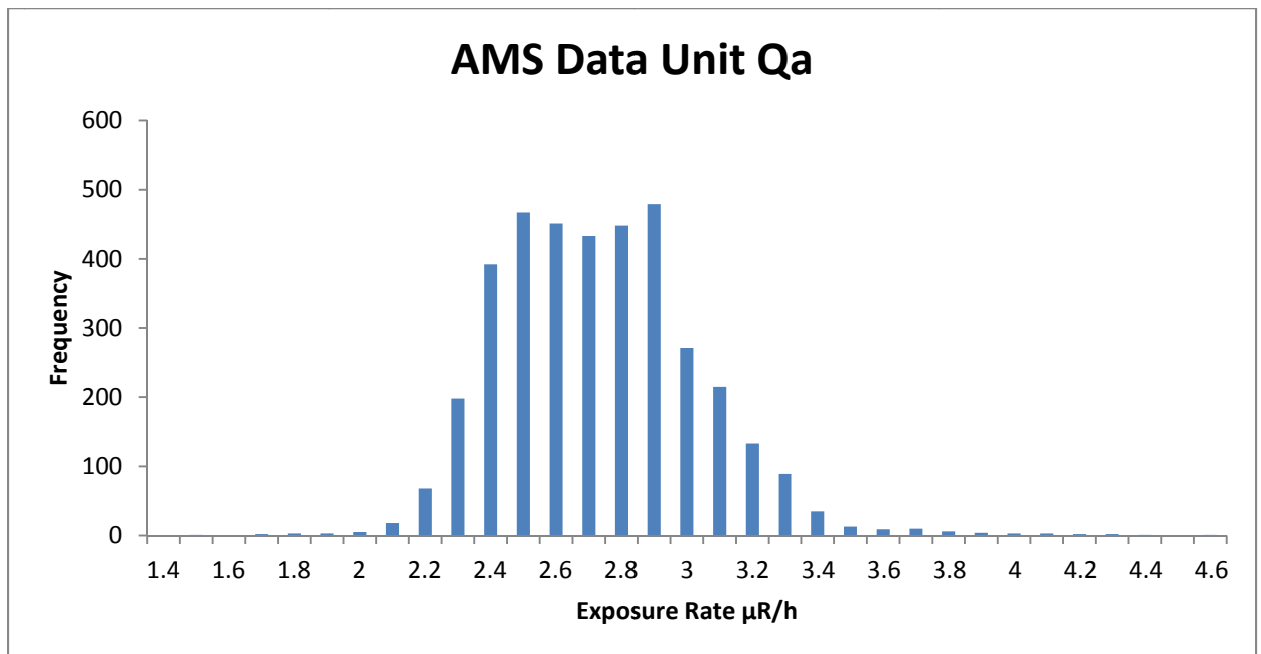
This unit is composed of Holocene to Pleistocene alluvium. Portions of the fan are contemporarily active and are intermixed with older terraced surfaces. Clasts range from boulder to sand size on terraces and sand to silt within active washes and fan surfaces (Duebendorfer, 2003). This unit has a heterogeneous mix of rock types sourced from units such as the Kaibab Formation (Pk), Aztec Sandstone (Ja), and members of the Horse Springs Formation in the northwest. It also has some contribution from units along its margins; notably the lower member of the Muddy Creek Formation (Tmcl).

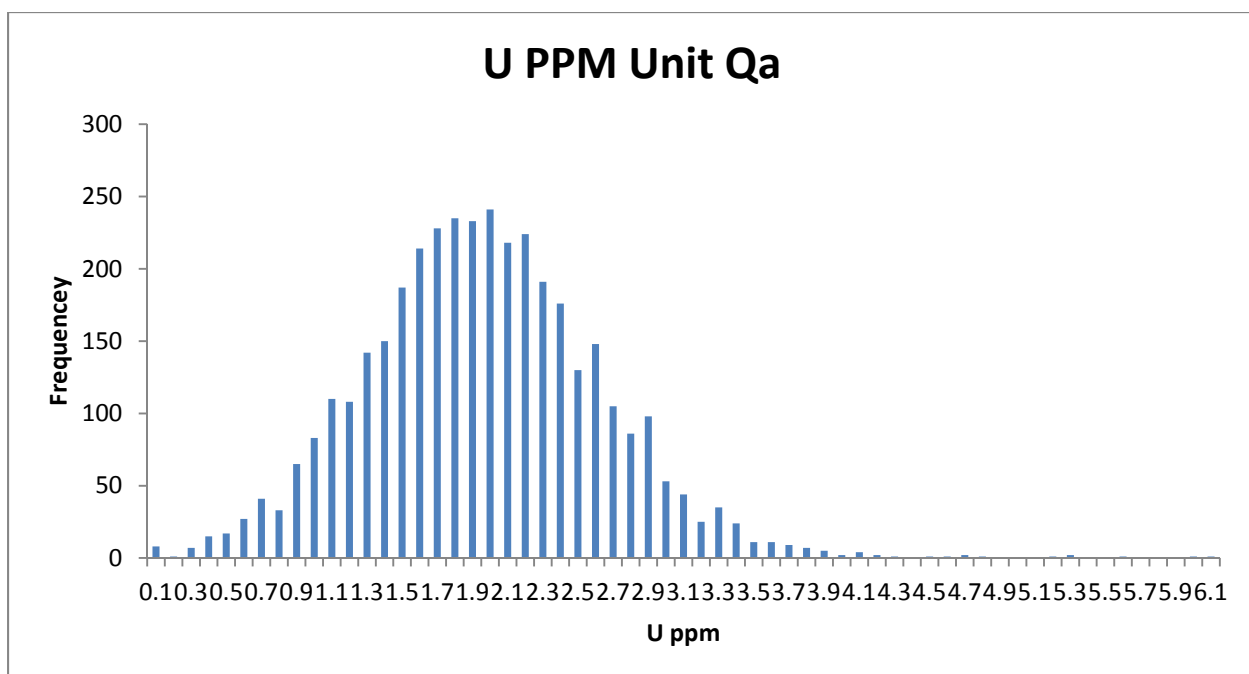
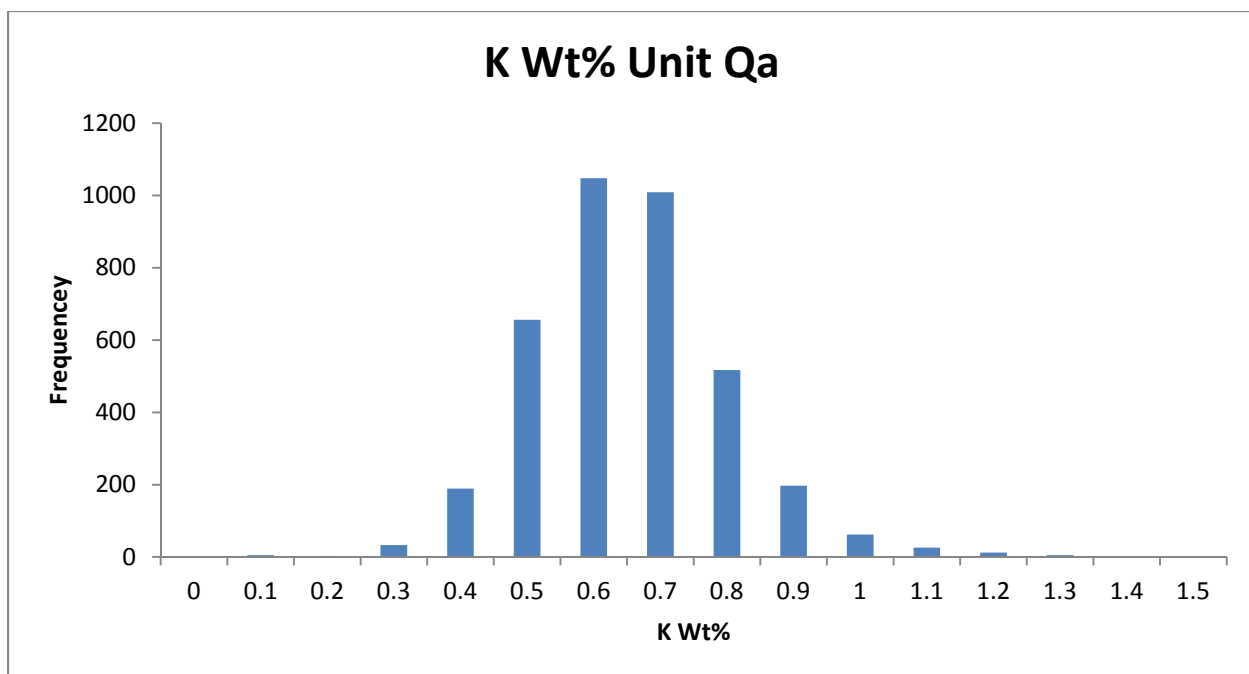
AMS Data

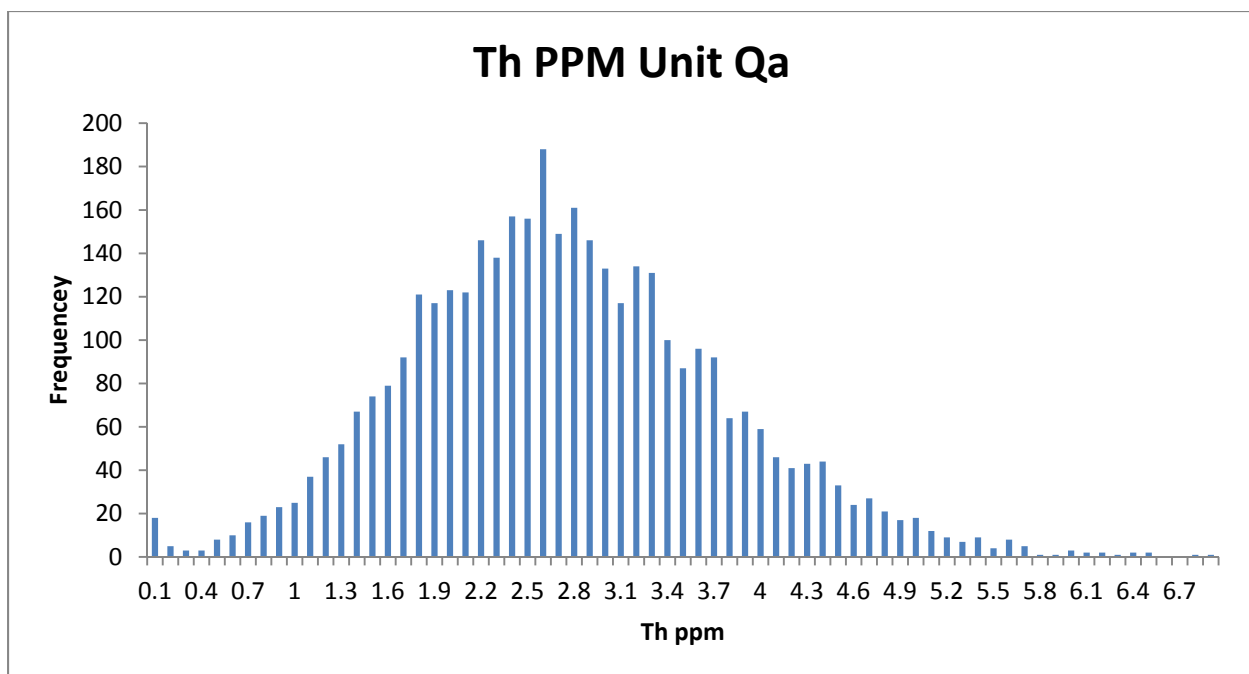
There is variability in exposure rate across Qa with two peaks in the data near 2.5 $\mu\text{R/h}$ and 2.9 $\mu\text{R/h}$. The average exposure rate for this unit falls in between at 2.68 $\mu\text{R/r}$ with a standard deviation of 0.3 $\mu\text{R/h}$ or 11% of the mean. The histogram of the exposure rate data suggests that this unit is more homogenous than it actually is. In terms of spatial distribution of exposure rate, this unit is fairly complex. In the north eastern portion of the fan exposure rates are on the lower end of the spectrum and represent more active portions of the fan. The south eastern portion is largely made up of older terraced surfaces. The cooler active washes are bisected by a tail of material from the hotter Tmcl. This tail of material adds hotter sediment to the southern portion of the fan in the direction of transport.

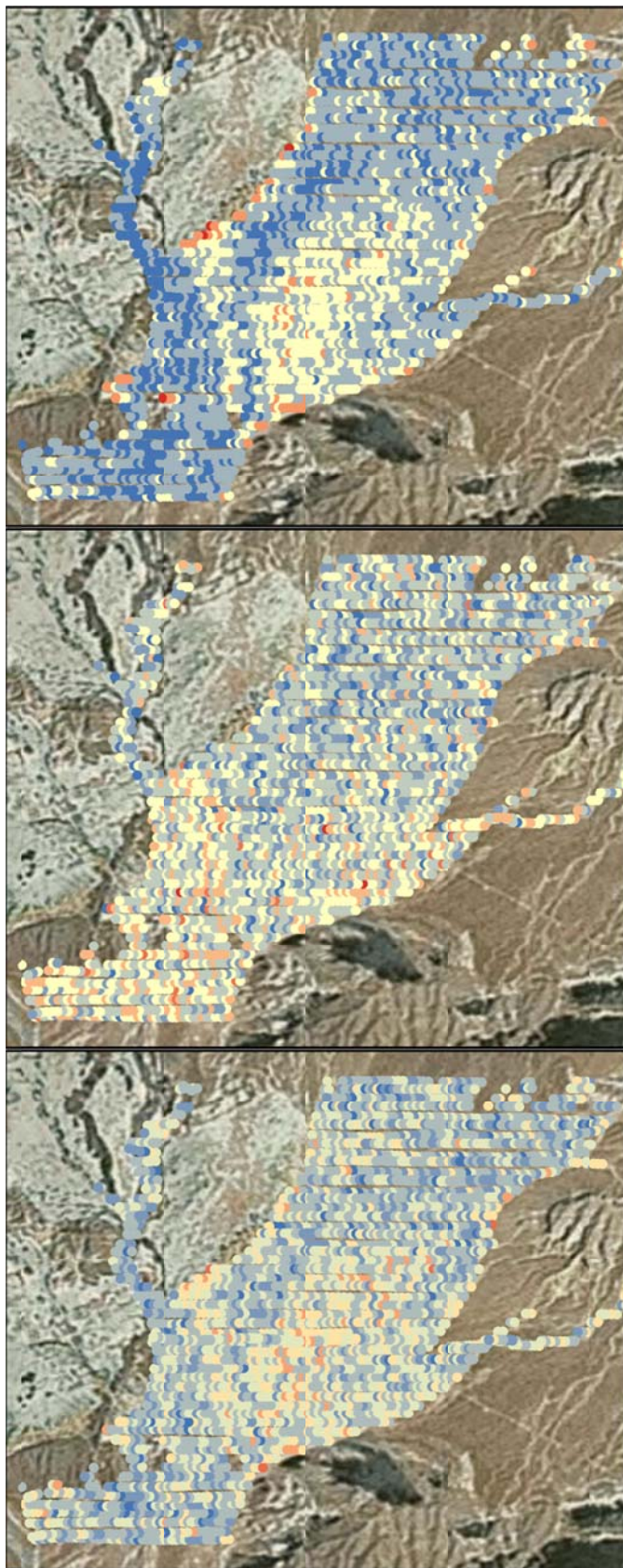
The K, U, and Th concentrations in this fan are also subject to this variability. Many of the same structural components remain in this dataset. K and Th are the nuclides most heavily correlated with exposure and in both datasets the cooler washes, hotter terraces and tail of hot material from Tmcl are all present. Interestingly, the area west of the hotter tail has relatively lower concentrations of K and Th despite the influence of the tail. In this region U appears to be controlling the exposure rate suggesting preferential U weathering in Tmcl. All of the histograms

show normal distribution of exposure, K, U, and Th but the distribution covers a very wide range which is not ideal for this work.









Government Wash Radioelement Concentration Images Unit Qa

K Wt%

- 0 - 0.485574
- 0.485575 - 0.679890
- 0.679891 - 0.902579
- 0.902580 - 1.234061
- 1.234062 - 2.271017

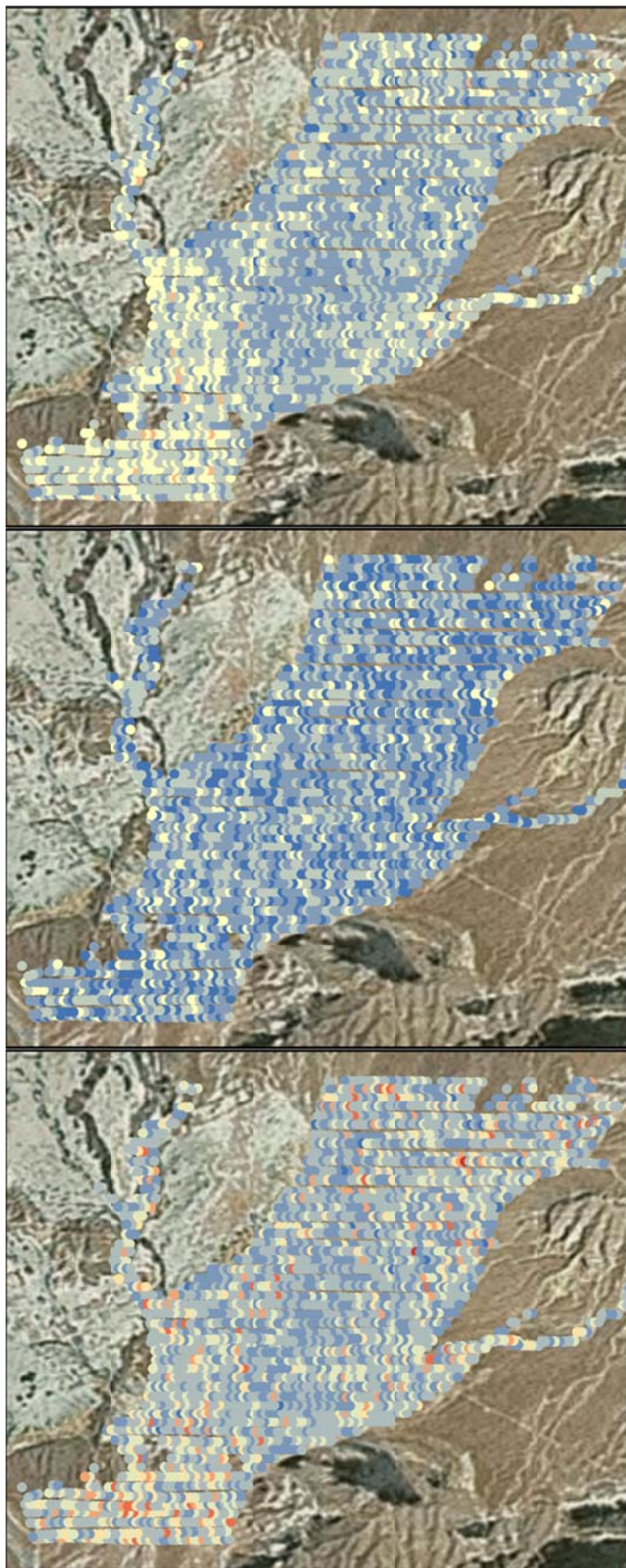
U PPM

- 0 - 0.818232
- 0.818233 - 1.415482
- 1.415483 - 2.069242
- 2.069243 - 2.679219
- 2.679220 - 3.502989
- 3.502990 - 4.043893
- 4.043894 - 7.910720

Th PPM

- 0 - 0.942384
- 0.942385 - 1.784504
- 1.784505 - 2.810072
- 2.810073 - 3.763784
- 3.763785 - 4.843144
- 4.843145 - 6.364771
- 6.364772 - 8.949389
- 8.949390 - 14.238856





Government Wash Radioelement Ratio Images Unit Qa

K/U Ratio

- 0 - 1.000000
- 1.000001 - 2.776200
- 2.776201 - 4.814531
- 4.814532 - 9.199804
- 9.199805 - 26.562074
- 26.562075 - 67.621020
- 67.621021 - 229.055746

Th/K Ratio

- 0 - 3.307556
- 3.307557 - 5.092326
- 5.092327 - 7.271497
- 7.271498 - 15.387768
- 15.387769 - 38.153590
- 38.153591 - 74.386013
- 74.386014 - 164.297821

U/Th Ratio

- 0 - 0.100000
- 0.100001 - 0.500000
- 0.500001 - 1.000000
- 1.000001 - 1.500000
- 1.500001 - 2.000000
- 2.000001 - 3.000000
- 3.000001 - 9.114520
- 9.114521 - 242.489933



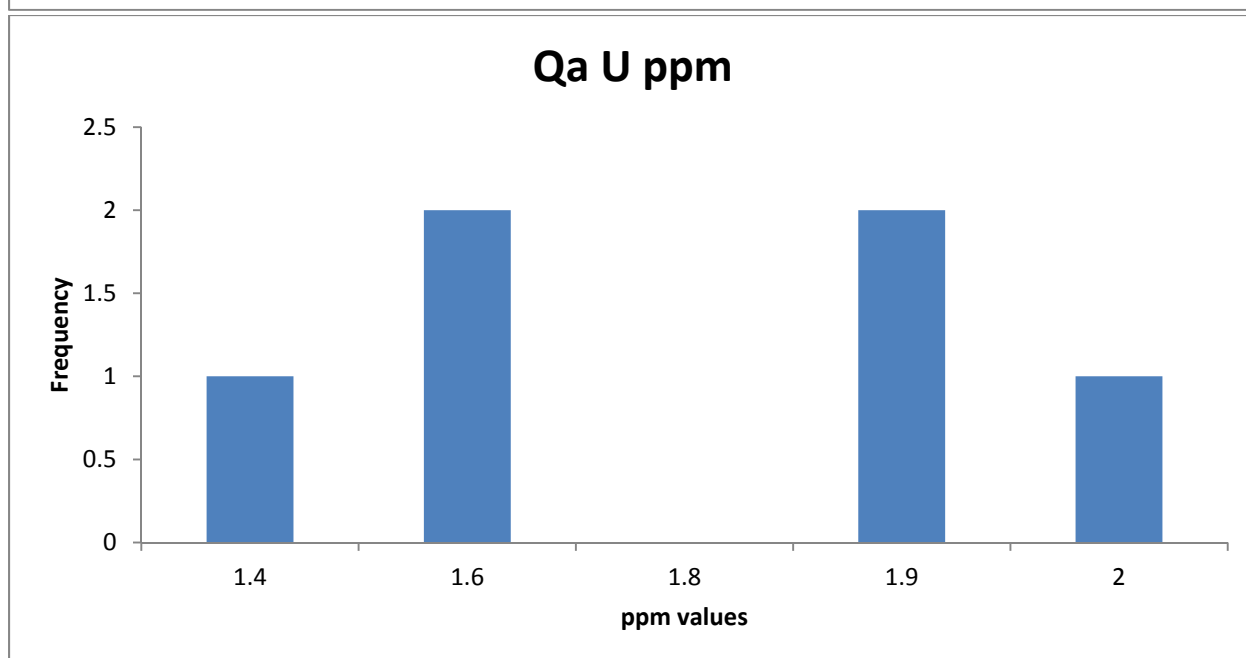
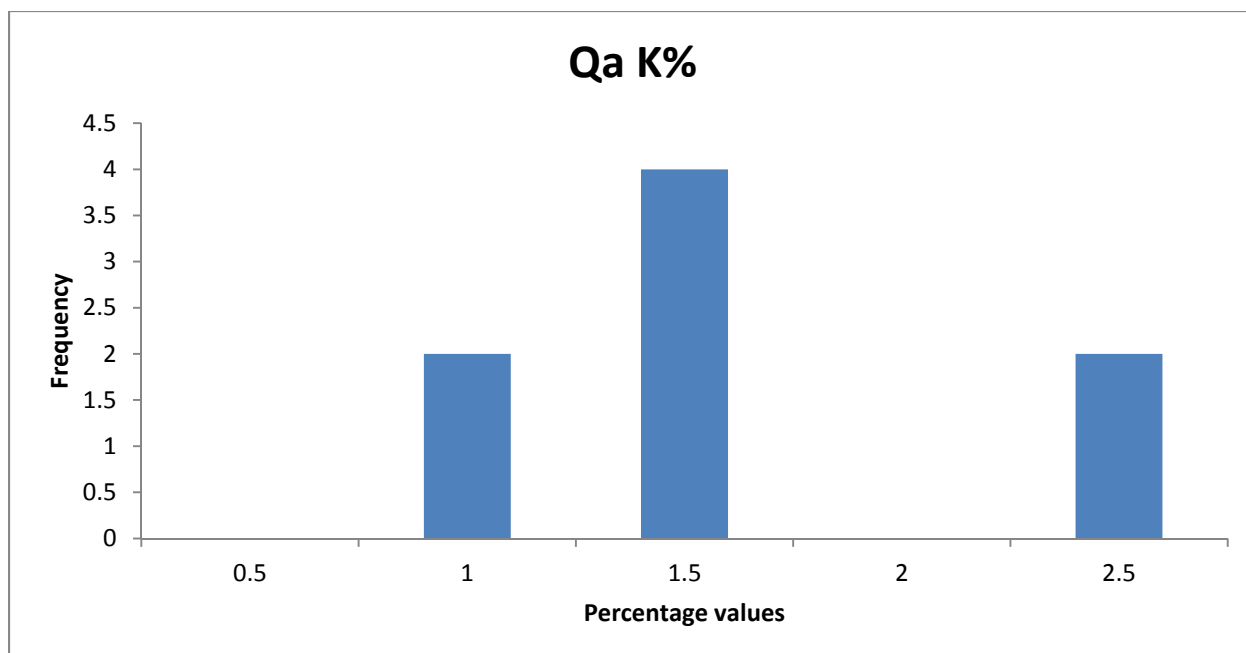
0 0.5 1 2
Kilometers

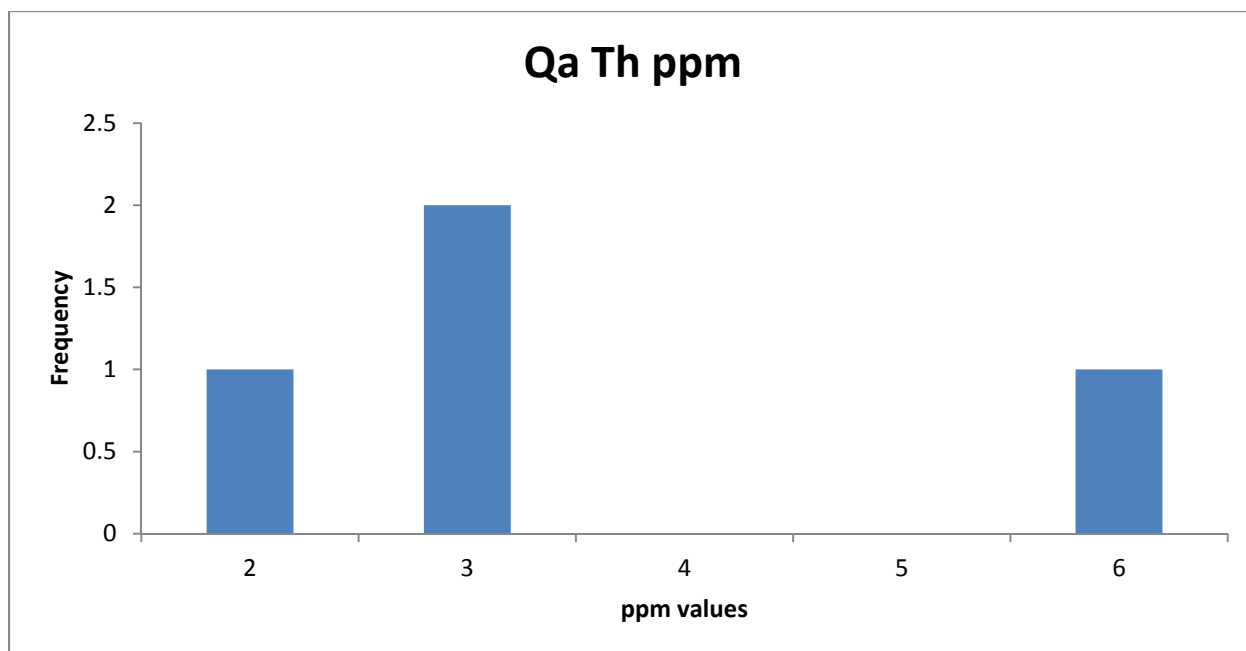
Traditional Geochemistry

Ten traditional geochemical data points occur within this unit. It is not clear whether these data points represent singular rocks taken from the fan or representative samples at each location. The potassium values range from 0.8% to 2.2%; the uranium values are tighter ranging from 1.35-1.98 ppm; the thorium values range from 1.6-5.1 ppm. When an exposure rate is calculated for this unit using these data the result is 3.58 $\mu\text{R/h}$ which contrasts with the mean of the AMS data of 2.68 $\mu\text{R/h}$. This is just within our stated goal of a difference of 1 $\mu\text{R/h}$.

Geochemical Data	K%	U ppm	Th ppm
Mean	1.3817	1.661667	3.09875
Median	1.336	1.685	2.774
Standard Deviation	0.487365	0.223861	1.270838
Range	0.7751-2.217	1.35-1.98	1.686-5.161

Sample ID	Latitude	Longitude	K %	U ppm	Th ppm
M201806	36.175	-114.808	2.217		
M201807	36.175	-114.808	2.061		
M201808	36.175	-114.808	1.352		
M201809	36.175	-114.808	1.356		
21143	36.1838	-114.841	1.32	1.82	2.759
21144	36.1514	-114.841	1.152	1.81	5.161
21151	36.2193	-114.81	0.7751	1.56	1.686
21152	36.2169	-114.826		1.45	
21153	36.2397	-114.837		1.35	
21155	36.1759	-114.801	0.8205	1.98	2.789

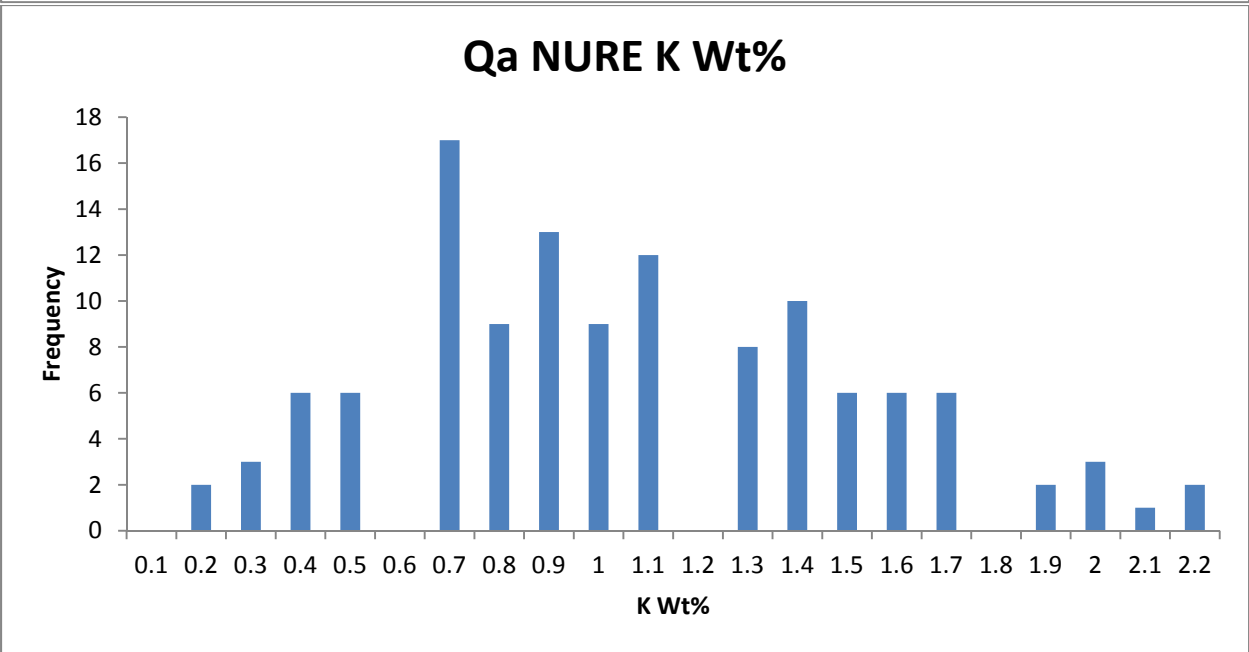
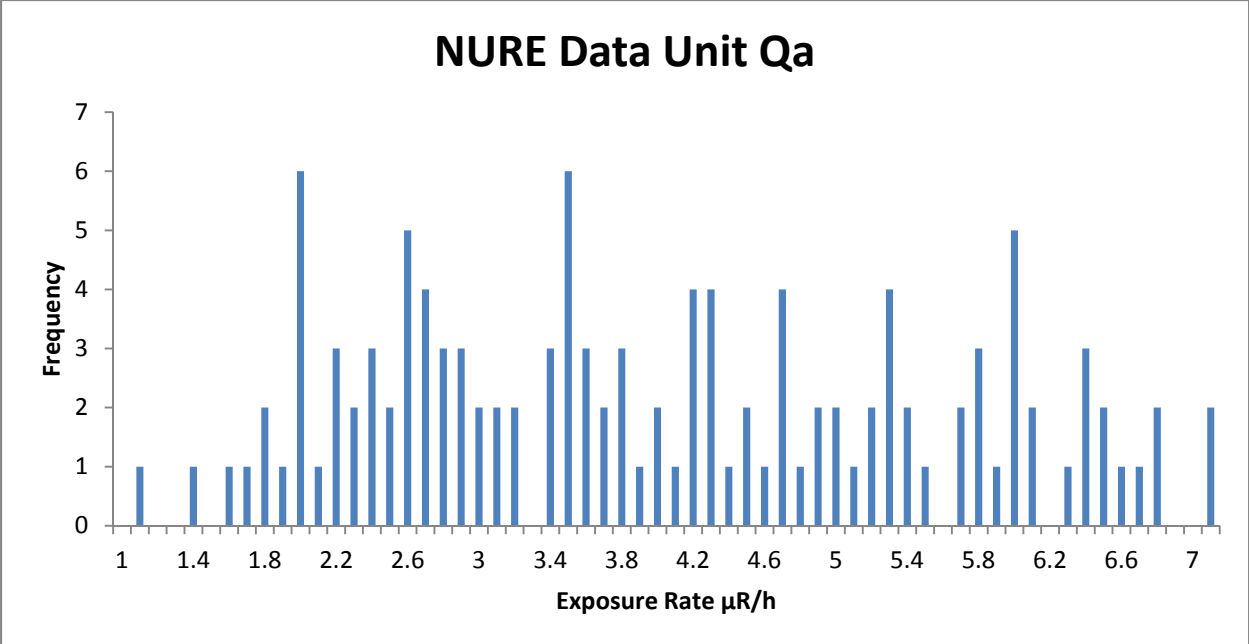


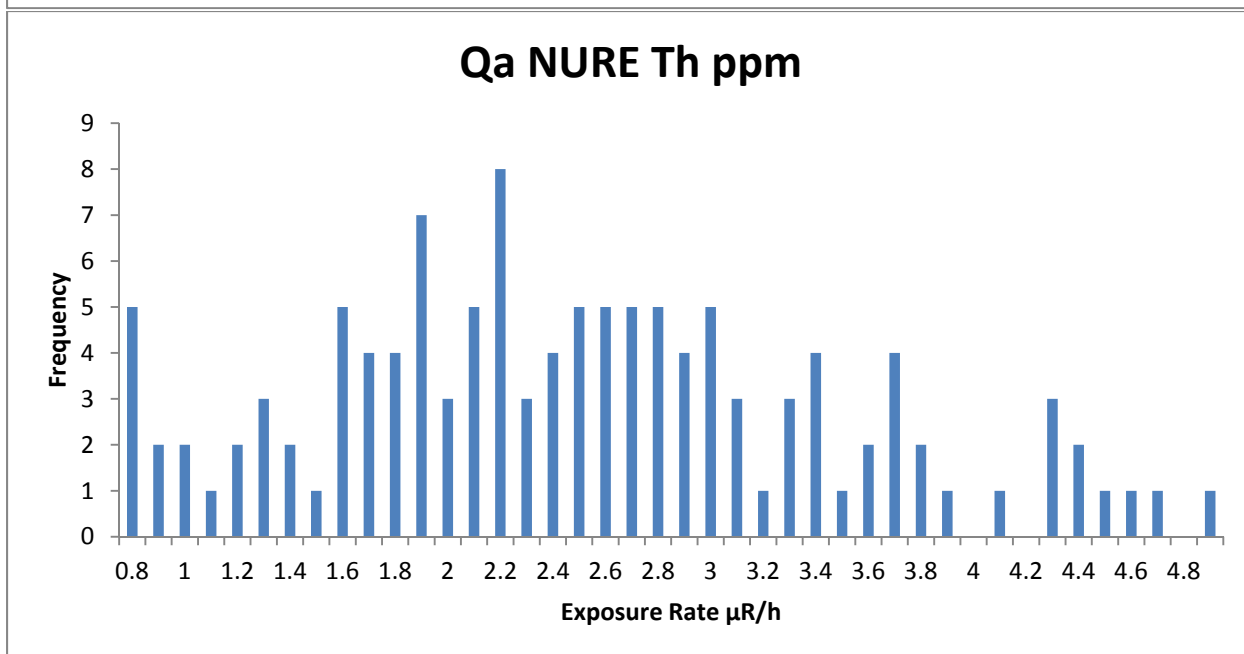
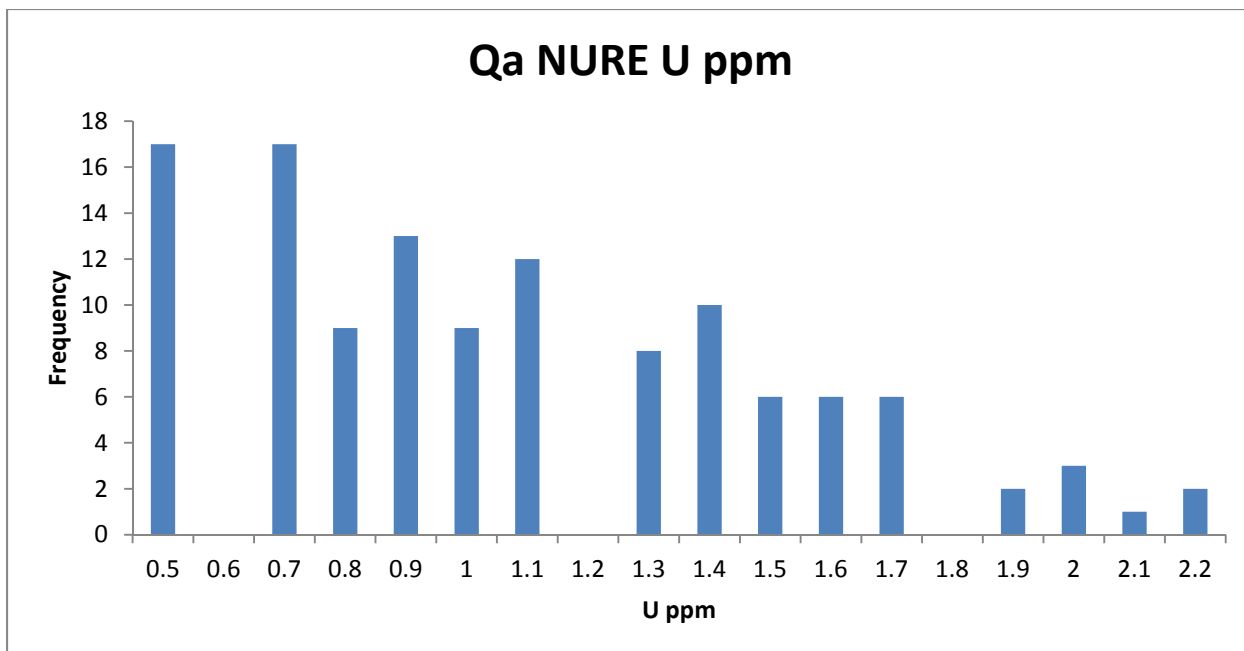


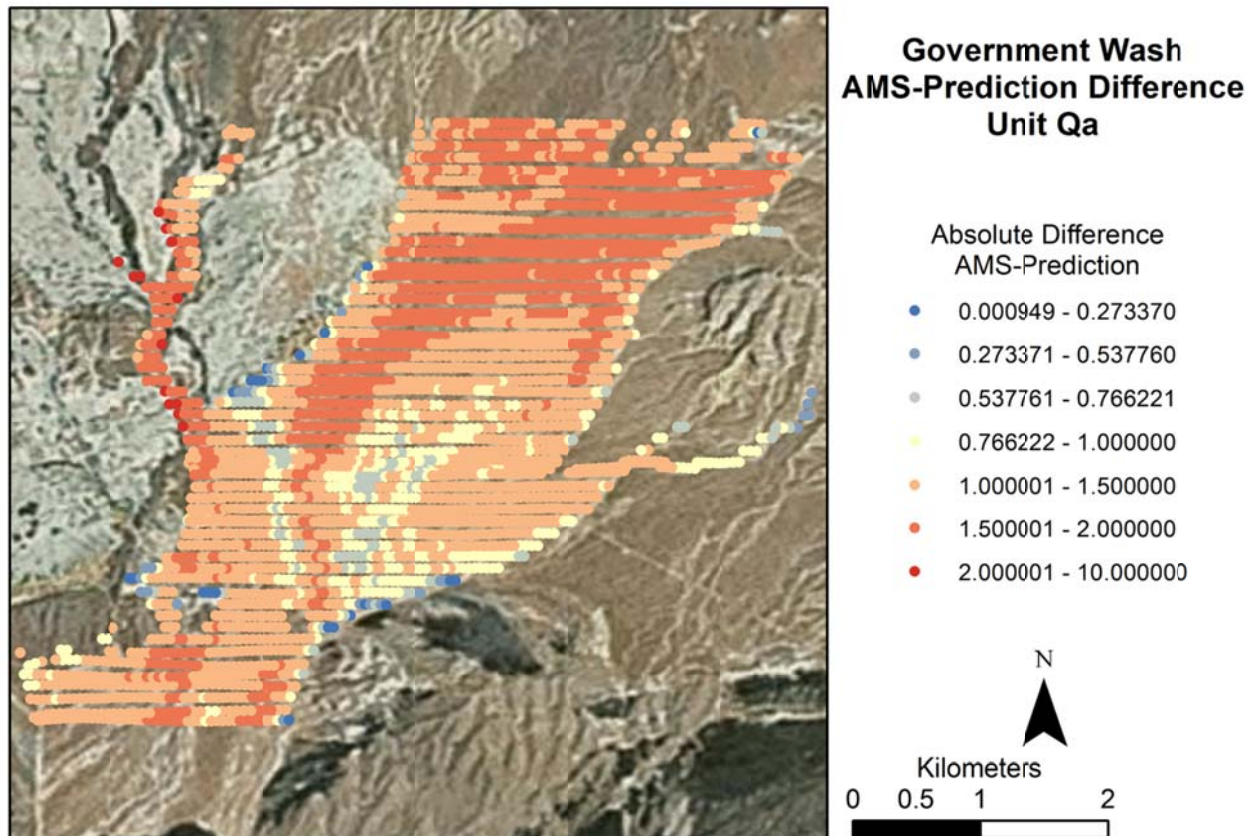
NURE Data

The NURE data that occurs within this unit is quite variable. Much of the data comes from the southern NURE line which as previously discussed, does not agree well with the AMS dataset. The average NURE exposure rate for this unit is 3.96 $\mu\text{R/h}$ which compares with the average AMS exposure rate of 2.68 $\mu\text{R/h}$ or the traditional geochemistry of 3.58 $\mu\text{R/h}$. As expected based on the distribution of exposure rates the NURE dataset also has quite variable concentrations of K, U, and Th.

When the AMS data is subtracted from the NURE prediction on a point by point basis the hotter terrace surfaces and erosional tail from Tmcl are in fairly good agreement with the NURE prediction. However, most of the spatial area of the fan is cooler and falls outside of the desired ± 1 $\mu\text{R/h}$ range.







Data Summary

Exposure Rate Comparison $\mu\text{R/h}$	Average	Median	STD	Range
AMS Data	2.68132571	2.663549	0.30407348	1.471689-4.522169
NURE Data	3.961944	3.761975	1.531062	1.022-7.047
Geochemical Prediction	3.58	3.441428	N/A	2.221524-5.415272

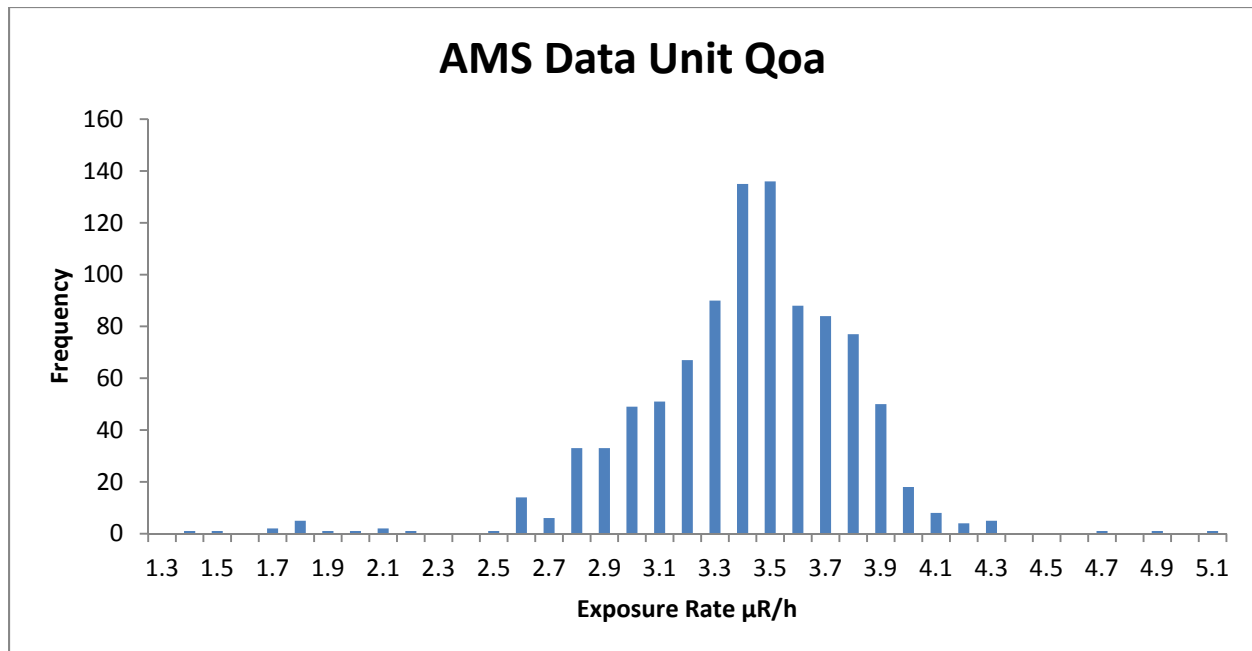
Qoa

Composition

This unit is an older alluvial fan that is Pleistocene in age. The surface consists of well-developed desert pavements that are present on elevated terrace surfaces. Poorly sorted and variability rounded clasts that range from boulder to silt in size and are largely composed of carbonate rocks. This unit is inconsistently cemented across the area; well cemented by calcrete in some areas and unconsolidated in others. Significant eolian addition has inflated pavement surfaces. Clasts are largely sourced from the Kaibab and Horse Springs Formations to the north east (Duebendorfer, 2003).

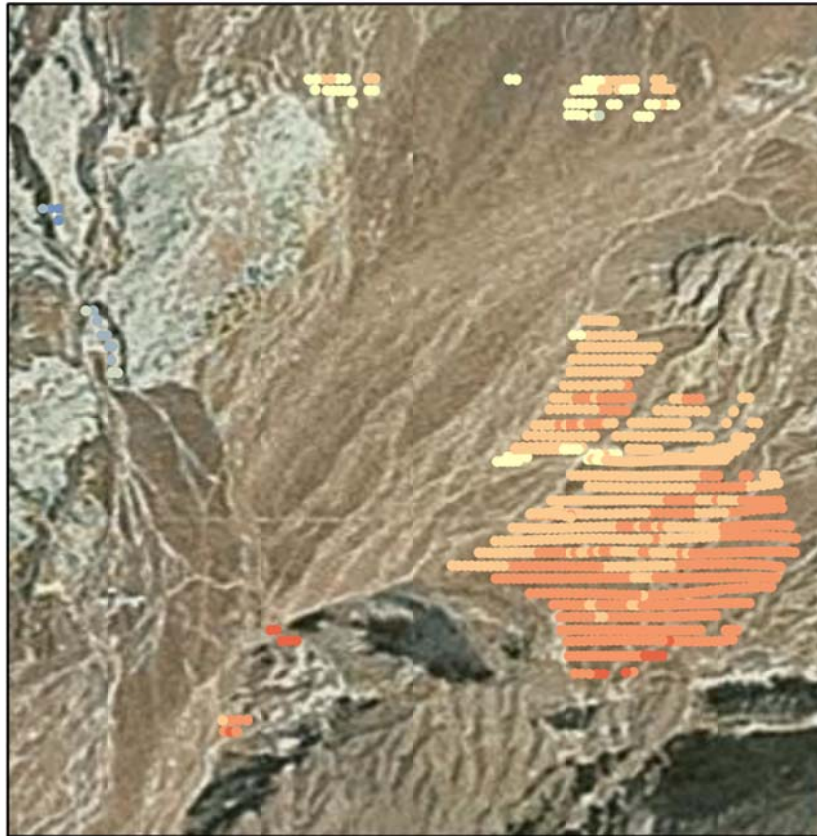
AMS Data

This unit is largely homogenous in terms of exposure rate. It ranges from 1.3-5.1 $\mu\text{R/h}$ but has a strong peak from 3.4-3.5 $\mu\text{R/h}$. The average exposure rate is 3.36 $\mu\text{R/h}$ with a standard deviation of 0.39 or 12% of the mean. The homogeneity can be attributed to several factors: the unit is of sufficient age that any disequilibrium effects in the U and Th decay chain should be minimal, the unit also consists of eolian inflated desert pavements that have likely very cool carbonate clasts that sit on top. Reheis et al. studied eolian dust in Southern Nevada in 2009 and found that much of the dust is homogenous in terms of radionuclides and generally hotter than we would expect carbonate material to be. This means that the relatively hot dust sitting under the cooler limestone is dominating the signal.



In terms of spatial distribution Qoa is spread throughout government wash as it is a remnant alluvial fan that once buried older units. This means erosional remnants appear in patches across the area of interest. A large portion of the fan resides in the eastern portion of the area and is quite homogenous in exposure ranging from 3.3-3.6 $\mu\text{R/h}$. In the western portion of the area there are two small outcrops of this fan as mapped by Duebendorfer that are very cool in the AMS data. However, while working in the field these outcrops were indistinguishable from the units that surrounded them. The data that occurs in these areas are significantly cooler than the other portions of Qoa ($<2 \mu\text{R/h}$) further suggesting that they may not actually belong to Qoa.

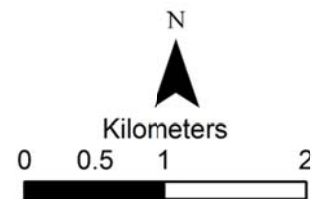
The exposure rate in this unit is controlled primarily by K; U and Th have variable concentrations across the unit which is further expressed in the ratio images. Indeed the cooler portions of the fan express the lowest K values while the hotter portions have higher K values.

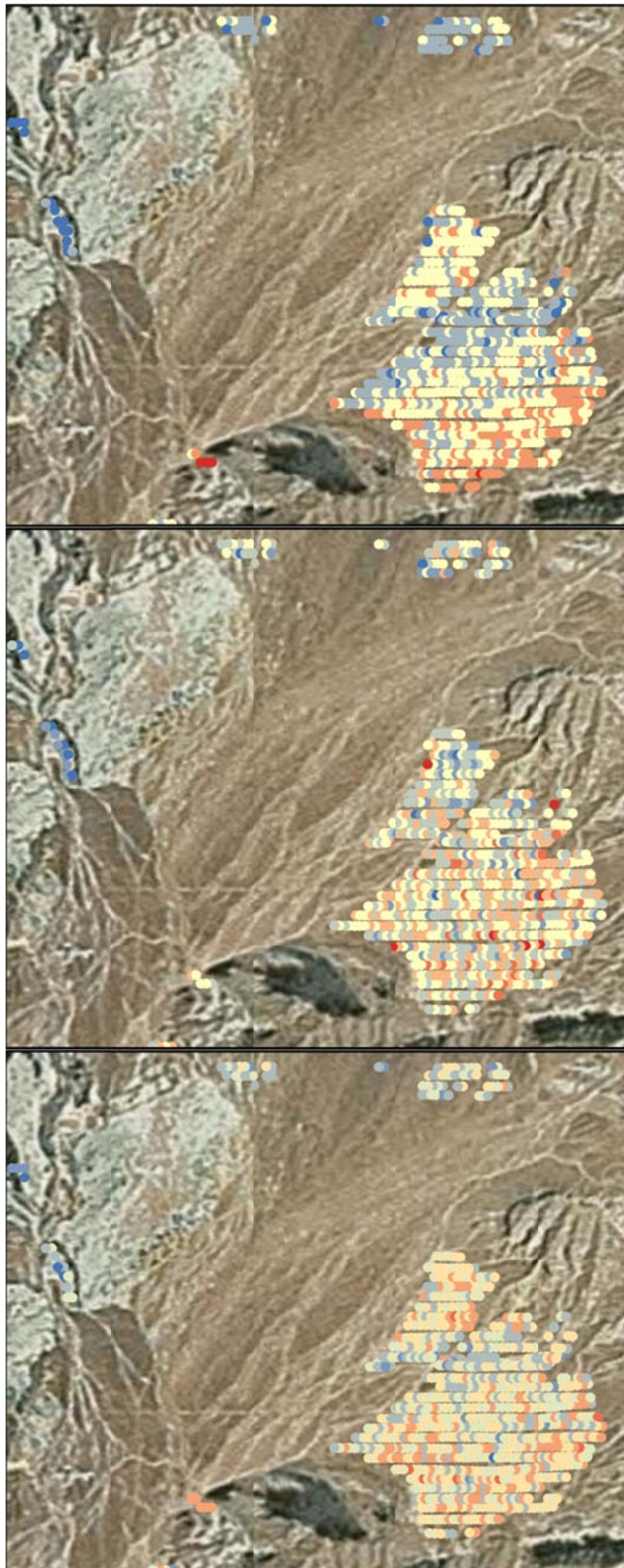


Government Wash AMS Data Unit Qoa

Exposure Rate ($\mu\text{R/h}$)

- 0 - 1.230088
- 1.230089 - 1.633850
- 1.633851 - 2.037611
- 2.037612 - 2.441372
- 2.441373 - 2.845133
- 2.845134 - 3.450774
- 3.450775 - 4.056416
- 4.056417 - 5.670907
- 5.670908 - 10.768856





Government Wash Radioelement Concentration Images Unit Qoa

K Wt%

- 0 - 0.485574
- 0.485575 - 0.679890
- 0.679891 - 0.902579
- 0.902580 - 1.234061
- 1.234062 - 2.271017

U PPM

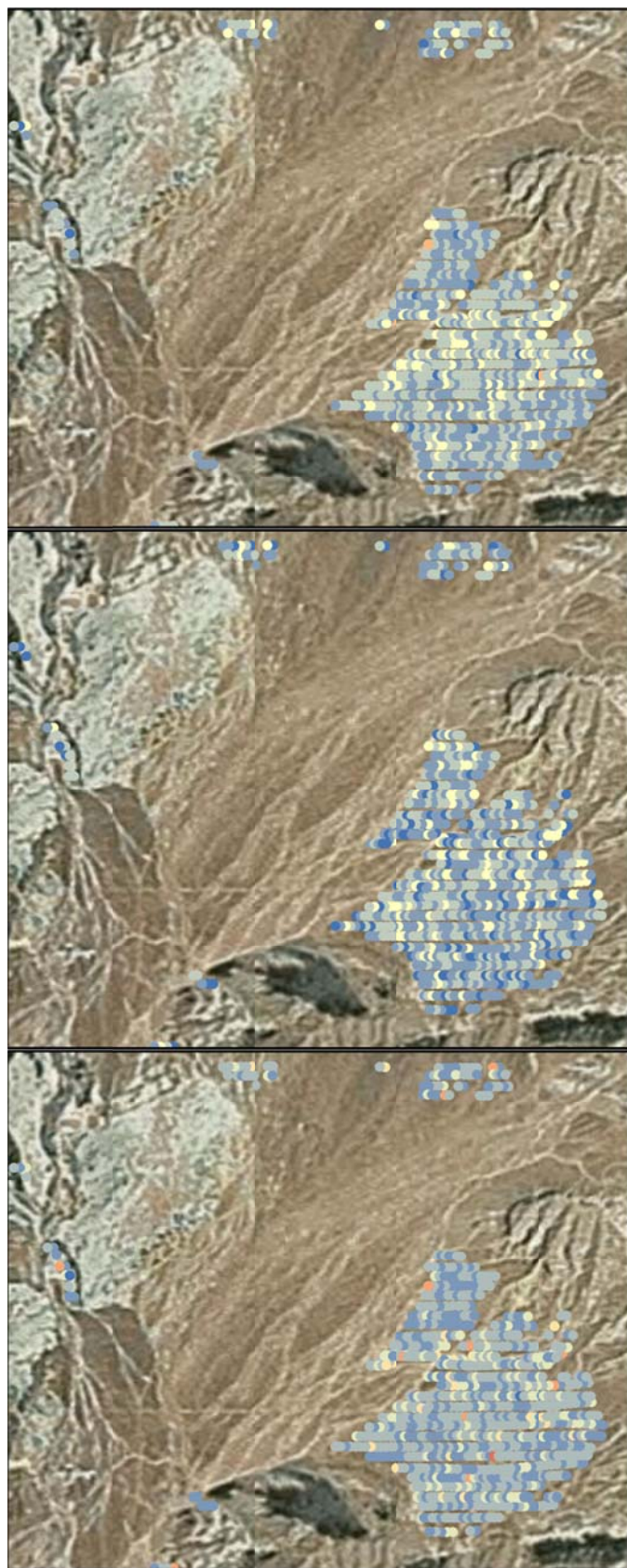
- 0 - 0.818232
- 0.818233 - 1.415482
- 1.415483 - 2.069242
- 2.069243 - 2.679219
- 2.679220 - 3.502989
- 3.502990 - 4.043893
- 4.043894 - 7.910720

Th PPM

- 0 - 0.942384
- 0.942385 - 1.784504
- 1.784505 - 2.810072
- 2.810073 - 3.763784
- 3.763785 - 4.843144
- 4.843145 - 6.364771
- 6.364772 - 8.949389
- 8.949390 - 14.238856



0 0.450.9 1.8
Kilometers



Government Wash Radioelement Ratio Images Unit Qoa

K/U Ratio

- 0 - 1.000000
- 1.000001 - 2.776200
- 2.776201 - 4.814531
- 4.814532 - 9.199804
- 9.199805 - 26.562074
- 26.562075 - 67.621020
- 67.621021 - 229.055746

Th/K Ratio

- 0 - 3.307556
- 3.307557 - 5.092326
- 5.092327 - 7.271497
- 7.271498 - 15.387768
- 15.387769 - 38.153590
- 38.153591 - 74.386013
- 74.386014 - 164.297821

U/Th Ratio

- 0 - 0.100000
- 0.100001 - 0.500000
- 0.500001 - 1.000000
- 1.000001 - 1.500000
- 1.500001 - 2.000000
- 2.000001 - 3.000000
- 3.000001 - 9.114520
- 9.114521 - 242.489933



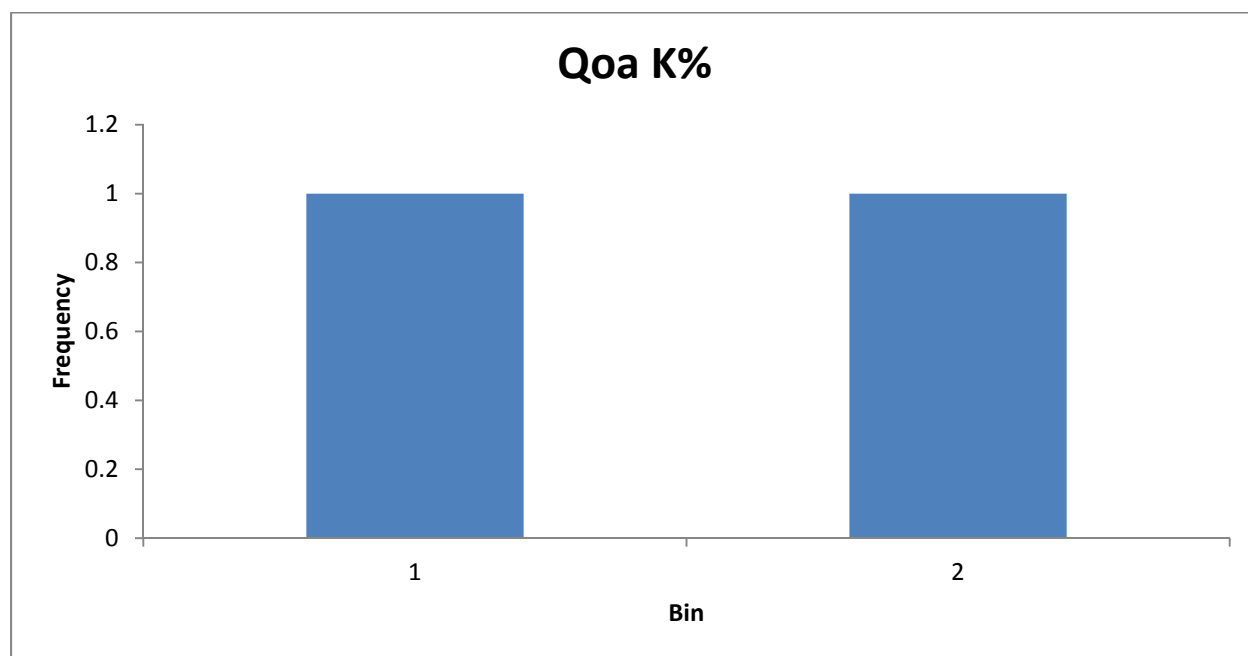
0 0.450.9 1.8
Kilometers

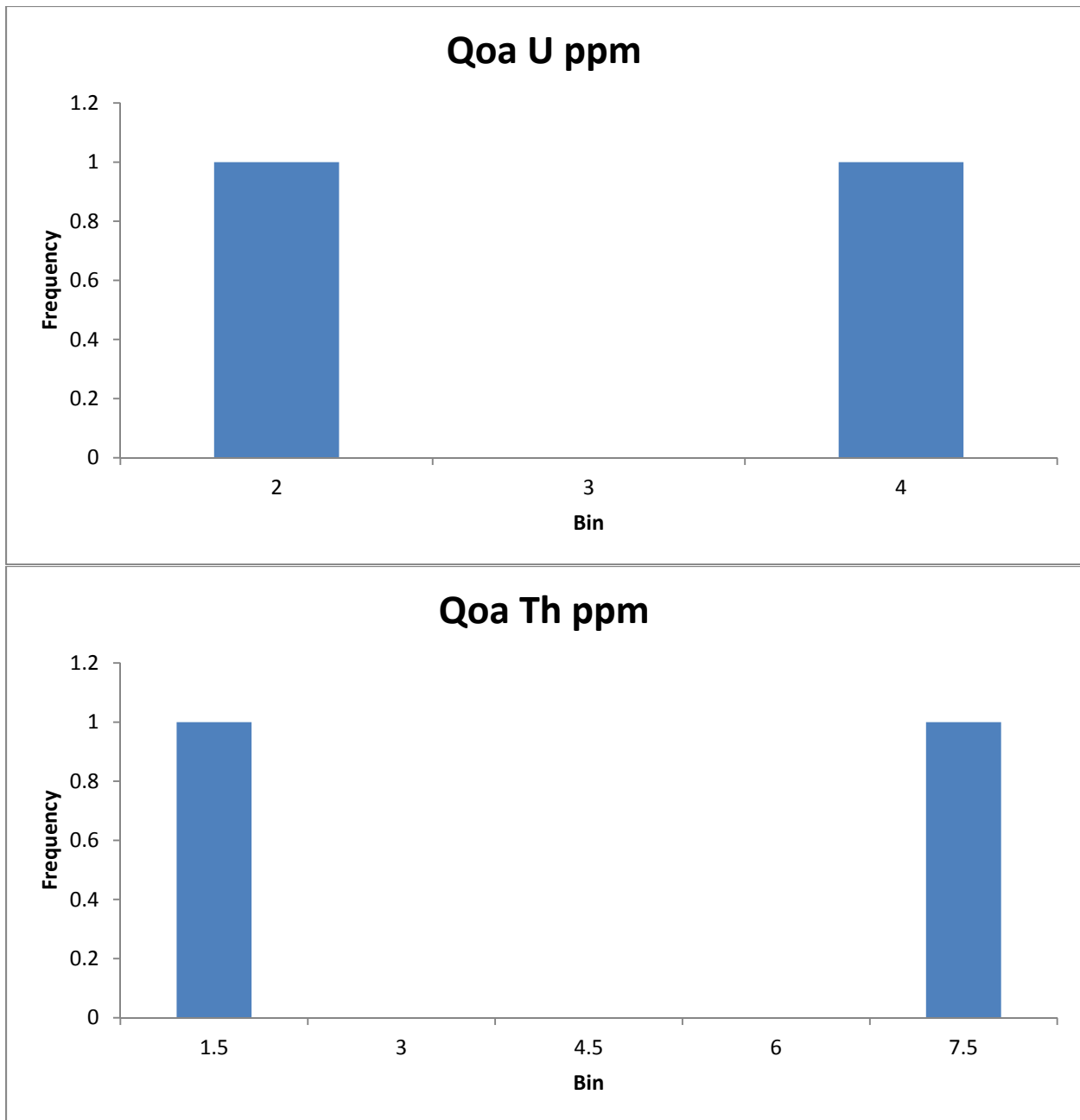
Traditional Geochemistry

There are two traditional geochemical points in Qoa. The data for each point are quite different in terms of concentrations. The first point a has K weight percent of 1.99% vs the other at 0.7%, U is 3.224 ppm vs 1.51 ppm and Th is 6 ppm vs 1.2 ppm. The predicted exposure rate using this data is 4.06 $\mu\text{R/h}$ which compares with the AMS mean of 3.39 $\mu\text{R/h}$.

Sample ID	Latitude	Longitude	K %	U ppm	Th ppm
21120	36.1398	-114.897	1.99	3.224	6.028
21150	36.2252	-114.784	0.7123	1.51	1.172

	K%	U ppm	Th ppm
Mean	1.35115	2.367	3.6
Median	1.35115	2.367	3.6
Standard Deviation	N/A	N/A	N/A
Range	0.7123-1.99	1.51-3.224	1.172-6.028



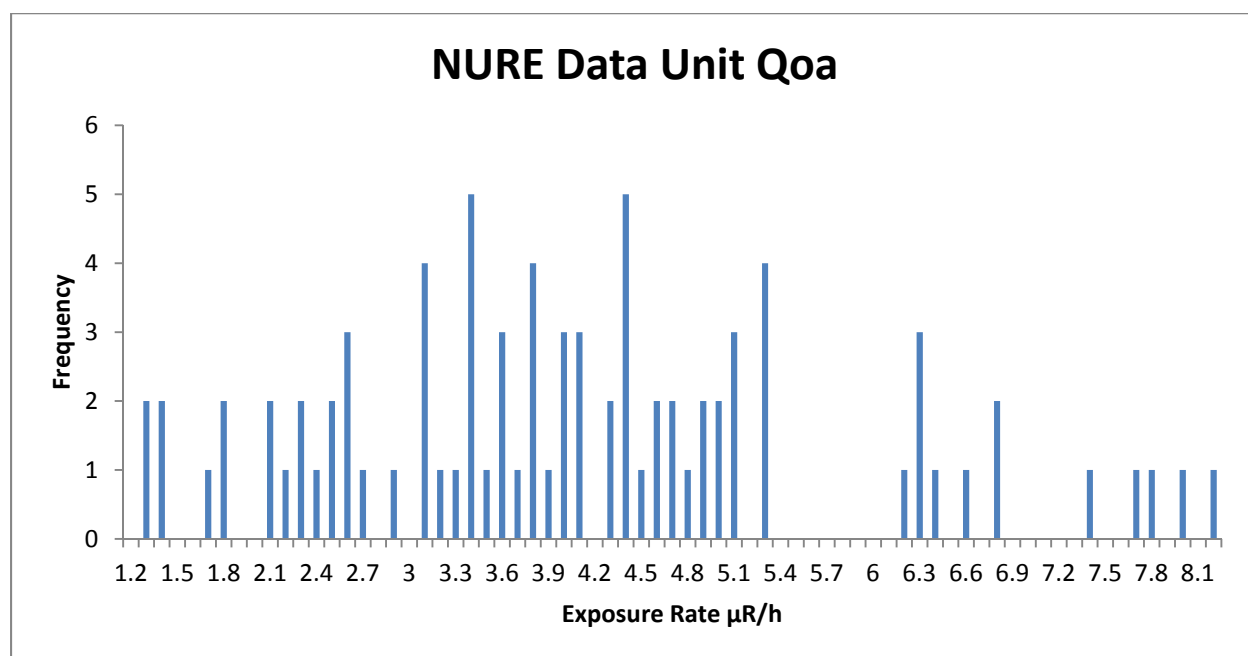


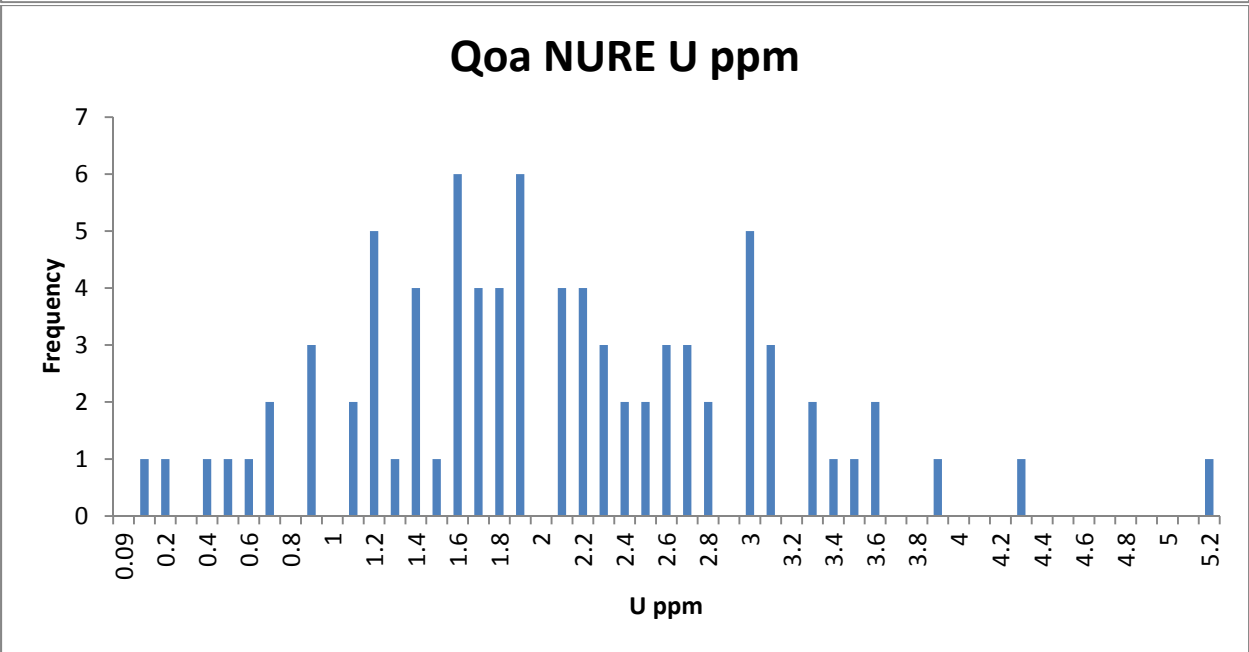
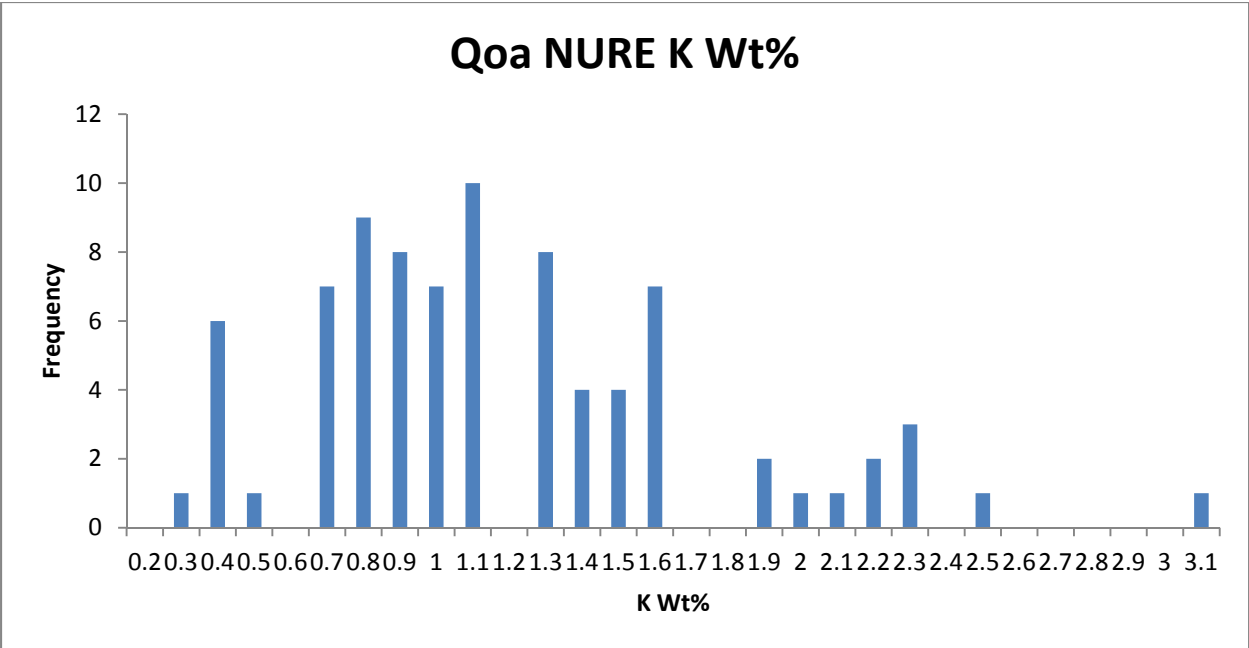
NURE Data

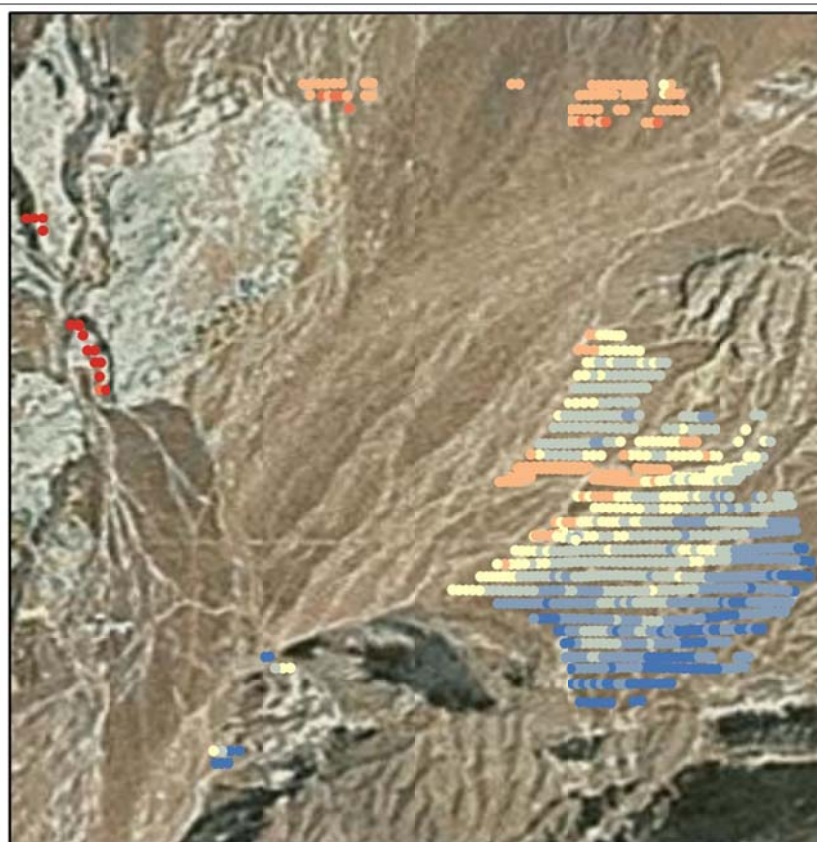
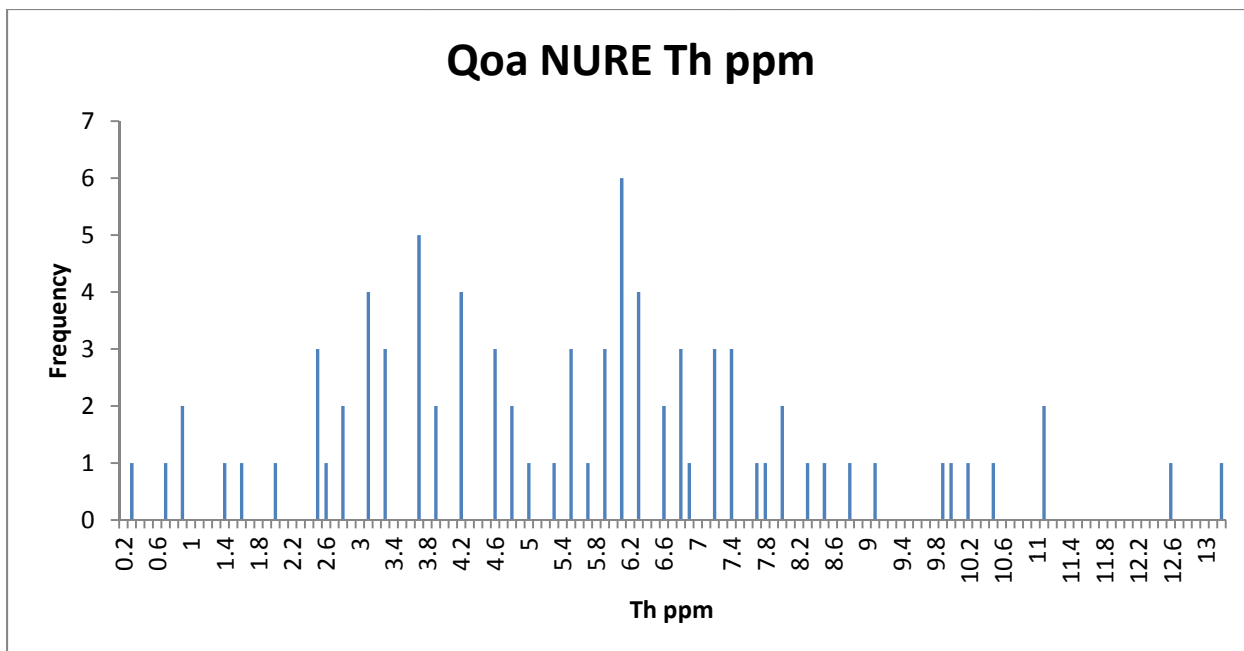
The NURE data for this unit are spread quite widely in terms of both exposure and K, U, and Th concentrations. There are no clear peaks in exposure rate or concentrations. The spread in this unit is a function of the southern NURE line which has no correlation to the AMS data. However, the modeled exposure rate based on this data is within the desired $\pm 1 \mu\text{R/h}$. The

modeled rate is 4.06 $\mu\text{R/h}$ vs the average AMS rate of 3.36 $\mu\text{R/h}$. The predicted rate using NURE data is very similar to the rate from the geochemical prediction.

When comparing the AMS data to the predicted NURE exposure rate on a point by point basis the southern portion appears to be modeled fairly well. However the points that are near the northern unit boundary and the points in the northern portion of the area of interest are not modeled very well.



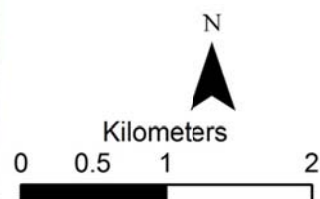




**Government Wash
AMS-Prediction Difference
Unit Qoa**

Absolute Difference
AMS-Prediction

- 0.000949 - 0.273370
- 0.273371 - 0.537760
- 0.537761 - 0.766221
- 0.766222 - 1.000000
- 1.000001 - 1.500000
- 1.500001 - 2.000000
- 2.000001 - 10.000000



Summary

Exposure Rate Comparison $\mu\text{R/h}$	Mean	Median	STD	Range
AMS Data	3.36077664	3.3921685	0.38608314	1.374765-5.041857
NURE Data	4.057899	3.91073	1.625402	1.24076-8.15724
Geochemical Prediction	4.059834	4.059834	N/A	2.0865-6.033168

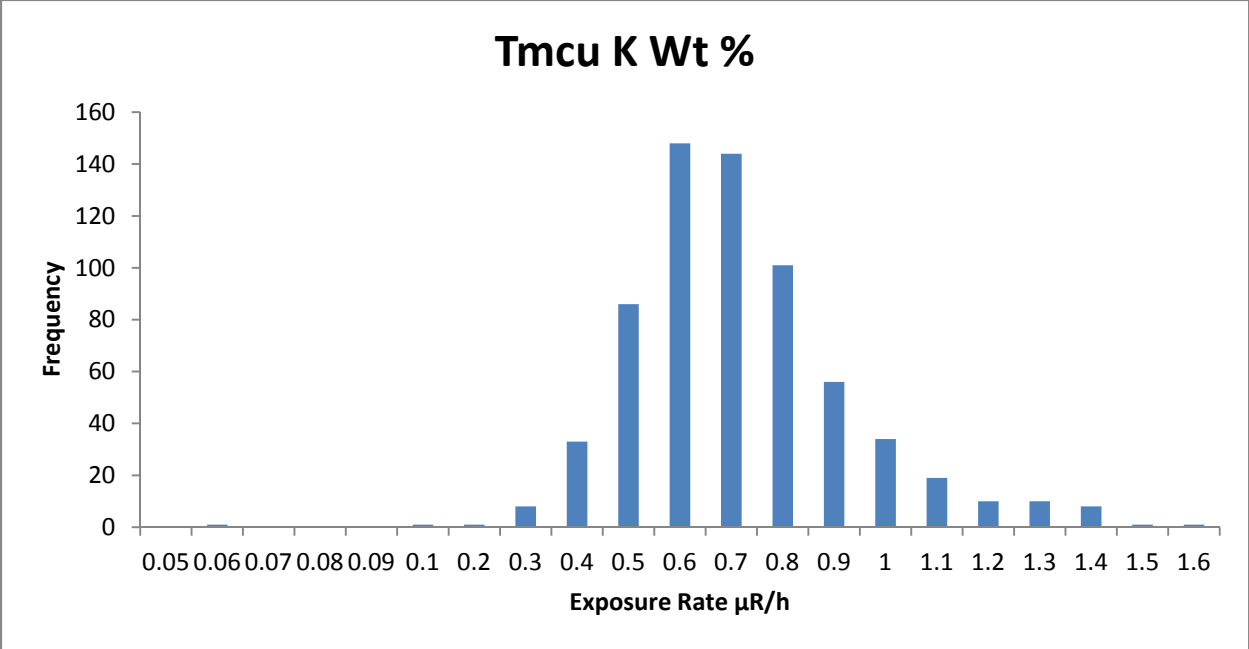
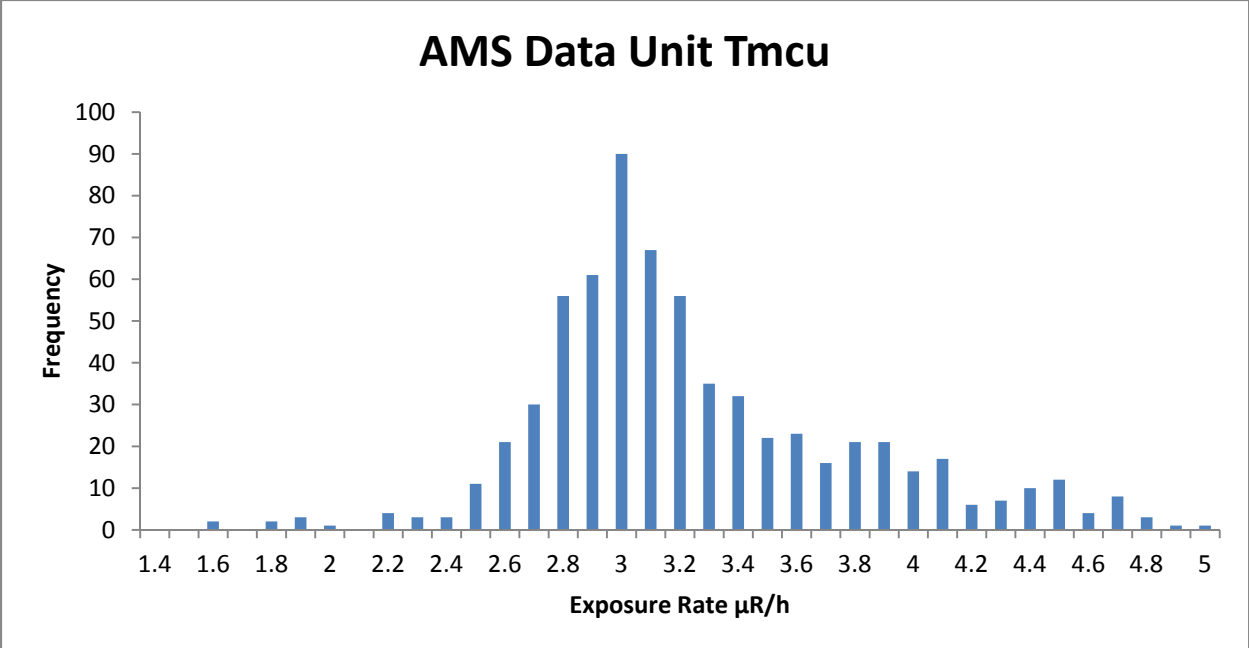
Tmcu

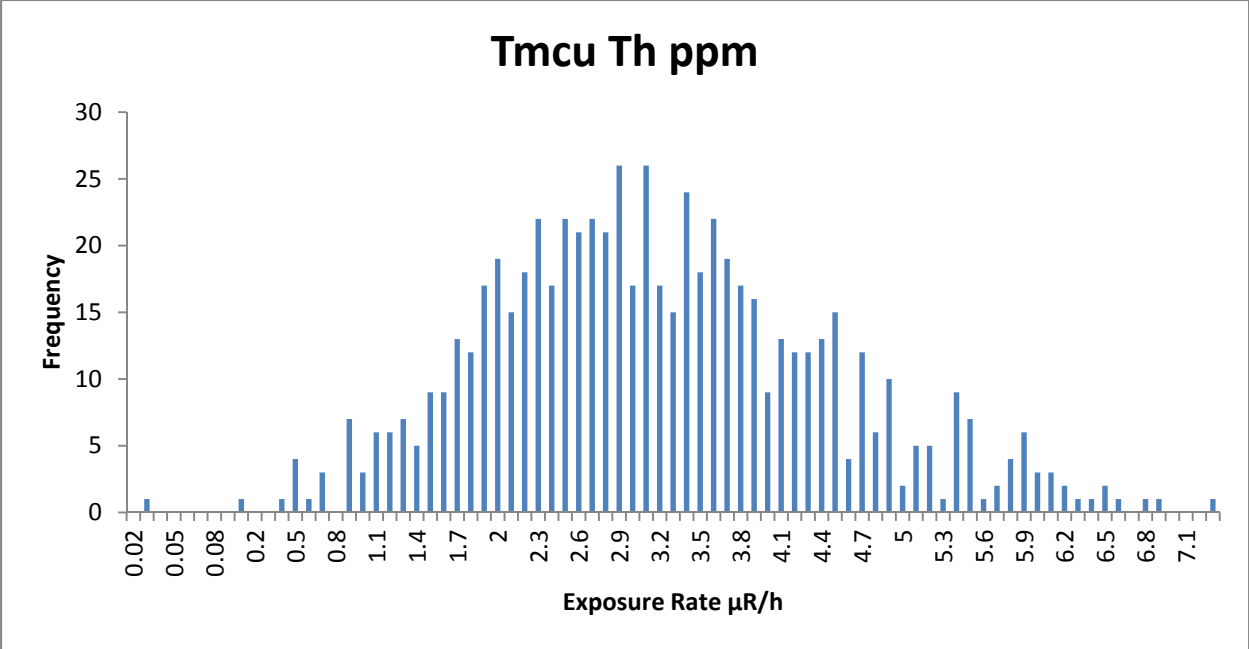
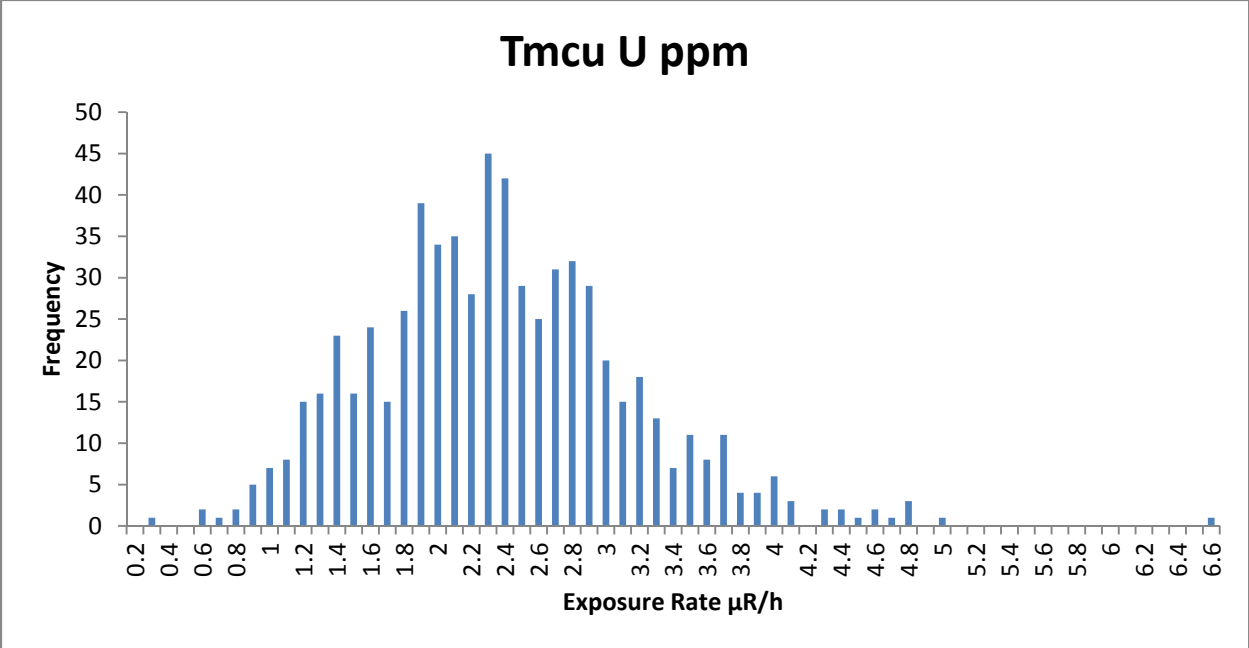
Composition

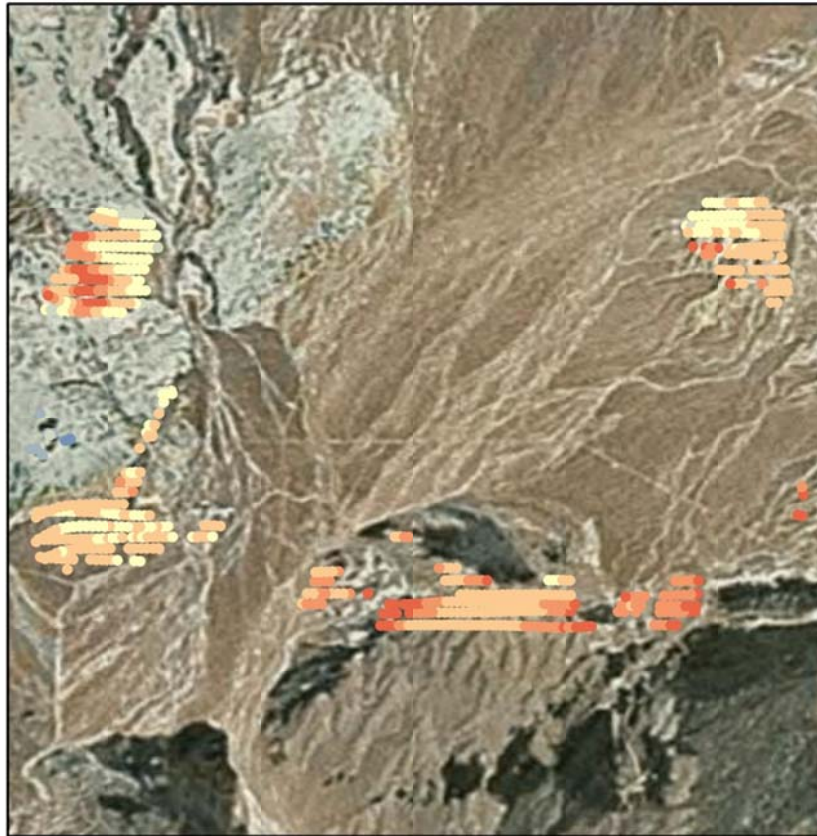
Tmcu is the upper member of the Muddy Creek Formation and is late Miocene in age. It consists of boulder to cobble conglomerate with areas of minor sandstone and siltstone. Clasts are light brown to tan, poorly sorted and fairly well indurated. Clast and matrix supported conglomerate are present. Clasts are heterogeneous in nature and subangular, ranging from Paleozoic to Mesozoic in age. Rocks are sourced from sandstone, siltstone, mudstone and limestone from the Willow Tank Formation, Aztec Sandstone, Moenkopi Formation and older Permian units. It also contains dacite from Lava Butte and minor contributions from the Horse Springs Formation. (Duebendorfer, 2003)

AMS Data

The AMS data within Tmcu has a fairly normal distribution with a strong peak at 3 $\mu\text{R/h}$. The average exposure rate is 3.2 $\mu\text{R/h}$ with a standard deviation of 0.55 $\mu\text{R/h}$ or 17% of the mean. There is a tail at the high end of the data that occurs near unit boundaries suggesting a detector footprint effect. The K, U, and Th concentrations are also normally distributed.







**Government Wash
AMS Data
Unit TmCu**

Exposure Rate ($\mu\text{R/h}$)

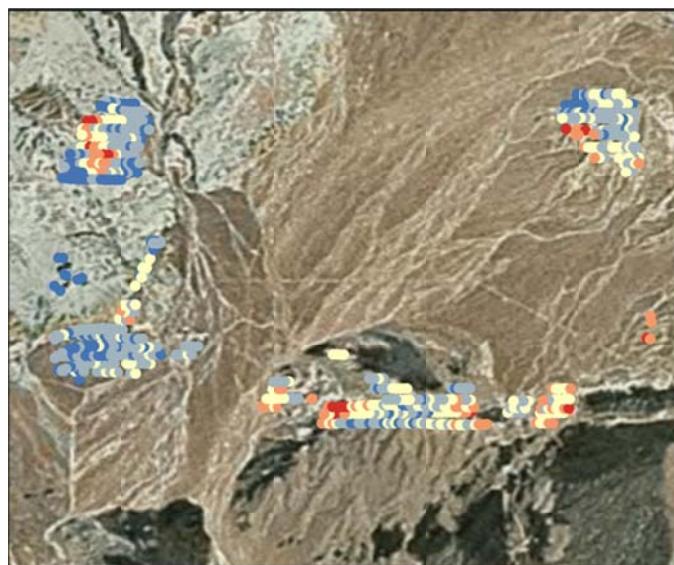
- 0 - 1.230088
- 1.230089 - 1.633850
- 1.633851 - 2.037611
- 2.037612 - 2.441372
- 2.441373 - 2.845133
- 2.845134 - 3.450774
- 3.450775 - 4.056416
- 4.056417 - 5.670907
- 5.670908 - 10.768856

N

Kilometers

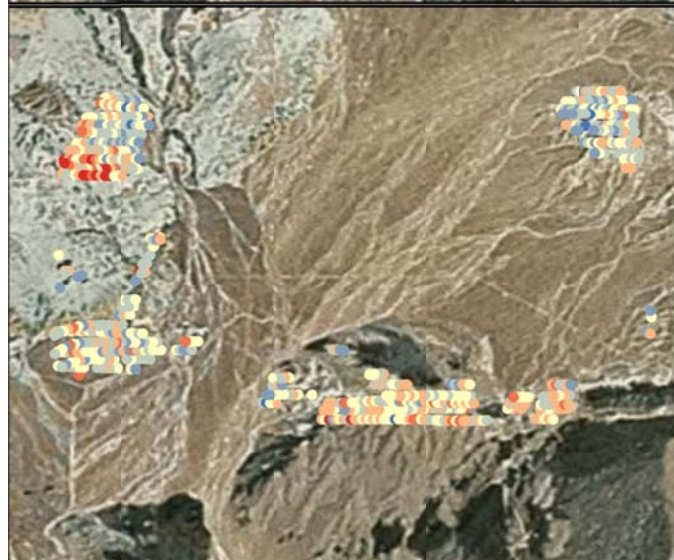
0 0.75 1.5 3

Government Wash Radioelement Concentration Images Unit Tmcu



K Wt%

- 0 - 0.485574
- 0.485575 - 0.679890
- 0.679891 - 0.902579
- 0.902580 - 1.234061
- 1.234062 - 2.271017



U PPM

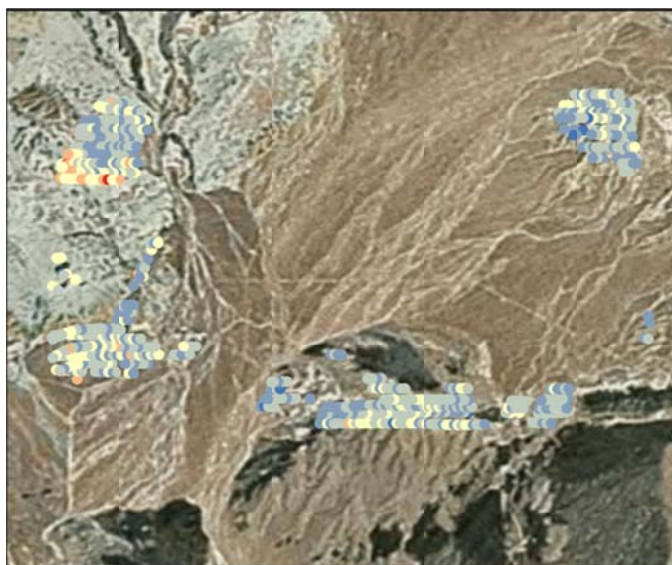
- 0 - 0.818232
- 0.818233 - 1.415482
- 1.415483 - 2.069242
- 2.069243 - 2.679219
- 2.679220 - 3.502989
- 3.502990 - 4.043893
- 4.043894 - 7.910720



Th PPM

- 0 - 0.942384
- 0.942385 - 1.784504
- 1.784505 - 2.810072
- 2.810073 - 3.763784
- 3.763785 - 4.843144
- 4.843145 - 6.364771
- 6.364772 - 8.949389
- 8.949390 - 14.238856





Government Wash Radioelement Ratio Images Unit Tmcu

U/K Ratio

- 0 - 1.000000
- 1.000001 - 2.776200
- 2.776201 - 4.814531
- 4.814532 - 9.199804
- 9.199805 - 26.562074
- 26.562075 - 67.621020
- 67.621021 - 229.055746



Th/K Ratio

- 0 - 3.307556
- 3.307557 - 5.092326
- 5.092327 - 7.271497
- 7.271498 - 15.387768
- 15.387769 - 38.153590
- 38.153591 - 74.386013
- 74.386014 - 164.297821



U/Th Ratio

- 0 - 0.100000
- 0.100001 - 0.500000
- 0.500001 - 1.000000
- 1.000001 - 1.500000
- 1.500001 - 2.000000
- 2.000001 - 3.000000
- 3.000001 - 9.114520
- 9.114521 - 242.489933

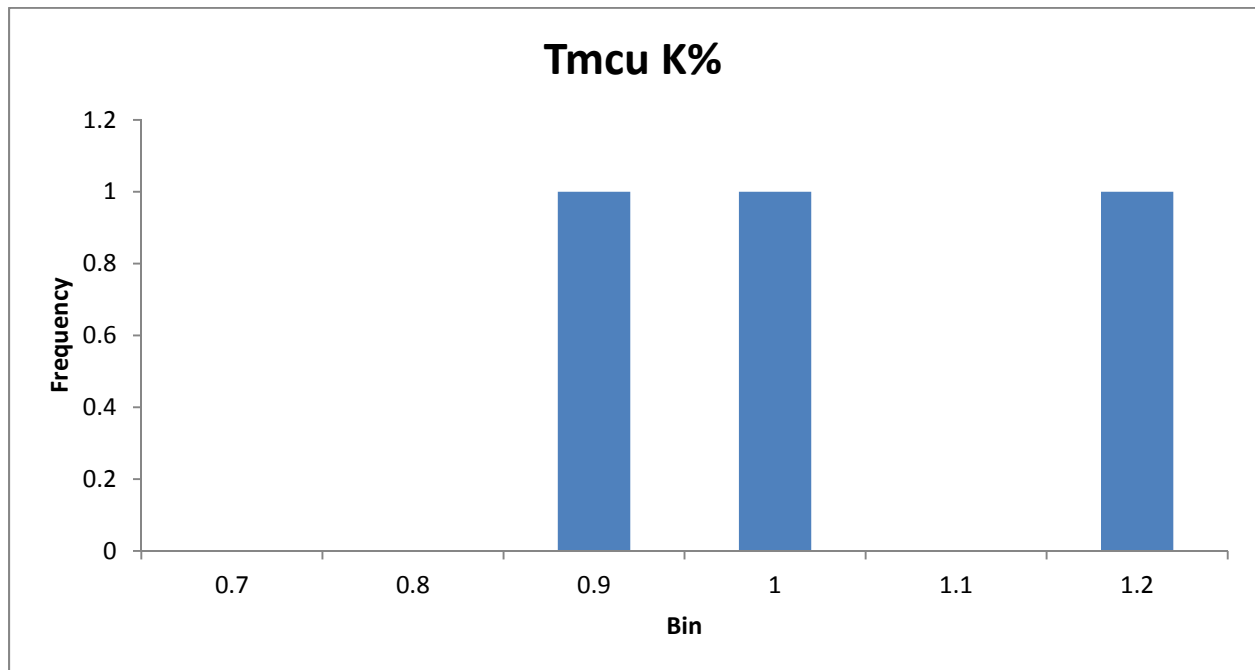


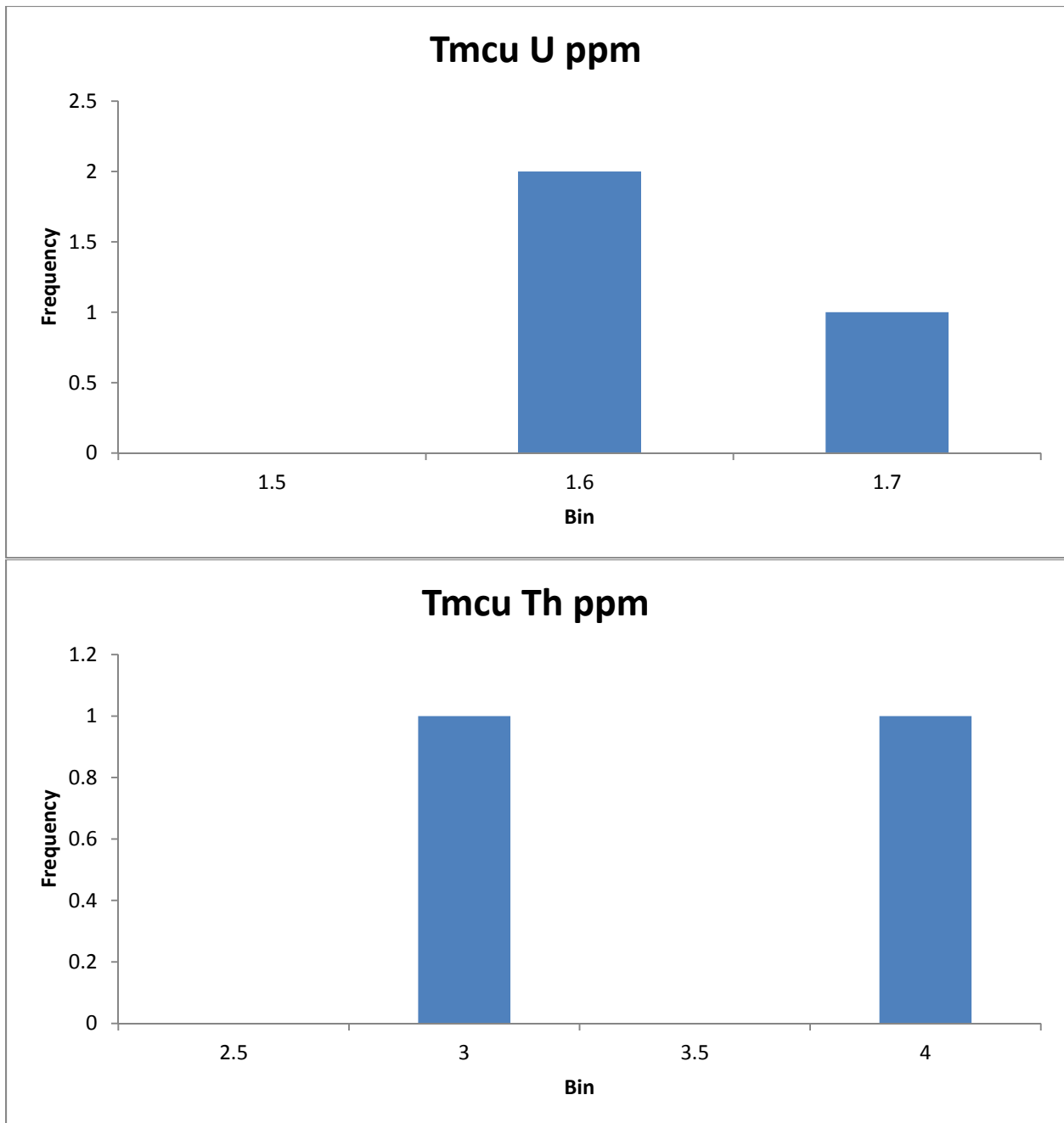
Traditional Geochemistry

There are three data points that occur in this unit and they all report similar values. The exposure rate derived from these values is 3 μ R/h compared to the AMS mean of 3.2 μ R/h.

Sample ID	Latitude	Longitude	K %	U ppm	Th ppm
21156	36.1801	-114.785	0.8336	1.59	
21157	36.1818	-114.777	1.132	1.65	2.637
21158	36.1879	-114.767	0.9569	1.57	3.539

	K%	U ppm	Th ppm
Mean	0.974167	1.603333	3.088
Median	0.9569	1.59	3.088
Standard Deviation	0.122432	0.033993	0.451
Range	0.8336-1.132	1.57-1.65	2.637-3.539

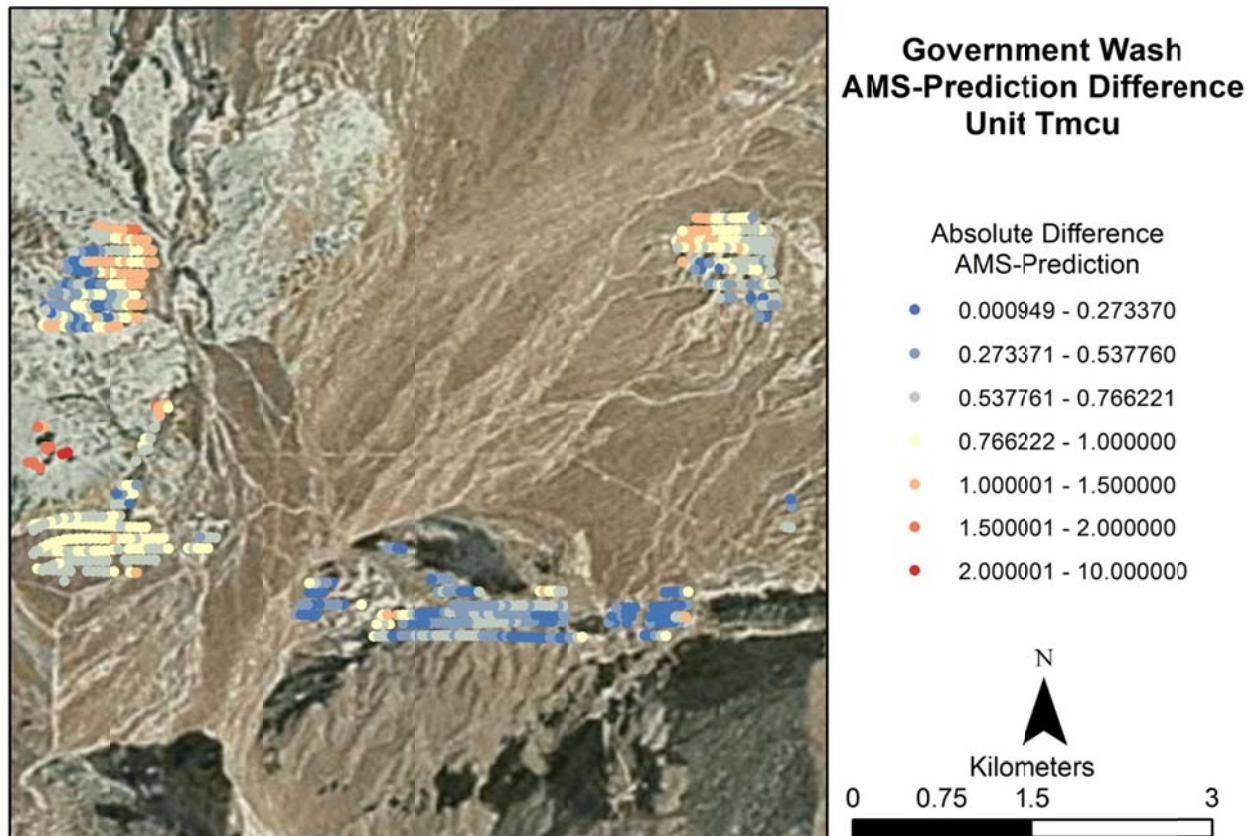


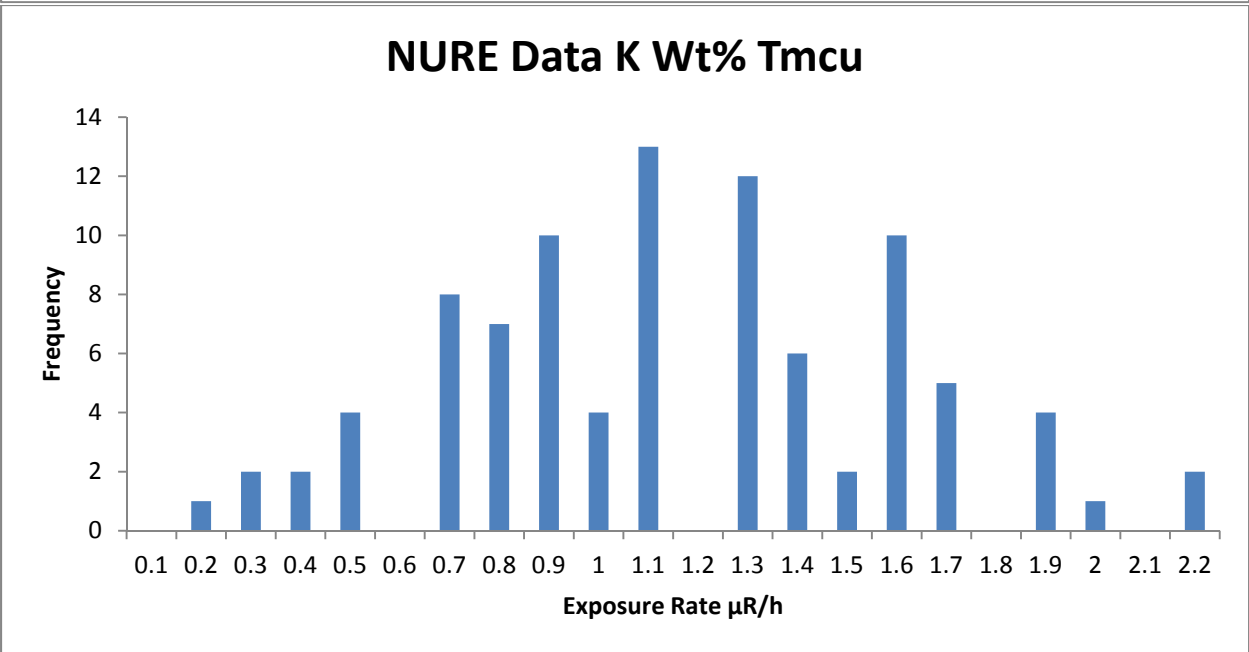
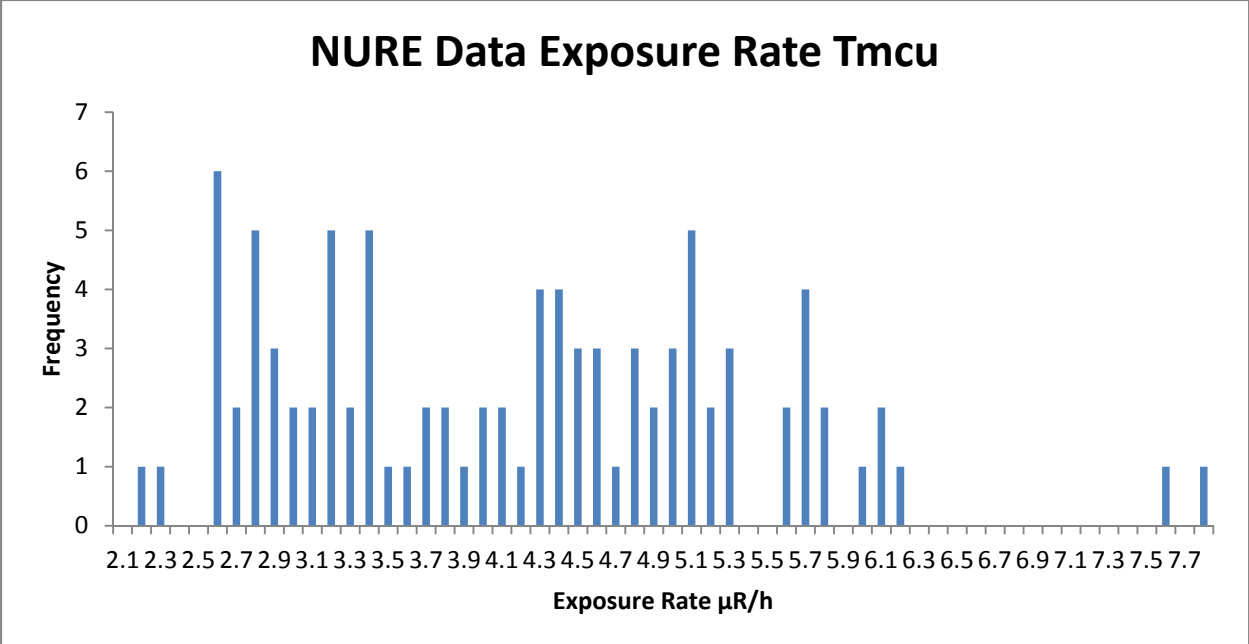


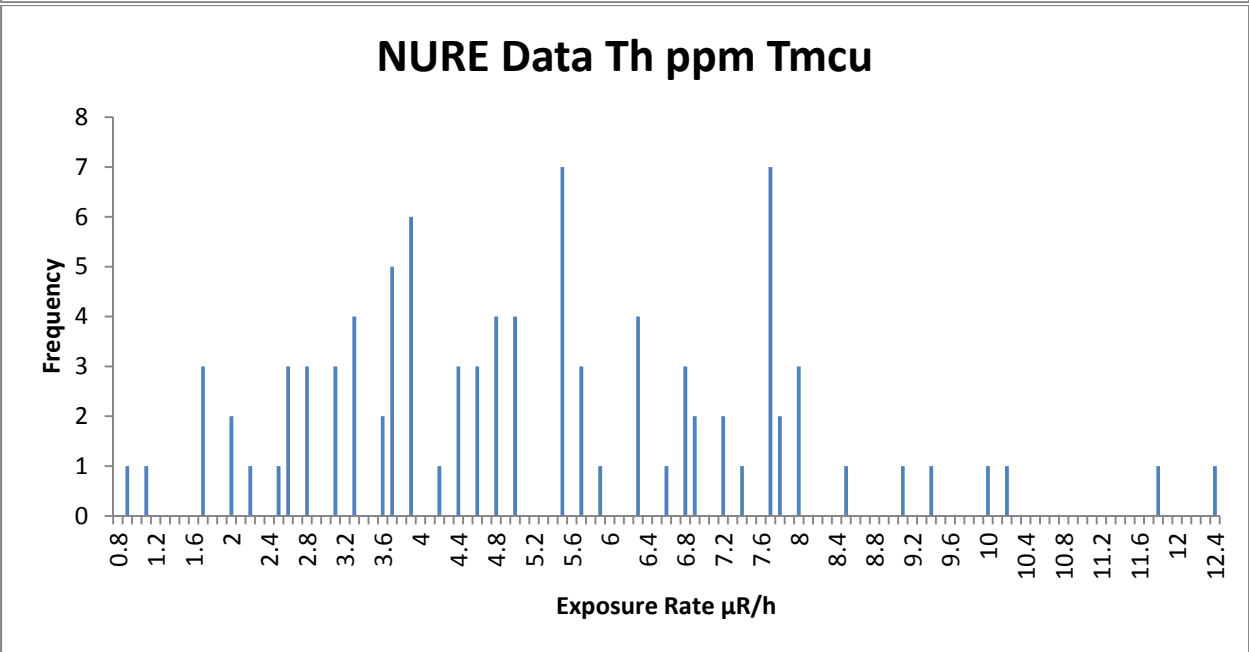
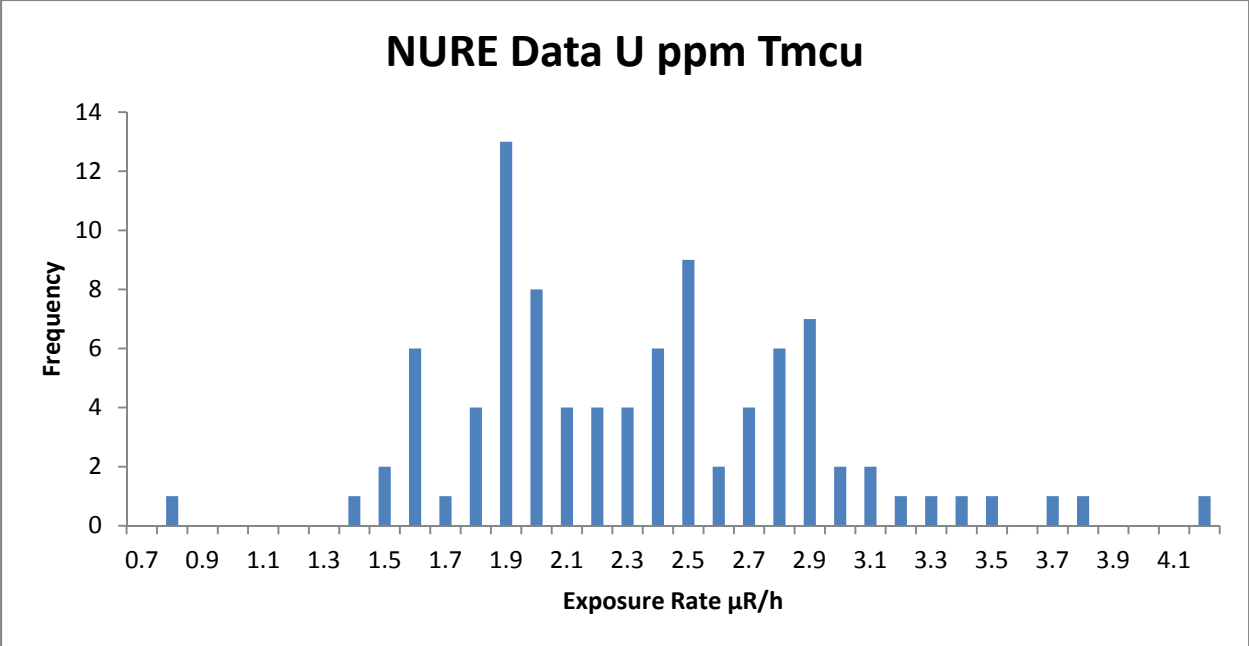
NURE Data

The NURE data that occurs in this unit has wide variability. Much of the data for this unit comes from the southern NURE line that is in disagreement with the AMS data. The mean exposure rate of this data is 3.7 $\mu\text{R/h}$ which compares with the AMS mean of 3.2 $\mu\text{R/h}$. This data falls within the desired ± 1 $\mu\text{R/h}$ range.

When comparing the NURE mean against each AMS point there are areas with fairly good agreement. The southern portion of the unit generally shows less than 0.5 $\mu\text{R/h}$ difference while greater differences occur in the western portion of the unit. In the western areas there are only small outcroppings of the unit and are nearly the size of the detector footprint.







Summary

Exposure Rate Comparison μR/h	Average	Median	STD	Range
AMS Data	3.20053391	3.064148	0.55323723	1.522792-4.971656
NURE Data	3.691962	4.21533	1.187289	2.15237-7.74172
Geochemical Prediction	3.004463	2.974364	N/A	2.677976-3.361048

Tmcg

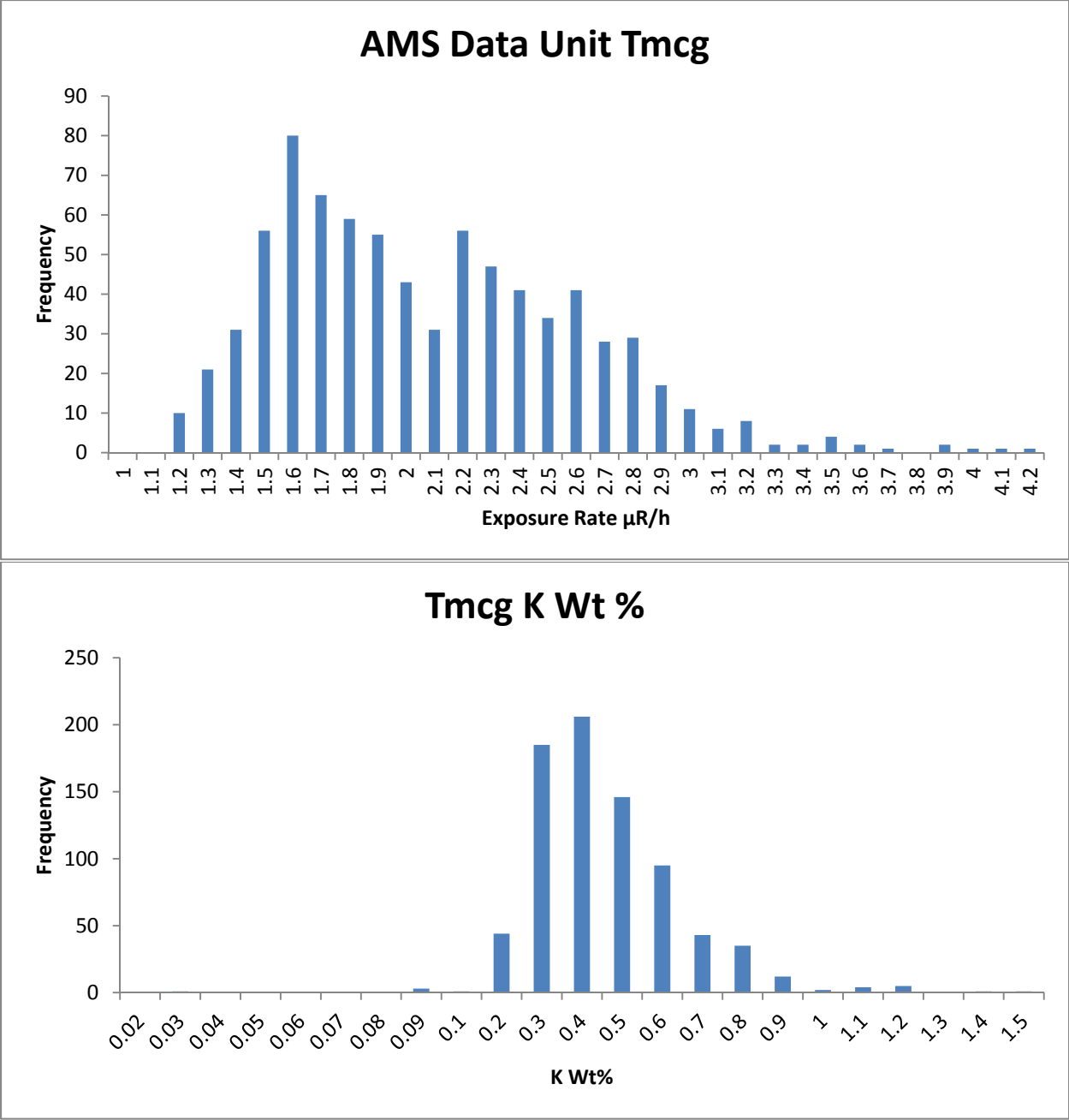
Composition

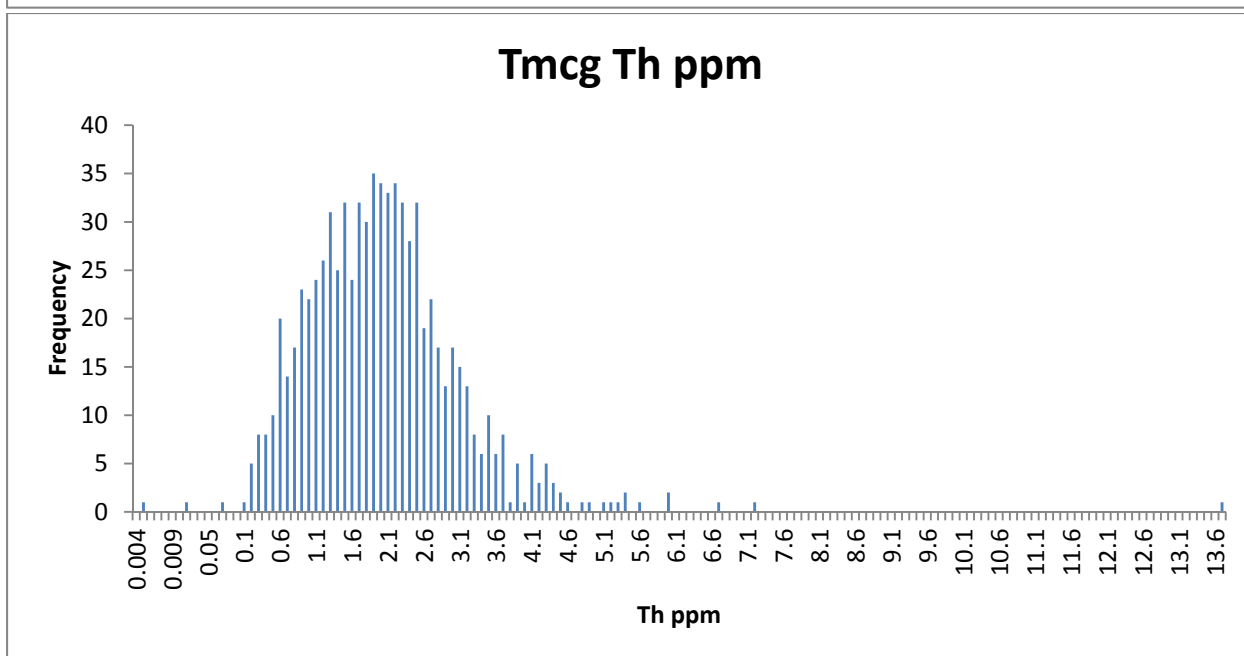
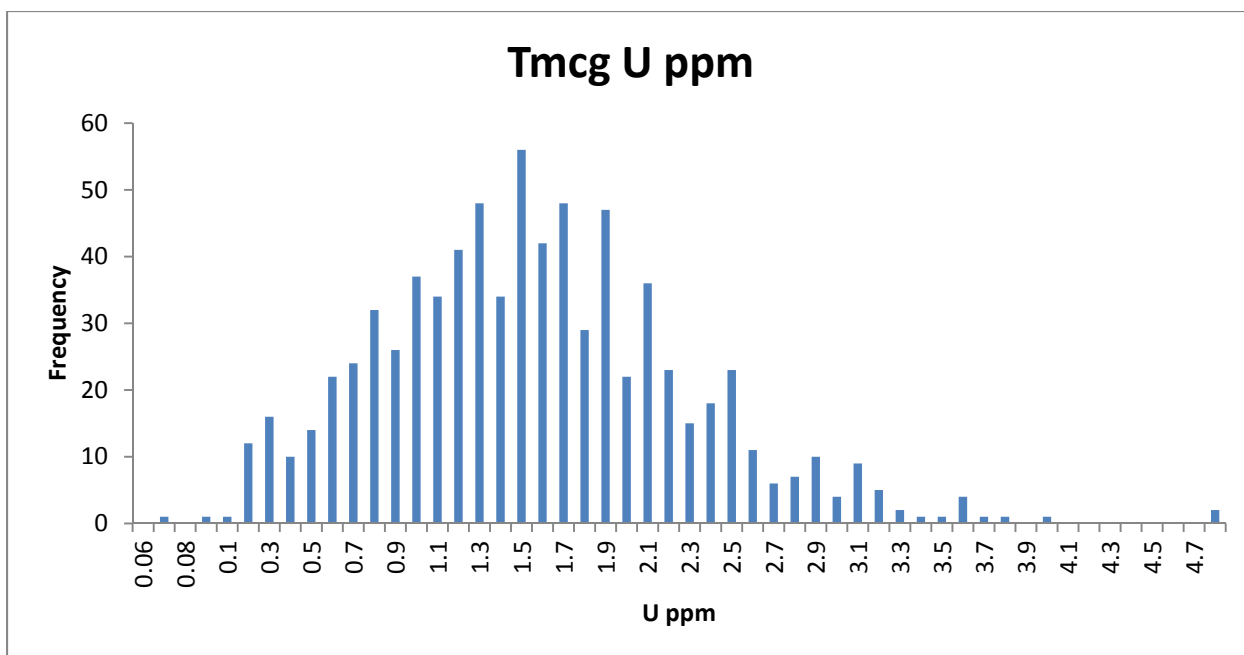
Tmcg is the middle unit in the Muddy Creek Formation and is late Miocene in age. It consists largely of gypsum with some variable amounts of silt and clay. The color ranges from white/grey to pale yellow/orange. Resistant to weathering relative to the lower unit Tmcl and forms weakly resistant ledges on top of Tmcl. Currently mined for gypsum by Pabco Gypsum. (Duebendorfer, 2003) Pabco Gypsum, a local gypsum mining company, has measured the concentration of gypsum in Tmcg for commercial mining purposes and found that it consists of 91.3% gypsum and is 19.1% water by weight (Pabco Gypsum, 2011).

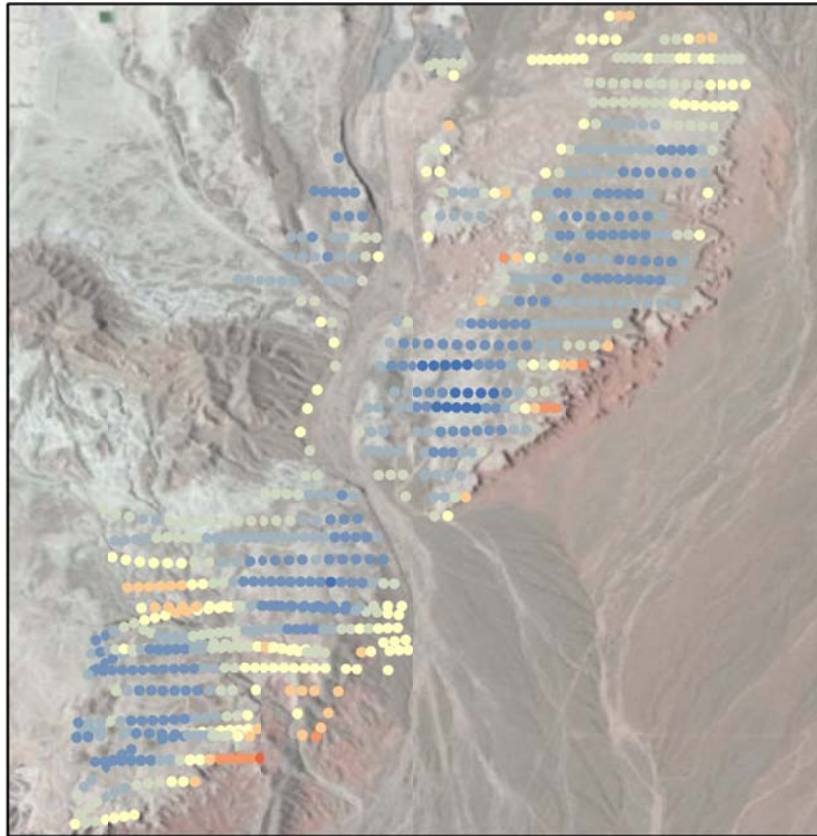
AMS Data

The AMS data shows a strong peak at 1.6 $\mu\text{R/h}$ and trails off toward the high end with one significant peak at 2.2 $\mu\text{R/h}$. The average exposure rate is 2.02 $\mu\text{R/h}$ with a standard deviation of 0.52 $\mu\text{R/h}$ or 25% of the mean. The majority of the points with higher exposure rate values occur around the margins of the unit and in places where the unit has thinned due to erosion. In these places, there are exposures of Tmcl, a significantly hotter unit, that may be influencing the signal.

The distributions of K, U, and Th are however closer to normal but have a wider spread in the data. Data points with higher U and Th values occur along the margins of the unit much like the higher exposure rate values. K however is relatively homogenous across the unit. K peaks at 0.4%, U peaks at 1.5 ppm and Th peaks at 1.9 ppm.



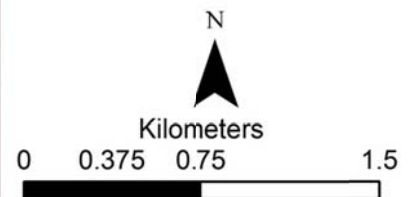


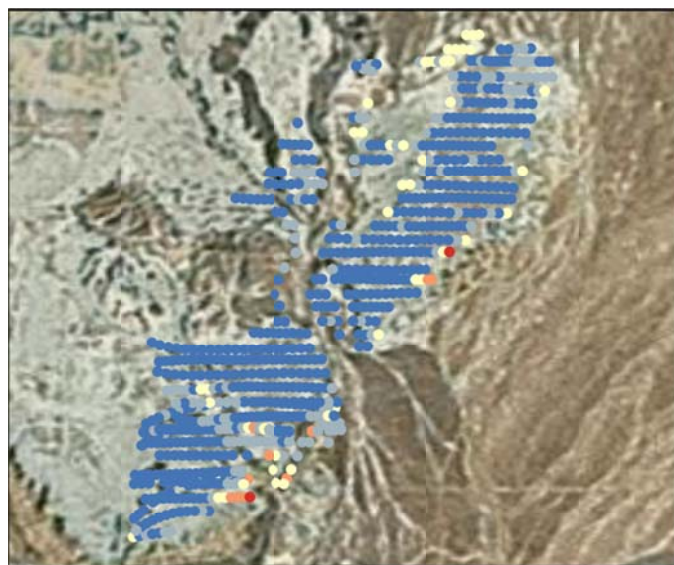


**Government Wash
AMS Data
Unit Tmcg**

Exposure Rate ($\mu\text{R/h}$)

- 0 - 1.230088
- 1.230089 - 1.633850
- 1.633851 - 2.037611
- 2.037612 - 2.441372
- 2.441373 - 2.845133
- 2.845134 - 3.450774
- 3.450775 - 4.056416
- 4.056417 - 5.670907
- 5.670908 - 10.768856

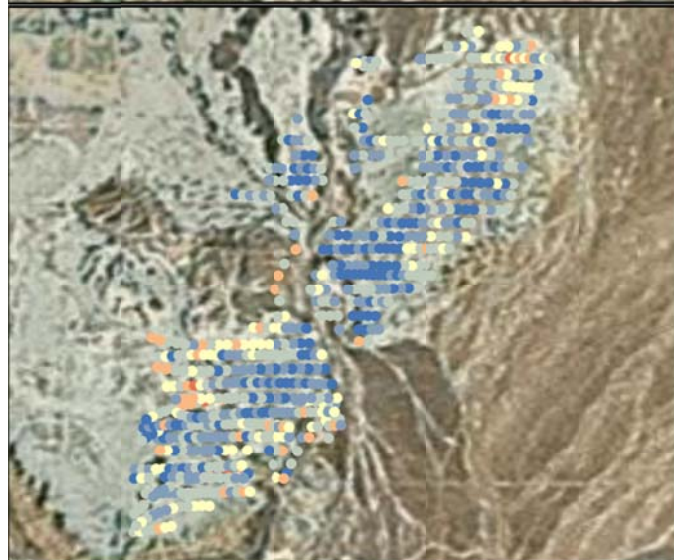




Government Wash Radioelement Concentration Images Unit Tmcg

K Wt%

- 0 - 0.485574
- 0.485575 - 0.679890
- 0.679891 - 0.902579
- 0.902580 - 1.234061
- 1.234062 - 2.271017



U PPM

- 0 - 0.818232
- 0.818233 - 1.415482
- 1.415483 - 2.069242
- 2.069243 - 2.679219
- 2.679220 - 3.502989
- 3.502990 - 4.043893
- 4.043894 - 7.910720

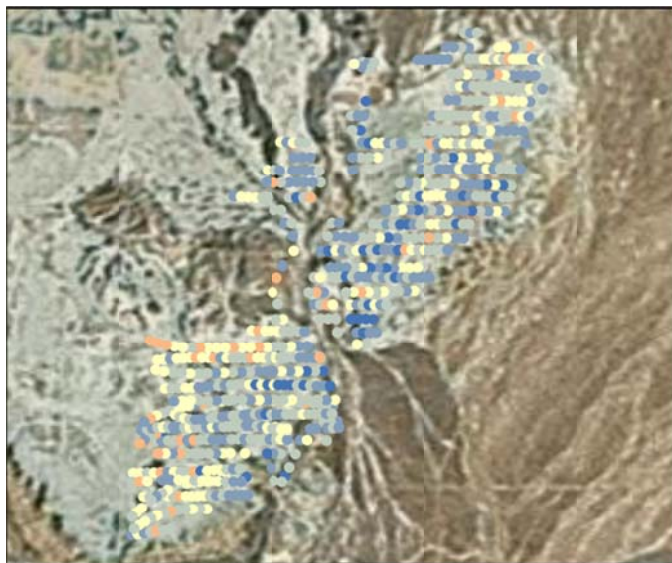


Th PPM

- 0 - 0.942384
- 0.942385 - 1.784504
- 1.784505 - 2.810072
- 2.810073 - 3.763784
- 3.763785 - 4.843144
- 4.843145 - 6.364771
- 6.364772 - 8.949389
- 8.949390 - 14.238856



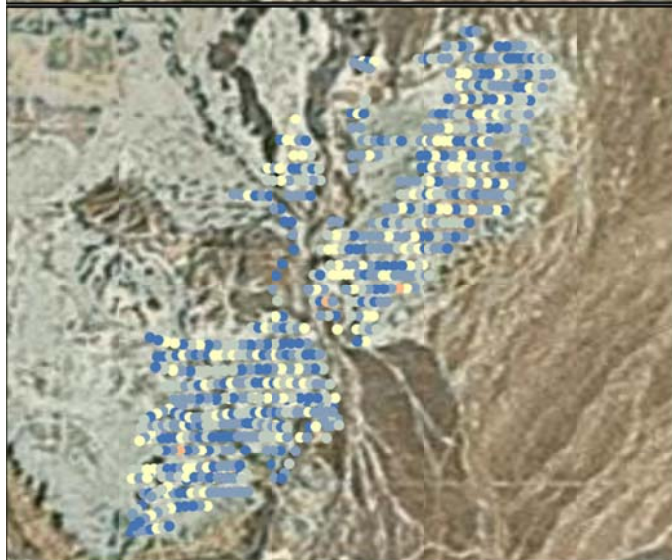
0 0.350.7 1.4
Kilometers



Government Wash Radioelement Ratio Images Unit Tmcg

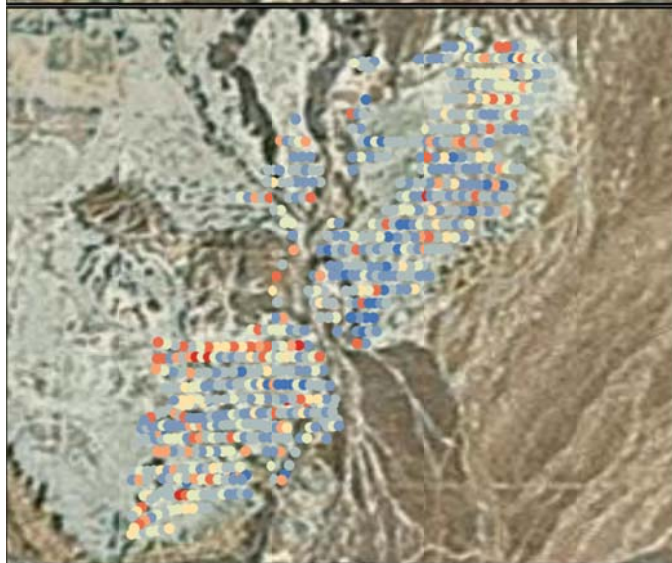
U/K Ratio

- 0 - 1.000000
- 1.000001 - 2.776200
- 2.776201 - 4.814531
- 4.814532 - 9.199804
- 9.199805 - 26.562074
- 26.562075 - 67.621020
- 67.621021 - 229.055746



Th/K Ratio

- 0 - 3.307556
- 3.307557 - 5.092326
- 5.092327 - 7.271497
- 7.271498 - 15.387768
- 15.387769 - 38.153590
- 38.153591 - 74.386013
- 74.386014 - 164.297821



U/Th Ratio

- 0 - 0.100000
- 0.100001 - 0.500000
- 0.500001 - 1.000000
- 1.000001 - 1.500000
- 1.500001 - 2.000000
- 2.000001 - 3.000000
- 3.000001 - 9.114520
- 9.114521 - 242.489933



0 0.350.7 1.4
Kilometers

Traditional Geochemistry

There are no data points for Tmcg that occur within the primary geologic map. Therefore, in order to get data for this unit, the adjacent Frenchman Mountain Geologic Map was used (Castor, Faulds et al. 2000). Unfortunately, the adjacent map has different unit definitions and is mapped at a different scale. The result appears to be that this unit was lumped together with another Muddy Creek unit and the only data point that was recoverable is questionably usable as it contains no metadata to verify that it belongs within this unit. The one data point on the adjacent map has potassium, uranium and thorium values that are very high relative to AMS and NURE concentrations.

Sample ID	Latitude	Longitude	K %	U ppm	Th ppm
15103	36.1077	-114.969	2.715	1.26	4.188

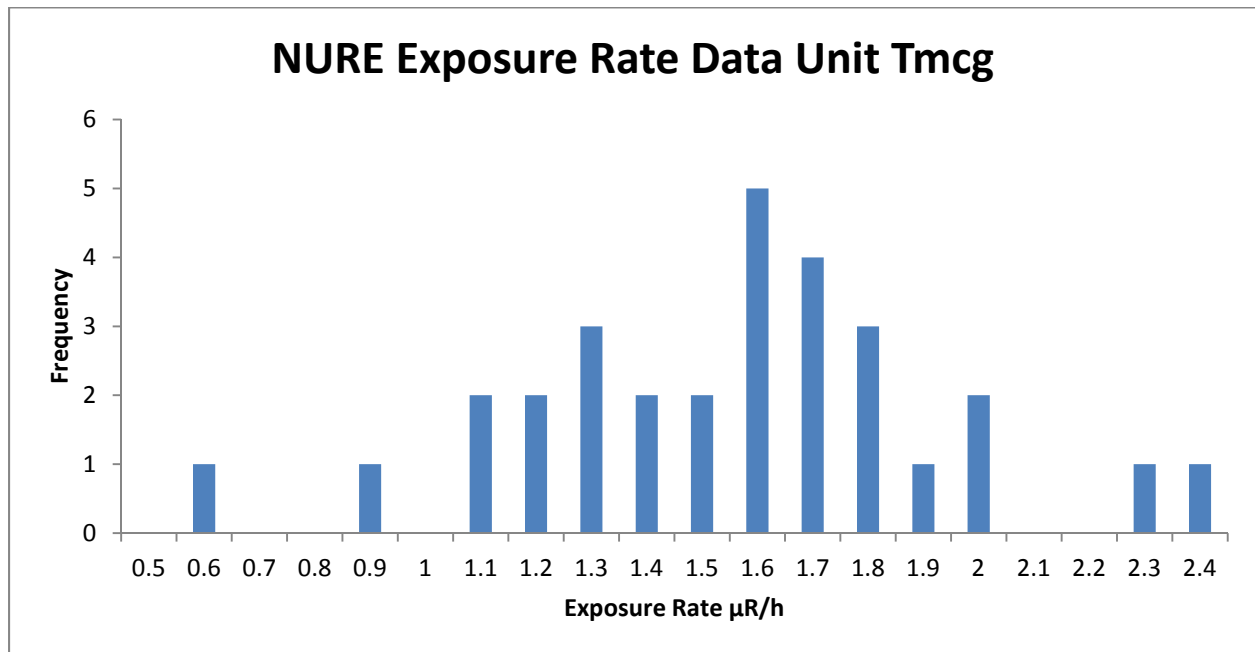
NURE Data

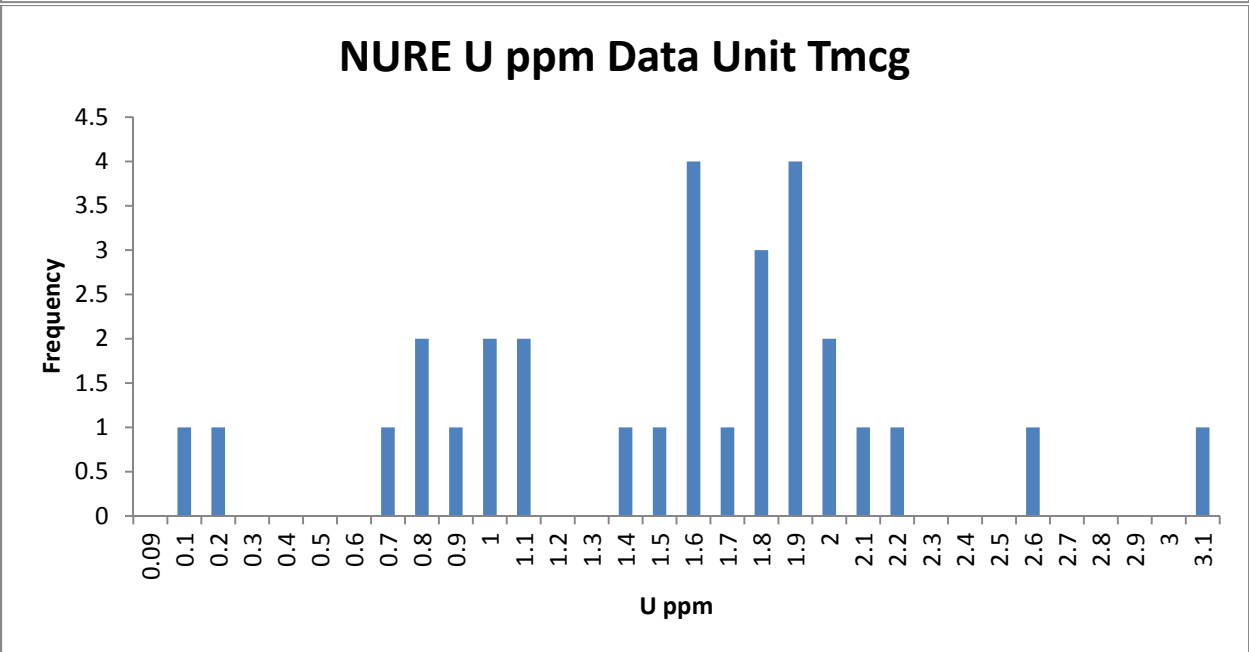
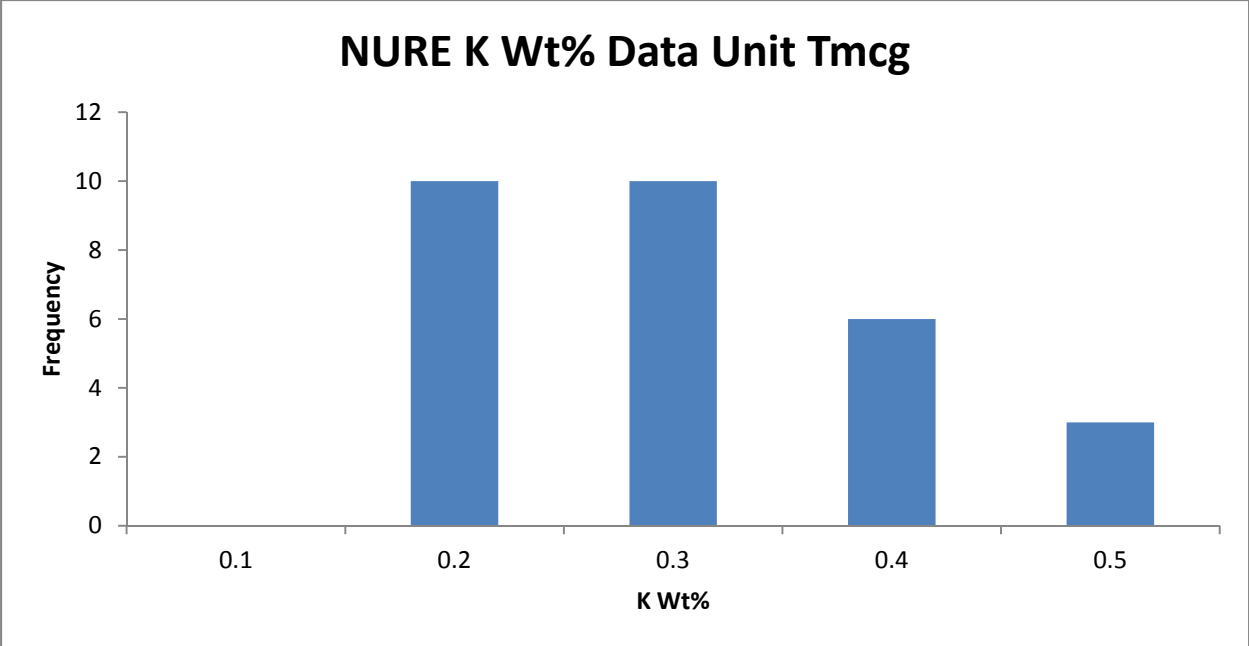
NURE data in Tmcg has considerable spread; however, there are similarities with the AMS data. While the distributions of exposure, K, U, and Th are not normal, they all contain significant peaks at or near the same locations as the AMS data. The exposure rate peak in the NURE data is at 1.6 $\mu\text{R/h}$ which is the same location as the AMS data. K has no significant peak but most points occur between 0.2-0.4% which compares with the AMS peak at 0.4%. The majority of the U points are between 1.4 and 2 ppm which compares to the AMS peak at 1.5 ppm. Th on the other hand is spread fairly widely in the NURE data set and has data on either side of the AMS peak of 1.9 ppm.

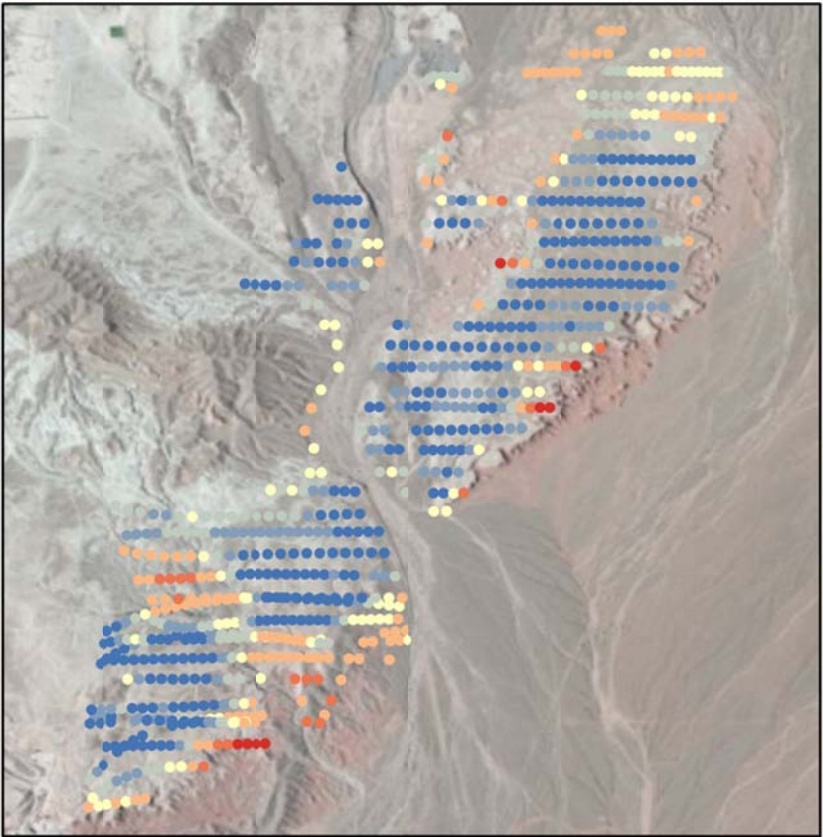
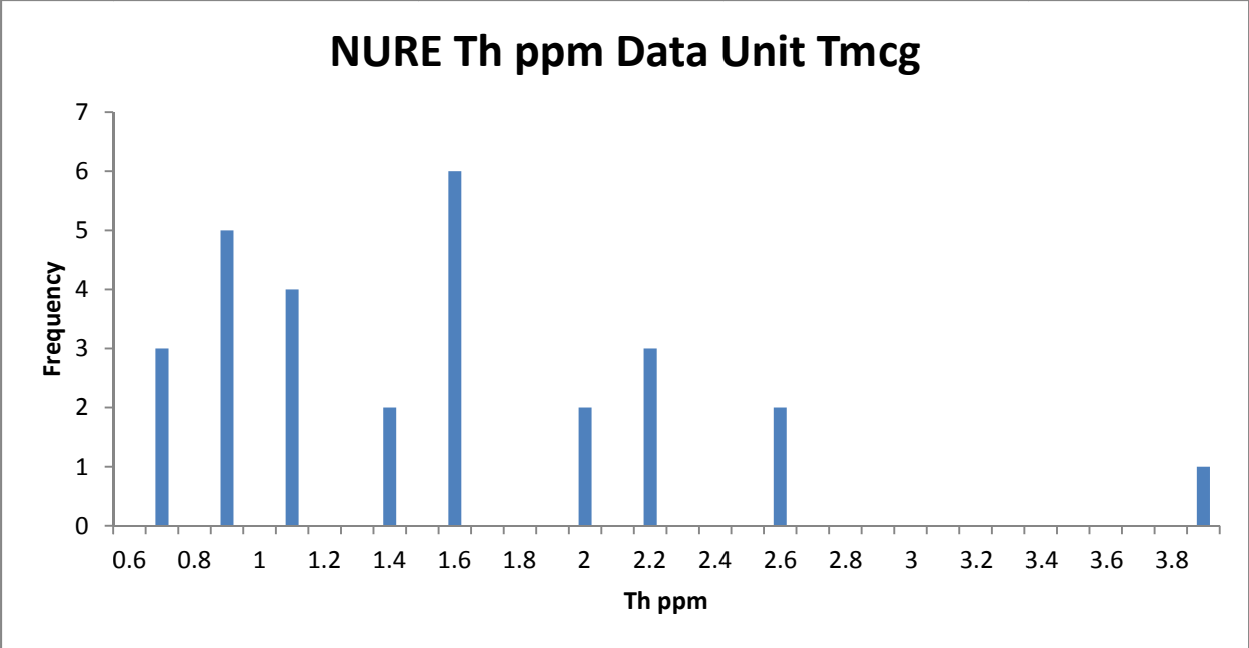
The exposure rate calculated for Tmcg is 1.5 $\mu\text{R/h}$ which compares to the AMS mean of 2.02 $\mu\text{R/h}$. Considering the effect of the hotter points near the margins of the unit the exposure can also be compared to the median of the AMS data at 1.9 $\mu\text{R/h}$ or the exposure rate peak in

the AMS histogram at 1.6 $\mu\text{R/h}$. In every case the average NURE exposure rate is within the ± 1 $\mu\text{R/h}$ success range.

When comparing the NURE exposure rate and the AMS data on a point by point basis it becomes clear that the NURE exposure rate represents the majority of the unit interior. The margins of the unit and areas that have experienced thinning due to erosion are not well modeled with this exposure rate.



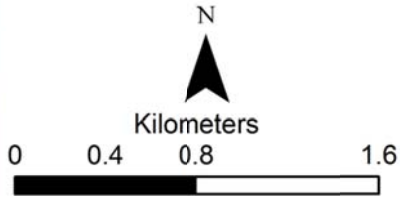




**Government Wash
AMS-Prediction Difference
Unit Tmcg**

Absolute Difference
AMS-Prediction

- 0.000949 - 0.273370
- 0.273371 - 0.537760
- 0.537761 - 0.766221
- 0.766222 - 1.000000
- 1.000001 - 1.500000
- 1.500001 - 2.000000
- 2.000001 - 10.000000



Summary

Exposure Rate Comparison μR/h	Average	Median	STD	Range
AMS Data	2.02534721	1.9271	0.52562249	1.107517-4.1228
NURE Data	1.50422007	1.55627	0.376307713	0.52414-2.34739
Geochemical Prediction	5.413416	N/A	N/A	N/A

Tmcl

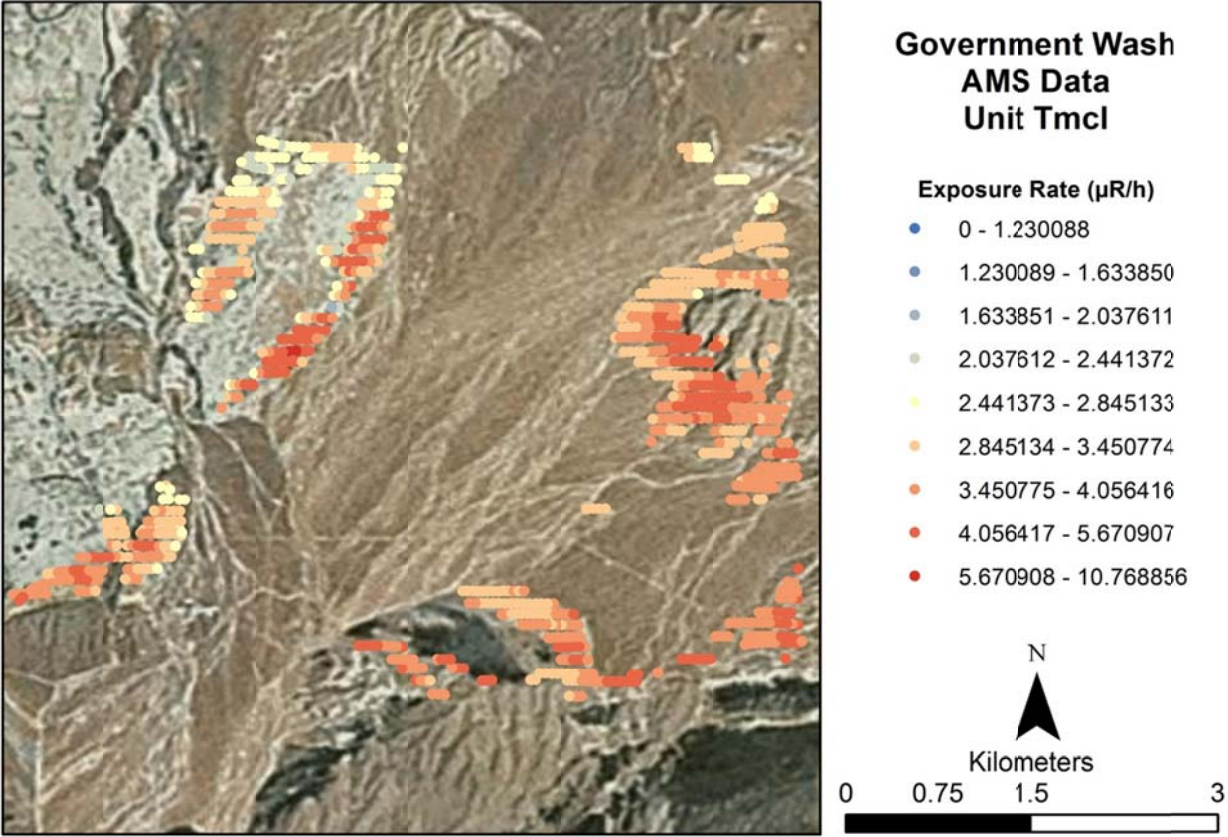
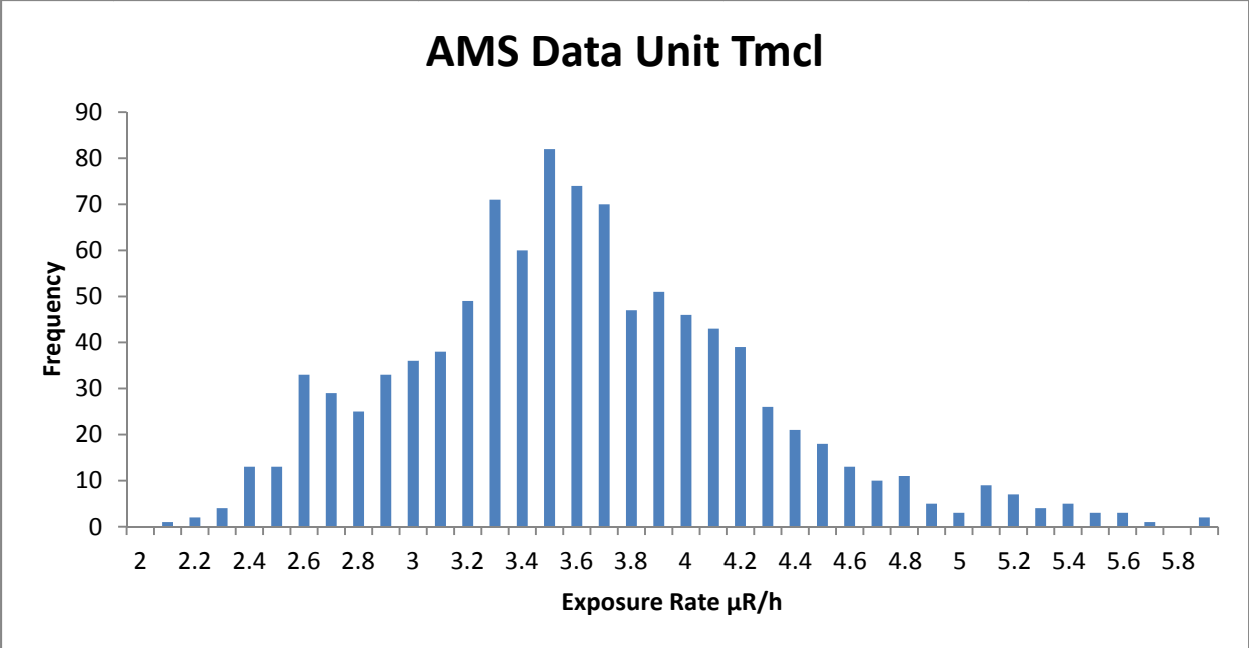
Composition

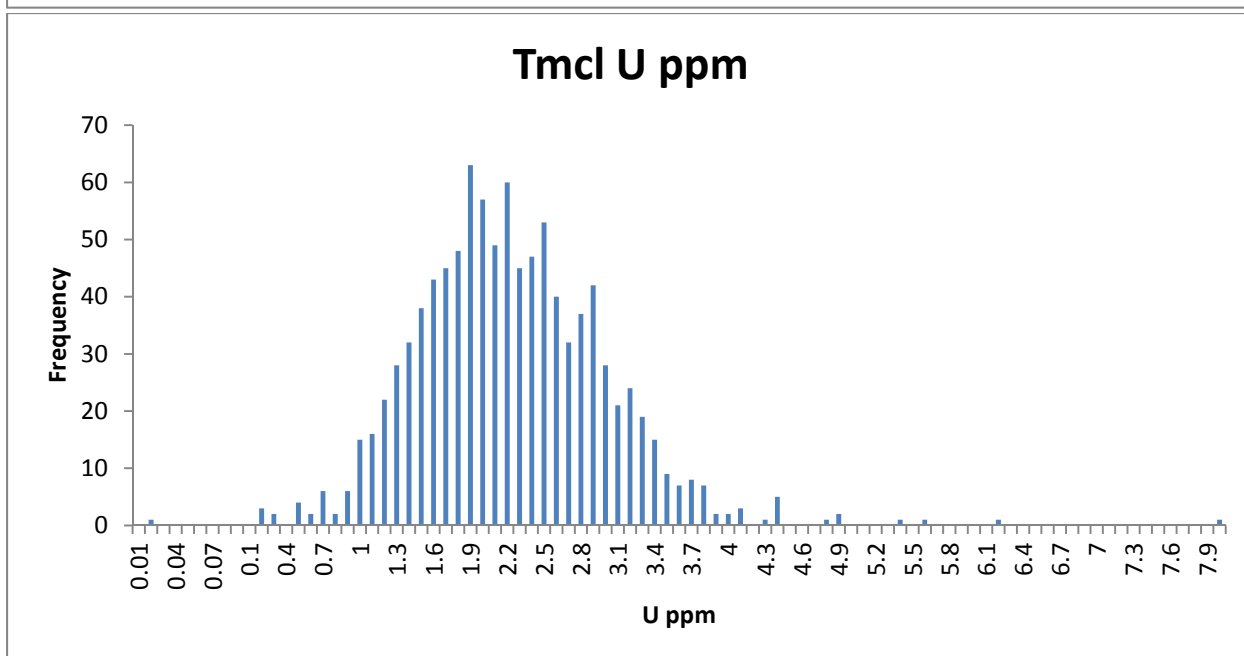
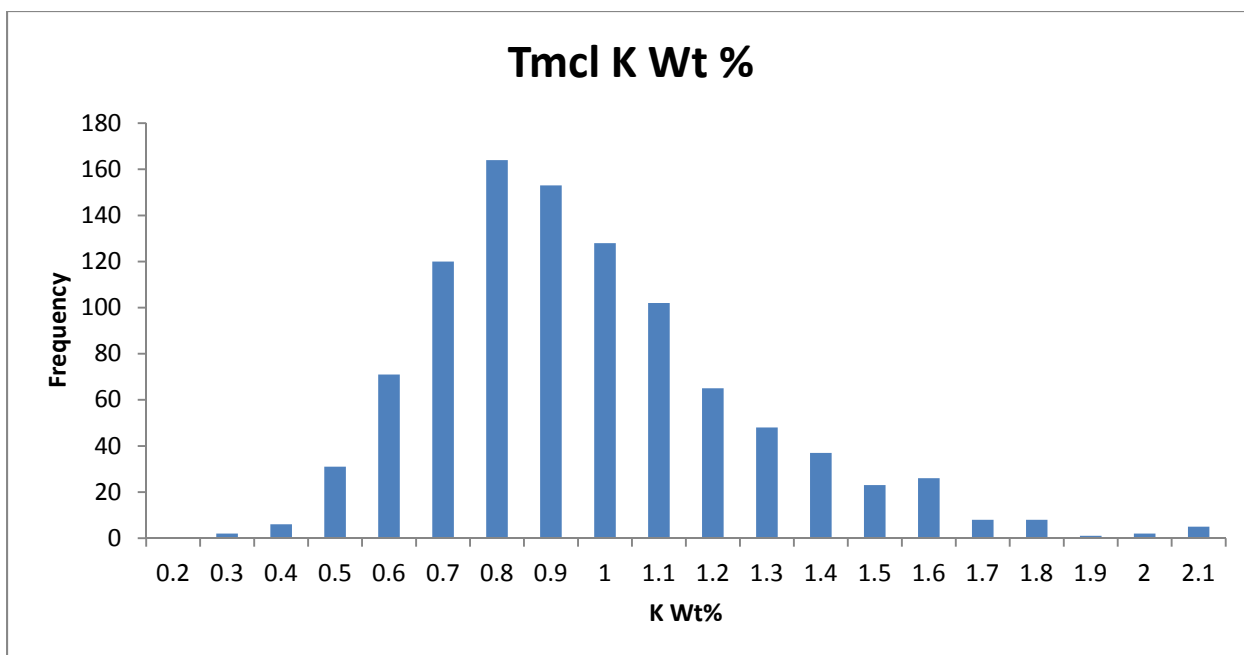
Tmcl is the lowest member of the Muddy Creek Formation and is late Miocene in age. It consists of tan to red-brown mudstone with silt to clay size clasts. It is variably gypsiferous throughout but generally much less gypsum present than in Tmcg. Parts are conglomeratic at the base quickly grading upward to gypsiferous mudstone. (Duebendorfer, 2003)

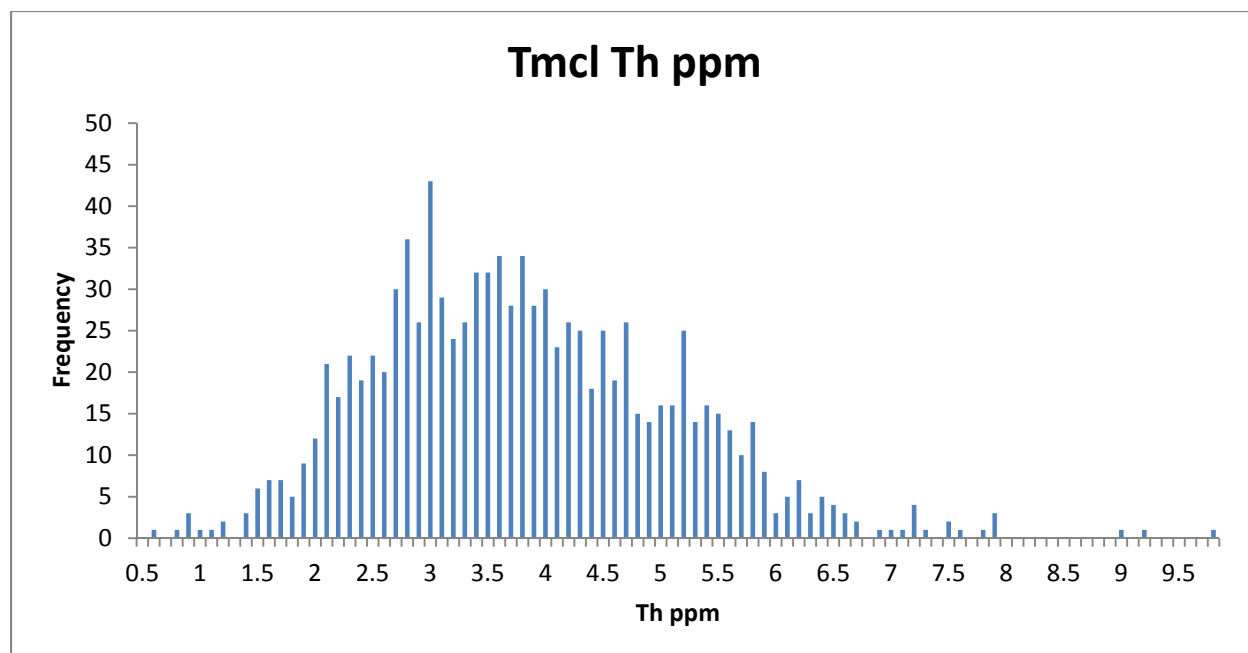
AMS Data

The AMS data for this unit are close to normally distributed. The exposure rate has a peak near 3.5 $\mu\text{R/h}$ with a higher end tail that is $>5 \mu\text{R/h}$. The average exposure rate is 3.56 $\mu\text{R/h}$ with a standard deviation of 0.64 $\mu\text{R/h}$ or 18% of the mean. There are also a significant number of points with lower exposure rates that occur in the northwest portion of the map where the unit has blurred borders with Tmcg. In this region Tmcg has thinned to expose Tmcl and therefore the AMS data in this area may be influenced by remaining Tmcg material.

The K and U distributions for this unit are also close to normal with peaks at 0.8-0.9% and 2 ppm respectively. The Th distribution is less normal with a median of 3.6 ppm. Spatially the distribution of K, U, and Th follow similar patterns to the exposure rate. The areas that may be influenced by eolian addition from Tmcg report lower values of K, U, and Th; while the areas with high exposure generally report higher K, U, and Th. Like most units in this area, K controls the exposure rate.









Government Wash Radioelement Concentration Images Unit Tmcl

K Wt%

- 0 - 0.485574
- 0.485575 - 0.679890
- 0.679891 - 0.902579
- 0.902580 - 1.234061
- 1.234062 - 2.271017

U PPM

- 0 - 0.818232
- 0.818233 - 1.415482
- 1.415483 - 2.069242
- 2.069243 - 2.679219
- 2.679220 - 3.502989
- 3.502990 - 4.043893
- 4.043894 - 7.910720

Th PPM

- 0 - 0.942384
- 0.942385 - 1.784504
- 1.784505 - 2.810072
- 2.810073 - 3.763784
- 3.763785 - 4.843144
- 4.843145 - 6.364771
- 6.364772 - 8.949389
- 8.949390 - 14.238856



0 0.375 1.5
Kilometers



Government Wash Radioelement Ratio Images Unit Tmcl

U/K Ratio

- 0 - 1.000000
- 1.000001 - 2.776200
- 2.776201 - 4.814531
- 4.814532 - 9.199804
- 9.199805 - 26.562074
- 26.562075 - 67.621020
- 67.621021 - 229.055746

Th/K Ratio

- 0 - 3.307556
- 3.307557 - 5.092326
- 5.092327 - 7.271497
- 7.271498 - 15.387768
- 15.387769 - 38.153590
- 38.153591 - 74.386013
- 74.386014 - 164.297821

U/Th Ratio

- 0 - 0.100000
- 0.100001 - 0.500000
- 0.500001 - 1.000000
- 1.000001 - 1.500000
- 1.500001 - 2.000000
- 2.000001 - 3.000000
- 3.000001 - 9.114520
- 9.114521 - 242.489933



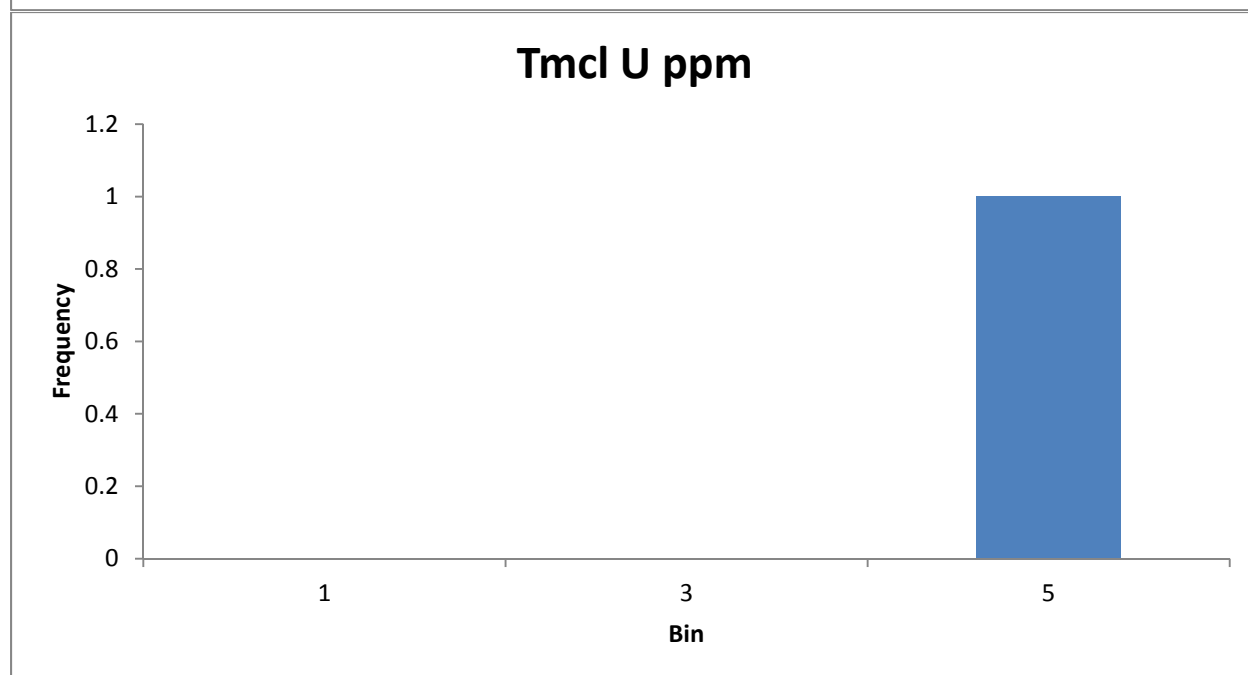
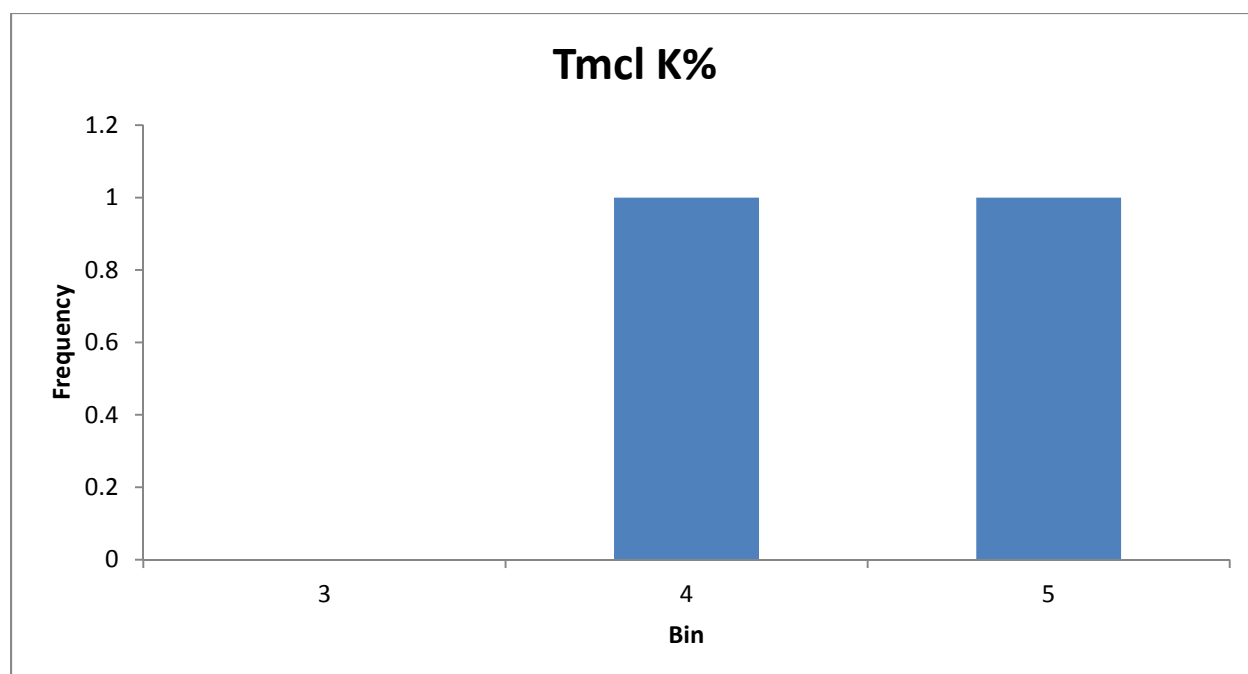
0 0.375 1.5
Kilometers

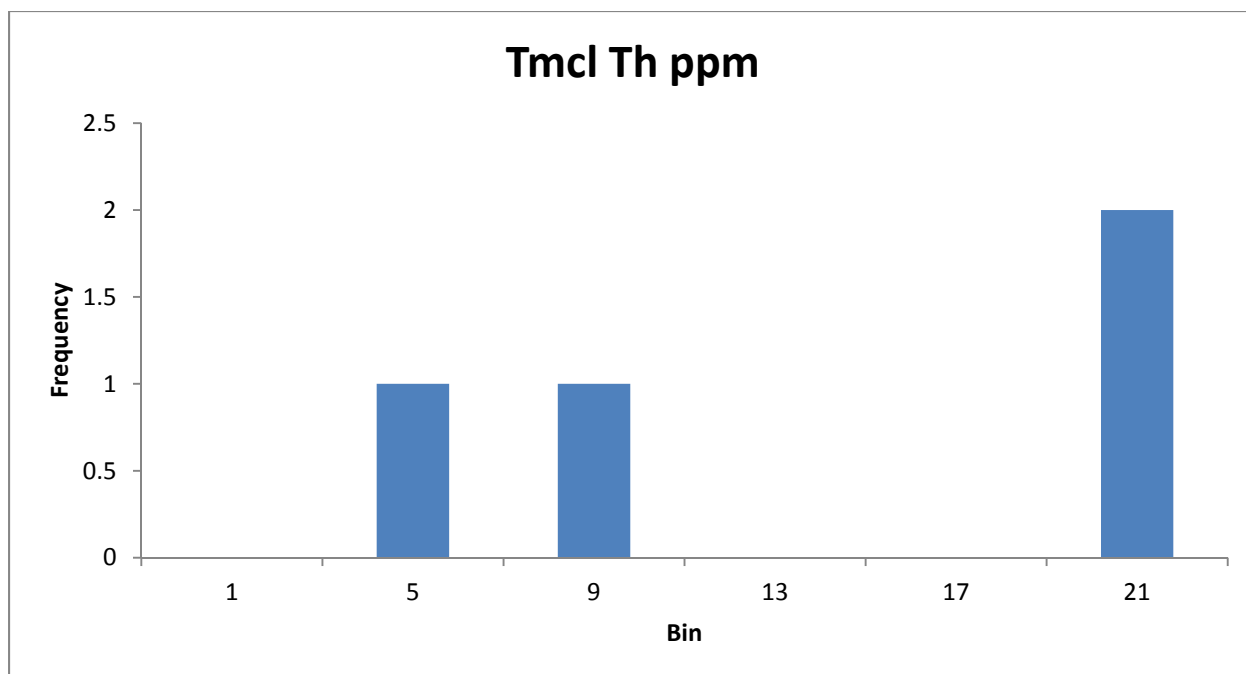
Traditional Geochemistry

The geochemistry data for this unit do not agree with the AMS data. Two of the data points occur within the primary geologic map by Duebendorfer while the other three are taken from an adjacent map by Castor et al. The metadata, where available, does not provide good sample descriptions so it is difficult to say exactly what these points represent. All values: K, U, Th and exposure rate from these data are significantly higher than both the AMS data and NURE data.

Sample ID	Latitude	Longitude	K %	U ppm	Th ppm
D265845	36.125	-114.875			19
D265847	36.125	-114.875			4
D187810	36.16667	-114.9	5		
21119	36.1304	-114.926	3.025	4.62	5.432
D265848	36.125	-114.875			19

	K%	U ppm	Th ppm
Mean	4.0125	4.62	11.858
Median	4.0125	4.62	12.216
Standard Deviation	0.9875	N/A	7.159923
Range	3.025-5.0	4.62	4-19

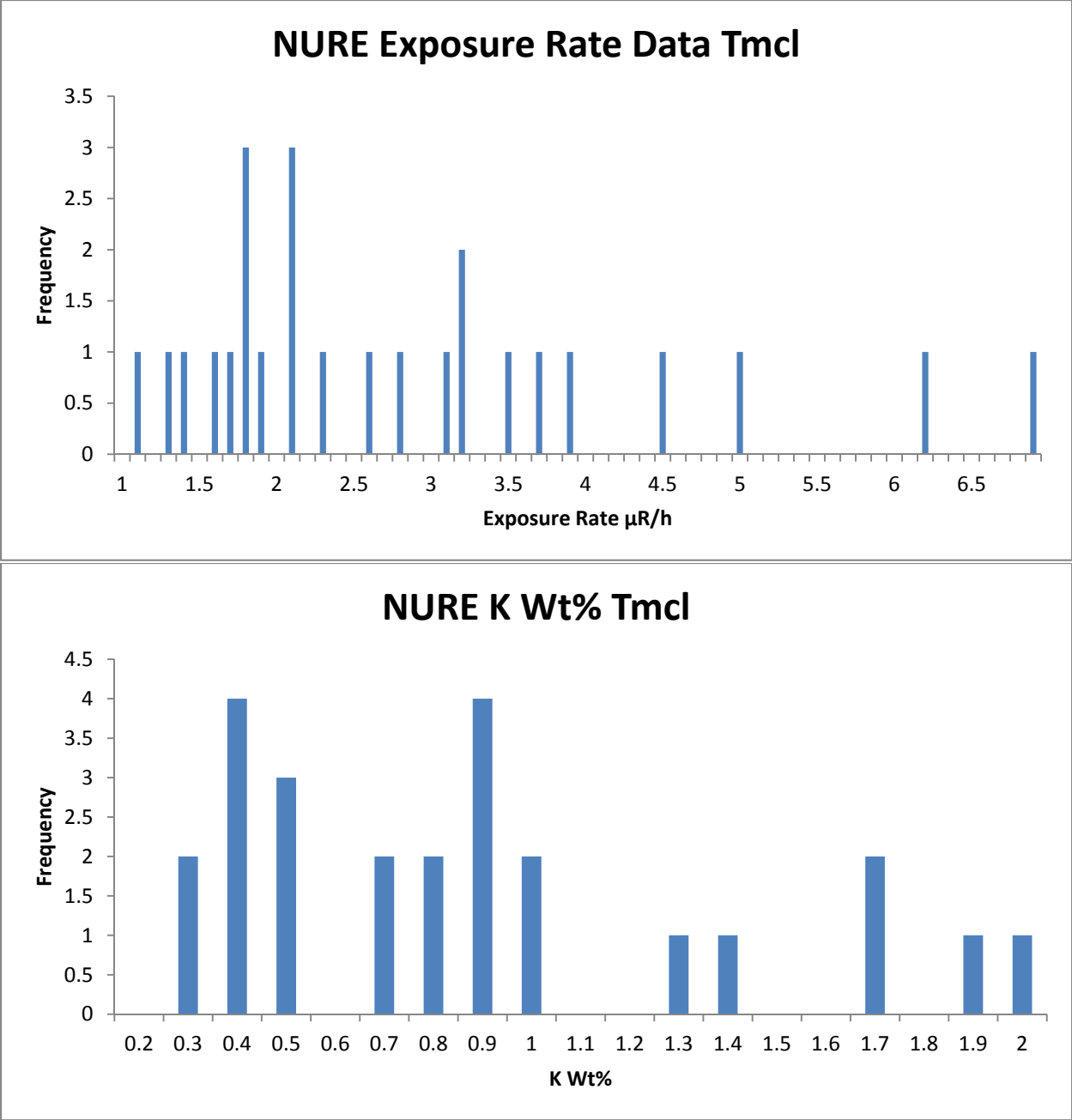


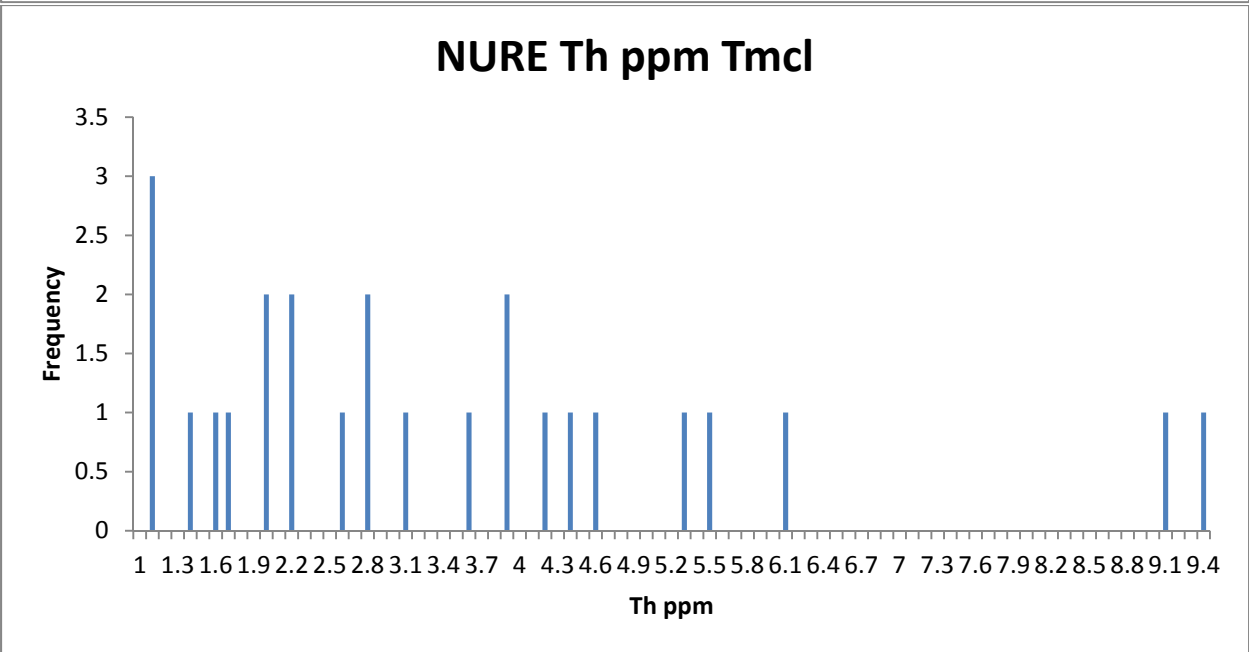
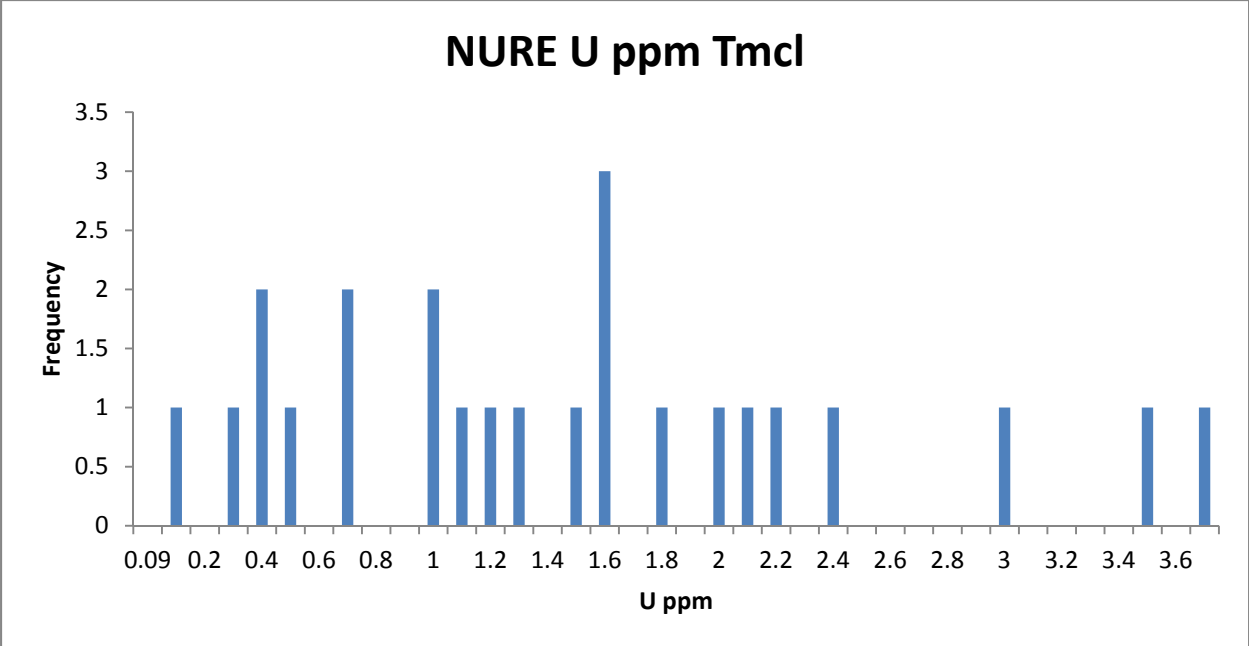


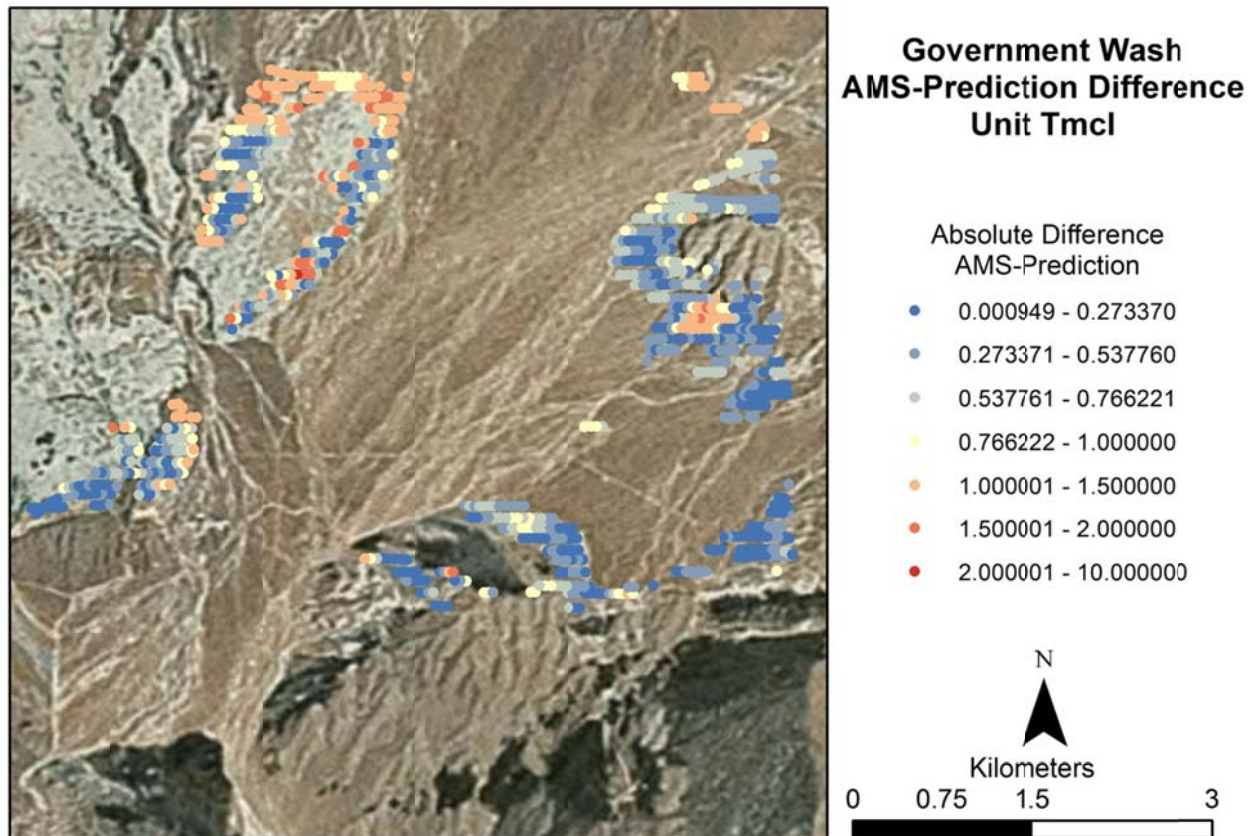
NURE Data

The NURE exposure rate data for this unit have no distinct features and are spread from 1 $\mu\text{R/h}$ to 7 $\mu\text{R/h}$ with most of the data occurring lower than 4 $\mu\text{R/h}$. There are also no significant peaks in K, U, or Th concentration. This is likely a product of the fact that most of the data comes from the southern NURE line that is not in agreement with AMS data.

However, the exposure rate prediction with the NURE data is much better than the traditional geochemistry. The NURE mean in Tmcl is 3.86 $\mu\text{R/h}$ which compares with the AMS mean of 3.56 $\mu\text{R/h}$. This means the unit falls within the desired ± 1 $\mu\text{R/h}$ range. Further, when comparing the AMS data point by point to the NURE mean, the majority of the unit is modeled very well with less than 0.5 $\mu\text{R/h}$ difference. Areas that are potentially influenced by addition by Tmcg generally have a larger difference but mostly fall within the ± 1 $\mu\text{R/h}$ range.







Summary

Exposure Rate Comparison $\mu\text{R/h}$	Average	Median	STD	Range
AMS Data	3.56107986	3.521703	0.64510227	2.035527-5.875
NURE Data	3.857995	2.23944	1.475567	1.07158-6.89808
Geochemical Prediction	11.05364	11.15101	N/A	7.61276-14.29976

Tvc

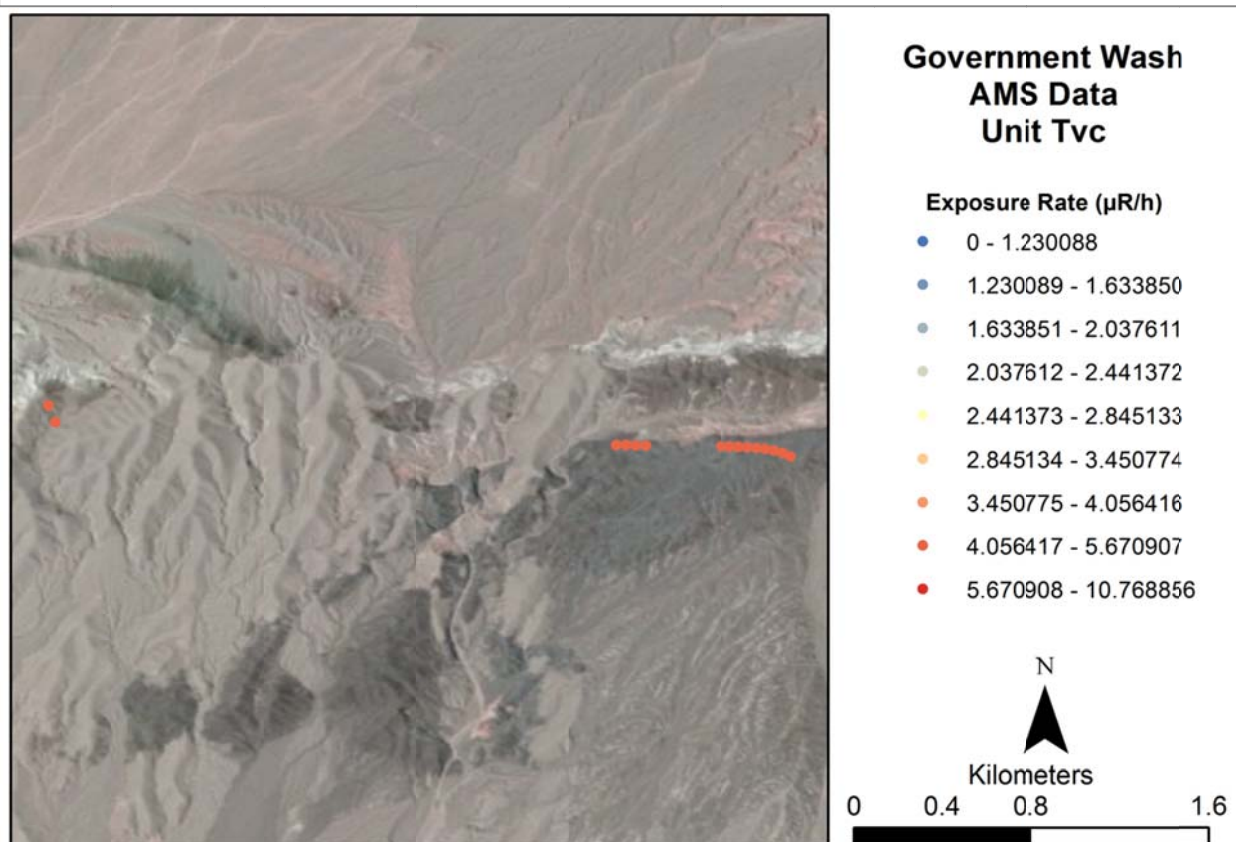
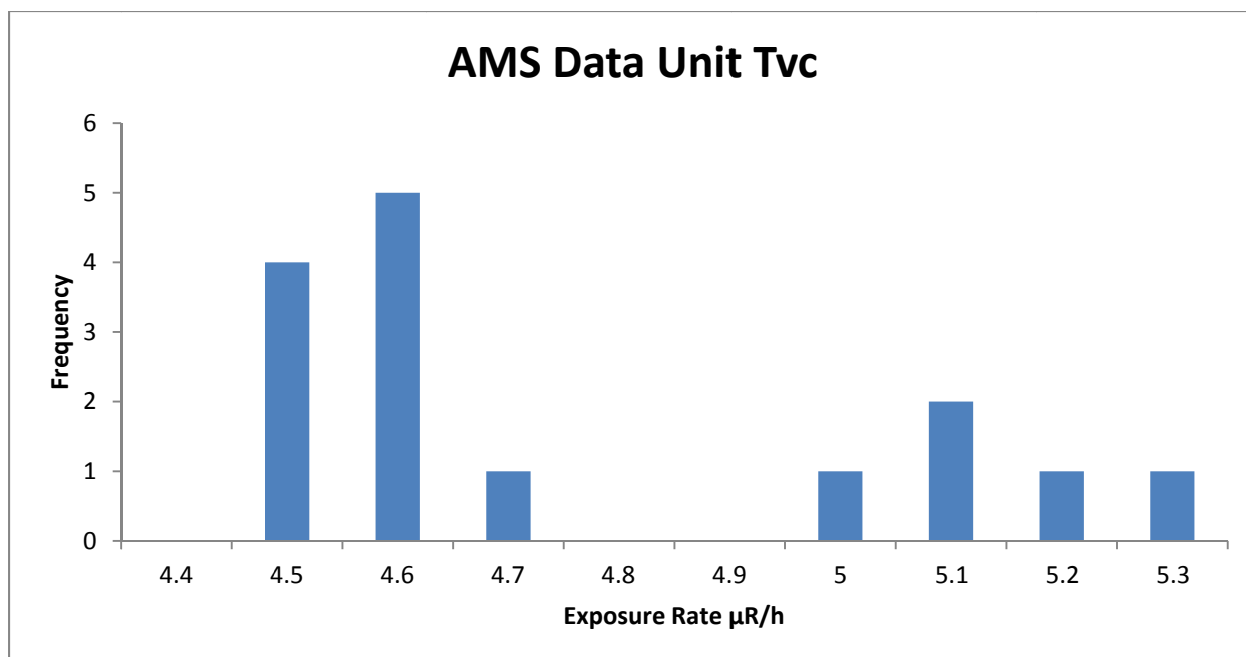
Composition

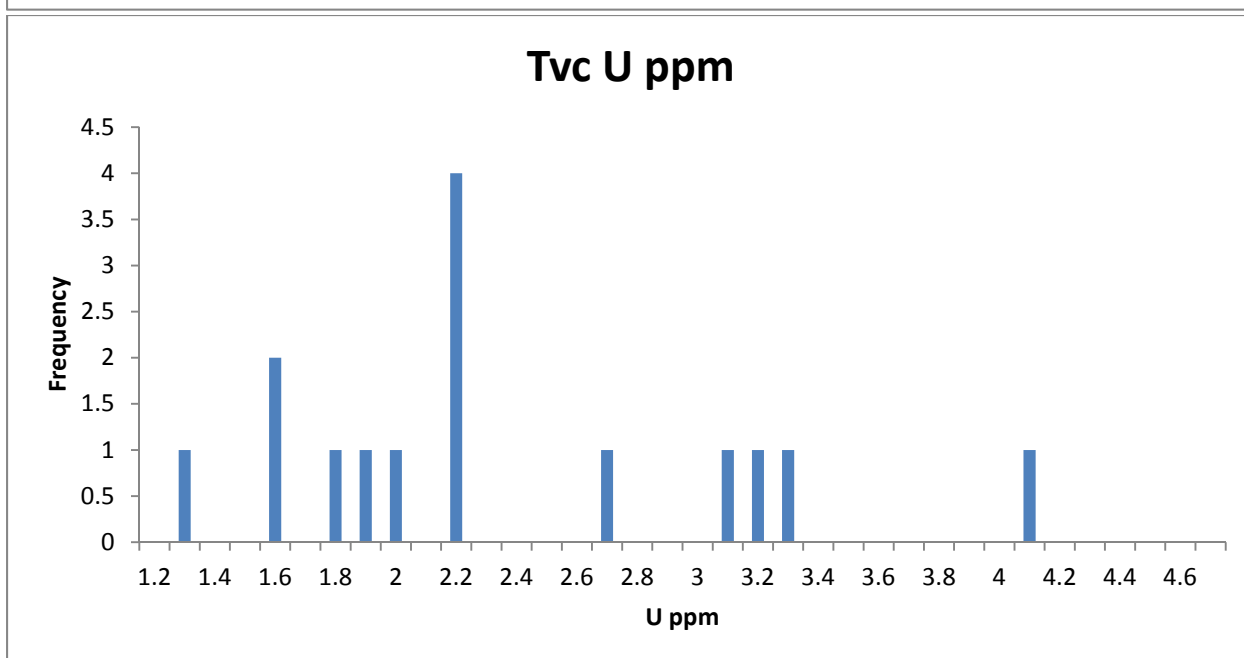
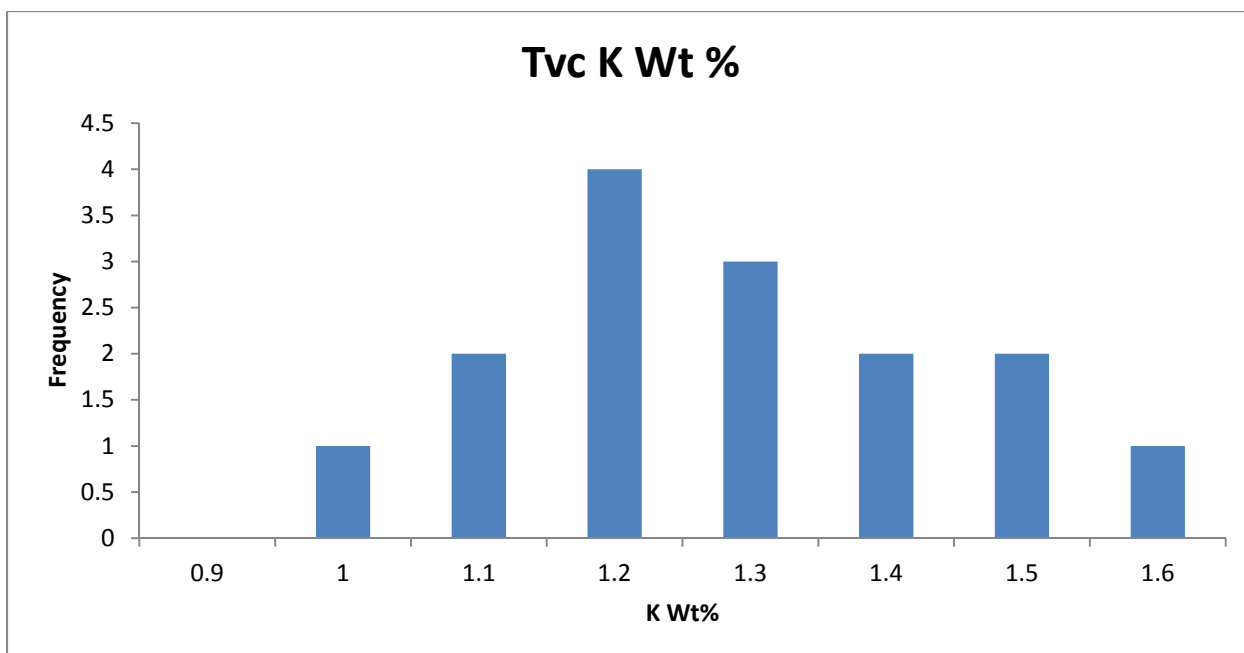
Tvc is middle Miocene in age and composed of basaltic andesite flows, breccias, and plugs. The texture is aphyric to porphyritic and contains phenocrysts of olivine, clinopyroxene, and plagioclase. The color is dark gray to black or purple. In some locations there are xenocrysts of quartz and alkali feldspars. Breccias are locally interbedded with red sandstone and siltstone. The flows are 11.4 to 8.5 Ma in age. (Duebendorfer, 2003)

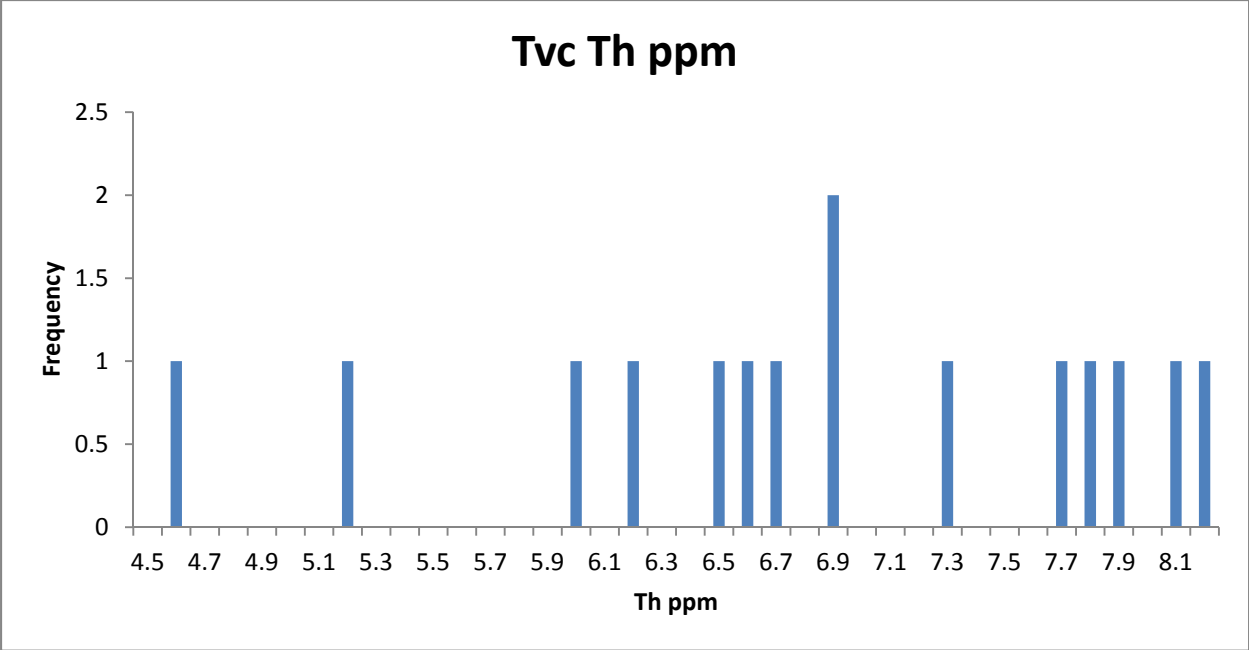
AMS Data

Spatially Tvc is very thin and occurs in three small outcrops. Exposure rates range from 4.5 to 5.3 $\mu\text{R/h}$. Most of the data is centered between 4.5-4.7 $\mu\text{R/h}$. The mean exposure rate is 4.7 $\mu\text{R/h}$ with a standard deviation of 0.28 $\mu\text{R/h}$ or 6% of the mean. The standard deviation is only 6% of the mean.

K percentages are concentrated between 1.1 and 1.5 percent. U and Th values are much more broadly spread with no clear features in the data. These relationships are also apparent in the concentration images as K tends to follow the exposure rate and U and Th are more randomly spread.







**Government Wash Radioelement
Concentration Images
Unit Tvc**



K Wt%

- 0 - 0.485574
- 0.485575 - 0.679890
- 0.679891 - 0.902579
- 0.902580 - 1.234061
- 1.234062 - 2.271017



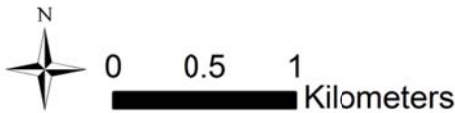
U PPM

- 0 - 0.818232
- 0.818233 - 1.415482
- 1.415483 - 2.069242
- 2.069243 - 2.679219
- 2.679220 - 3.502989
- 3.502990 - 4.043893
- 4.043894 - 7.910720



Th PPM

- 0 - 0.942384
- 0.942385 - 1.784504
- 1.784505 - 2.810072
- 2.810073 - 3.763784
- 3.763785 - 4.843144
- 4.843145 - 6.364771
- 6.364772 - 8.949389
- 8.949390 - 14.238856





Government Wash Radioelement Ratio Images Unit Tvc

U/K Ratio

- 0 - 1.000000
- 1.000001 - 2.776200
- 2.776201 - 4.814531
- 4.814532 - 9.199804
- 9.199805 - 26.562074
- 26.562075 - 67.621020
- 67.621021 - 229.055746



Th/K Ratio

- 0 - 3.307556
- 3.307557 - 5.092326
- 5.092327 - 7.271497
- 7.271498 - 15.387768
- 15.387769 - 38.153590
- 38.153591 - 74.386013
- 74.386014 - 164.297821



U/Th Ratio

- 0 - 0.100000
- 0.100001 - 0.500000
- 0.500001 - 1.000000
- 1.000001 - 1.500000
- 1.500001 - 2.000000
- 2.000001 - 3.000000
- 3.000001 - 9.114520
- 9.114521 - 242.489933



Traditional Geochemistry

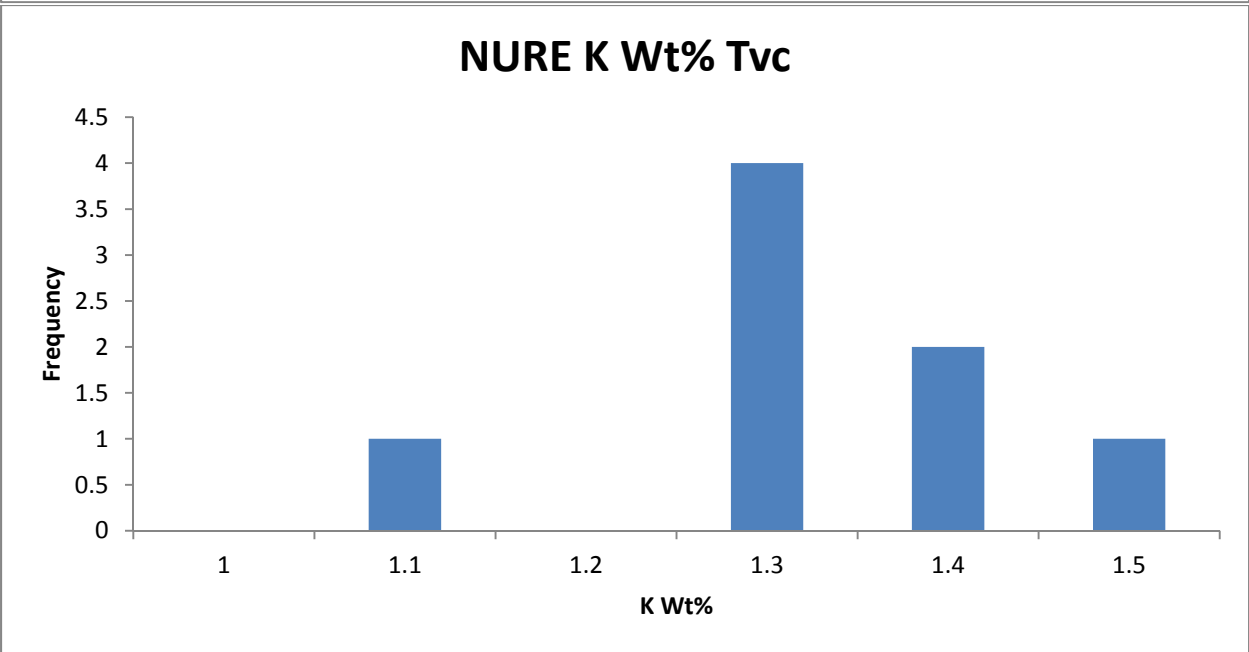
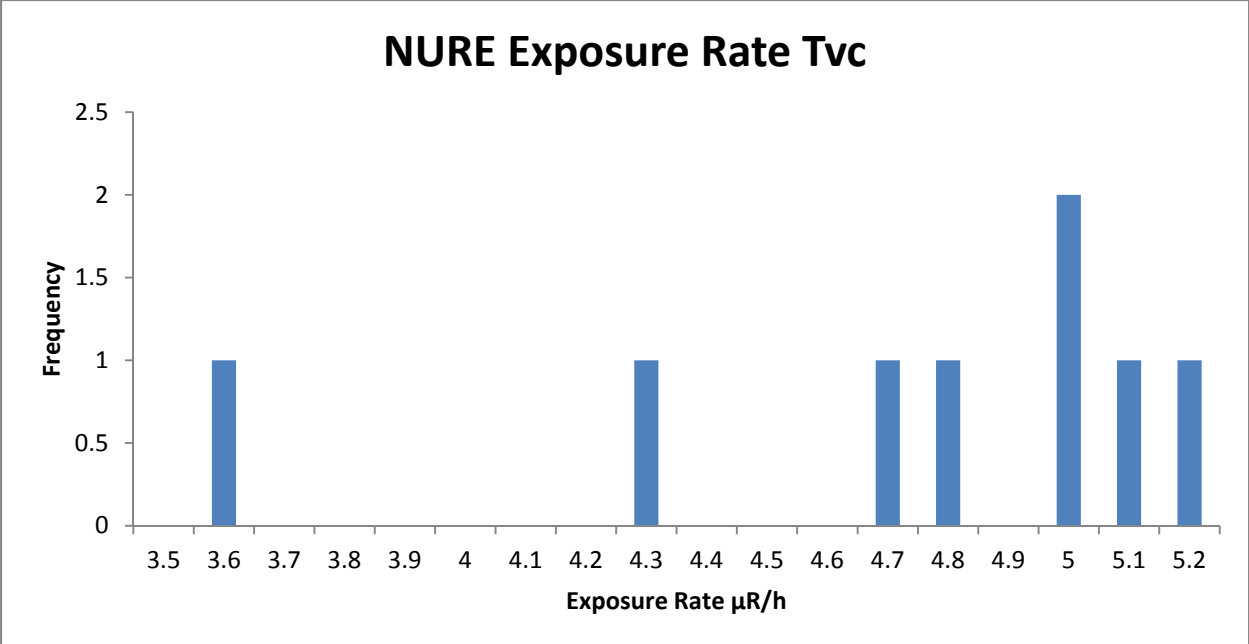
There are 4 geochemical data points that occur in Tvc. All of these points only provide K% data, therefore an exposure rate prediction cannot be made for this unit. The K values range from 2.4-3.1% which are much higher than the AMS data that ranges from 1.1 and 1.5%.

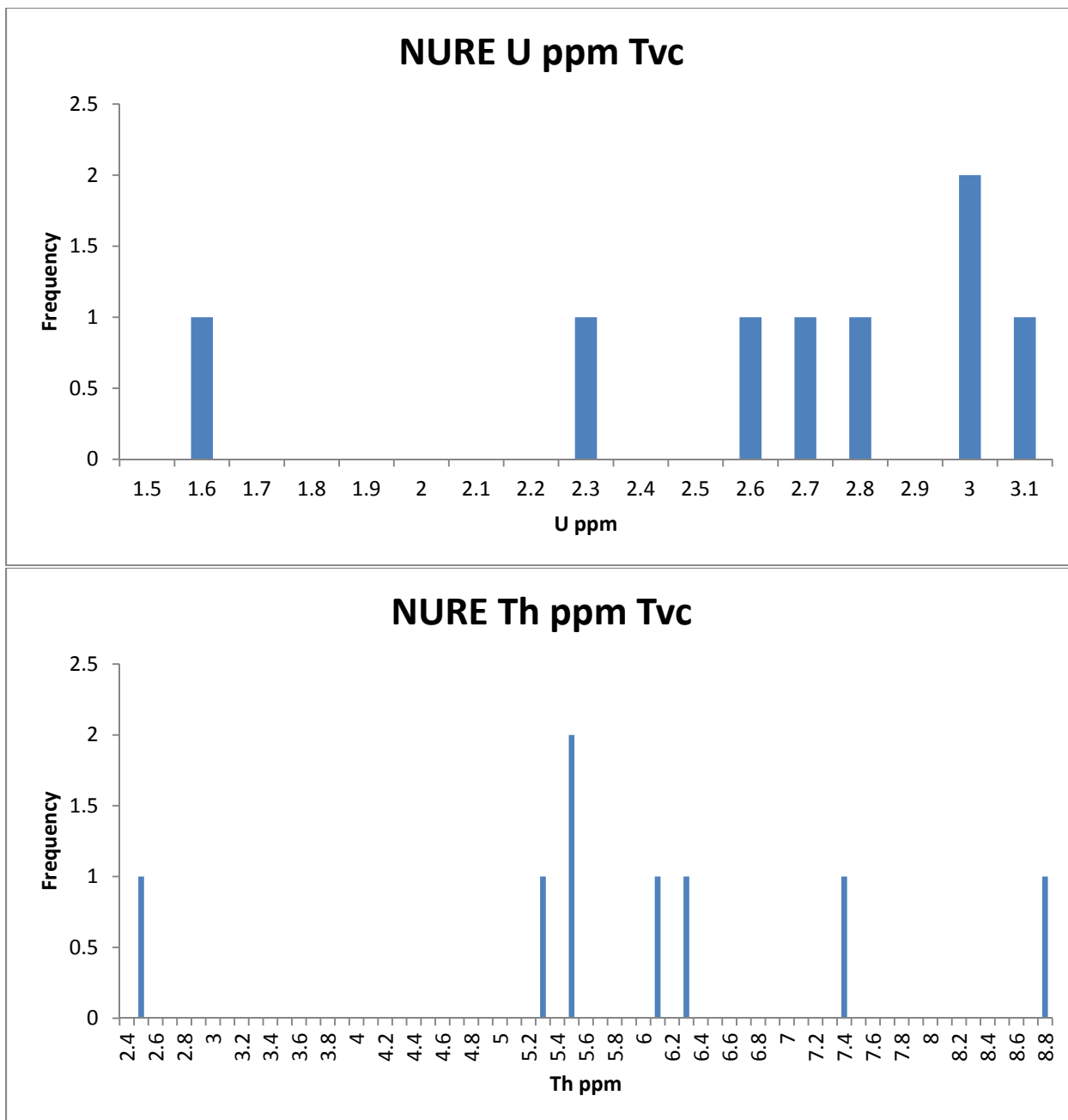
Sample ID	Latitude	Longitude	K %	U ppm	Th ppm
2-93-3	36.1653	-114.767	2.56		
24	36.1653	-114.77	2.39		
M201804	36.15	-114.858	3.09		
M201804	36.175	-114.808	3.09		

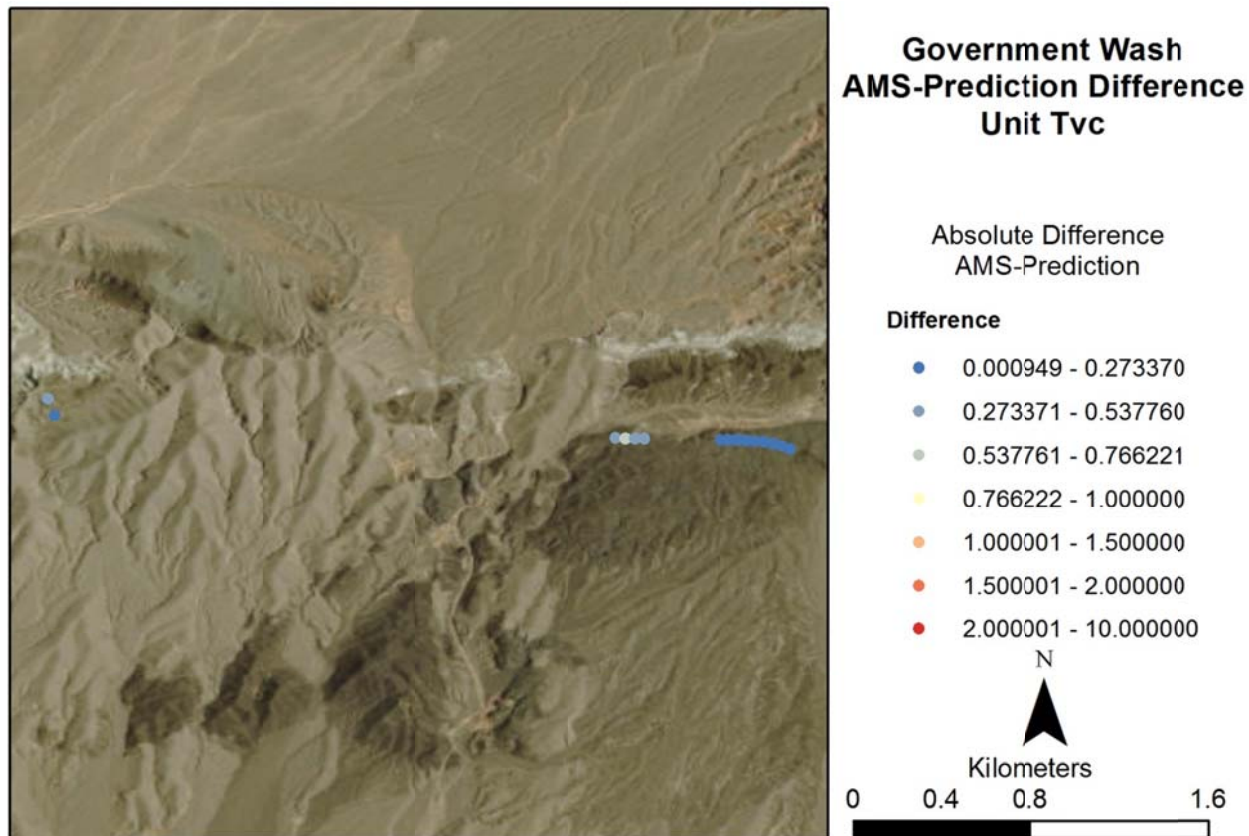
NURE Data

NURE exposure rates in Tvc are relatively high compared to the AMS exposure rates. There is however a point that is cool, 3.6 $\mu\text{R/h}$, that brings the average NURE exposure rate down. The result is that both the predicted exposure rate and AMS exposure rate are very similar at 4.67 $\mu\text{R/h}$ and 4.71 $\mu\text{R/h}$ respectively. When you compare the NURE prediction against the AMS data point by point almost every point has a difference of less than 0.5 $\mu\text{R/h}$.

K values in the NURE data set are also quite similar to values in the AMS data with both having most of the data between 1.2 and 1.4%. U and Th data in the AMS data set are largely featureless and the same holds true for the NURE data. Despite the seeming randomness of this result, this unit is modeled very well.







Summary

Exposure Rate Comparison $\mu\text{R/h}$	Average	Median	STD	Range
AMS Data	4.71007107	4.548371	0.28345726	4.444988-5.225004
NURE Data	4.671961	4.85185	0.515011	3.50488-5.1761
Geochemical Prediction	N/A	N/A	N/A	N/A

Trs

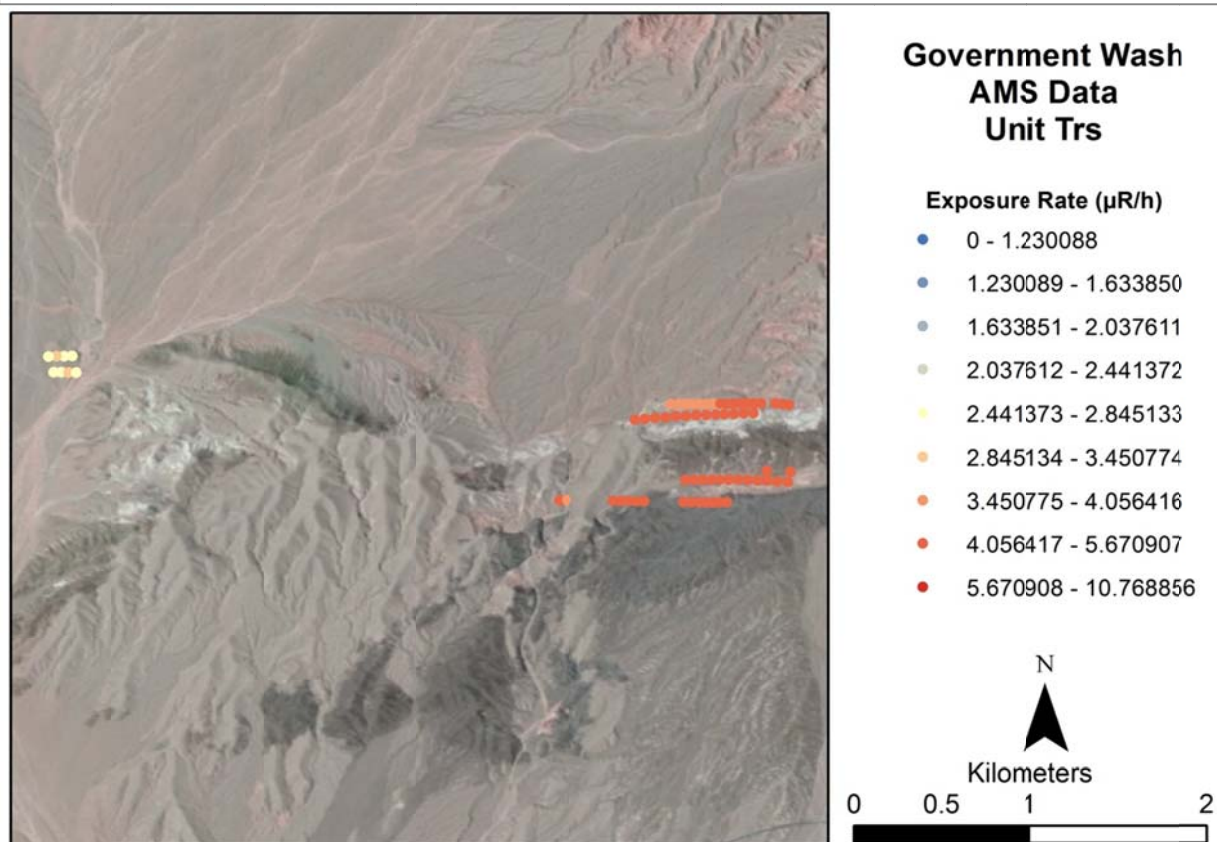
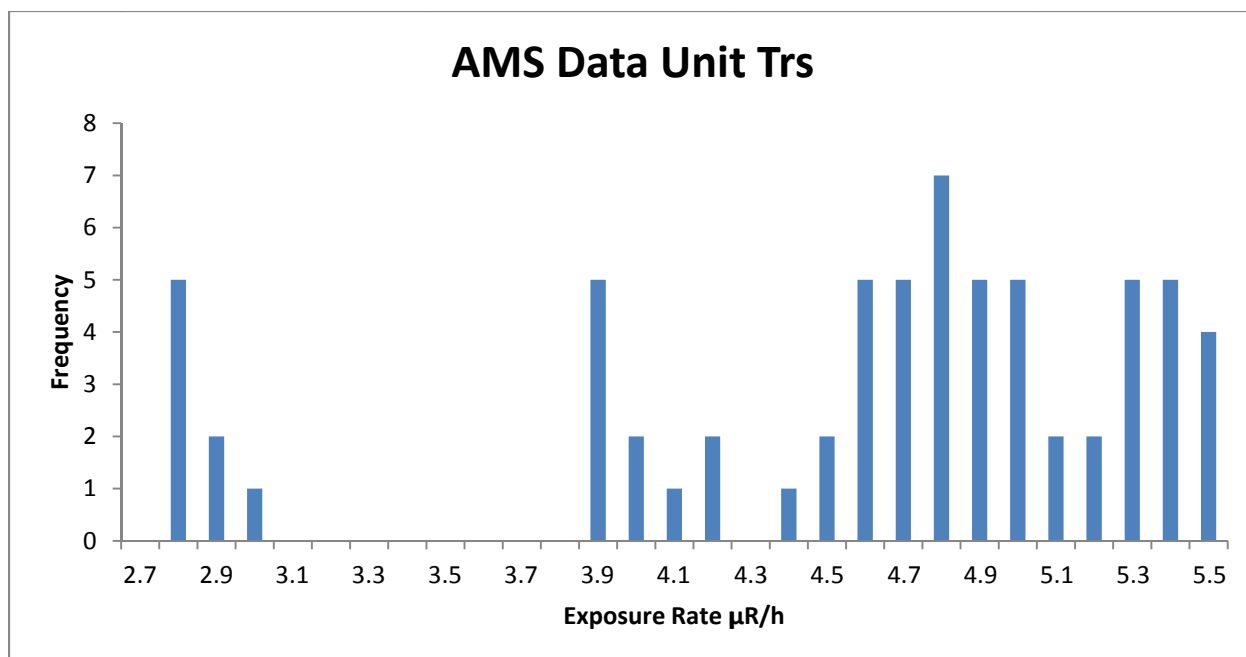
Composition

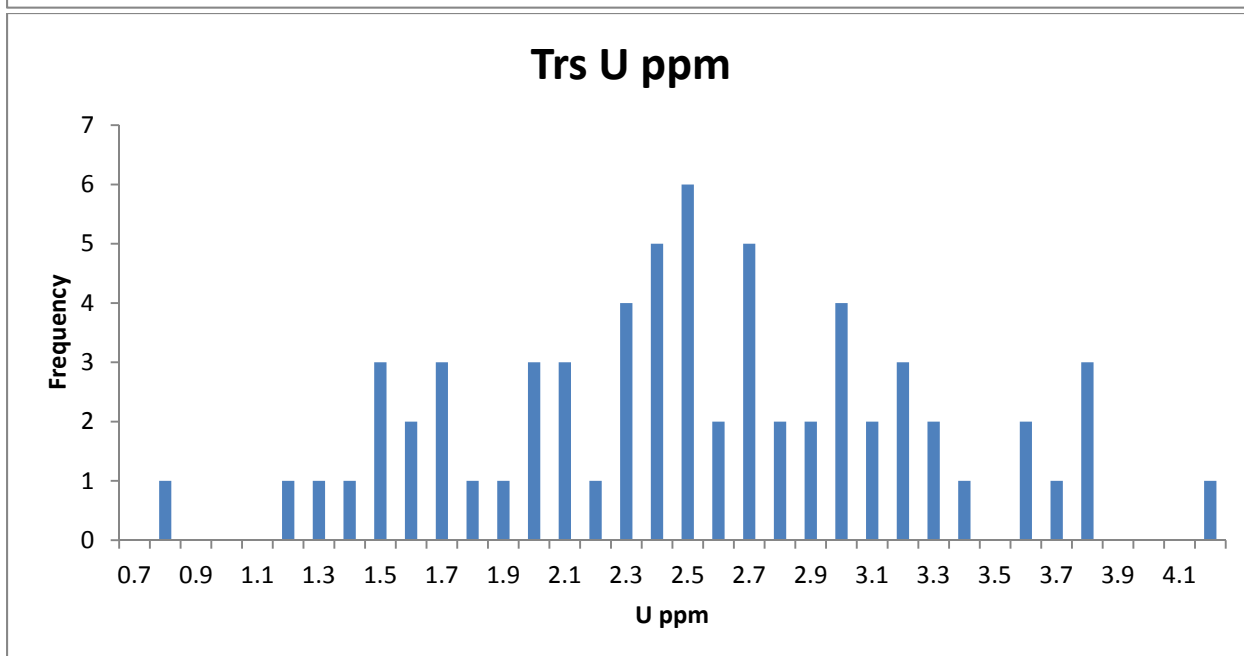
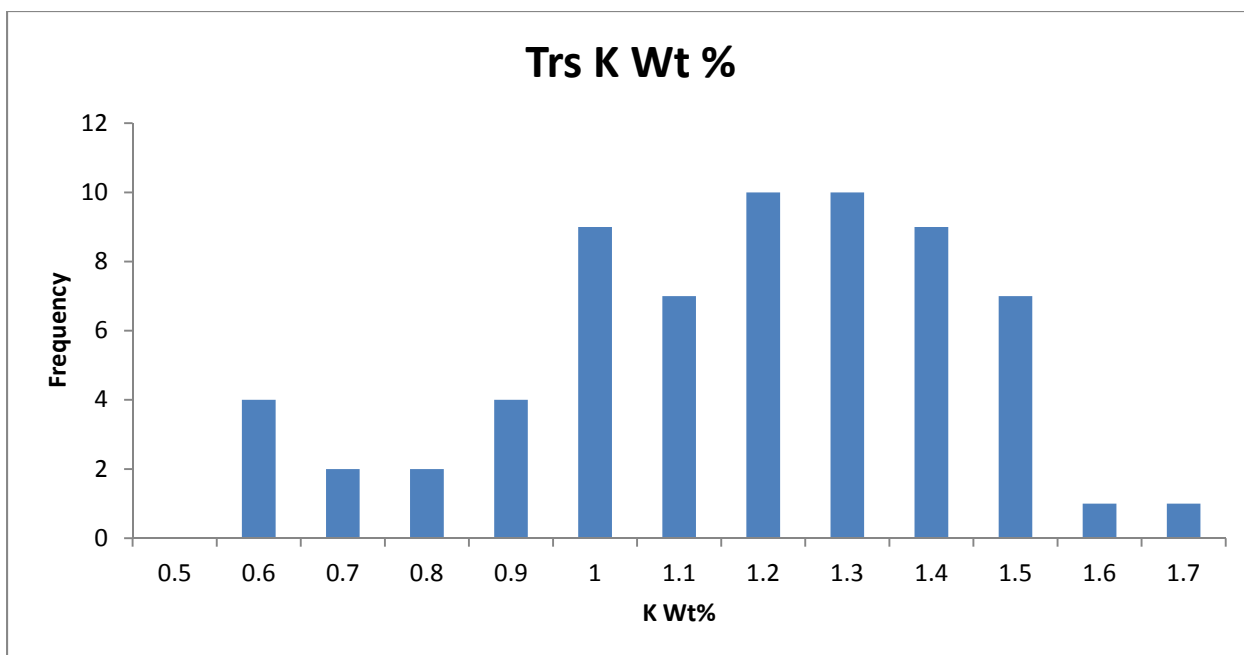
Trs is a red sandstone unit of the Boulder Basin that is Miocene in age. It consists of conglomerate, sandstone, siltstone and gypsiferous siltstone. It is interbedded with flows of basaltic andesite of the volcanic rocks of Callville Mesa. Conglomerate clasts consist of limestone and siltstone, which are well indurated, poorly sorted and subrounded. Sandstone is fine to medium grain, tan, weakly indurated and friable with sedimentary structures such as ripples. (Duebendorfer, 2003)

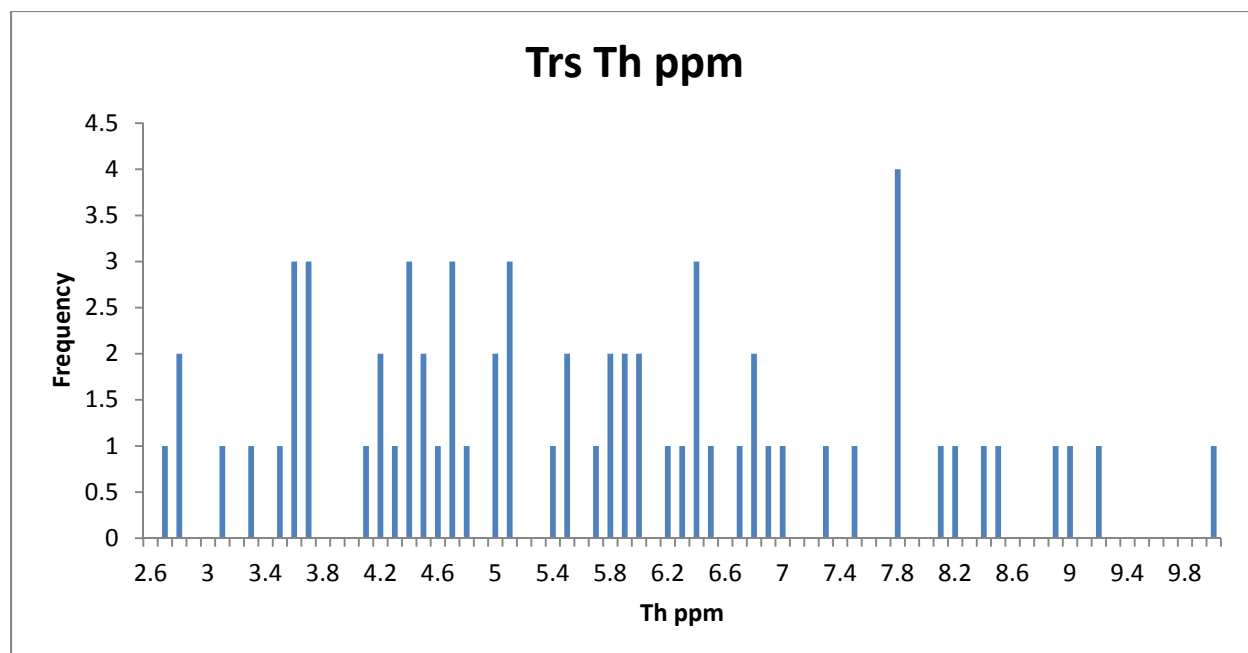
AMS Data

Trs is a spatially limited sedimentary unit that is rarely more than two AMS data points thick. The spatial thinness of the unit implies that it may be influenced by surrounding units due to the detector footprint. There are several points that occur in an outcrop that is surrounded by Qa to the west. These points are significantly cooler than other portions of the unit. There are no clear patterns in the AMS exposure rate data other than the cooler peak that is associated with the outcrop within Qa. The remainder of the unit has exposure rates from 3.9 to 5.5 $\mu\text{R/h}$ with the strongest peak at 4.8 $\mu\text{R/h}$. The average exposure rate in Trs is 4.52 $\mu\text{R/h}$ with a standard deviation of 0.78 $\mu\text{R/h}$. The standard deviation is 17% of the mean.

K values range from 0.6 to 1.7 percent with the majority of the data occurring in the 1-1.5 percent range. U ppm values have a wider range than the K % values but has a somewhat normal shape peaking at 2.5 ppm. Th ppm values are widely distributed and show no discernable pattern. In the concentration images the K values vary most closely with exposure rate, U values are mostly scattered and Th has some correlation with exposure and K.









Government Wash Radioelement Concentration Images Unit Trs

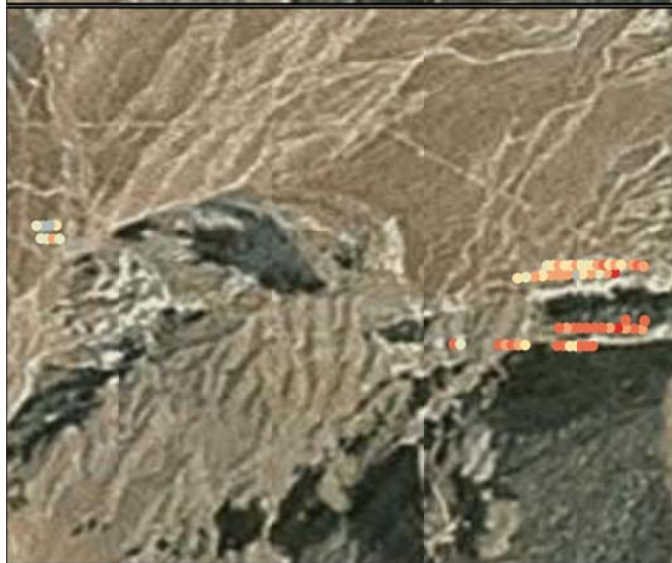
K Wt%

- 0 - 0.485574
- 0.485575 - 0.679890
- 0.679891 - 0.902579
- 0.902580 - 1.234061
- 1.234062 - 2.271017



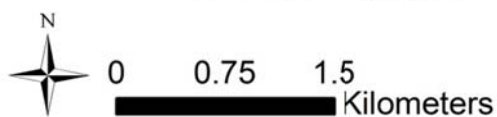
U PPM

- 0 - 0.818232
- 0.818233 - 1.415482
- 1.415483 - 2.069242
- 2.069243 - 2.679219
- 2.679220 - 3.502989
- 3.502990 - 4.043893
- 4.043894 - 7.910720



Th PPM

- 0 - 0.942384
- 0.942385 - 1.784504
- 1.784505 - 2.810072
- 2.810073 - 3.763784
- 3.763785 - 4.843144
- 4.843145 - 6.364771
- 6.364772 - 8.949389
- 8.949390 - 14.238856





Government Wash Radioelement Ratio Images Unit Trs

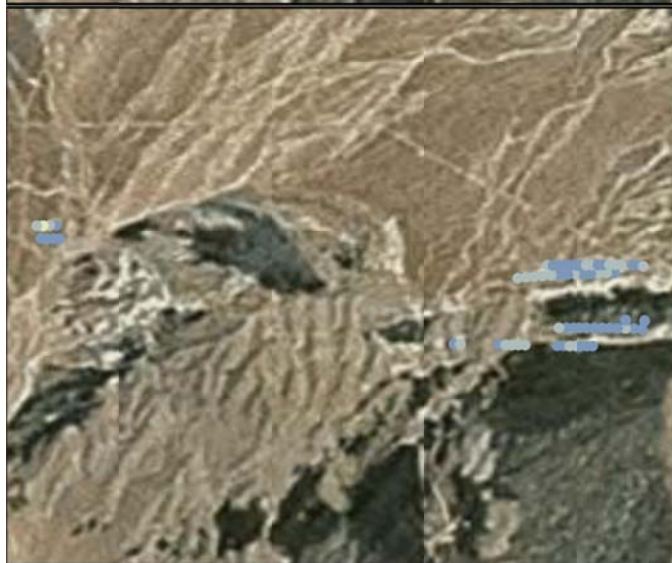
U/K Ratio

- 0 - 1.000000
- 1.000001 - 2.776200
- 2.776201 - 4.814531
- 4.814532 - 9.199804
- 9.199805 - 26.562074
- 26.562075 - 67.621020
- 67.621021 - 229.055746



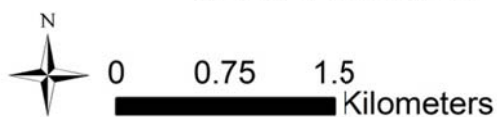
Th/K Ratio

- 0 - 3.307556
- 3.307557 - 5.092326
- 5.092327 - 7.271497
- 7.271498 - 15.387768
- 15.387769 - 38.153590
- 38.153591 - 74.386013
- 74.386014 - 164.297821



U/Th Ratio

- 0 - 0.100000
- 0.100001 - 0.500000
- 0.500001 - 1.000000
- 1.000001 - 1.500000
- 1.500001 - 2.000000
- 2.000001 - 3.000000
- 3.000001 - 9.114520
- 9.114521 - 242.489933



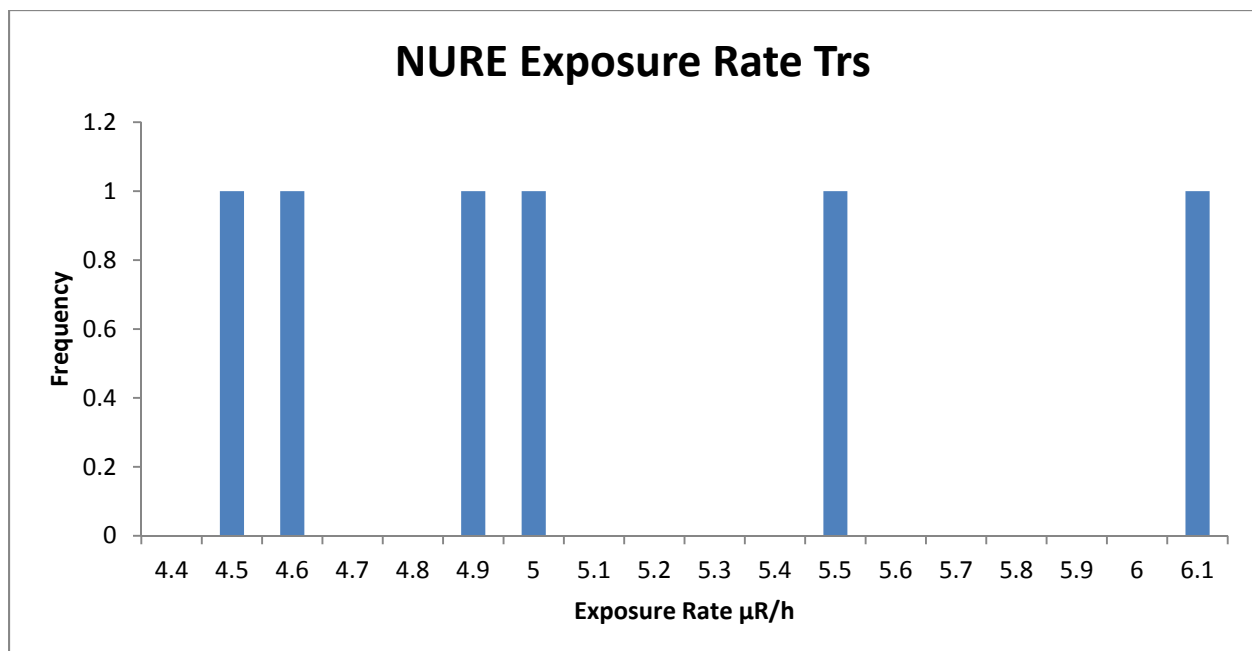
Traditional Geochemistry

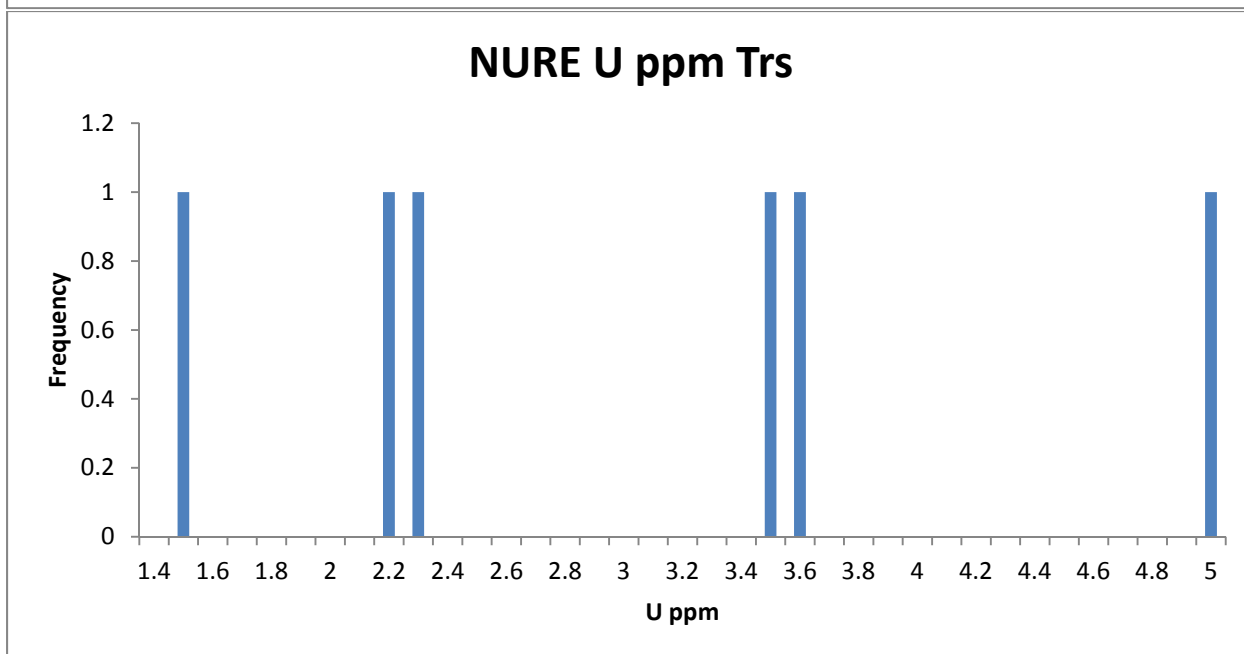
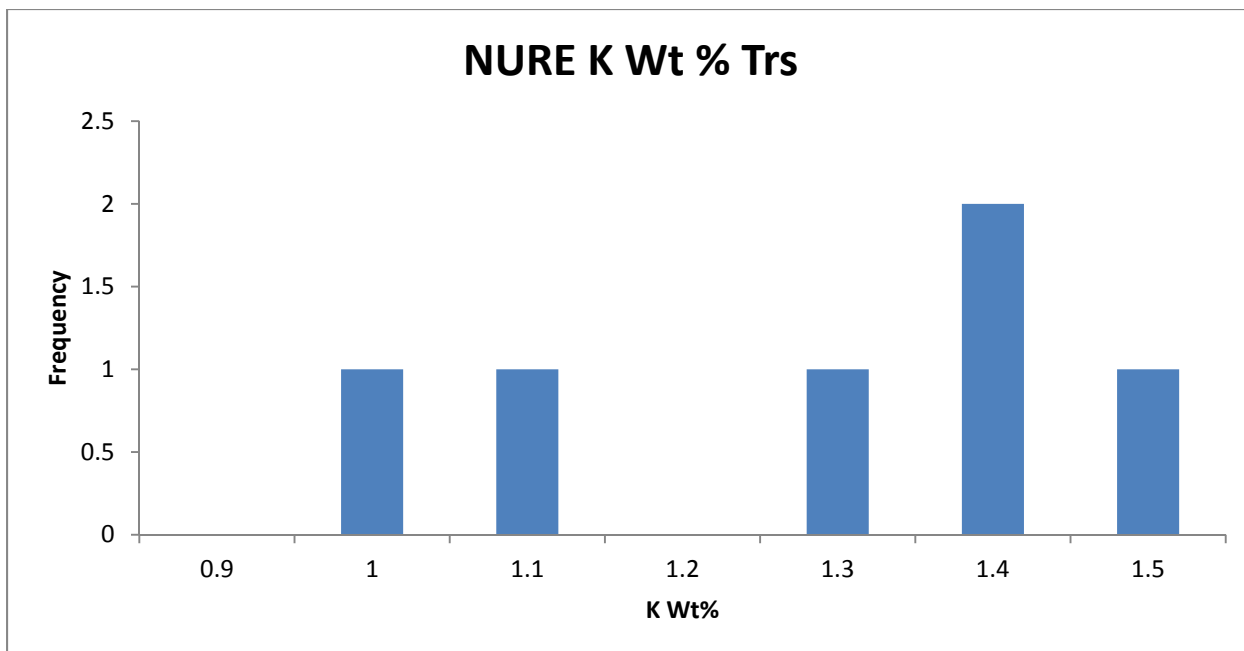
There is only one geochemical data point associated with Trs. This data point does provide U and Th values but does not provide K. The U and Th values from this data point are significantly lower than the AMS data.

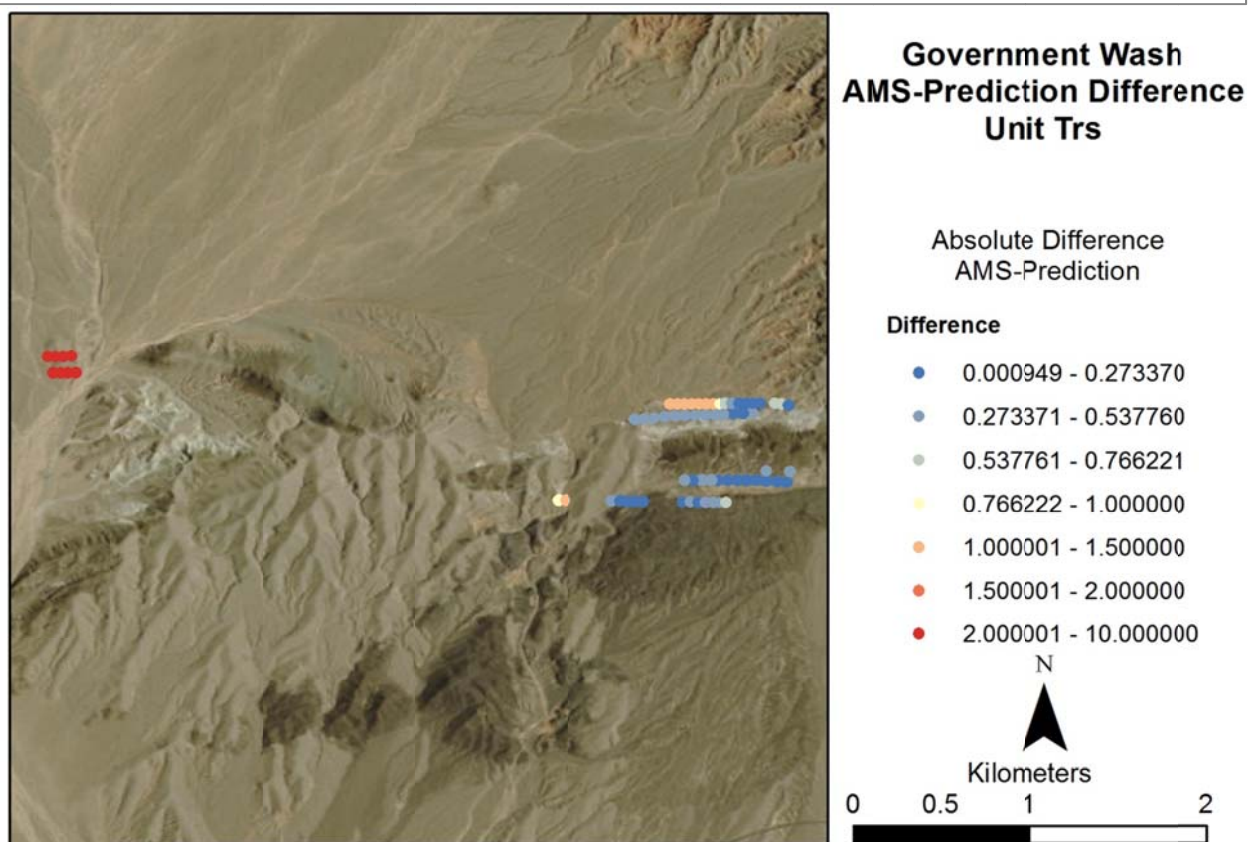
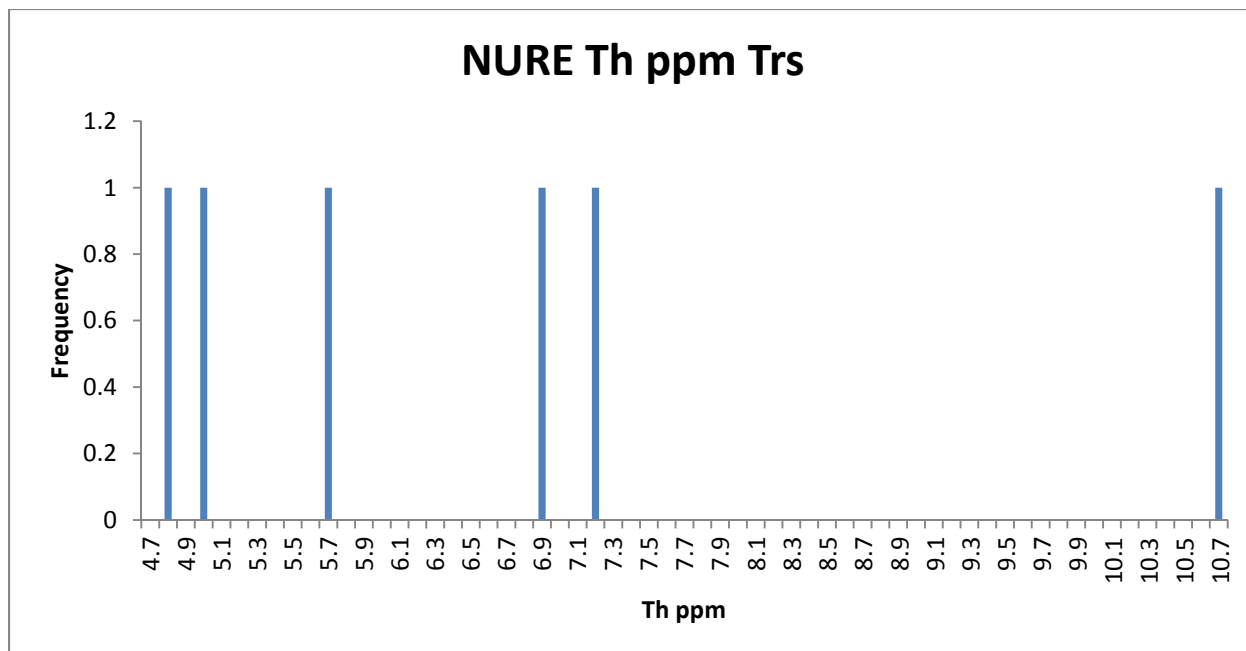
Sample ID	Latitude	Longitude	K %	U ppm	Th ppm
21006	36.3245	-114.651		0.83	2.104

NURE Data

The NURE data for Trs is entirely from the southern line that disagrees with the AMS data. The exposure rate, K, U, and Th data are featureless. However, the average exposure rate derived from the NURE data is 5.06 $\mu\text{R/h}$ which compares to an average AMS exposure rate of 4.52 $\mu\text{R/h}$. This means that this unit falls within the ± 1 $\mu\text{R/h}$ desired range. When comparing the NURE prediction against the AMS data point by point the cool exposure surrounded by Qa shows the most difference while the hotter portion of the unit to the east is most similar with a difference generally less than 0.5 $\mu\text{R/h}$.







Summary

Exposure Rate Comparison μR/h	Average	Median	STD	Range
AMS Data	4.52748005	4.738715	0.77830827	2.762918-5.531483
NURE Data	5.062002	4.931405	0.524303	4.46901-6.0109
Geochemical Prediction	N/A	N/A	N/A	N/A

ThI

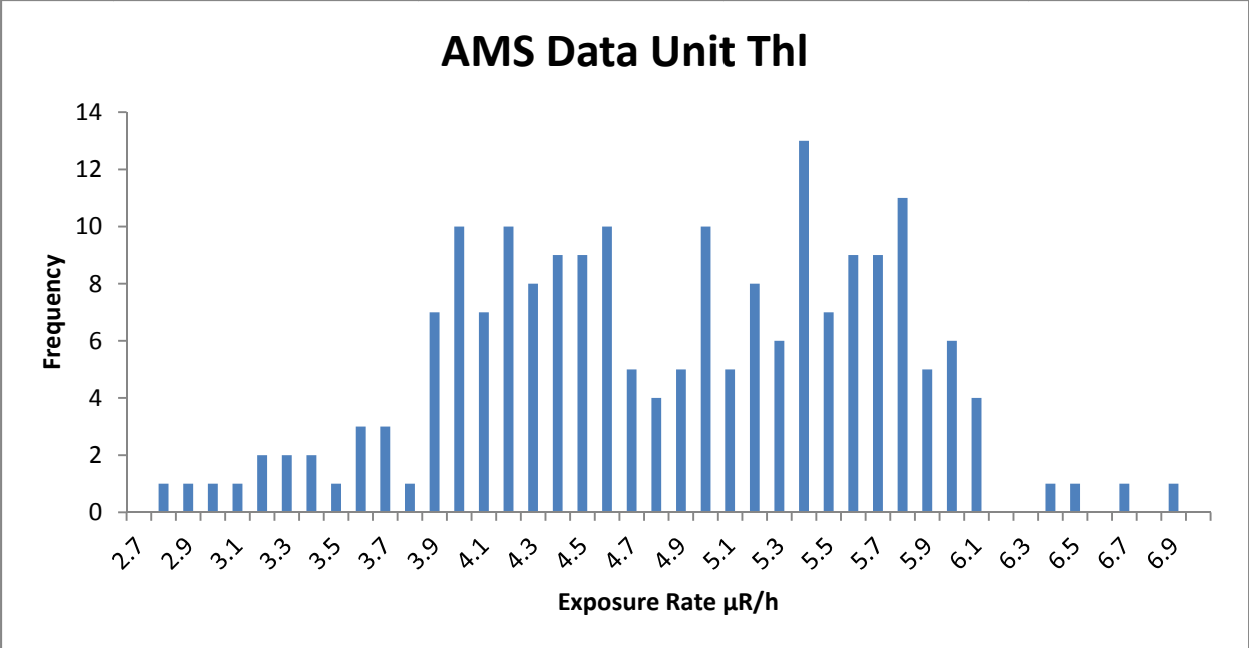
Composition

ThI is a paleo-alluvial fan of Miocene age that is composed of a variety of rock types including white to tan limestone, calcareous sandstone, tuffaceous sandstone and siltstone, and minor pebble conglomerate with clasts up to 5mm. In some locations, white tuffaceous sandstone grades upward into white tuffaceous siltstone. (Duebendorfer, 2003)

AMS Data

The AMS data that occurs in ThI is not normally distributed. The data mostly clusters in the 3.9-6.1 $\mu\text{R/h}$ range with an average of 4.8 $\mu\text{R/h}$. The standard deviation of these data is 0.82 $\mu\text{R/h}$ which is 17% of the mean. Exposure rates in the eastern portion of the unit are higher than the western. In those western areas the data points are thinly spread and may be influenced by surrounding units. This can account for some of the variability in the data.

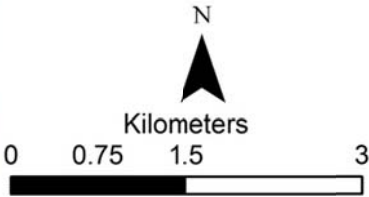
K values are close to normally distributed. It follows some similar patterns to the exposure rate data as the areas with higher density of data report similar values while areas that are thinly spread show more variability. U and Th data are more variable. The histogram for the U data seems to be somewhat close to normal however, in the image below it becomes apparent that U values follow no particular pattern in their spatial distribution. Th has more spread in the histogram but spatially it follows a pattern more similar to the exposure rate and K data. The ratio images show that there is no clear pattern in how the nuclide concentrations covary.

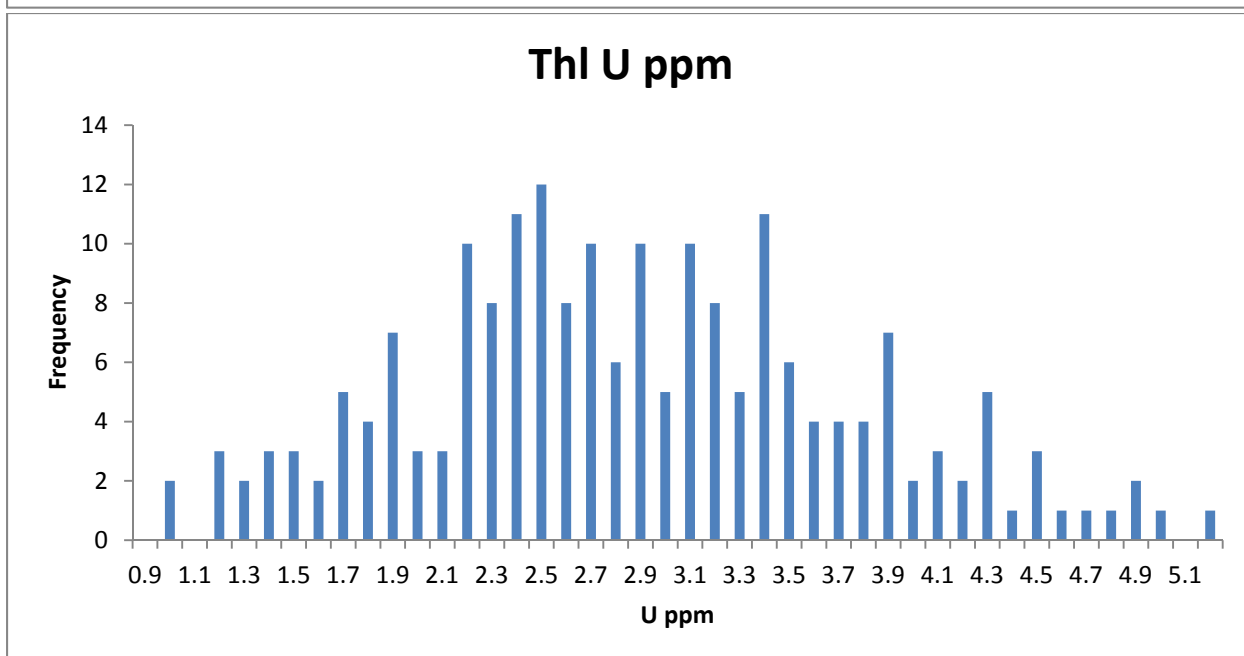
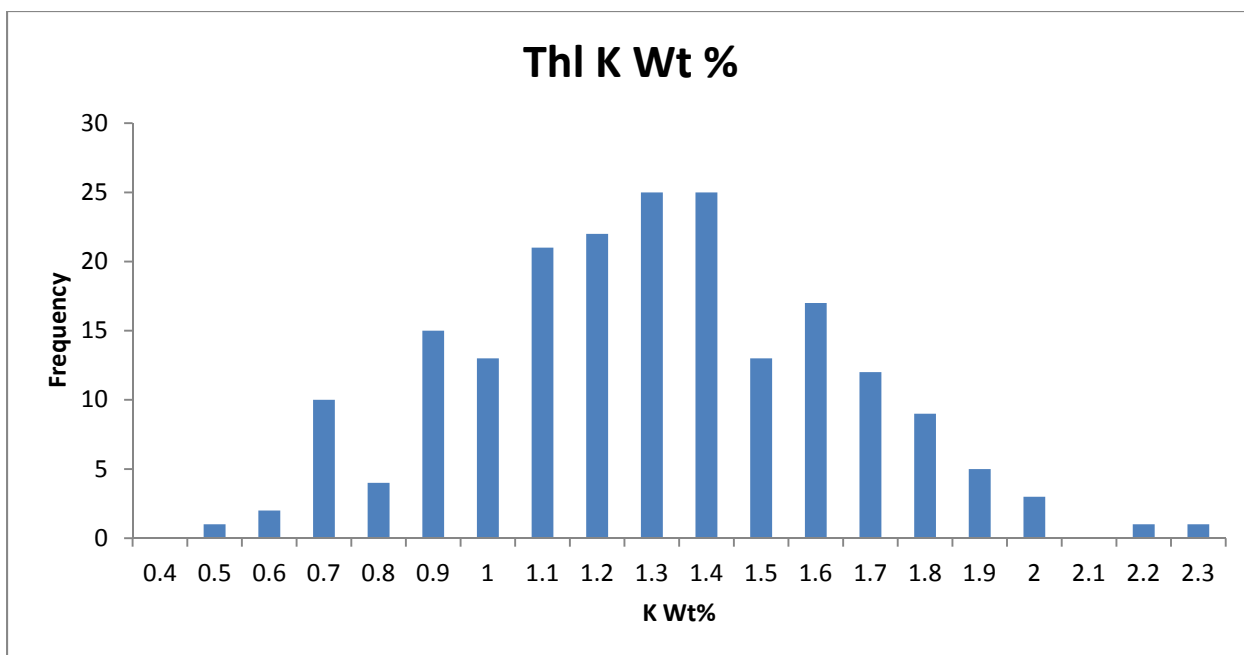


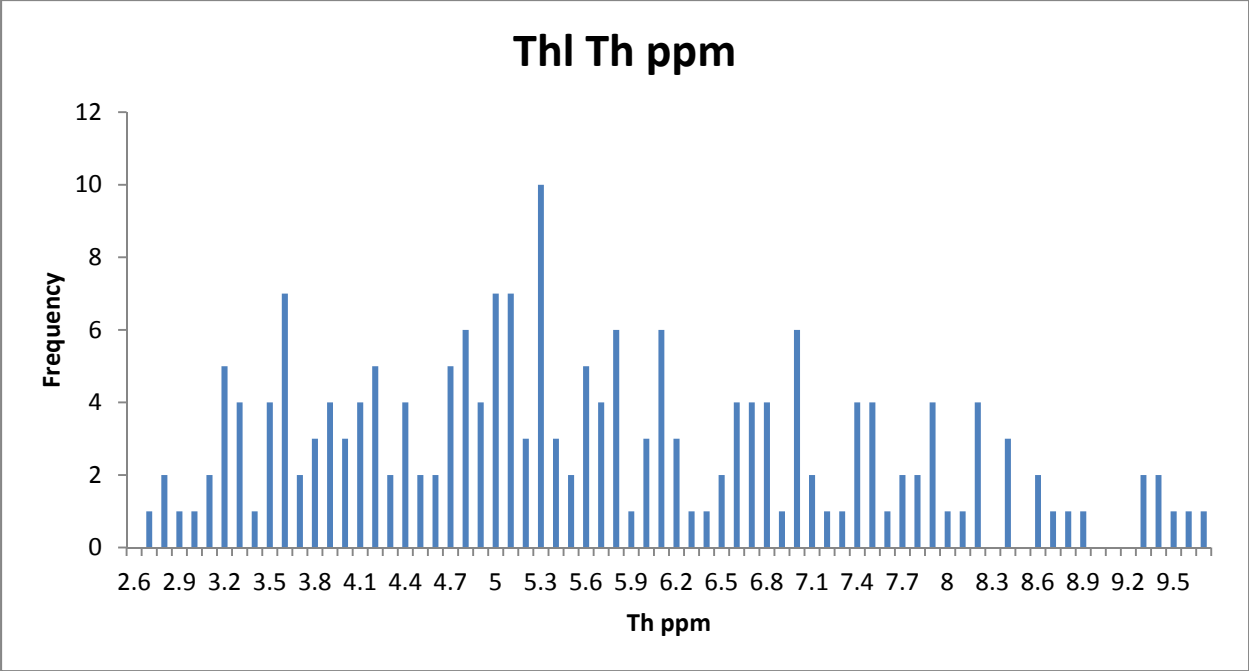
**Government Wash
AMS Data
Unit Th1**

Exposure Rate ($\mu\text{R/h}$)

- 0 - 1.230088
- 1.230089 - 1.633850
- 1.633851 - 2.037611
- 2.037612 - 2.441372
- 2.441373 - 2.845133
- 2.845134 - 3.450774
- 3.450775 - 4.056416
- 4.056417 - 5.670907
- 5.670908 - 10.768856







**Government Wash Radioelement
Concentration Images
Unit Th1**



K Wt%

- 0 - 0.485574
- 0.485575 - 0.679890
- 0.679891 - 0.902579
- 0.902580 - 1.234061
- 1.234062 - 2.271017



U PPM

- 0 - 0.818232
- 0.818233 - 1.415482
- 1.415483 - 2.069242
- 2.069243 - 2.679219
- 2.679220 - 3.502989
- 3.502990 - 4.043893
- 4.043894 - 7.910720



Th PPM

- 0 - 0.942384
- 0.942385 - 1.784504
- 1.784505 - 2.810072
- 2.810073 - 3.763784
- 3.763785 - 4.843144
- 4.843145 - 6.364771
- 6.364772 - 8.949389
- 8.949390 - 14.238856

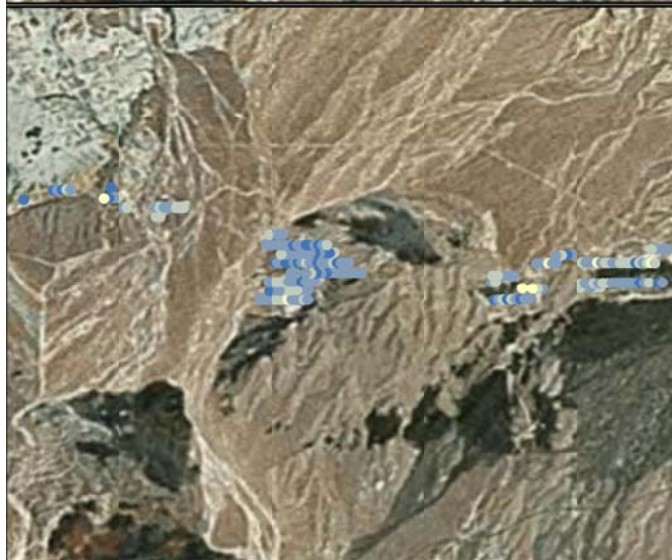




Government Wash Radioelement Ratio Images Unit ThI

U/K Ratio

- 0 - 1.000000
- 1.000001 - 2.776200
- 2.776201 - 4.814531
- 4.814532 - 9.199804
- 9.199805 - 26.562074
- 26.562075 - 67.621020
- 67.621021 - 229.055746



Th/K Ratio

- 0 - 3.307556
- 3.307557 - 5.092326
- 5.092327 - 7.271497
- 7.271498 - 15.387768
- 15.387769 - 38.153590
- 38.153591 - 74.386013
- 74.386014 - 164.297821



U/Th Ratio

- 0 - 0.100000
- 0.100001 - 0.500000
- 0.500001 - 1.000000
- 1.000001 - 1.500000
- 1.500001 - 2.000000
- 2.000001 - 3.000000
- 3.000001 - 9.114520
- 9.114521 - 242.489933



Traditional Geochemistry

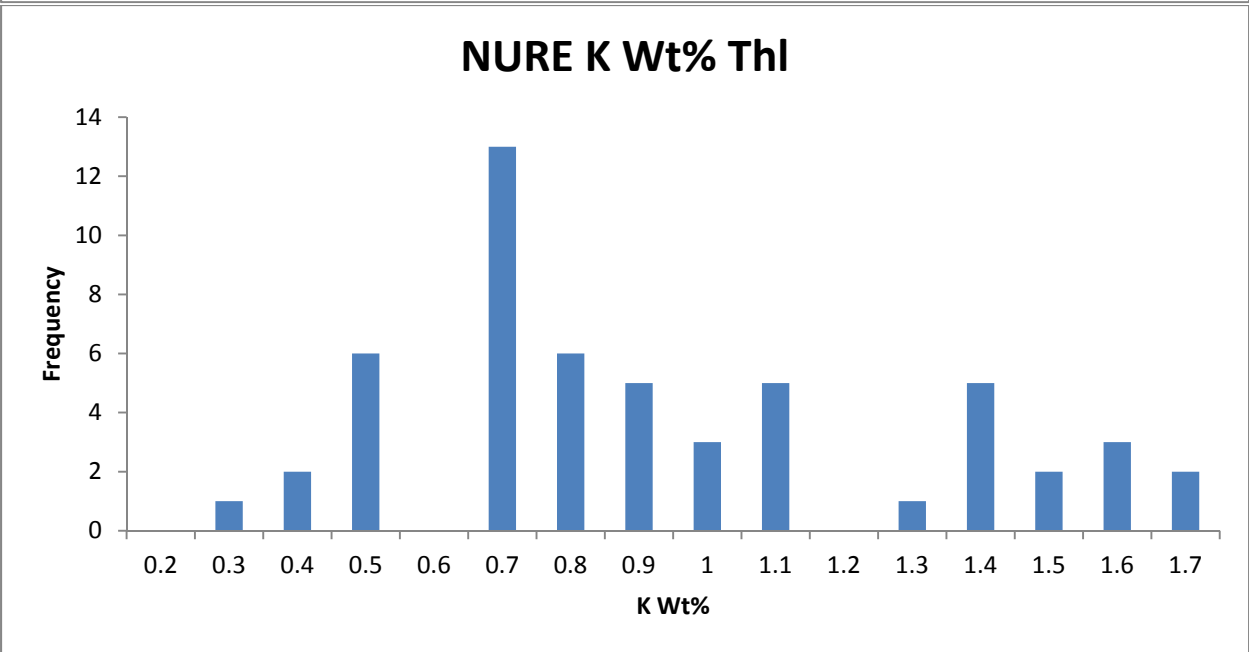
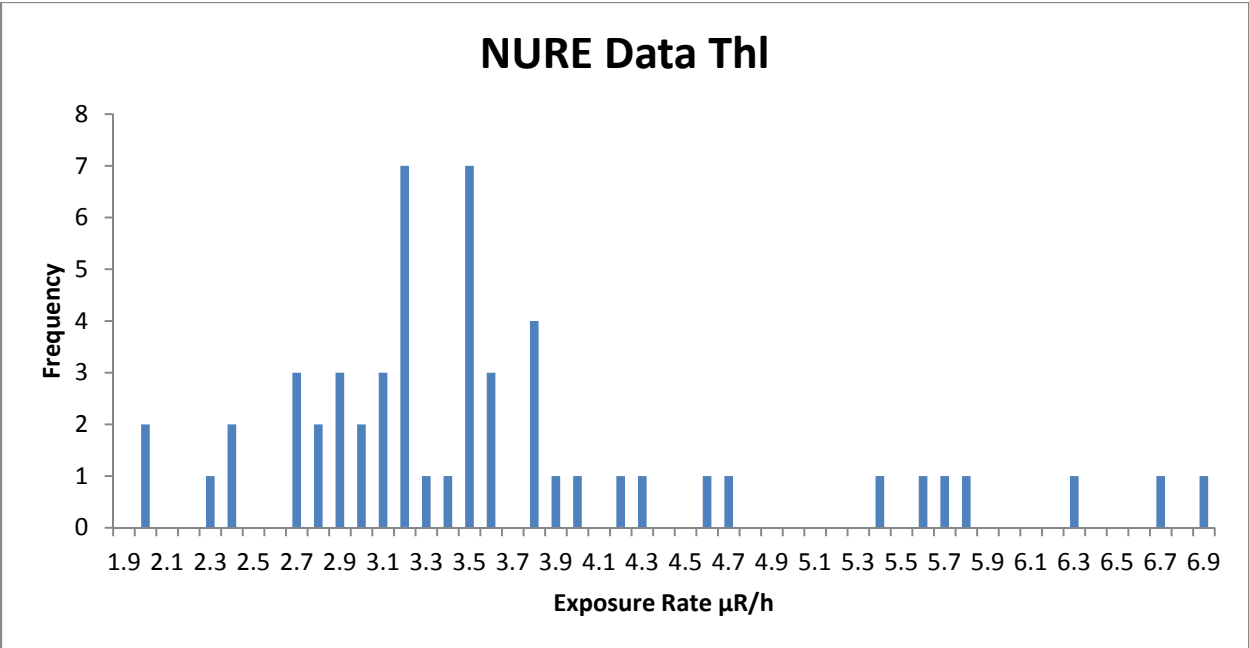
There is only a single geochemical data point for this Thl. The potassium and thorium concentrations are low while the uranium concentration is analogous to other units in the area. The predicted exposure rate from the geochemistry is 2.5 $\mu\text{R/h}$ which compares with the AMS data of 4.8 $\mu\text{R/h}$; this places this unit outside the desired ± 1 $\mu\text{R/h}$ range.

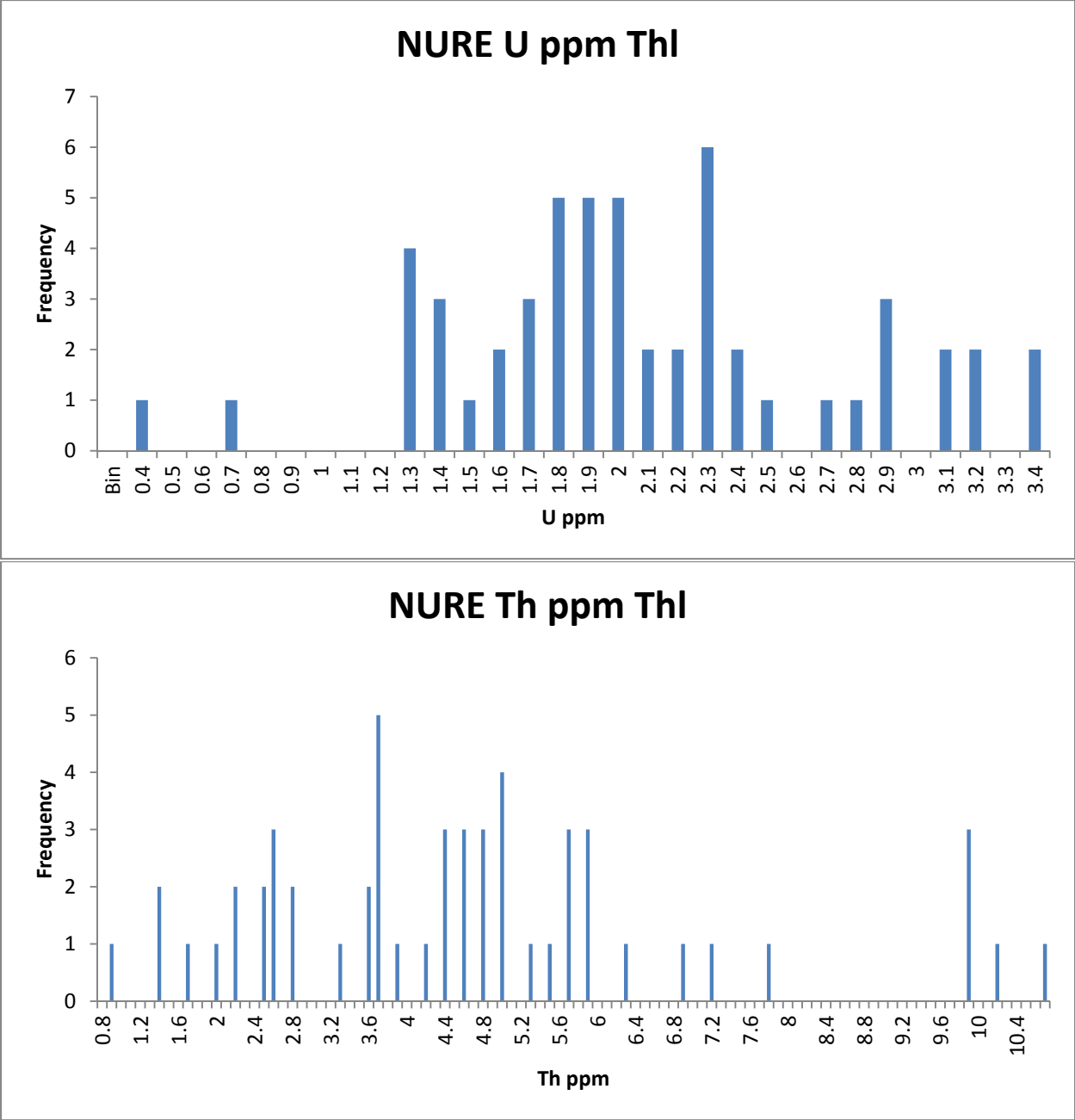
Sample ID	Latitude	Longitude	K %	U ppm	Th ppm
21154	36.1779	-114.808	0.6306	1.71	2.62

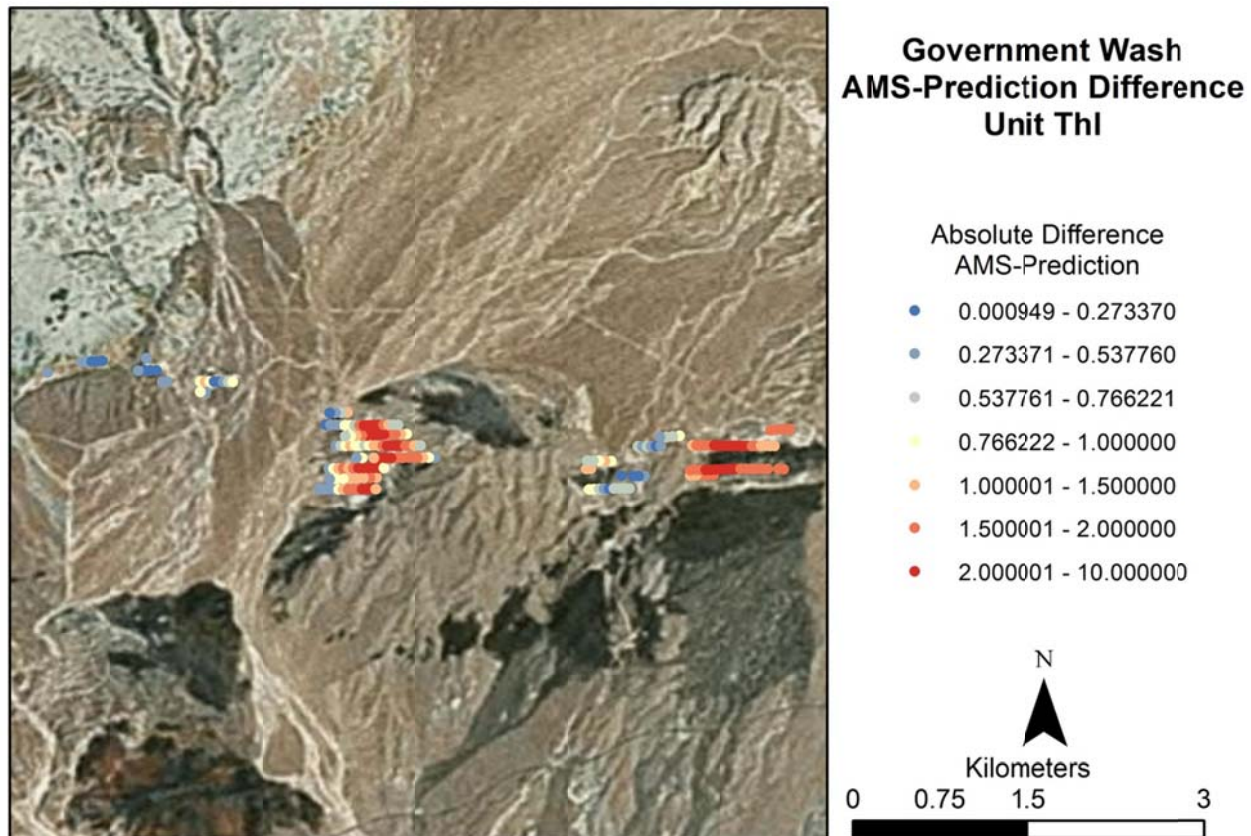
NURE Data

The NURE data for this unit primarily comes from the southern line. All of the histograms of the NURE data for Thl show no discernable pattern. Indeed the average NURE exposure rate for Thl is 3.6 $\mu\text{R/h}$ which compares with the AMS mean of 4.8 $\mu\text{R/h}$, placing this unit outside of the ± 1 $\mu\text{R/h}$ desired range.

When comparing the NURE prediction against the AMS data on a point by point basis the portions of the unit that have larger surface area have the greatest disagreement with the prediction >2 $\mu\text{R/h}$. However, portions of the unit that are near the margins or have small surface area tend to agree more with the prediction. This however is likely due to either the footprint effect of the detector or addition from surrounding materials.







Summary

Exposure Rate Comparison $\mu\text{R/h}$	Average	Median	STD	Range
AMS Data	4.80505004	4.873038	0.81652835	2.787857-6.85045
NURE Data	3.590308	3.398475	1.100896	1.96252-6.84678
Geochemical Prediction	2.482112	N/A	N/A	N/A

Thlv

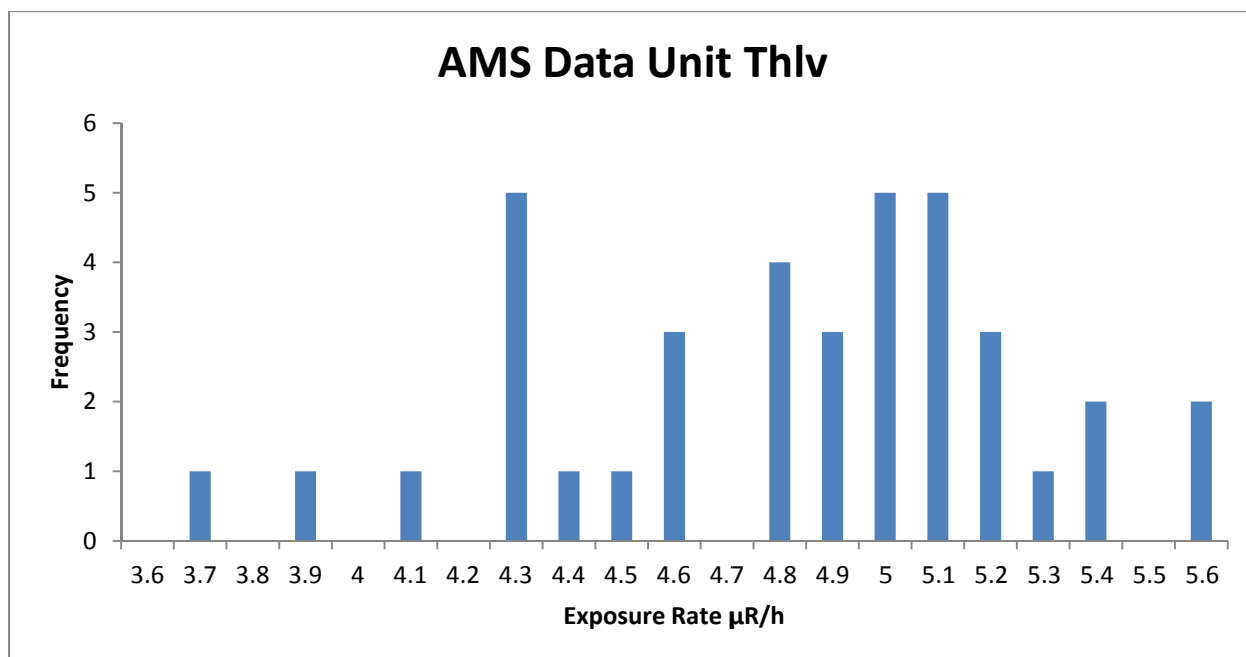
Composition

Thlv is a subunit of Thl and is therefore also Miocene in age. Both are paleo-alluvial fans that contain significant limestone as well as volcanic components. The primary difference between Thl and Thlv is that Thlv has a much greater basaltic component. (Duebendorfer, 2003) Otherwise the units are very similar in composition. There are no traditional geochemical data for this unit.

AMS Data

Much like Thl, Thlv has significant spread in the AMS exposure rate data. Exposure rates mostly cluster between 4.3 and 5.1 $\mu\text{R/h}$ but there is no clear peak in the data. The average exposure rate is 4.7 $\mu\text{R/h}$ with a standard deviation of 0.45 $\mu\text{R/h}$ which is only 9% of the mean.

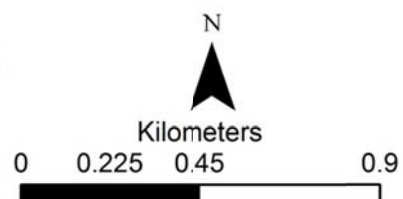
Similarly, K, U, and Th values show little pattern and are spread fairly widely. All of the data occurs in a thin strip that is mostly one data point in thickness. This means the data may be heavily influenced by surrounding units because of the detector footprint. Considering its small surface area, it is difficult to say whether it is geochemically homogenous.

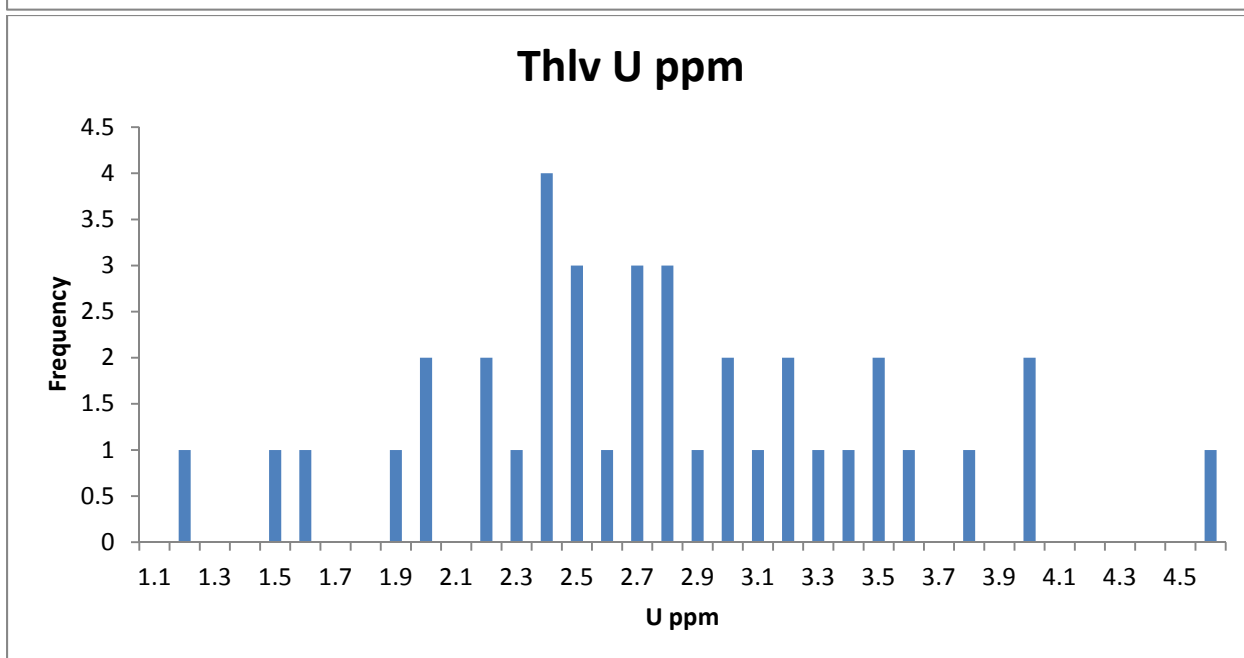
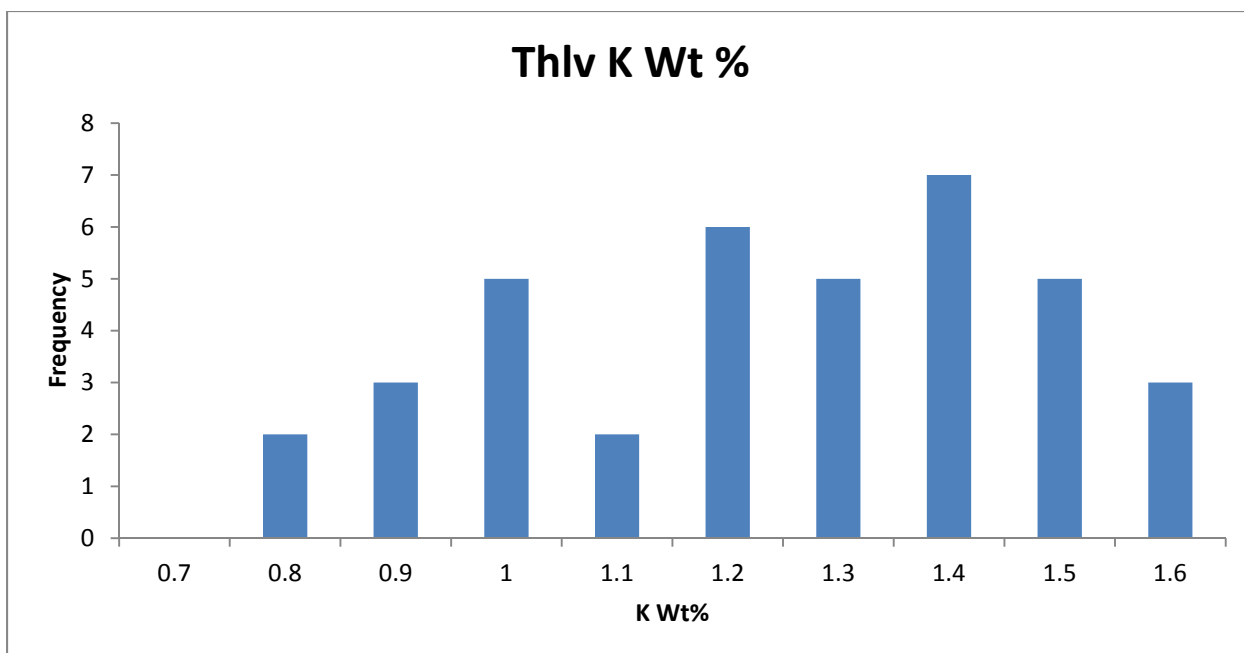


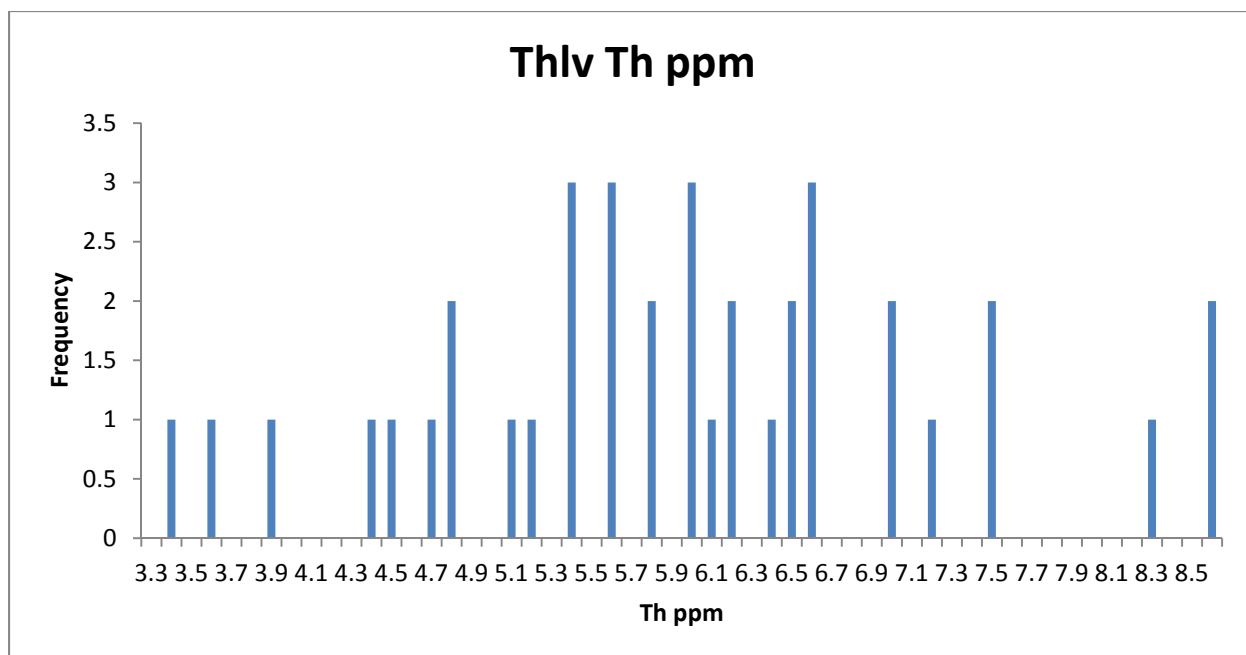
Government Wash AMS Data Unit Thlv

Exposure Rate ($\mu\text{R/h}$)

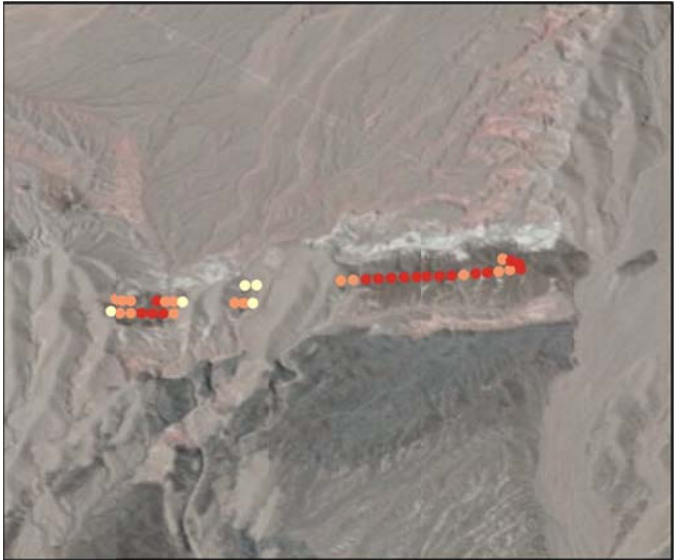
- 0 - 1.230088
- 1.230089 - 1.633850
- 1.633851 - 2.037611
- 2.037612 - 2.441372
- 2.441373 - 2.845133
- 2.845134 - 3.450774
- 3.450775 - 4.056416
- 4.056417 - 5.670907
- 5.670908 - 10.768856







**Government Wash Radioelement
Concentration Images
Unit Thlv**



K Wt%

- 0 - 0.485574
- 0.485575 - 0.679890
- 0.679891 - 0.902579
- 0.902580 - 1.234061
- 1.234062 - 2.271017



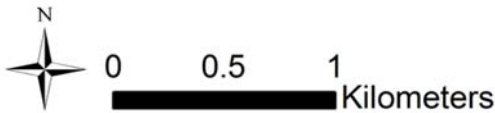
U PPM

- 0 - 0.818232
- 0.818233 - 1.415482
- 1.415483 - 2.069242
- 2.069243 - 2.679219
- 2.679220 - 3.502989
- 3.502990 - 4.043893
- 4.043894 - 7.910720



Th PPM

- 0 - 0.942384
- 0.942385 - 1.784504
- 1.784505 - 2.810072
- 2.810073 - 3.763784
- 3.763785 - 4.843144
- 4.843145 - 6.364771
- 6.364772 - 8.949389
- 8.949390 - 14.238856





Government Wash Radioelement Ratio Images Unit Thlv

U/K Ratio

- 0 - 1.000000
- 1.000001 - 2.776200
- 2.776201 - 4.814531
- 4.814532 - 9.199804
- 9.199805 - 26.562074
- 26.562075 - 67.621020
- 67.621021 - 229.055746



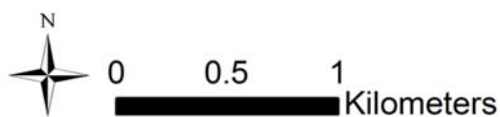
Th/K Ratio

- 0 - 3.307556
- 3.307557 - 5.092326
- 5.092327 - 7.271497
- 7.271498 - 15.387768
- 15.387769 - 38.153590
- 38.153591 - 74.386013
- 74.386014 - 164.297821



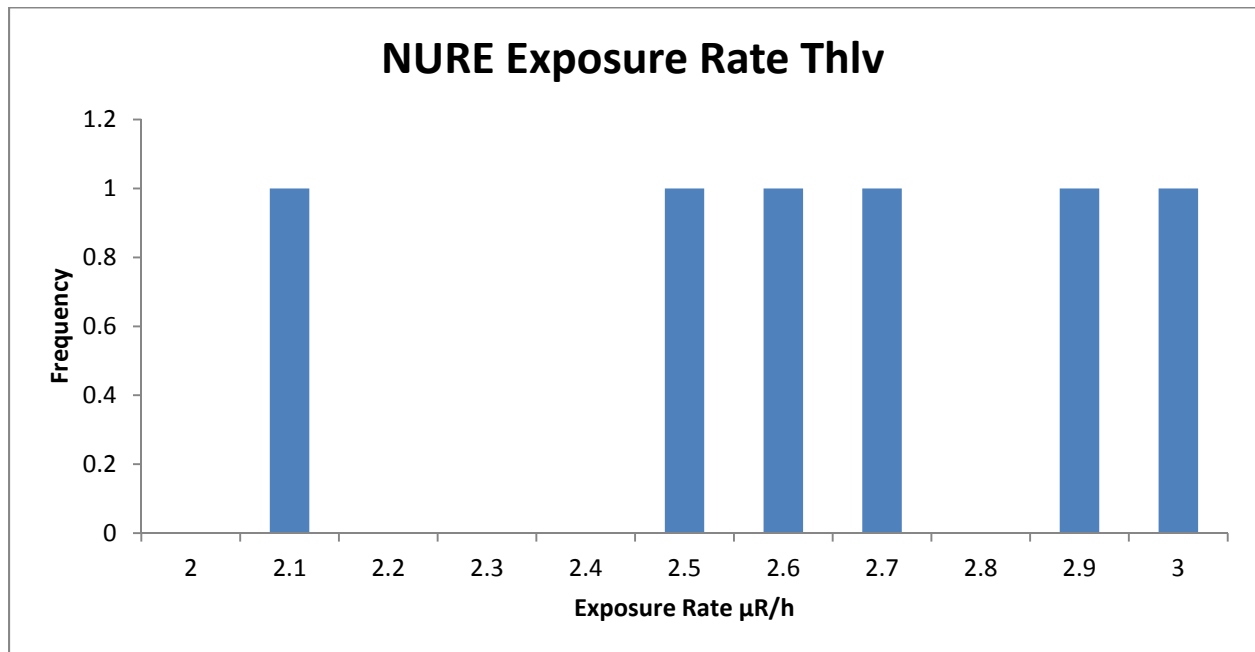
U/Th Ratio

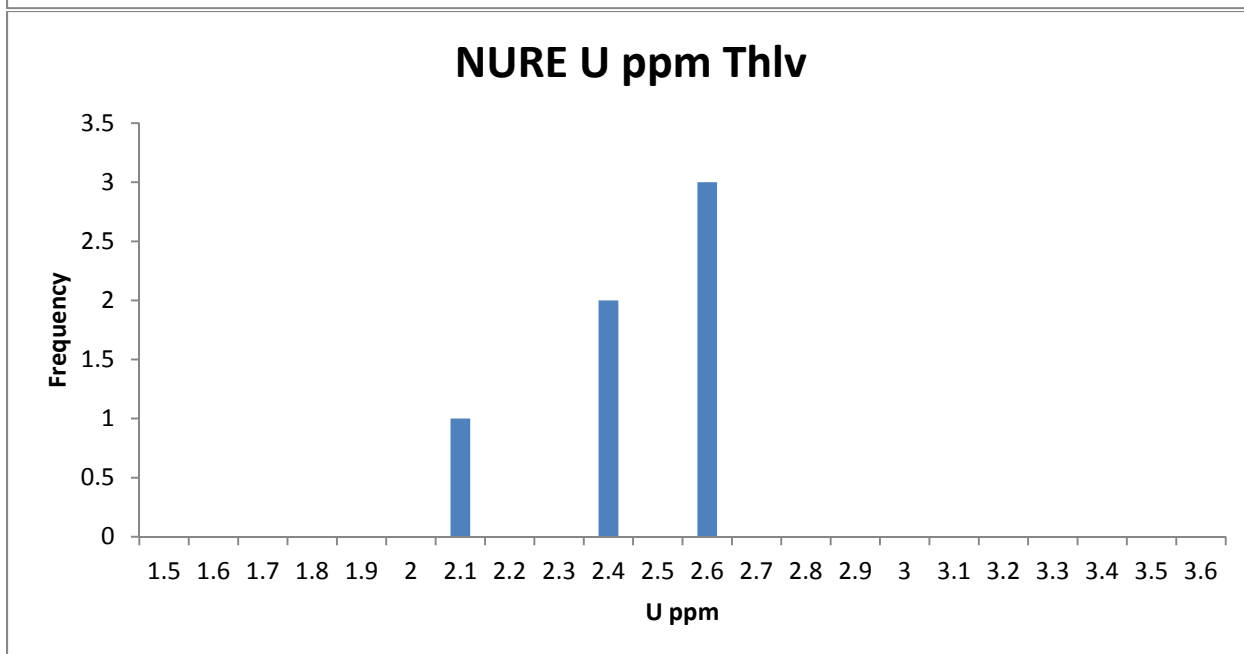
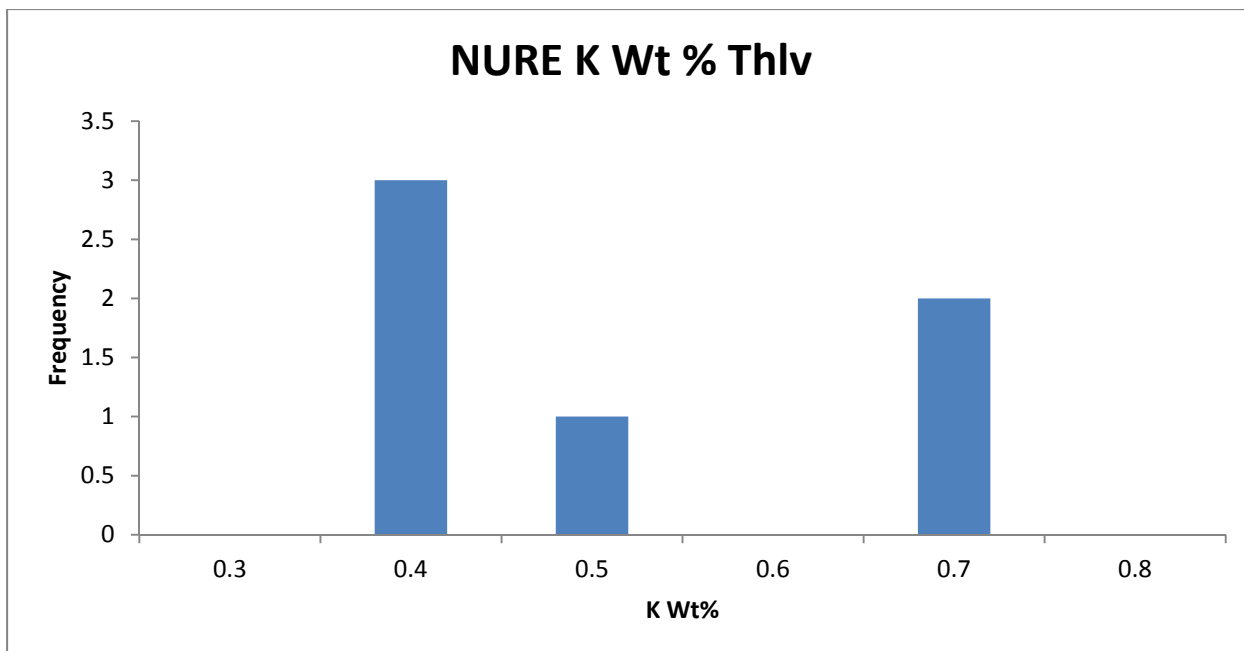
- 0 - 0.100000
- 0.100001 - 0.500000
- 0.500001 - 1.000000
- 1.000001 - 1.500000
- 1.500001 - 2.000000
- 2.000001 - 3.000000
- 3.000001 - 9.114520
- 9.114521 - 242.489933

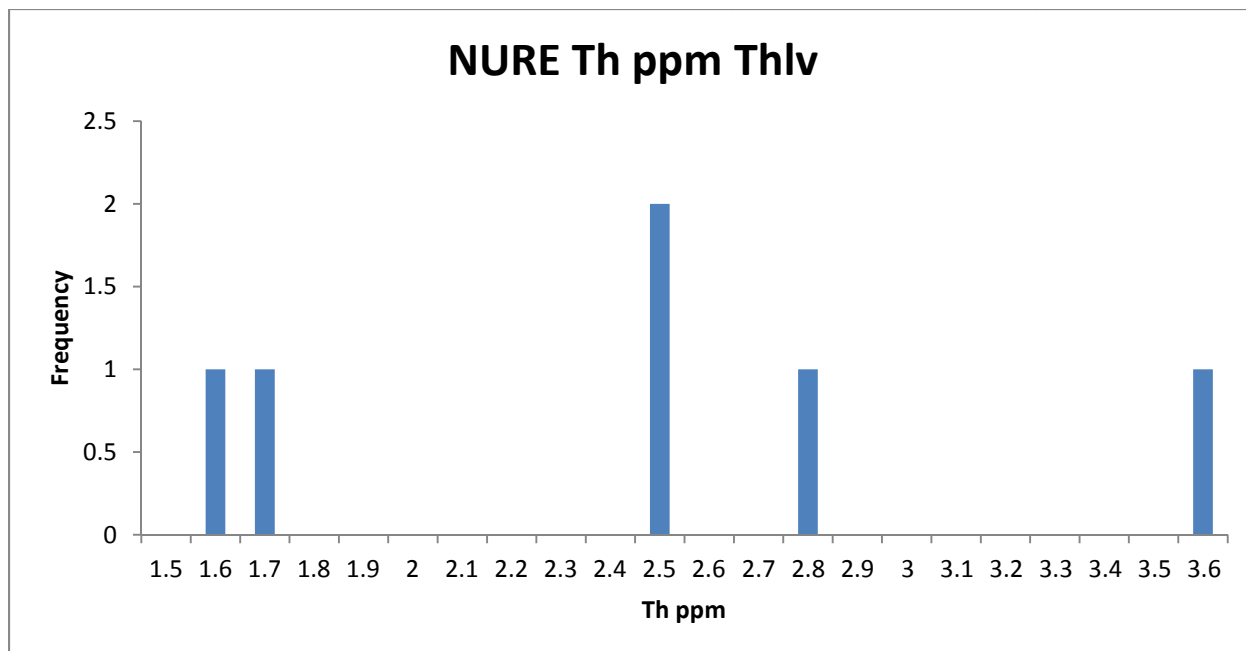


NURE Data

Thlv gets all of its NURE data from the southern line. There is no discernable pattern in the data. The NURE mean exposure rate is 2.59 $\mu\text{R/h}$ which compares with the AMS mean of 4.77 $\mu\text{R/h}$. In this case the predicted exposure is much less than the AMS mean. Similarly, the K, U, and Th data are not well represented by the NURE data. This unit is not modeled well by the NURE data.



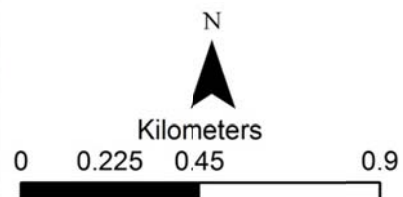




Government Wash AMS-Prediction Difference Unit Thlv

Absolute Difference
AMS-Prediction

- 0.000949 - 0.273370
- 0.273371 - 0.537760
- 0.537761 - 0.766221
- 0.766222 - 1.000000
- 1.000001 - 1.500000
- 1.500001 - 2.000000
- 2.000001 - 10.000000



Summary

Exposure Rate Comparison μR/h	Average	Median	STD	Range
AMS Data	4.77180942	4.8630825	0.45430035	3.629267-5.563032
NURE Data	2.592547	2.601315	0.304651	2.05234-2.99895
Geochemical Prediction	N/A	N/A	N/A	N/A

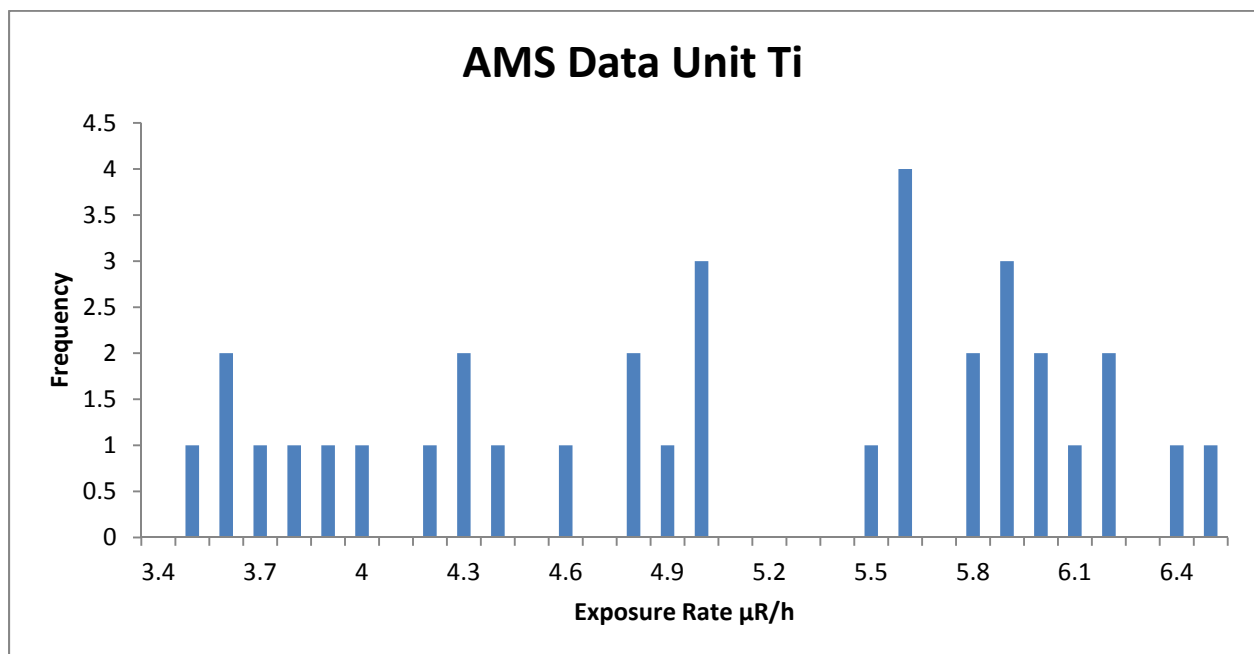
Ti

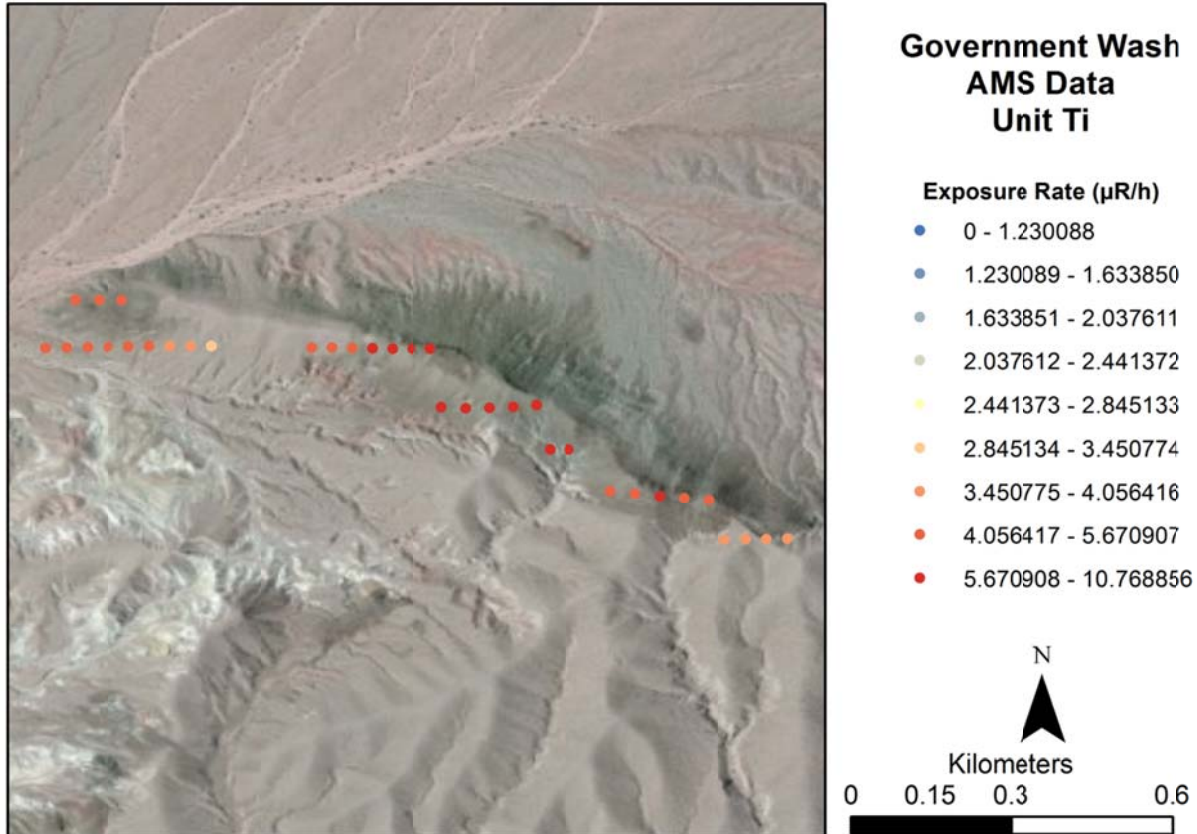
Composition

Duebendorfer (2003) mapped this unit as a small intrusive basaltic dike of Miocene age in the Horse Spring Formation that consists of mafic rock with hornblende, plagioclase, clinopyroxene and olivine with minor sphene. However, field work in the area found that at least a significant portion of the unit is reworked into dark basaltic sandstone. It is not clear if portions of the unit are still in place.

AMS Data

The AMS data in this unit is spread fairly widely from 3.4 to 6.5 $\mu\text{R/h}$. The majority of the data occurs after 4.8 $\mu\text{R/h}$ and the mean of the data is 5.03 $\mu\text{R/h}$. The standard deviation is 0.93 or 18% of the mean. This is a thin unit with a very limited spatial extent and is likely influenced by surrounding units due to the detector footprint effect. There are no geochemical or NURE data for this unit. Because of this no prediction can be made.





Summary

Exposure Rate Comparison μR/h	Average	Median	STD	Range
AMS Data	5.035238	4.98544	0.930856	3.43611-6.49247
NURE Data	N/A	N/A	N/A	N/A
Geochemical Prediction	N/A	N/A	N/A	N/A

Tht

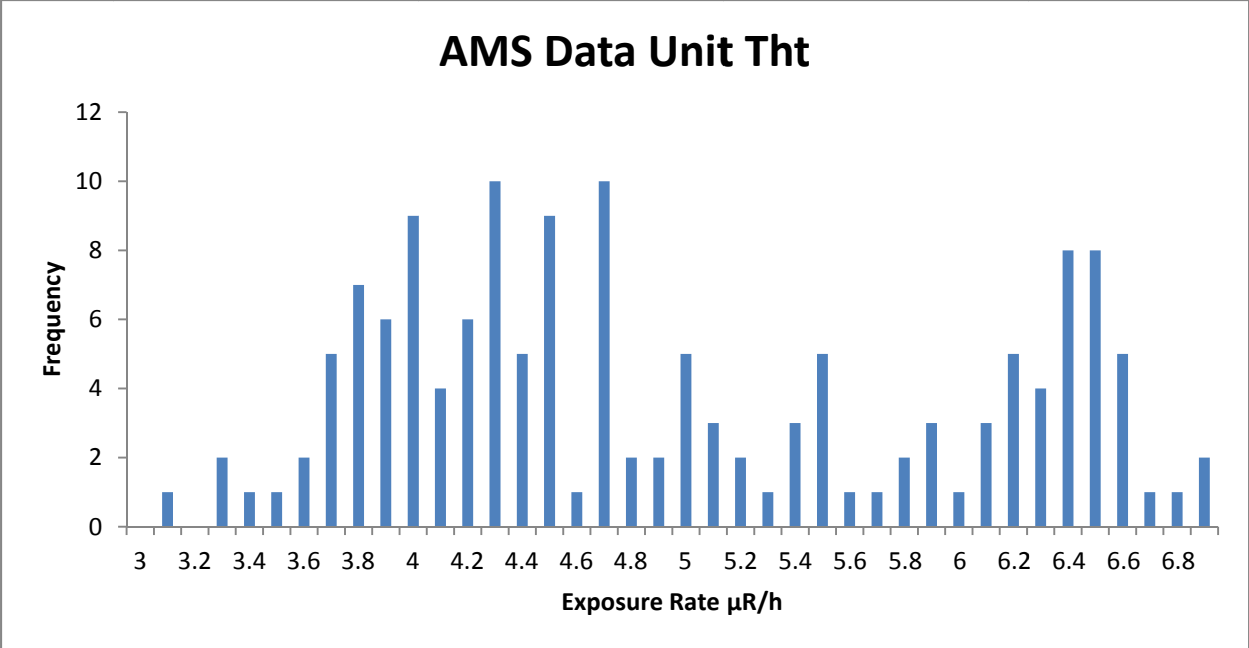
Composition

Tht is a member of the Horse Spring Formation and Miocene in age. It consists of conglomerate, megabreccia, sandstone, siltstone, gypsum, gypsiferous siltstone, with minor limestone, tuff, and tuffaceous and calcareous sandstone. Conglomerate occurs as discontinuous layers interbedded with sandstone and siltstone. Conglomerate and sandstone are brown, gray, red, and yellow. Clast types in the conglomerate include Paleozoic carbonates and sandstones and Mesozoic sandstone, mostly Aztec Sandstone. (Duebendorfer, 2003)

AMS Data

The AMS exposure rate data for Tht has two distinct clusters. The first peaks near 4.3 $\mu\text{R/h}$ but has considerable spread and is not normally distributed. The second peaks near 6.5 $\mu\text{R/h}$. The second cluster all occurs within the spatial center of the unit while the lower exposure rates occur near the margins of the unit. The average exposure rate is 4.92 $\mu\text{R/h}$ with a standard deviation of 1.03 $\mu\text{R/h}$ or 21% of the mean.

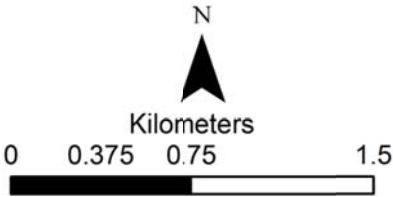
The distributions of K, U, and Th are wide and are not normal. This is likely driven by the fact that the unit is spatially thin and heavily influenced by surrounding units. In the composition images K and Th vary with exposure rate while U seems to have little relationship with exposure.

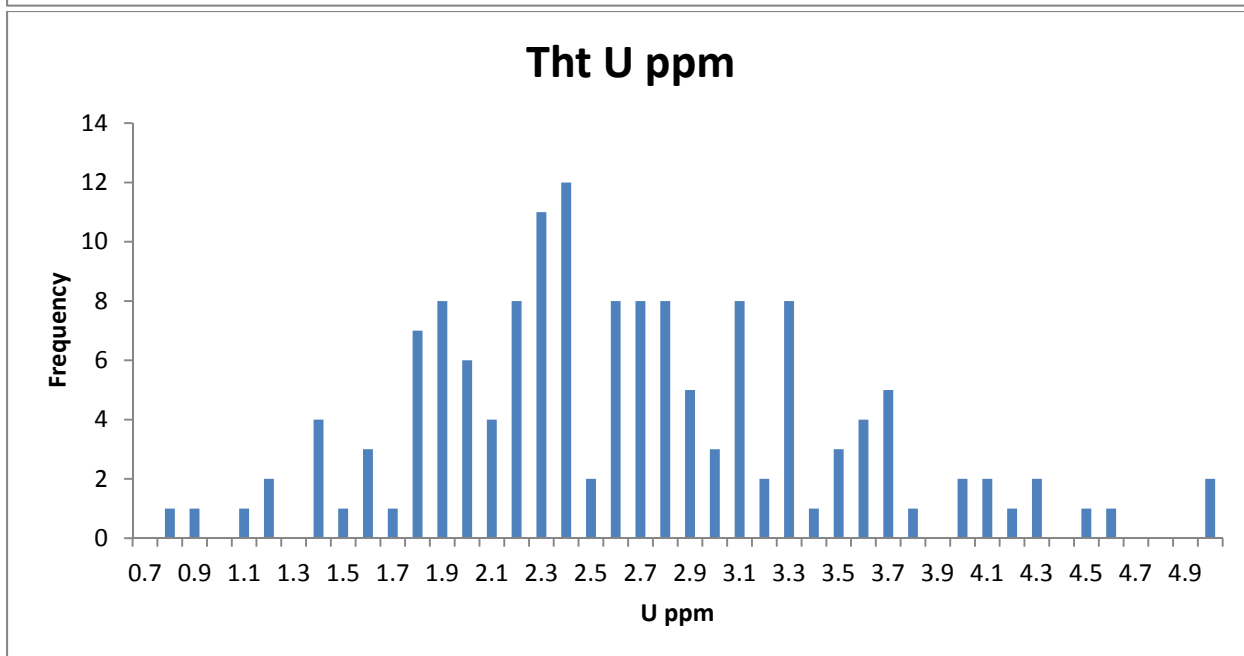
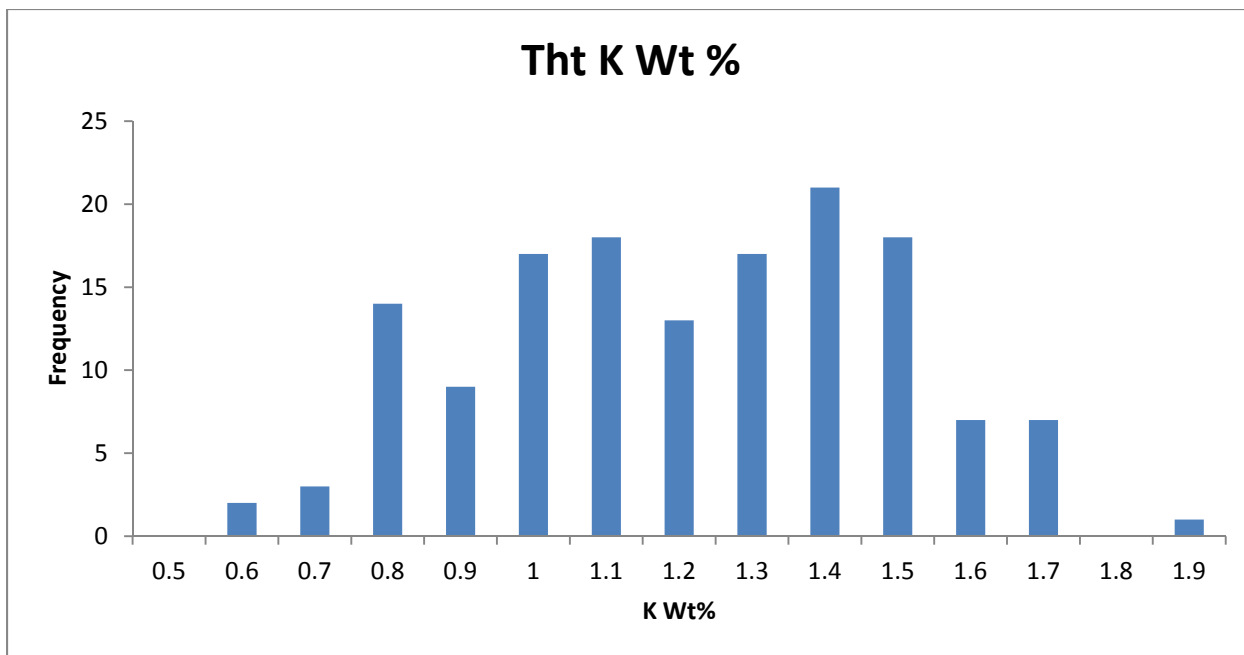


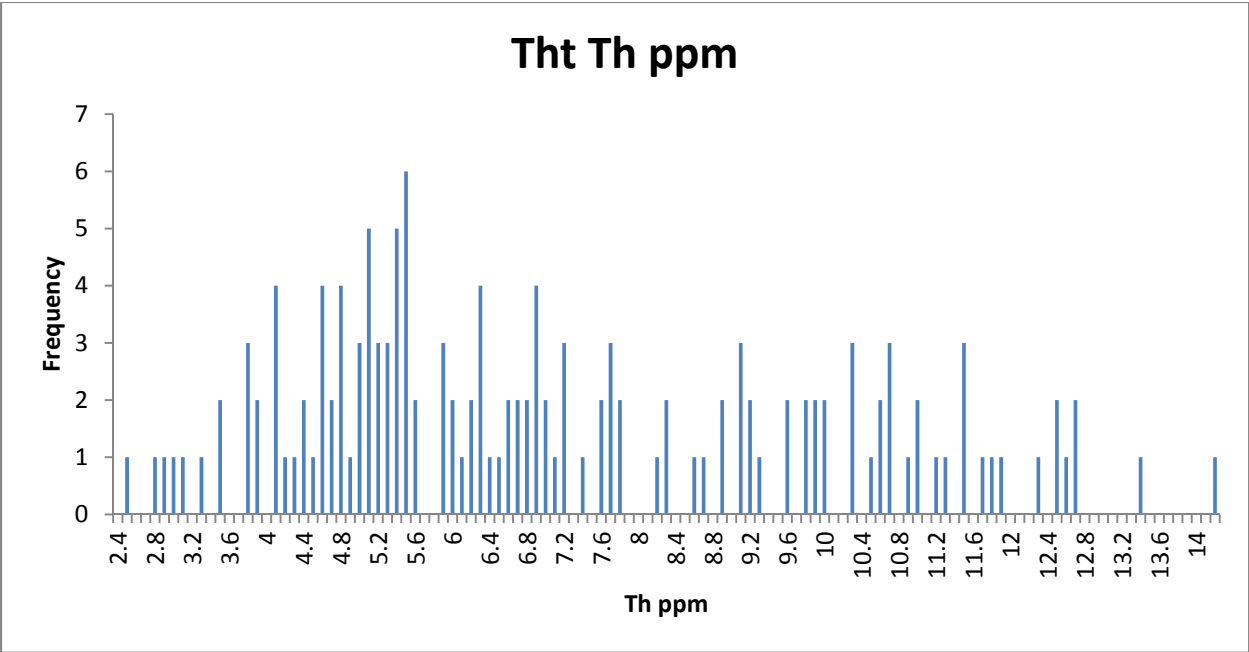
Government Wash AMS Data Unit Tht

Exposure Rate ($\mu\text{R/h}$)

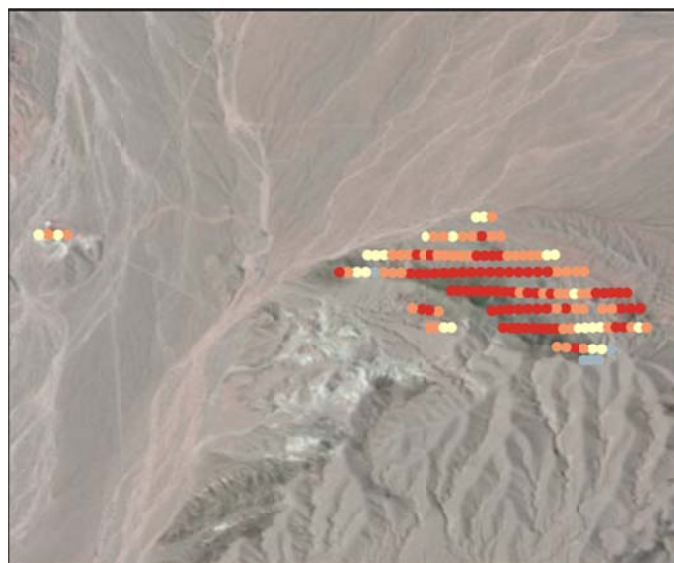
- 0 - 1.230088
- 1.230089 - 1.633850
- 1.633851 - 2.037611
- 2.037612 - 2.441372
- 2.441373 - 2.845133
- 2.845134 - 3.450774
- 3.450775 - 4.056416
- 4.056417 - 5.670907
- 5.670908 - 10.768856







Government Wash Radioelement Concentration Images Unit Tht



K Wt%

- 0 - 0.485574
- 0.485575 - 0.679890
- 0.679891 - 0.902579
- 0.902580 - 1.234061
- 1.234062 - 2.271017



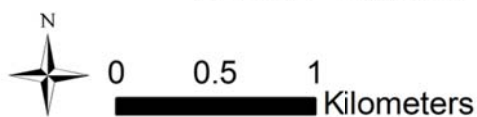
U PPM

- 0 - 0.818232
- 0.818233 - 1.415482
- 1.415483 - 2.069242
- 2.069243 - 2.679219
- 2.679220 - 3.502989
- 3.502990 - 4.043893
- 4.043894 - 7.910720



Th PPM

- 0 - 0.942384
- 0.942385 - 1.784504
- 1.784505 - 2.810072
- 2.810073 - 3.763784
- 3.763785 - 4.843144
- 4.843145 - 6.364771
- 6.364772 - 8.949389
- 8.949390 - 14.238856





Government Wash Radioelement Ratio Images Unit Tht

U/K Ratio

- 0 - 1.000000
- 1.000001 - 2.776200
- 2.776201 - 4.814531
- 4.814532 - 9.199804
- 9.199805 - 26.562074
- 26.562075 - 67.621020
- 67.621021 - 229.055746



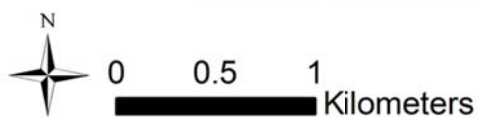
Th/K Ratio

- 0 - 3.307556
- 3.307557 - 5.092326
- 5.092327 - 7.271497
- 7.271498 - 15.387768
- 15.387769 - 38.153590
- 38.153591 - 74.386013
- 74.386014 - 164.297821



U/Th Ratio

- 0 - 0.100000
- 0.100001 - 0.500000
- 0.500001 - 1.000000
- 1.000001 - 1.500000
- 1.500001 - 2.000000
- 2.000001 - 3.000000
- 3.000001 - 9.114520
- 9.114521 - 242.489933

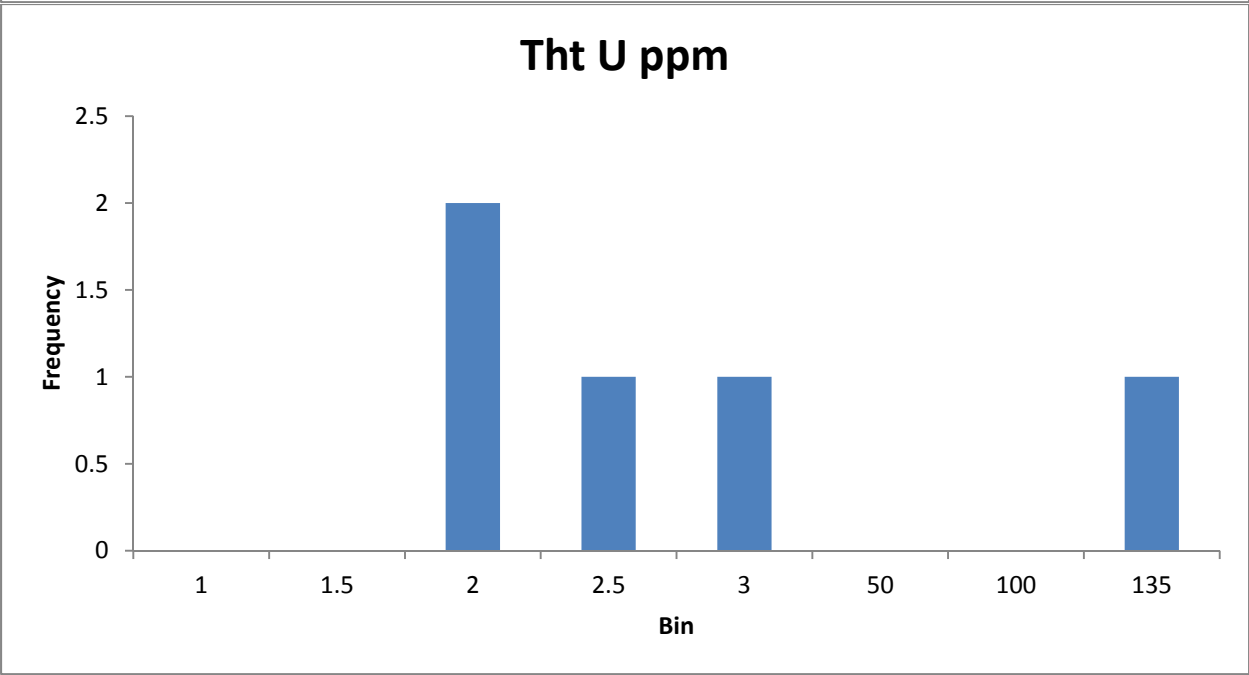
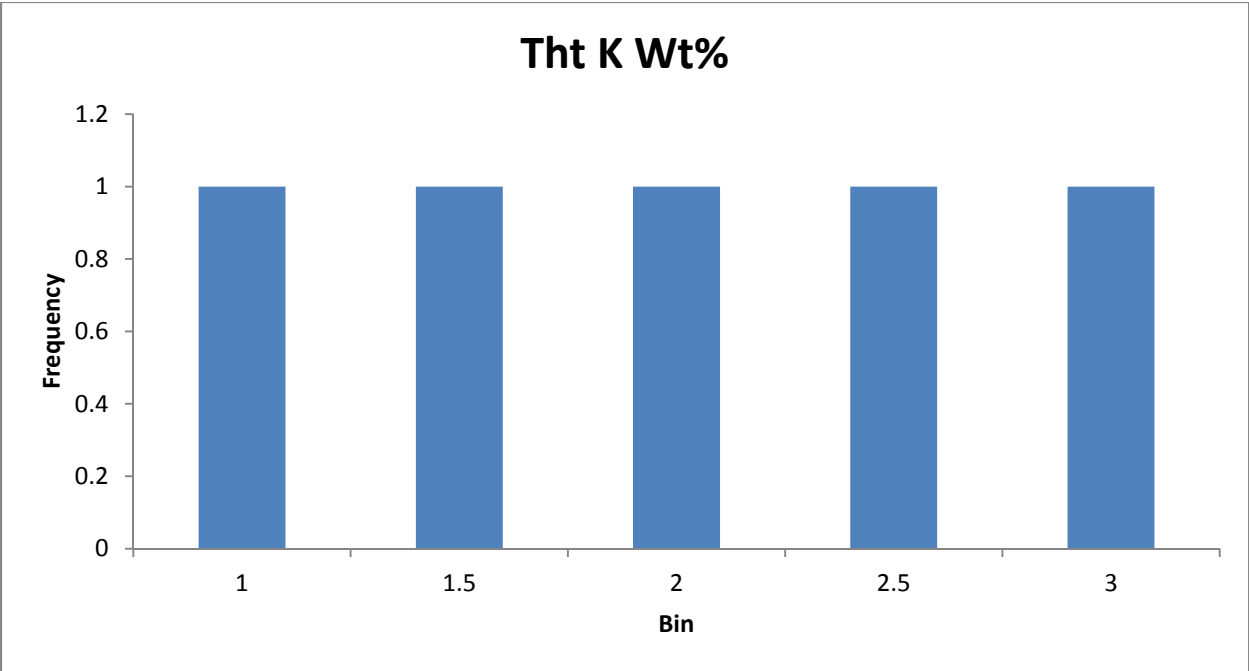


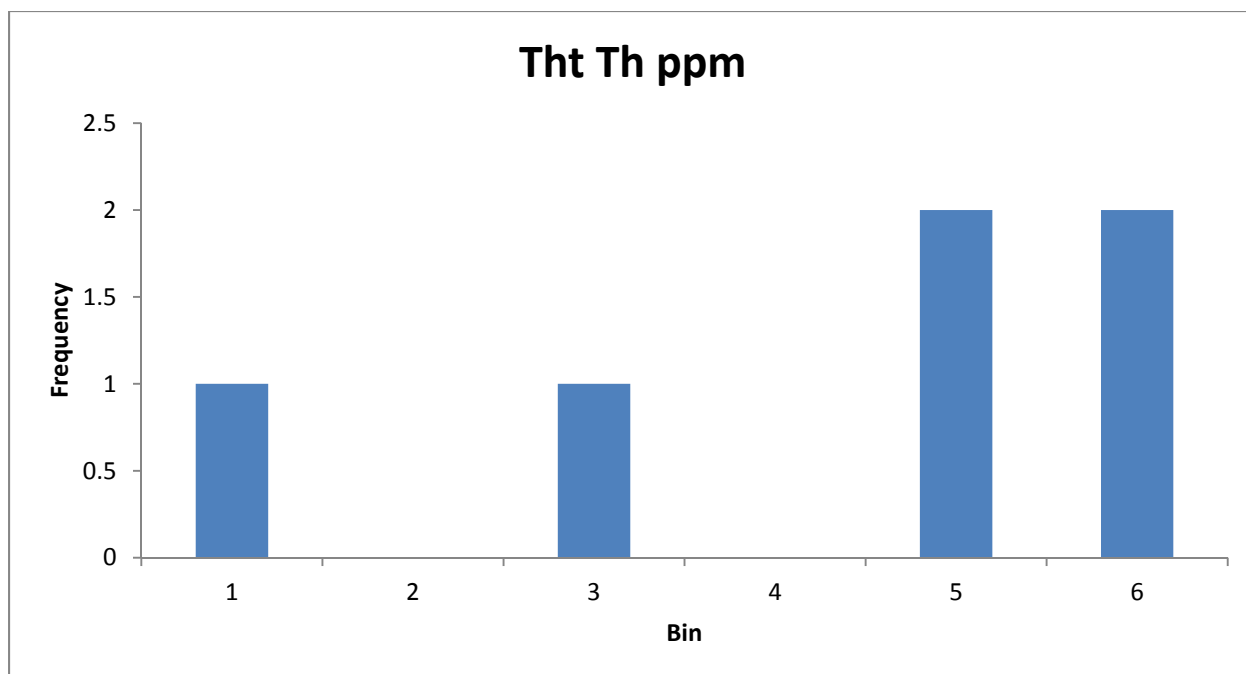
Traditional Geochemistry

There are 7 geochemical data points that occur in Tht. The K percentage values range from <1 to >2.5 with an average of 1.68. The Th values also have a broad range from <1 to >5.4 ppm with an average of 3.88. However, most of the Th data is centered between 4.5-5.5 ppm so the lower values pull down the average. For the most part, U values are near 2 ppm but there is however one data point that is greater than 130 ppm. Therefore, the median value for U is used to calculate exposure rate while mean values are used for K and Th. The exposure rate derived from these data is 4.46 $\mu\text{R/h}$ which compares with the AMS mean of 4.9 $\mu\text{R/h}$. This places this unit well within the ± 1 $\mu\text{R/h}$ success range.

Sample ID	Latitude	Longitude	K %	U ppm	Th ppm
21145	36.1716	-114.765	1.508	2.17	5.017
21147	36.2091	-114.727		1.62	0.9625
CM24-68	36.1719	-114.708	2.54		5.46
CM24-49	36.17	-114.71	2.33		4.89
21164	36.1643	-114.71	1.456	1.56	4.457
15101	36.2077	-114.913	0.5671	2.9	2.54
1-121-1	36.1861	-114.912		134	

	K%	U ppm	Th ppm
Mean	1.68022	28.45	3.88775
Median	1.508	2.17	4.6735
Standard Deviation	0.70433	52.7772	1.604641
Range	0.5671-2.54	1.56-134	0.9625-5.46

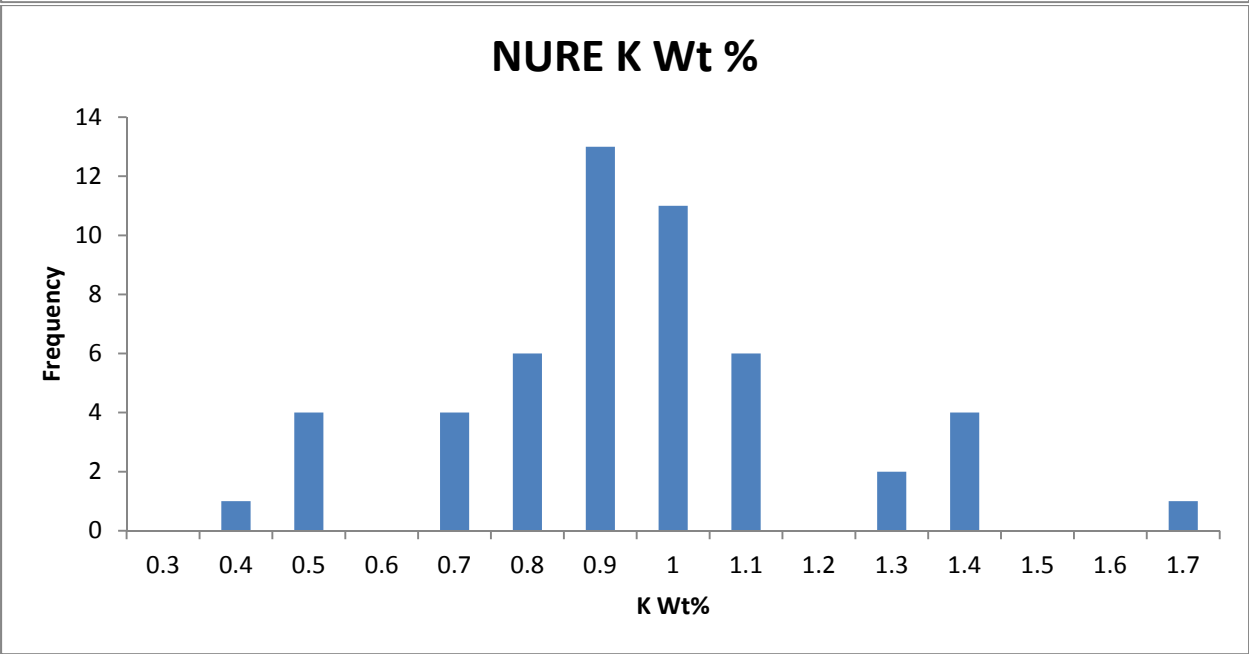
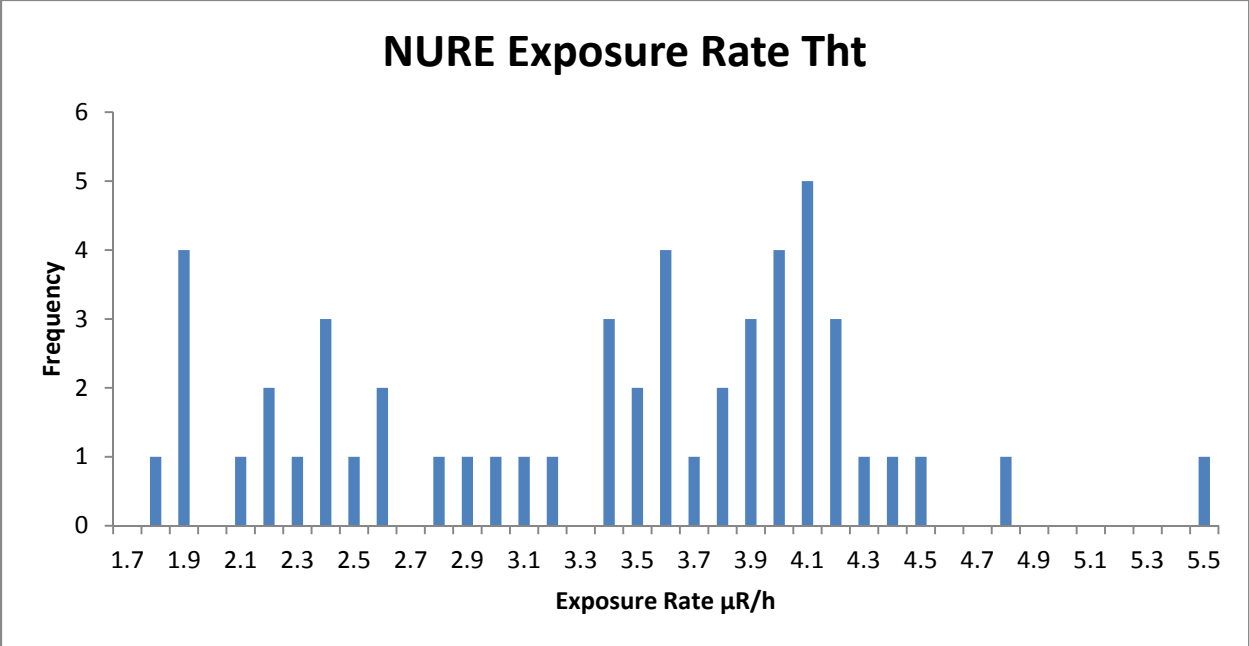


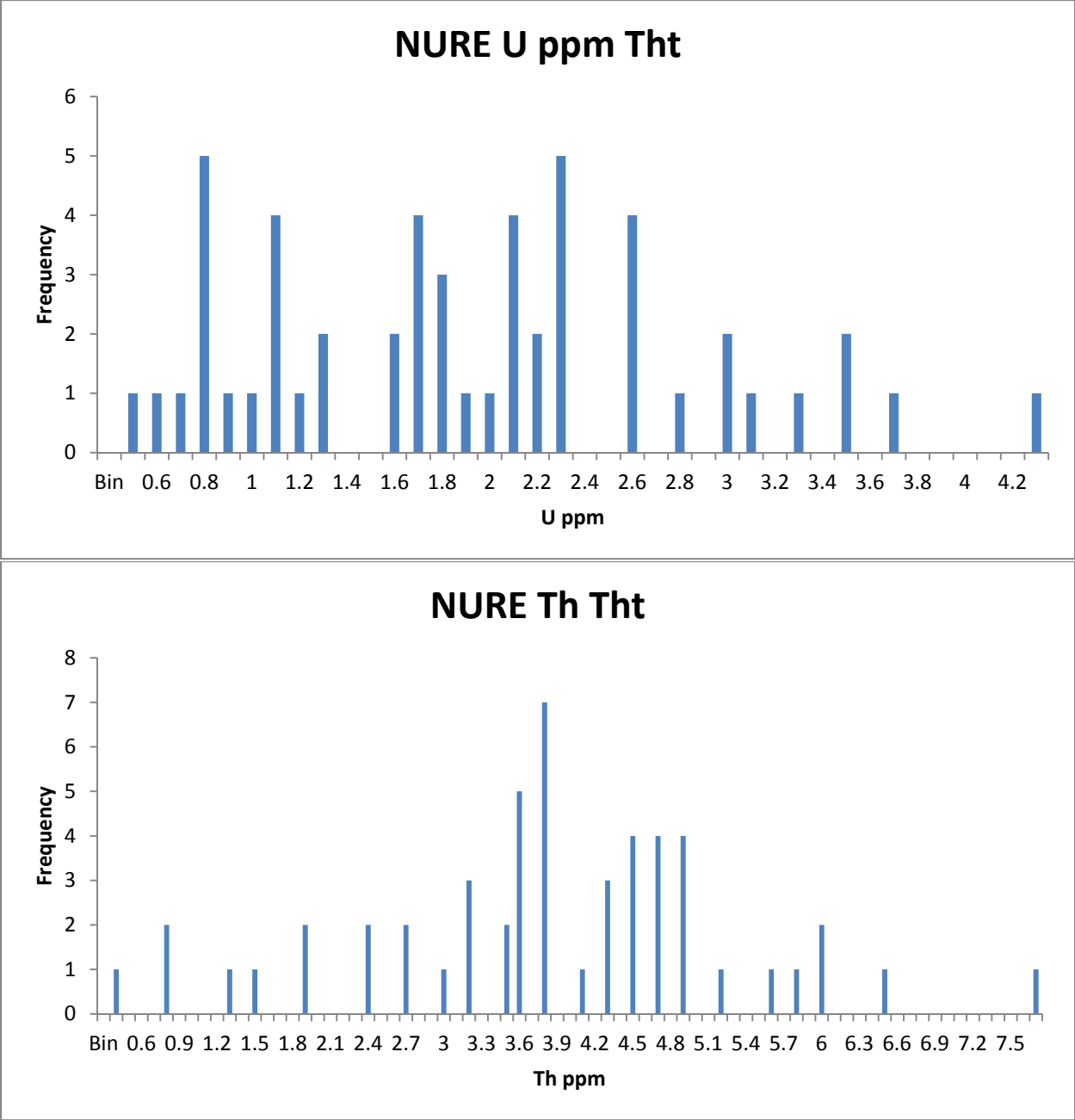


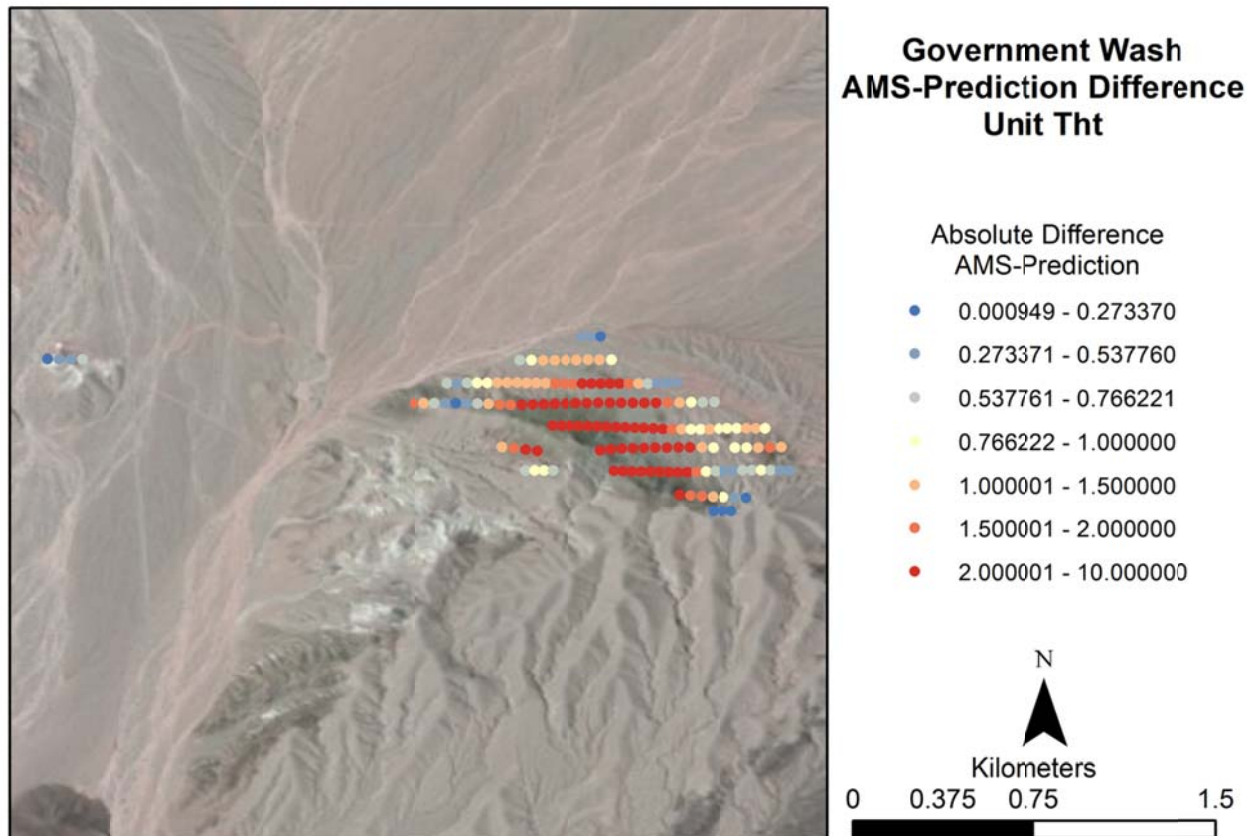
NURE Data

Similar to other units that occur in the southern portion of the area of interest, NURE data for Tht are derived from the problematic southern line. Therefore, the spread in the NURE data is fairly wide. The exposure rate values have several peaks; some near 2-2.5 $\mu\text{R/h}$ and others near 3.5-4 $\mu\text{R/h}$. Similarly, U and Th values vary with only Th having a strong peak near 3.8 ppm. K values on the other hand are centered near a peak between 0.9-1%.

The exposure rate prediction based on the NURE data is 3.32 $\mu\text{R/h}$ which compares with the AMS mean of 4.9 $\mu\text{R/h}$. This places this unit outside of the ± 1 $\mu\text{R/h}$ desired range. When comparing the NURE prediction against the AMS data point by point the interior of the unit has significant differences with the prediction while the margins of the unit are closer to agreement.







Summary

Exposure Rate Comparison $\mu\text{R/h}$	Average	Median	STD	Range
AMS Data	4.91894216	4.659219	1.03176904	3.075872-6.89516
NURE Data	3.322575	3.52182	0.874311	1.70576-5.41447
Geochemical Prediction	4.4645	4.450912	N/A	1.865252-78.26992

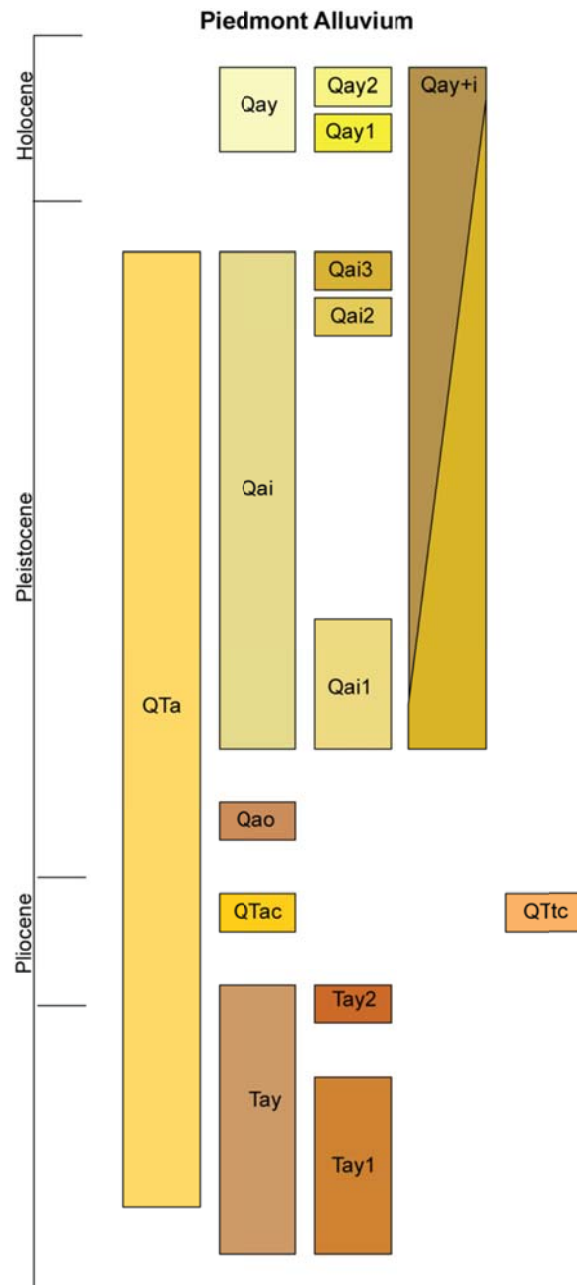
Appendix B: Lake Mohave Unit Report

Abstract

The western shore Lake Mohave is dominated by Quaternary alluvium whose source material is derived from igneous and metamorphic sources to the west. The alluvium is characterized by many stages of deposition, terracing and incision. Modeling the geochemical distribution on many of the surfaces has proven challenging. In most areas, the surface material is dominated by a single source class, e.g., felsic igneous rocks, but is heavily mixed with material from other sources. Additionally, some older surfaces are buried by younger surfaces and still others are dissected by very recent activity.

This report characterizes the distribution of exposure rate, K, U, and Th across the alluvial units that are defined by the geologic map titled, "Preliminary Geologic Map of the North Half of the Spirit Mtn. NW Quadrangle" mapped by House and Faulds in 2009 and published by the Nevada Bureau of Mines and Geology.

All predicted exposure rates are calculated using Equation 4-1 from geochemical or previously existing gamma ray survey data points collected from national databases. The measured exposure rates are averages from the AMS data points that occur within each unit. Units are listed in stratigraphic order.



Introduction

Lake Mohave is an artificial lake on the Colorado River located south of Lake Mead in Southern Nevada and Arizona. This area has experienced significant tectonic and volcanic activity since the Miocene (House and Faulds, 2009). On the western shore of Lake Mohave there are extensive alluvial deposits that are composed of rocks derived from the plutonic, volcanic and metamorphic rocks to the west. The mountain range that is the source of the alluvial material is part of the El Dorado Mountains.

In the southern portion of the source mountain range there is a mix of Proterozoic age crystalline basement and Miocene age felsic and intermediate igneous rocks. The crystalline basement rocks are composed of metamorphic rocks that are granitic to dioritic in composition. The felsic and intermediate igneous rocks are composed of rhyolite, diorite and tuff and are intermixed in overlapping veins.

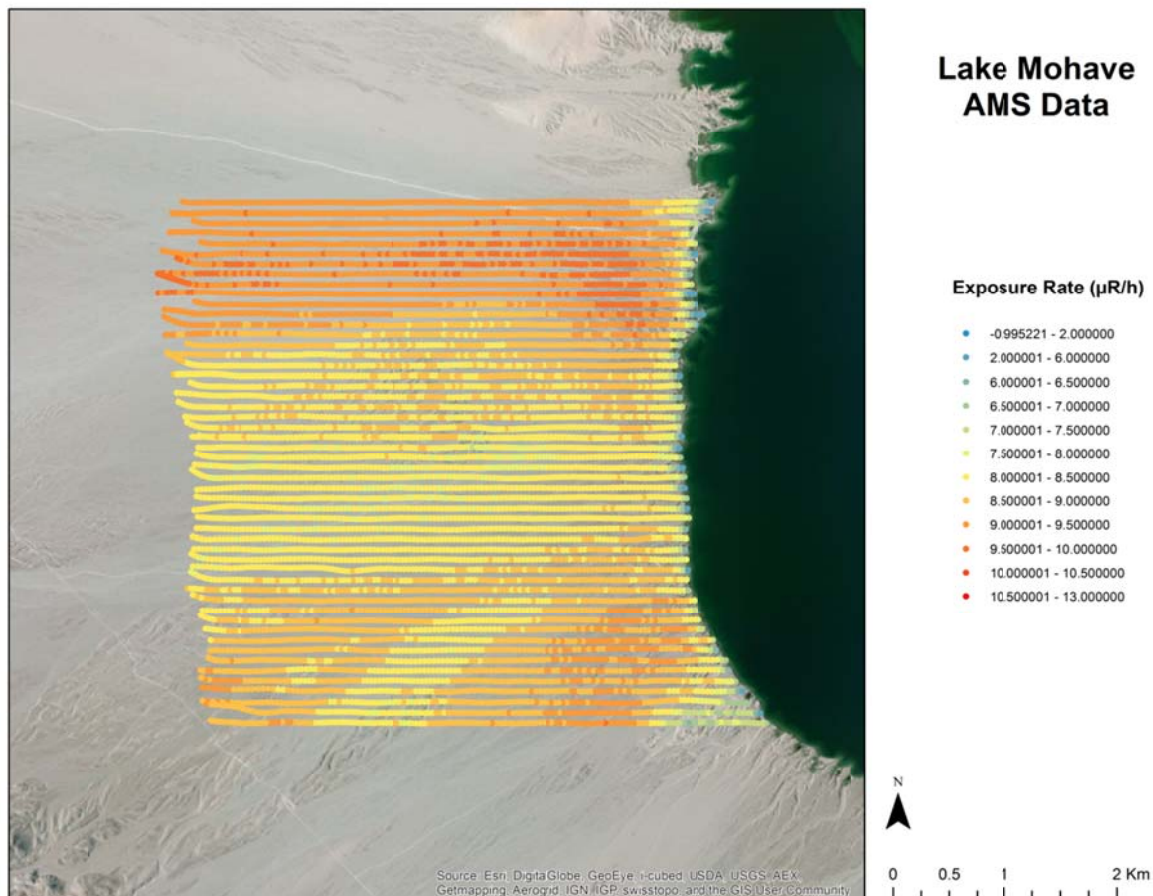
In the center of the range there are intermediate and mafic, igneous and metamorphic rocks such as andesite, dacite, amphibolite and basalt that are Miocene in age that contribute to the fans. The northern section is dominated by felsic igneous and metamorphic rocks including quartz monzonite, granite, gneiss and contains minor mafic rocks that are all Miocene in age.

Aside from materials derived from the range to the west there are significant components related to river deposits. Lake Mohave sits above the recent flood plain of the Colorado River; however, there are deposits related to the rivers evolutionary past intermixed with alluvium as late as early Holocene in age. Generally, these deposits sit near the shore of Lake Mohave, with some cases of material further inland.

General Trends

The area of interest (AOI) for the Lake Mohave field area is the western shore of the lake. The northern third of the AOI is the hottest; the middle third is cooler and the southern third

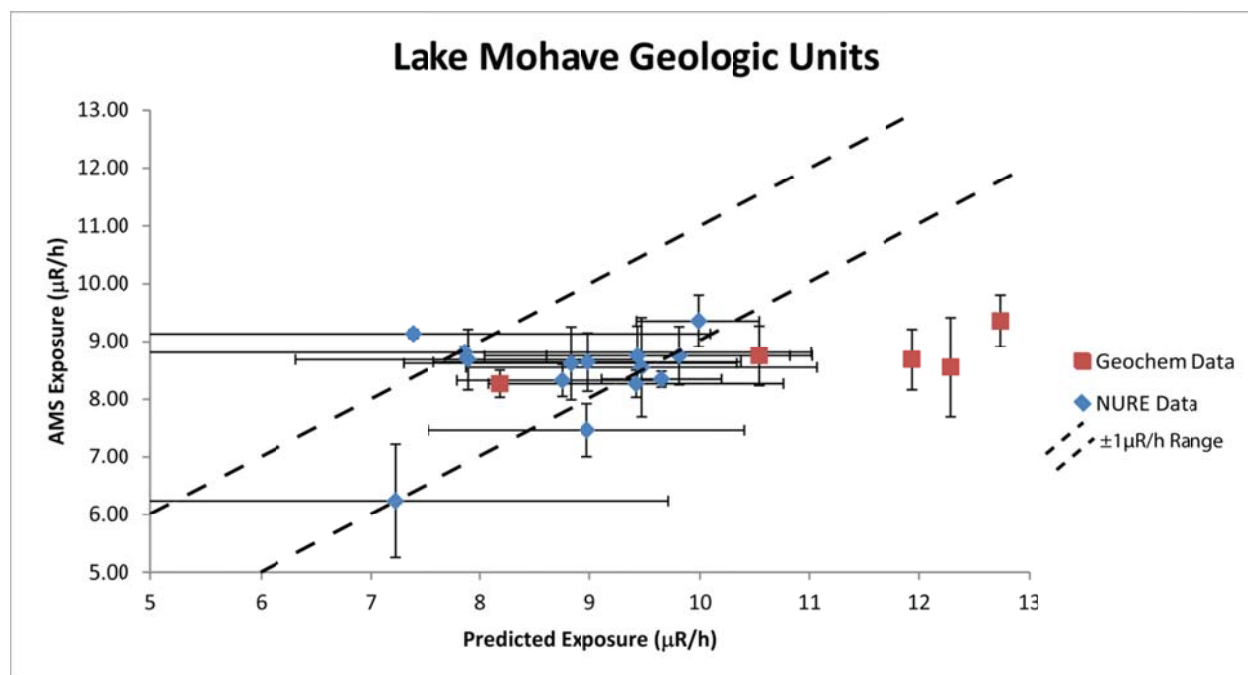
is in between. The trend is directly related to the source material of the alluvial fans. The areas with higher exposure rate are composed primarily of felsic igneous and metamorphic rocks while the cooler areas are dominated by intermediate and mafic igneous and metamorphic rocks. There is however some mixing of material throughout. There is also a trend related to surface age and exposure rate. Older terraced surfaces have higher exposure rates, while younger loosely consolidated surfaces have lower exposure rates. This could be related to surface inflation due to eolian addition or it may be related to the equilibrium condition of the U and Th decay chains. Finally, there is an east-west trend whereby the points closest to the lake have the lowest exposure rates. This may be due to the influence of subsurface water, near-shore vegetation or related to river gravels and deposits.



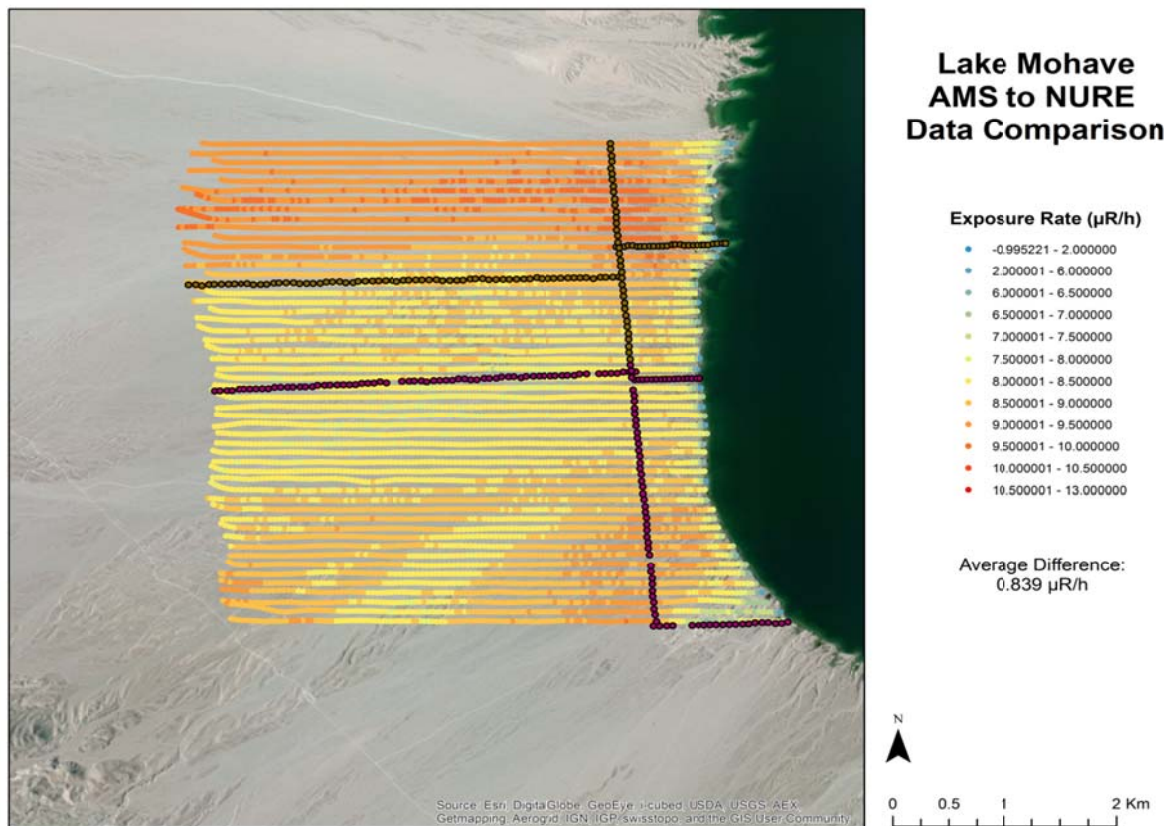
Data Sources

There are two major sources of geochemical data used in this study. In general we refer to the two major sources of data as traditional geochemistry, and NURE data. Traditional geochemistry is sourced from several online databases including: the National Uranium Resource Evaluation (NURE) Survey (geochemical section), Geochemical Rock Database (GeoRoc), and Integrated Earth Data Applications (IEDA). NURE aerial survey data consists of data derived from a national scale aerial gamma ray survey. Since the traditional geochemistry and NURE data are derived using different techniques they are used to create separate models.

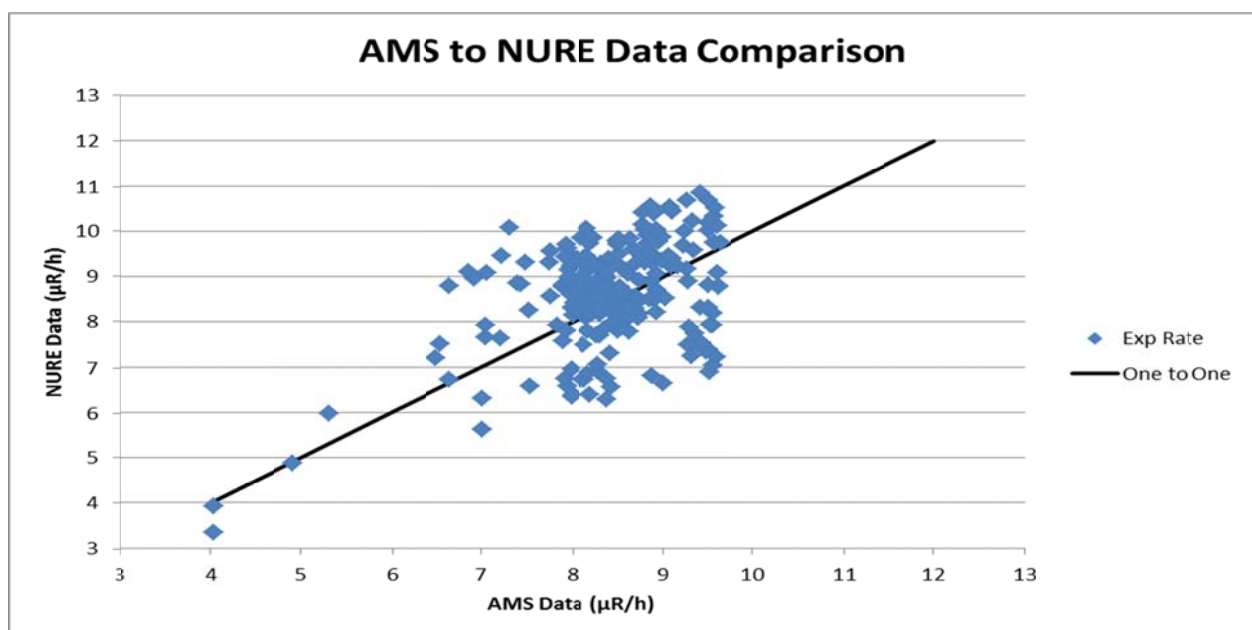
In the figure below, the predicated exposure rate for each geologic unit is plotted against the mean of the AMS data within that unit; error bars represent one standard deviation. The traditional geochemistry is generally more spread out when compared to the NURE data.



The NURE data is the result of a series of aerial gamma ray surveys flown in the 1970's to assess the distribution of U across the contemporaneous United States. Several NURE flight lines overlap with the AMS survey in Lake Mohave and a comparison was made between these two datasets.

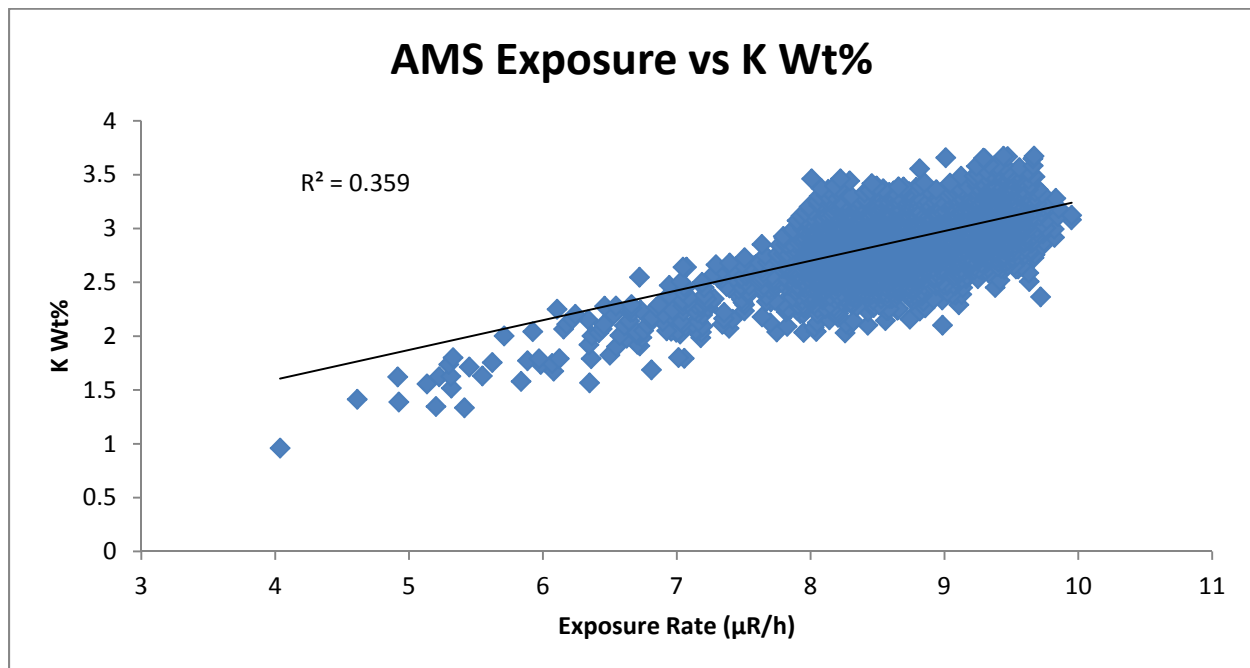


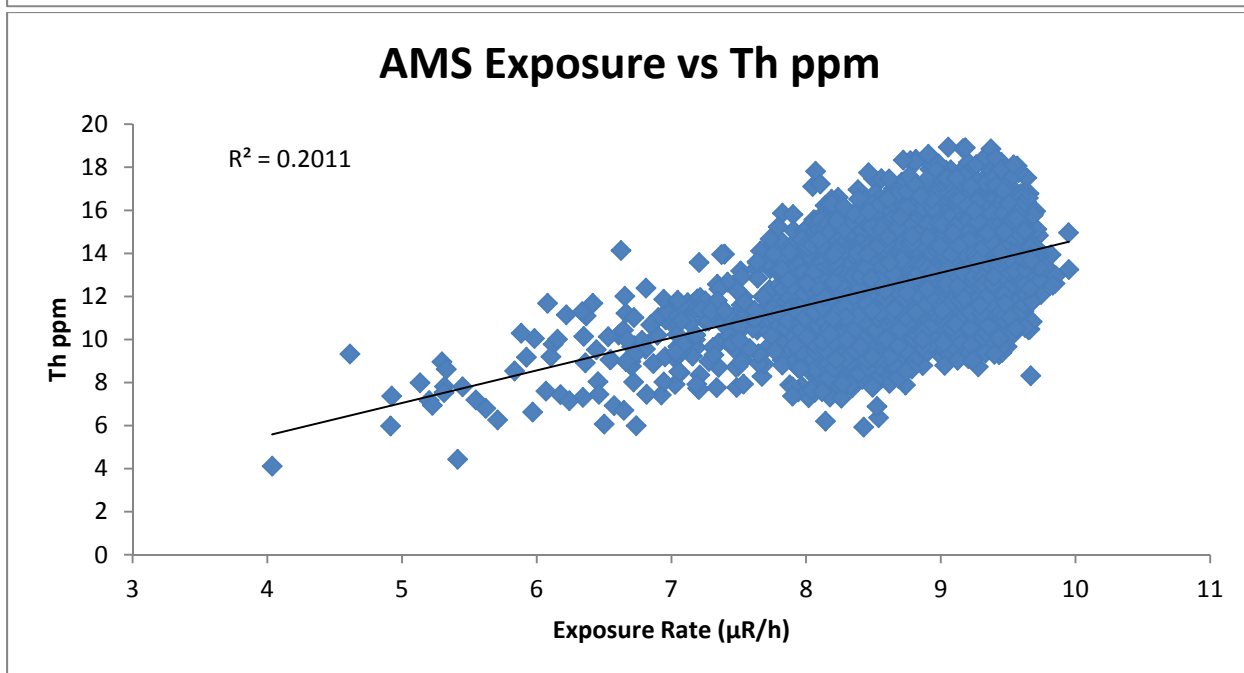
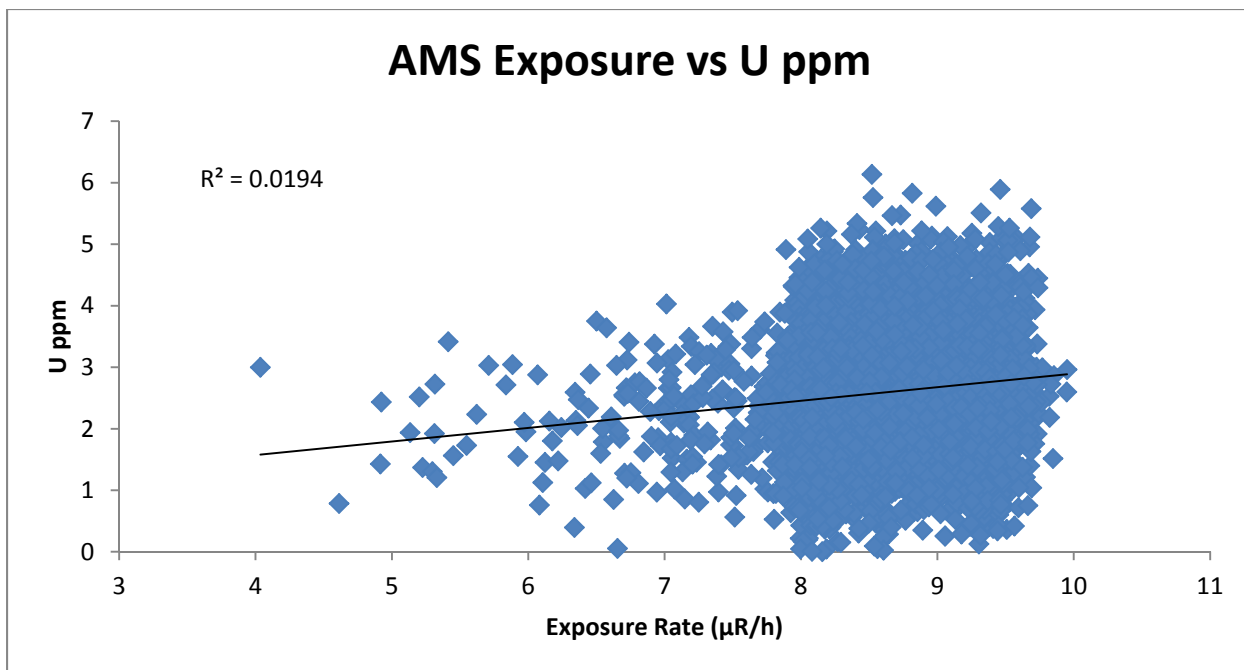
When the NURE data is compared to the closest AMS data point in the figure below there is a scattered but consistent relationship between the data. While the data have some amount of correlation there is no systemic offset that can be corrected for.



K, U, and Th Distribution

The exposure rate at Lake Mohave does not correlate strongly with either K, U, or Th. However, it tends to have the strongest correlation with K concentration with an R^2 value of 0.36. Th has a lower but still significant R^2 value 0.2 while U has little to no correlation with exposure rate with an R^2 of less than 0.02. This relationship can be seen when comparing the exposure rate map to the concentration and ratio images below. K values tend to be highest in the northern third of the AOI and are mixed to low further south. This has some correlation to the exposure rate in that the northern third has the highest exposure rates. Th values also show a similar relationship; however, Th is also high in the southern third of the AOI and correlates well with the higher exposure rates in that area. Both K and Th values are low in the middle third with also expresses the lowest exposure rates. High Th/K ratios in the southern third show that Th tends to control the exposure rate in that area. U seems to be randomly distributed throughout the area.





Lake Mohave Radioelement Concentration Images

K Wt%

- 0.960459 - 2.243253
- 2.243254 - 2.723497
- 2.723498 - 2.956414
- 2.956415 - 3.187128
- 3.187129 - 3.672559

U PPM

- 0 - 1.581498
- 1.581499 - 2.338019
- 2.338020 - 3.035367
- 3.035368 - 3.852008
- 3.852009 - 6.135812

Th PPM

- 4.118740 - 9.969537
- 9.969538 - 10.905588
- 10.905589 - 11.949598
- 11.949599 - 13.168826
- 13.168827 - 14.872976
- 14.872977 - 18.871453



Lake Mohave Radioelement Ratio Images

U/K Ratio

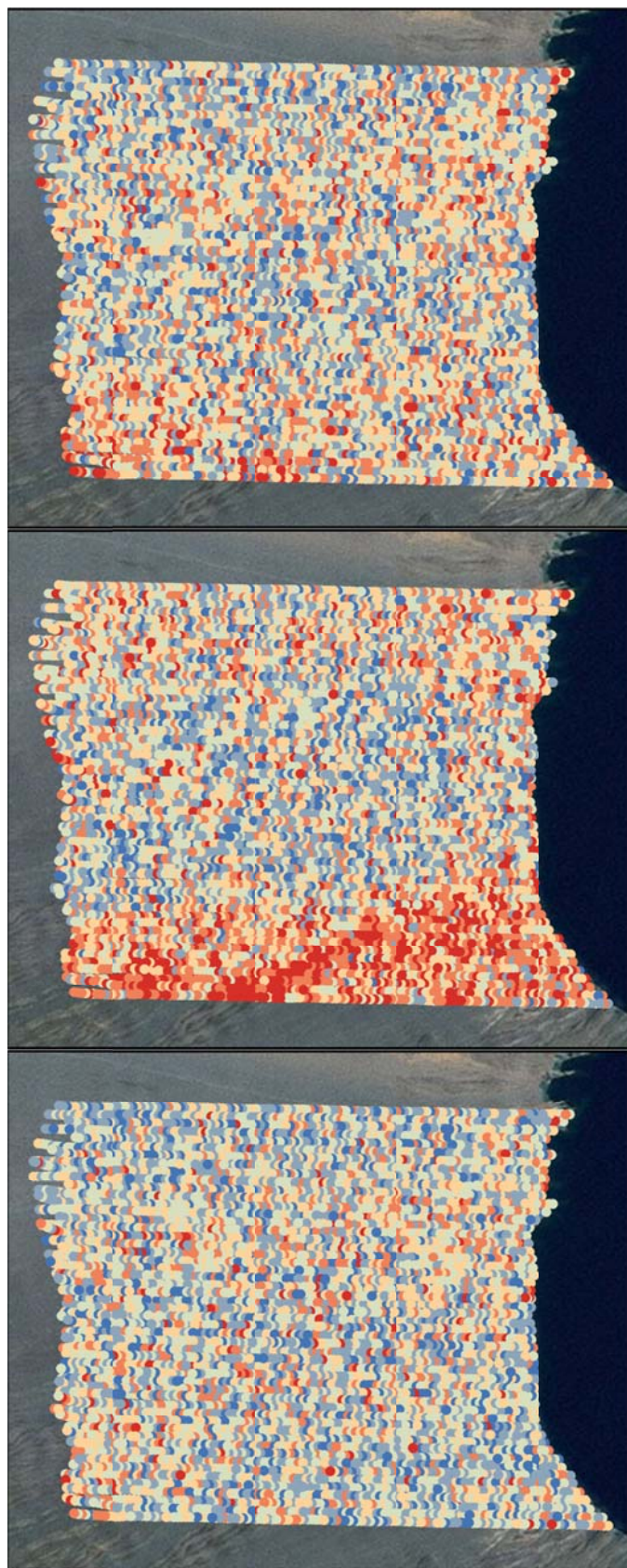
- 0 - 0.498470
- 0.498471 - 0.745602
- 0.745603 - 0.968045
- 0.968046 - 1.208879
- 1.208880 - 1.542684
- 1.542685 - 3.123242

Th/K Ratio

- 2.090277 - 3.461301
- 3.461302 - 3.942091
- 3.942092 - 4.348792
- 4.348793 - 4.786292
- 4.786293 - 5.355216
- 5.355217 - 8.000000

U/Th Ratio

- 0 - 0.117615
- 0.117616 - 0.182165
- 0.182166 - 0.244454
- 0.244455 - 0.316216
- 0.316217 - 0.426078
- 0.426079 - 0.803350



Unit Data Summary

Unit	AMS Mean	AMS Median	AMS STD	AMS Low	AMS High	Nure Exp	Avg ABS Diff	Avg Diff
Qai	8.756	8.716	0.507	6.36	9.855	9.797	1.042	-1.042
Qai+y	8.347	8.341	0.137	8.07	8.922	9.652	1.3052	-1.305
Qai1	8.554	8.719	0.861	5.547	9.414	9.472	0.918	-0.918
Qai3	8.624	8.652	0.633	4.915	9.768	8.820	0.476	-0.196
Qao	9.360	9.506	0.444	8.364	9.663	9.987	0.627	-0.627
Qay	8.689	8.610	0.526	5.449	9.951	7.896	0.817	0.794
Qay+i	8.815	8.827	0.1002	8.679	8.984	7.866	0.949	0.949
Qay1	8.645	8.486	0.5045	7.937	9.832	8.984	0.5510	-0.339
Qay2	8.754	8.679	0.5176	7.518	9.819	9.434	0.736	-0.680
Qby	6.239	6.531	0.985	4.035	7.688	7.219	1.045	-0.980
Qch	7.464	7.346	0.459	6.895	8.592	8.975	1.511	-1.511
QTa	8.268	8.265	0.235	7.464	9.066	9.422	1.155	-1.155
Tay1	8.326	8.333	0.2814	7.793	8.877	8.741	0.415	-0.415

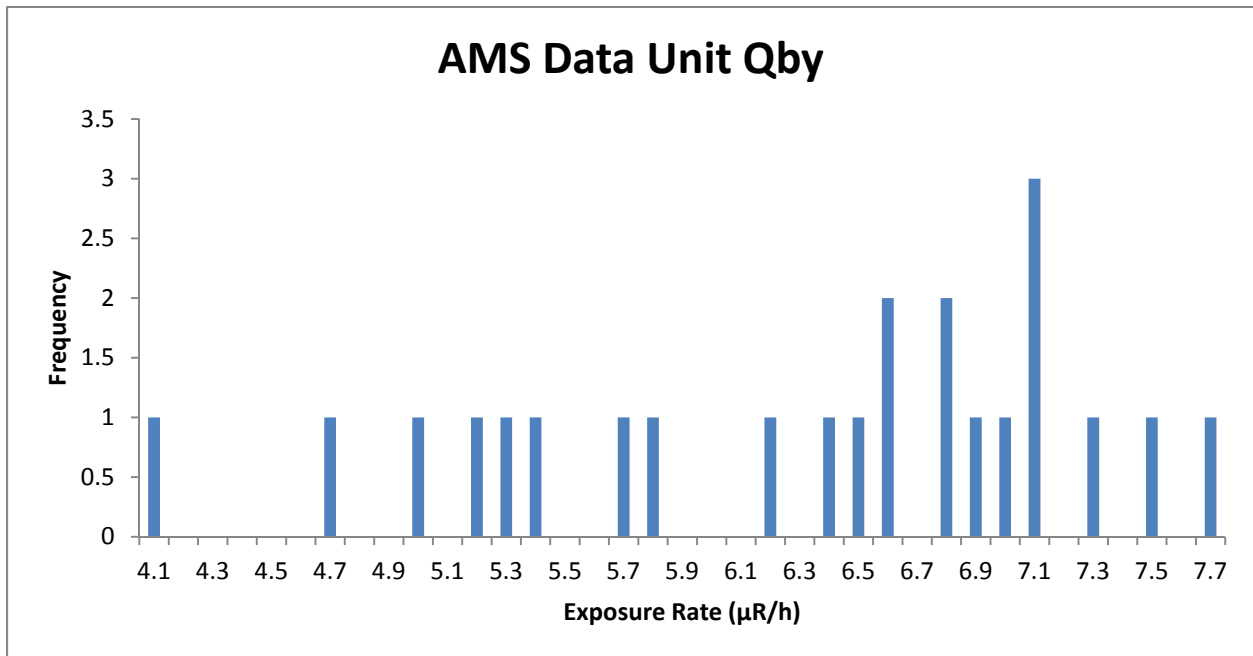
Qby

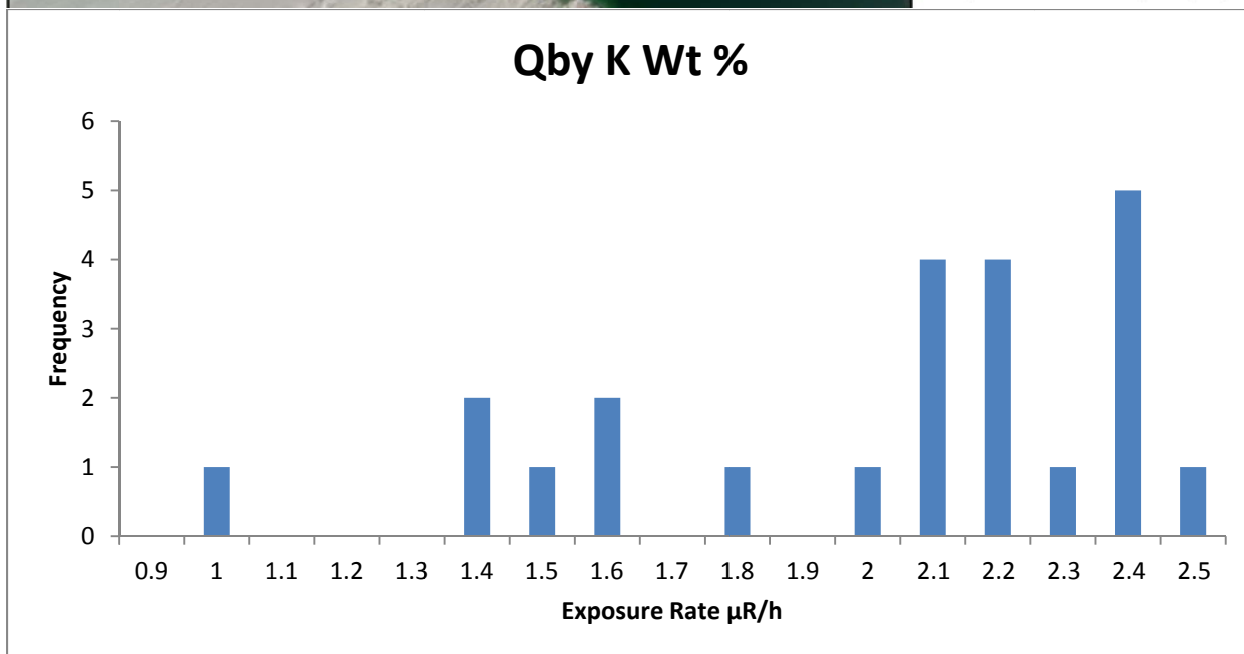
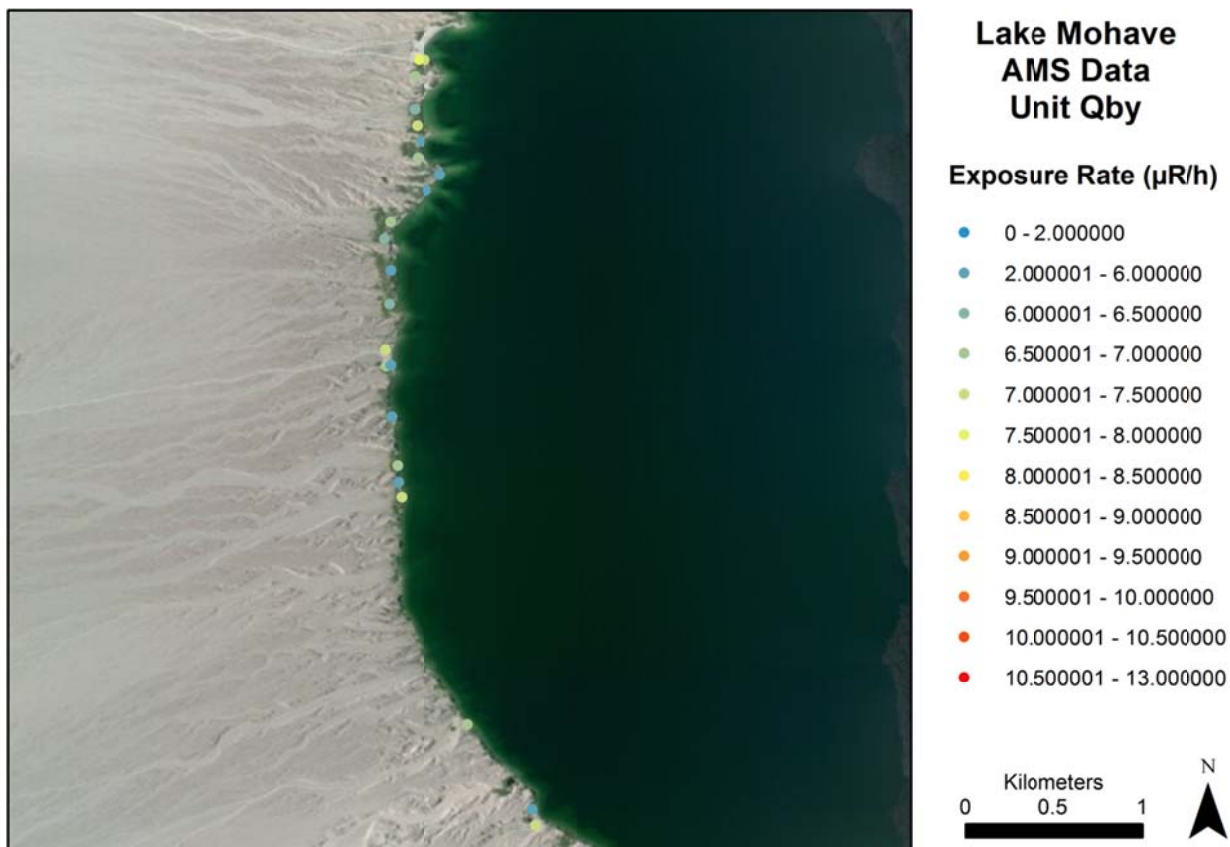
Composition

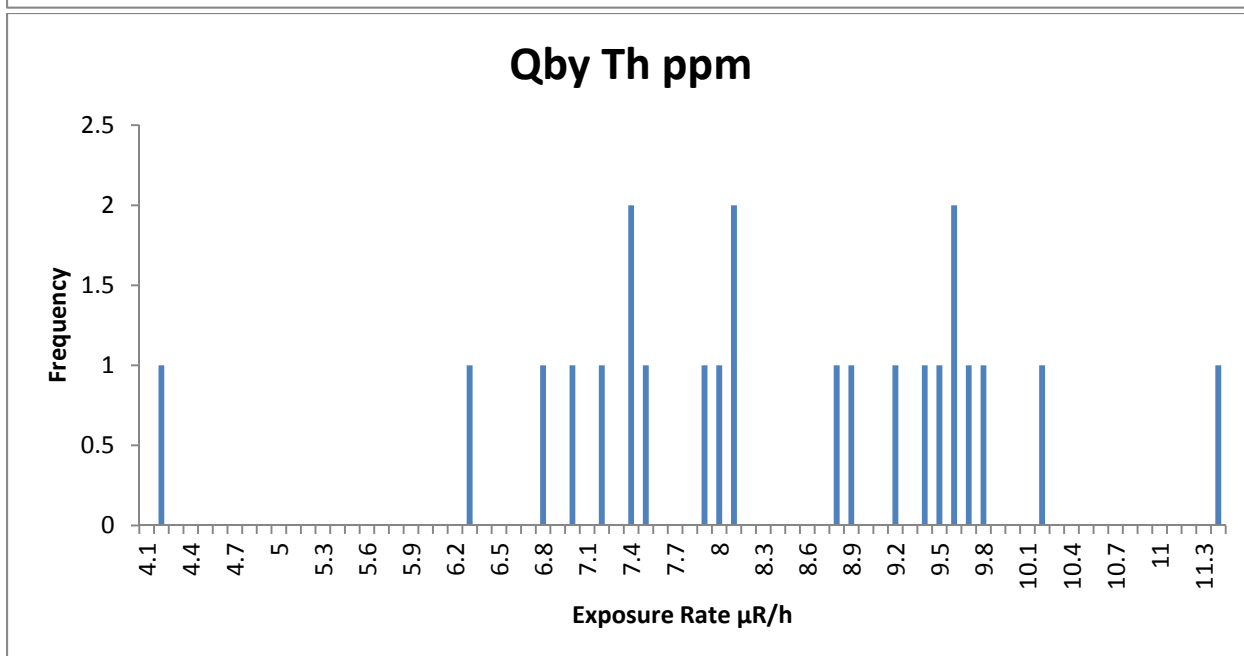
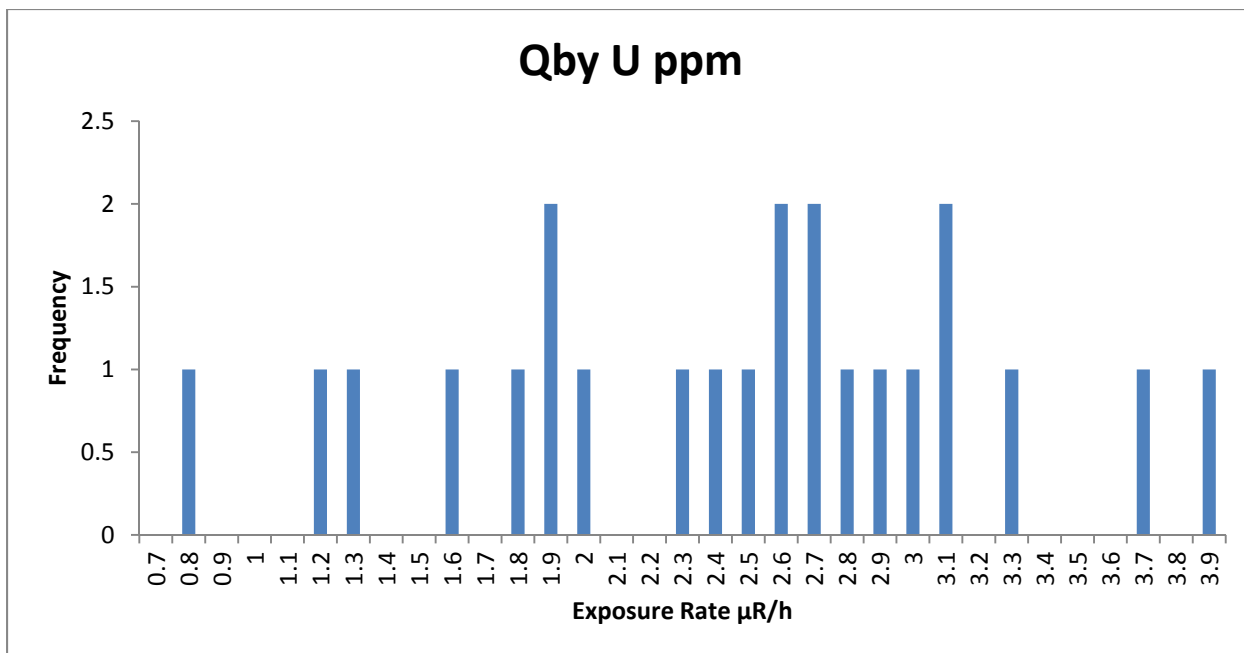
Qby is the most recent, Holocene deposits along the shoreline of Lake Mohave. It is composed of locally derived gravels that are wave worked, subangular and moderately to well sorted. (House and Faulds, 2009)

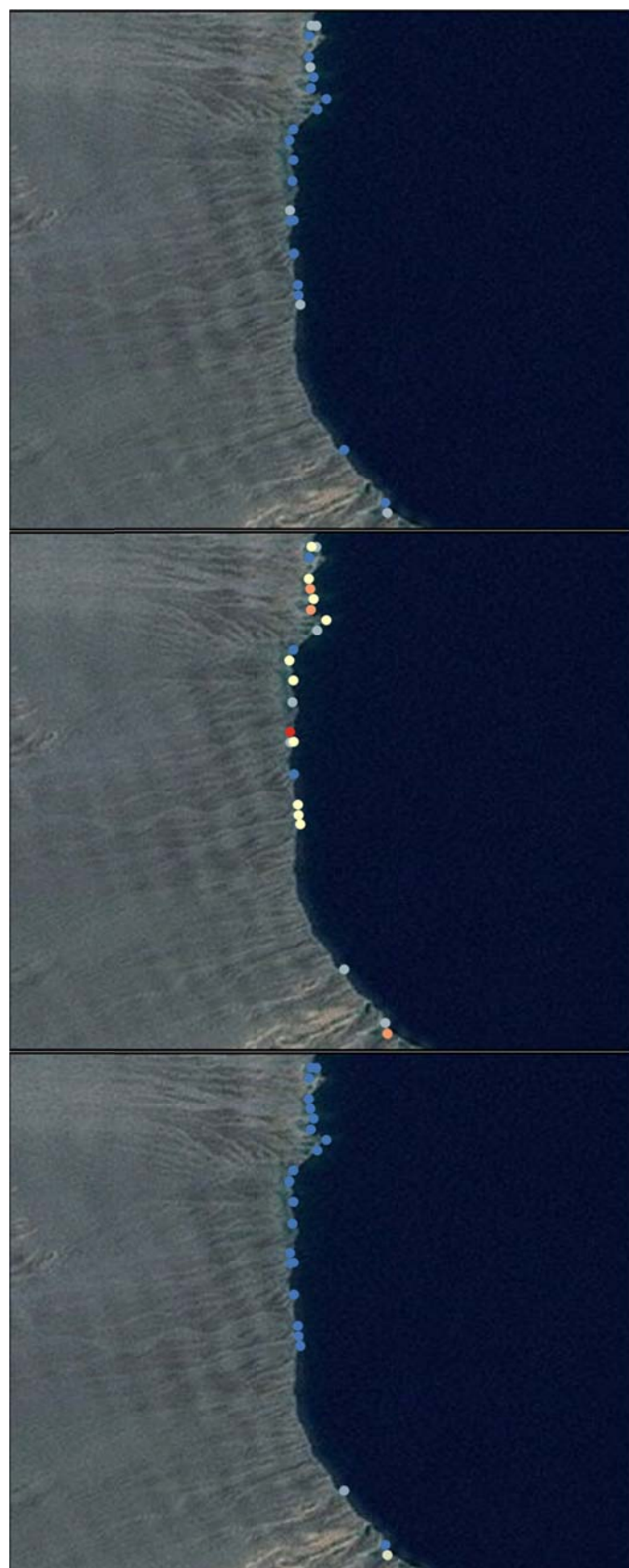
AMS Data

The AMS data in Qby is randomly distributed and generally lower in exposure rate than the rest of the area. The average exposure rate is 6.24 $\mu\text{R/h}$ with a standard deviation of 0.99 $\mu\text{R/h}$ or 16% of the mean. The K, U, and Th concentrations are also randomly distributed and are likely influenced by the presence of water. There are no distinct features present in the histograms of exposure rate, K, U, or Th.









Lake Mohave Radioelement Concentration Images Unit Qby

K Wt%

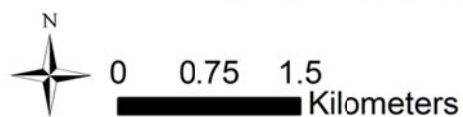
- 0.960459 - 2.243253
- 2.243254 - 2.723497
- 2.723498 - 2.956414
- 2.956415 - 3.187128
- 3.187129 - 3.672559

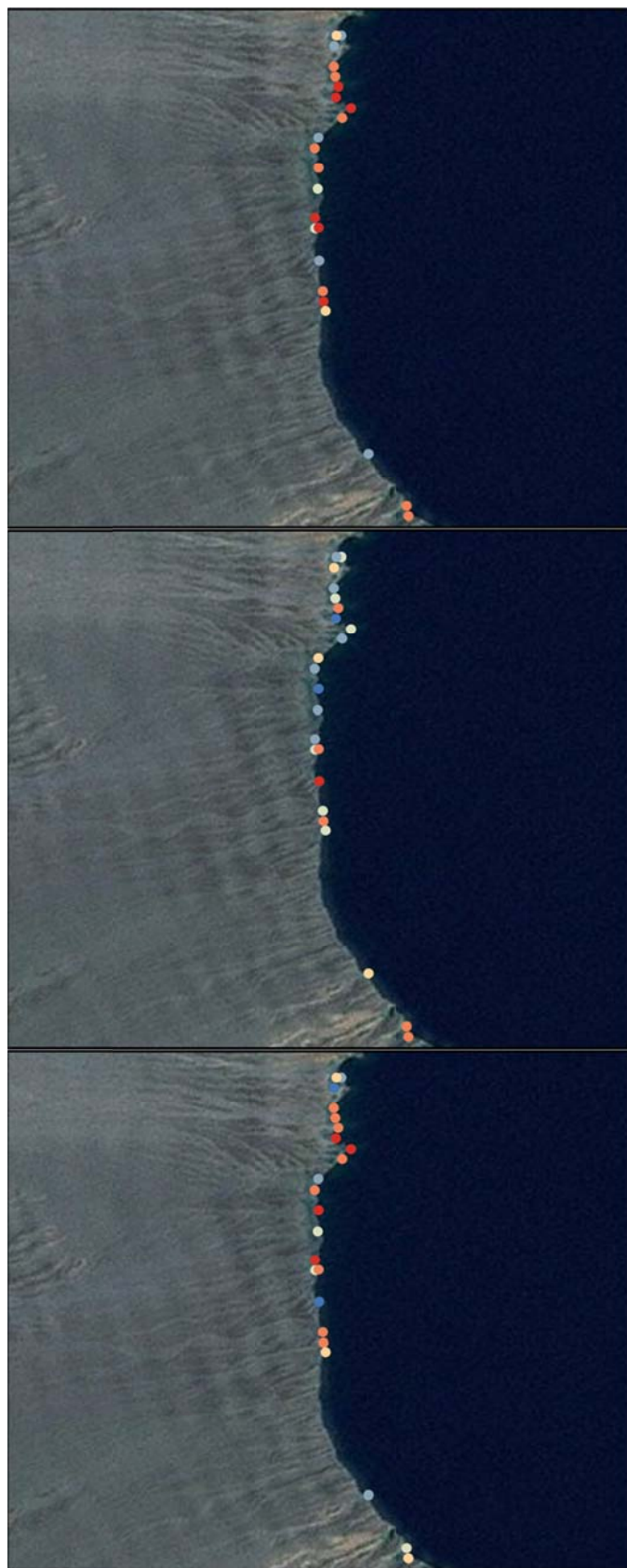
U PPM

- 0 - 1.581498
- 1.581499 - 2.338019
- 2.338020 - 3.035367
- 3.035368 - 3.852008
- 3.852009 - 6.135812

Th PPM

- 4.118740 - 9.969537
- 9.969538 - 10.905588
- 10.905589 - 11.949598
- 11.949599 - 13.168826
- 13.168827 - 14.872976
- 14.872977 - 18.871453





Lake Mohave Radioelement Ratio Images Unit Qby

U/K Ratio

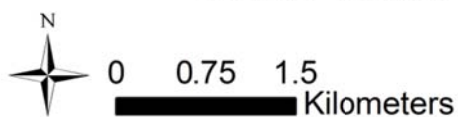
- 0 - 0.498470
- 0.498471 - 0.745602
- 0.745603 - 0.968045
- 0.968046 - 1.208879
- 1.208880 - 1.542684
- 1.542685 - 3.123242

Th/K Ratio

- 2.090277 - 3.461301
- 3.461302 - 3.942091
- 3.942092 - 4.348792
- 4.348793 - 4.786292
- 4.786293 - 5.355216
- 5.355217 - 8.000000

U/Th Ratio

- 0 - 0.117615
- 0.117616 - 0.182165
- 0.182166 - 0.244454
- 0.244455 - 0.316216
- 0.316217 - 0.426078
- 0.426079 - 0.803350

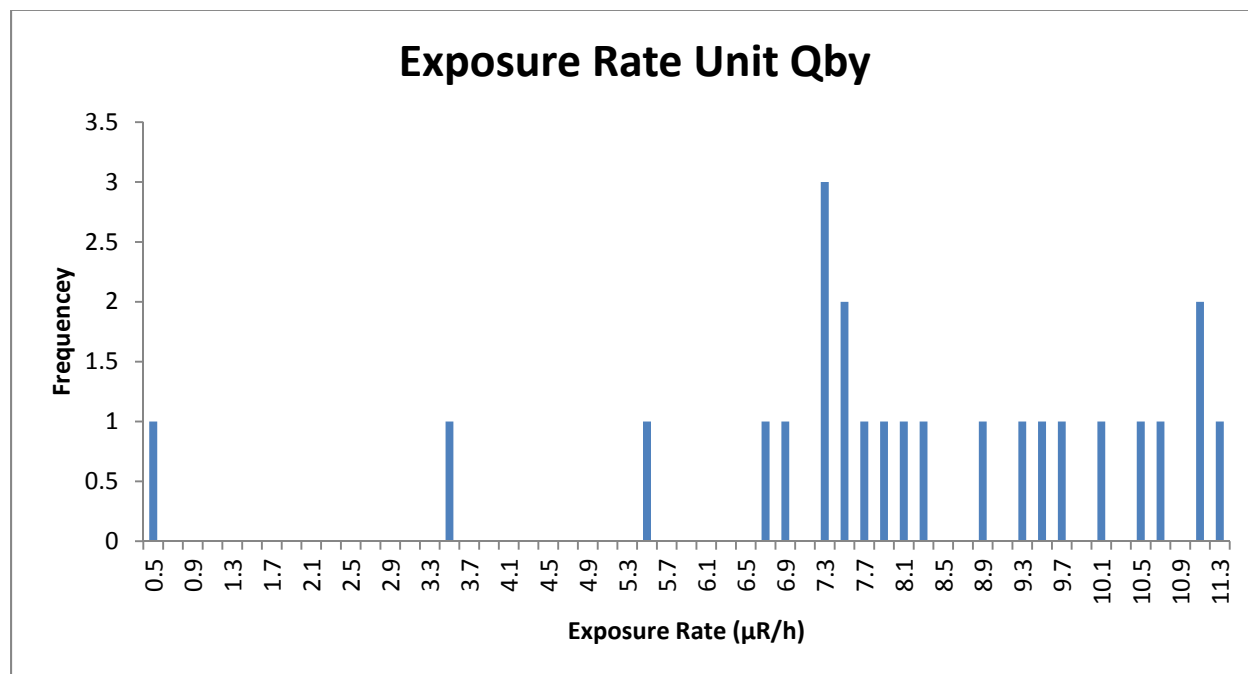


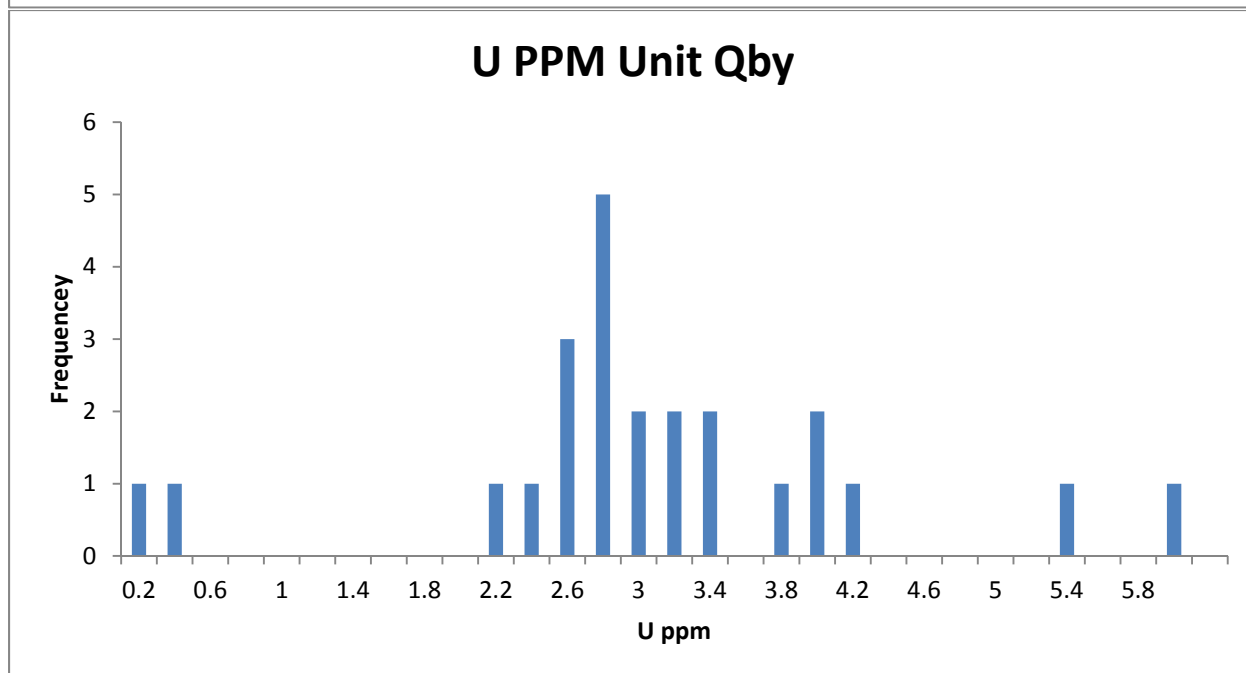
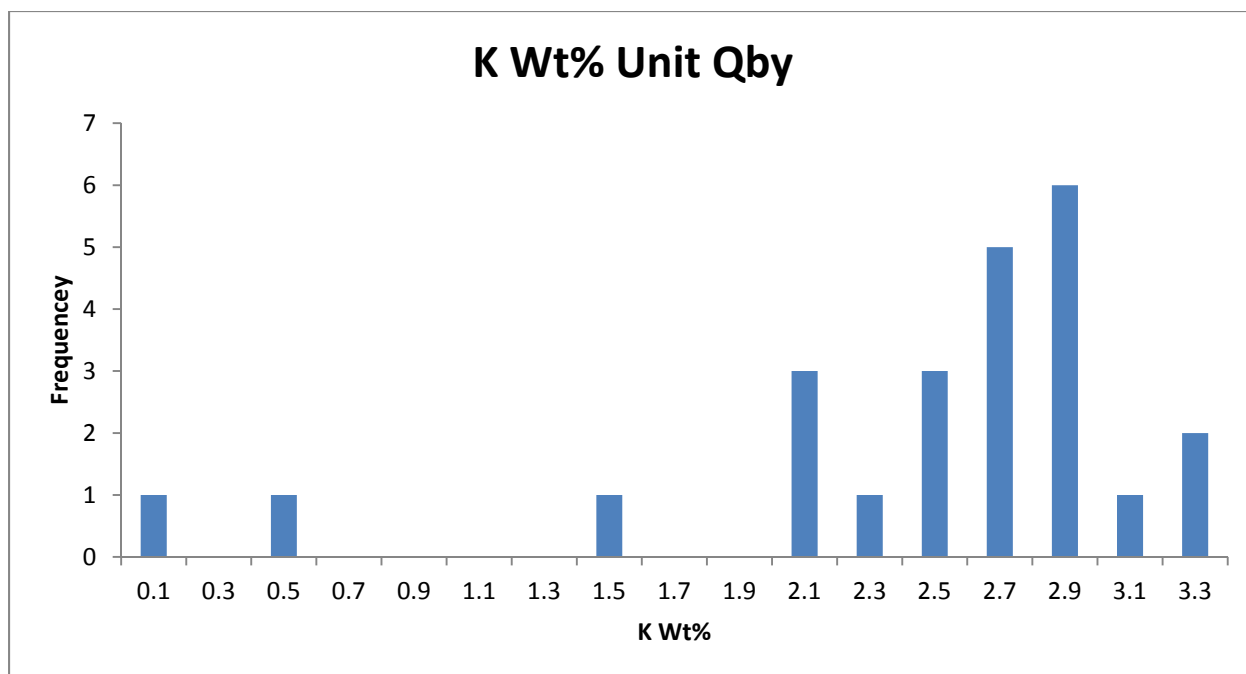
Traditional Geochemistry

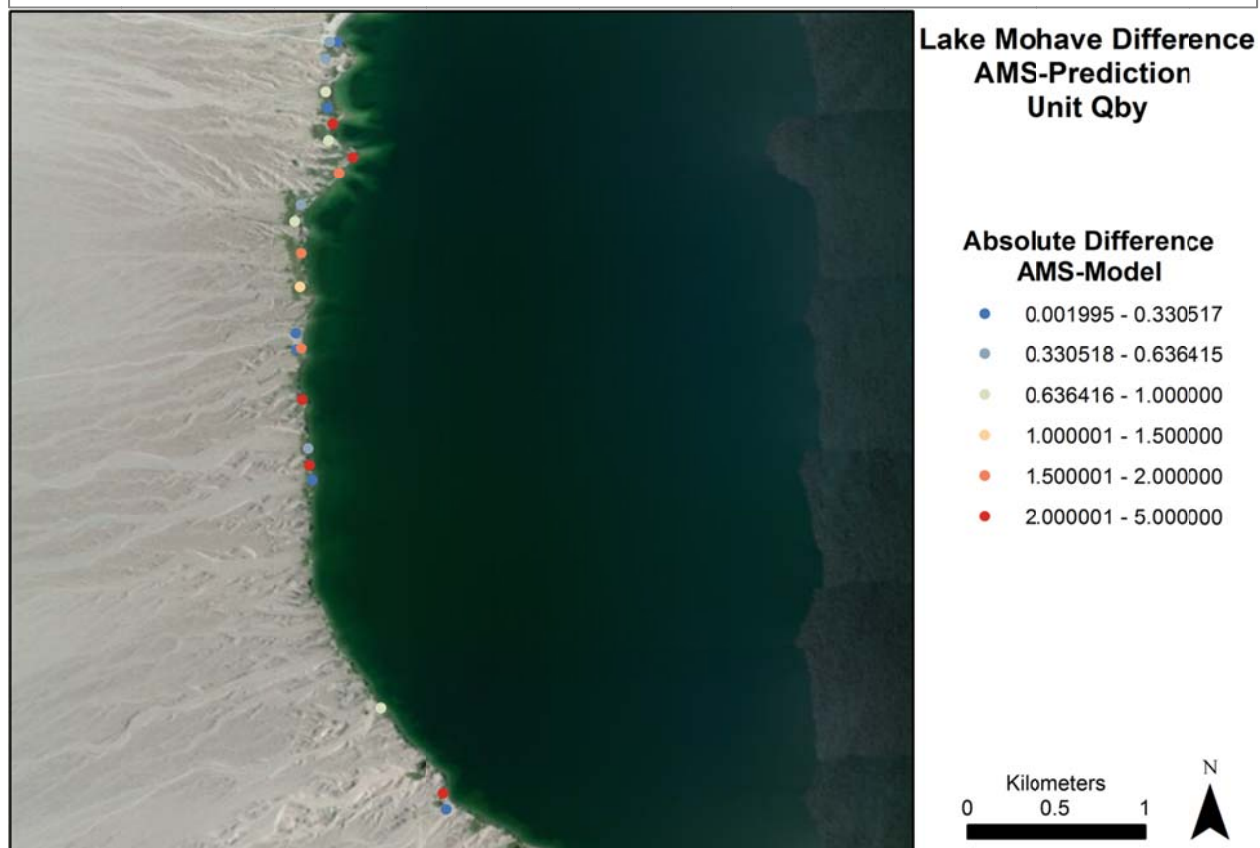
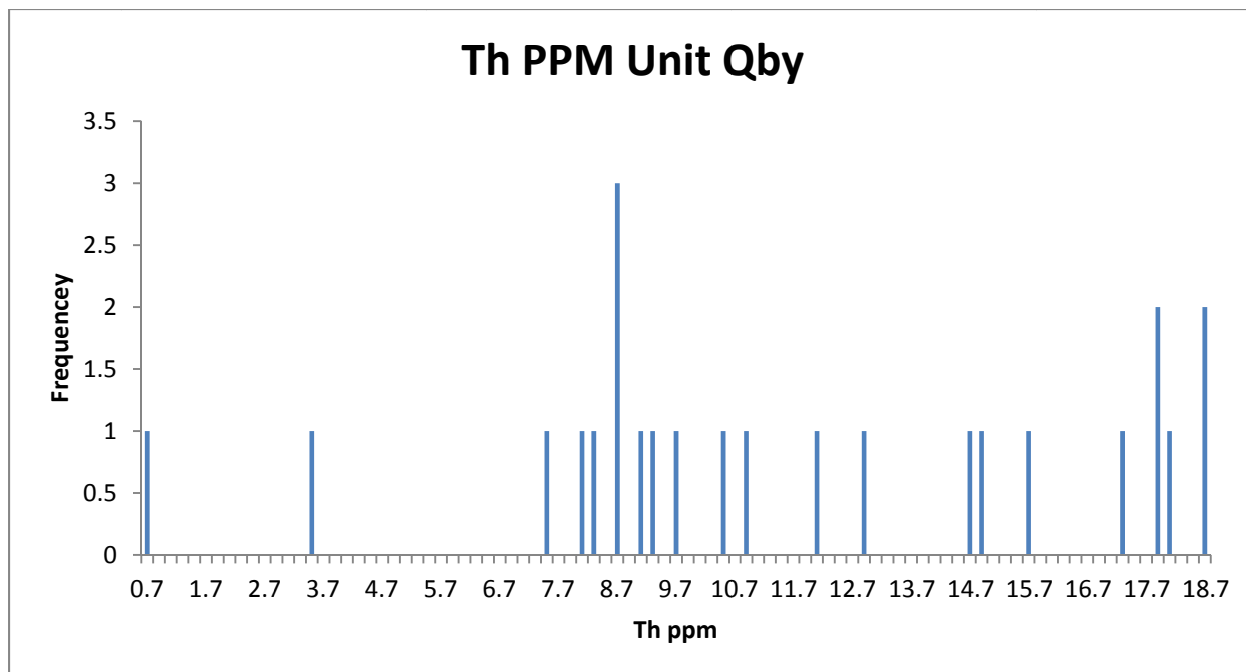
There are no traditional geochemical data for Qby.

NURE Data

The NURE data, like the AMS data, are randomly distributed in Qby. The average NURE exposure rate in Qby is 8.03 $\mu\text{R/h}$ which compares to the AMS value of 6.24 $\mu\text{R/h}$ meaning that on average Qby is outside of the ± 1 $\mu\text{R/h}$ success range. Most of the K data centers between 2.5 and 2.9 Wt%. The U data has a small peak near 2.9 ppm. The Th data has no peak or distinct features. When comparing the difference between the AMS exposure rate points and NURE exposure rate some points are within the success range and others are well outside. There is no clear pattern to these differences.







Data Summary

Exposure Rate Comparison μR/h	Average	Median	STD	Range
AMS Data	6.238756	6.5306	0.985298	4.03596-7.68887
NURE Data	8.029283	7.9562	2.493656	0.5416-11.3144

Qay

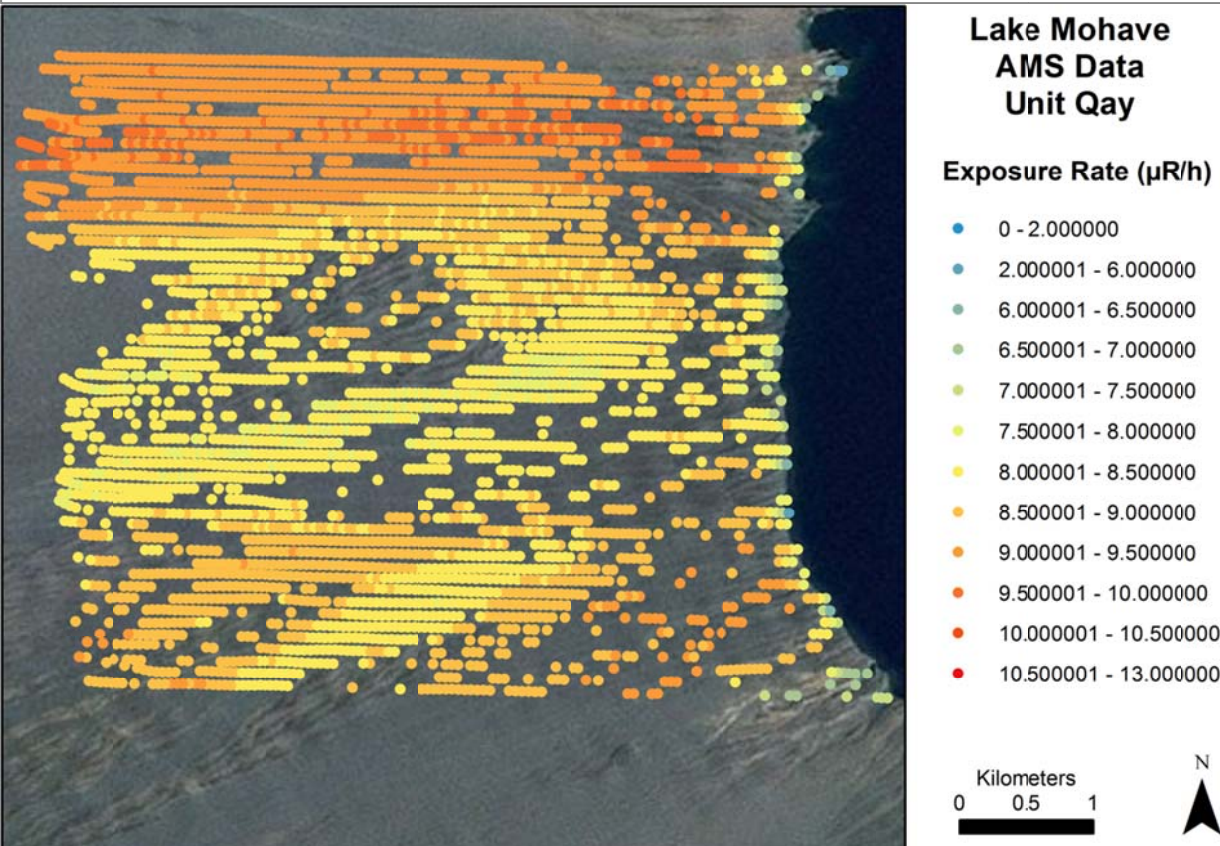
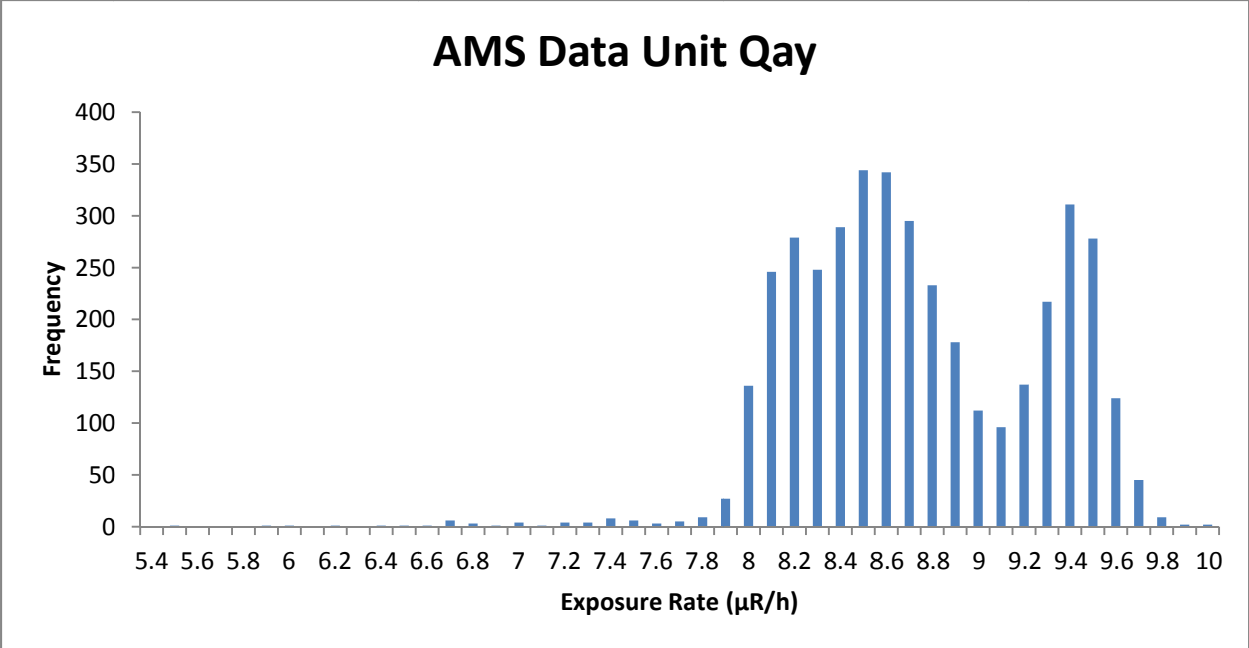
Composition

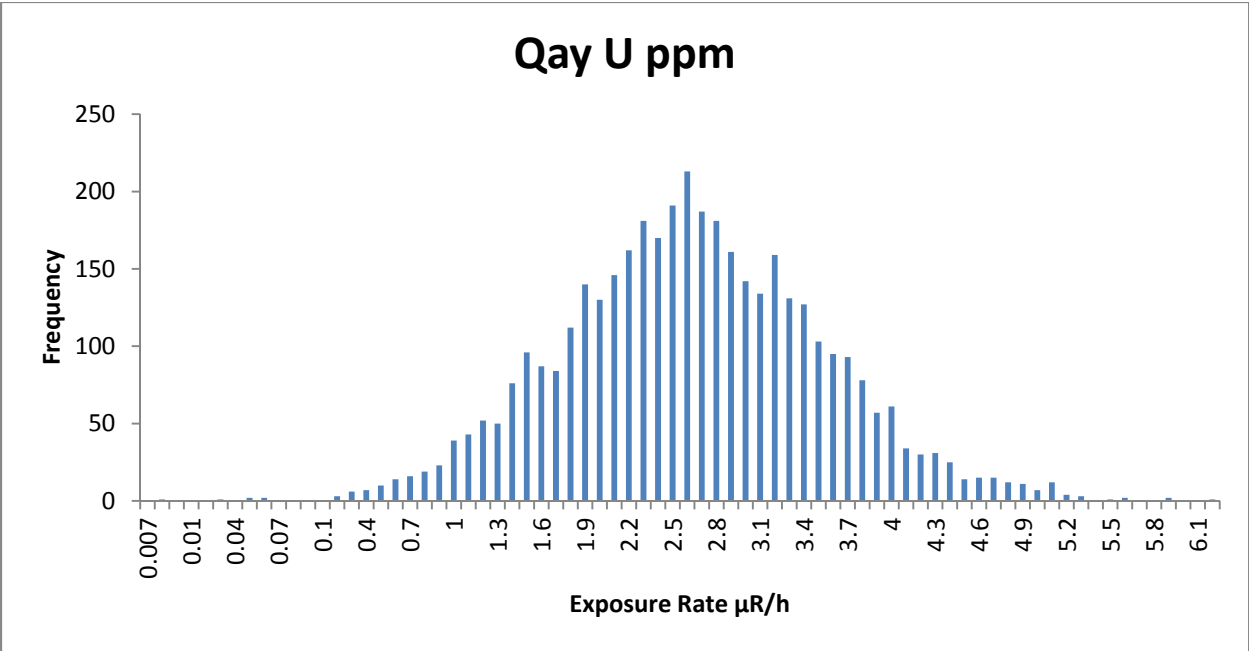
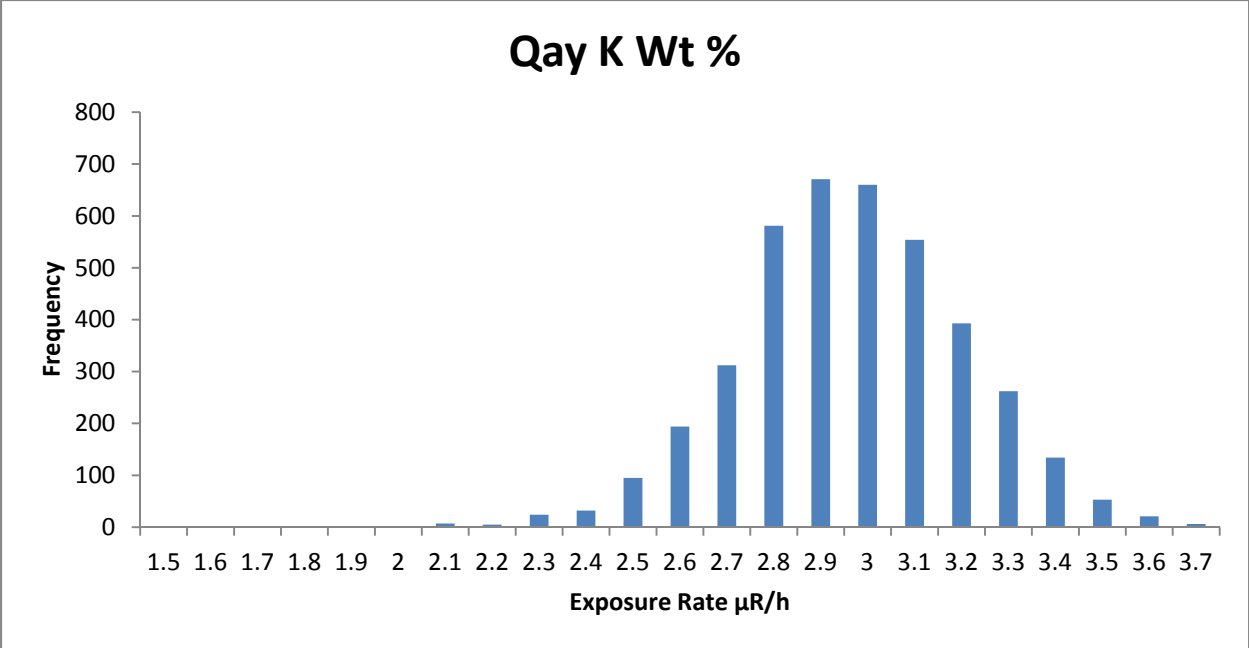
Qay is middle to late Holocene age alluvial deposits that consist of active channels and recently terraced surfaces. This unit is undivided and frequently interspersed with older deposits (House and Faulds, 2009). The source material is variable across the area. In southern portions the unit is composed of material that is more mafic igneous and metamorphic. The northern portions contain more felsic rocks such as tuffs and granitic rocks.

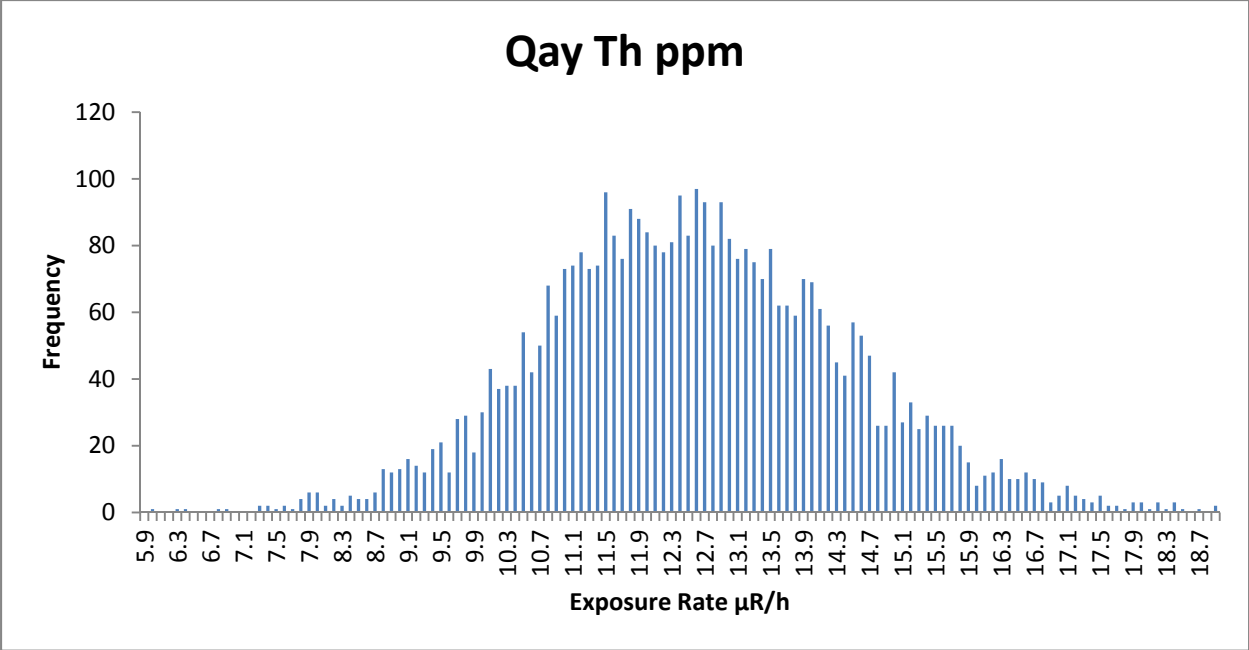
AMS Data

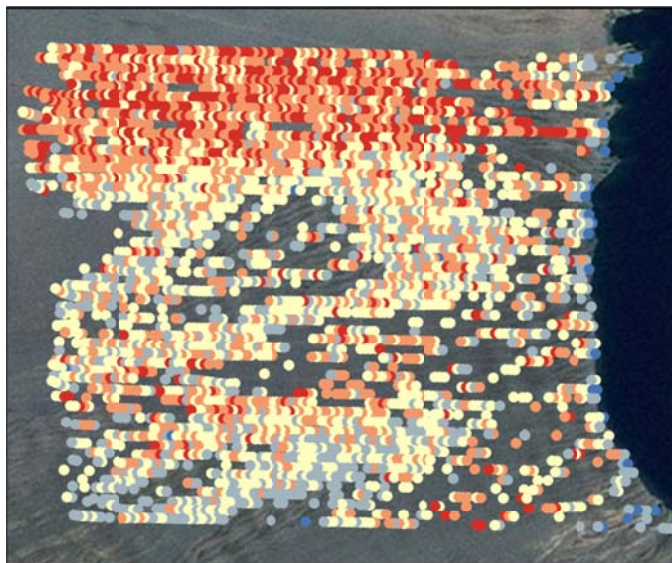
Qay is the spatially largest unit within the AOI. Across the area the exposure rate varies widely with source materials. The only parameter that is constant across this unit is the relative young age. The average exposure rate is 8.69 $\mu\text{R/h}$ with a standard deviation of 0.53 which is 6.01% of the mean. This low standard deviation is deceptive and become apparent when analyzing the exposure rate distribution. There are two major peaks in this data; the first is wide and is between 8.2 and 8.8 and the second between 9.4 and 9.6. The majority of the data is centered around the first peak and occurs in the southern two thirds of the unit. The higher exposure rates are concentrated in the northern third of the unit while the southern two thirds are generally cooler. The area nearest to the shore of Lake Mohave have the lowest exposure rates and may be influenced by near-shore effects.

The K, U, and Th distributions are generally normal in appearance but are very widely distributed. This type of distribution is not unexpected considering the large spatial area that this unit covers. In terms of spatial distribution, K and Th are both high in the northern third of the unit while Th is high and K is low in the southern third. The middle third has lower values of K and Th than the northern third of the unit. U values are randomly distributed throughout.





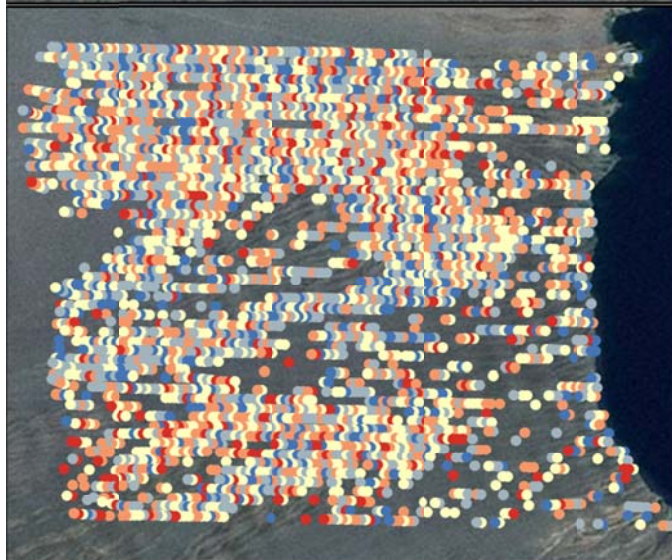




Lake Mohave Radioelement Concentration Images Unit Qay

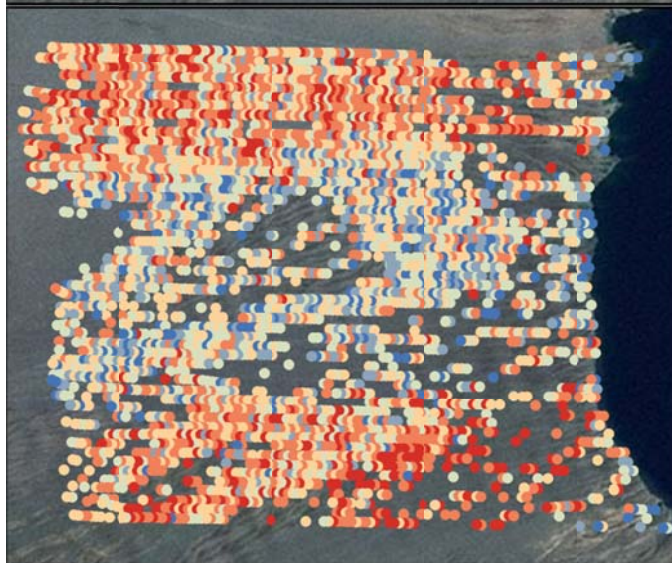
K Wt%

- 0.960459 - 2.243253
- 2.243254 - 2.723497
- 2.723498 - 2.956414
- 2.956415 - 3.187128
- 3.187129 - 3.672559



U PPM

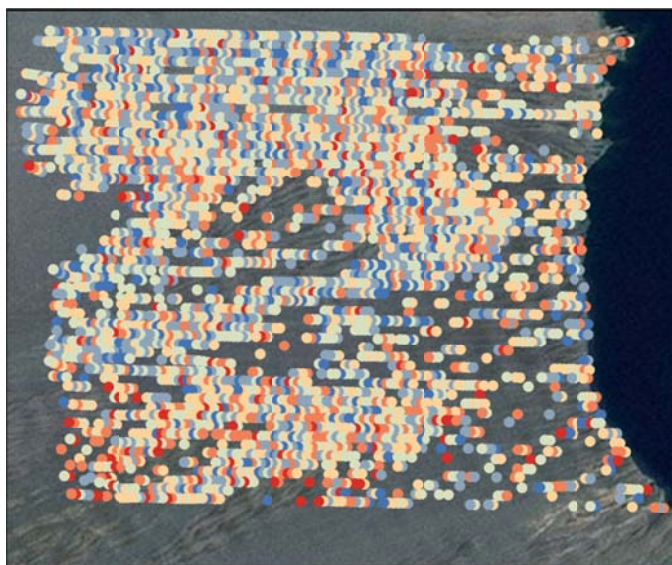
- 0 - 1.581498
- 1.581499 - 2.338019
- 2.338020 - 3.035367
- 3.035368 - 3.852008
- 3.852009 - 6.135812



Th PPM

- 4.118740 - 9.969537
- 9.969538 - 10.905588
- 10.905589 - 11.949598
- 11.949599 - 13.168826
- 13.168827 - 14.872976
- 14.872977 - 18.871453





Lake Mohave Radioelement Ratio Images Unit Qay

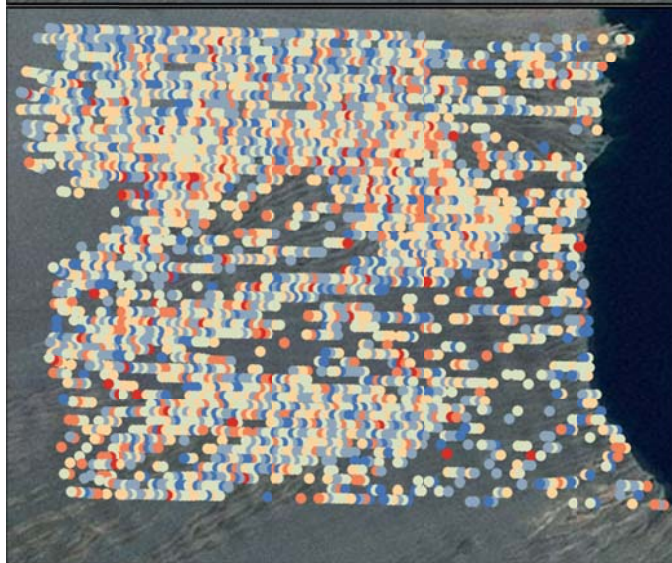
U/K Ratio

- 0 - 0.498470
- 0.498471 - 0.745602
- 0.745603 - 0.968045
- 0.968046 - 1.208879
- 1.208880 - 1.542684
- 1.542685 - 3.123242



Th/K Ratio

- 2.090277 - 3.461301
- 3.461302 - 3.942091
- 3.942092 - 4.348792
- 4.348793 - 4.786292
- 4.786293 - 5.355216
- 5.355217 - 8.000000



U/Th Ratio

- 0 - 0.117615
- 0.117616 - 0.182165
- 0.182166 - 0.244454
- 0.244455 - 0.316216
- 0.316217 - 0.426078
- 0.426079 - 0.803350

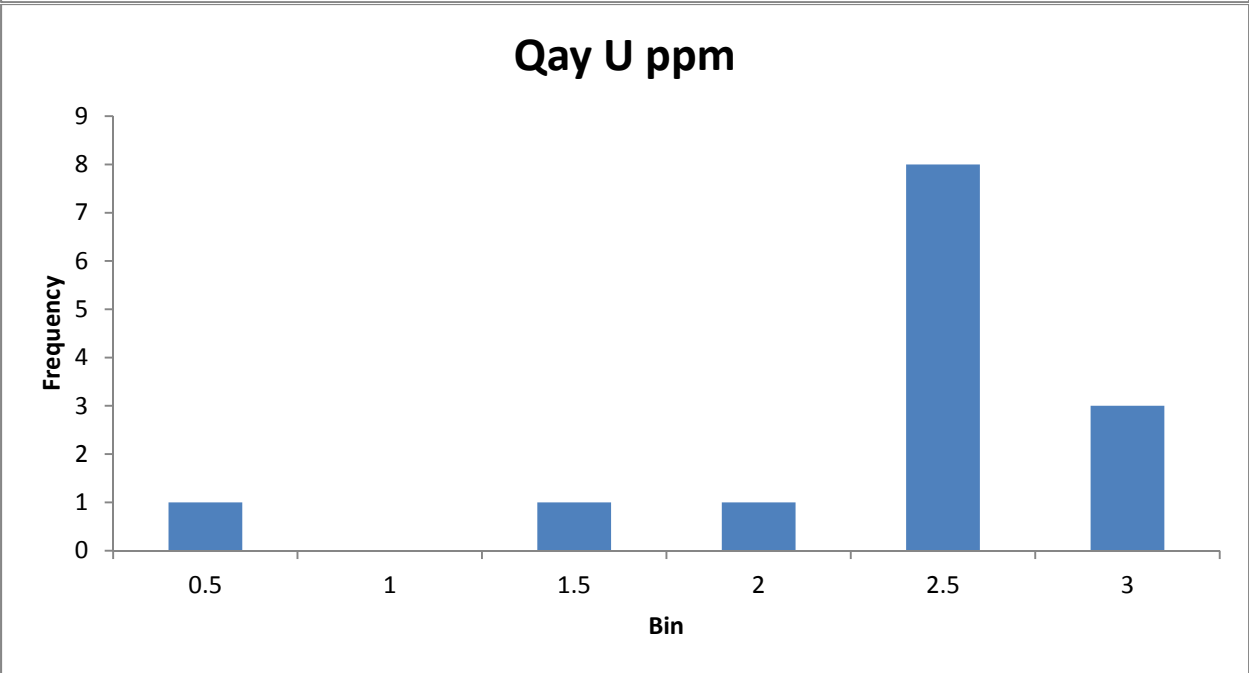
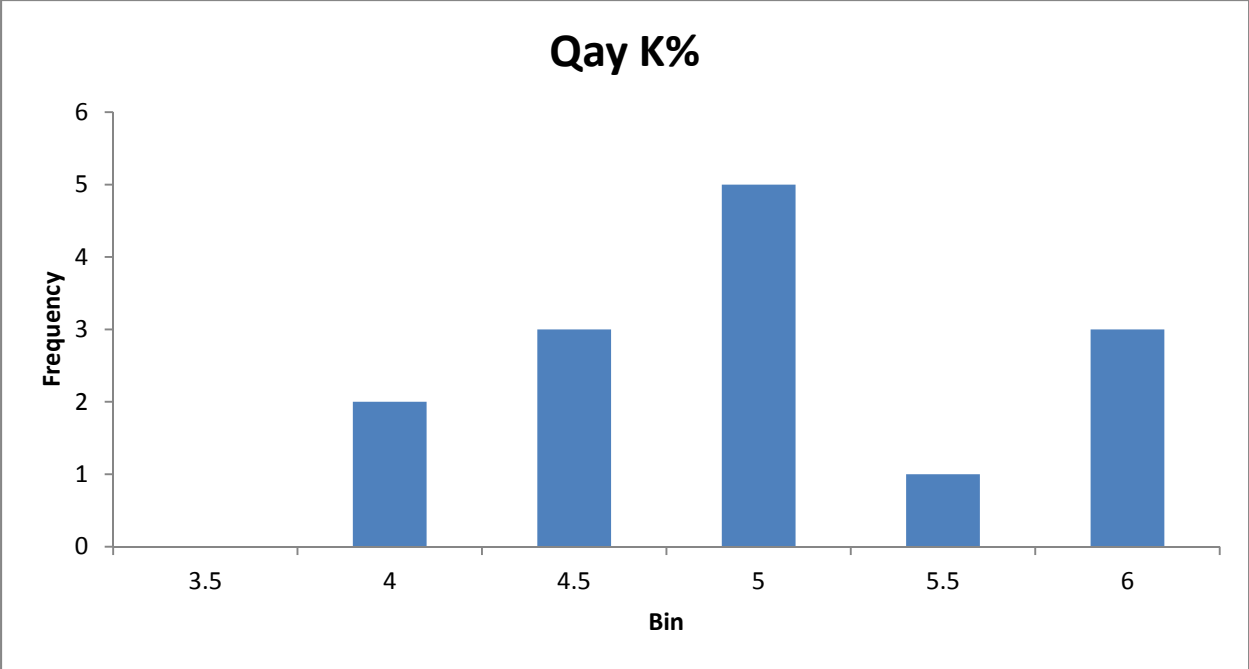


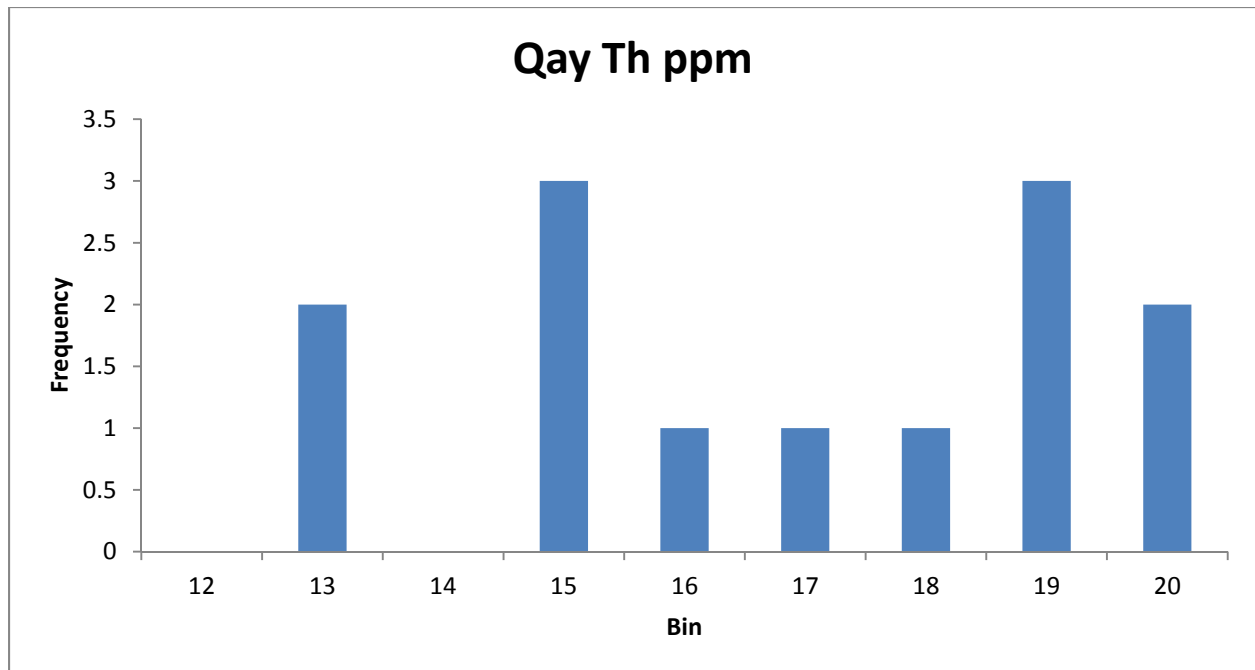
Traditional Geochemistry

There are 15 traditional geochemical data points that occur in Qay. The K Wt% values range from 3.5 to 5.9; the U ppm values range from .05 to 2.7 and the Th ppm values range from 12.7 to 19.7. When an exposure rate is calculated from the mean of these values it is higher than the AMS mean in the unit; 11.9 $\mu\text{R/h}$ and 8.69 $\mu\text{R/h}$ respectively. This is outside the desired ± 1 $\mu\text{R/h}$ range.

Sample ID	Latitude	Longitude	K %	U ppm	Th ppm
9642	35.4753	-114.839	5.441	2.36	18.79
9513	35.5323	-114.802	3.58	1.83	15.64
9673	35.4248	-114.74	4.361	2.41	19.68
M167556	35.435	-114.969	4.63		
9633	35.4662	-114.939	4.974	2.22	14.85
9634	35.473	-114.967	4.441	2.45	14.44
9636	35.4014	-114.943	4.515	1.44	12.7
9638	35.4477	-114.911	5.95	2.64	17.53
9649	35.4337	-114.882	4.491	2.73	18.57
9652	35.3754	-114.897	5.545	2.58	18.73
9465	35.4443	-114.819	5.581	2.05	14.43
9645	35.4921	-114.774	3.951	2.11	19.04
9646	35.4839	-114.769	4.946	2.21	16.07
9647	35.4432	-114.761	4.814	2.05	12.67
7377	35.4737	-114.852		0.0551	

	K%	U ppm	Th ppm
Mean	4.801429	2.081079	16.39538
Median	4.722	2.215	16.07
Standard Deviation	0.637323	0.650374	2.374041
Range	3.58-5.95	0.0551-2.73	12.67-19.68

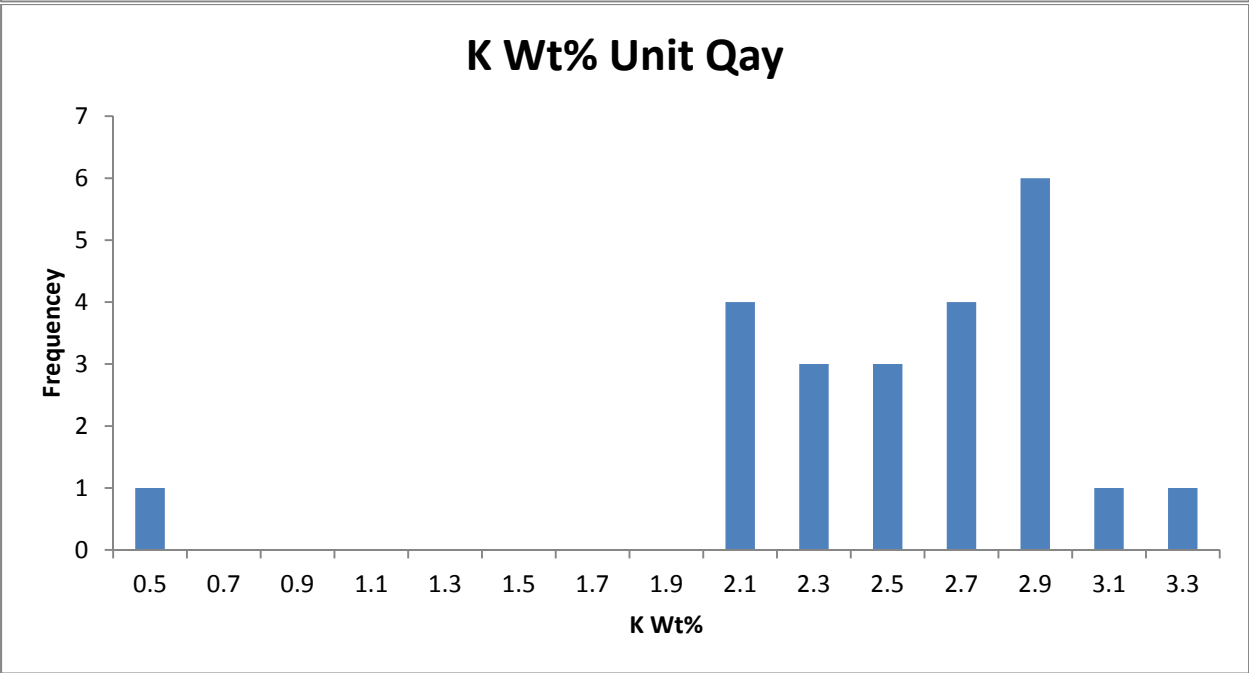
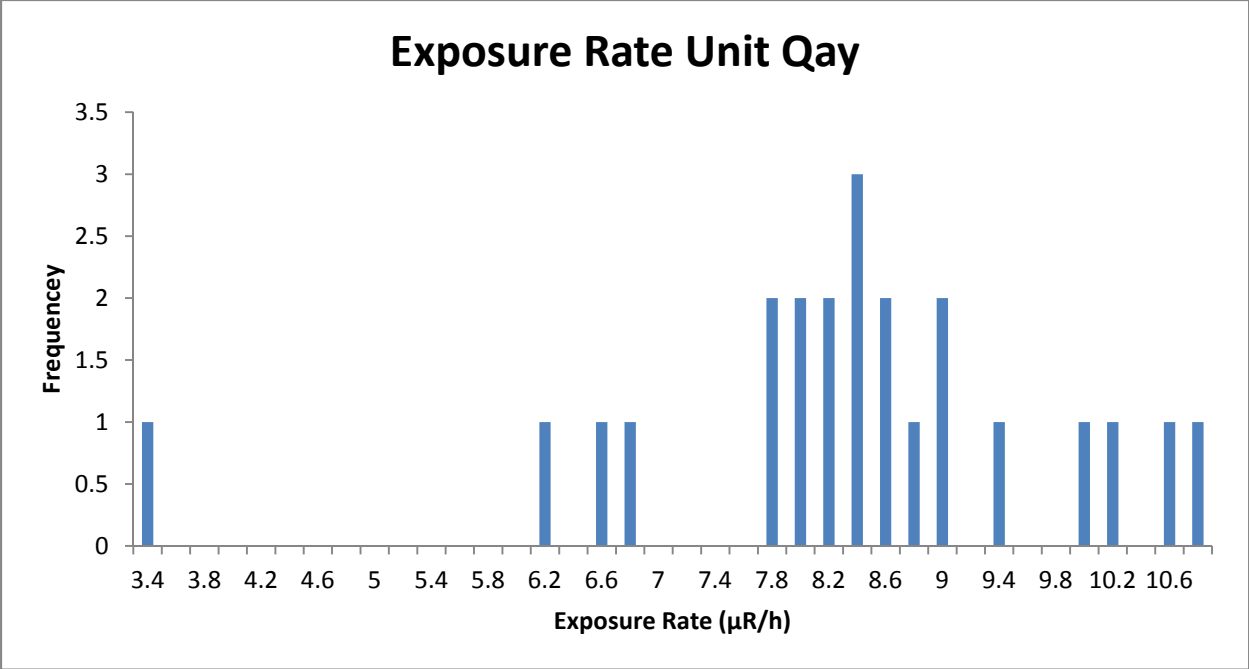


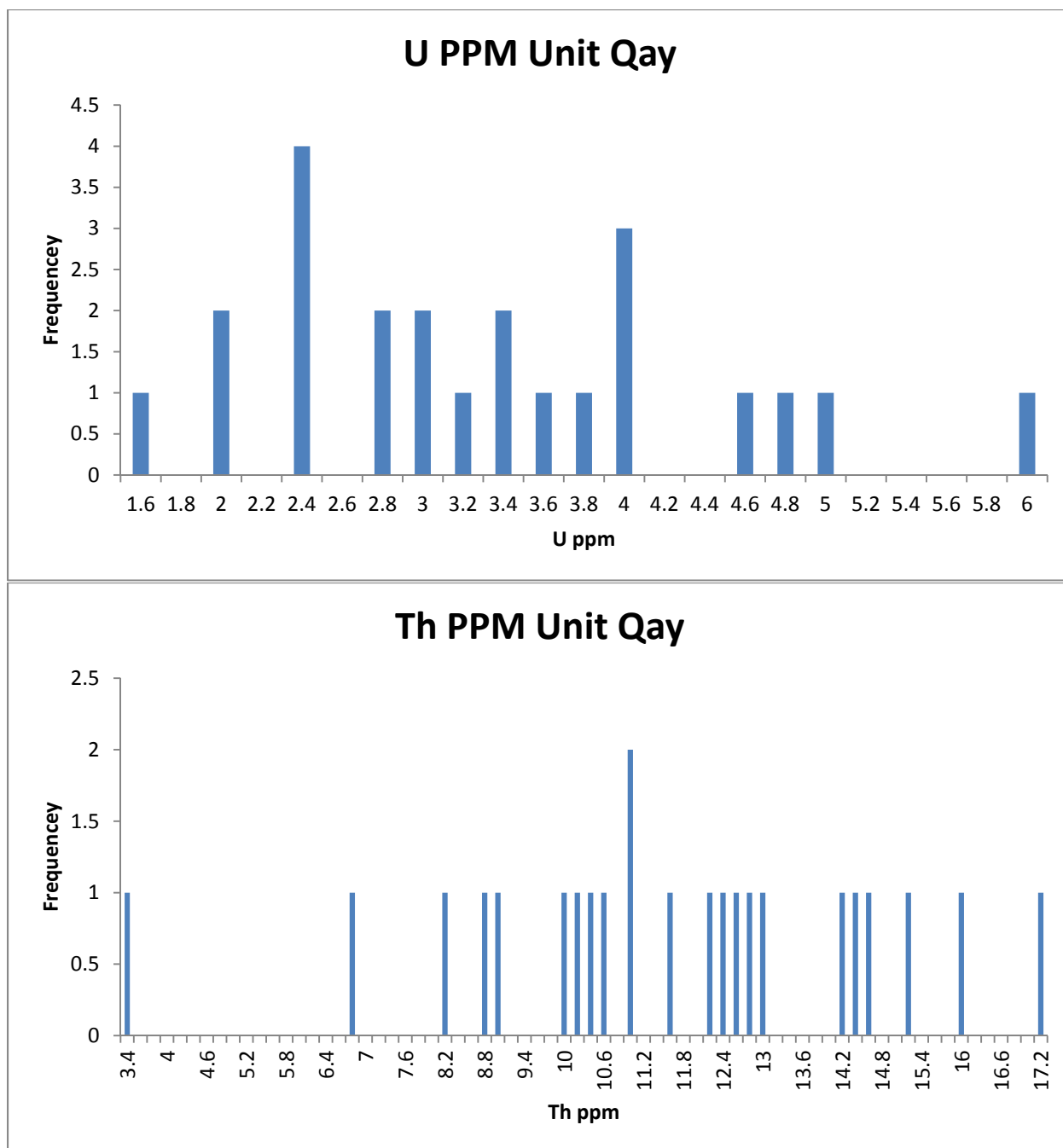


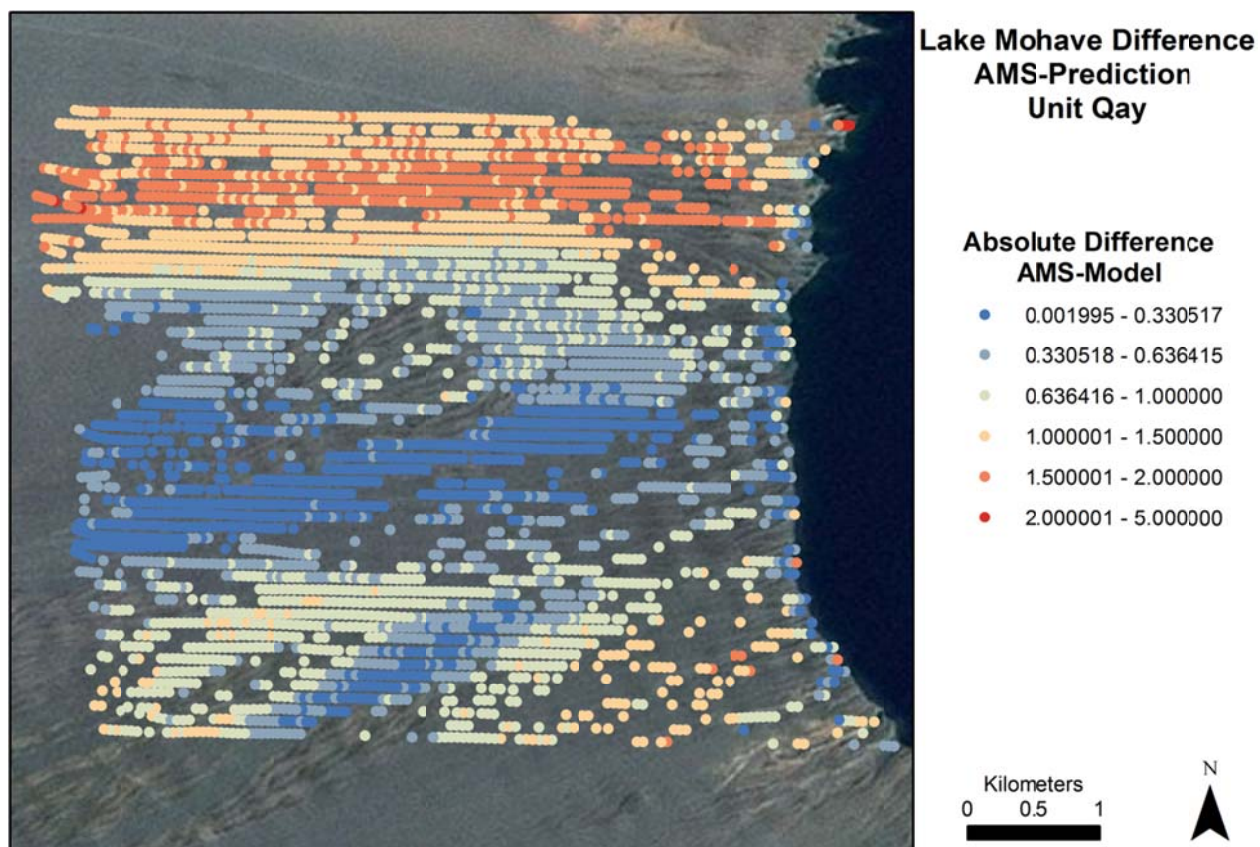
NURE Data

The NURE data for Qay has no distinct features in terms of exposure rate, K , U, or Th. The exposure rate derived from the NURE data is 8.19 $\mu\text{R/h}$ which compares to the AMS exposure rate mean of 8.69 $\mu\text{R/h}$. This means that in terms of mean exposure this unit is within the ± 1 $\mu\text{R/h}$ desired range.

However, when comparing the AMS data points to the NURE mean on a point by point basis it is clear that this modeled exposure rate only works for portions of Qay. The hotter northern third of the unit is outside to far outside the desired range. The southern two thirds of the unit are however within the desired range.







Data Summary

Exposure Rate Comparison $\mu\text{R/h}$	Average	Median	STD	Range
AMS Data	8.689358	8.61033	0.525939	5.44996-9.95081
NURE Data	8.192417	8.2632	1.573618	3.3932-10.6436
Geochemical Prediction	11.93786139	11.8179	N/A	8.2020348-14.703

Qay2

Composition

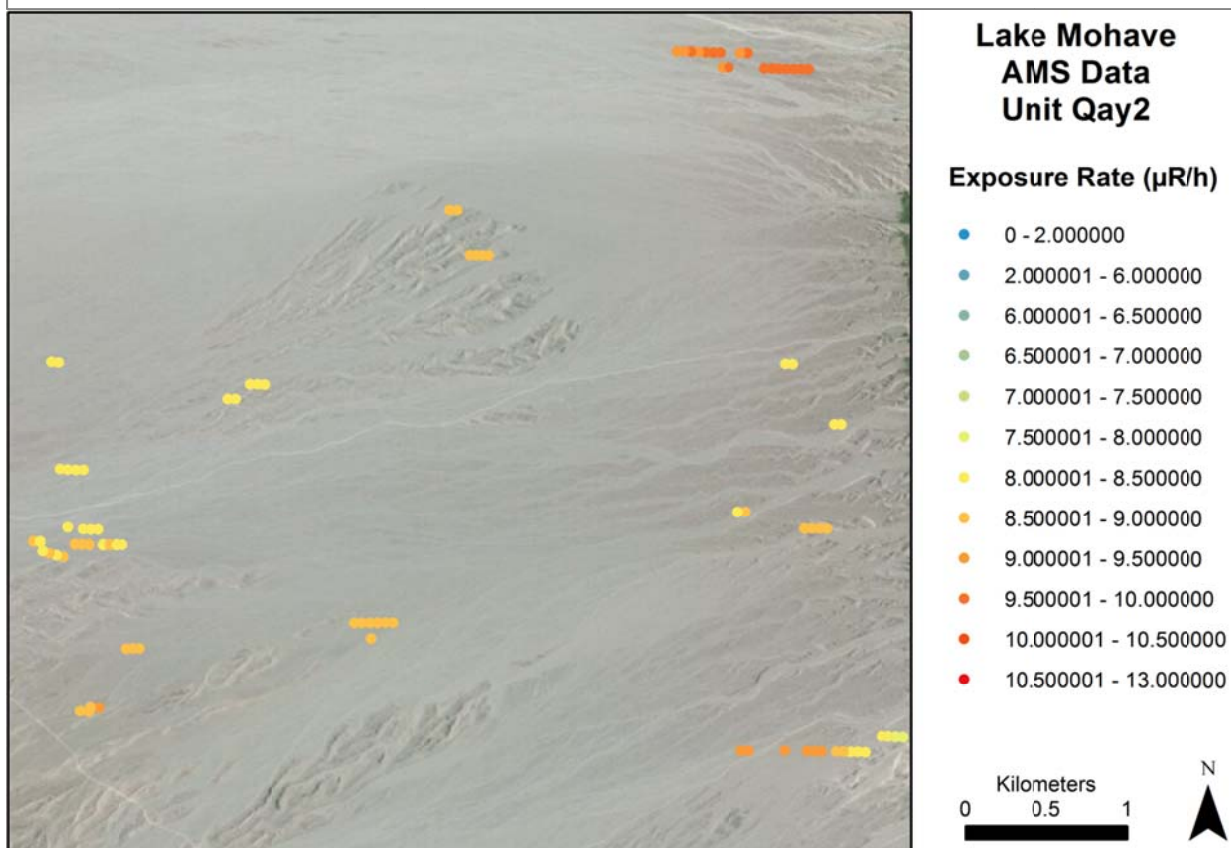
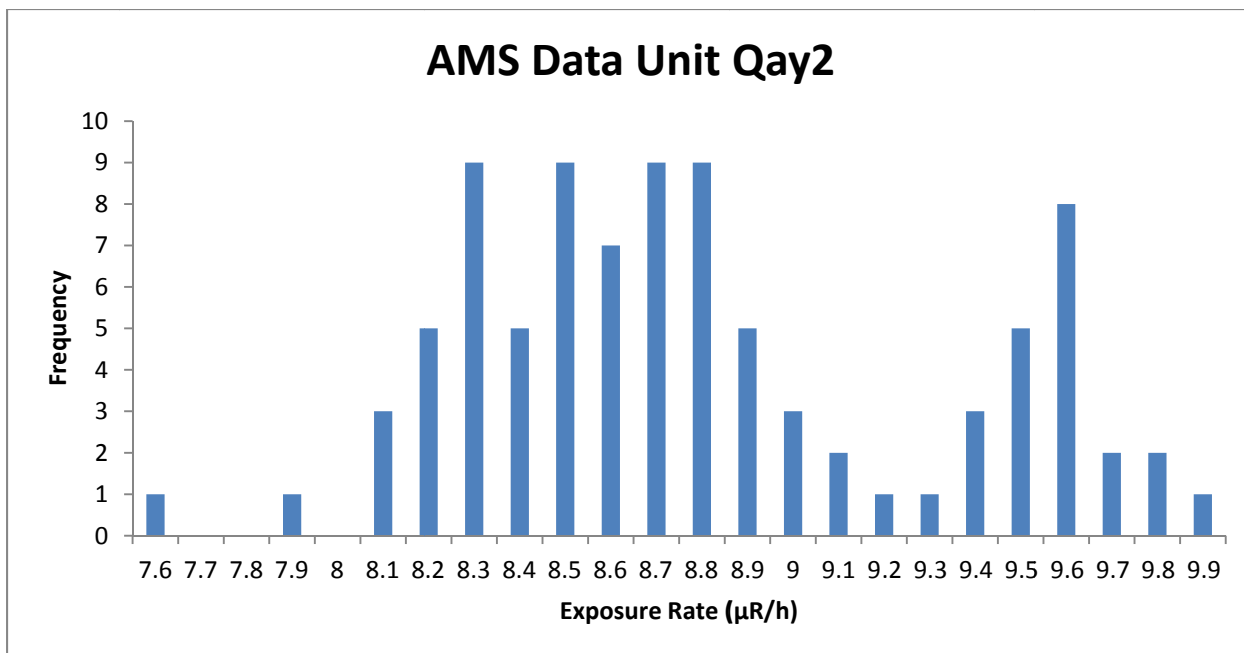
Qay2 is a middle to late Holocene alluvial unit that consists of inactive to intermittently active alluvial fans and washes. The unit is spatially discontinuous and is only mapped where it is spatially large enough to be properly mapped. Where it does exist it consists of weak desert pavements with angular clasts. (House and Faulds, 2009) Compositionally Qay2 consists of mafic igneous and metamorphic clasts as well as tuffs and granitic. Composition varies with source material.

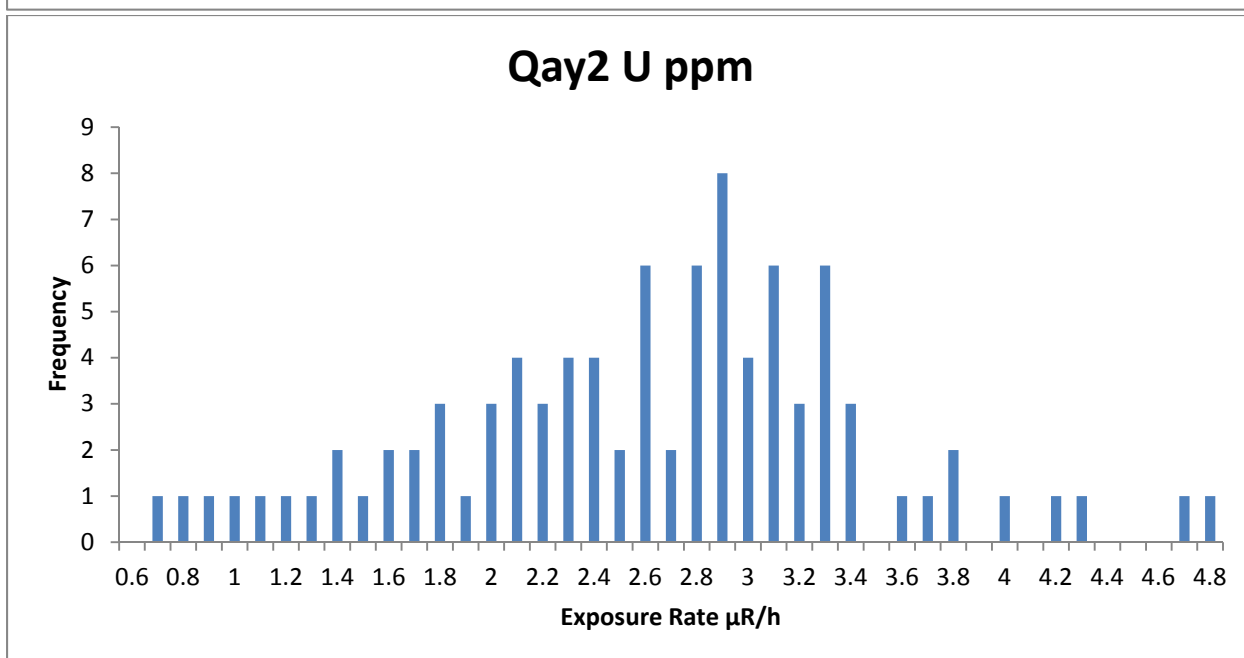
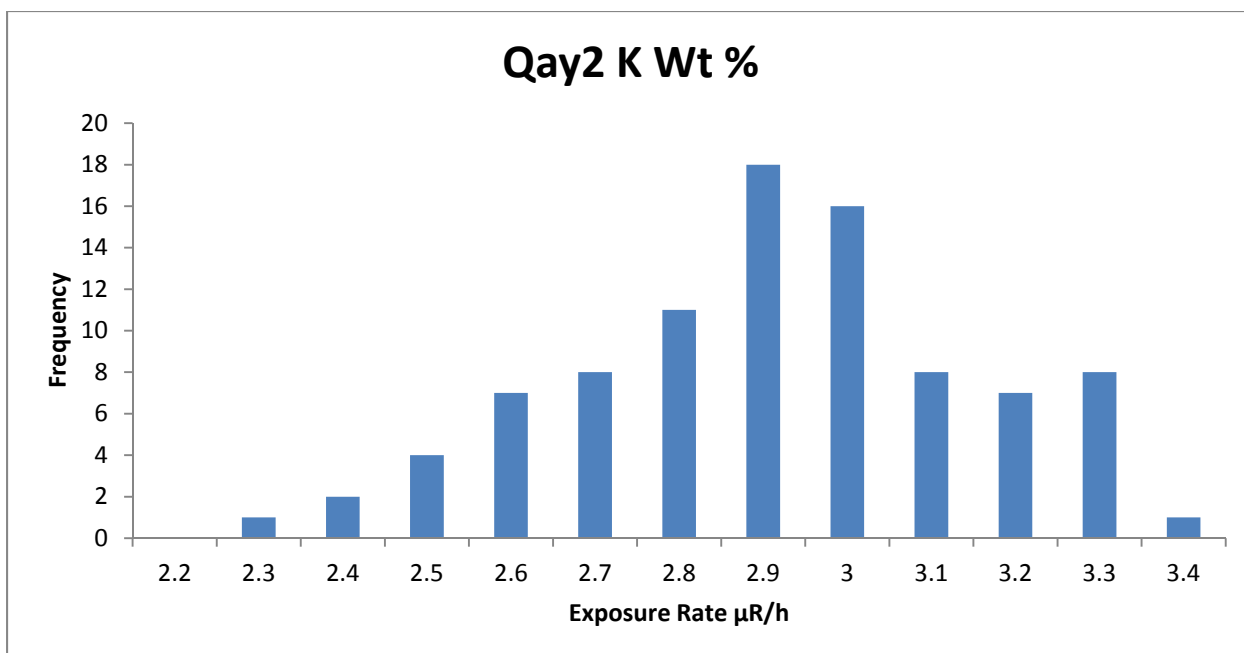
AMS Data

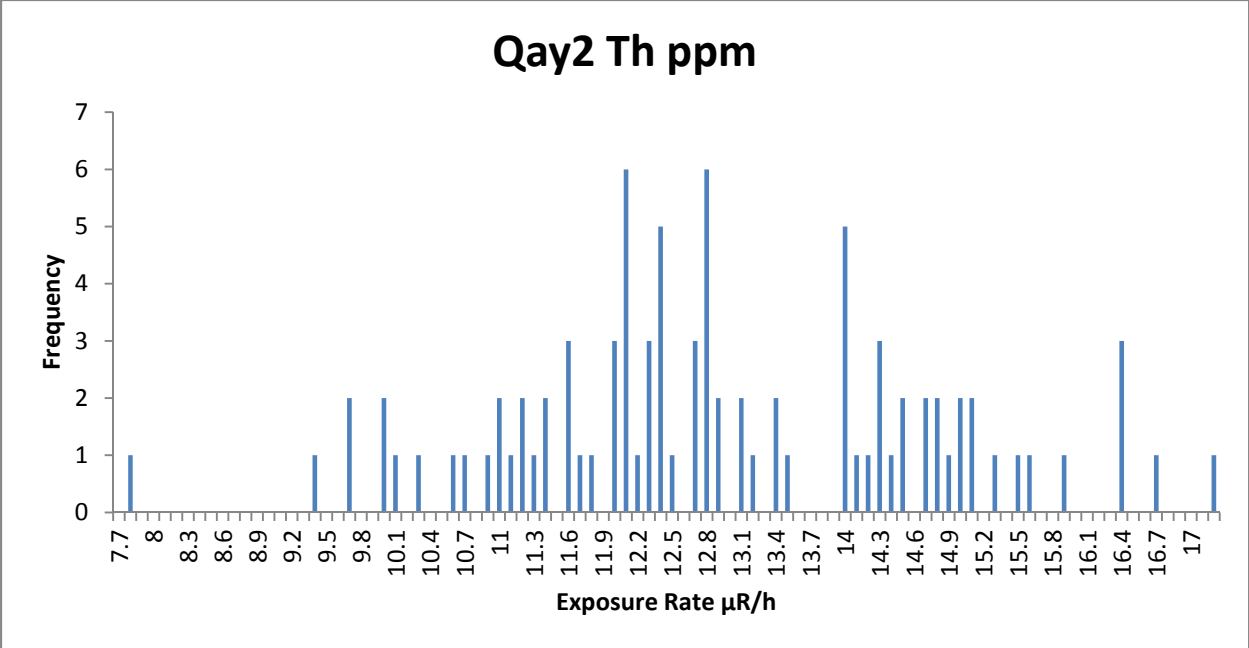
This unit is very spatially discontinuous and has variable composition in each location that it occurs. The northern portions are composed of hotter felsic derived material and therefore express higher exposure rates. The southern portions are largely composed of more mafic materials that have lower exposure rates.

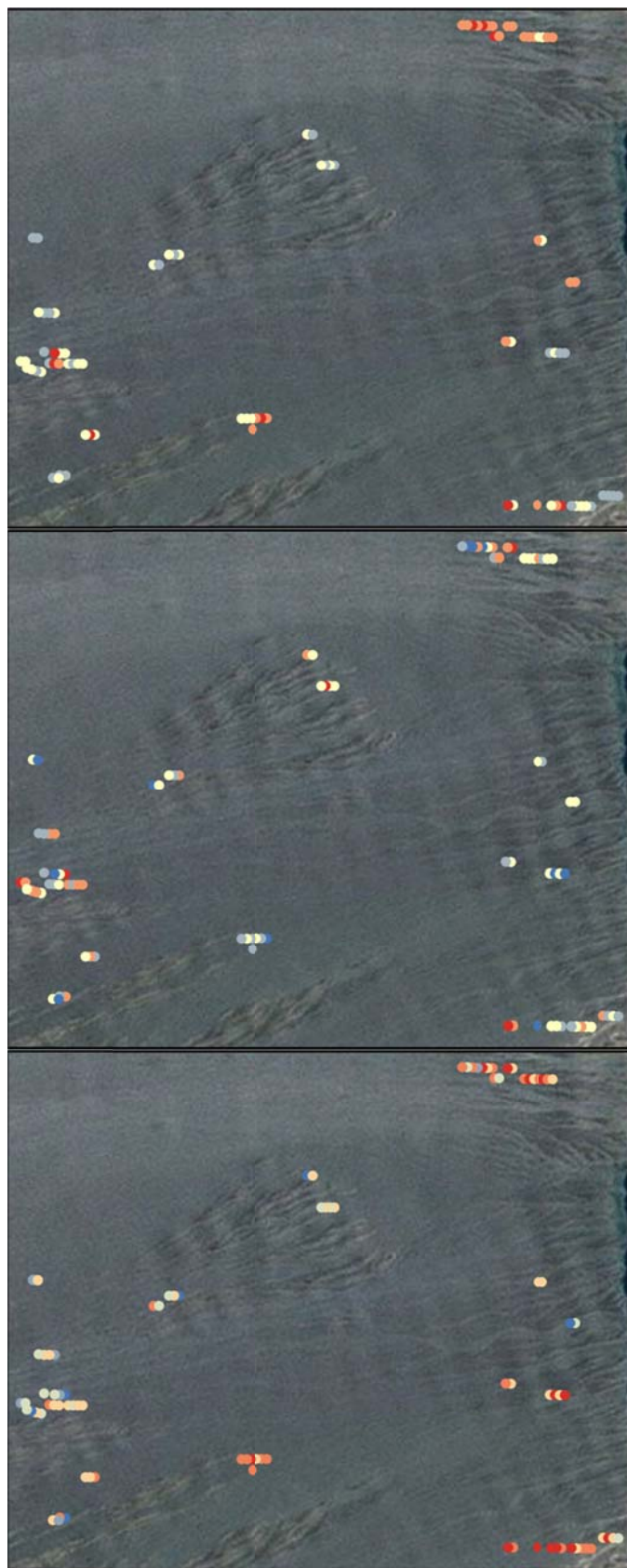
The average AMS exposure rate is 8.75 $\mu\text{R/h}$ with a standard deviation of 0.52 or 6% of the mean. The low standard deviation is deceptive; when looking at the distribution of exposure rate data there is a wide peak from 8.2 to 8.9 $\mu\text{R/h}$ with a second peak near 9.6 $\mu\text{R/h}$. The majority of the data lie within the wide peak. The peak at 9.6 $\mu\text{R/h}$ represents the northern portion of the unit.

The distribution of K, U, and Th all have peak ranges where most of the data are concentrated but generally the distribution cannot be called normal. Spatially, K, U, and Th are randomly distributed. The notable exceptions are high K in the hotter northern portion of the unit and high Th in the southern portions.









Lake Mohave Radioelement Concentration Images Unit Qay2

K Wt%

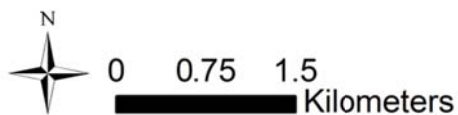
- 0.960459 - 2.243253
- 2.243254 - 2.723497
- 2.723498 - 2.956414
- 2.956415 - 3.187128
- 3.187129 - 3.672559

U PPM

- 0 - 1.581498
- 1.581499 - 2.338019
- 2.338020 - 3.035367
- 3.035368 - 3.852008
- 3.852009 - 6.135812

Th PPM

- 4.118740 - 9.969537
- 9.969538 - 10.905588
- 10.905589 - 11.949598
- 11.949599 - 13.168826
- 13.168827 - 14.872976
- 14.872977 - 18.871453





Lake Mohave Radioelement Ratio Images Unit Qay2

U/K Ratio

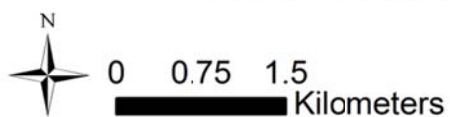
- 0 - 0.498470
- 0.498471 - 0.745602
- 0.745603 - 0.968045
- 0.968046 - 1.208879
- 1.208880 - 1.542684
- 1.542685 - 3.123242

Th/K Ratio

- 2.090277 - 3.461301
- 3.461302 - 3.942091
- 3.942092 - 4.348792
- 4.348793 - 4.786292
- 4.786293 - 5.355216
- 5.355217 - 8.000000

U/Th Ratio

- 0 - 0.117615
- 0.117616 - 0.182165
- 0.182166 - 0.244454
- 0.244455 - 0.316216
- 0.316217 - 0.426078
- 0.426079 - 0.803350

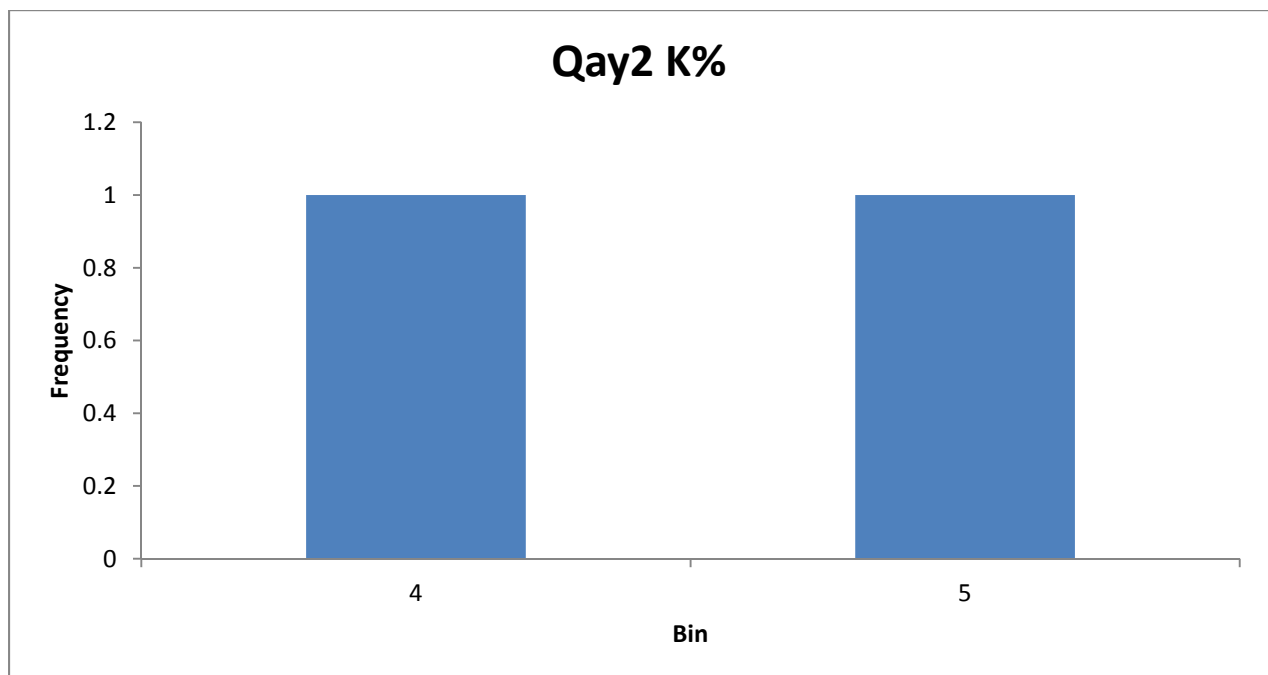


Traditional Geochemistry

There are two traditional geochemical points that occur in Qay2. One of the points only provides K data and therefore U and Th concentrations are based off one measurement. Of the two points the K values are about 1% different from each other. The exposure rate derived from this data is 10.55 $\mu\text{R/h}$ which compares to the AMS data of 8.75 $\mu\text{R/h}$. This means the geochemistry puts this unit well outside the ± 1 $\mu\text{R/h}$ range.

Sample ID	Latitude	Longitude	K %	U ppm	Th ppm
M167555	35.395	-114.965	3.82	2.24	13.6
TP23	35.6167	-114.87	4.7		

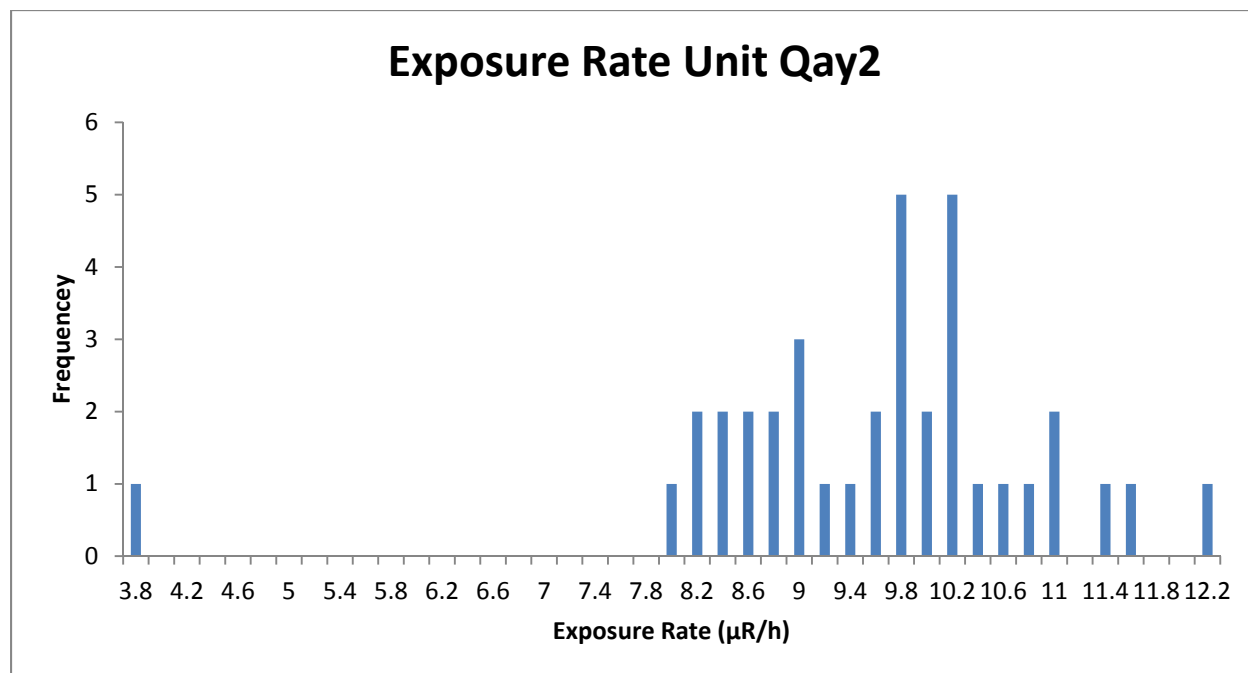
	K%	U ppm	Th ppm
Mean	4.26	2.24	13.6
Median	4.26	2.24	13.6
Standard Deviation	0.44	N/A	N/A
Range	3.82-4.7	N/A	N/A

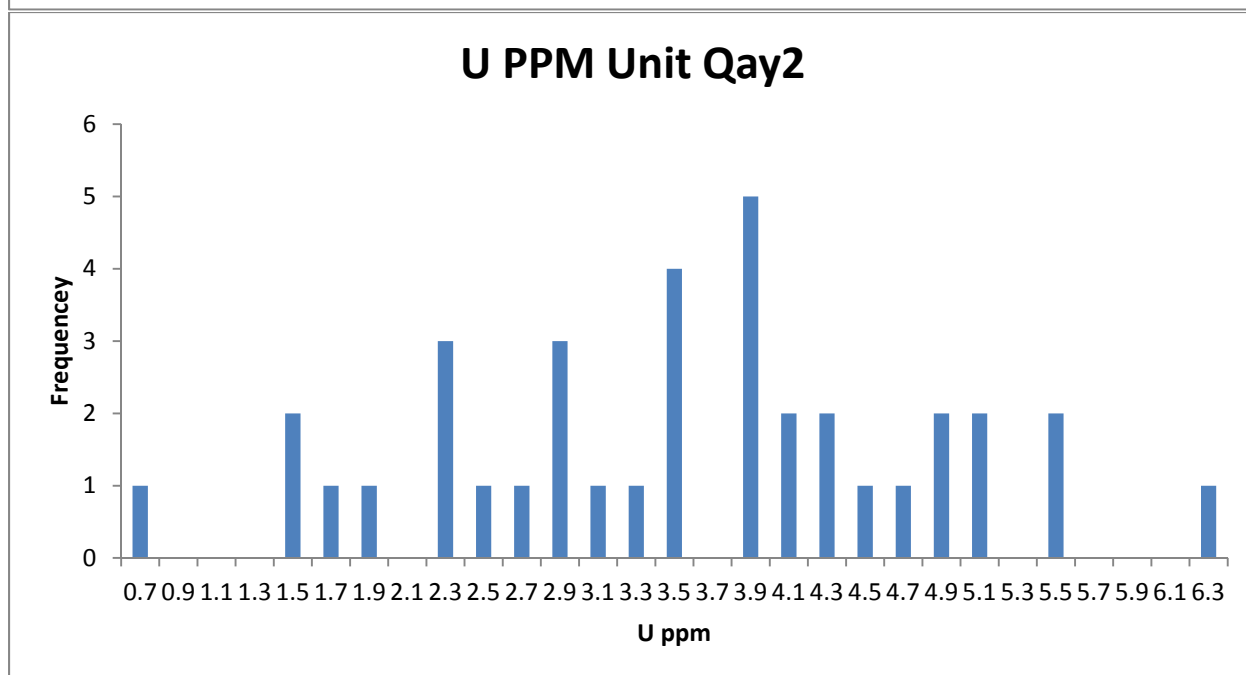
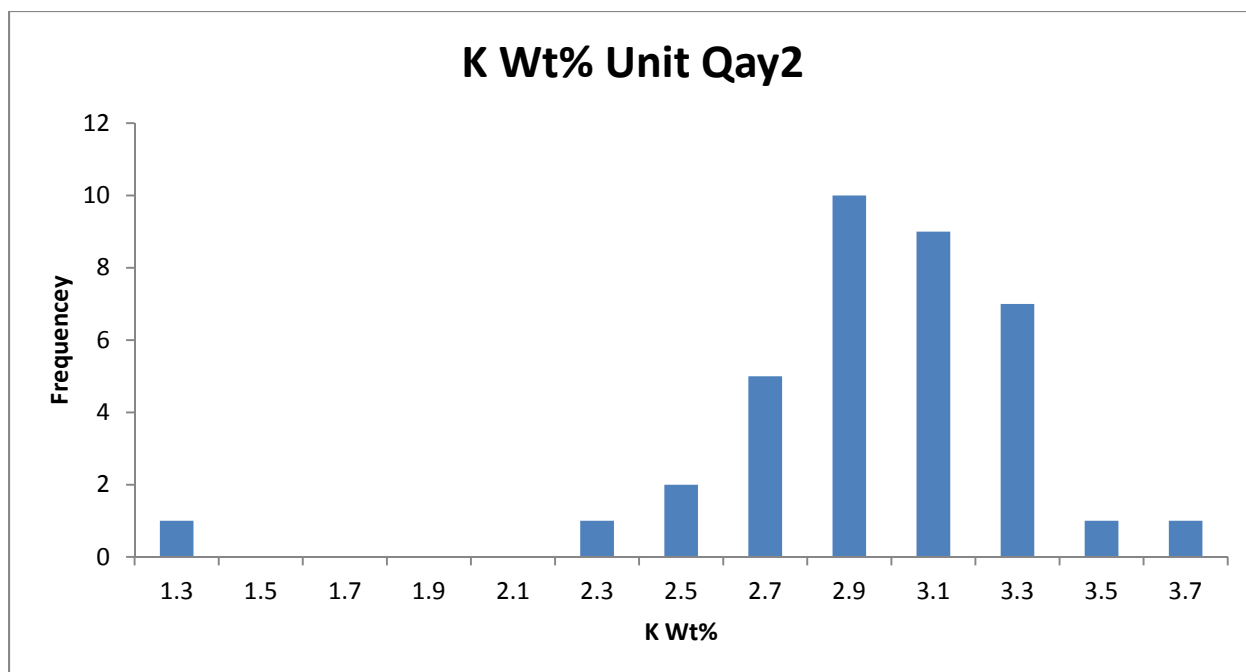


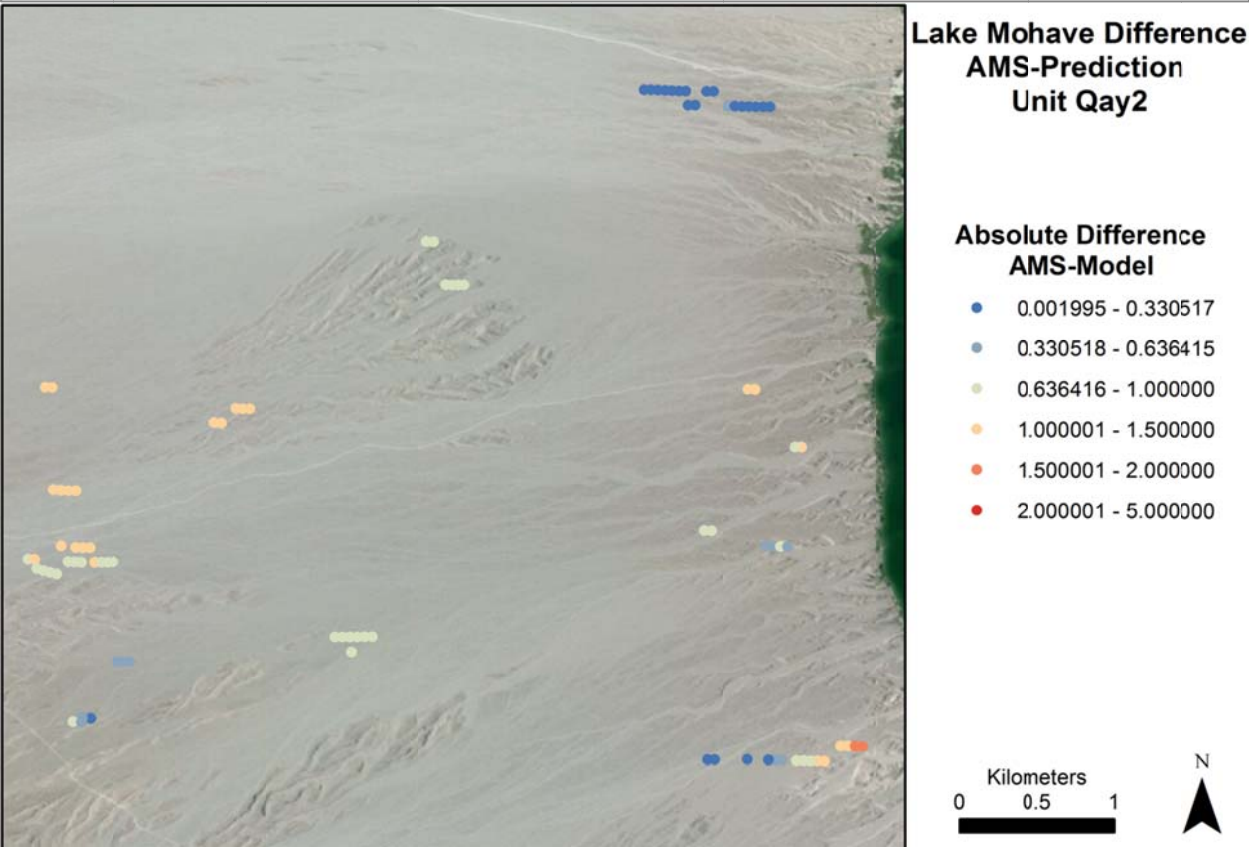
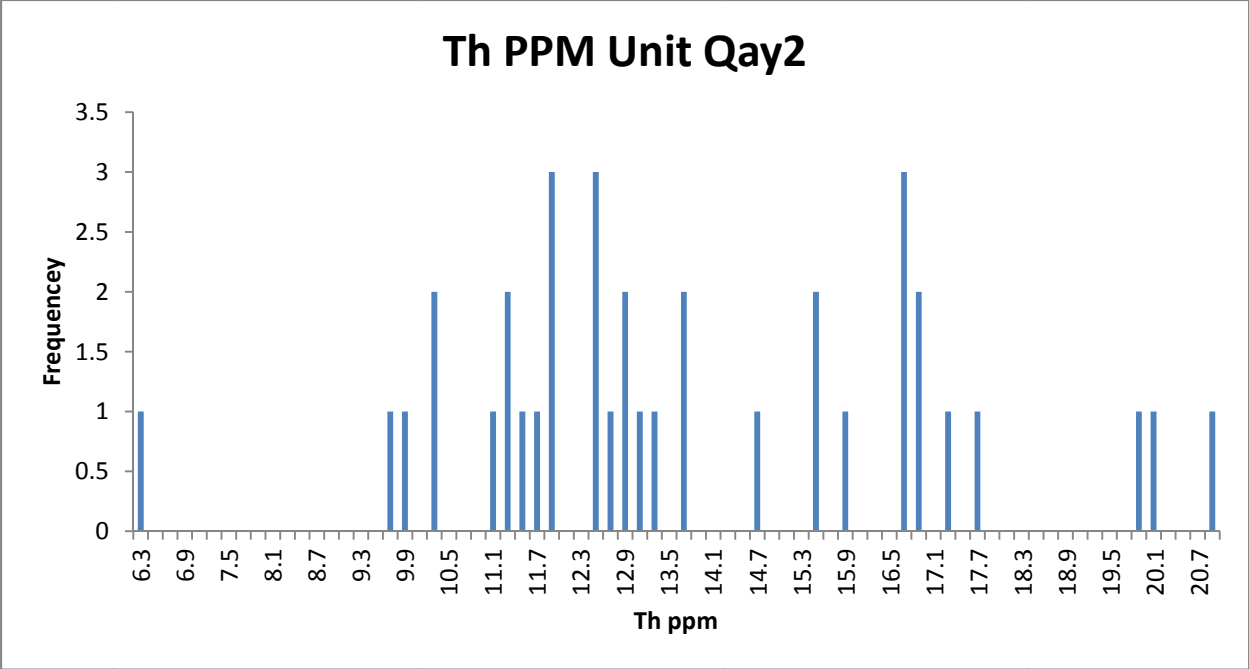
NURE Data

The NURE exposure rate data in Qay2 is mostly $>9 \mu\text{R/h}$. The average NURE exposure rate is $9.47 \mu\text{R/h}$ which compares to the AMS average of $8.75 \mu\text{R/h}$. This unit is within the desired $\pm 1 \mu\text{R/h}$ range. The K, U, and Th data are widely distributed with only K having something resembling a normal distribution.

When comparing the NURE derived exposure rate to the AMS data points that occur within Qay2 most of the unit falls within the $\pm 1 \mu\text{R/h}$ range. The portions of the unit that are best represented by these data are the northern hot portions of the unit that are largely composed of felsic materials.







Data Summary

Exposure Rate Comparison μR/h	Average	Median	STD	Range
AMS Data	8.754271	8.67957	0.5177	7.51876-9.81942
NURE Data	9.473946	9.7304	1.39044	3.8132-12.058
Geochemical Prediction	10.54992	10.54992	N/A	9.96912-11.13072

Qay1

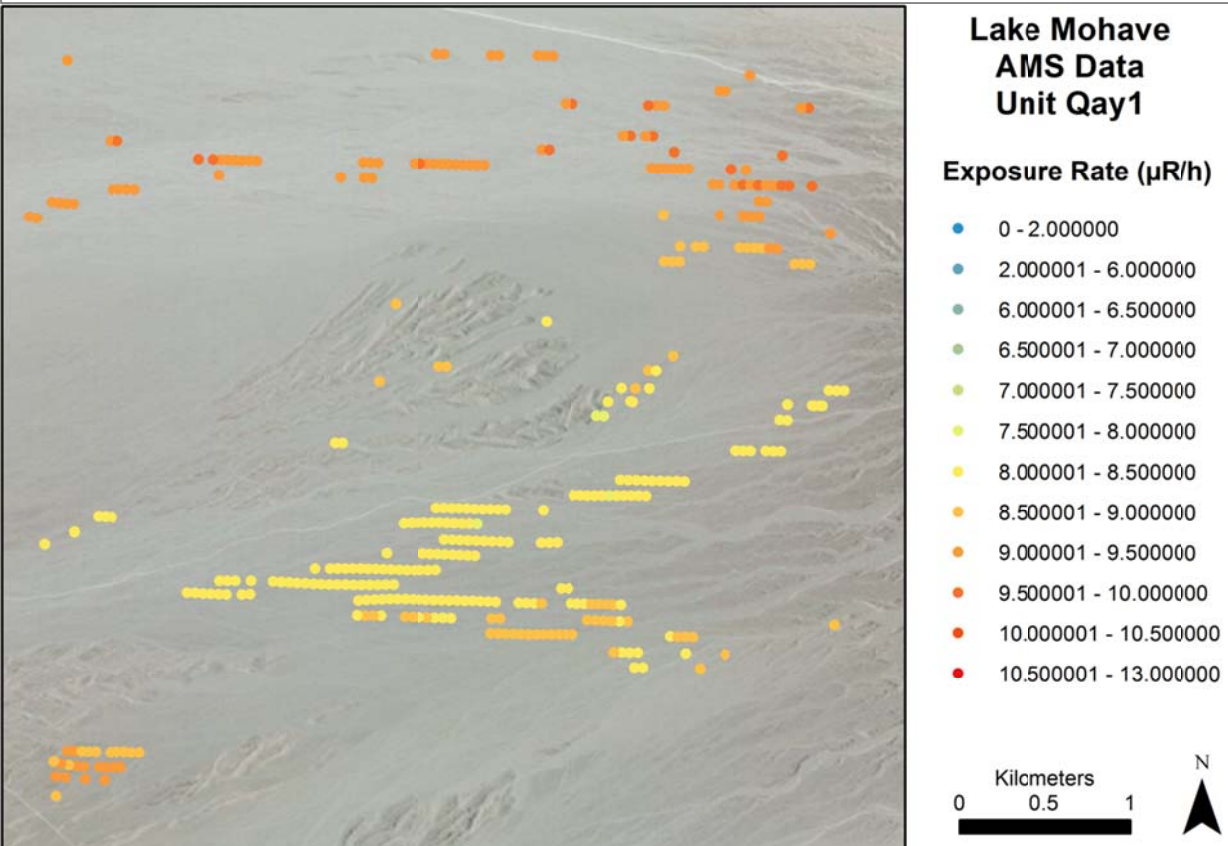
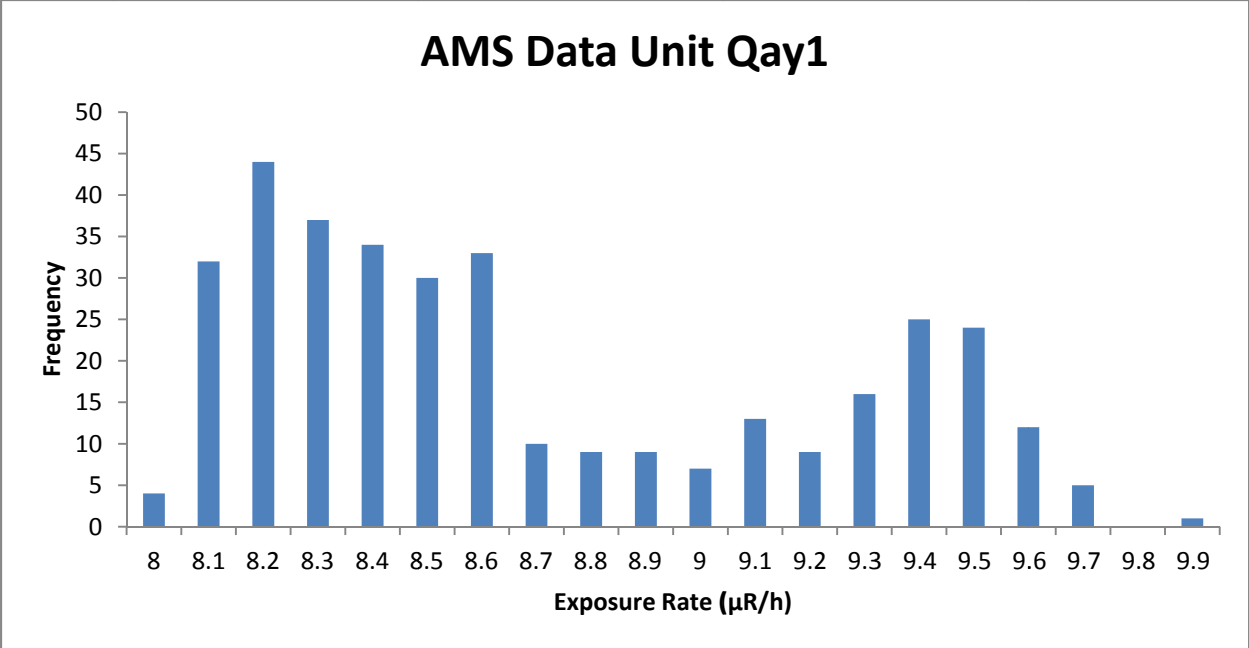
Composition

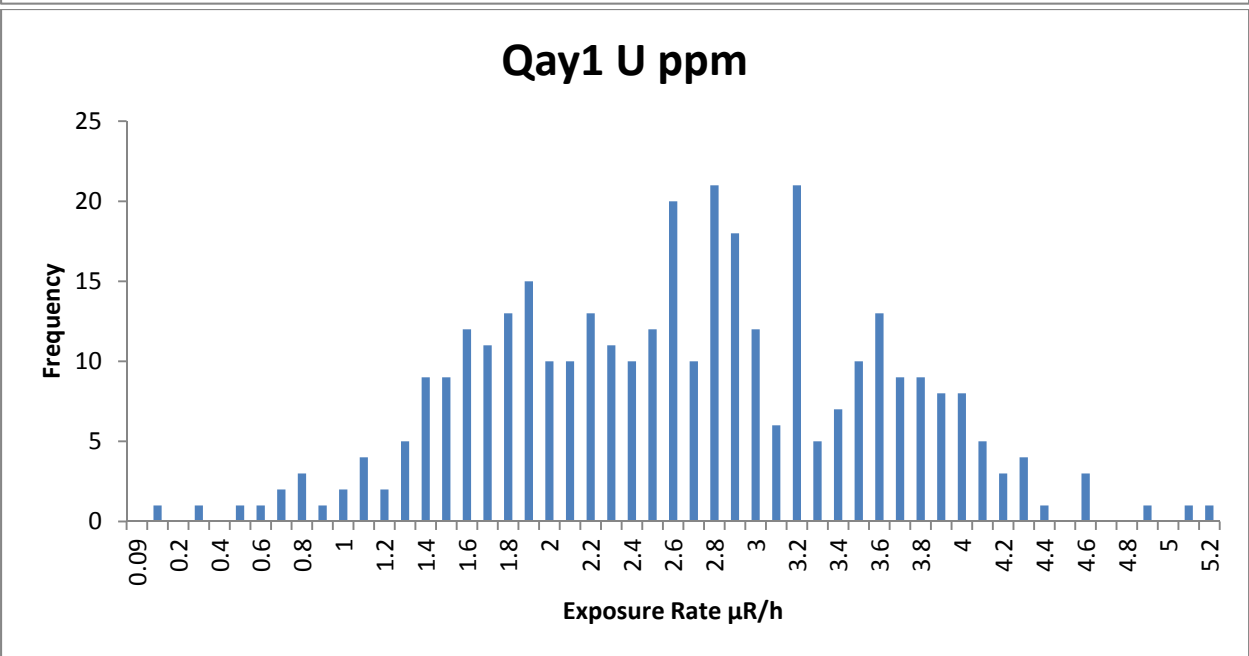
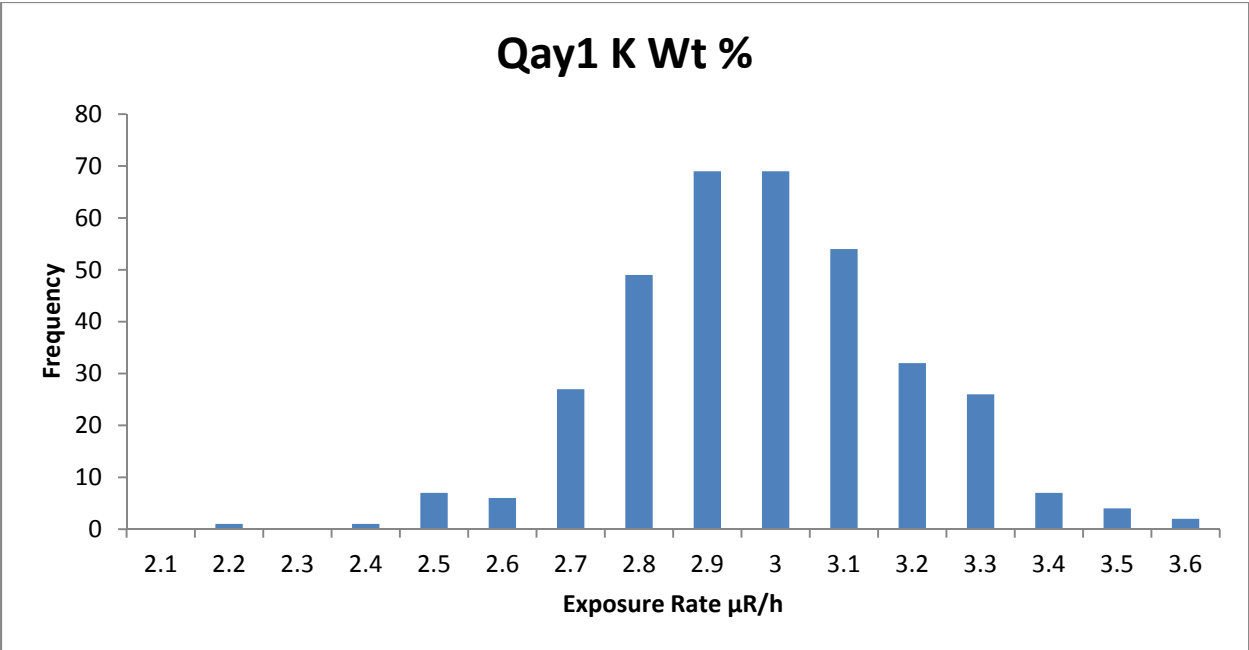
Qay1 a Holocene age alluvial deposit consisting of inactive alluvial fans, alluvial terraces and moderate to strong desert pavements. Pavement surfaces are typically varnished. (House and Faulds, 2009) Compositionally Qay1 contains tuff and granitic rocks in the northern half of the AOI and more mafic rocks in the southern portion.

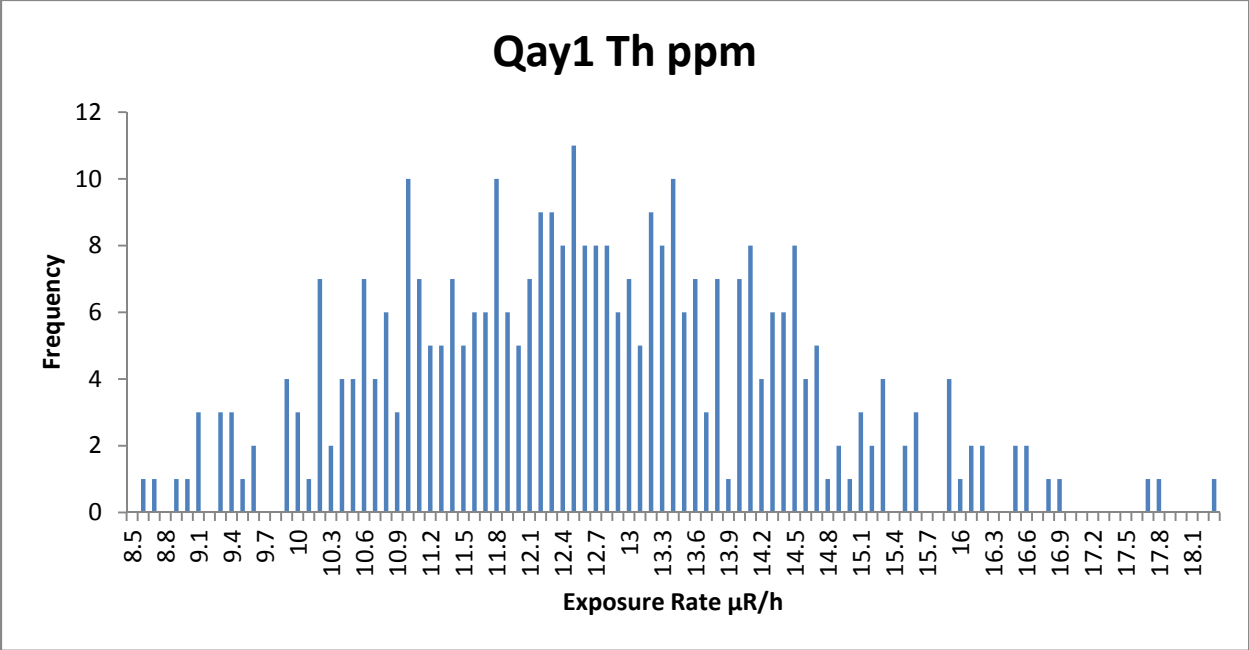
AMS Data

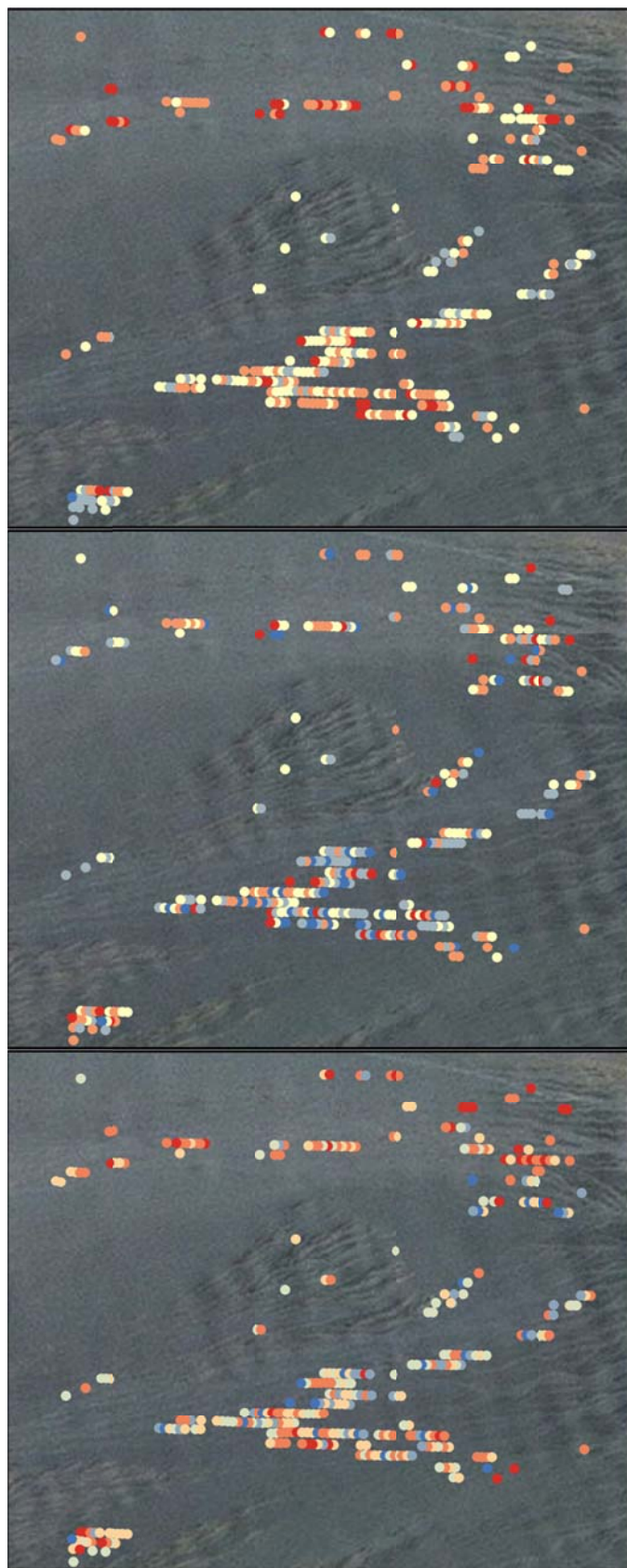
In terms of exposure rate, Qay1 has two distinct regions. The first region is centered around 8.3 $\mu\text{R/h}$ and occurs in the areas with more mafic components. The second region is higher in exposure rate centering near 9.4 $\mu\text{R/h}$ and represents the hotter tuffs and granites in the northern portion of the unit. The average exposure rate is 8.64 $\mu\text{R/h}$ with a standard deviation of 0.5 or 6% of the mean.

K has a close to normal distribution with most of the data falling into a narrow 2.7% to 3.2% range. U and Th however both have wide distributions and are not normal. Spatially, the northern half of the unit tends to have higher values of K, although there are some high values further south. Th follows a similar pattern to K but is more randomized. U appears to be randomly distributed.









Lake Mohave Radioelement Concentration Images Unit Qay1

K Wt%

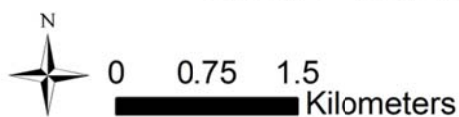
- 0.960459 - 2.243253
- 2.243254 - 2.723497
- 2.723498 - 2.956414
- 2.956415 - 3.187128
- 3.187129 - 3.672559

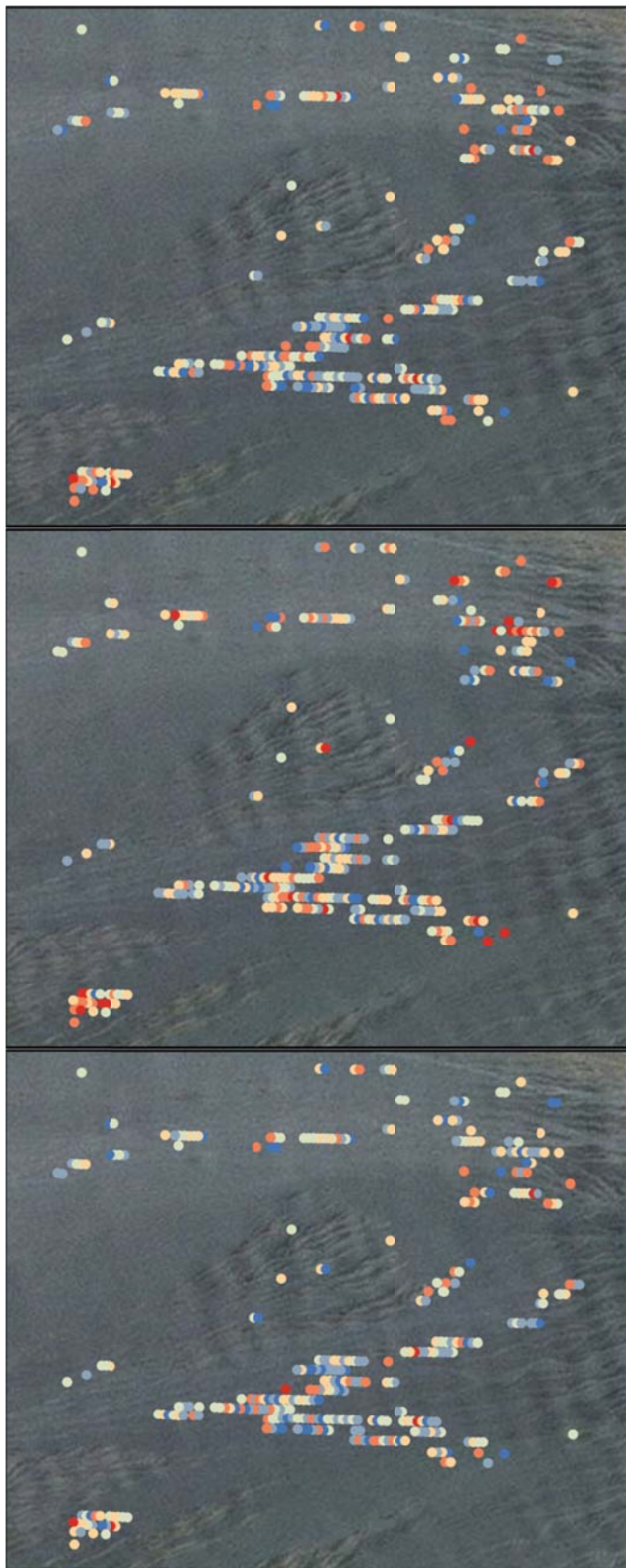
U PPM

- 0 - 1.581498
- 1.581499 - 2.338019
- 2.338020 - 3.035367
- 3.035368 - 3.852008
- 3.852009 - 6.135812

Th PPM

- 4.118740 - 9.969537
- 9.969538 - 10.905588
- 10.905589 - 11.949598
- 11.949599 - 13.168826
- 13.168827 - 14.872976
- 14.872977 - 18.871453





Lake Mohave Radioelement Ratio Images Unit Qay1

U/K Ratio

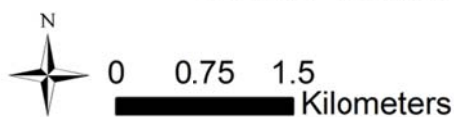
- 0 - 0.498470
- 0.498471 - 0.745602
- 0.745603 - 0.968045
- 0.968046 - 1.208879
- 1.208880 - 1.542684
- 1.542685 - 3.123242

Th/K Ratio

- 2.090277 - 3.461301
- 3.461302 - 3.942091
- 3.942092 - 4.348792
- 4.348793 - 4.786292
- 4.786293 - 5.355216
- 5.355217 - 8.000000

U/Th Ratio

- 0 - 0.117615
- 0.117616 - 0.182165
- 0.182166 - 0.244454
- 0.244455 - 0.316216
- 0.316217 - 0.426078
- 0.426079 - 0.803350



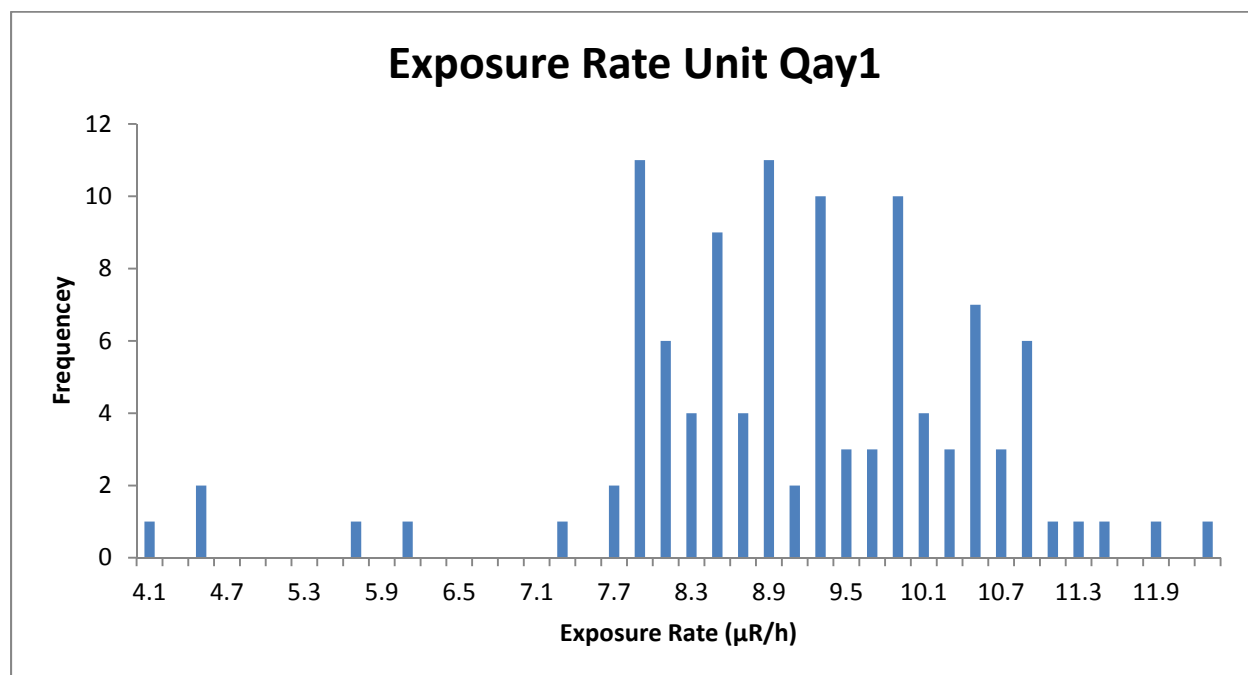
Traditional Geochemistry

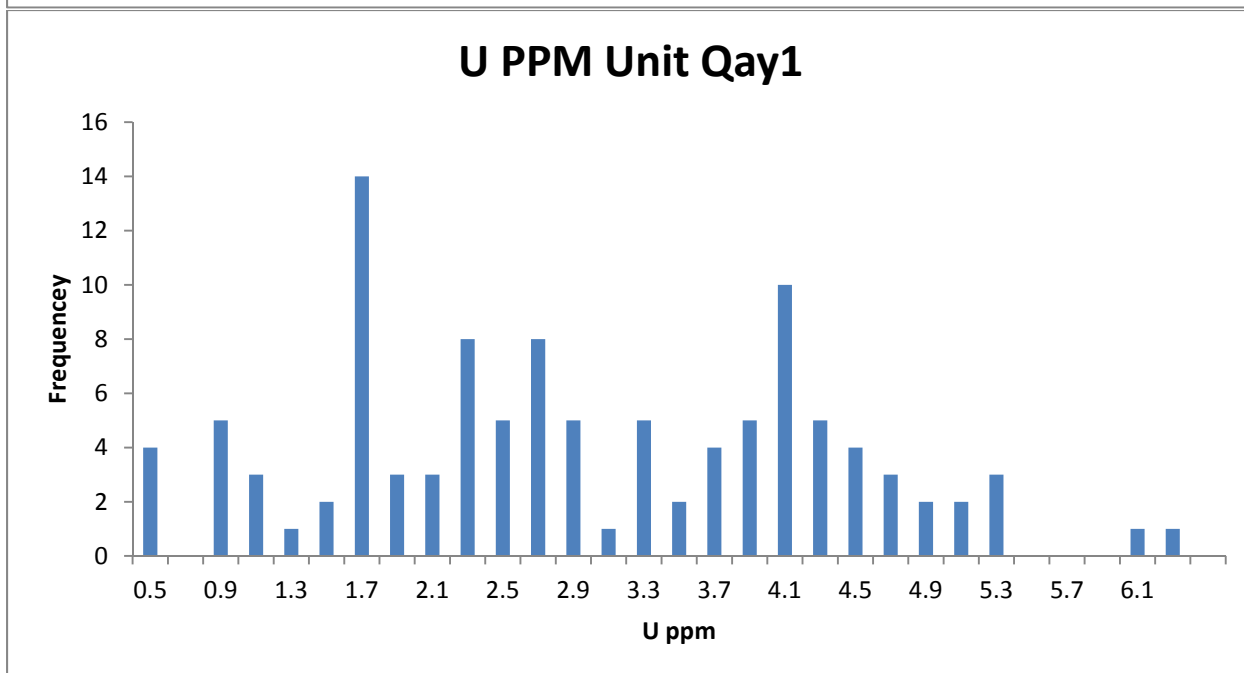
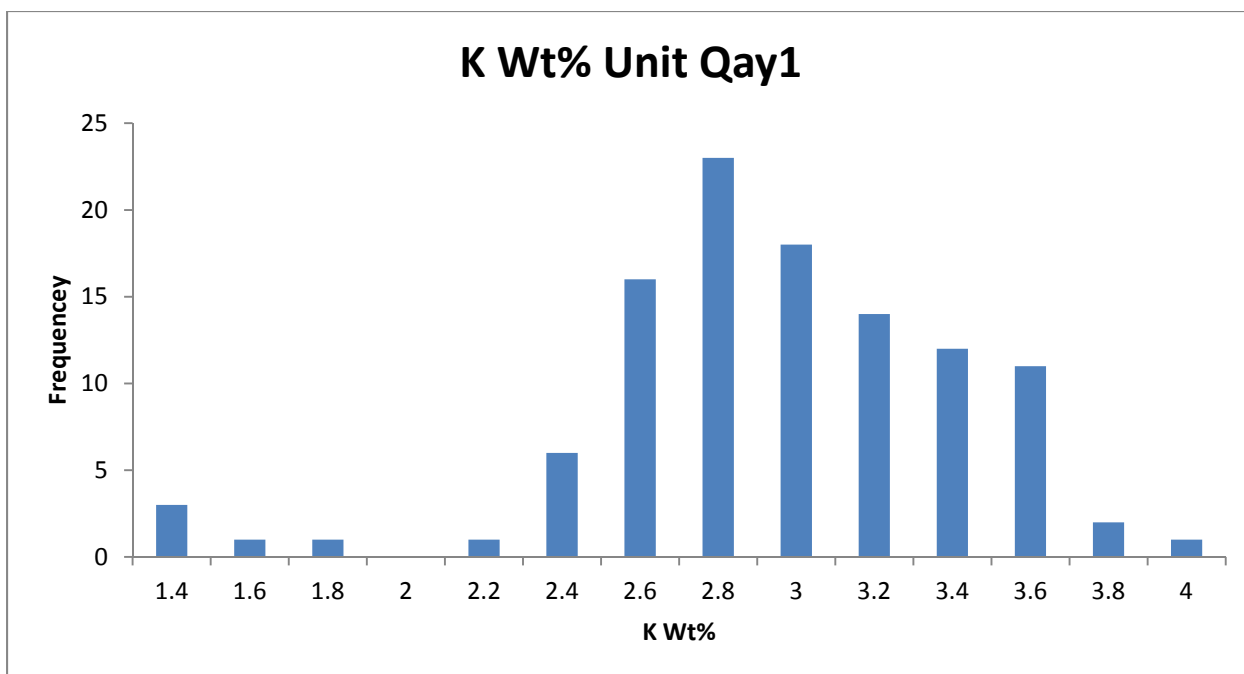
There are no traditional geochemical data for Qay1.

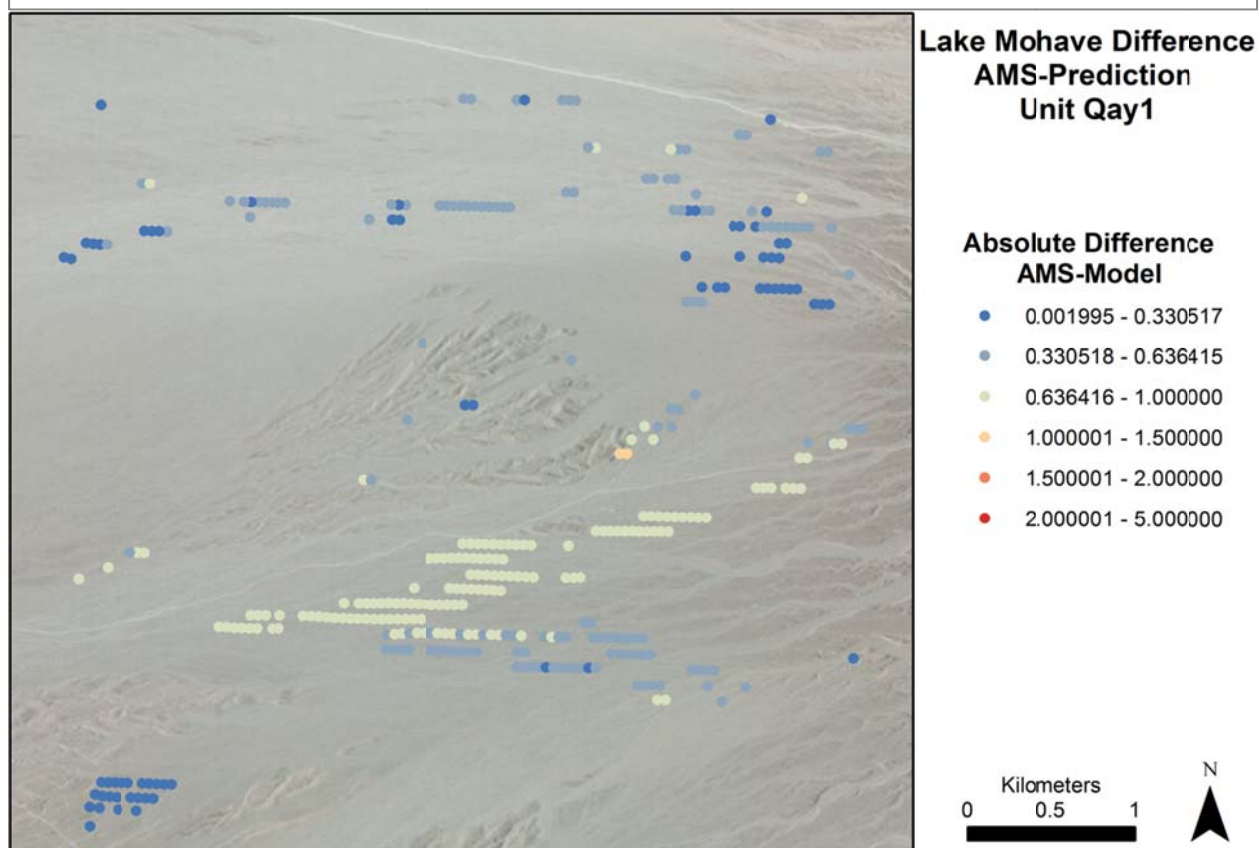
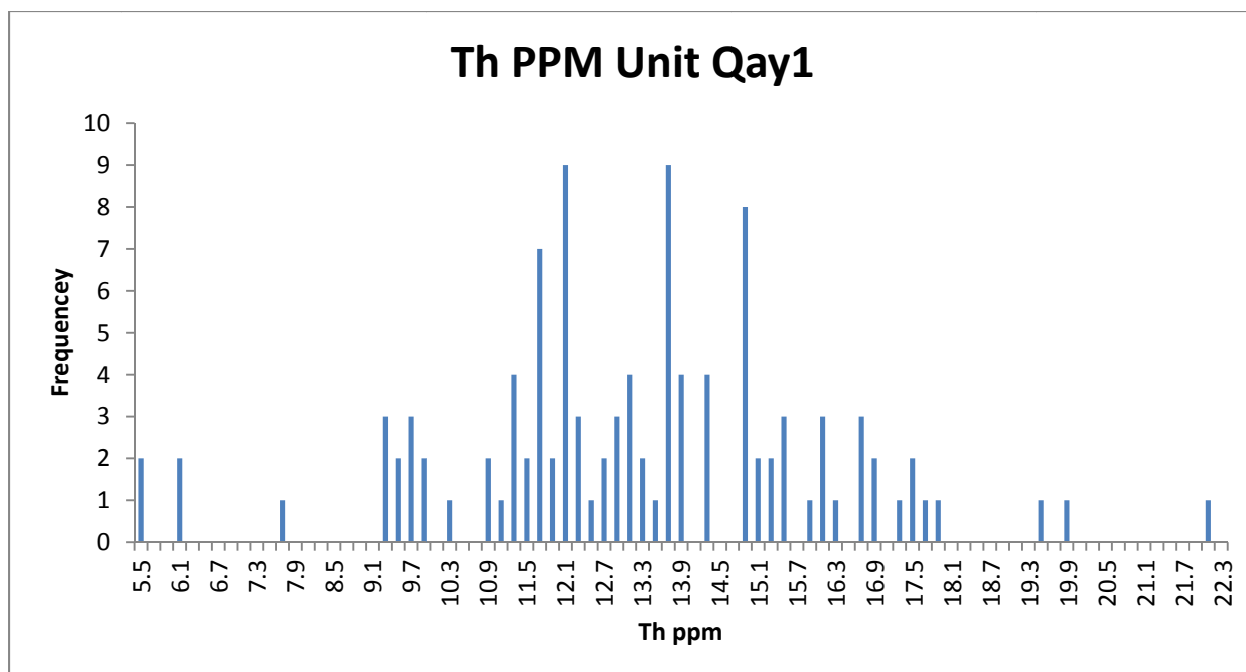
NURE Data

The NURE exposure rate data for Qay1 ranges mostly from 7.9 to 10.9 $\mu\text{R/h}$ with an average of 8.97 $\mu\text{R/h}$. This compares with the AMS exposure rate of 8.64 $\mu\text{R/h}$ and is within the desired ± 1 $\mu\text{R/h}$ range. The majority of the K data are $> 2.6\%$ and tend to peak near 2.8% with a strong tail towards higher percentages. U and Th data are more randomly distributed than the K data are.

When comparing the AMS data points to the NURE mean the majority of the unit is modeled very well. The hotter portions of the unit in the north are particularly well modeled while the cooler center portion, while still well modeled, is further from the NURE rate.







Data Summary

Exposure Rate Comparison μR/h	Average	Median	STD	Range
AMS Data	8.644988	8.48574	0.504485	7.93725-9.83221
NURE Data	8.975508	8.9828	1.401636	4.0564-12.058

Qai3

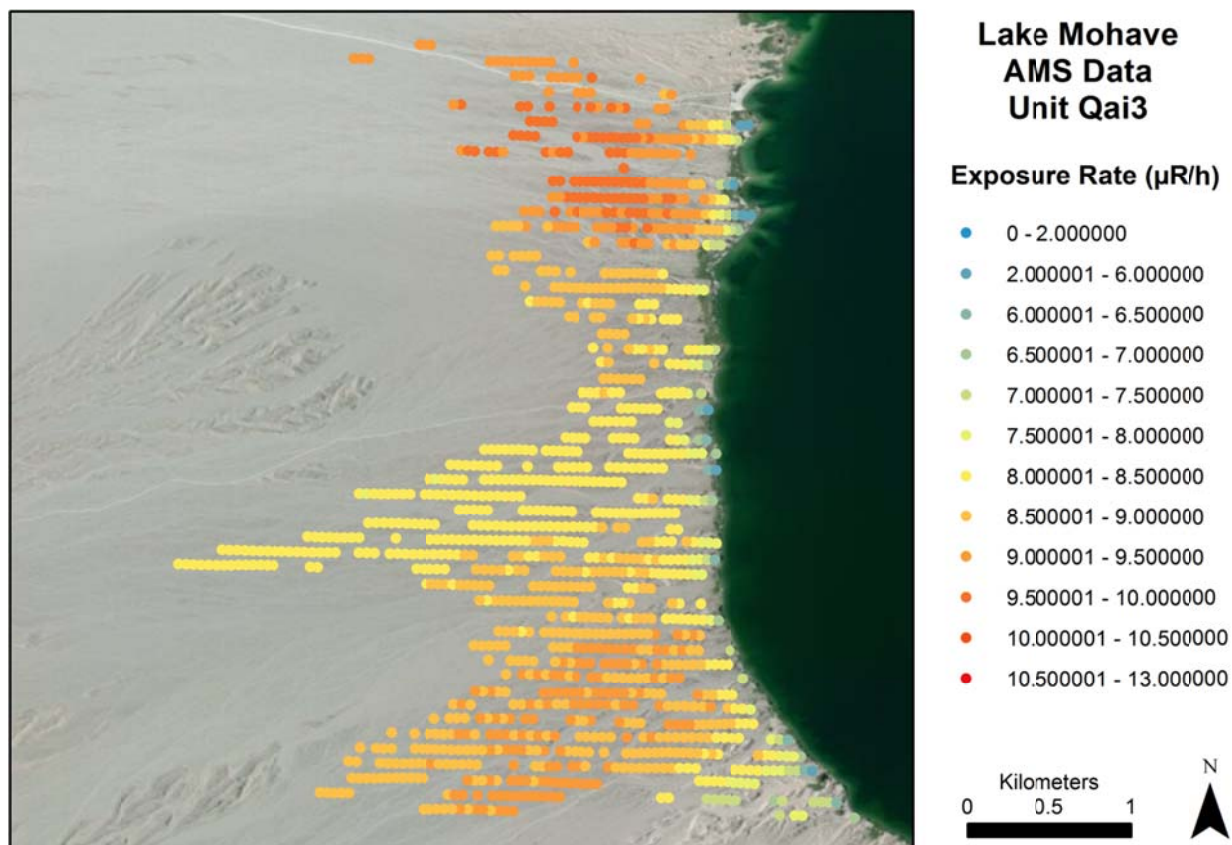
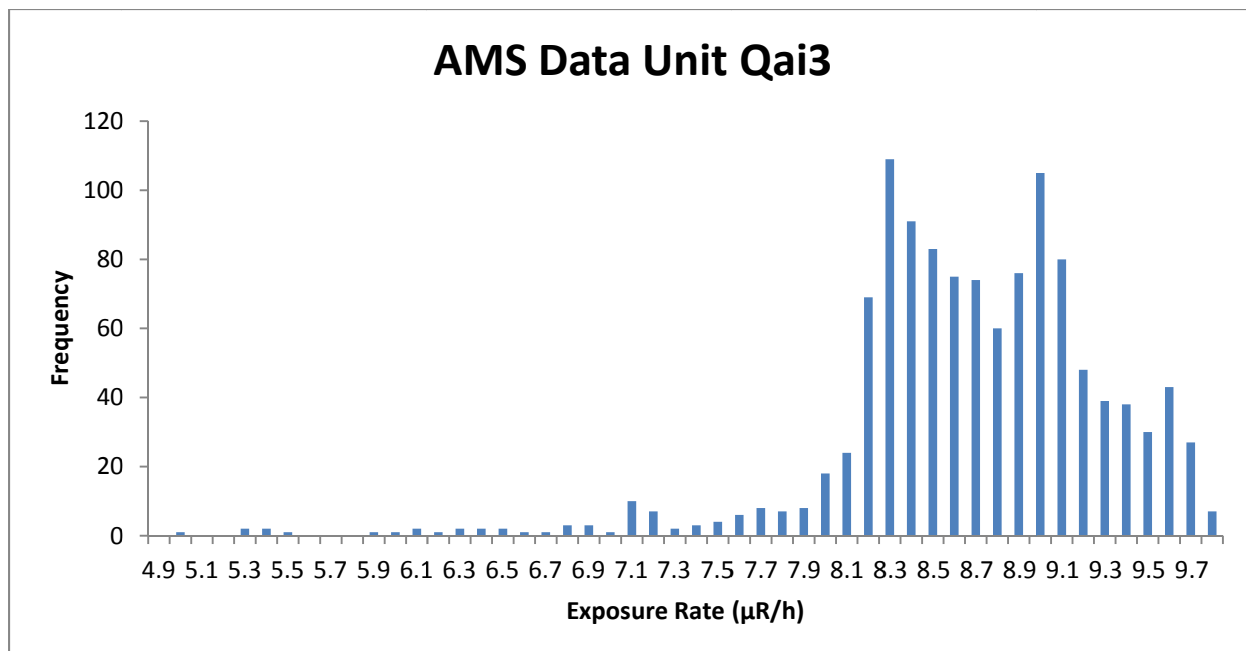
Composition

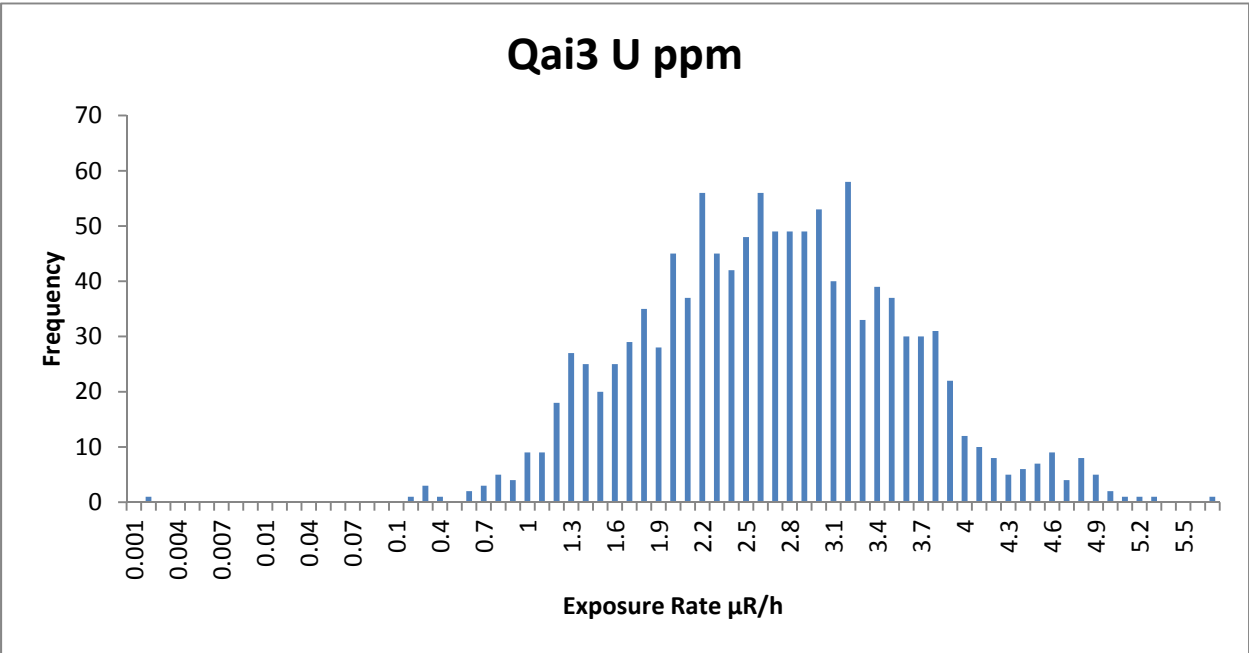
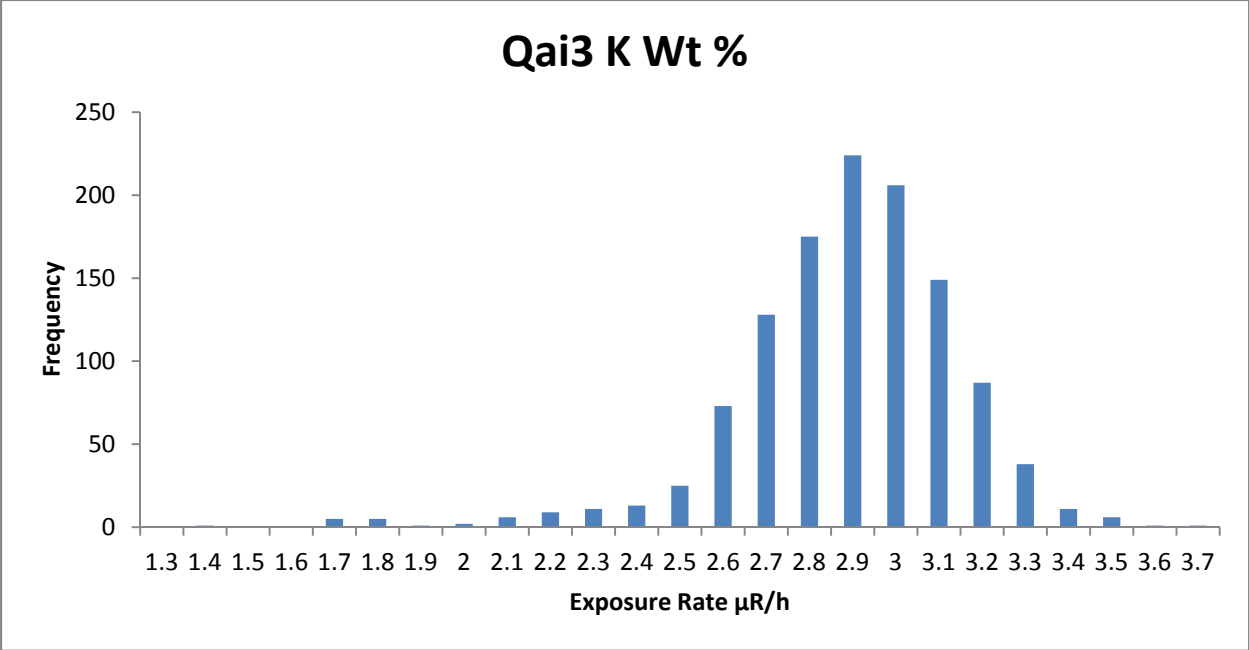
Qai3 is an alluvial unit that is late Pleistocene to early Holocene in age. It is the youngest in a series of relict inactive alluvial fan and terrace surfaces. The unit is graded to past Colorado River levels that were higher than the current surface of Lake Mohave. Bar and swale topography is present in a muted state. Cobble size clasts present on bar crests while lows contain smaller clasts and sand. Strong to moderate desert pavements present across the unit with moderate to dark varnish. (House and Faulds, 2009) Composition varies over the unit. In the southern portion mafic rocks consisting of schist, gabbro and amphibolite are dominate with minor granite, quartzite and red tuffs. The center of the unit is more recently reworked and consists of clasts of primarily basalt with some minor red to white tuff. The northern portion consists primarily of clasts of white tuff.

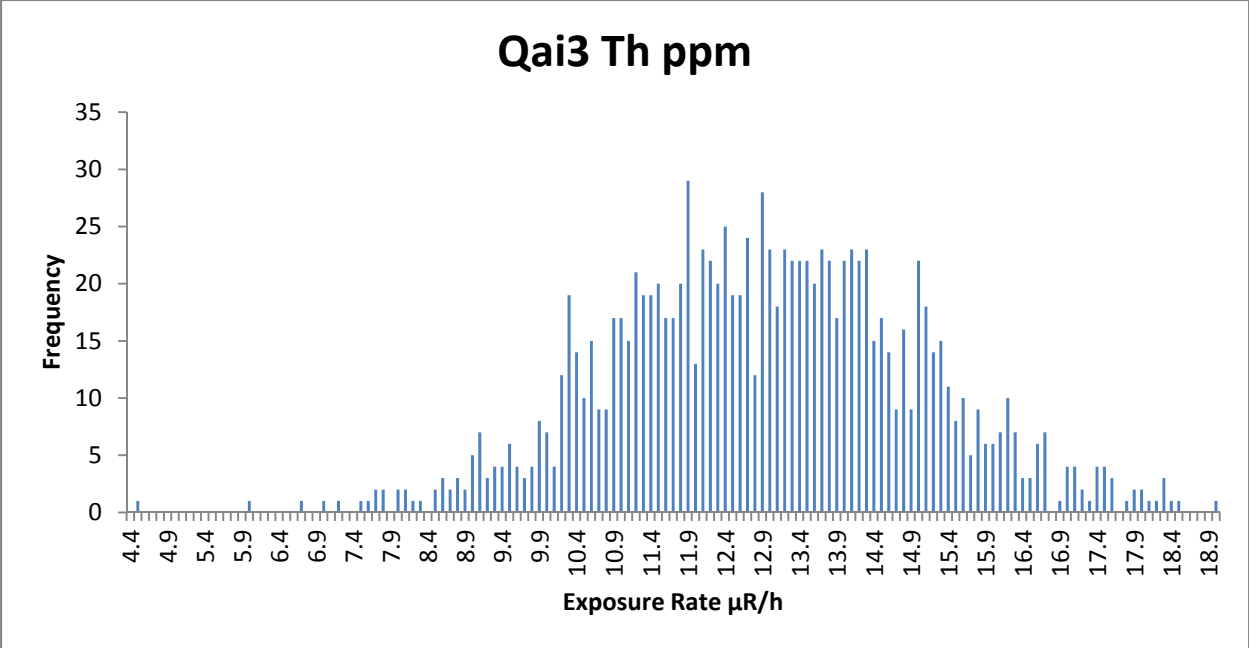
AMS Data

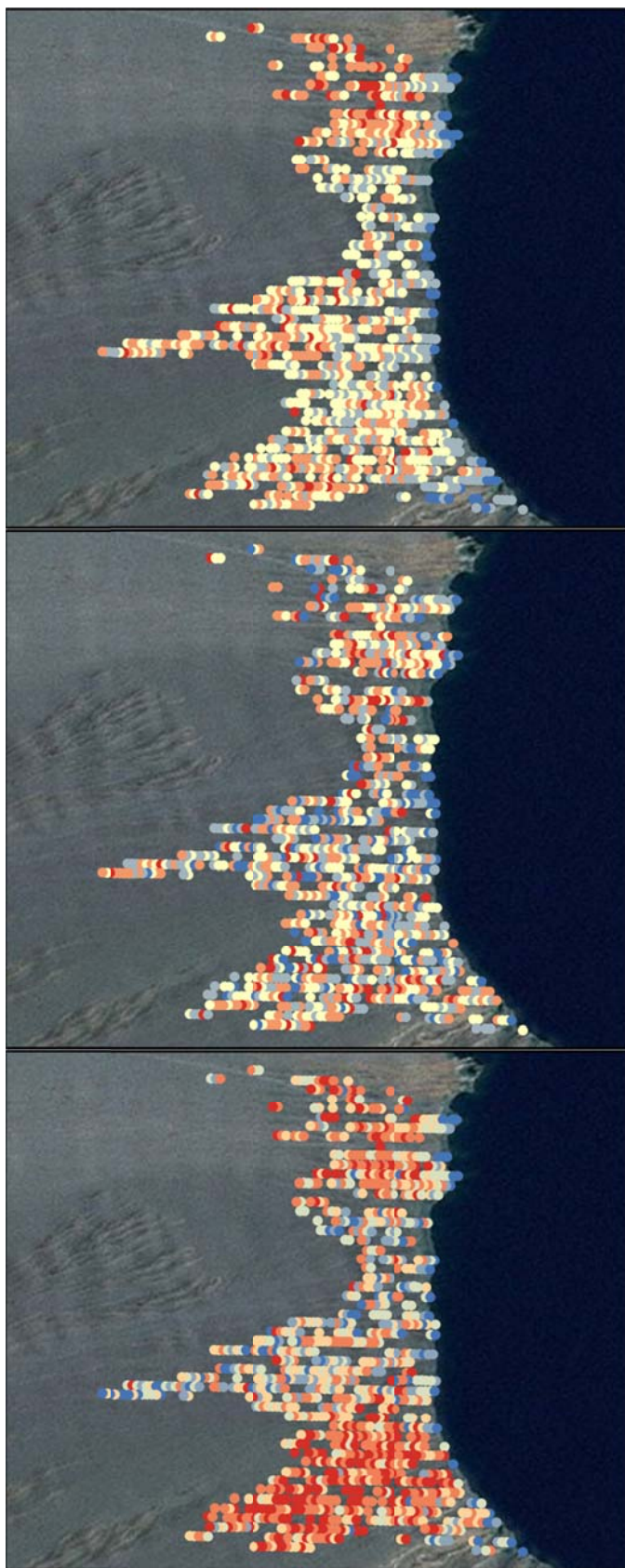
The AMS exposure rate data has a long low exposure tail that represents points near the shore of Lake Mohave that are likely influenced by groundwater. Otherwise there are two main peaks in the data; the first near 8.2 $\mu\text{R/h}$ and the second near 9 $\mu\text{R/h}$. These two peaks represent the cooler center and southern portions of the unit while the higher exposure peak represents the hotter northern portion of the unit and some parts of the southern portion. The average exposure rate is 8.62 $\mu\text{R/h}$ with a standard deviation of 0.63 or 7% of the mean.

K, U, and Th all have distributions that approach normal; however, all of their distributions are widely set. In terms of spatial distribution, K is highest in the northern portion of the unit but is otherwise randomly distributed. Th is high in both the northern and southern portions of the unit and is lower in the cooler center of the unit. U is randomly distributed throughout the unit.









Lake Mohave Radioelement Concentration Images Unit Qai3

K Wt%

- 0.960459 - 2.243253
- 2.243254 - 2.723497
- 2.723498 - 2.956414
- 2.956415 - 3.187128
- 3.187129 - 3.672559

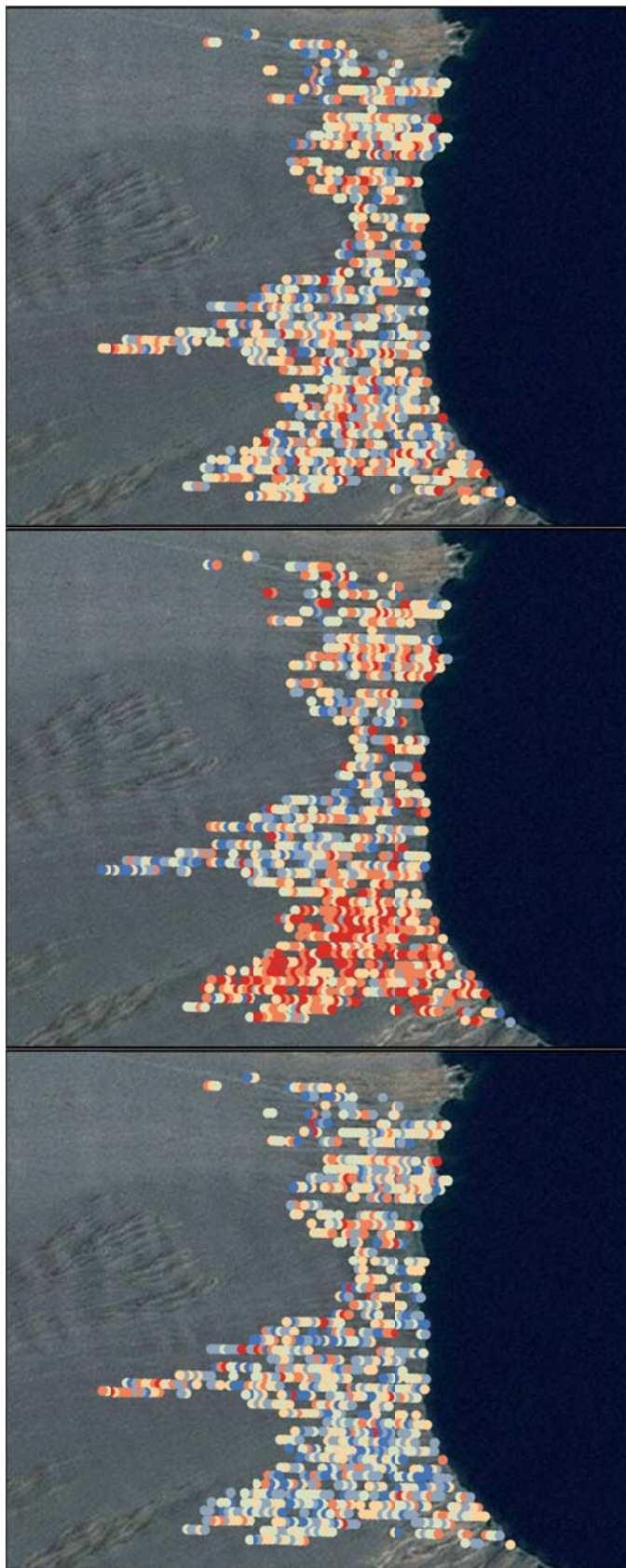
U PPM

- 0 - 1.581498
- 1.581499 - 2.338019
- 2.338020 - 3.035367
- 3.035368 - 3.852008
- 3.852009 - 6.135812

Th PPM

- 4.118740 - 9.969537
- 9.969538 - 10.905588
- 10.905589 - 11.949598
- 11.949599 - 13.168826
- 13.168827 - 14.872976
- 14.872977 - 18.871453





Lake Mohave Radioelement Ratio Images Unit Qai3

U/K Ratio

- 0 - 0.498470
- 0.498471 - 0.745602
- 0.745603 - 0.968045
- 0.968046 - 1.208879
- 1.208880 - 1.542684
- 1.542685 - 3.123242

Th/K Ratio

- 2.090277 - 3.461301
- 3.461302 - 3.942091
- 3.942092 - 4.348792
- 4.348793 - 4.786292
- 4.786293 - 5.355216
- 5.355217 - 8.000000

U/Th Ratio

- 0 - 0.117615
- 0.117616 - 0.182165
- 0.182166 - 0.244454
- 0.244455 - 0.316216
- 0.316217 - 0.426078
- 0.426079 - 0.803350



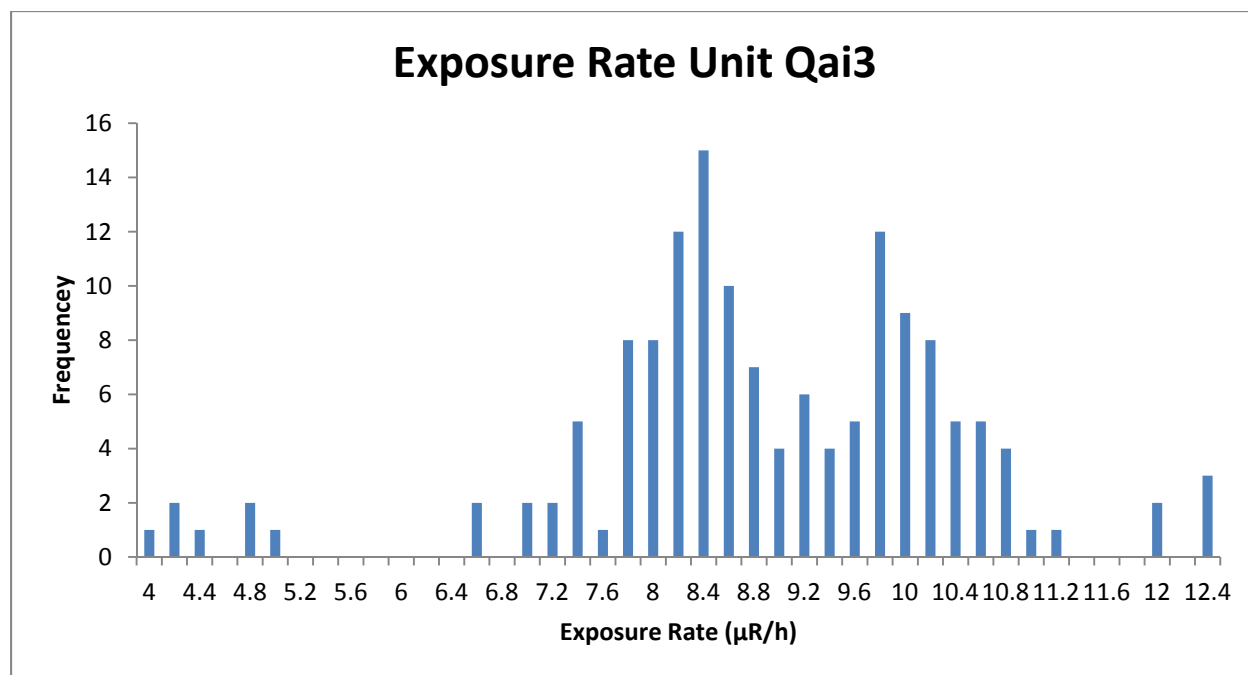
Traditional Geochemistry

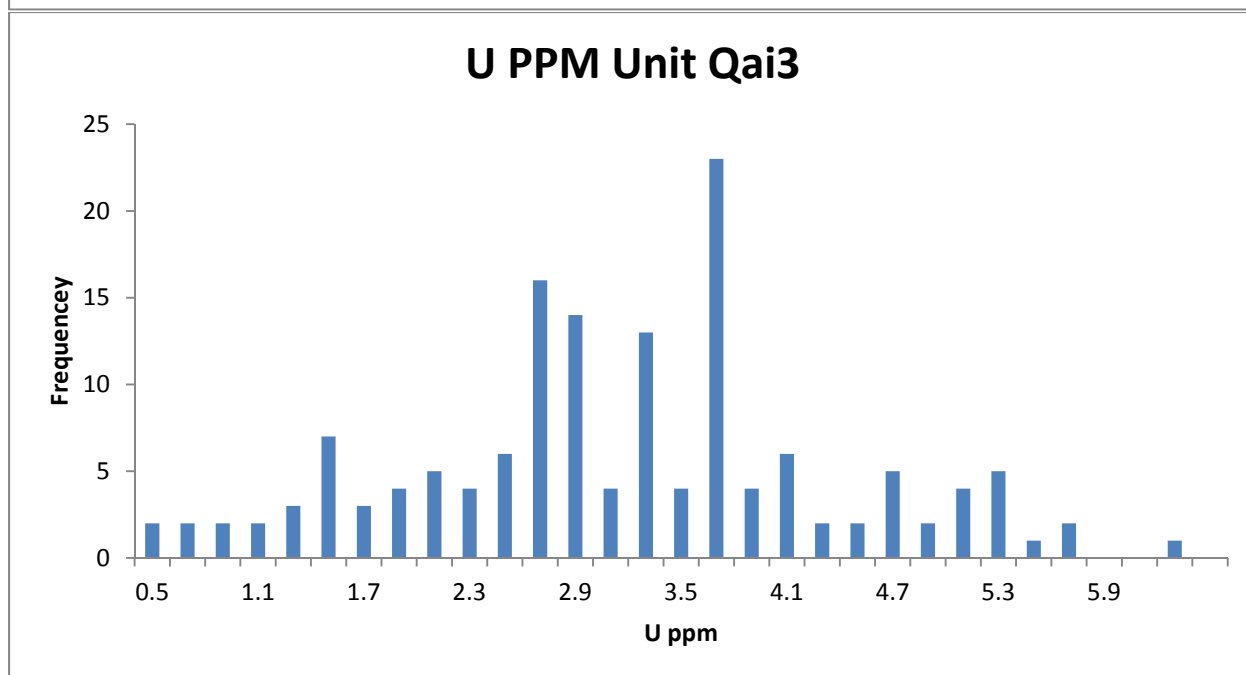
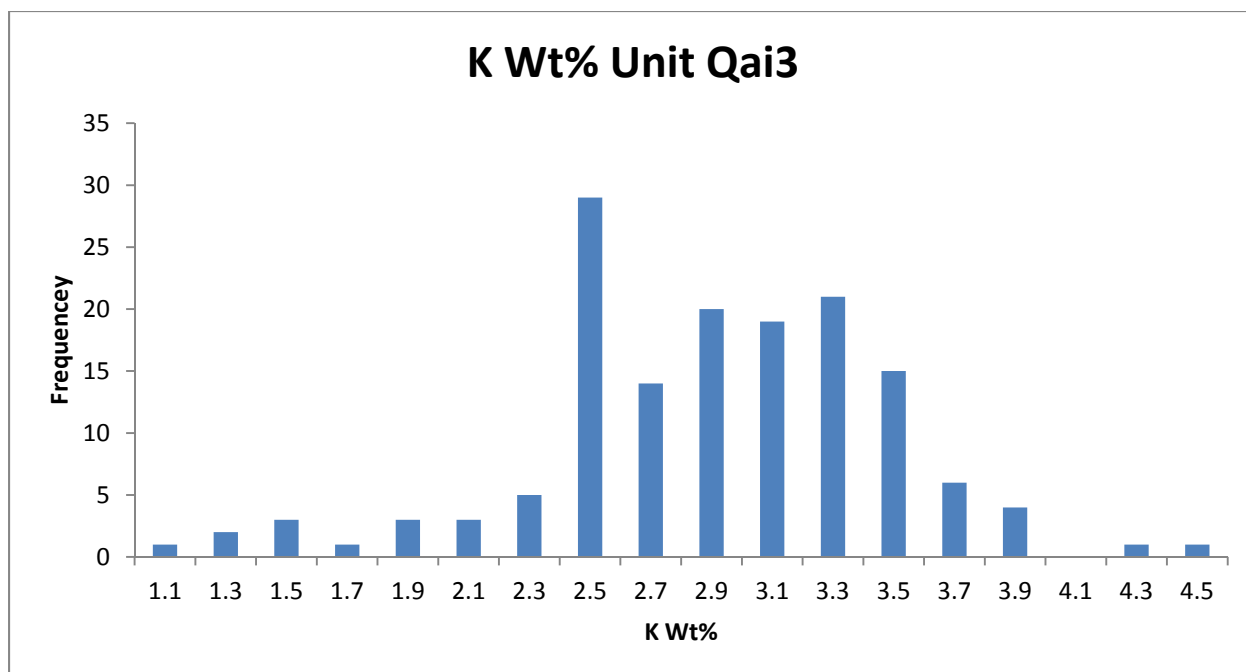
There are no traditional geochemical data available for Qai3.

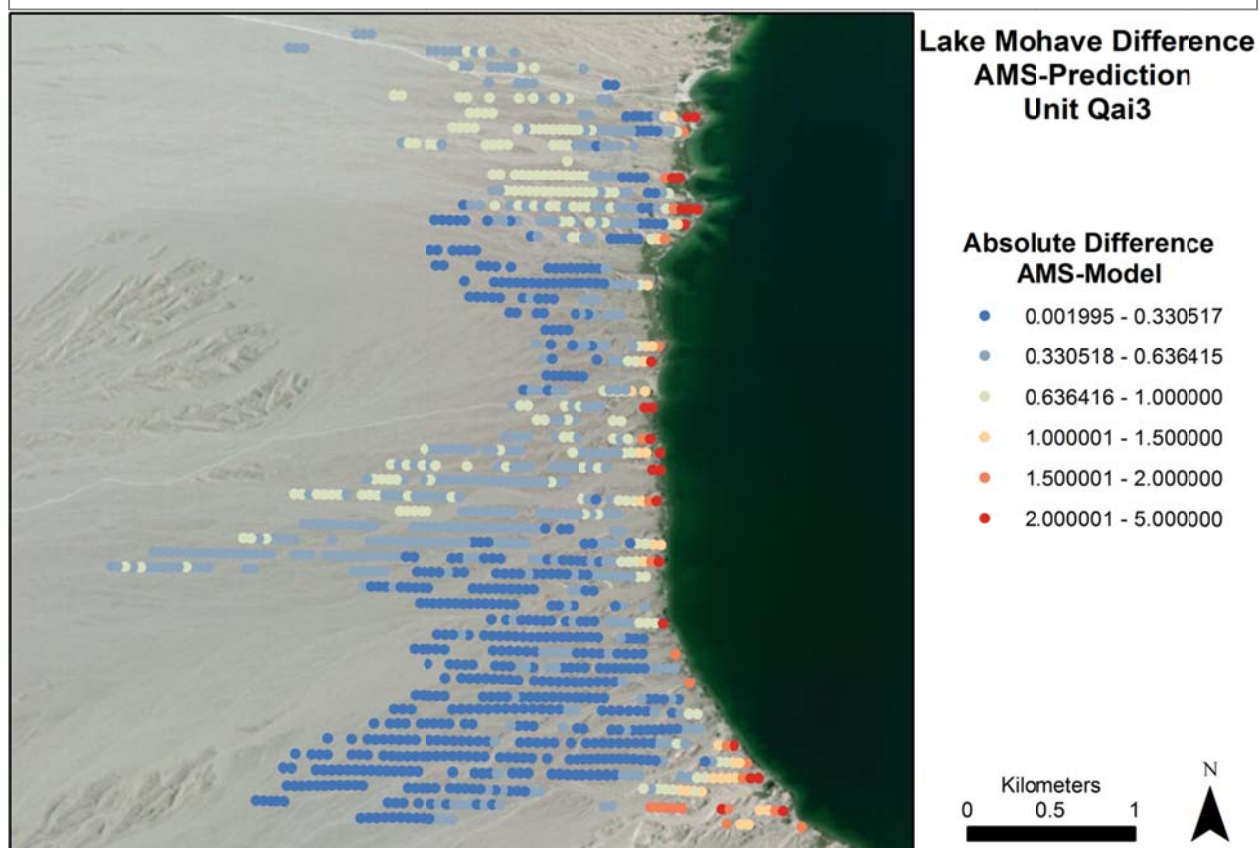
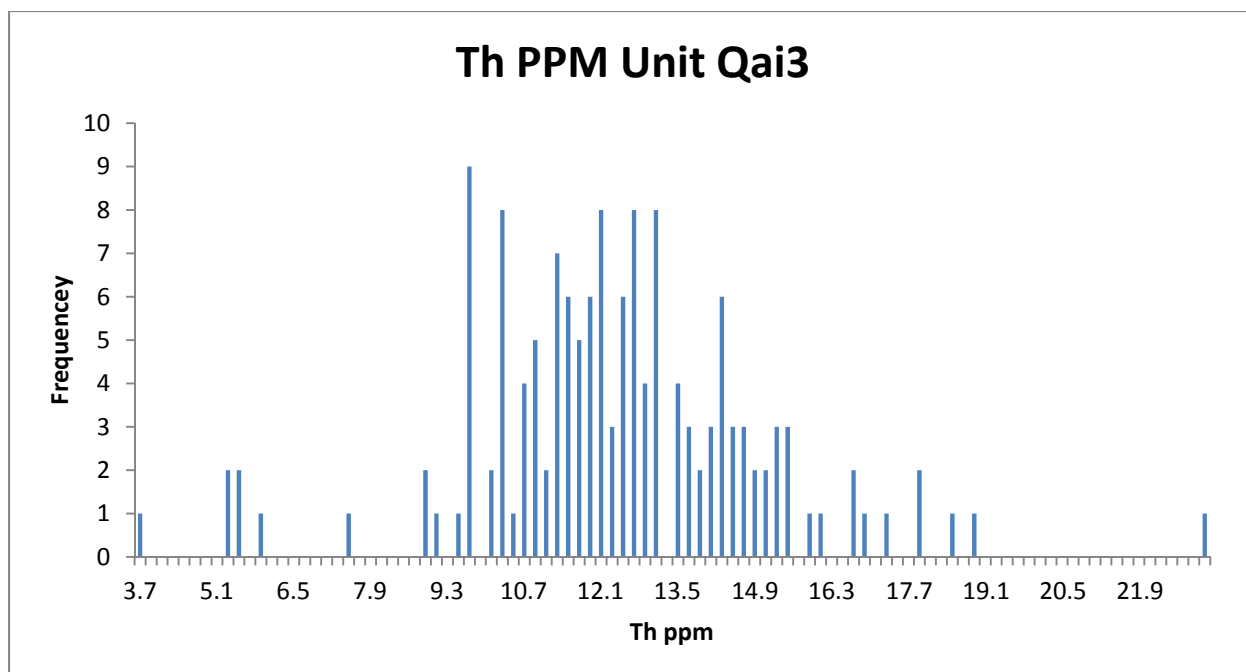
NURE Data

The NURE exposure rate data have two strong peaks near 8.4 $\mu\text{R/h}$ and 9.9 $\mu\text{R/h}$. The average NURE exposure rate is 8.82 $\mu\text{R/h}$ which compares to the AMS exposure average of 8.62 $\mu\text{R/h}$. These exposure values put this unit well into the ± 1 $\mu\text{R/h}$ desired range. K, U, and Th are all widely distributed. The majority of K values are between 2.5 and 3.5%. U values are more widely distributed than K but much of the data is between 2.8 and 3.6 ppm. Th very widely distributed with most of the data occurring between 9.3 and 15 ppm.

When comparing the AMS exposure rate points against the NURE exposure rate most of the unit modeled very well. The southern portion of the unit with moderate exposure rates is modeled best while the cool center and hot northern portion, while still well modeled are further from the NURE model. The points with very low exposure near the shore of Lake Mohave are the least well modeled.







Data Summary

Exposure Rate Comparison μR/h	Average	Median	STD	Range
AMS Data	8.624481	8.6517	0.632859	4.91559-9.76859
NURE Data	8.820435	8.6452	1.526452	4.042-12.4104

Qai1

Composition

Qai is middle to late Pleistocene in age and is a series of relict alluvial fans and terraces that are interbedded with Qch and Qcw. Surfaces have strong desert pavements with dark desert varnish. Strong carbonate development at depth. (House and Faulds, 2009)

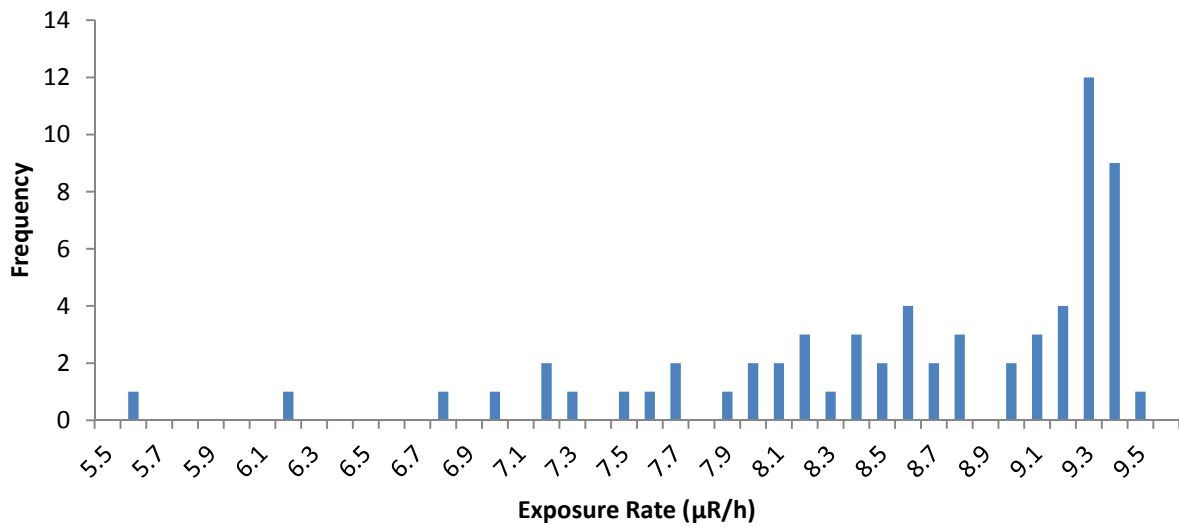
Compositionally, Qai1 is principally composed of clasts of white tuff within the AOI. Composition outside of this area is not well understood.

AMS Data

The exposure rate data for Qai1 has a long low end tail that ends with the majority of the data above 9 $\mu\text{R/h}$. Qai1 extends from the shoreline of Lake Mohave inland toward the west. The points near the shore have low exposure rates while the points further out have much higher exposure rates. This suggests influence on exposure from groundwater near the shore. The average AMS exposure rate for Qai1 is 8.55 $\mu\text{R/h}$ and has a standard deviation of 0.86 or 10% of the mean.

K has a similar low end tail with the majority of the data above 2.8%. U and Th are more widely and randomly distributed. Spatially, K and Th follow a similar pattern to the exposure rate in that the points near the shore have the lowest values while the points farther from shore are much higher. U is more randomly distributed.

AMS Data Unit Qai1



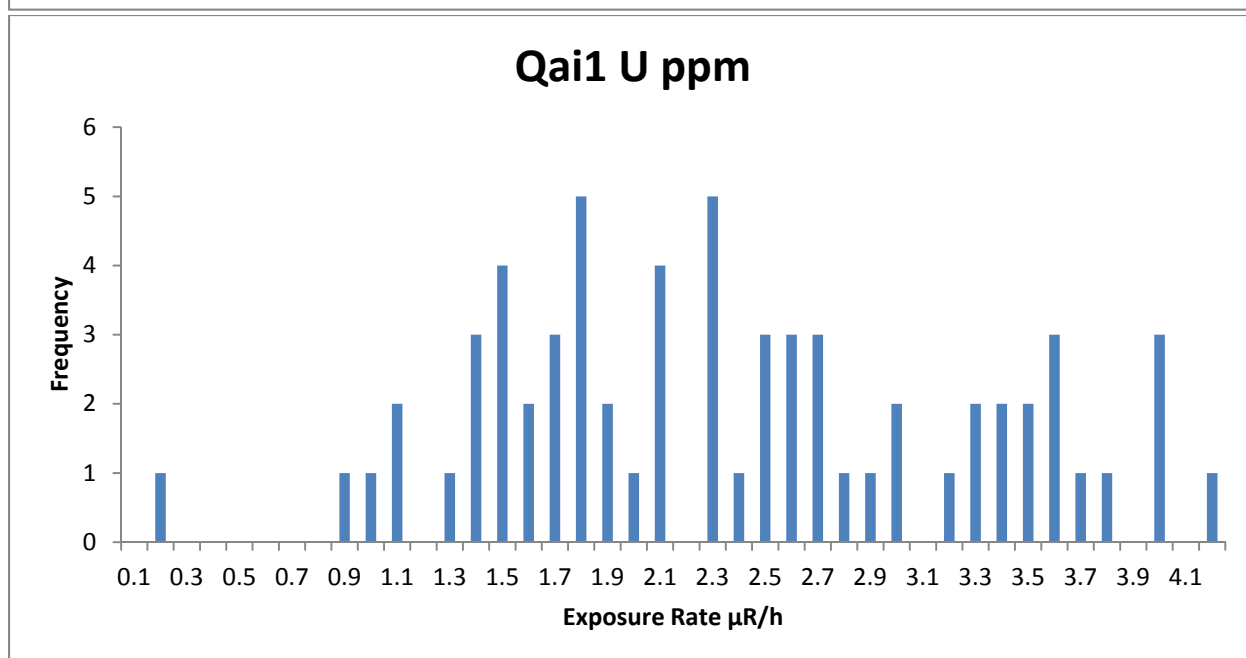
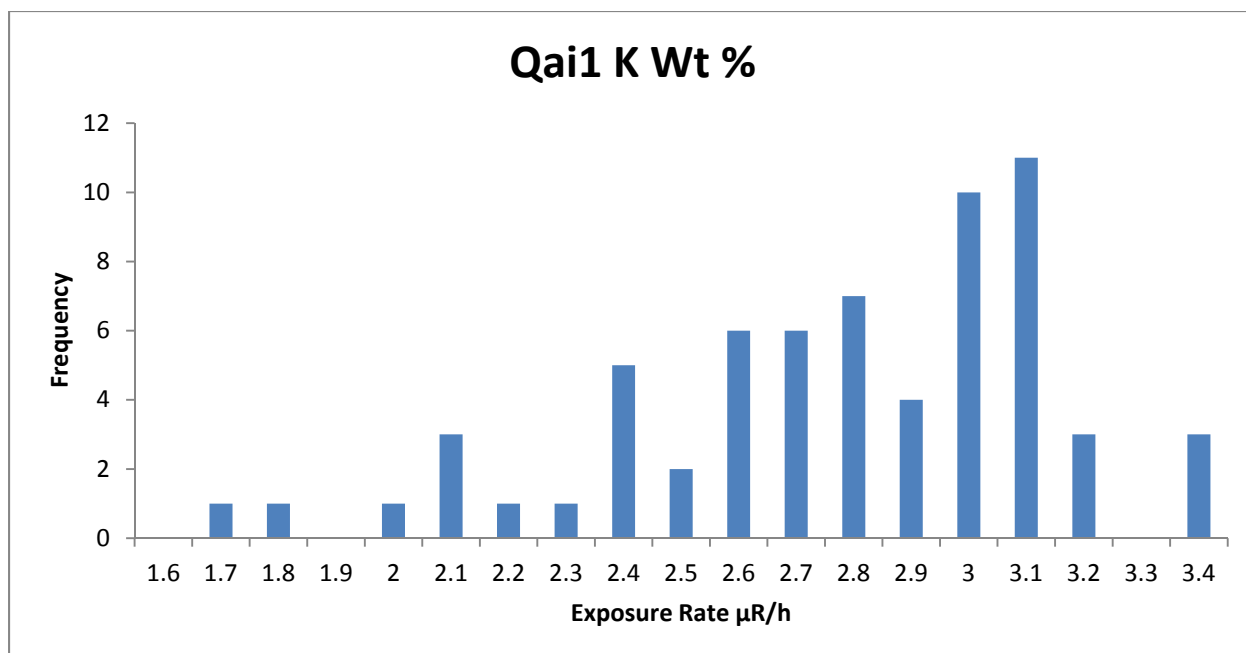
Lake Mohave AMS Data Unit Qai1

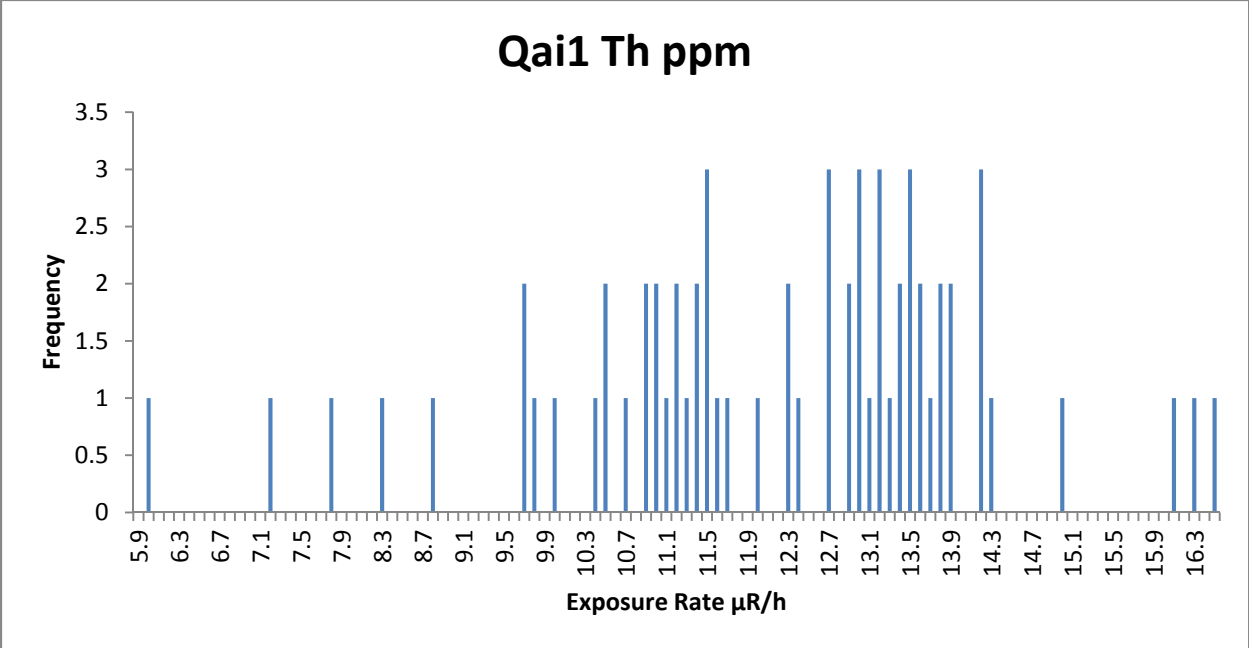
Exposure Rate ($\mu\text{R/h}$)

- 0 - 2.000000
- 2.000001 - 6.000000
- 6.000001 - 6.500000
- 6.500001 - 7.000000
- 7.000001 - 7.500000
- 7.500001 - 8.000000
- 8.000001 - 8.500000
- 8.500001 - 9.000000
- 9.000001 - 9.500000
- 9.500001 - 10.000000
- 10.000001 - 10.500000
- 10.500001 - 13.000000

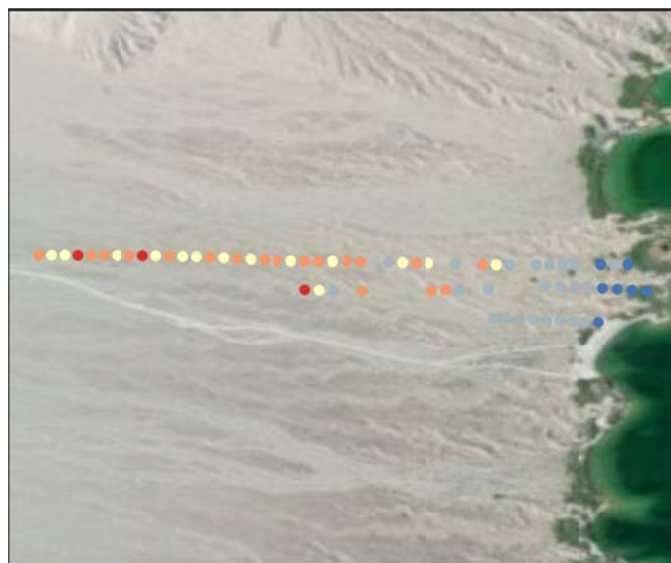
Kilometers
0 0.2 0.4





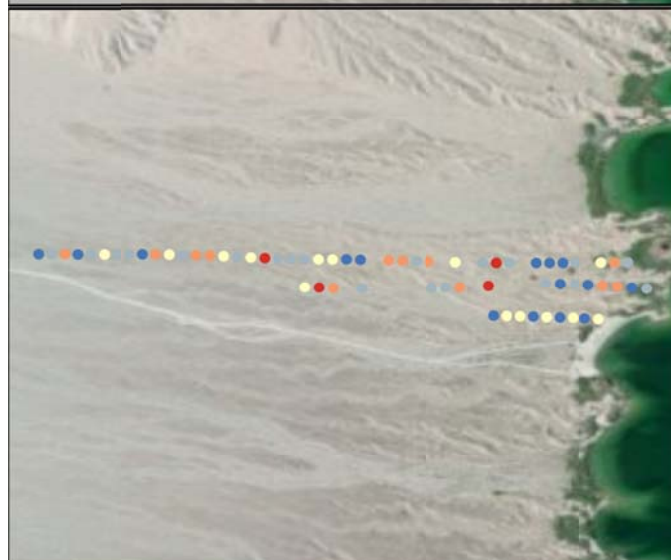


Lake Mohave Radioelement Concentration Images Unit Qai1



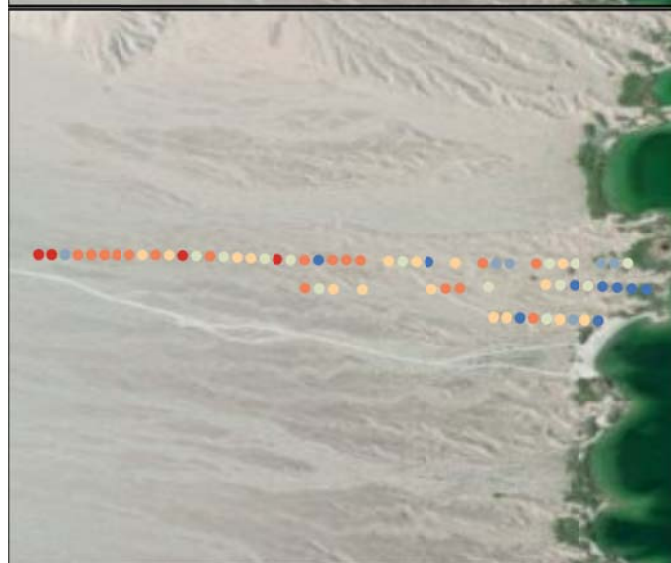
K Wt%

- 0.960459 - 2.243253
- 2.243254 - 2.723497
- 2.723498 - 2.956414
- 2.956415 - 3.187128
- 3.187129 - 3.672559



U PPM

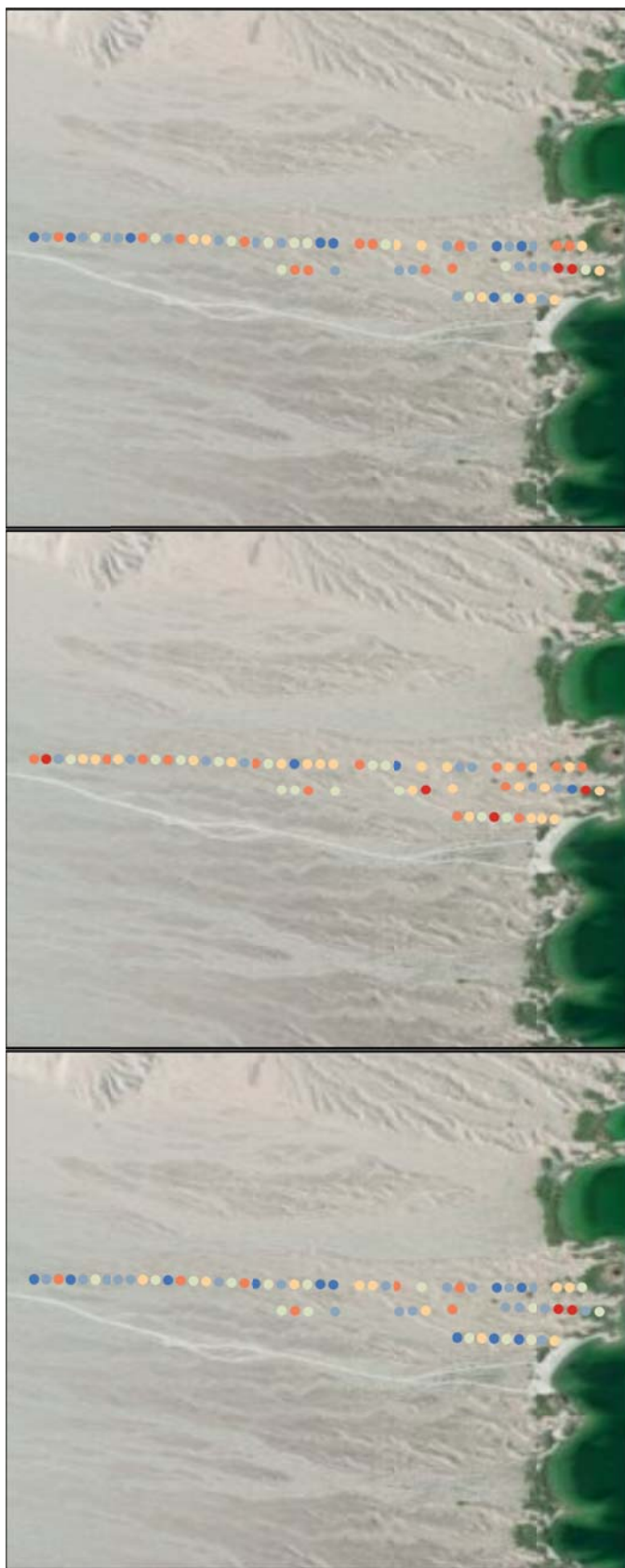
- 0 - 1.581498
- 1.581499 - 2.338019
- 2.338020 - 3.035367
- 3.035368 - 3.852008
- 3.852009 - 6.135812



Th PPM

- 4.118740 - 9.969537
- 9.969538 - 10.905588
- 10.905589 - 11.949598
- 11.949599 - 13.168826
- 13.168827 - 14.872976
- 14.872977 - 18.871453





Lake Mohave Radioelement Ratio Images Unit Qai1

U/K Ratio

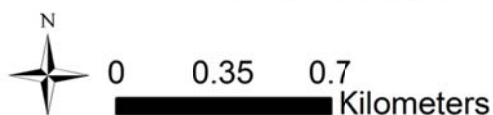
- 0 - 0.498470
- 0.498471 - 0.745602
- 0.745603 - 0.968045
- 0.968046 - 1.208879
- 1.208880 - 1.542684
- 1.542685 - 3.123242

Th/K Ratio

- 2.090277 - 3.461301
- 3.461302 - 3.942091
- 3.942092 - 4.348792
- 4.348793 - 4.786292
- 4.786293 - 5.355216
- 5.355217 - 8.000000

U/Th Ratio

- 0 - 0.117615
- 0.117616 - 0.182165
- 0.182166 - 0.244454
- 0.244455 - 0.316216
- 0.316217 - 0.426078
- 0.426079 - 0.803350



Traditional Geochemistry

There are two traditional geochemical data points that occur within Qai1. K values range from 4 to 4.7%; U values are very similar ranging from 2.8 to 3.01 ppm and Th values range from 17.5 to 18.5 ppm. The exposure rate calculated from these values is 12.28 $\mu\text{R/h}$ which compares with the AMS mean of 8.55 $\mu\text{R/h}$. This does put this unit outside the desired ± 1 $\mu\text{R/h}$ range.

Sample ID	Latitude	Longitude	K %	U ppm	Th ppm
9635	35.4212	-114.943	4.081	3.01	17.52
9650	35.4075	-114.88	4.704	2.8	18.49

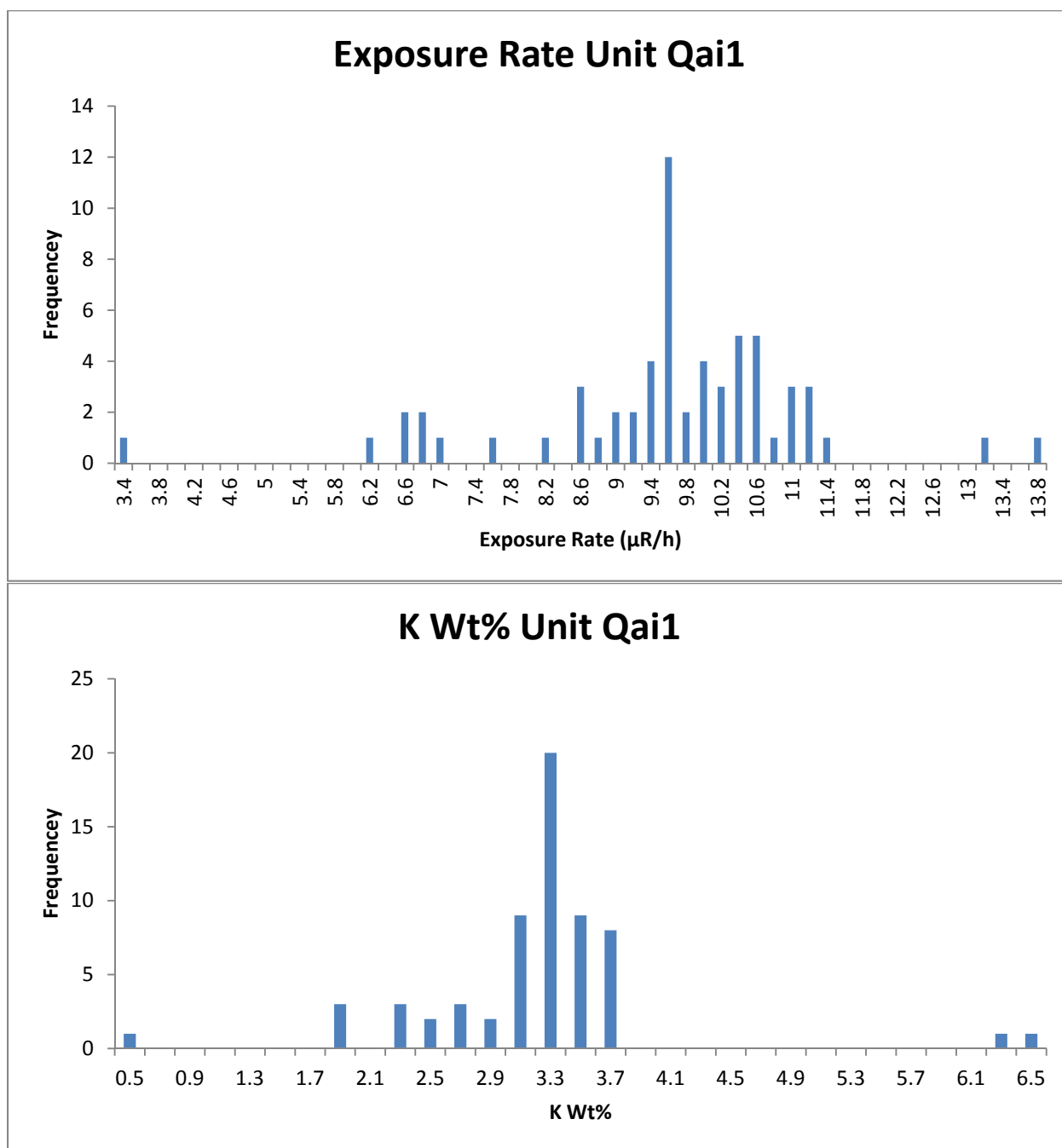
	K%	U ppm	Th ppm
Mean	4.3925	2.905	18.005
Median	4.3925	2.905	18.005
Standard Deviation	0.3115	0.105	0.485
Range	4.081-4.704	2.8-3.01	17.52-18.49

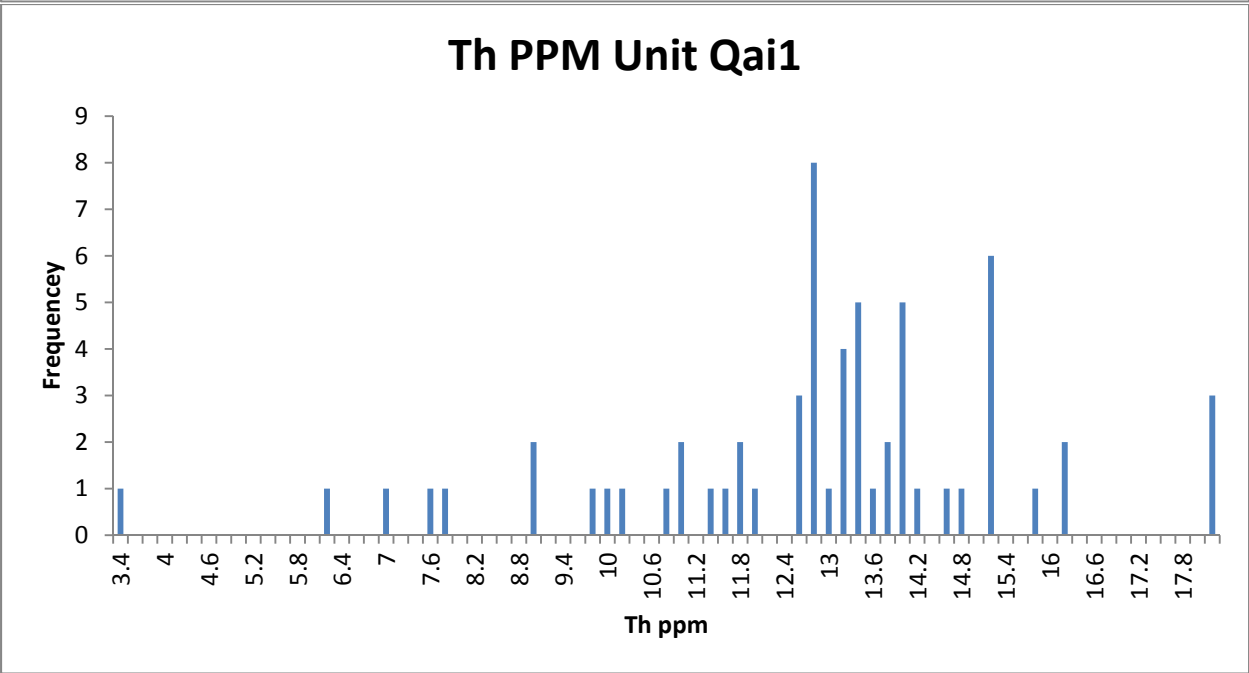
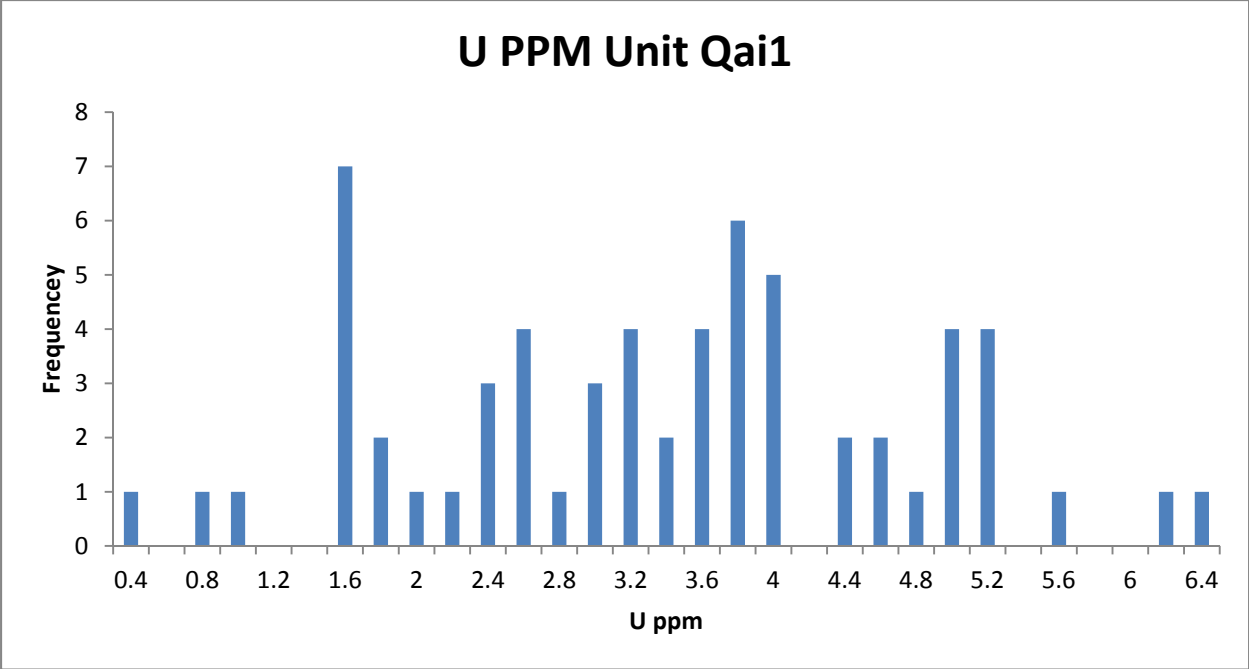
NURE Data

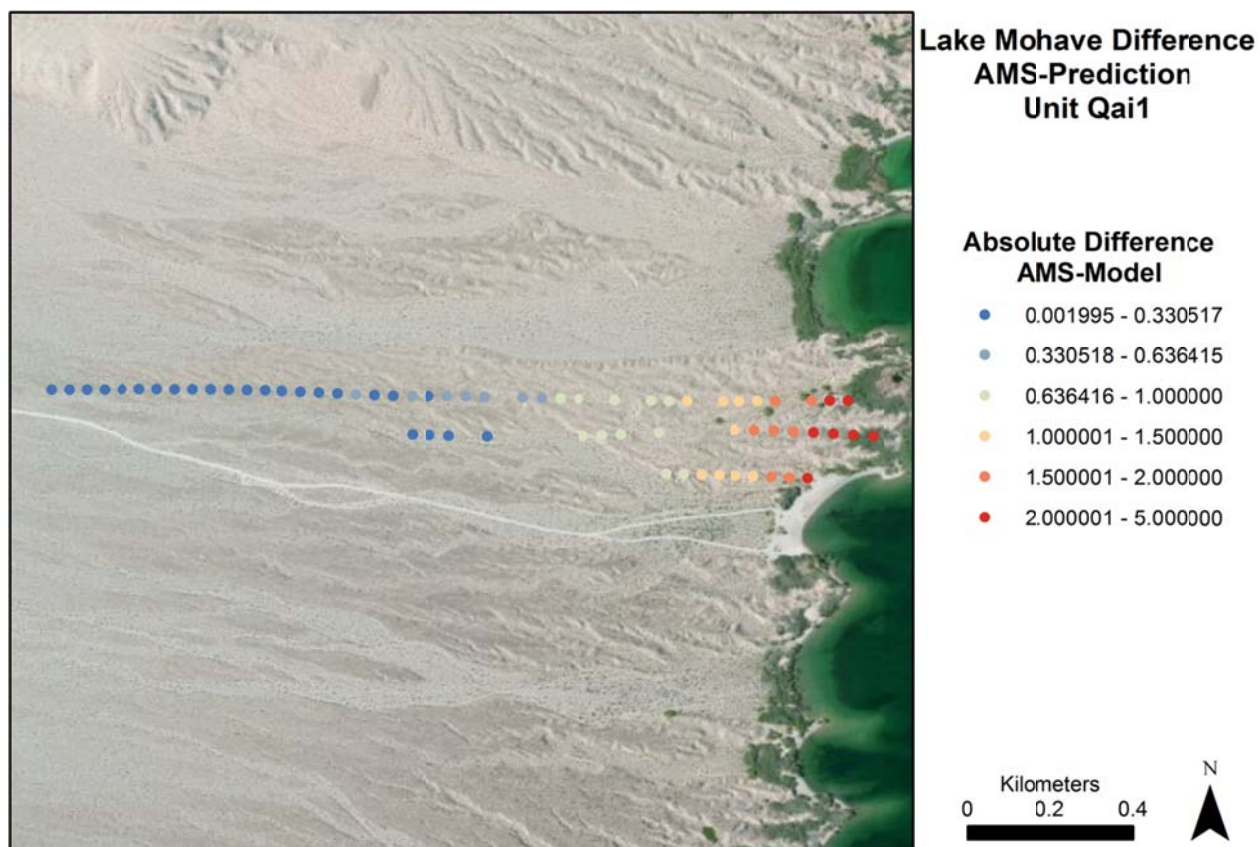
The NURE exposure rate data are widely distributed with the majority of the data falling between 9 and 11 $\mu\text{R/h}$ with a strong peak at 9.6 $\mu\text{R/h}$. The average NURE exposure rate in this unit is 9.48 $\mu\text{R/h}$ which compares with the AMS mean of 8.55 $\mu\text{R/h}$. This is just inside the ± 1 $\mu\text{R/h}$ desired range. However, considering the influence of groundwater on the AMS exposure rate the NURE rate is very close to the majority of the data that sits away from the shore. Overall, this rate fits the majority of the data within the unit. K values mostly sit between 3 and 3.7% while U and Th values are more broadly distributed.

When comparing the NURE exposure rate to the AMS exposure rate data points it is clear that the NURE rate represents the portion of the unit that sits away from the shore very

well. However, points near the shore that exhibit very low exposure rates are not well represented.







Data Summary

Exposure Rate Comparison $\mu\text{R/h}$	Average	Median	STD	Range
AMS Data	8.554239	8.71963	0.860953	5.54778-9.4143
NURE Data	9.482258	9.5676	1.595275	3.3932-13.6244
Geochemical Prediction	12.2874	12.2874	N/A	11.68676-12.88804

Qai

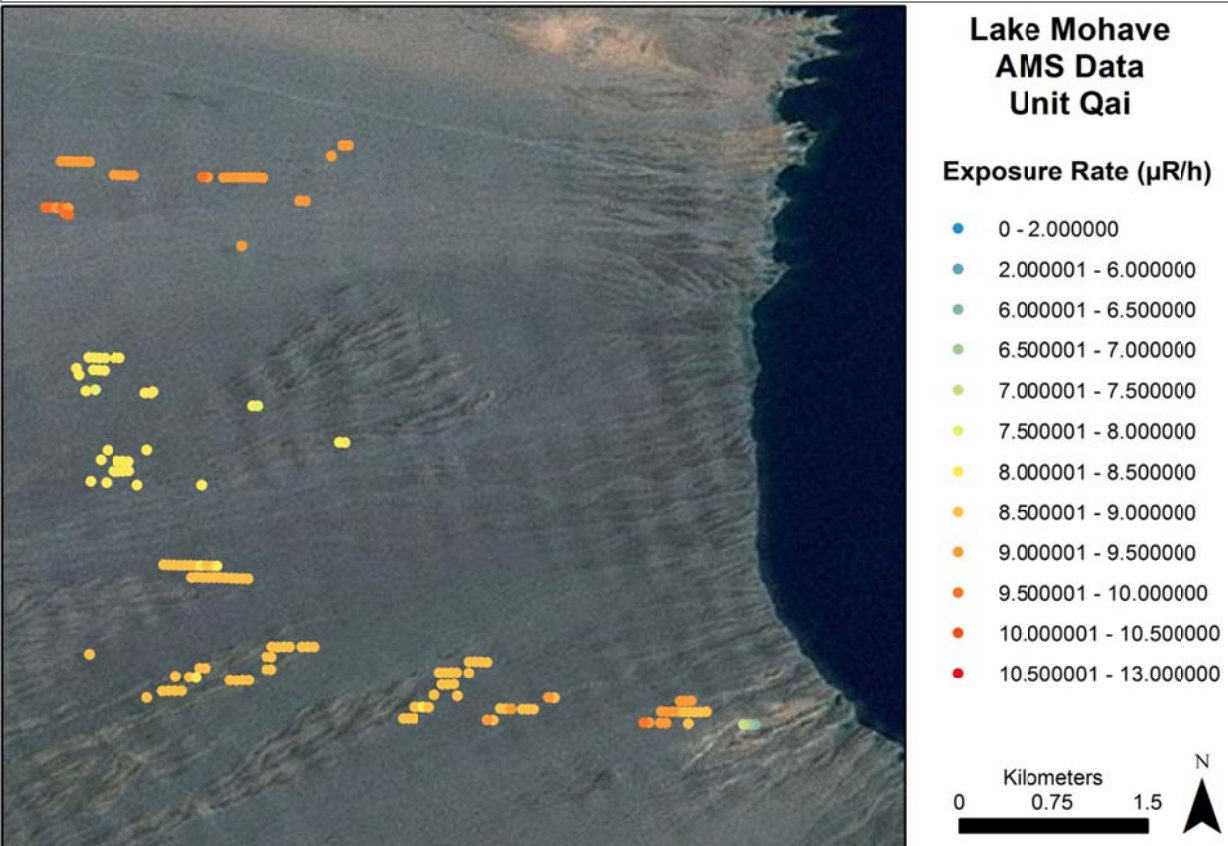
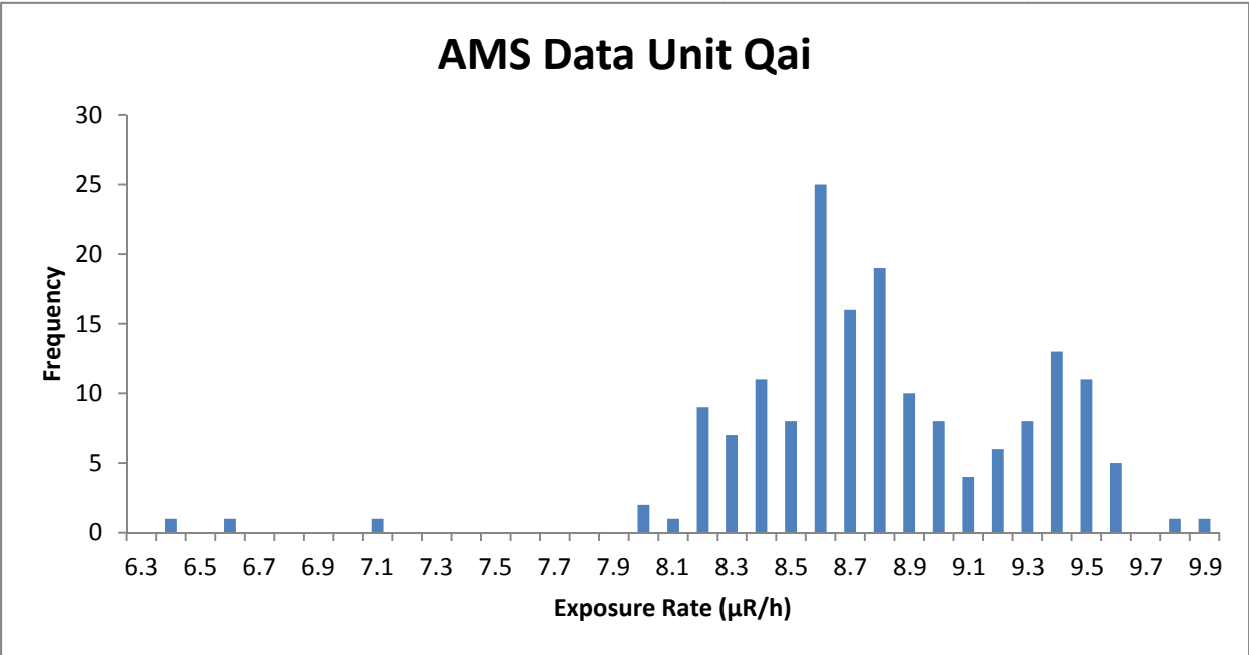
Composition

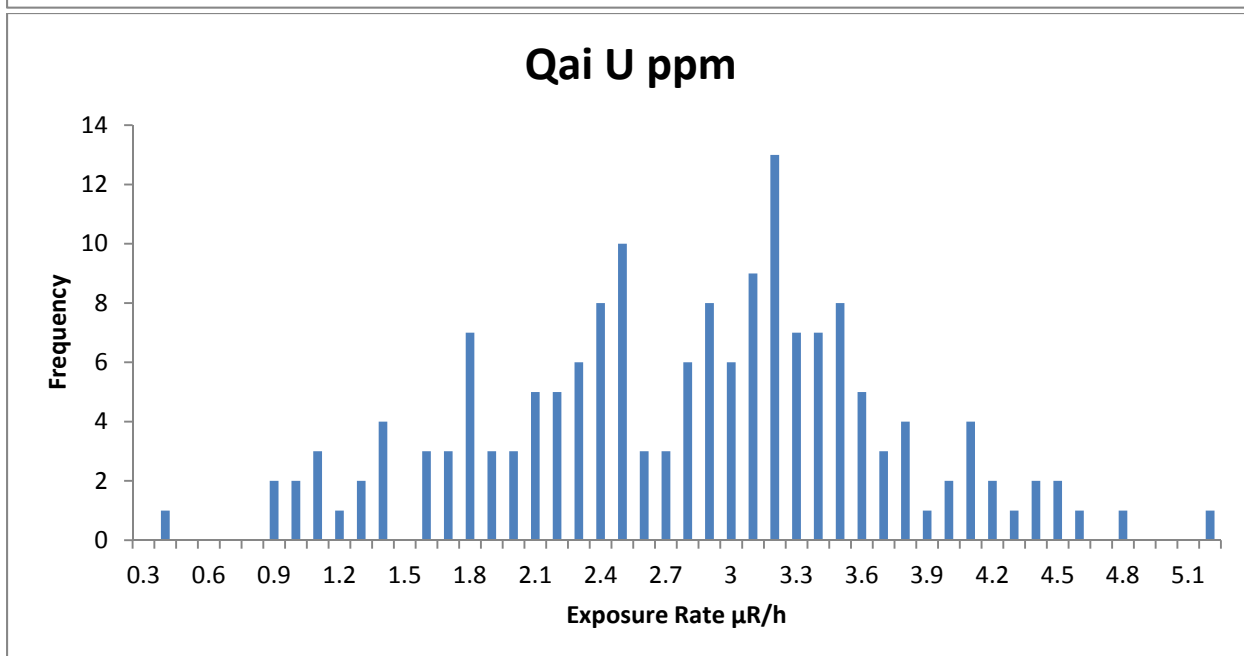
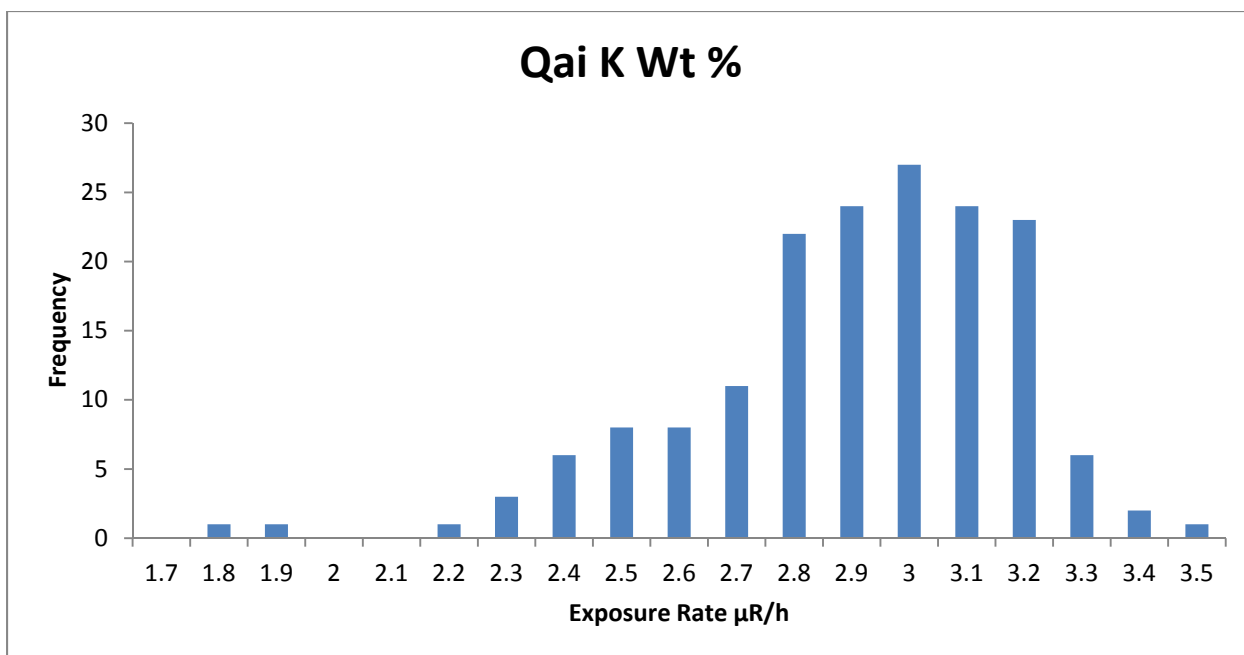
Qai is the oldest Quaternary age relict alluvial deposits. Qai is early Pleistocene in age and truncates Colorado River deposits in Qch and Qcts. The unit contains high standing alluvial terraces that are typically deeply incised. Well devolved desert pavements on terraced surfaces that have dark desert varnish. Very strong carbonate formation at depth. (House and Faulds, 2009) In terms of composition, this unit was not documented during field work and published descriptions do not provide compositional information. However, if this unit follows the trends exhibited in other similar units then the clasts in the south should be largely composed of mafic igneous and metamorphic rocks while further north the unit should be dominated by felsic igneous rocks.

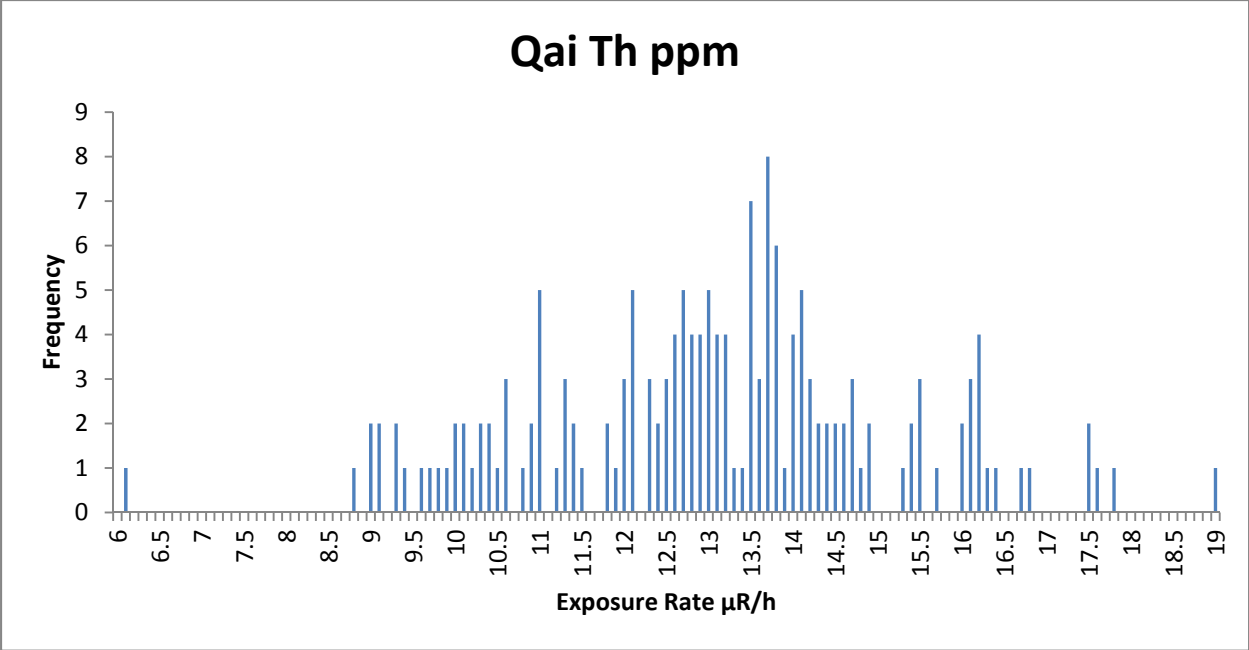
AMS Data

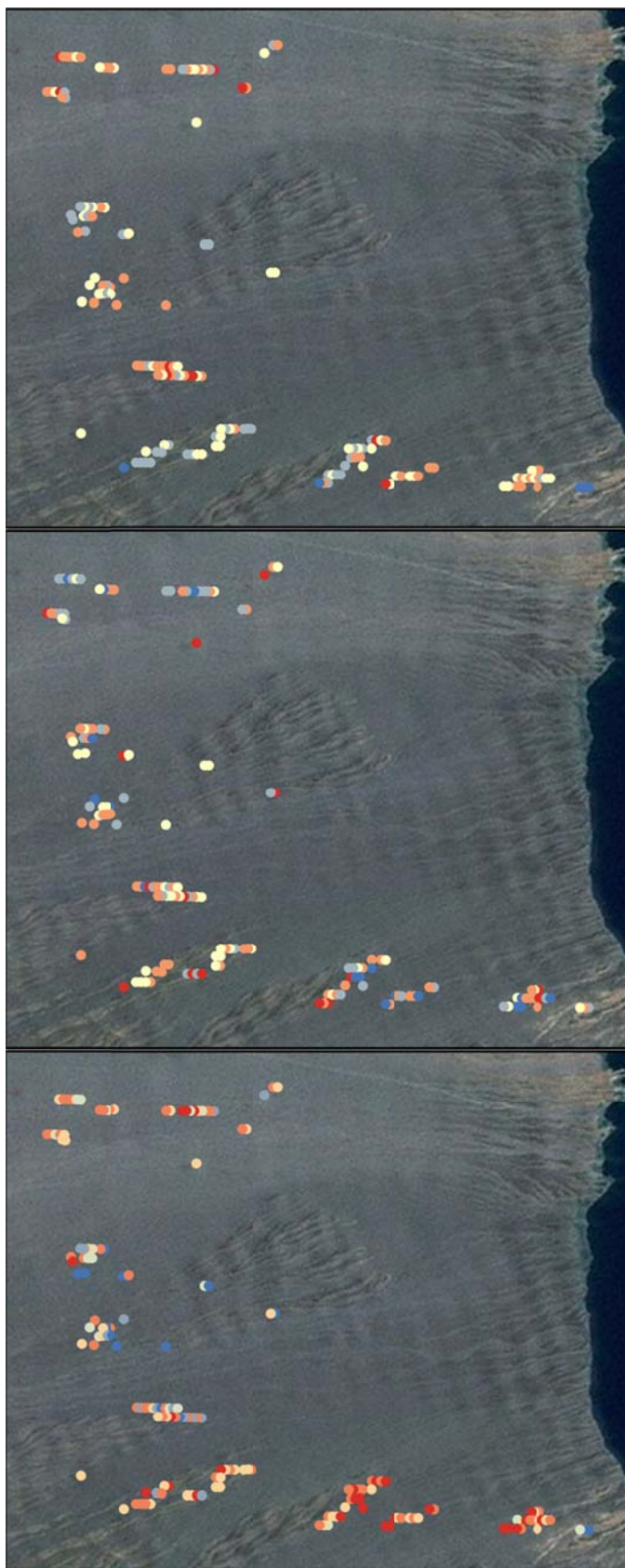
The AMS data in Qai has a strong peak near 8.6 $\mu\text{R/h}$ and a secondary peak near 9.4 $\mu\text{R/h}$. Spatially, the lower peak represents the majority of the southern as well as the central portions of the unit. The secondary peak better represents the hotter portion of the unit in the northern section. The average AMS exposure rate for this unit is 8.75 $\mu\text{R/h}$ with a standard deviation of 0.5 which is 6% of the mean.

K values have a strong center between 2.8 and 3.2% with a significant low end tail. U values are widely spread with peaks at 1.8, 2.5 and 3.2 ppm. Th values are also widely distributed with some significant peaks near 13.5-13.7 ppm. Spatially, K is high in the hotter northern portion of the unit and in other portions with higher exposure rates; U is randomly distributed across the unit; and Th is high in both the northern and southern portions of the unit and low in the center.









Lake Mohave Radioelement Concentration Images Unit Qai

K Wt%

- 0.960459 - 2.243253
- 2.243254 - 2.723497
- 2.723498 - 2.956414
- 2.956415 - 3.187128
- 3.187129 - 3.672559

U PPM

- 0 - 1.581498
- 1.581499 - 2.338019
- 2.338020 - 3.035367
- 3.035368 - 3.852008
- 3.852009 - 6.135812

Th PPM

- 4.118740 - 9.969537
- 9.969538 - 10.905588
- 10.905589 - 11.949598
- 11.949599 - 13.168826
- 13.168827 - 14.872976
- 14.872977 - 18.871453





Lake Mohave Radioelement Ratio Images Unit Qai

U/K Ratio

- 0 - 0.498470
- 0.498471 - 0.745602
- 0.745603 - 0.968045
- 0.968046 - 1.208879
- 1.208880 - 1.542684
- 1.542685 - 3.123242



Th/K Ratio

- 2.090277 - 3.461301
- 3.461302 - 3.942091
- 3.942092 - 4.348792
- 4.348793 - 4.786292
- 4.786293 - 5.355216
- 5.355217 - 8.000000



U/Th Ratio

- 0 - 0.117615
- 0.117616 - 0.182165
- 0.182166 - 0.244454
- 0.244455 - 0.316216
- 0.316217 - 0.426078
- 0.426079 - 0.803350



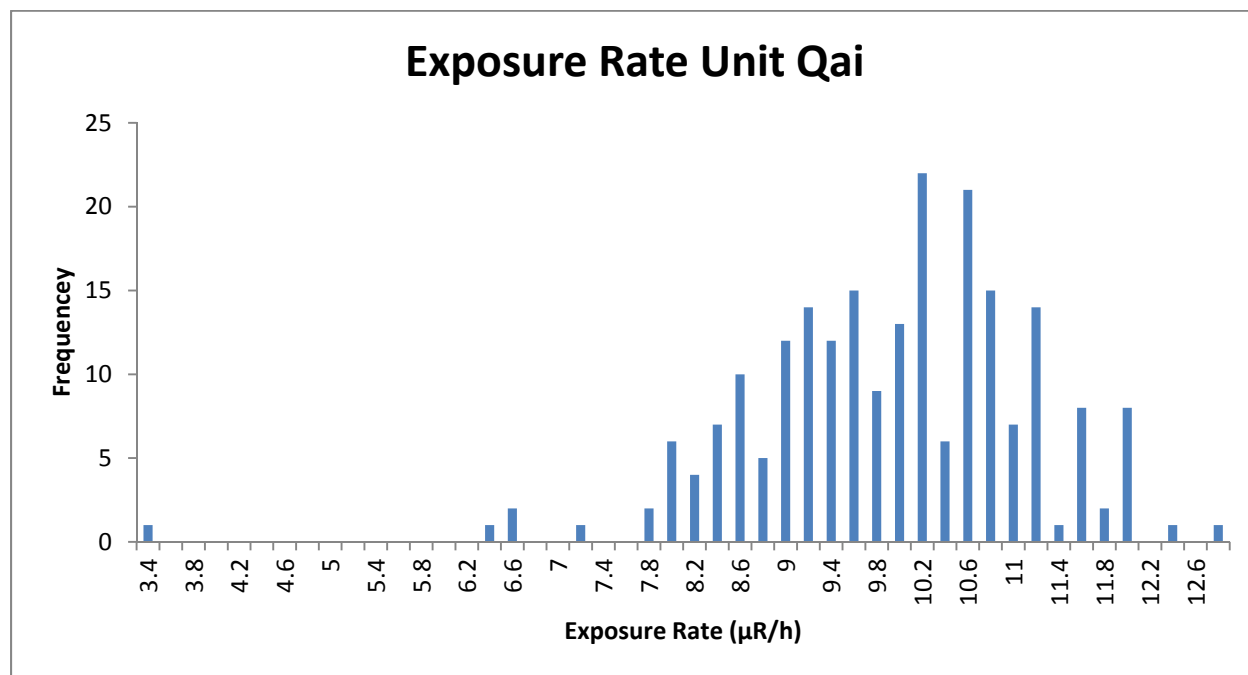
Traditional Geochemistry

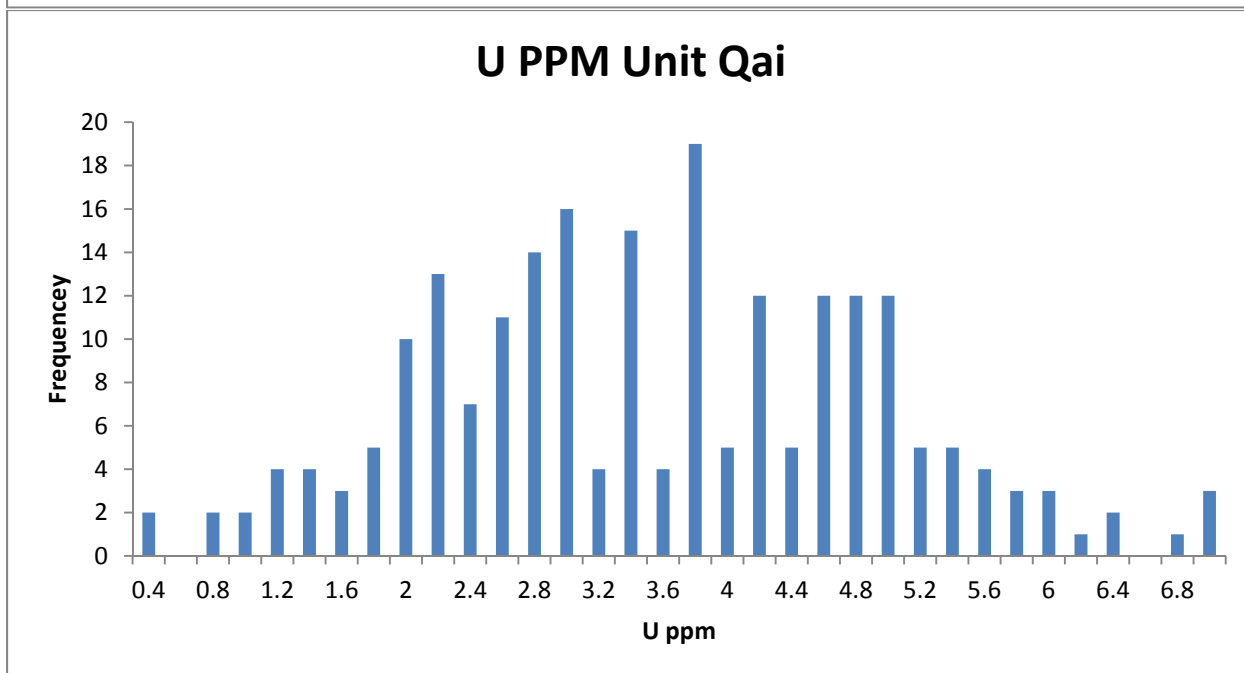
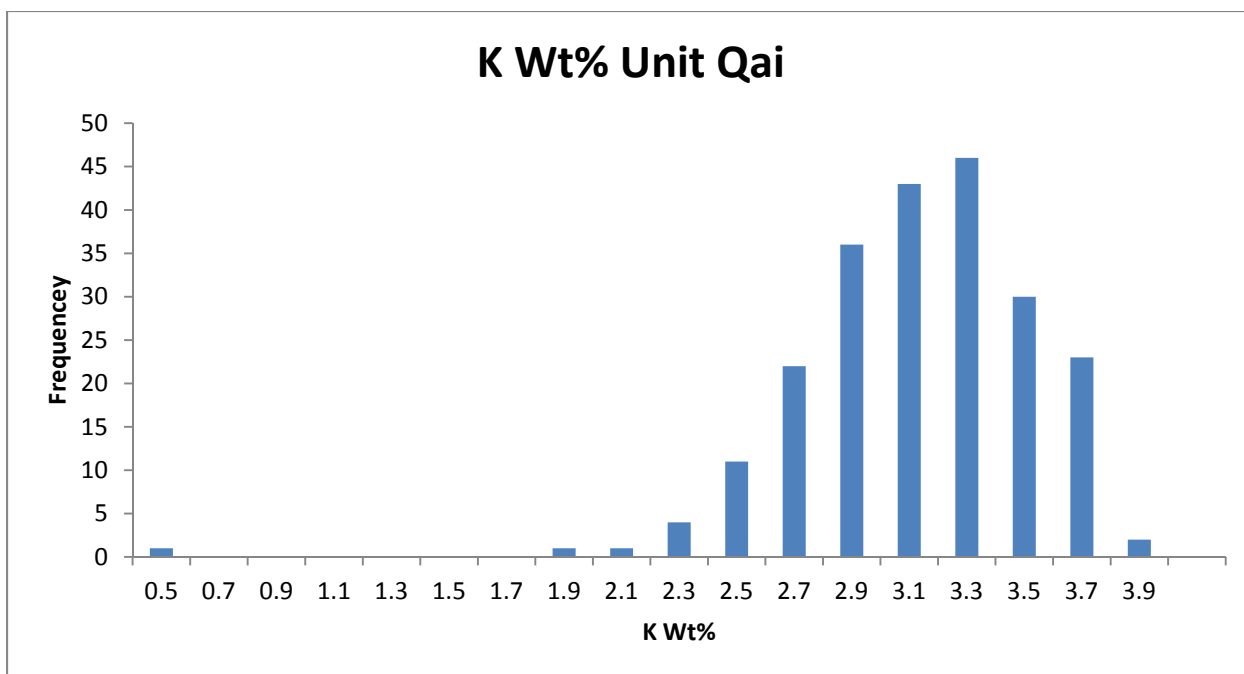
There are no traditional geochemical data for Qai.

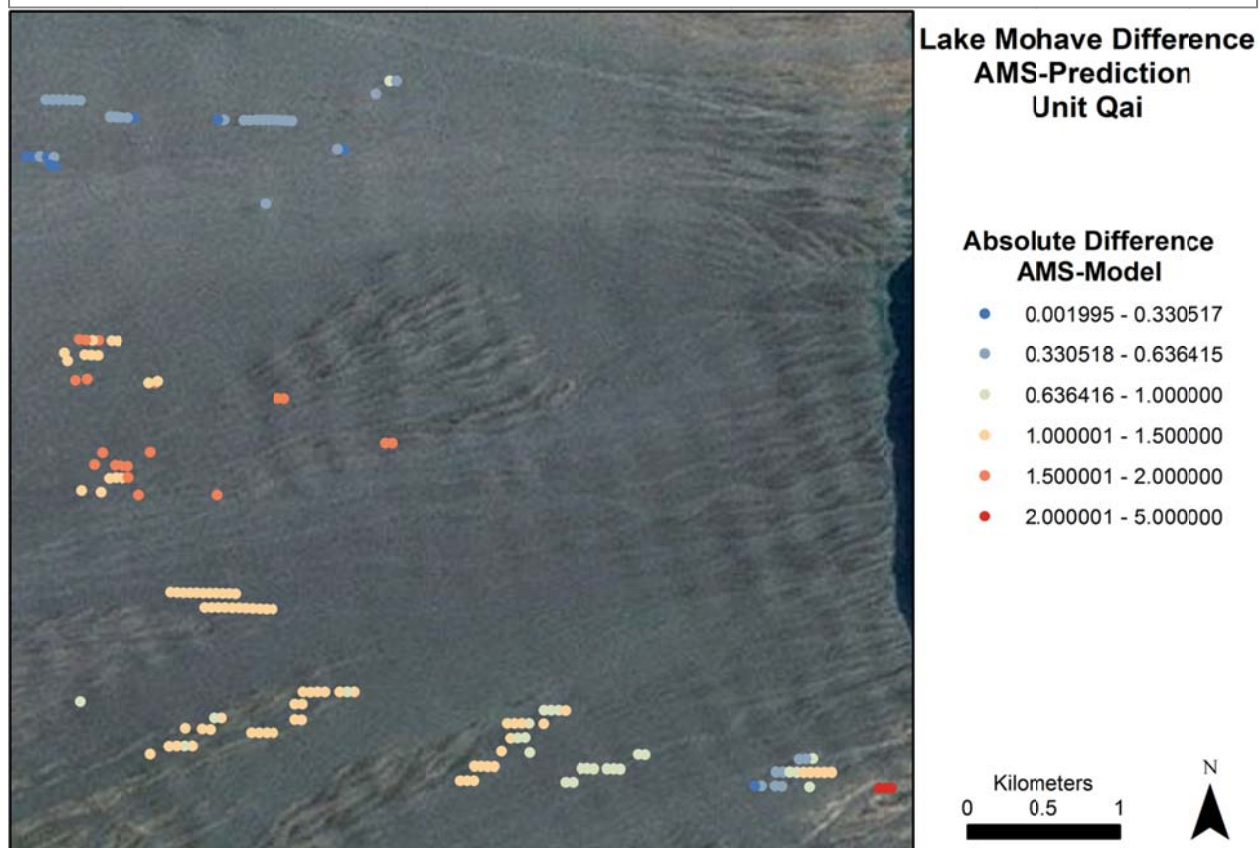
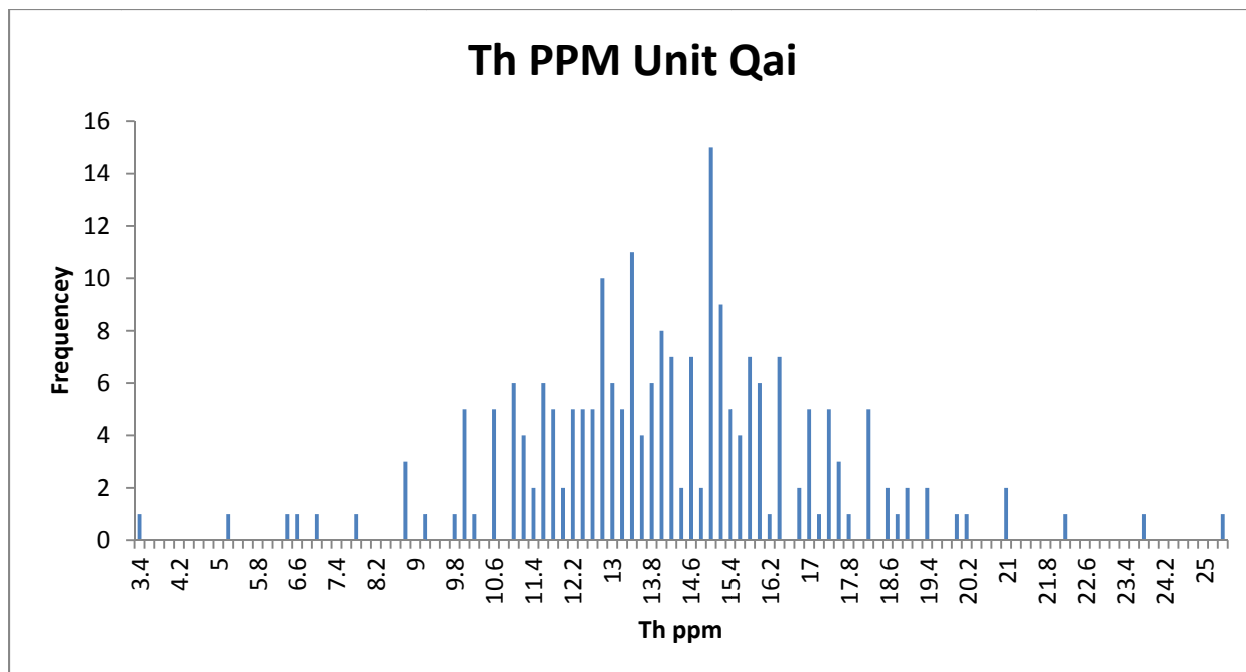
NURE Data

The NURE exposure rate data in Qai is broadly set but has a clear peak in the 10.2-10.6 $\mu\text{R/h}$ range. The average NURE exposure rate is 9.81 $\mu\text{R/h}$ which compares to the AMS mean of 8.75 $\mu\text{R/h}$. This places this unit just within the desired ± 1 $\mu\text{R/h}$ range. The distribution of K values is very similar in the NURE and AMS data. Most of the NURE K values are between 2.7 and 3.5%. The U values are fairly evenly spread among a broad distribution with the majority of the data between 2 and 5 ppm. The values are also widely distributed with the majority of the data falling between 10.5 and 18 ppm.

Comparing the NURE derived exposure rate to the AMS data points the hotter portion of the unit in the north appears to be represented best. The central and southern portions are generally below the ± 1 $\mu\text{R/h}$ range but are generally much closer to the edge.







Data Summary

Exposure Rate Comparison μR/h	Average	Median	STD	Range
AMS Data	8.755665	8.71646	0.507095	6.36096-9.85464
NURE Data	9.811149	9.9304	1.214169	3.3932-12.614

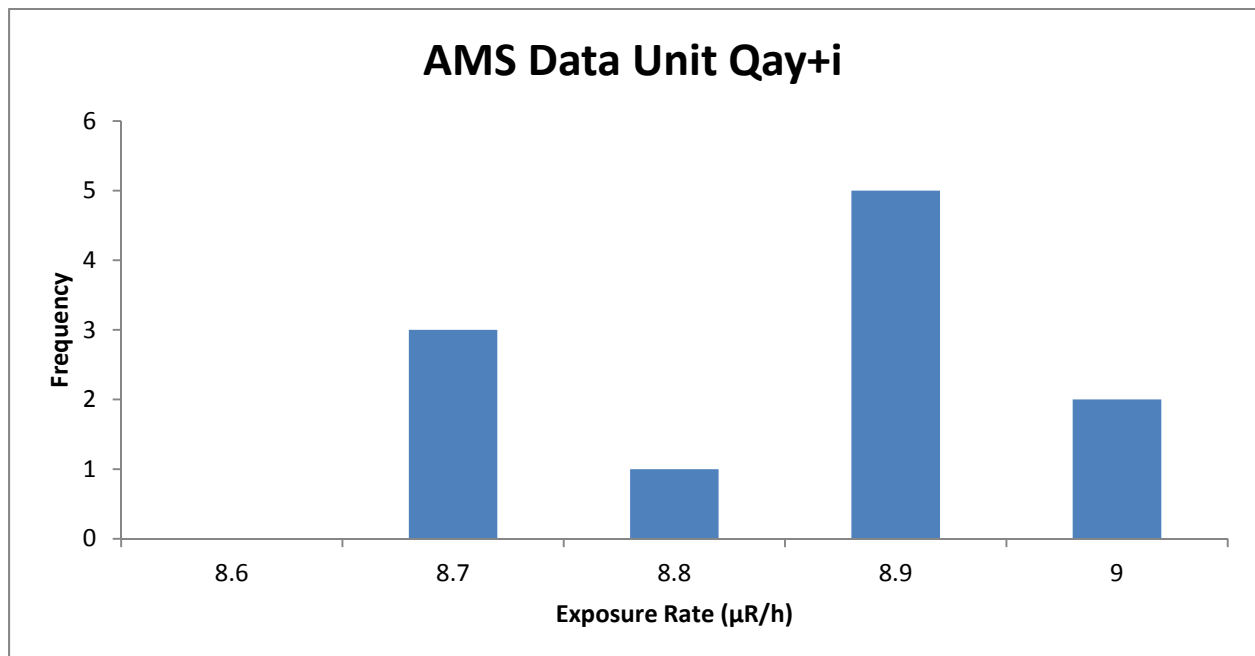
Qay+i

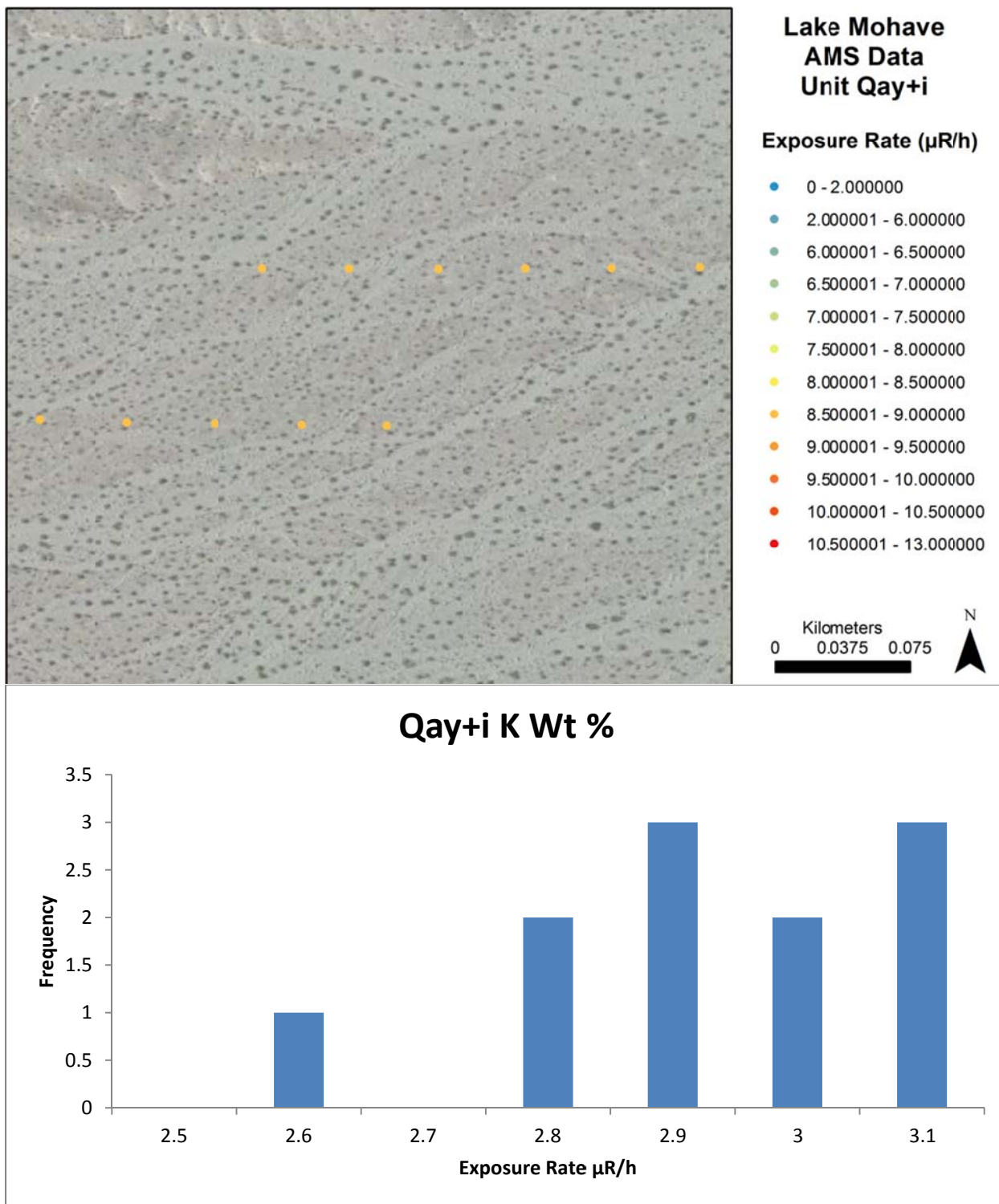
Composition

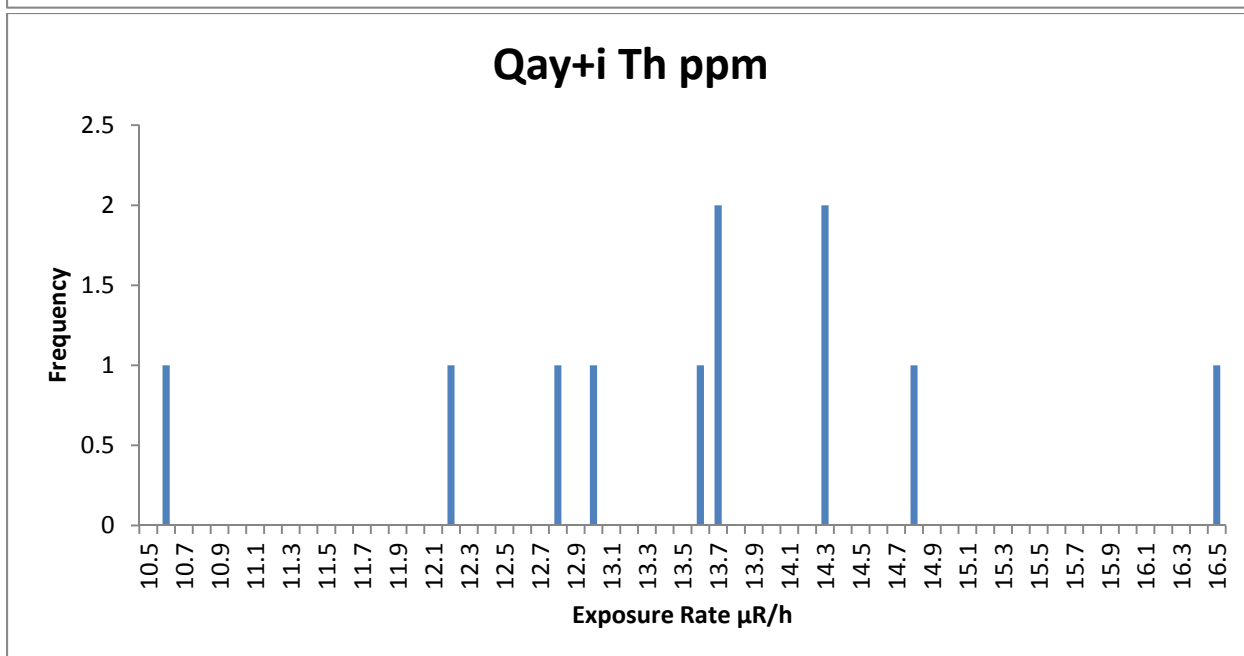
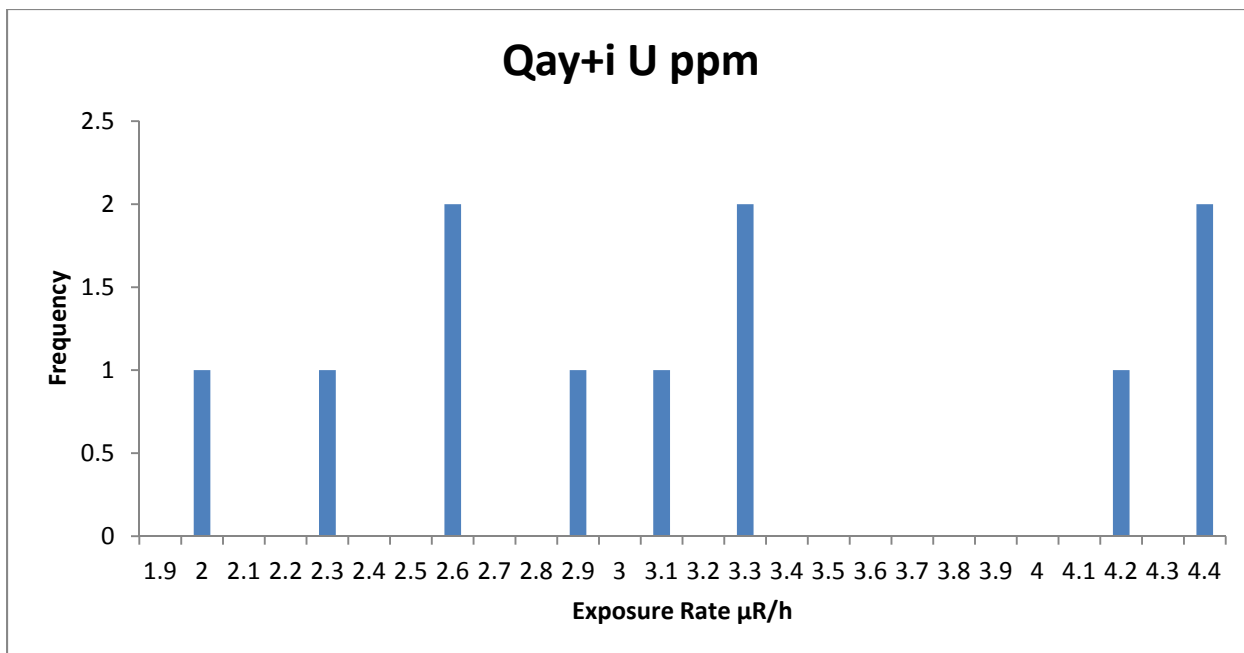
Qay+i is a mixed unit that contains both Qay and Qai deposits. It ranges in age from Holocene to Pleistocene. In this unit Qay is the dominate contributor. (House and Faulds, 2009) Compositional information is unknown but can likely be compared to units Qay and Qai.

AMS Data

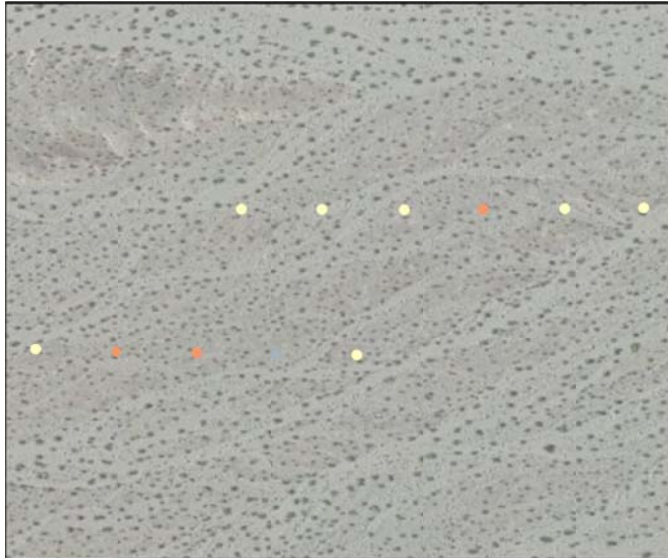
The AMS data in this unit is limited due to the limited spatial extent of this unit. Generally, histograms of exposure, K, U, and Th are featureless and provide little insight into this unit. The average AMS exposure rate in this unit is 8.81 $\mu\text{R/h}$ with a standard deviation of 0.1 or 1% of the mean. There are no clear patterns to the spatial distribution of exposure rate, K, U, or Th.





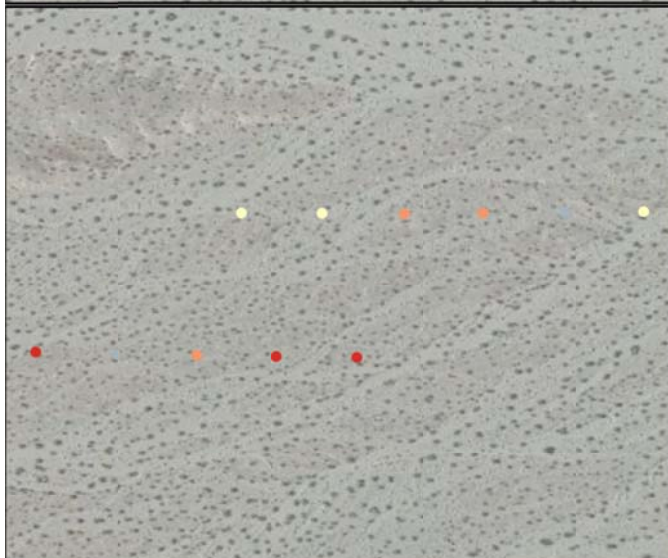


Lake Mohave Radioelement Concentration Images Unit Qay+i



K Wt%

- 0.960459 - 2.243253
- 2.243254 - 2.723497
- 2.723498 - 2.956414
- 2.956415 - 3.187128
- 3.187129 - 3.672559



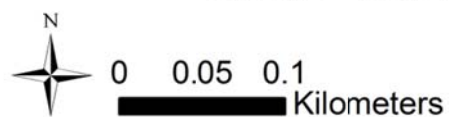
U PPM

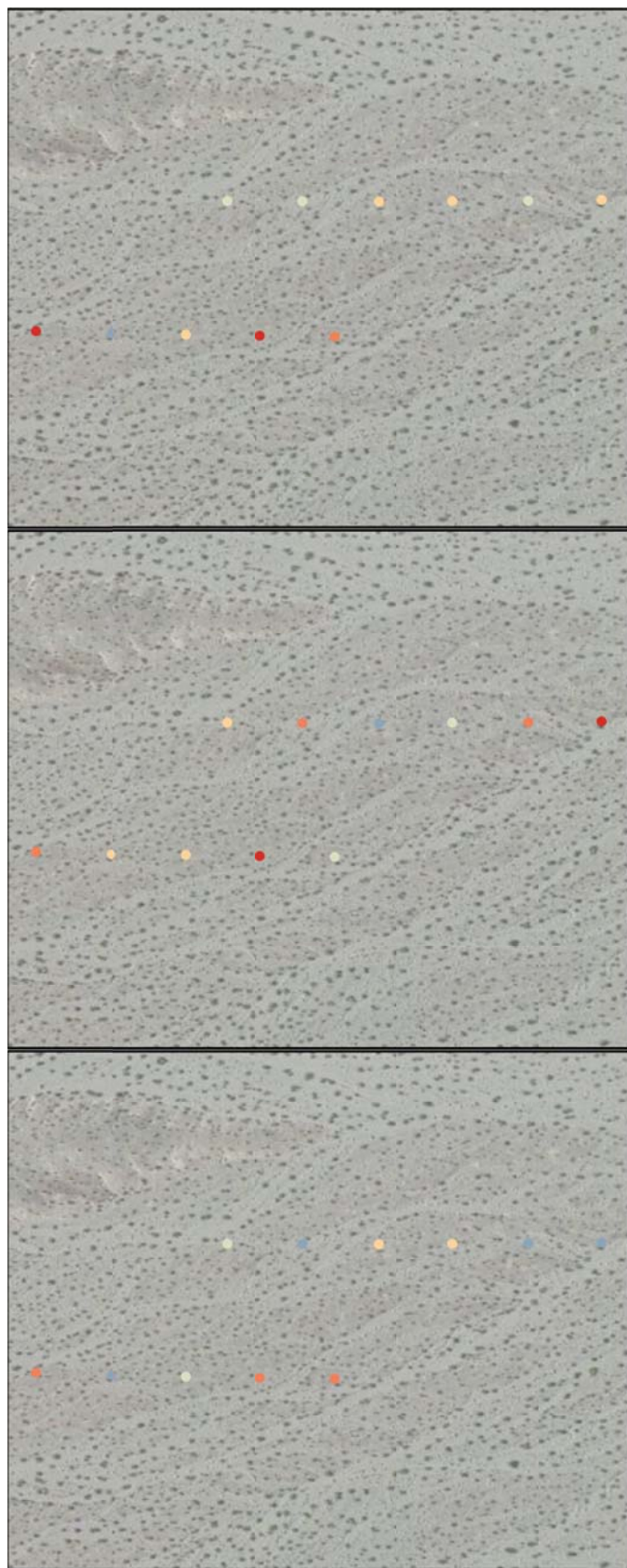
- 0 - 1.581498
- 1.581499 - 2.338019
- 2.338020 - 3.035367
- 3.035368 - 3.852008
- 3.852009 - 6.135812



Th PPM

- 4.118740 - 9.969537
- 9.969538 - 10.905588
- 10.905589 - 11.949598
- 11.949599 - 13.168826
- 13.168827 - 14.872976
- 14.872977 - 18.871453





Lake Mohave Radioelement Ratio Images Unit Qay+i

U/K Ratio

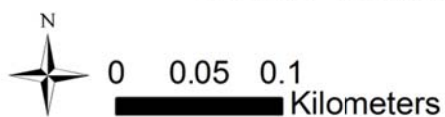
- 0 - 0.498470
- 0.498471 - 0.745602
- 0.745603 - 0.968045
- 0.968046 - 1.208879
- 1.208880 - 1.542684
- 1.542685 - 3.123242

Th/K Ratio

- 2.090277 - 3.461301
- 3.461302 - 3.942091
- 3.942092 - 4.348792
- 4.348793 - 4.786292
- 4.786293 - 5.355216
- 5.355217 - 8.000000

U/Th Ratio

- 0 - 0.117615
- 0.117616 - 0.182165
- 0.182166 - 0.244454
- 0.244455 - 0.316216
- 0.316217 - 0.426078
- 0.426079 - 0.803350

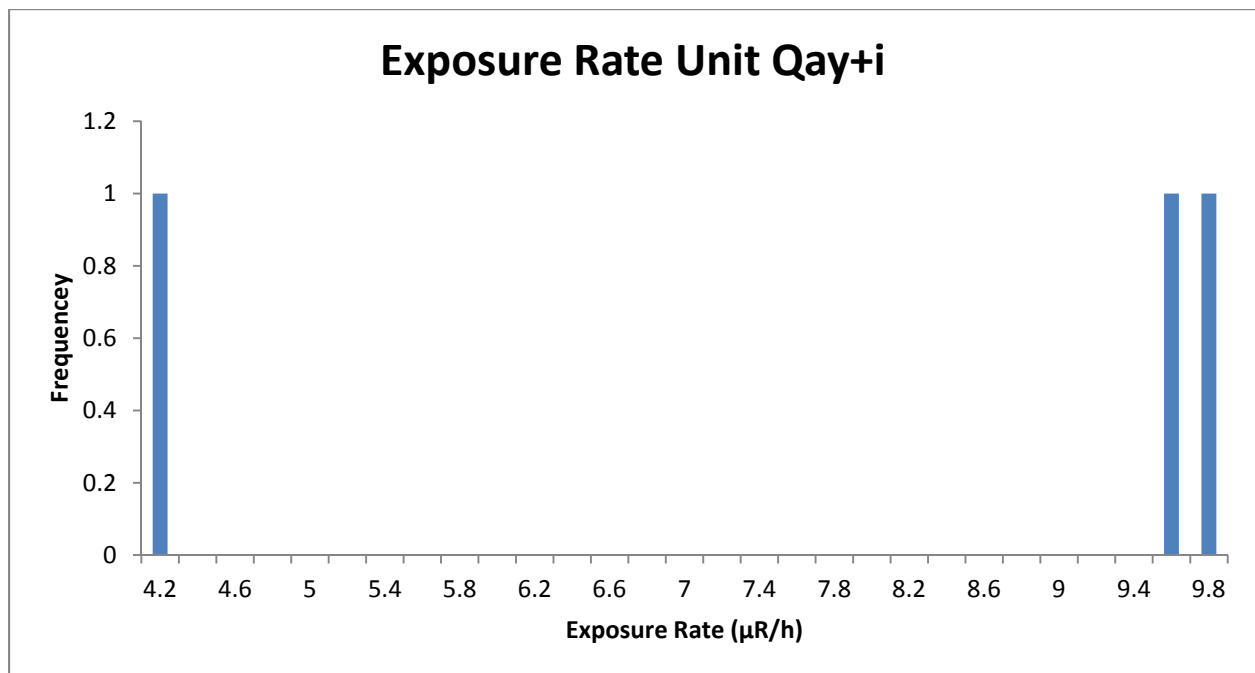


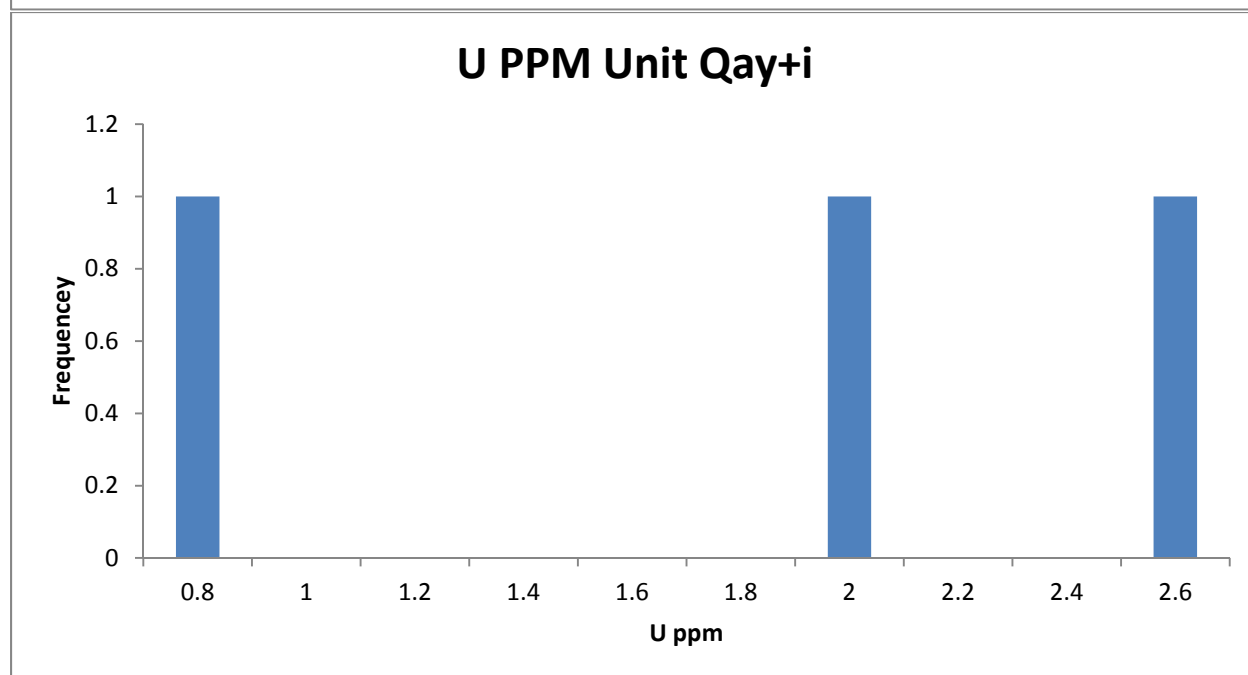
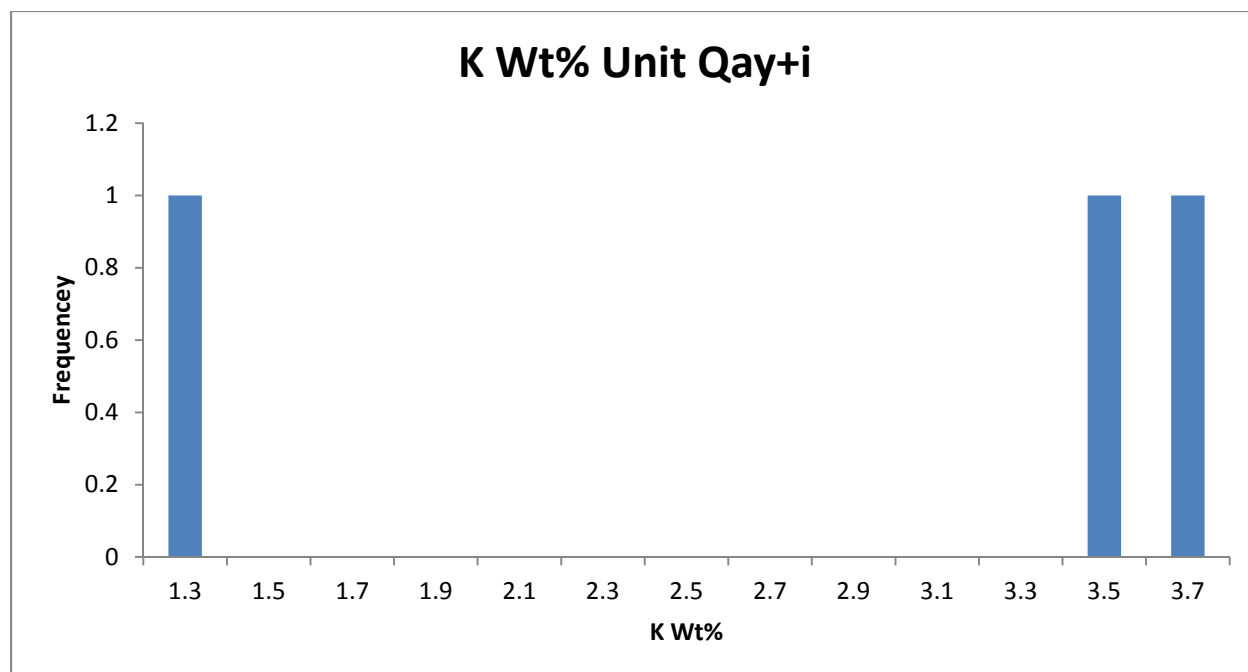
Traditional Geochemistry

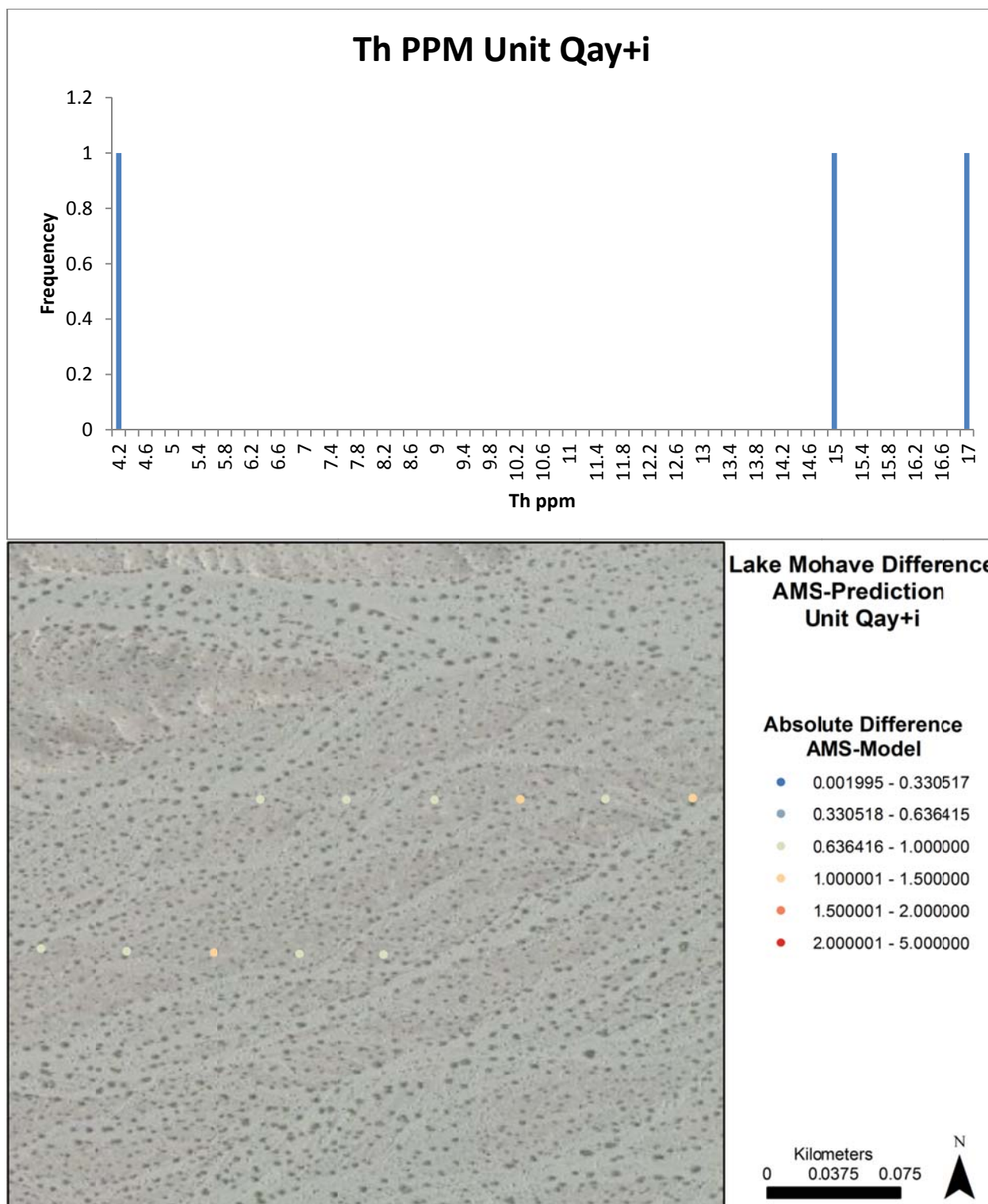
There are no traditional geochemical data that occur within Qay+i.

NURE Data

The NURE data for Qay+1 is featureless and does not provide any additional insight into this unit. The average NURE exposure rate is 7.86 $\mu\text{R/h}$ which compares with the AMS average exposure rate of 8.81 $\mu\text{R/h}$. This places this unit within the ± 1 $\mu\text{R/h}$ desired range.







Data Summary

Exposure Rate Comparison μR/h	Average	Median	STD	Range
AMS Data	8.815052	8.82704	0.100297	8.67933-8.98405
NURE Data	7.865867	9.582	3.151809	4.2284-9.7872

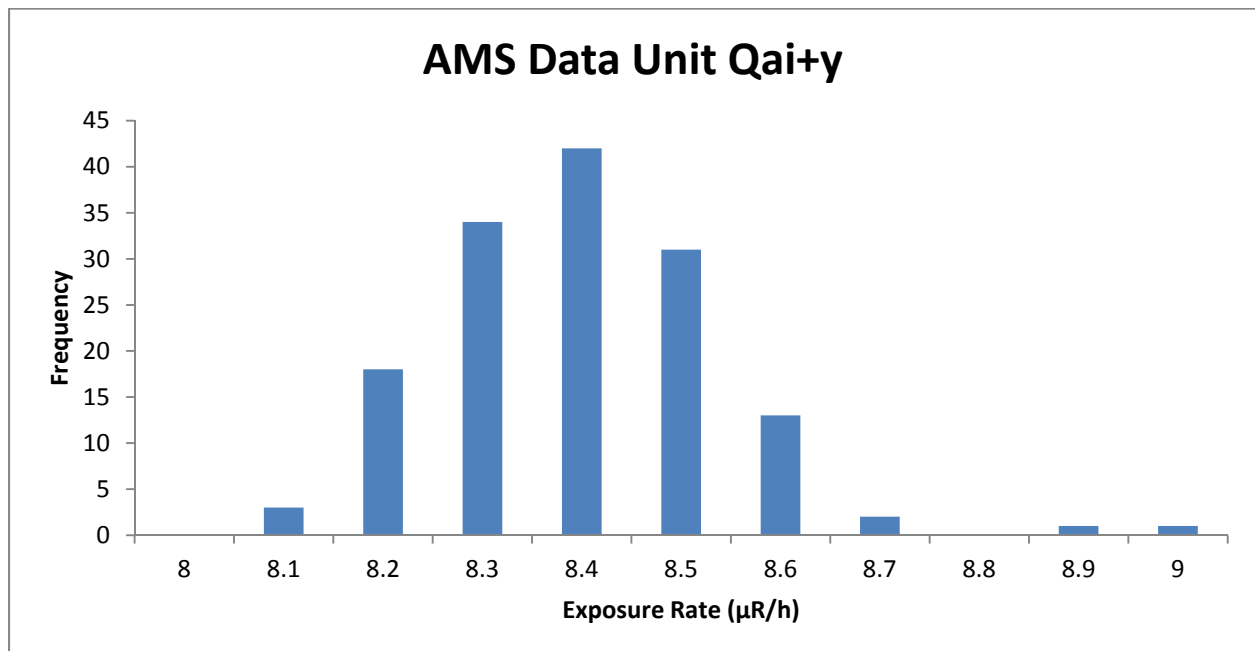
Qai+y

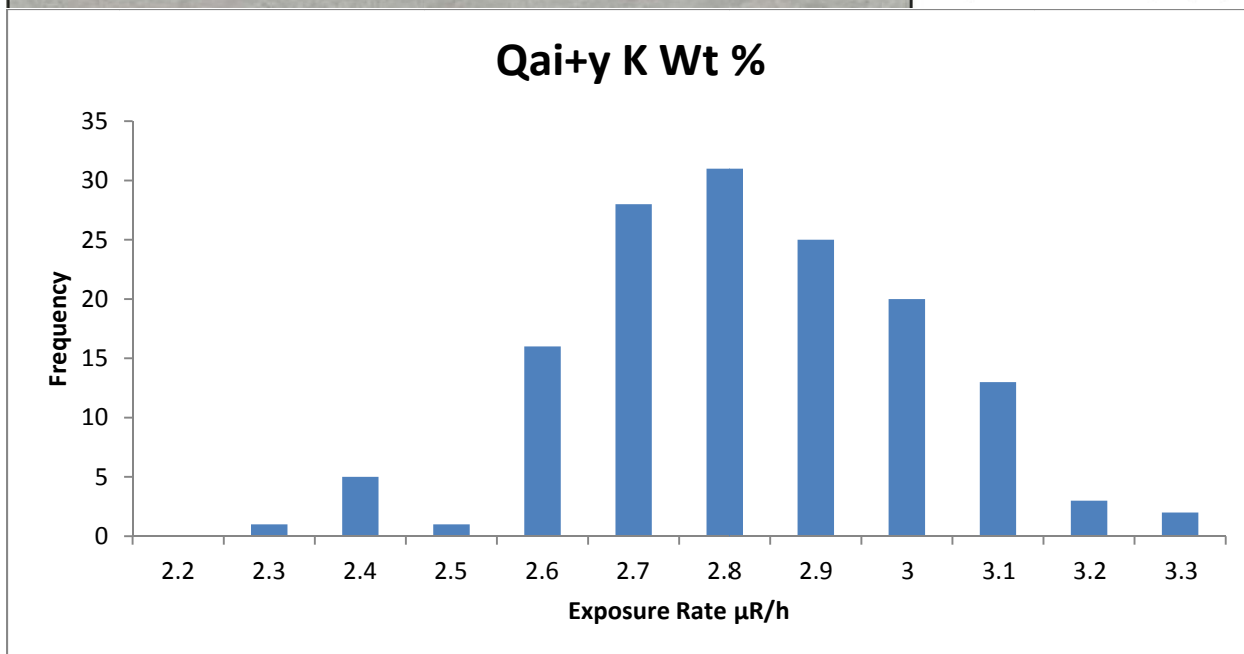
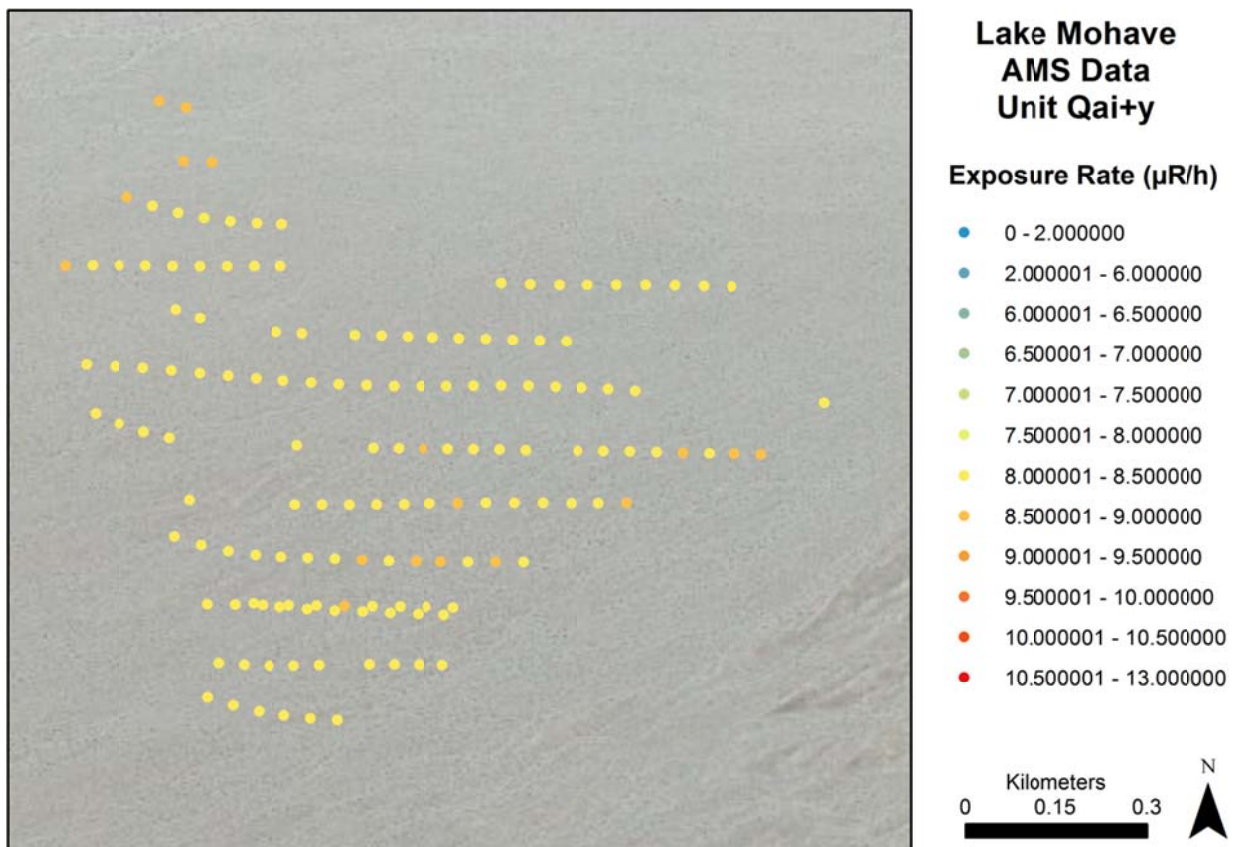
Composition

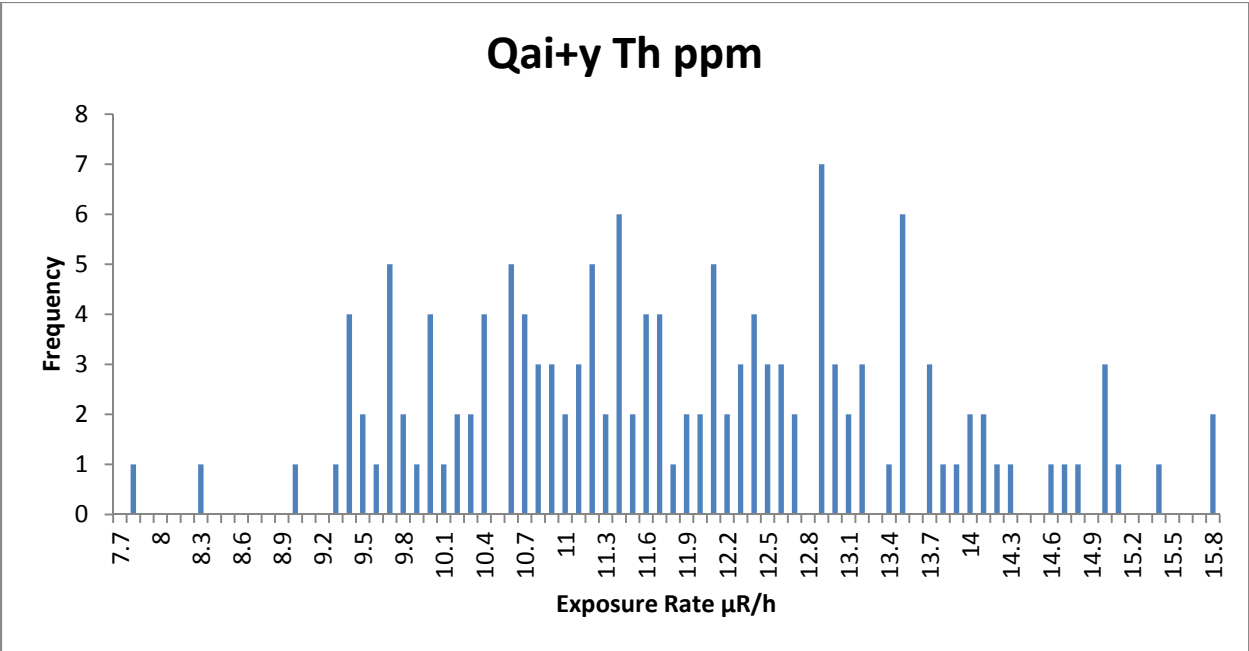
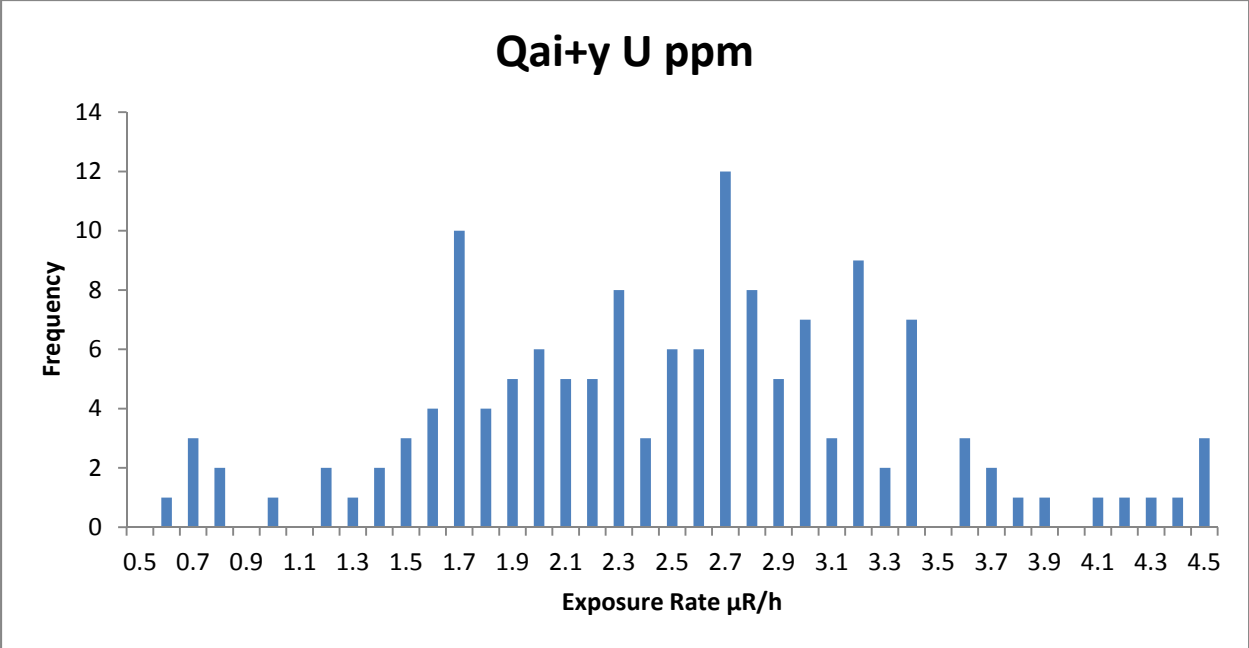
Qai+y is a mixed unit that contains both Qay and Qai deposits. It ranges in age from Holocene to Pleistocene. In this unit Qai is the dominate contributor. (House and Faulds, 2009) Compositional information is unknown but can likely be compared to units Qay and Qai.

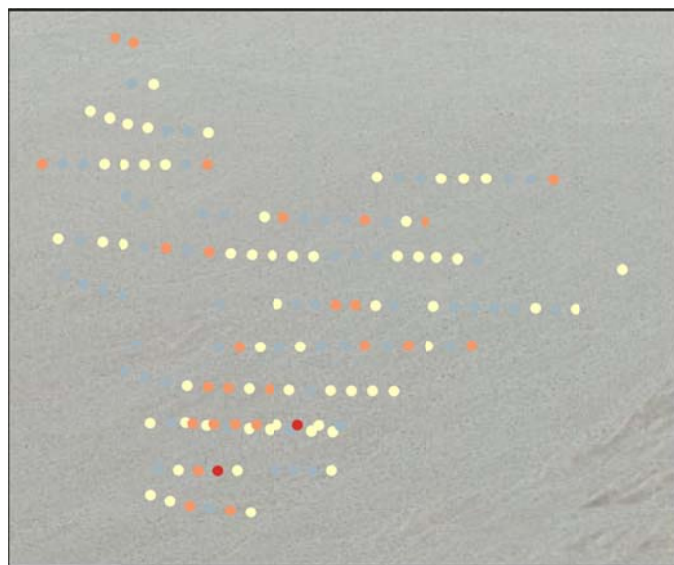
AMS Data

Qai+y is a small unit that appears to be quite homogenous. The AMS exposure rate data in Qai+y is nearly normally distributed around a mean of 8.35 $\mu\text{R/h}$. The associated standard deviation is 0.14 or 2% of the mean. K values are also near a normal distribution with a peak near 2.8%. U and Th values are spread widely and have few features in their distribution. Spatially, K, U, and Th values appear to be randomly distributed throughout the unit. Because of this units limited spatial extent it is difficult to say if this unit is truly homogenous or if there are other factors such as eolian addition that have influenced this unit.





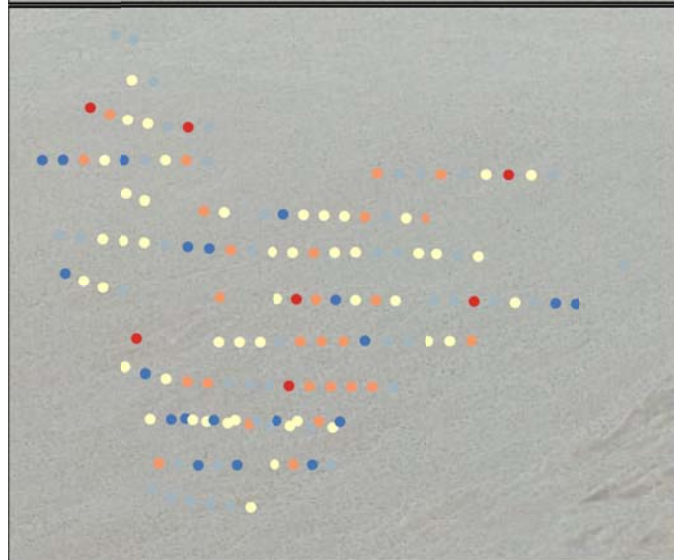




Lake Mohave Radioelement Concentration Images Unit Qai+y

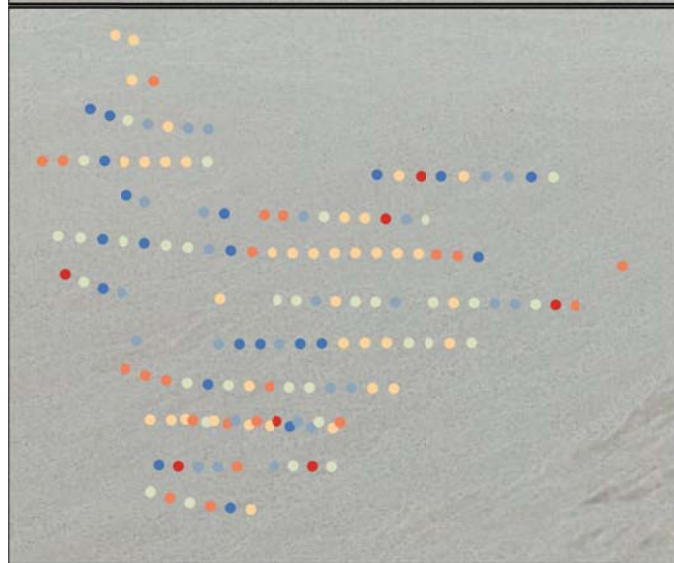
K Wt%

- 0.960459 - 2.243253
- 2.243254 - 2.723497
- 2.723498 - 2.956414
- 2.956415 - 3.187128
- 3.187129 - 3.672559



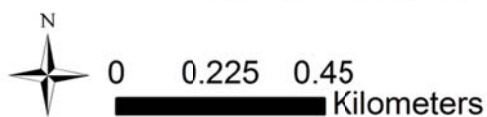
U PPM

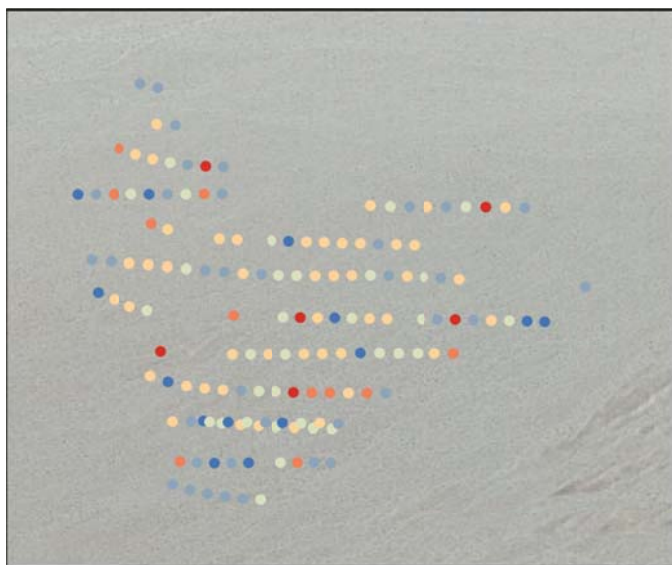
- 0 - 1.581498
- 1.581499 - 2.338019
- 2.338020 - 3.035367
- 3.035368 - 3.852008
- 3.852009 - 6.135812



Th PPM

- 4.118740 - 9.969537
- 9.969538 - 10.905588
- 10.905589 - 11.949598
- 11.949599 - 13.168826
- 13.168827 - 14.872976
- 14.872977 - 18.871453

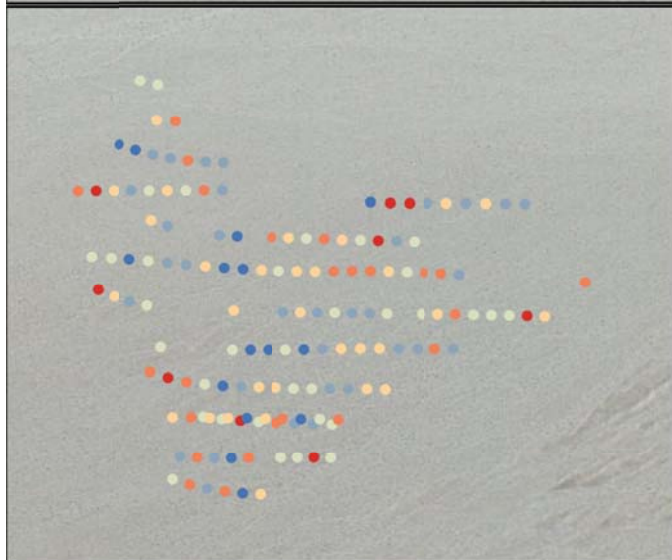




Lake Mohave Radioelement Ratio Images Unit Qai+y

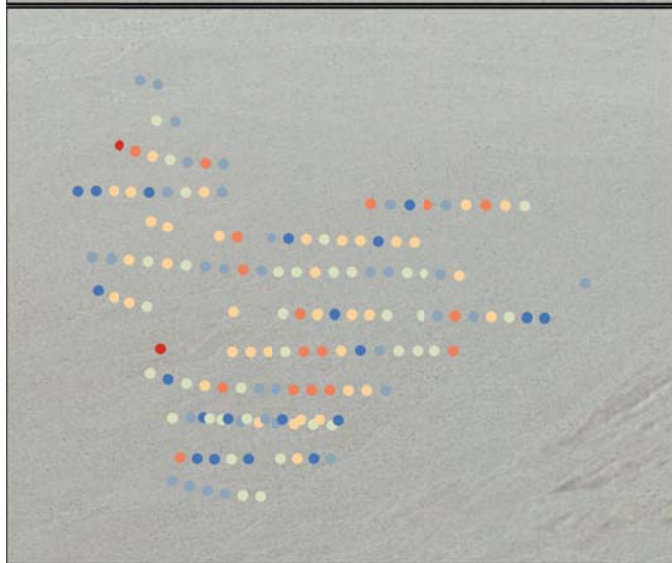
U/K Ratio

- 0 - 0.498470
- 0.498471 - 0.745602
- 0.745603 - 0.968045
- 0.968046 - 1.208879
- 1.208880 - 1.542684
- 1.542685 - 3.123242



Th/K Ratio

- 2.090277 - 3.461301
- 3.461302 - 3.942091
- 3.942092 - 4.348792
- 4.348793 - 4.786292
- 4.786293 - 5.355216
- 5.355217 - 8.000000



U/Th Ratio

- 0 - 0.117615
- 0.117616 - 0.182165
- 0.182166 - 0.244454
- 0.244455 - 0.316216
- 0.316217 - 0.426078
- 0.426079 - 0.803350

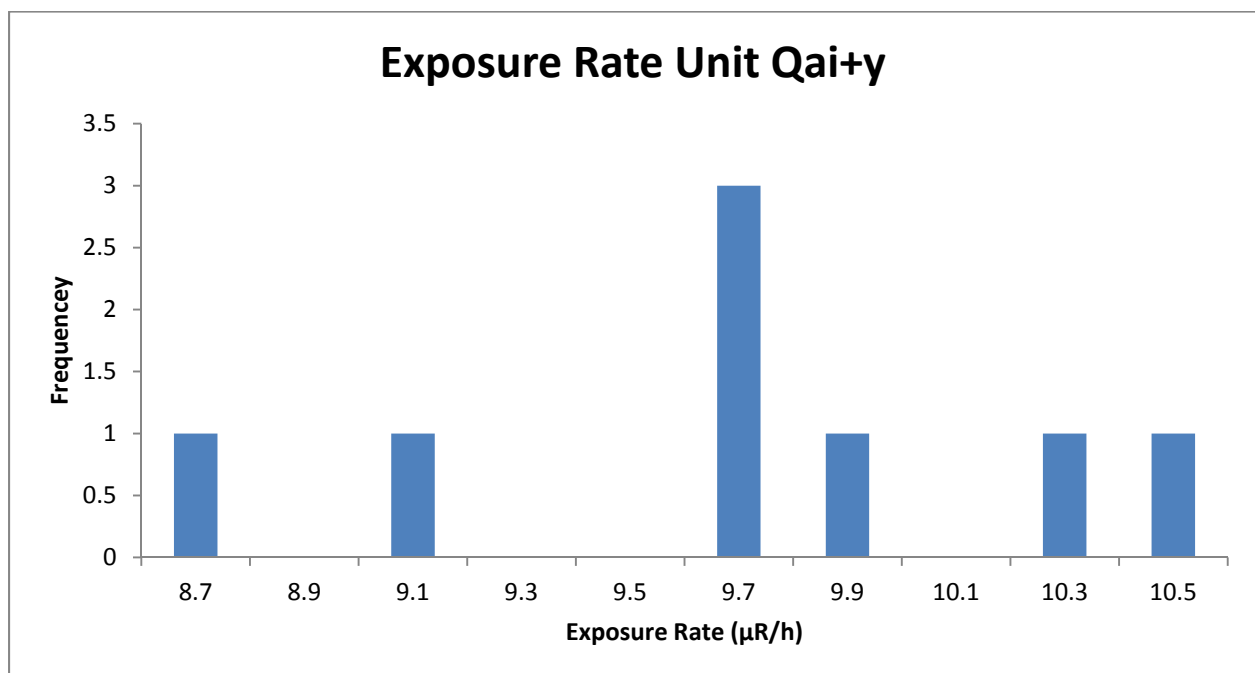


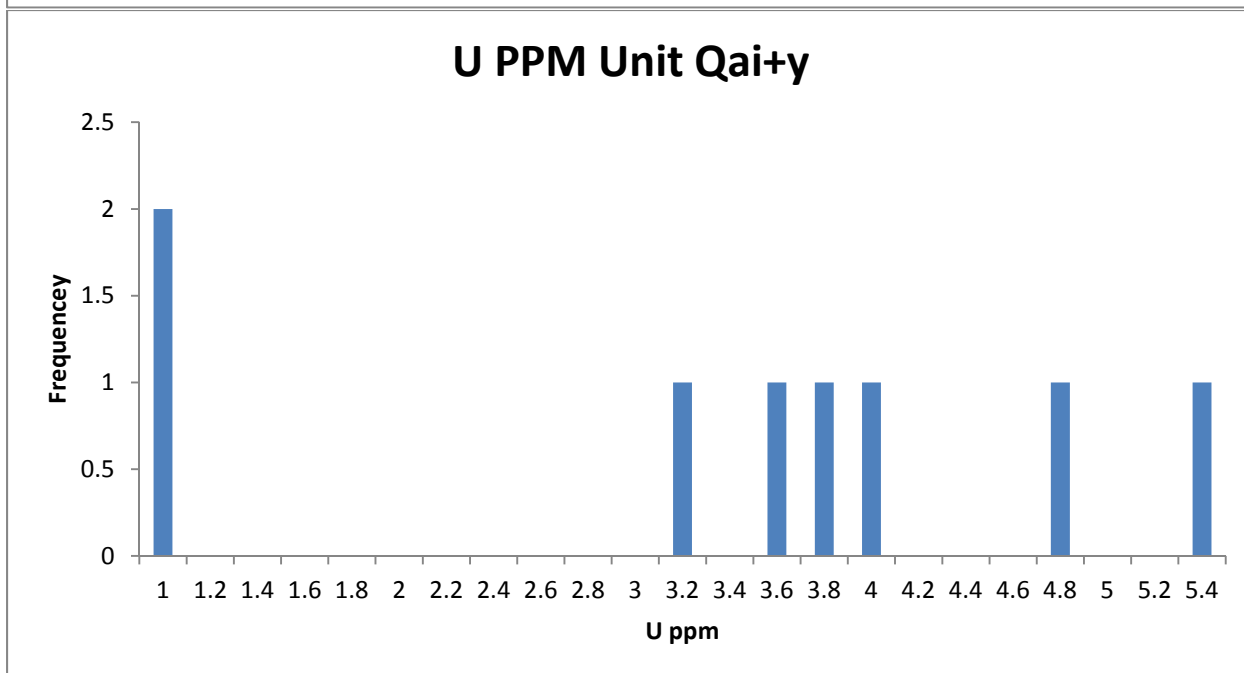
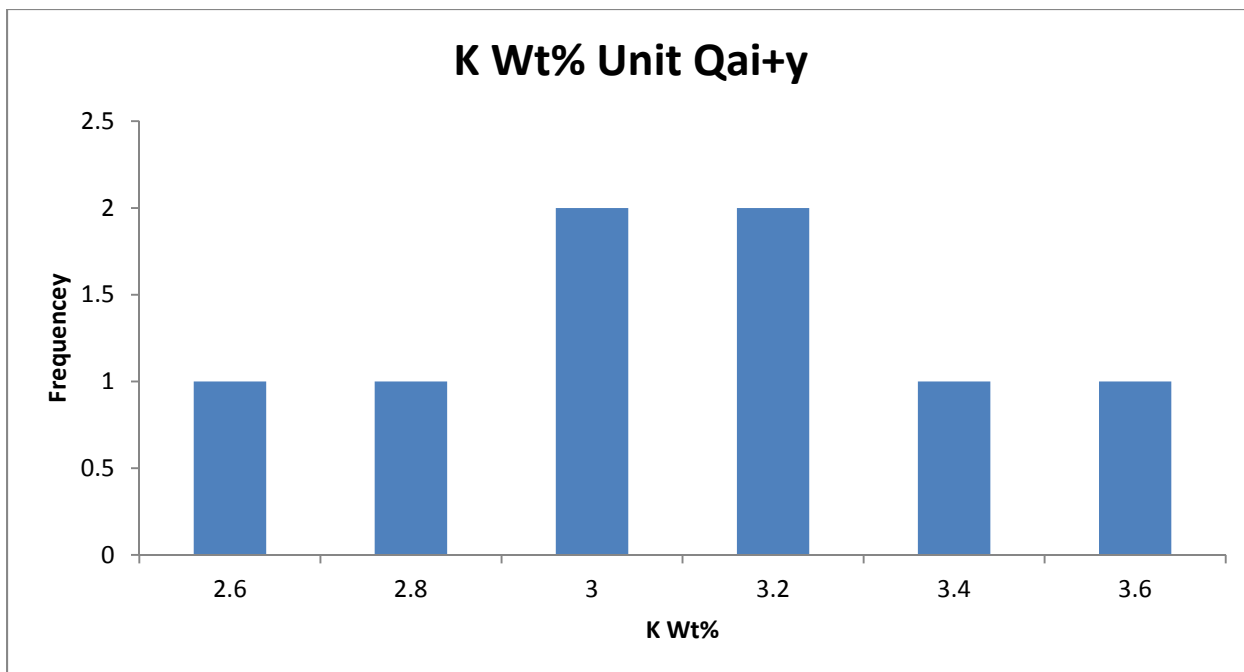
Traditional Geochemistry

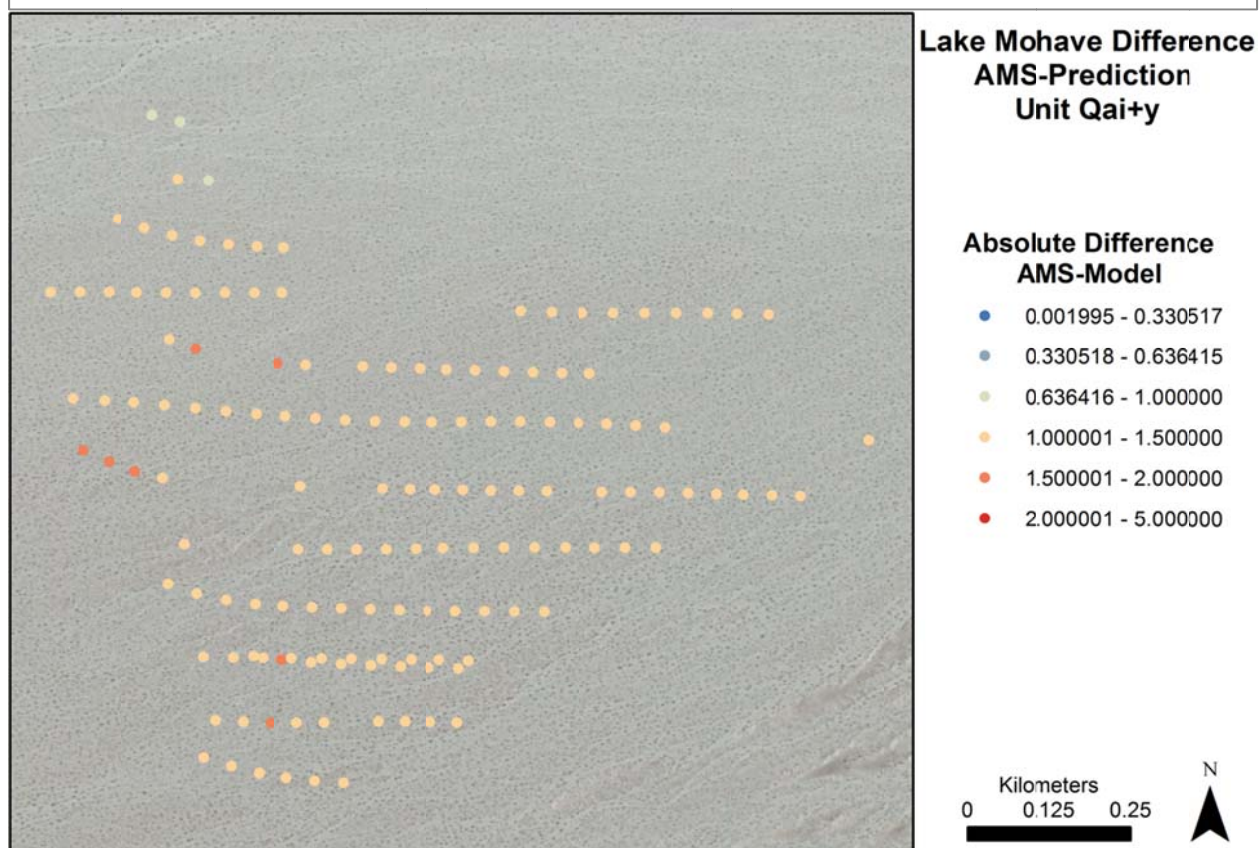
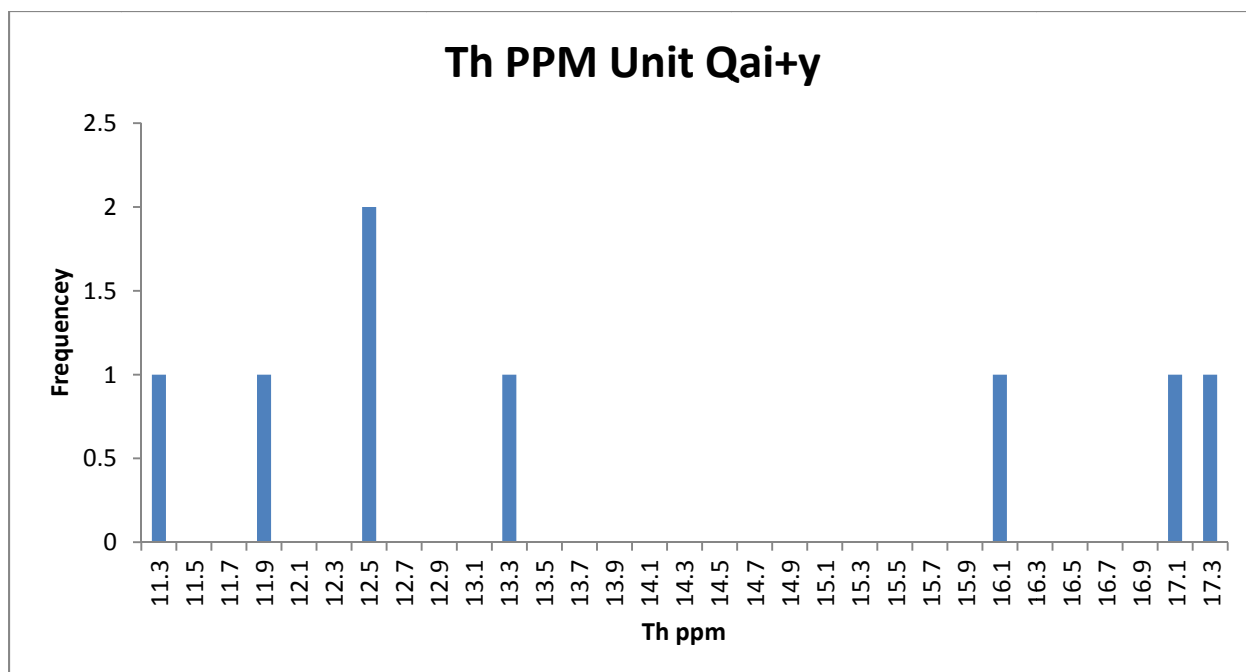
There are no traditional geochemical data points that occur in Qai+y.

NURE Data

NURE exposure rate data in Qai+y are widely spread with few features. The average NURE exposure rate for this unit is 9.65 $\mu\text{R/h}$ which compares with the AMS mean of 8.34 $\mu\text{R/h}$. This places the unit outside the desired range of ± 1 $\mu\text{R/h}$. K, U, and Th data are also distributed in a way that they provide no insight into the properties of the unit. When comparing the AMS data points to the NURE exposure rate it is clear that the majority of the data points have a difference between 1 and 1.5 $\mu\text{R/h}$.







Data Summary

Exposure Rate Comparison μR/h	Average	Median	STD	Range
AMS Data	8.347032	8.34071	0.136833	8.0702-8.92244
NURE Data	9.6522	9.667	0.541897	8.724-10.4168

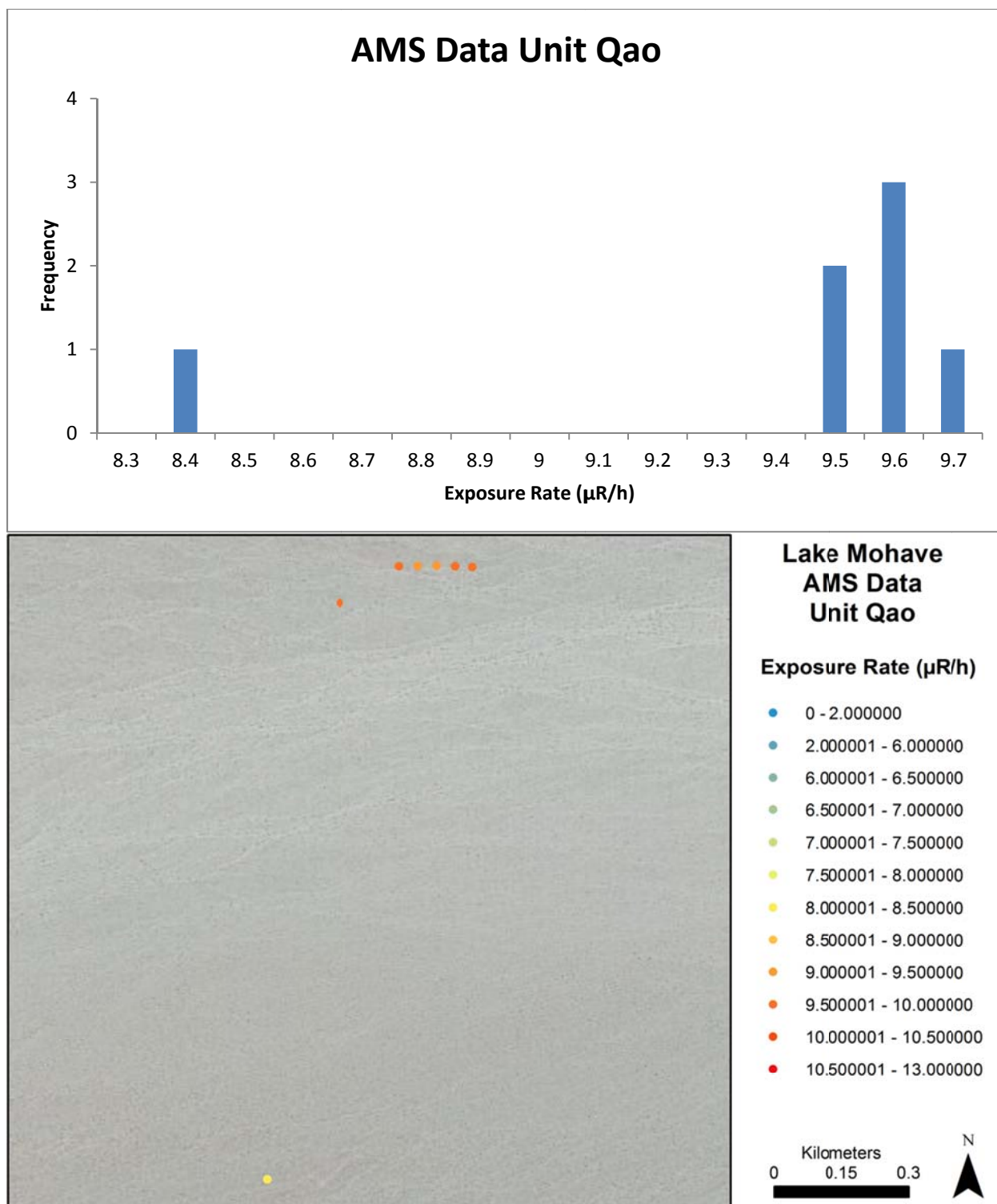
Qao

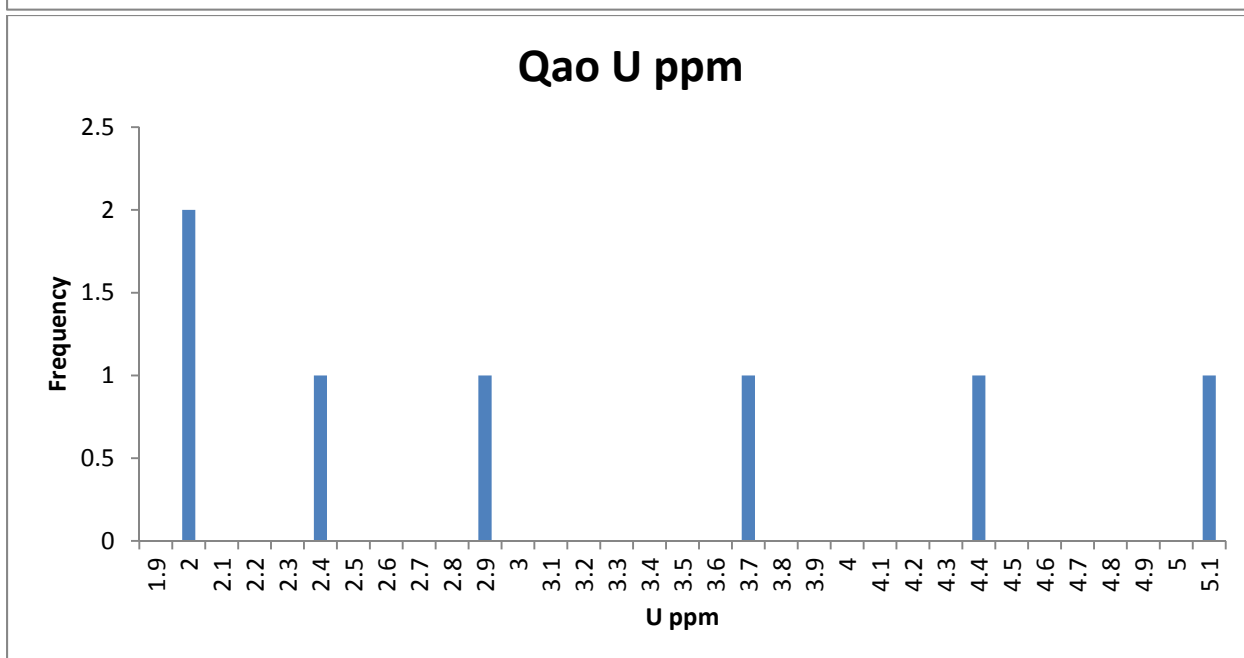
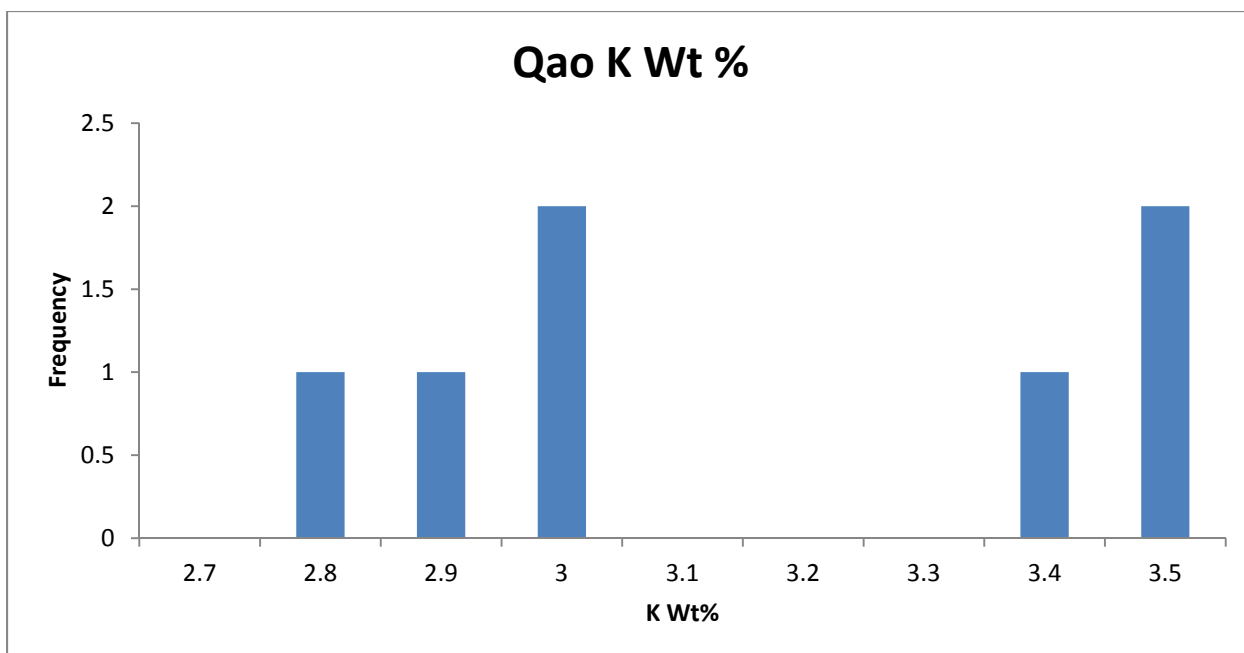
Composition

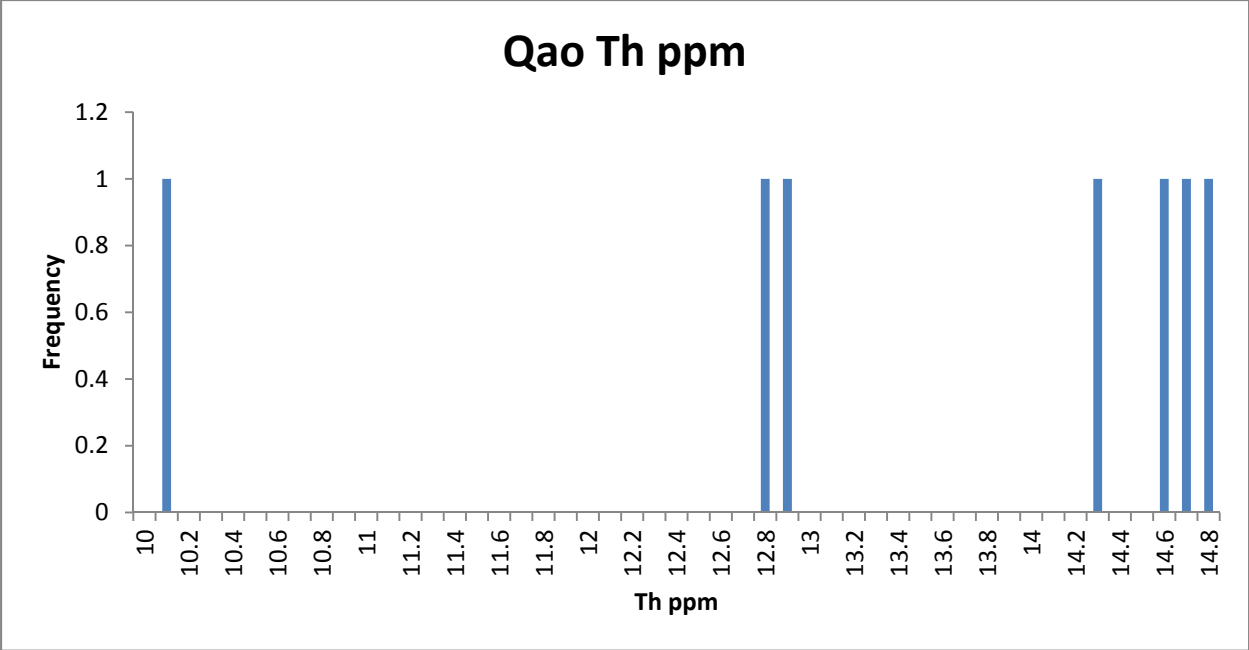
Qao is an alluvial unit that is middle Pleistocene in age. It consists of relict alluvial fans that are deeply incised and contain strong carbonate development. Shallow bar and swale topography that is sporadically covered with river gravels. Qao is limited in spatial extent. (House and Faulds, 2009) Published descriptions do not discuss the composition of the materials that compose Qao. However, if this unit follows similar trends in composition then it is likely composed largely of felsic igneous rock.

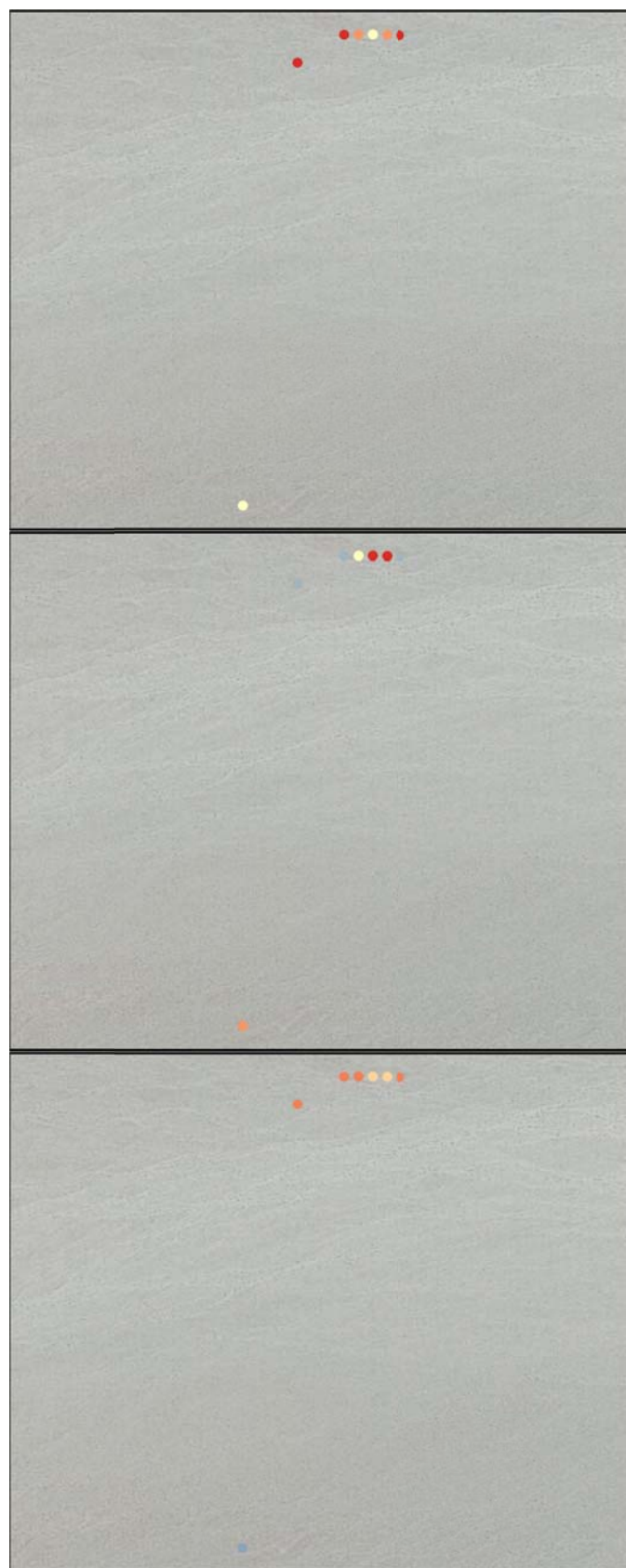
AMS Data

There are limited data AMS available for Qao. The AMS exposure rates are mostly grouped between 9.5 and 9.7 $\mu\text{R/h}$. There is one outlier with an exposure rate of 8.4 $\mu\text{R/h}$. The AMS mean for Qao is 9.36 $\mu\text{R/h}$ with a standard deviation of 0.44 or 5% of the mean. The single outlier occurs approximately 1 km south from the other points and may be composed of other materials. K, U, and Th distributions are largely featureless and provide no additional insight into this unit.









Lake Mohave Radioelement Concentration Images Unit Qao

K Wt%

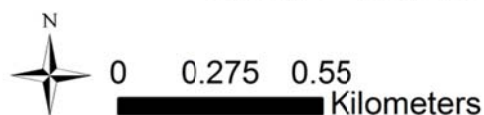
- 0.960459 - 2.243253
- 2.243254 - 2.723497
- 2.723498 - 2.956414
- 2.956415 - 3.187128
- 3.187129 - 3.672559

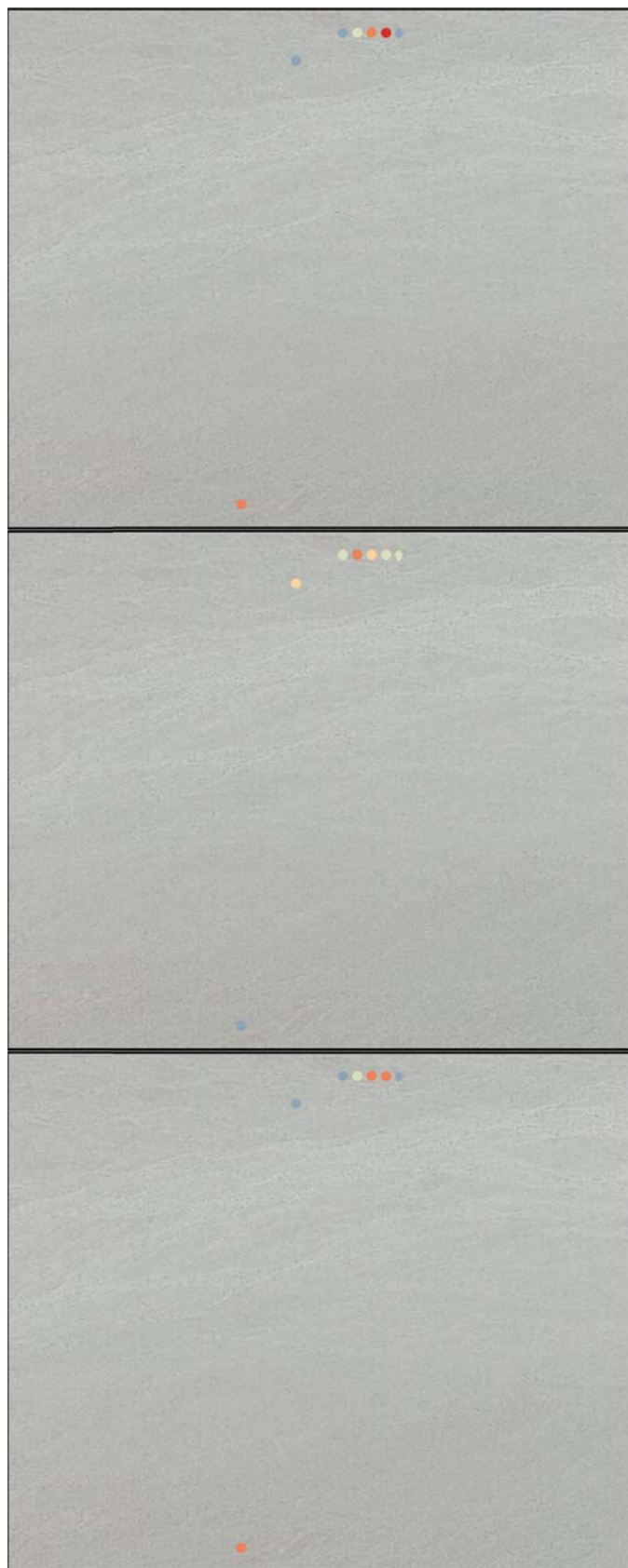
U PPM

- 0 - 1.581498
- 1.581499 - 2.338019
- 2.338020 - 3.035367
- 3.035368 - 3.852008
- 3.852009 - 6.135812

Th PPM

- 4.118740 - 9.969537
- 9.969538 - 10.905588
- 10.905589 - 11.949598
- 11.949599 - 13.168826
- 13.168827 - 14.872976
- 14.872977 - 18.871453





Lake Mohave Radioelement Ratio Images Unit Qao

U/K Ratio

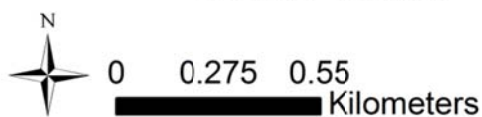
- 0 - 0.498470
- 0.498471 - 0.745602
- 0.745603 - 0.968045
- 0.968046 - 1.208879
- 1.208880 - 1.542684
- 1.542685 - 3.123242

Th/K Ratio

- 2.090277 - 3.461301
- 3.461302 - 3.942091
- 3.942092 - 4.348792
- 4.348793 - 4.786292
- 4.786293 - 5.355216
- 5.355217 - 8.000000

U/Th Ratio

- 0 - 0.117615
- 0.117616 - 0.182165
- 0.182166 - 0.244454
- 0.244455 - 0.316216
- 0.316217 - 0.426078
- 0.426079 - 0.803350



Traditional Geochemistry

There are two geochemical data points that occur in Qao. One of the points does not provide K data. U values agree with each other while Th varies by about 2 ppm. The exposure rate calculated from these data is 12.73 $\mu\text{R/h}$ which compares with the AMS mean of 9.36 $\mu\text{R/h}$ which is outside the success range of ± 1 $\mu\text{R/h}$.

Sample ID	Latitude	Longitude	K %	U ppm	Th ppm
9466	35.4416	-114.819	5.538	2.3	16.48
9506	35.566	-114.873		2.2	14.35

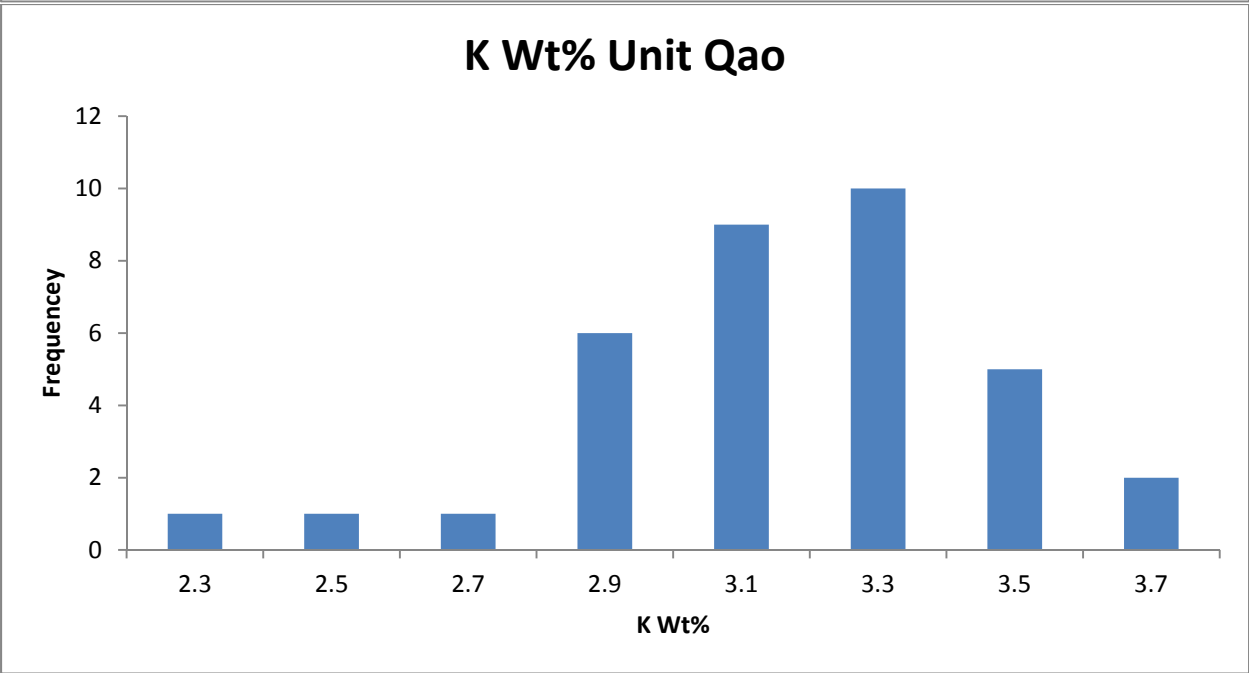
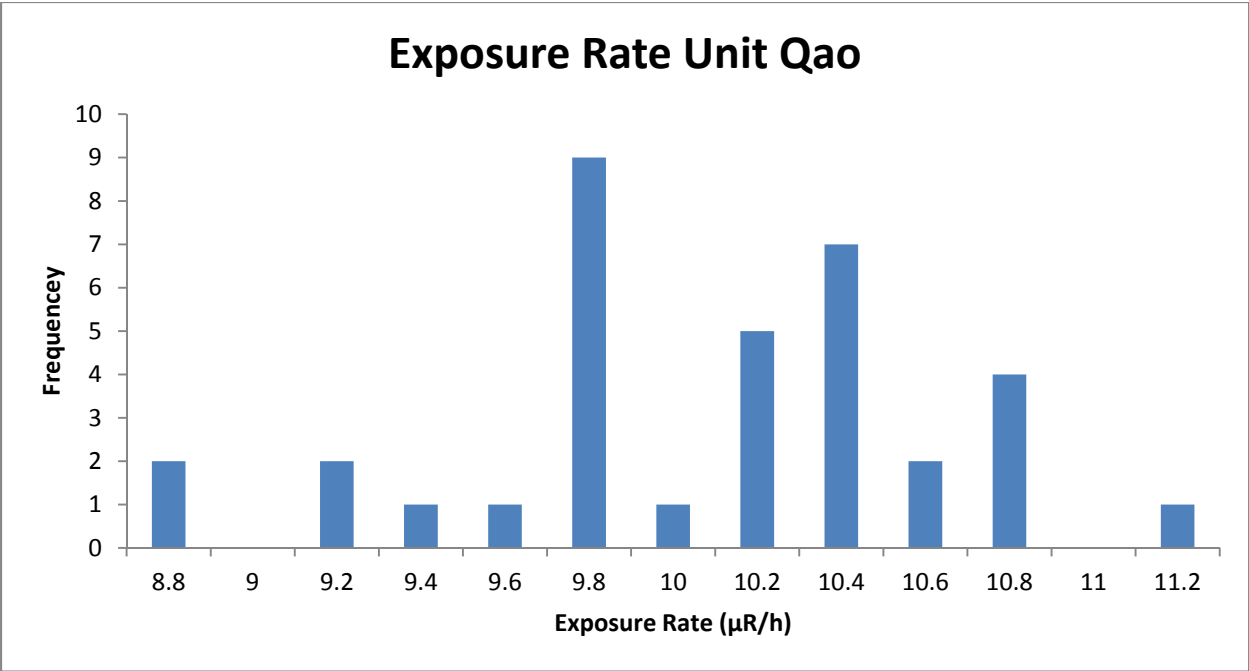
	K%	U ppm	Th ppm
Mean	5.538	2.25	15.415
Median	5.538	2.25	15.415
Standard Deviation	N/A	0.05	1.065
Range	5.538	2.2-2.3	14.35-16.48

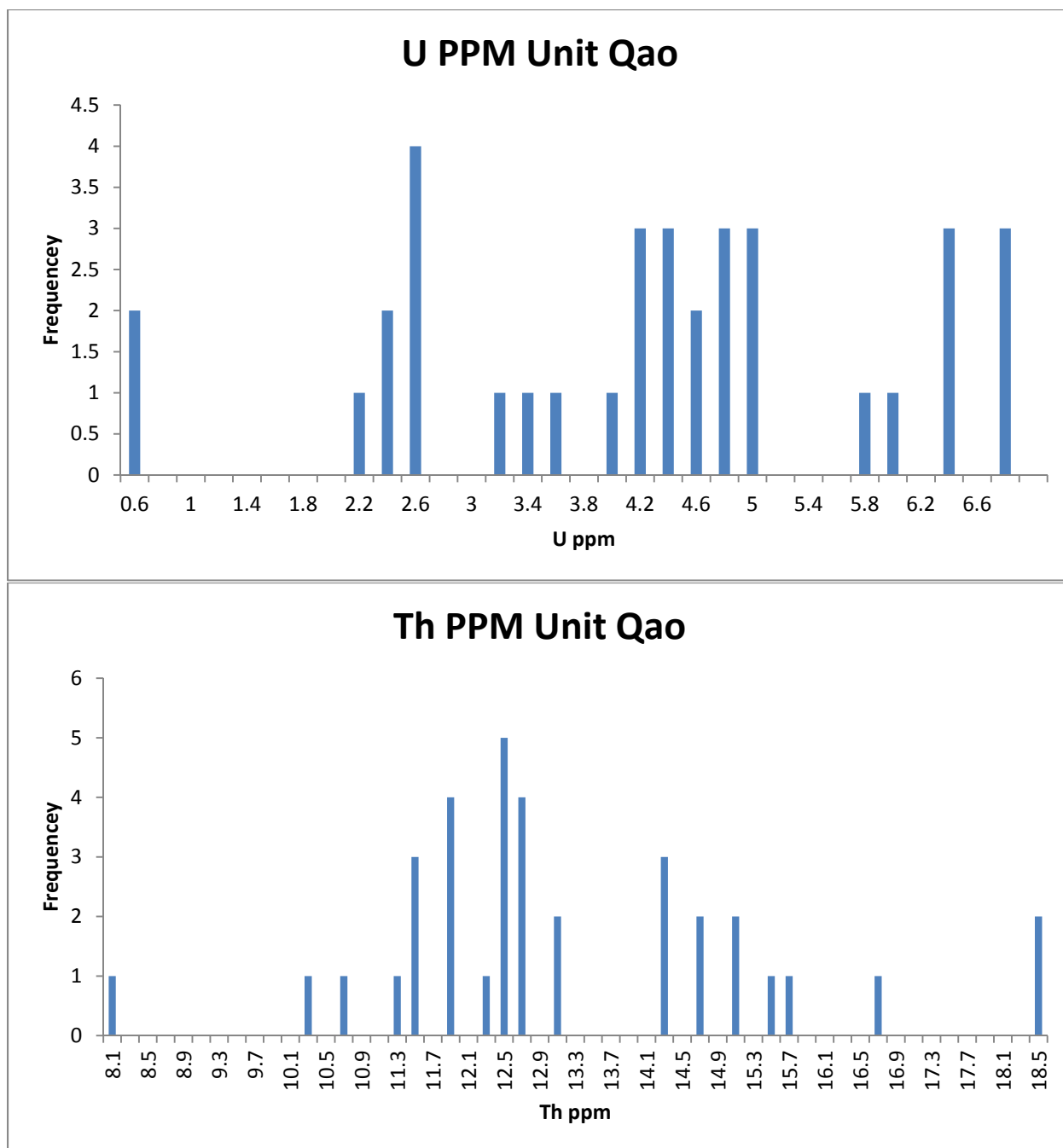
NURE Data

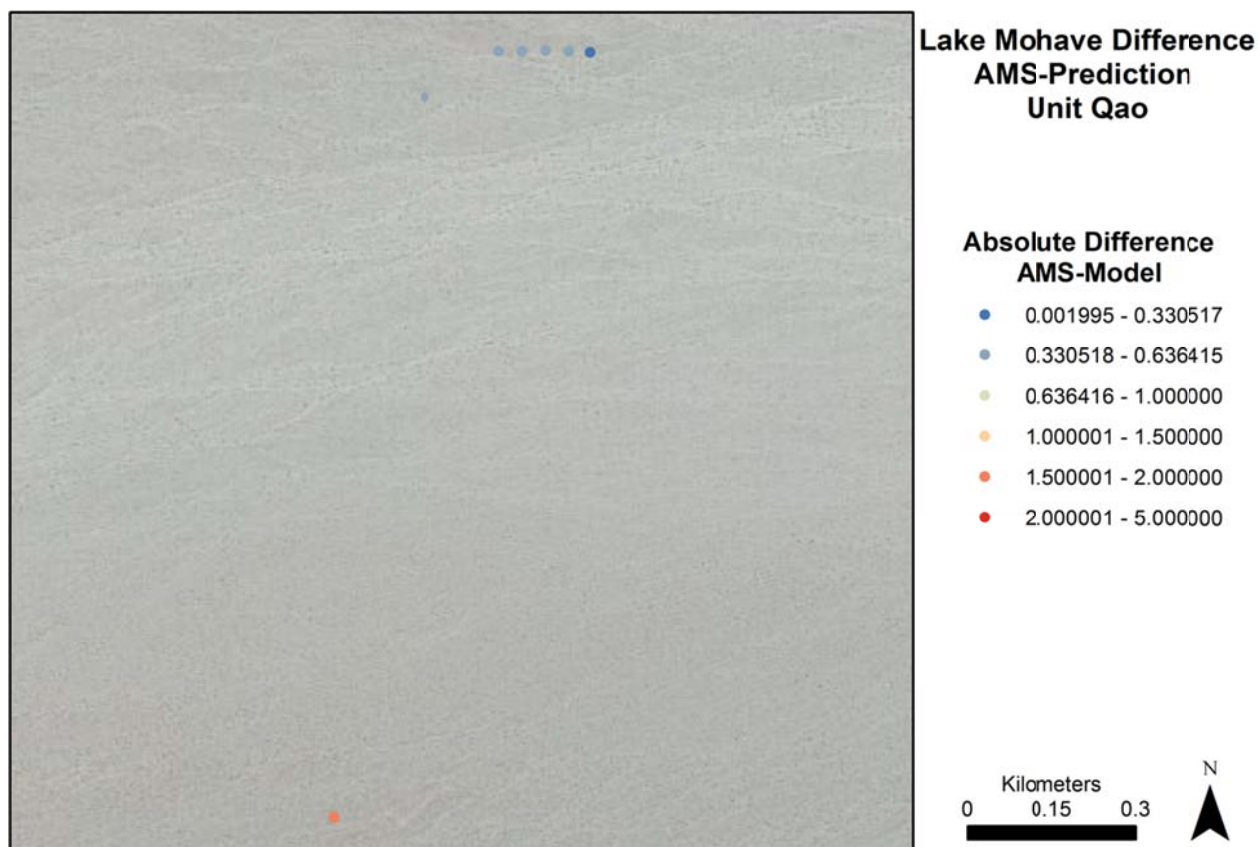
The NURE exposure rate data has no clear peaks but the majority of the data occurs between 9.8 and 10.4 $\mu\text{R/h}$. The average NURE exposure rate is 9.98 $\mu\text{R/h}$ which compares to the AMS mean of 9.36 $\mu\text{R/h}$. This unit is within the desired ± 1 $\mu\text{R/h}$ range.

K values peak at 3.3% and have a near normal distribution. Th values are more widely distributed but peak near 12.5 ppm. U values are randomly distributed.

When comparing the NURE exposure rate to the AMS data points the majority of the points are modeled very well. The outlier point in the south is the exception to this otherwise well modeled unit.







Data Summary

Exposure Rate Comparison μR/h	Average	Median	STD	Range
AMS Data	9.360434	9.50585	0.444505	8.36452-9.66293
NURE Data	9.987417	10.122	0.56223	8.8112-11.0712
Geochemical Prediction	12.73604	12.73604	N/A	12.41896-13.05312

QTa

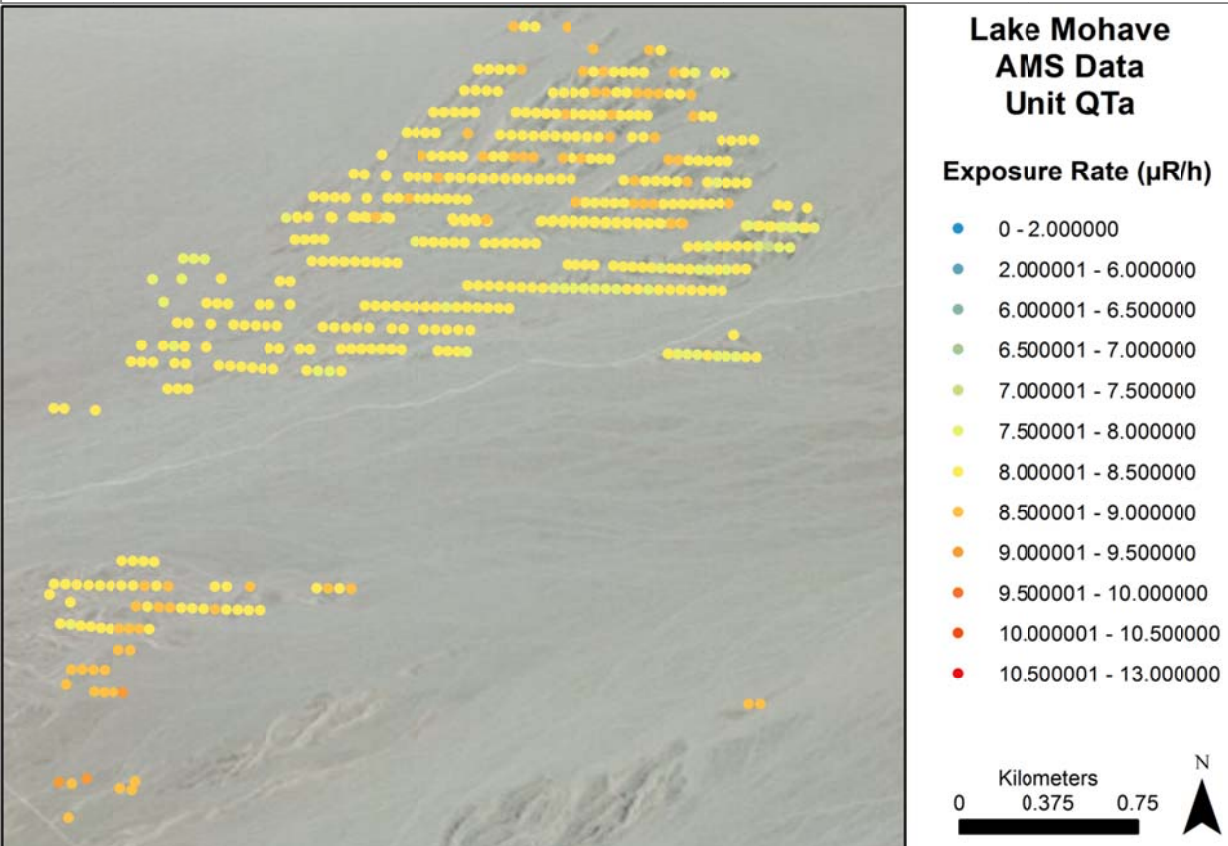
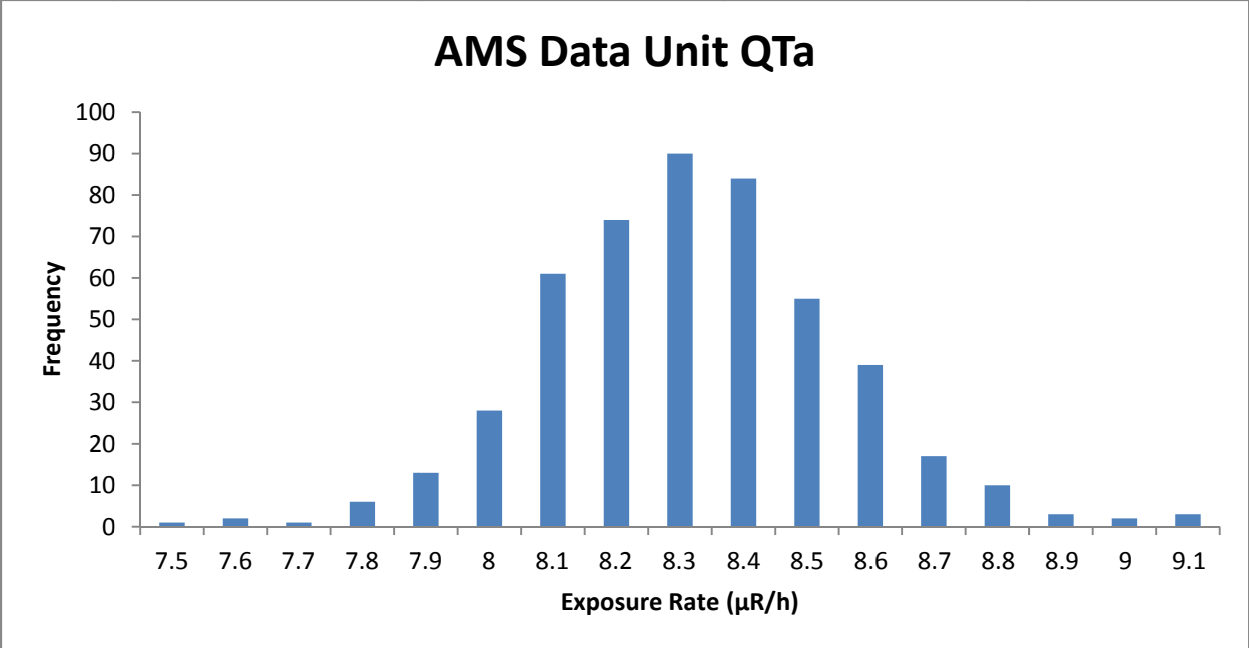
Composition

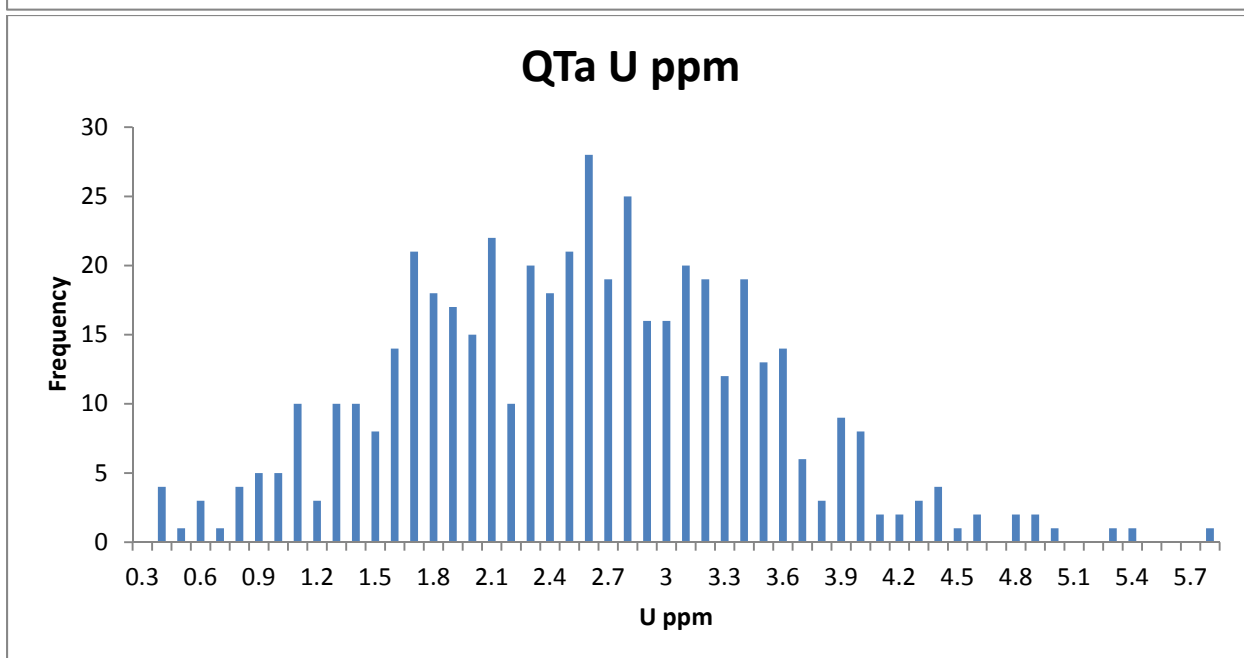
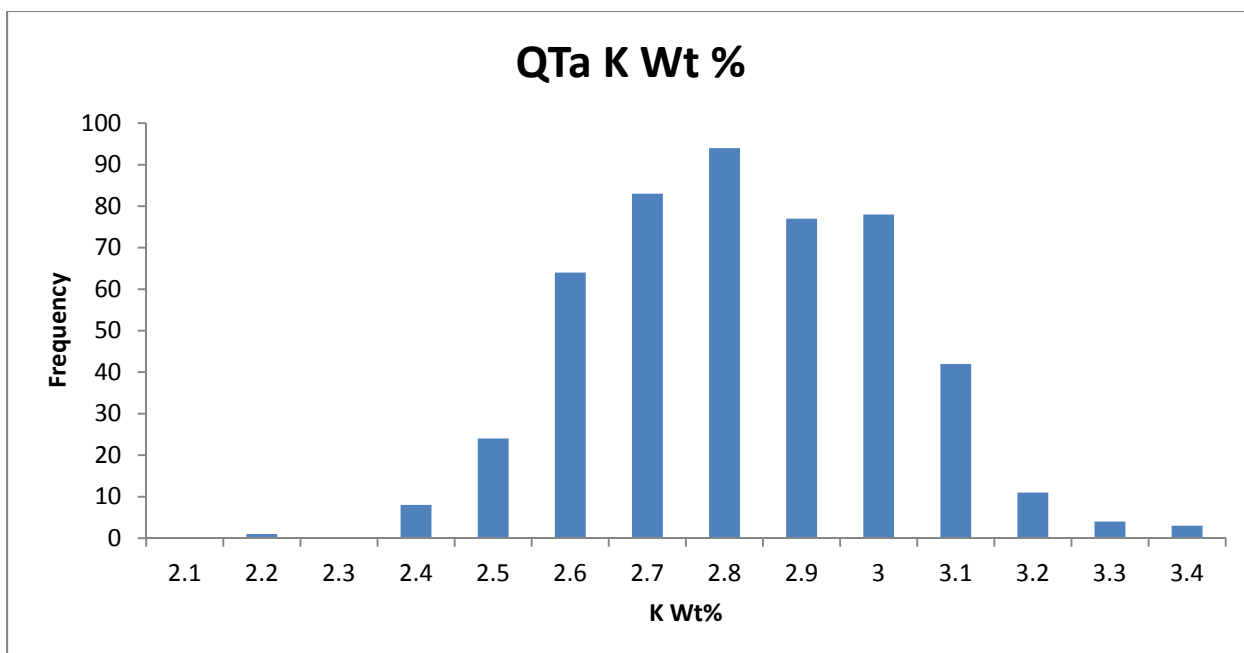
QTa is an erosional relict alluvial fan. Highly weathered with moderately to deeply weathered gravel lag deposits. There are large broken up fragments of calcrete in the soil. (House and Faulds, 2009) There is no published information as to the composition of QTa. However, if QTa follows general trends in the area it is likely to be composed largely of intermediate igneous and metamorphic rocks.

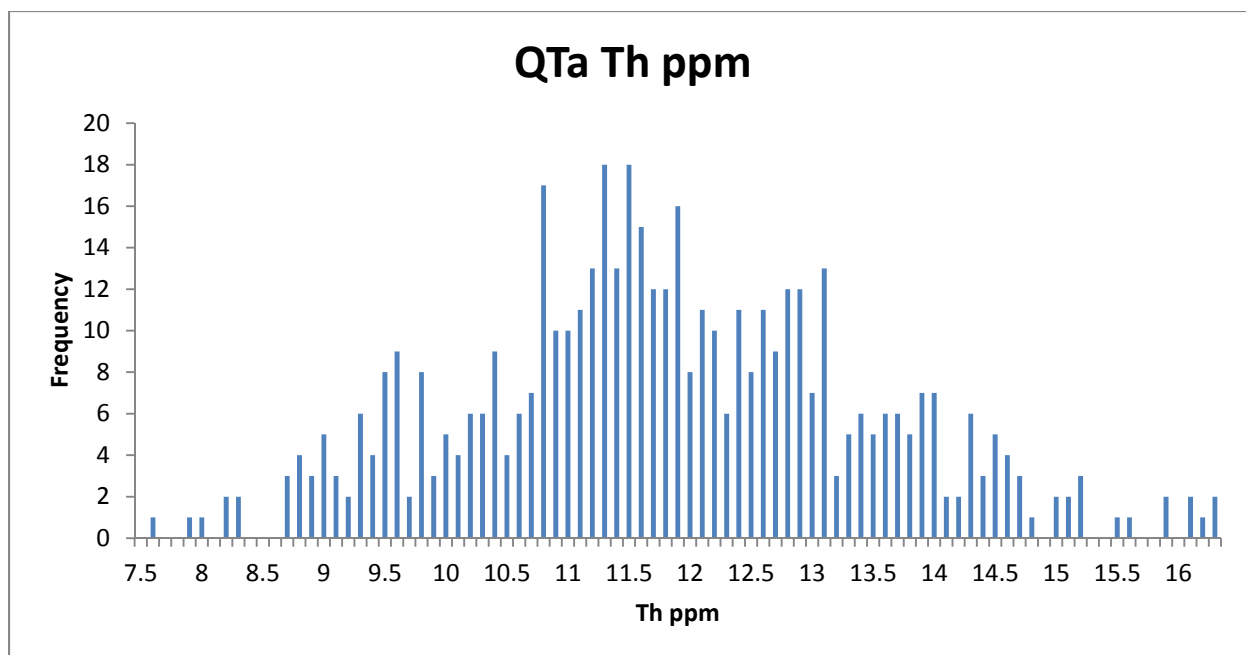
AMS Data

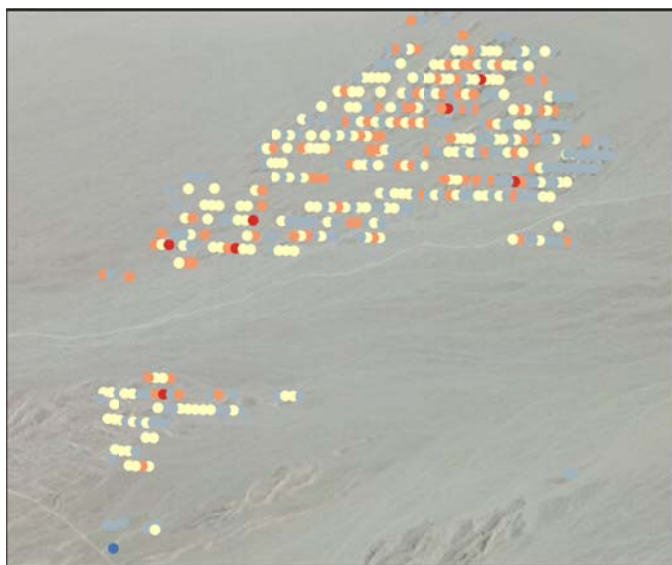
The AMS exposure rate data in QTa is normally distributed between 7.8 and 8.8 $\mu\text{R/h}$ with a mean of 8.3 $\mu\text{R/h}$. The standard deviation of the data is 0.23 or 2.7% of the mean. The unit is generally homogenous in terms of exposure rate with some higher values near the southern portion of the unit.

K values have a near normal distribution with a peak at 2.8%. U values are broadly set with a peak near 2.6 ppm. Th values are also broadly set and has a series of peaks near 10.8, 11.3, 11.5 and 11.9 ppm. K values are homogenously distributed spatially within the unit. U and Th values are randomly distributed with high U values near the hotter southern points.





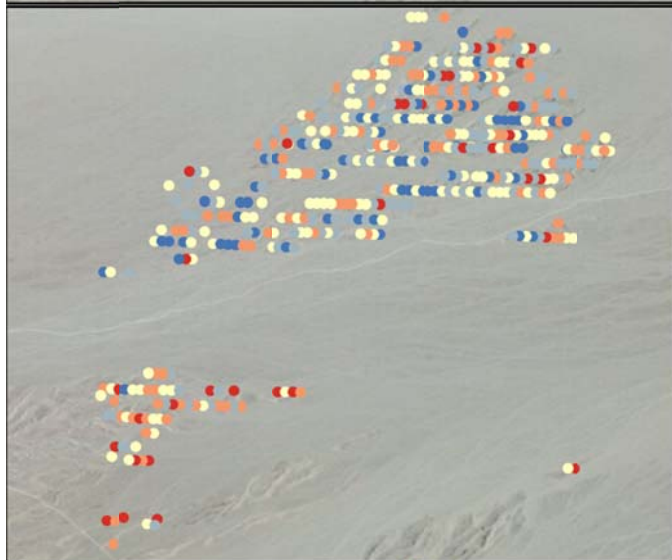




Lake Mohave Radioelement Concentration Images Unit QTa

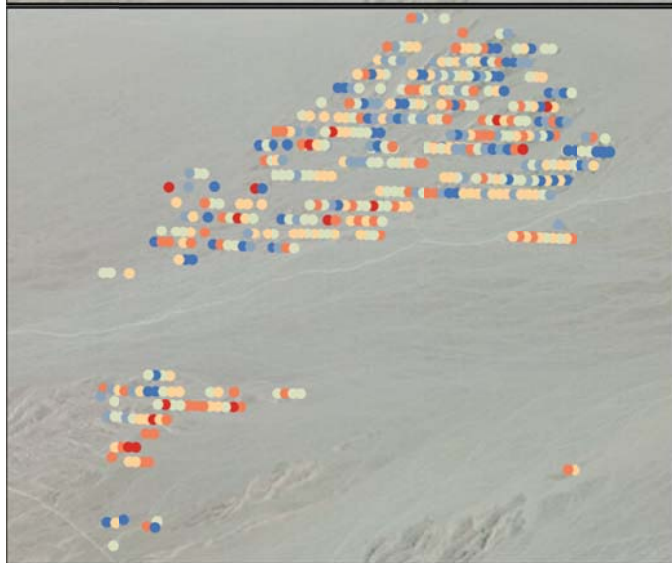
K Wt%

- 0.960459 - 2.243253
- 2.243254 - 2.723497
- 2.723498 - 2.956414
- 2.956415 - 3.187128
- 3.187129 - 3.672559



U PPM

- 0 - 1.581498
- 1.581499 - 2.338019
- 2.338020 - 3.035367
- 3.035368 - 3.852008
- 3.852009 - 6.135812



Th PPM

- 4.118740 - 9.969537
- 9.969538 - 10.905588
- 10.905589 - 11.949598
- 11.949599 - 13.168826
- 13.168827 - 14.872976
- 14.872977 - 18.871453





Lake Mohave Radioelement Ratio Images Unit QTa

U/K Ratio

- 0 - 0.498470
- 0.498471 - 0.745602
- 0.745603 - 0.968045
- 0.968046 - 1.208879
- 1.208880 - 1.542684
- 1.542685 - 3.123242



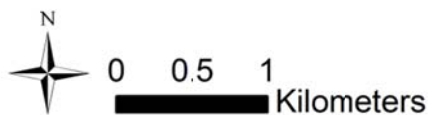
Th/K Ratio

- 2.090277 - 3.461301
- 3.461302 - 3.942091
- 3.942092 - 4.348792
- 4.348793 - 4.786292
- 4.786293 - 5.355216
- 5.355217 - 8.000000



U/Th Ratio

- 0 - 0.117615
- 0.117616 - 0.182165
- 0.182166 - 0.244454
- 0.244455 - 0.316216
- 0.316217 - 0.426078
- 0.426079 - 0.803350



Traditional Geochemistry

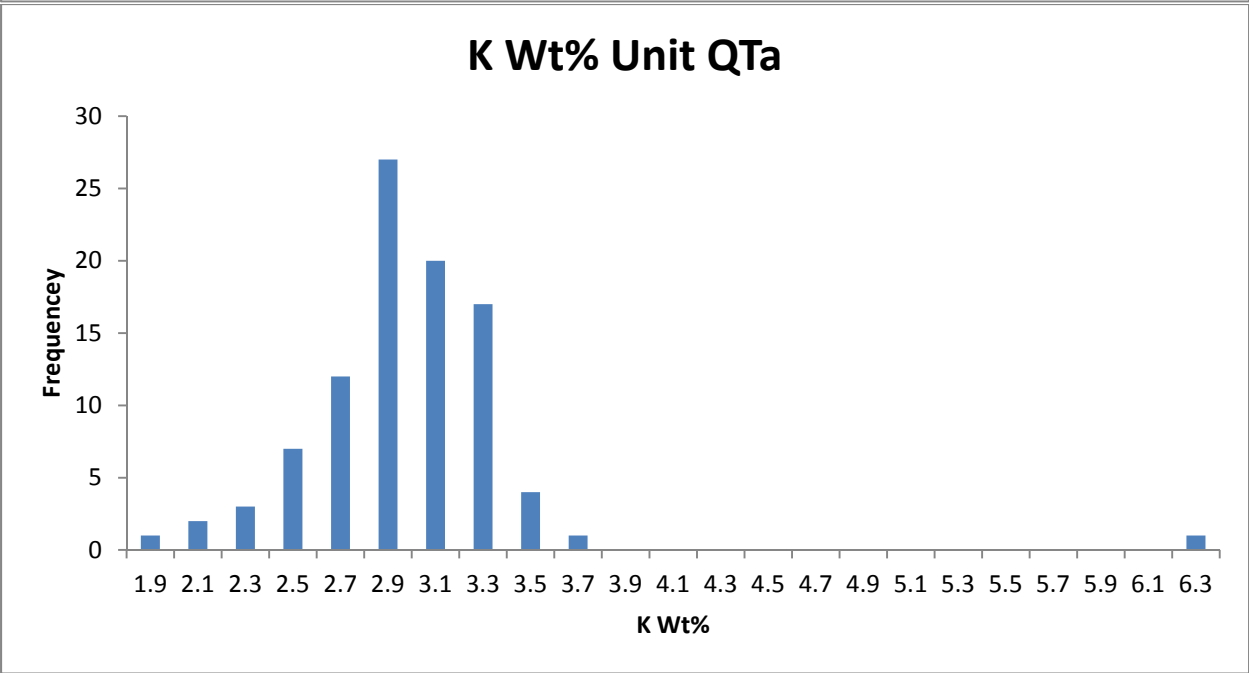
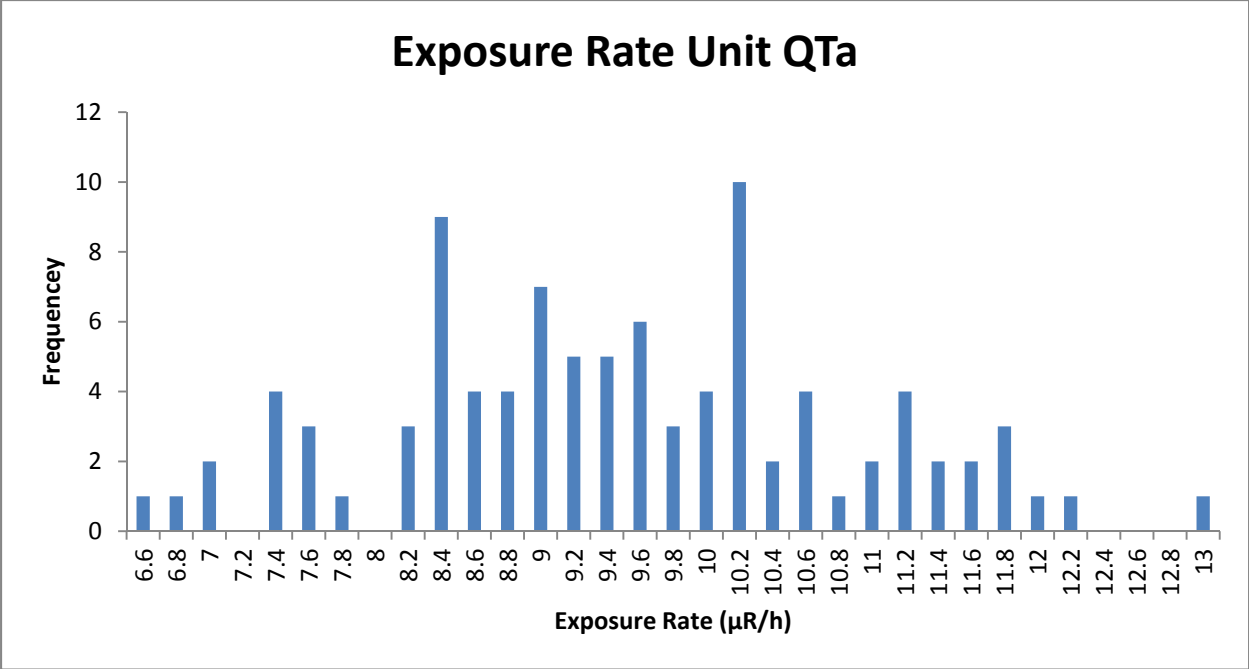
There is only one traditional geochemical data point within QTa. This point has a K value of 4.1% and U and Th values of 1.6 and 6.8 ppm respectively. The exposure rate calculated from these data is 8.2 $\mu\text{R/h}$ which is very close to the AMS mean of 8.3 $\mu\text{R/h}$ placing this unit well within the ± 1 $\mu\text{R/h}$ range.

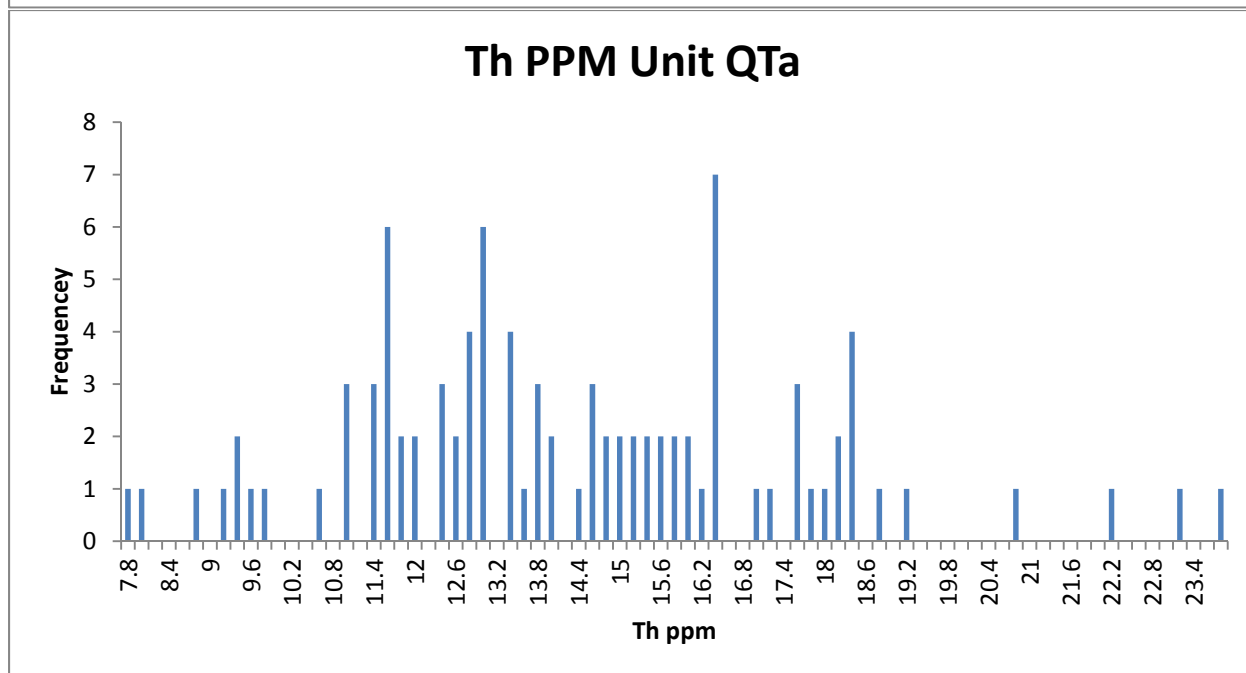
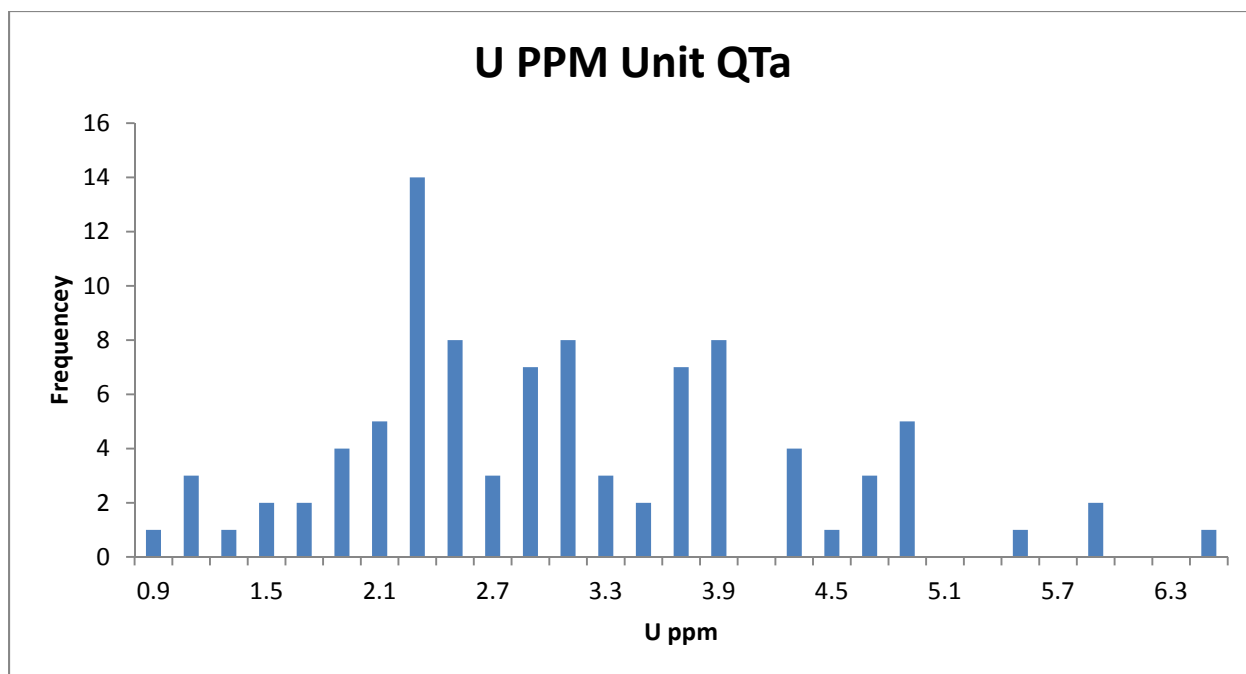
Sample ID	Latitude	Longitude	K %	U ppm	Th ppm
9674	35.3815	-114.693	4.135	1.6	6.785

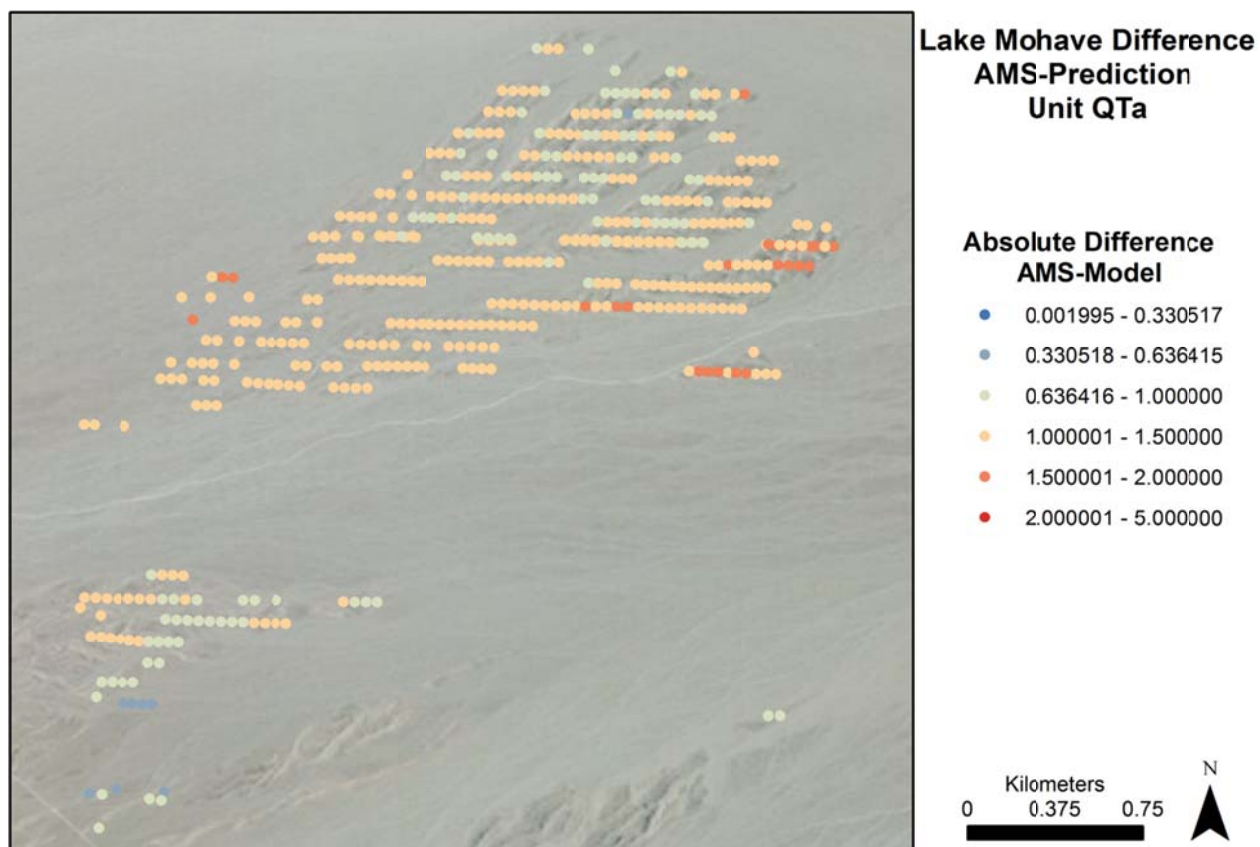
NURE Data

NURE exposure rate values for QTA are randomly distributed across a spectrum of values that run from 6.6 to 13 $\mu\text{R/h}$. The average NURE exposure rate is 9.4 $\mu\text{R/h}$ which compares to the AMS exposure rate of 8.3 $\mu\text{R/h}$. This places the NURE prediction in this unit outside the desired ± 1 $\mu\text{R/h}$ range. NURE K data is very similar to the AMS K data in this unit. U and Th values are however not consistent with AMS concentrations.

When comparing the NURE derived exposure rate to the AMS data points the hotter southern points are modeled well while much of the rest of the homogenous unit is just outside the desired range.







Data Summary

Exposure Rate Comparison $\mu\text{R/h}$	Average	Median	STD	Range
AMS Data	8.268	8.26518	0.235501	7.46408-9.06672
NURE Data	9.428872	9.4036	1.343939	6.6268-13.0084
Geochemical Prediction	8.18052	8.18052	N/A	N/A

Qch

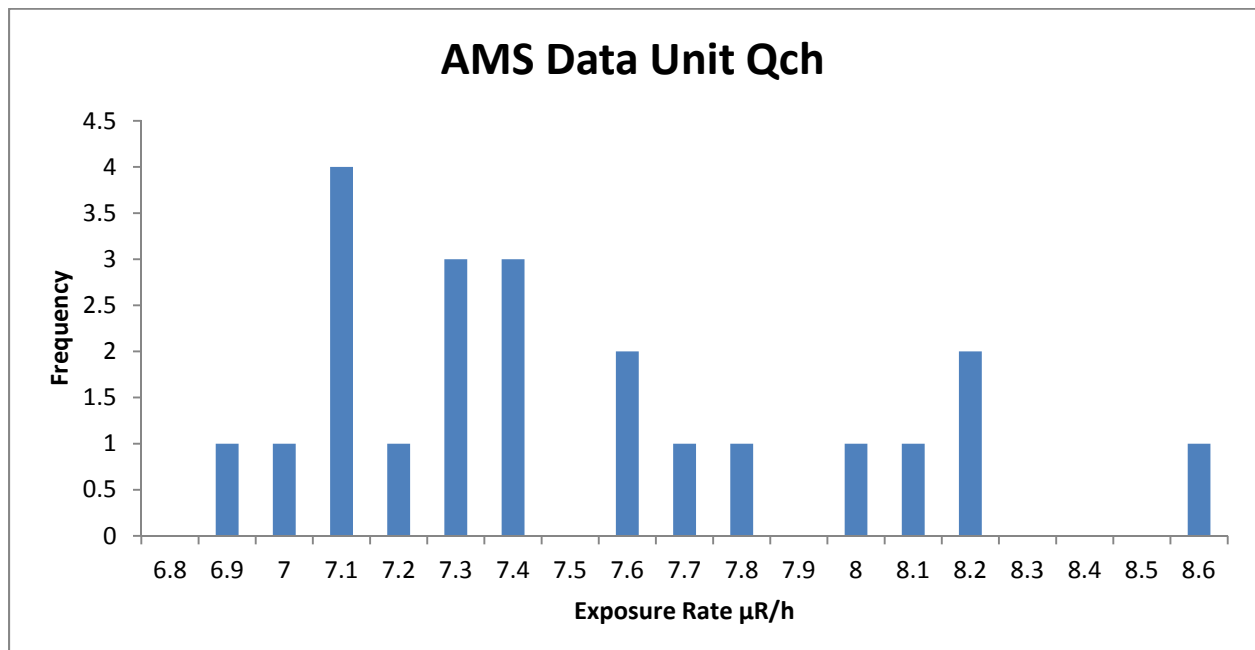
Composition

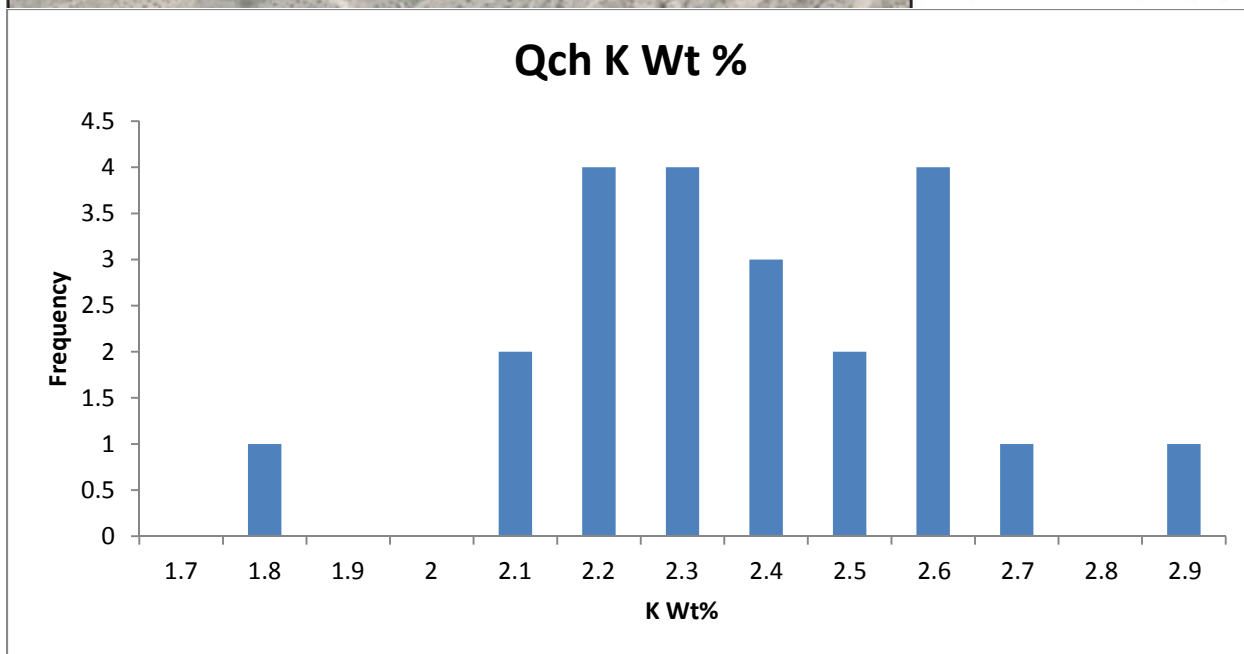
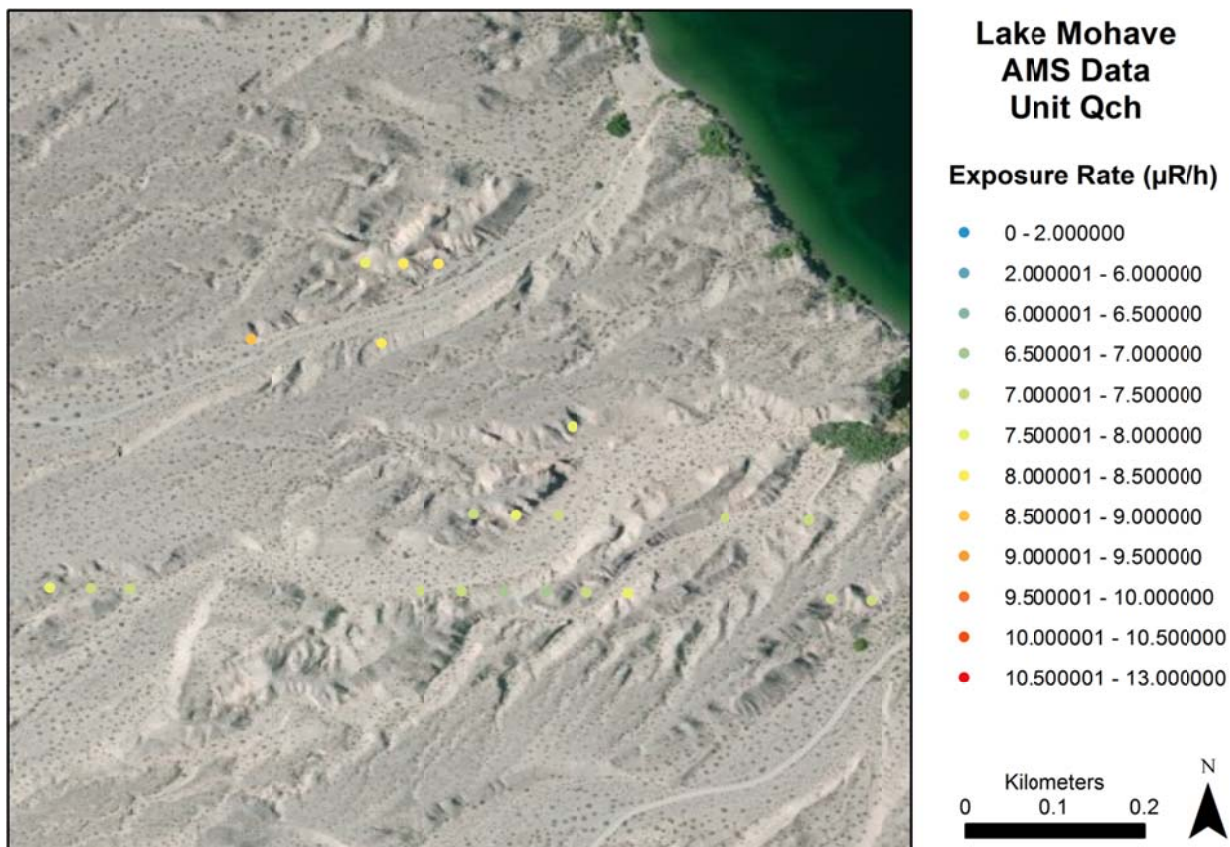
Qch is a late Pleistocene river gravel and sand deposit. This unit overlies older alluvial units such as Qai1 and Qcw. (House and Faulds, 2009) Compositional information for this unit is not available but it must contain gravel and sediment from further upstream of the Colorado River.

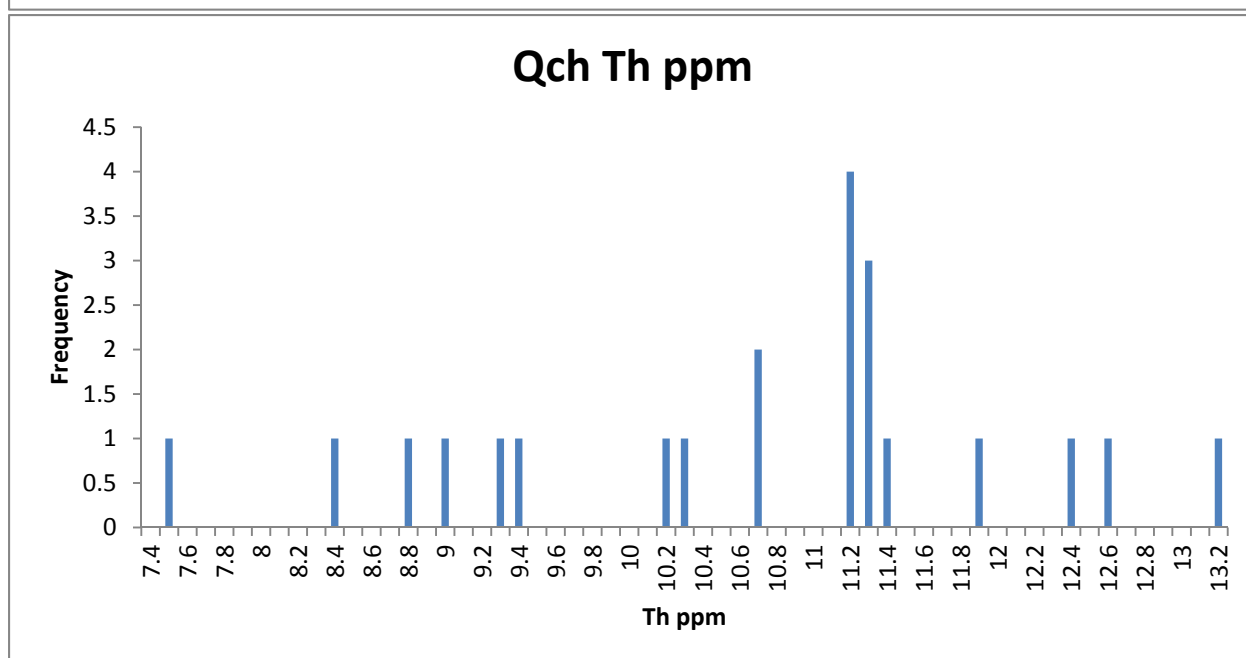
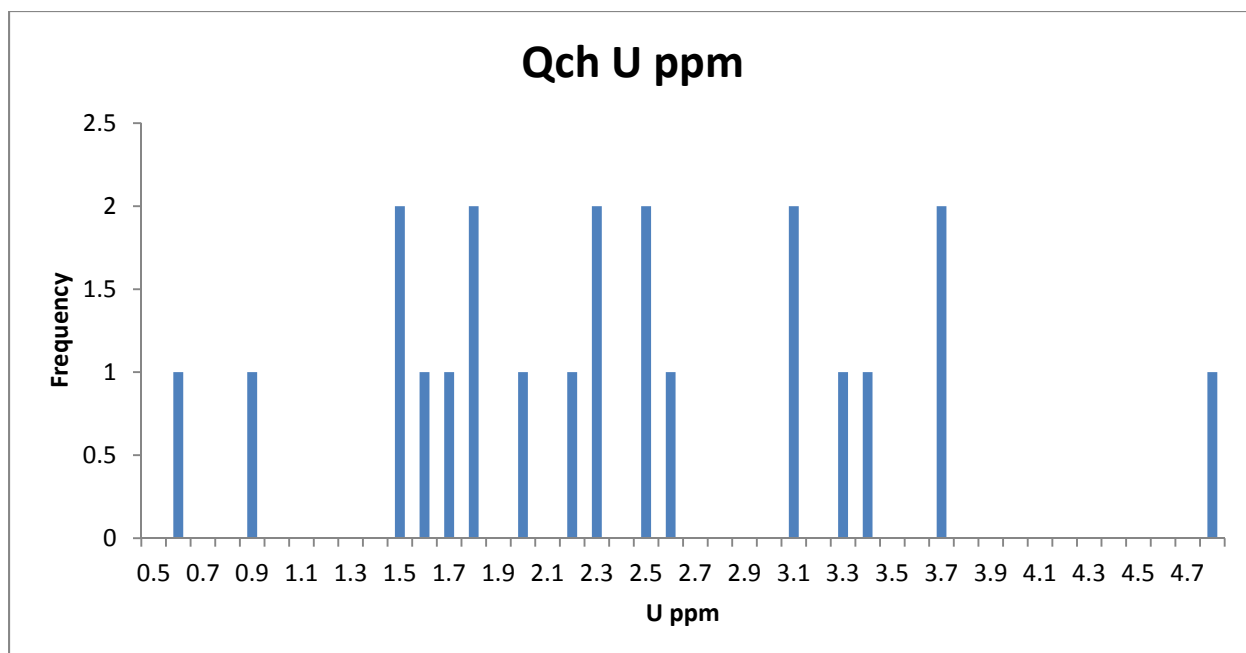
AMS Data

The AMS exposure rates for this unit are randomly distributed. There is little pattern in either the histogram distribution or the spatial distribution of the data. The average AMS exposure rate for Qch is 7.46 $\mu\text{R/h}$ with a standard deviation of 0.45 or 6% of the mean.

K, U, and Th values are also randomly distributed and have few notable features in both the histogram distribution and the spatial distribution.









Lake Mohave Radioelement Concentration Images Unit Qch

K Wt%

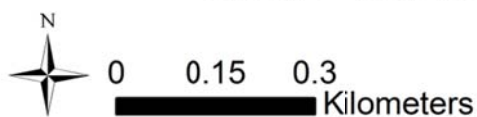
- 0.960459 - 2.243253
- 2.243254 - 2.723497
- 2.723498 - 2.956414
- 2.956415 - 3.187128
- 3.187129 - 3.672559

U PPM

- 0 - 1.581498
- 1.581499 - 2.338019
- 2.338020 - 3.035367
- 3.035368 - 3.852008
- 3.852009 - 6.135812

Th PPM

- 4.118740 - 9.969537
- 9.969538 - 10.905588
- 10.905589 - 11.949598
- 11.949599 - 13.168826
- 13.168827 - 14.872976
- 14.872977 - 18.871453





Lake Mohave Radioelement Ratio Images Unit Qch

U/K Ratio

- 0 - 0.498470
- 0.498471 - 0.745602
- 0.745603 - 0.968045
- 0.968046 - 1.208879
- 1.208880 - 1.542684
- 1.542685 - 3.123242



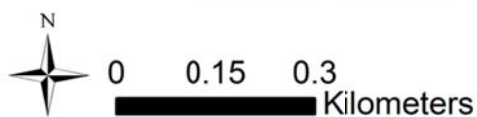
Th/K Ratio

- 2.090277 - 3.461301
- 3.461302 - 3.942091
- 3.942092 - 4.348792
- 4.348793 - 4.786292
- 4.786293 - 5.355216
- 5.355217 - 8.000000



U/Th Ratio

- 0 - 0.117615
- 0.117616 - 0.182165
- 0.182166 - 0.244454
- 0.244455 - 0.316216
- 0.316217 - 0.426078
- 0.426079 - 0.803350



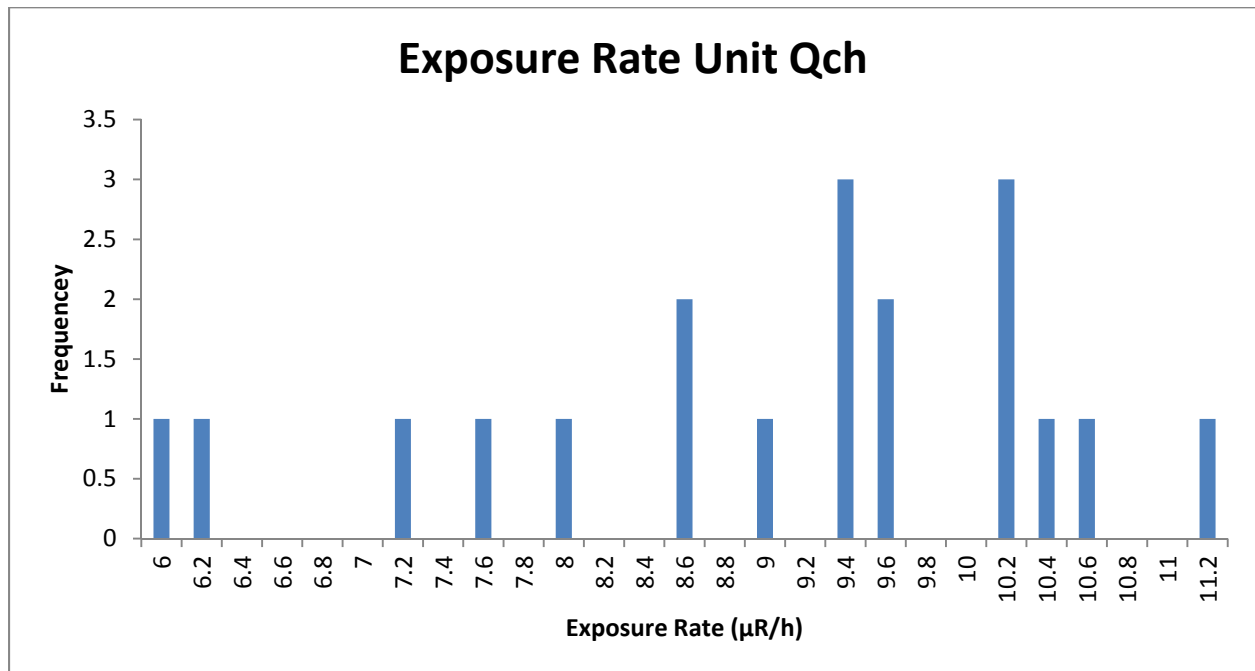
Traditional Geochemistry

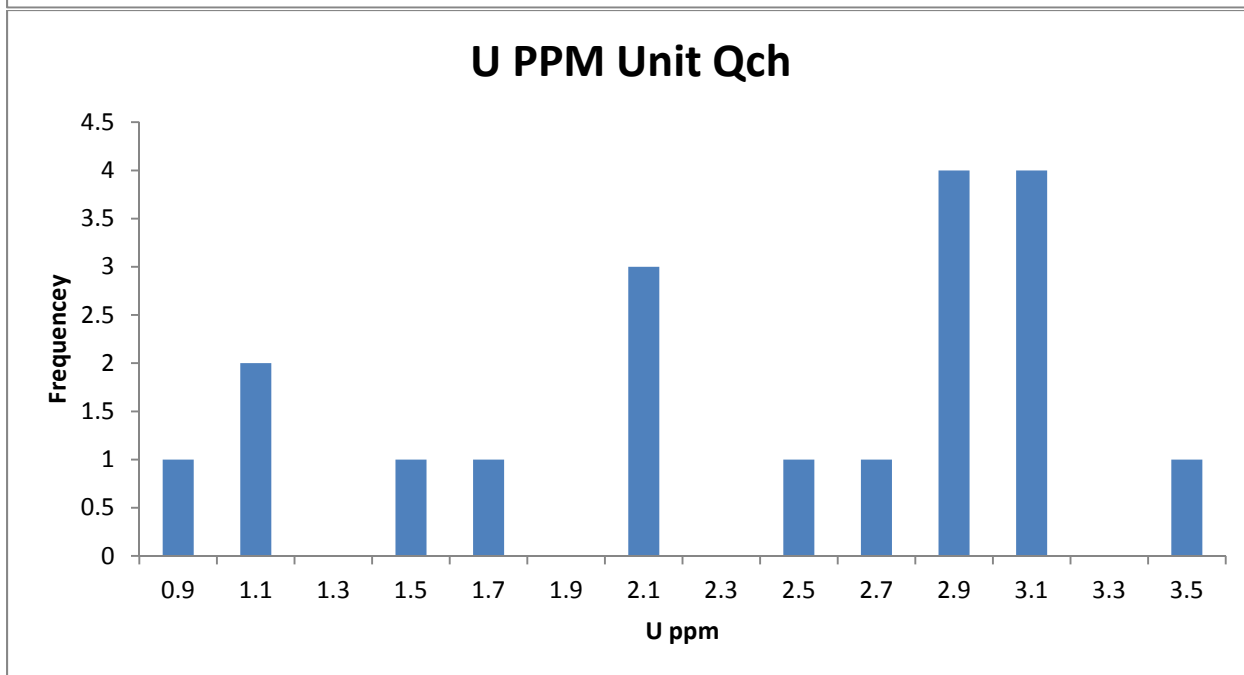
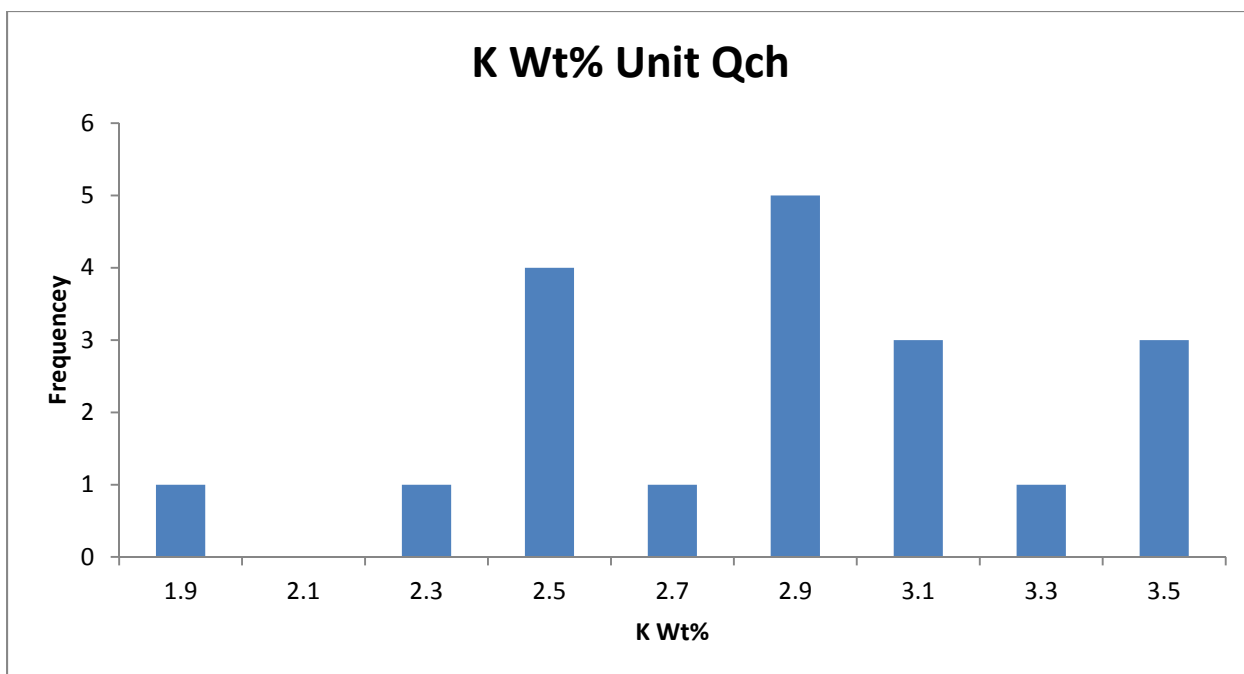
There are no traditional geochemical data for Qch.

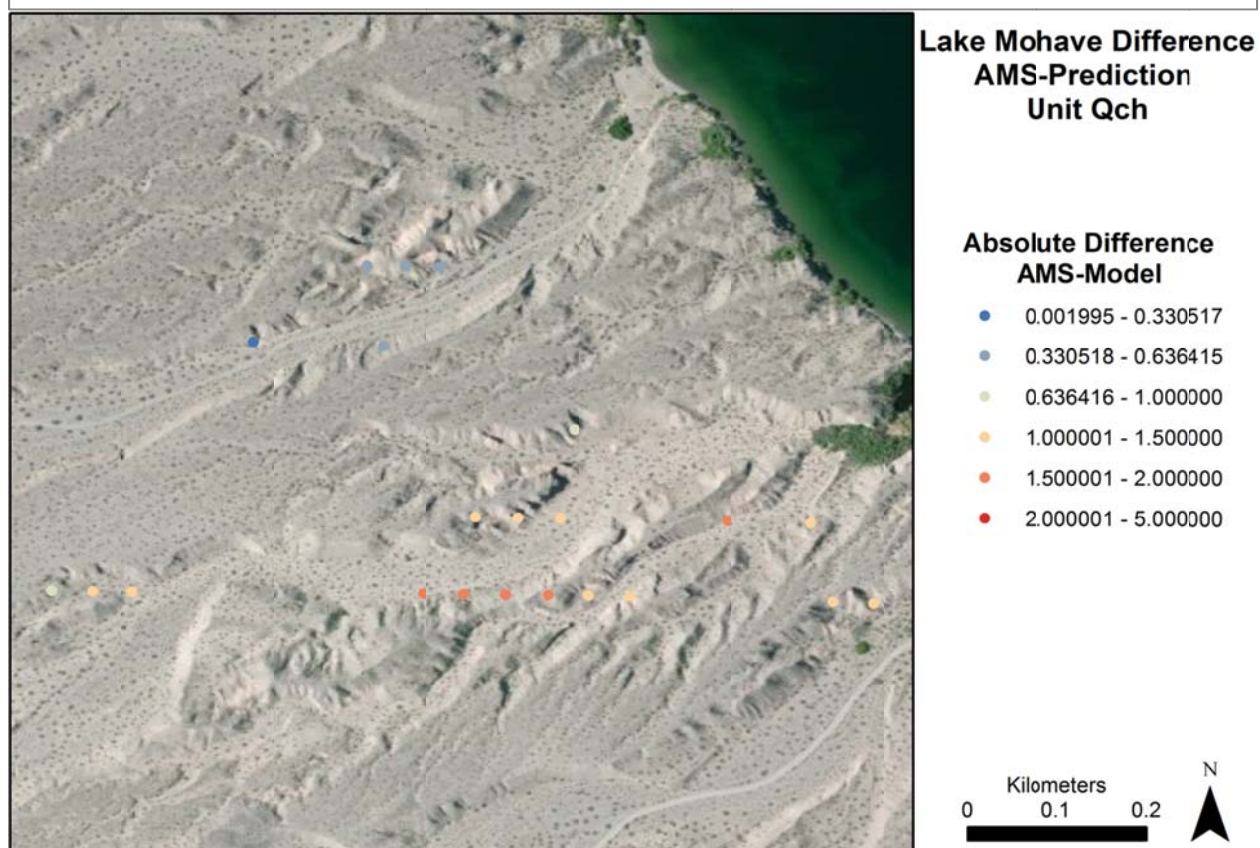
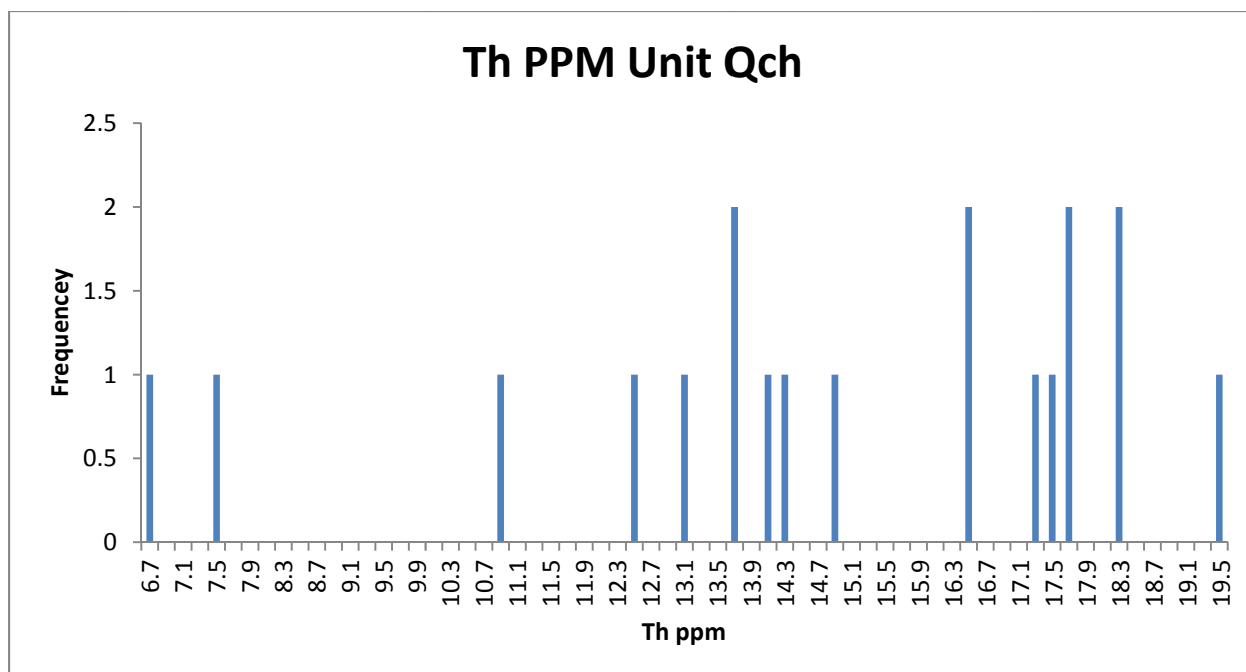
NURE Data

There are no notable features in the NURE exposure rate data for Qch. The NURE exposure rate for Qch is 8.97 $\mu\text{R/h}$ which compares with the AMS mean of 7.4 $\mu\text{R/h}$ placing this unit outside the desired ± 1 $\mu\text{R/h}$ range.

Comparing the NURE exposure rate to the AMS data points shows that the cooler portion of the unit are modeled well but the hotter portions are not.







Data Summary

Exposure Rate Comparison μR/h	Average	Median	STD	Range
AMS Data	7.464	7.346	0.459	6.8949-8.5917
NURE Data	8.974695	9.2492	1.43993	6.0416-11.1896

Tay1

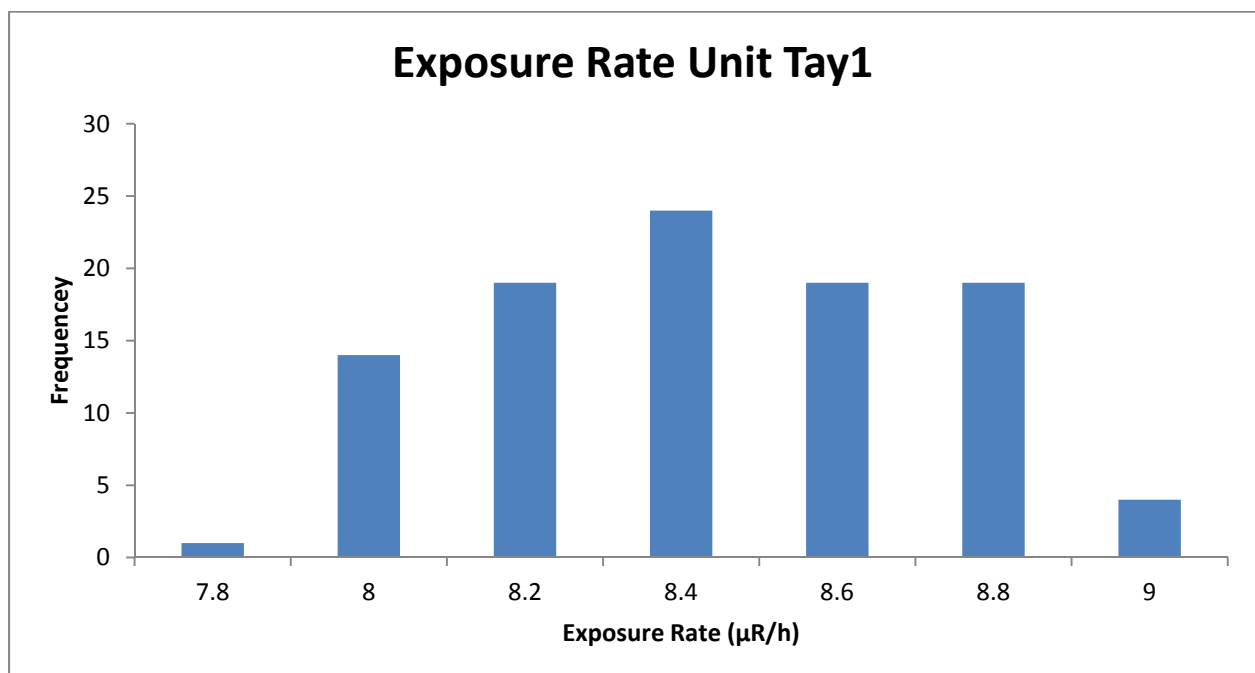
Composition

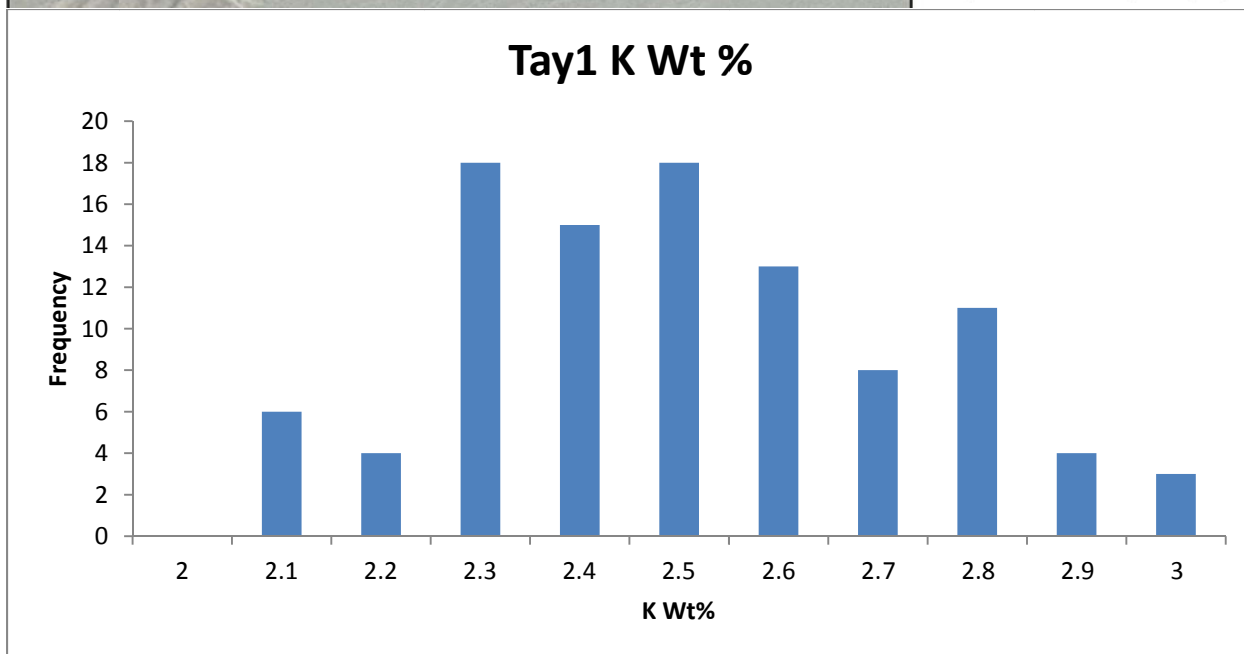
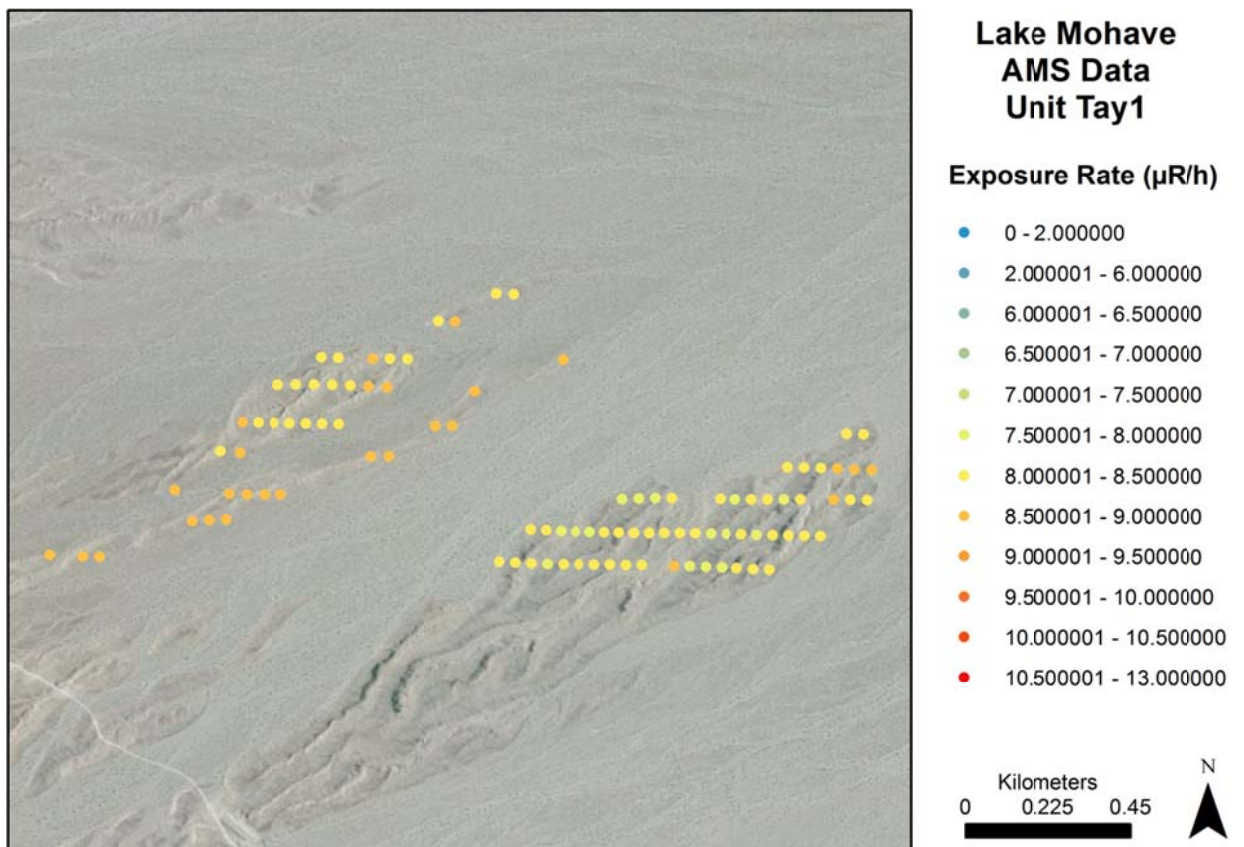
There are no published descriptions of Tay1. This unit was also not visited during field work. However, if this unit follows the trends in the area this unit should be an ancient alluvial fan that is early Pleistocene in age. It is likely composed of crystalline basement and felsic igneous rocks.

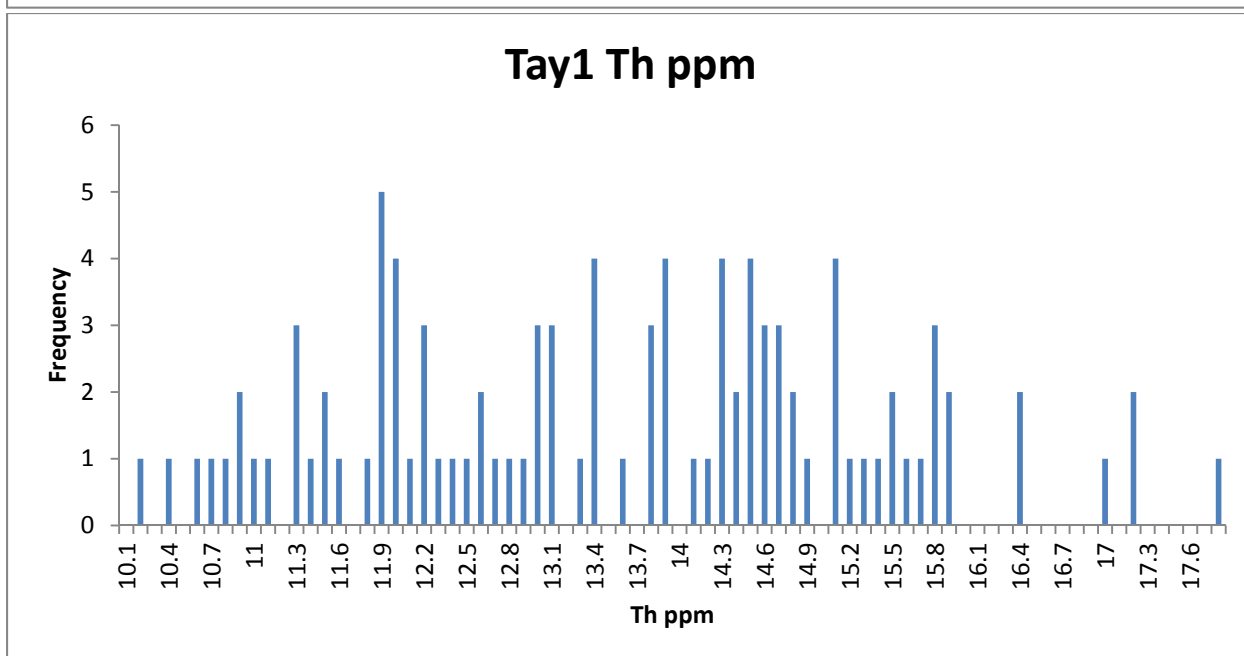
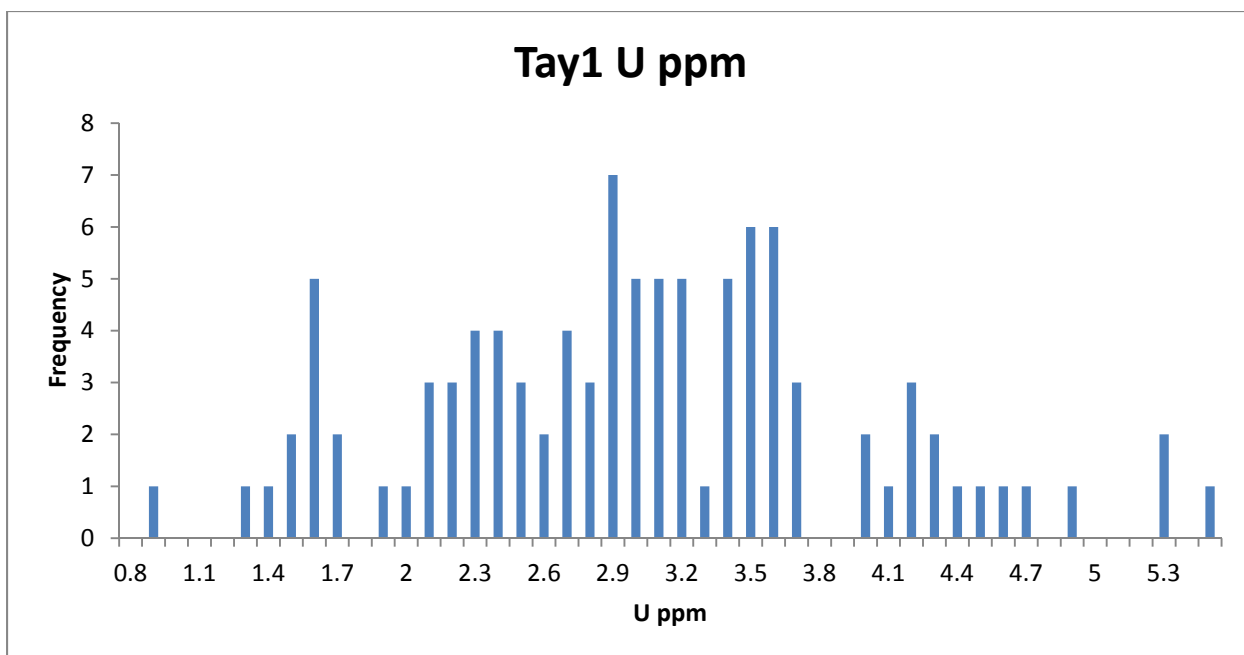
AMS Data

The AMS exposure rate data in Tay1 are homogenous and are mostly within ± 1 $\mu\text{R/h}$. The distribution is narrow with most of the data falling between 8 and 9 $\mu\text{R/h}$. The average exposure rate in Tay1 is 8.32 $\mu\text{R/h}$ with a standard deviation of 0.28 or 3% of the mean. There is very little spatial variation to the exposure rate.

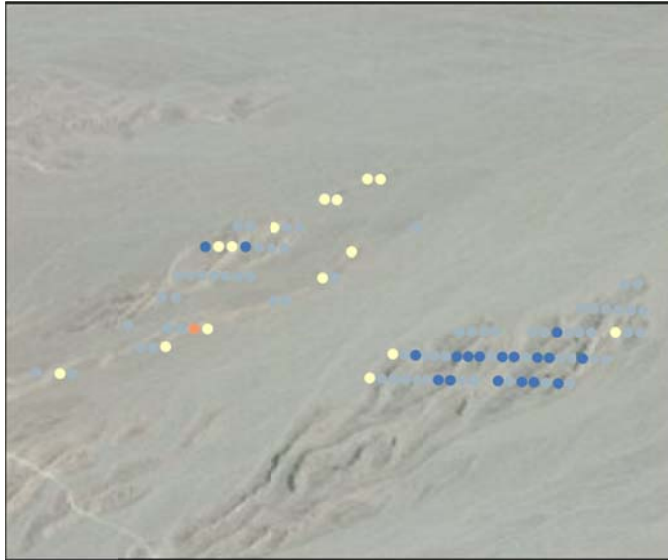
K values are between 2.3 and 2.8% with no strong peaks within that range. U and Th distributions are largely featureless. In terms of spatial distribution K, U, and Th show little discernable pattern.





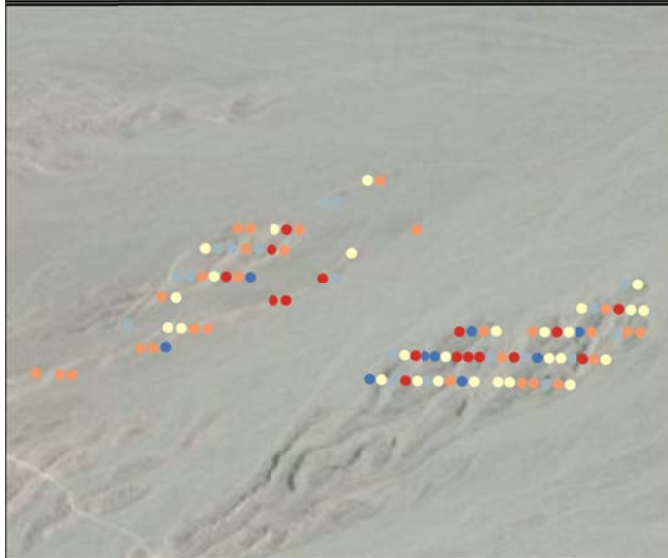


Lake Mohave Radioelement Concentration Images Unit Tay1



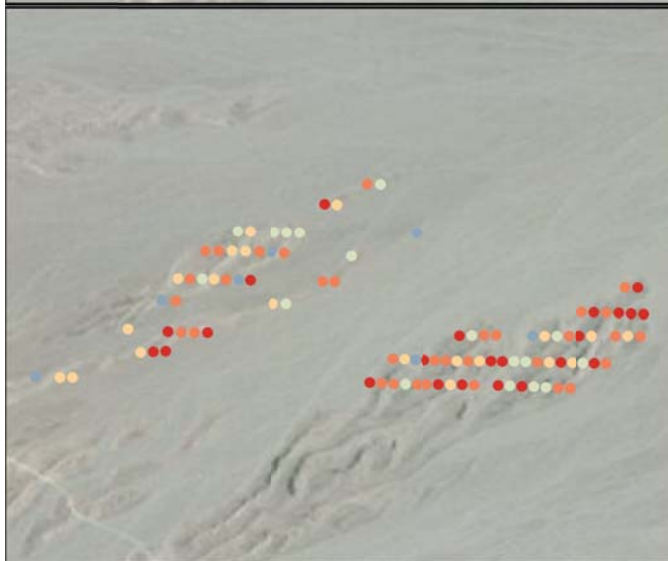
K Wt%

- 0.960459 - 2.243253
- 2.243254 - 2.723497
- 2.723498 - 2.956414
- 2.956415 - 3.187128
- 3.187129 - 3.672559



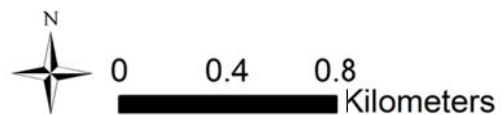
U PPM

- 0 - 1.581498
- 1.581499 - 2.338019
- 2.338020 - 3.035367
- 3.035368 - 3.852008
- 3.852009 - 6.135812



Th PPM

- 4.118740 - 9.969537
- 9.969538 - 10.905588
- 10.905589 - 11.949598
- 11.949599 - 13.168826
- 13.168827 - 14.872976
- 14.872977 - 18.871453



Lake Mohave Radioelement Ratio Images Unit Tay1

U/K Ratio

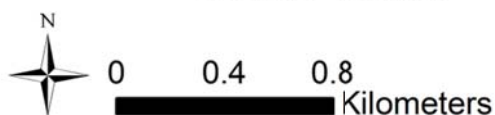
- 0 - 0.498470
- 0.498471 - 0.745602
- 0.745603 - 0.968045
- 0.968046 - 1.208879
- 1.208880 - 1.542684
- 1.542685 - 3.123242

Th/K Ratio

- 2.090277 - 3.461301
- 3.461302 - 3.942091
- 3.942092 - 4.348792
- 4.348793 - 4.786292
- 4.786293 - 5.355216
- 5.355217 - 8.000000

U/Th Ratio

- 0 - 0.117615
- 0.117616 - 0.182165
- 0.182166 - 0.244454
- 0.244455 - 0.316216
- 0.316217 - 0.426078
- 0.426079 - 0.803350



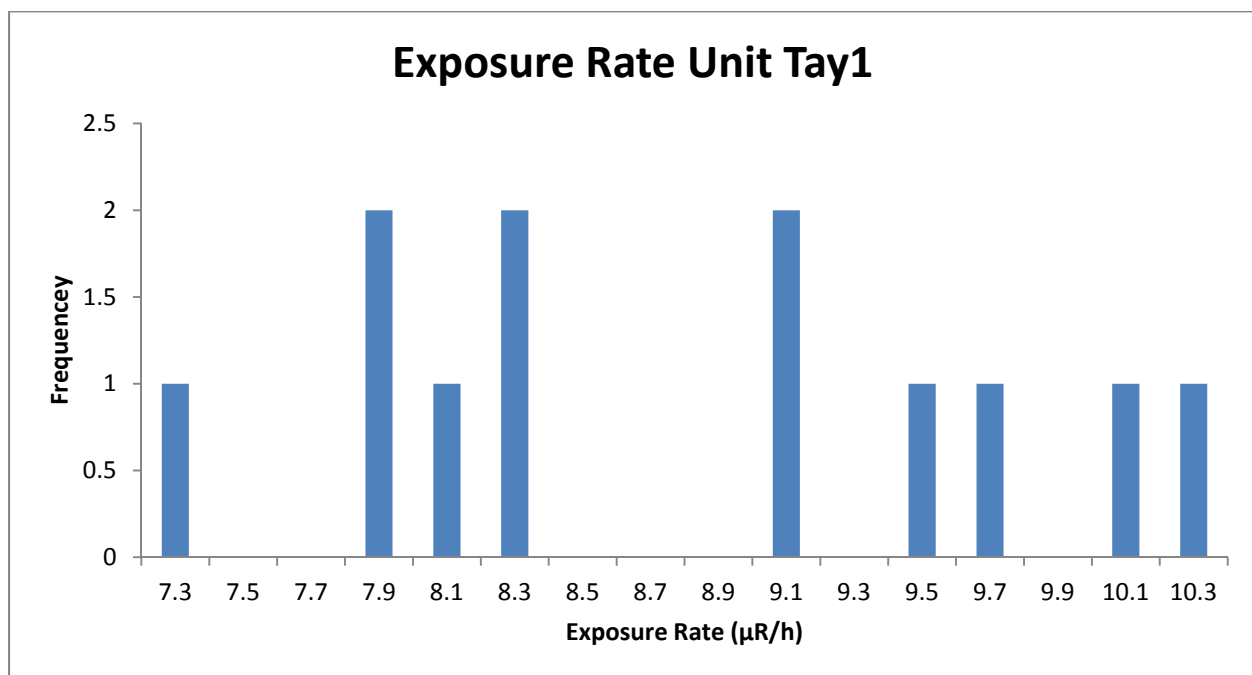
Traditional Geochemistry

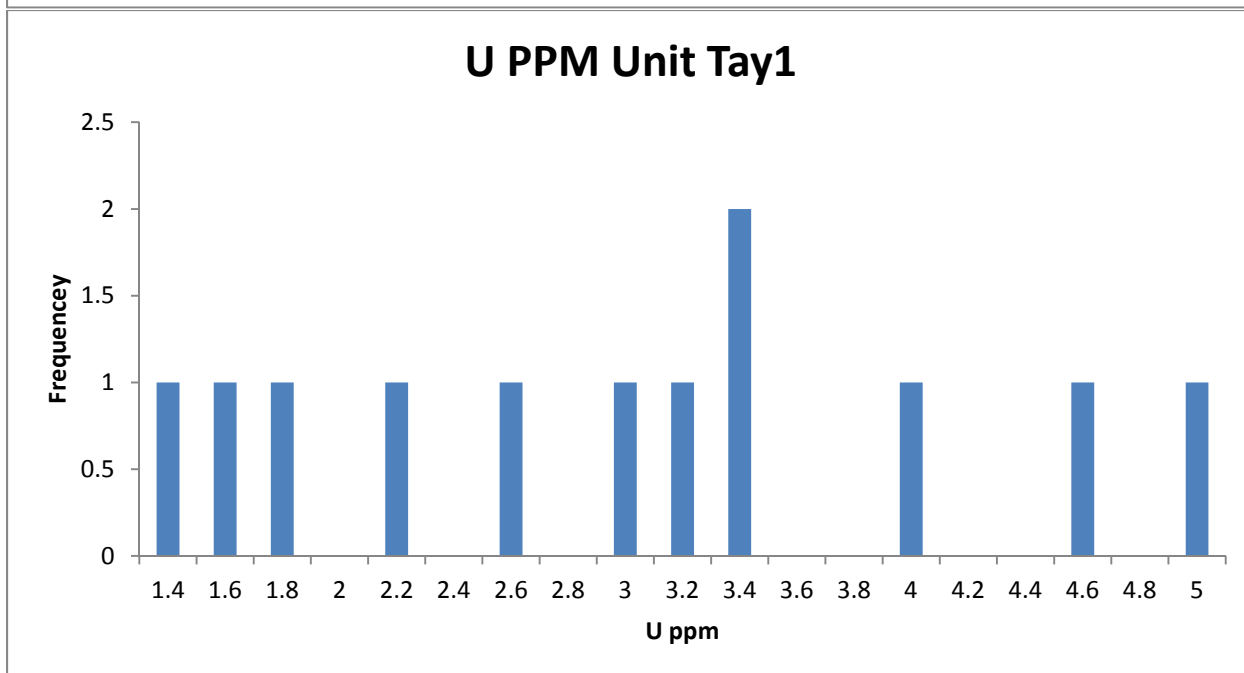
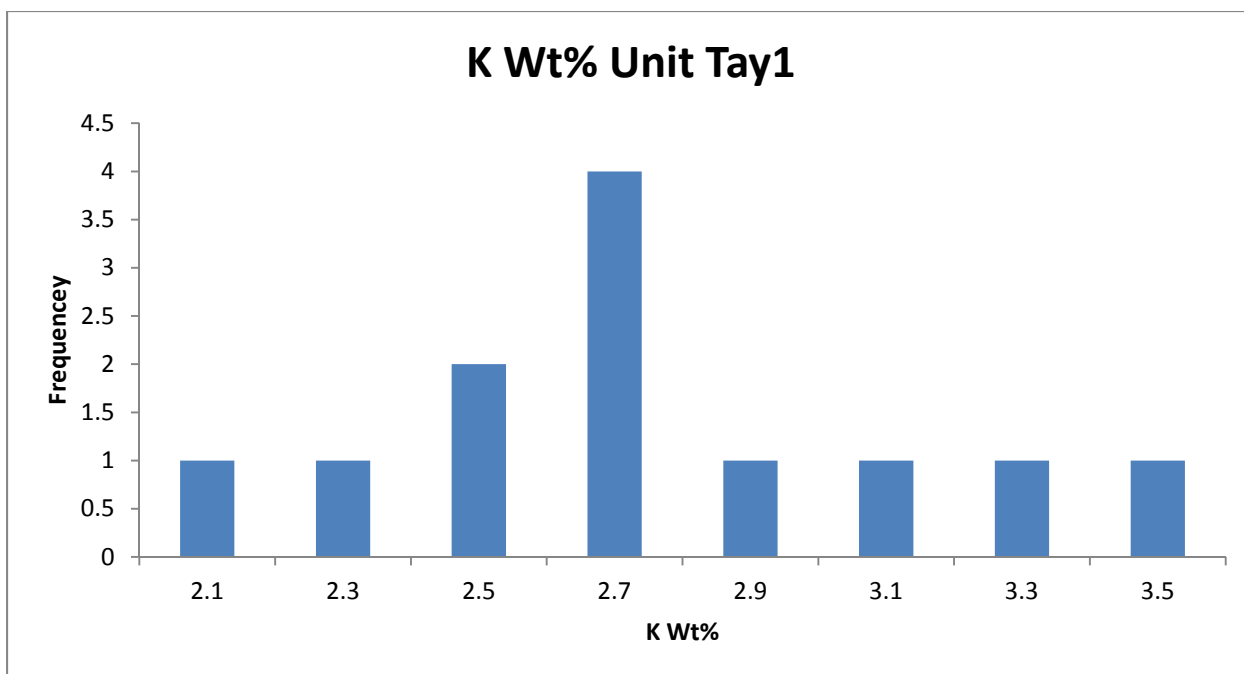
There are no traditional geochemical data for Tay1.

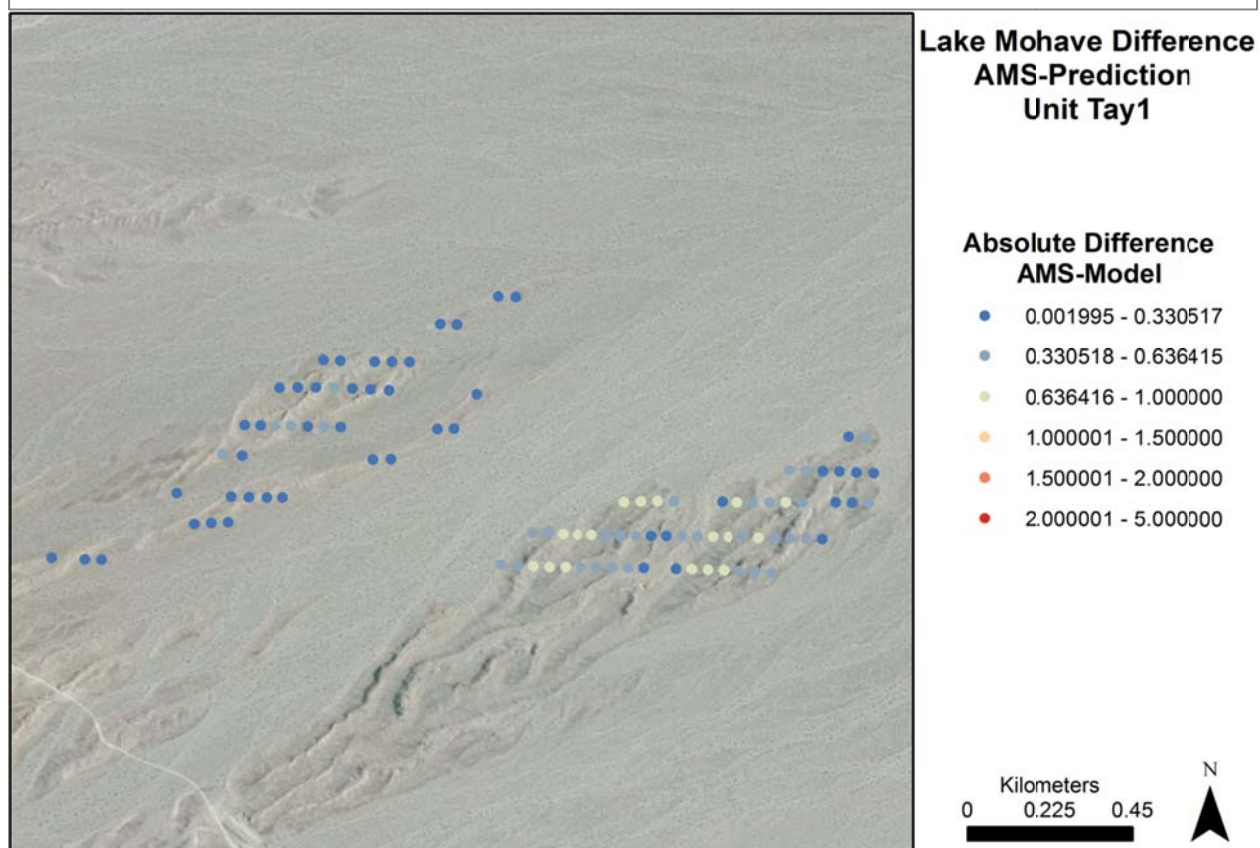
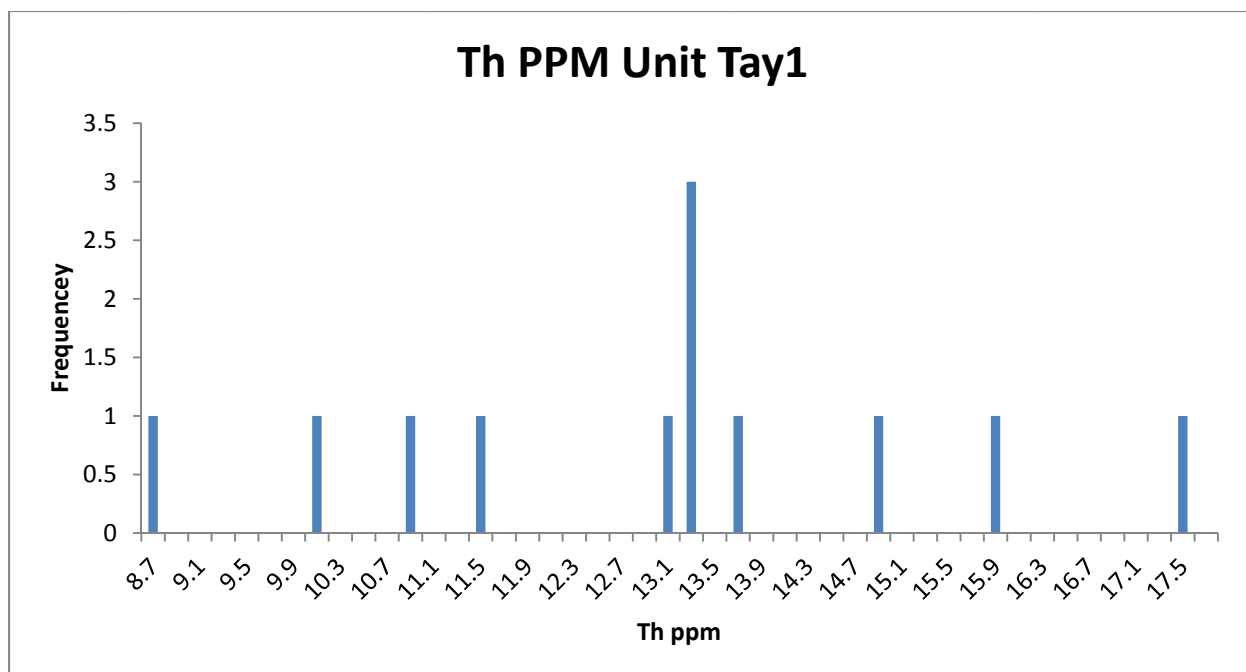
NURE Data

The NURE exposure rate data for Tay1 is largely featureless in terms of distribution. The average NURE exposure rate is 8.74 $\mu\text{R/h}$ which compares with the AMS average of 8.32 $\mu\text{R/h}$. This places this unit within the ± 1 $\mu\text{R/h}$ success range. K, U, and Th distributions have no distinct features to report.

When comparing the NURE exposure rate to the AMS data points in Tay1 it is clear that this unit is modeled well with this exposure rate. Most of the unit has a very small difference with the NURE mean with some small exceptions in the southeastern portion of the unit.







Data Summary

Exposure Rate Comparison μR/h	Average	Median	STD	Range
AMS Data	8.326431	8.332973	0.281439	7.793082-8.876783
NURE Data	8.741333	8.6474	0.946701	7.3048-10.1104

References

- Abrams, M. (2000). "The Advanced Spaceborne Thermal Emission and Reflection Radiometer (ASTER): Data products for the high spatial resolution imager on NASA's Terra platform." International Journal of Remote Sensing **21**(5).
- ASTM (2004). Standard Guide for High-Resolution Gamma-Ray Spectrometry of Soil Samples. ASTM Standard C1402-04. West Conshohocken, PA.
- ASTM (2005). Standard Practice for Soil Sample Preparation for the Determination of Radionuclides. ASTM Standard C999-05. West Conshohocken, PA.
- Beamish, David (2013). "Gamma ray attenuation in the soils of Northern Ireland, with special reference to peat." Journal of Environmental Radioactivity **115**: 13-27.
- Beck, H. L, J DeCampo, et al. (1972). In-situ Ge(Li) and NaI(Tl) gamma-ray spectrometry. Springfield, National Technical Information Service.
- Billingsley, G. H., S. S. Priest, et al. (2007). Geologic Map of the Cameron 30' x 60' Quadrangle, Coconino County, Northern Arizona. U. G. Survey.
- Books, Kenneth G. (1962). Aeroradioactivity survey and related surface geology of parts of the Los Angeles region, California.
- Breitner, Dániel, János Osán, et al. (2014). "Characteristics of uranium uptake of Boda Claystone Formation as the candidate host rock of high level radioactive waste repository in Hungary." Environmental Earth Science **73**: 209-219.
- BrooksRand (2007). Method 6020A - Inductively Coupled Plasma-mass Spectrometry.
- Burns, P. and R. Finch (1999). Uranium: Mineralogy, Geochemistry and the Environment. Washington, DC, Mineralogical Society of America.
- Castor, S.B., J.E. Faulds, et al. (2000). Geologic Map of the Frenchman Mountain Quadrangle, Clark County, Nevada. Reno, NV, Nevada Bureau of Mines and Geology.
- Cember, Herman and Thomas E. Johnson (2009). Introduction to Health Physics. New York, McGraw Hill Medical.
- Dickson, B.L. (1995). "U-series disequilibrium in Australian soils and its effect on aerial gamma-ray surveys." Journal of Geochemical Exploration **55**: 177-186.
- Dickson, B.L. and K.M. Scott (1997). "Interpretation of aerial gamma-ray surveys-adding the geochemical factors." AGSO Journal of Australian Geology and Geophysics **17**: 187-200.

Duebendorfer, Ernest M. (2003). Geologic Map of the Government Wash Quadrangle. Reno, NV, Nevada Bureau of Mines and Geology.

Duval, Joseph S., John M. Carson, et al. (2005). Terrestrial radioactivity and gamma-ray exposure in the United States and Canada: Open-File Report 2005-1413, U.S. Geological Survey.

Gasser, E., A. Nachab, et al. (2014). "Update of ^{40}K and ^{226}Ra and ^{232}Th series g-to-dose conversion factors for soil." Journal of Environmental Radioactivity **138**: 68-71.

George, David C., Edward F. Novak, et al. (1985). Calibration-Pad Parameter Assignments for In-Situ Gamma Ray Measurements of Radium, Thorium and Potassium. Grand Junction, CO.

Grasty, R., J. Carson, et al. (1984). Natural background radiation in Canada, Geological Survey of Canada Bulletin **360**: 39.

Griscom, Andrew and Donald L. Peterson (1961). "Aeromagnetic, aeroradioactivity, and gravity investigations of piedmont rocks in the Rockville Quadrangle Maryland." Short Papers in the Geologic and Hydrologic Sciences, Articles.

Hess, Paul C. (1989). Origins Of Igneous Rocks. Cambridge, Mass, Harvard University Press.

Hinz, Nicholas H., James E. Faulds, et al. (2012). Preliminary Geologic Map Of The North Half Of The Fourth Of July Mountain Quadrangle, Clark County, Nevada. N. B. o. M. a. Geology. Reno, NV.

Hinz, Nicholas H., James E. Faulds, et al. (2012). Preliminary Geologic Map Of The Ireteba Peaks Quadrangle, Clark County, Nevada. N. B. o. M. a. Geology and R. University of Nevada. Reno, NV.

House, P. Kyle and James E. Faulds (2008). Preliminary Geologic Map of the North Half of the Spirit Mtn. NW Quadrangle, Clark County, Nevada and Mohave County, Arizona. Reno, NV, Nevada Bureau of Mines and Geology.

IAEA (2003). Guidelines for radioelement mapping using gamma ray spectrometry data, International Atomic Energy Agency.

Knoll, Glenn F. (2000). Radiation Detection and Measurement. Ann Arbor, Mi, John Wiley & Sons, Inc.

Koons, R. D., P.A. Helmke, et al. (1980). "Association of Trace Elements with Iron Oxides During Rock Weathering." Soil Science Society of America **44**: 155-159.

Lambert, J.H. (1760) Photometria sive de mensura et gradibus luminis, colorum et umbrae.

Langenheim, V.E., R.C. Jachens, et al. (1997). Preliminary Location and Geometry of the Las Vegas Valley Shear Zone Based on Gravity and Aeromagnetic Data. Menlo Park, Ca, U.S. Geological Survey.

Lee, Seung Yeop and Min Hoon Baik (2009). "Uranium and other trace elements' distribution in Korean granite: implications for the influence of iron oxides on uranium migration." Environmental Geochemical Health **31**: 413-420.

Løvborg, L. and P. Kirkegaard (1974). "Response of 3" × 3" NaI(Tl) detectors to terrestrial gamma radiation." Nuclear Instruments and Methods **121**: 239-251.

Meer, Freek D. van der, Harald M.A. van der Werff, et al. (2011). "Multi- and hyperspectral geologic remote sensing: A review." International Journal of Applied Earth Observation and Geoinformation **14**: 112-128.

Michel, Jacqueline (1984). "Redistribution of uranium and thorium series isotopes during isovolumetric weathering of granite." Geochimica et Cosmochimica Acta **48**: 1249-1255.

Minty, B. (1997). "Fundamentals of airborne gamma-ray spectrometry." AGSO Journal of Australian Geology and Geophysics **17**: 39-50.

Moxham, R. (1963). "Natural Radioactivity In Washington County, Maryland." Geophysics **28**: 262-272.

Patino, Linda C., Michael A. Velbel, et al. (2003). "Trace element mobility during spheroidal weathering of basalts and andesites in Hawaii and Guatemala." Chemical Geology: 343-364.

Pelowitz, D.B. (2008). MCNPX User's Manual, Version 2.6.0.

Pitkin, J., R. Bates, et al. (1964). "Aeroradioactivity surveys and geologic mapping (Nuclear facility background gamma radiation measured by aerial radiological measurement)." The Natural Radiation Environment: 723-736.

Reheis, Marith C., James R. Budahn, et al. (2009). "Compositions of modern dust and surface sediments in the Desert Southwest, United States." JOURNAL OF GEOPHYSICAL RESEARCH **114**.

Schumacher, B. A, K. C. Shines, et al. (1990). A Comparison Of Soil Sample Homogenization Techniques. E. M. S. L. O. O. R. A. Development. Las Vegas, NV, U.S. Environmental Protection Agency.

Sloan, John (2011). Laboratory Report. North Las Vegas, NV, Silver State Analytical Laboratories; Pabco Gypsum.

Tosaka (2008). Decay chain 4n, Thorium series, https://en.wikipedia.org/wiki/File:Decay_chain%284n,Thorium_series%29.PNG.

Tosaka (2014). Uranium-238 Series Decay Chain, https://en.wikipedia.org/wiki/File:Decay_chain%284n%2B2,_Uranium_series%29.svg.

Tubas (2011). Potassium 40 decay scheme, <https://en.wikipedia.org/wiki/File:Potassium-40-decay-scheme.svg>.

Ulbrich, H. H. G. J, M. N. C. Ulbrich, et al. (2009). "Levantamentos Gamaespectrométricos Em Granitos Diferenciados: Revisão Da Metodologia E Do Comportamento Geoquímico Dos Elementos K, Th E U." Geologia USP. Série Científica **9**: 33-53.

Ward, D.L. (1978). Construction of the Calibration Pads Facility Walker Field Grand Junction, Colorado. U. D. o. Energy. Grand Junction.

Wilford, J., P. Bierwirth, et al. (1997). "Application Of Airborne Gamma-Ray Spectrometry In Soil/regolith Mapping And Applied Geomorphology." AGSO Journal of Australian Geology and Geophysics **17**: 201-216.

Wilford, J. and B. Minty (2007). The use of Airborne Gamma-Ray Imagery for Mapping Soils and Understanding Landscape Processes. Digital Soil Mapping: an Introductory Perspective. **31**: 207-218.

Winter, John D. (2010). Principles of Igneous and Metamorphic Petrology. New York, Prentice Hall.

YBG (2013). Uranium-235 Series Decay Chain, https://en.wikipedia.org/wiki/File:Decay_Chain_of_Actinium.svg.

Curriculum Vitae

Daniel A. Haber
1464 Creslow Ct #101
Las Vegas, NV 89102
(702) 378-3951
haberda@gmail.com

Education

University of Nevada Las Vegas, Las Vegas, NV

Expected Graduation: Fall 2015

Master of Science, Geoscience, GPA: 3.96

Thesis: Predictive Modeling of Terrestrial Radiation Exposure from Geologic Materials

University of Nevada Las Vegas, Las Vegas, NV

Graduation: Fall 2013

Bachelor of Science, Geology, GPA: 3.61

Advanced Technologies Academy, Las Vegas, NV

Graduated with Honors: May 2002

High School Diploma with Major, Computer Science, GPA: 3.5

Research and Relevant Work Experience

UNLV – Geoscience Department, Las Vegas NV, January 2014 – Present

Graduate Research Assistant – Supervised by Pamela C. Burnley, PhD.

R&D of technique to predict gamma ray emissions from geology

Creation of GIS models

Creation and interpretation of Monte Carlo N-Particle Transport models

Gamma spectra data reduction and analysis

Interpretation of geology and geochemistry

UNLV - NeRD Lab, Las Vegas NV, January 2013 - January 2014

Lab Assistant - Supervised by Pamela C. Burnley, PhD.

Peak fitting and data reduction

Writing of computer code

UNLV - LVIS Lab, Las Vegas NV, May 2012 - May 2013

Lab Assistant - Supervised by Matthew S. Lachniet, PhD.

Field sample collection followed by lab preparation and analysis

Operation of Kiel V device as well as mass spectrometer

UNLV – Independent Study, Las Vegas NV, Fall 2013

Undergraduate Student - Supervised by Ganqing Jiang, PhD.

Investigation of an early Mississippian carbon isotope excursion

UNLV – Independent Study, Las Vegas NV, Spring 2012

Undergraduate Student - Supervised by Stephen M. Rowland, PhD.

Characterizing Archeocyathan provinciality and the break-up of Rodinia

Relevant Coursework

- Remote Sensing
- GIS: Theory and Application
- Environmental Health Physics
- Radiation Detection
- Advanced Mineralogy
- Advanced Geochemistry
- ExxonMobil Geophysics Short Course

Other Work Experience

Rental Systems Incorporated, Las Vegas NV, August 2006 - September 2009

Production Department Head

- Maintain corporate LAN and file servers
- Managed large inventory of computers
- Supervised teams up to 10 in production and deployment of client machines

United States Marine Corps, Thurmont, MD, August 2002 - August 2006

Security Operations Controller\Rank Sergeant (E-5)

- Operated Security Operations Center at the Presidential Retreat, Camp David
- Handled classified information
- Conducted security for the President of the United States

Other Skills

Computer

- ESRI ArcGIS
- Microsoft Products
- Adobe Products
- Linux/Unix Environments
- General Computer Networking
- C++, Basic

Managerial

- Sergeant of Marines
- Head of Production Department
- Led teams up to 10

Honors and Awards

- Presidential Support Badge 2005
- White House Letter 2005
- Honorable Separation from the Marine Corps 2010

1st Place CSN Spring Public Speaking Festival 2010

L. Austin Weeks Grant Award 2012 \$500 Award

Outstanding Geoscience Undergraduate 2012

Abstracts

Haber, D., Burnley, P.C., Marsac, K. and Malchow, R. (2014) Predictive radiological background distributions from geochemical data. Abstract NH11B-3711, Fall Meeting, AGU, San Francisco, Calif.

Marsac, K., Burnley, P., Malchow, R. Haber, D. Hausrath, E., Adcock, C. (2014) Modeling background radiation in our environment using geochemical data. Geological Society of America, Abstracts with Programs. Vol. 46, No. 6, p.109

Haber, D., Burnley, P.C., Marsac, K. and Malchow, R. (2014) Predictive radiological background distributions from geochemical data. Abstract, AEG 2014 Annual Meeting - Program with Abstracts, Scottsdale, AZ, p. 58.

References

Andrew D. Hanson, PhD.

Associate Dean, Honors College
University of Nevada, Las Vegas
4505 S. Maryland Pkwy.
Las Vegas, NV 89154 LLB 3273
(702) 895-2263
andrew.hanson@unlv.edu

Matthew S. Lachniet, PhD.

Associate Professor of Geology
University of Nevada, Las Vegas
4505 S. Maryland Pkwy.
Las Vegas, NV 89154 SEB 3240
(702) 895-4388
matthew.lachniet@unlv.edu

Pamela C. Burnley, PhD.

Associate Research Professor
University of Nevada, Las Vegas
4505 S. Maryland Pkwy.
Las Vegas, NV 89154 LFG 212
(702) 895-5460
burnley@physics.unlv.edu

Stephen M. Rowland, PhD.

Professor of Geology
University of Nevada, Las Vegas
4505 S. Maryland Pkwy.
Las Vegas, NV 89154 LFG 210
(702) 895-3625
steve.rowland@unlv.edu